



United States Department of Agriculture

Proceedings

20th International Nondestructive Testing and Evaluation of Wood Symposium

Madison, Wisconsin USA
2017



Forest Service, Forest Products Laboratory
Forest Products Society
International Union of Forest Research Organizations

General Technical Report
FPL-GTR-246

September
2017

Abstract

The 20th International Nondestructive Testing and Evaluation of Wood Symposium was hosted by the USDA Forest Service Forest Products Laboratory in Madison, Wisconsin, USA, on September 12–15, 2017. This Symposium was a forum for those involved in nondestructive testing and evaluation (NDT/NDE) of wood and brought together many NDT/NDE users, suppliers, international researchers, representatives from various government agencies, and other groups to share research results, products, and technology for evaluating a wide range of wood products, including standing trees, logs, lumber, and wood structures. Networking among participants encouraged international collaborative efforts and fostered the implementation of NDT/NDE technologies around the world. The technical content of the 20th Symposium is captured in these proceedings.

Keywords: International Nondestructive Testing and Evaluation of Wood Symposium, nondestructive testing, nondestructive evaluation, wood, wood products

September 2017

Wang, Xiping; Senalik, C. Adam; Ross, Robert J., eds. 2017. Proceedings: 20th International Nondestructive Testing and Evaluation of Wood Symposium. General Technical Report FPL-GTR-246. Madison, WI: U.S. Department of Agriculture, Forest Service, Forest Products Laboratory. 539 p.

A limited number of free copies of this publication are available to the public from the Forest Products Laboratory, One Gifford Pinchot Drive, Madison, WI 53726–2398. This publication is also available online at www.fpl.fs.fed.us. Laboratory publications are sent to hundreds of libraries in the United States and elsewhere.

The Forest Products Laboratory is maintained in cooperation with the University of Wisconsin.

The use of trade or firm names in this publication is for reader information and does not imply endorsement by the United States Department of Agriculture (USDA) of any product or service.

In accordance with Federal civil rights law and U.S. Department of Agriculture (USDA) civil rights regulations and policies, the USDA, its Agencies, offices, and employees, and institutions participating in or administering USDA programs are prohibited from discriminating based on race, color, national origin, religion, sex, gender identity (including gender expression), sexual orientation, disability, age, marital status, family/parental status, income derived from a public assistance program, political beliefs, or reprisal or retaliation for prior civil rights activity, in any program or activity conducted or funded by USDA (not all bases apply to all programs). Remedies and complaint filing deadlines vary by program or incident.

Persons with disabilities who require alternative means of communication for program information (e.g., Braille, large print, audiotape, American Sign Language, etc.) should contact the responsible Agency or USDA's TARGET Center at (202) 720–2600 (voice and TTY) or contact USDA through the Federal Relay Service at (800) 877–8339. Additionally, program information may be made available in languages other than English.

To file a program discrimination complaint, complete the USDA Program Discrimination Complaint Form, AD-3027, found online at http://www.ascr.usda.gov/complaint_filing_cust.html and at any USDA office or write a letter addressed to USDA and provide in the letter all of the information requested in the form. To request a copy of the complaint form, call (866) 632–9992. Submit your completed form or letter to USDA by: (1) mail: U.S. Department of Agriculture, Office of the Assistant Secretary for Civil Rights, 1400 Independence Avenue, SW, Washington, D.C. 20250–9410; (2) fax: (202) 690–7442; or (3) email: program.intake@usda.gov.

USDA is an equal opportunity provider, employer, and lender.

Contents

General Session: Nondestructive Evaluation—
Application and Research Needs

Session 1: In-Forest Wood Property Assessment

Session 2: Evaluation of Structural Timber

Session 3: Evaluation of Engineered Wood Products

Session 4: Urban Tree Defect Assessment and
Risk Analysis I

Session 5: Condition Assessment and Evaluation
of Wood Structures I

Session 6: Wood Material Characterization I

Session 7: Urban Tree Defect Assessment and
Risk Analysis II

Session 8: Condition Assessment and Evaluation
of Wood Structures II

Session 9: Wood Material Characterization II

Session 10: Evaluation of Seedlings and Young Trees
for Genetic Improvement

Session 11: Evaluation of Roundwood

Session 12: Poster Session

Proceedings
**20th International Nondestructive Testing
and Evaluation of Wood Symposium**
Madison, Wisconsin, USA
2017

Edited by

Xiping Wang, Research Forest Products Technologist
Forest Products Laboratory, Madison, Wisconsin

C. Adam Senalik, Research General Engineer
Forest Products Laboratory, Madison, Wisconsin

Robert J. Ross, Supervisory Research General Engineer and Research Professor,
Forest Products Laboratory, Madison, Wisconsin and Michigan Technological University,
Houghton, Michigan

Preface

The International Nondestructive Testing and Evaluation of Wood Symposium Series started in Madison, Wisconsin, USA, in 1963. Since its inception, 19 symposia have been held in various countries around the world, including Brazil, China, Germany, Hungary, Switzerland, and the United States.

The 20th International Nondestructive Testing and Evaluation of Wood Symposium was hosted by the USDA Forest Service Forest Products Laboratory. It was held in Madison, Wisconsin, USA, on September 12–15, 2017. This symposium was a forum for those involved in nondestructive testing and evaluation (NDT/NDE) of wood and brought together many international researchers, NDT/NDE users, suppliers, representatives from various government agencies, and other groups to share research results, products, and technology for evaluating a wide range of wood products, including standing trees, logs, structural lumber, engineered wood products, and wood structures. Networking among participants encouraged international collaborative efforts and fostered the implementation of NDT/NDE technologies around the world.

The opening session, “Nondestructive Evaluation—Application and Research Needs,” included keynote speakers from around the globe who presented the state-of-the-art technologies in nondestructive testing and evaluation of wood.

The technical content of the 20th symposium is captured in the following proceedings. Full-length, in-depth technical papers for the oral presentations and several of the poster presentations

are published herein. The papers were not peer reviewed and are reproduced here as they were submitted by the authors.

The organization of the following proceedings follows that of the sessions at the 20th symposium. Technical sessions covered the following topics:

1. In-Forest Wood Property Assessment
2. Evaluation of Structural Timber
3. Evaluation of Engineered Wood Products
4. Urban Tree Defect Assessment and Risk Analysis I
5. Condition Assessment and Evaluation of Wood Structures I
6. Wood Material Characterization I
7. Urban Tree Defect Assessment and Risk Analysis II
8. Condition Assessment and Evaluation of Wood Structures II
9. Wood Material Characterization II
10. Evaluation of Seedlings and Young Trees for Genetic Improvement
11. Evaluation of Round Wood
12. Poster Session

We express our sincere appreciation and gratitude to members of the Organizing Committee, International Nondestructive Testing and Evaluation of Wood Symposium Series, for their efforts in making this symposium a success:

Dr. Ferenc Divos, University of West Hungary, Hungary
Dr. Raquel Goncalves, University of Campinas, Brazil
Dr. Francisco Arriaga Martitegui, Universidad Politécnic de Madrid, Spain
Roy F. Pellerin, Emeritus Professor, Washington State University, USA
Dr. Robert J. Ross, FPL and Michigan Technological University, USA
Dr. Laszlo Bejo, University of West Hungary, Hungary
Dr. C. Adam Senalik, FPL, USA
Dr. Xiping Wang, FPL, USA
Dr. Houjiang Zhang, Beijing Forestry University, China

We thank the International Union of Forest Research Organizations (IUFRO), Forest Products Society, and USDA Forest Products Laboratory for their support. Thanks also go to the following organizations for providing financial support in the form of sponsorships or who exhibited equipment: ABENDI; Allison Tree, LLC; Beijing Forestry University (BFU); FAKOPP Enterprise Bt.; International Wood Culture Society; Michigan Technological University; Midwest Section of the Forest Products Society; Mississippi State University; Nanjing Forestry University; Northeast Forestry University; The Morton Arboretum; University of Campinas(UNICAMP); and Washington State University. A special thanks to Dr. Laszlo Bejo for his personal financial support.

A very special thank you to Ms. Pamela Byrd (FPL) for her outstanding efforts—especially for serving as our main point of contact for speakers. Thank you, Pam!

We thank the following staff at FPL for their outstanding efforts in preparing these proceedings: Jim Anderson, Barb Hogan, and Karen Nelson.

A note of thanks to the many individuals who prepared papers for inclusion in the symposium. Your dedication and efforts make this Symposium Series a success!

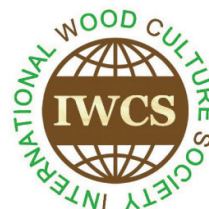
We hope that these proceedings provide inspiration to those who read its papers, and we welcome new participants in the global wood NDT/NDE family!

Dr. Xiping Wang
Dr. Adam Senalik
Dr. Robert J. Ross
Symposium Co-Chairs

*Thank you to this year's sponsors.
Your support has helped make this symposium possible!*



Forest
Products
Laboratory



Michigan Technological University
School of Forest Resources
and Environmental Science



László
Bejő

General Session

**Nondestructive Evaluation
Application and Research Needs**

Nondestructive Assessment of Wood Quality throughout Wood Supply Chain and Manufacturing Process

Udo H. Sauter

Department of Forest Utilisation, Forest Research Institute, Baden-Wuerttemberg, Wonnhaldestr. 4, Freiburg, Germany, udo.sauter@forst.bwl.de

Franka Bruechert

Department of Forest Utilisation, Forest Research Institute, Baden-Wuerttemberg, Wonnhaldestr. 4, Freiburg, Germany, franka.bruechert@forst.bwl.de

Joerg Staudenmaier

Department of Forest Utilisation, Forest Research Institute, Baden-Wuerttemberg, Wonnhaldestr. 4, Freiburg, Germany, Joerg.staudenmaier@forst.bwl.de

Abstract

For an optimized wood supply chain, a decisive factor is the proper allocation of raw wood materials to the mills. This includes aspects such as accurate volume, adequate quality, and timely delivery. Therefore a comprehensive resource allocation and raw material pre-sorting along the supply chain is the basis for successful process flows in any active forest- and wood enterprises. Log dimension, wood density and wood mechanical properties are key parameters for down-stream production decisions in wood processing industries. A second rationale is directed to the fundamental “stages” along the supply chain: forest stands, standing trees, roundwood after felling (on site, road side), logs (mill gate, log yard). Depending on the stages, a wide range of NDT methods can be applied.

Keywords: Logs, trees, dimension, volume, wood density, wood stiffness, nondestructive technologies

Introduction and background

Wood supply chain and demands

Technologies for forest assessment are focused on tree dimension, volume, and first attempts to derive tree quality criteria such as branch dimensions. Measurements rely on air-borne scanning systems with different resolutions. Technologies for individual tree assessment are terrestrial laser scanning by LiDAR systems for stem shape and knots. Other assessment tools for use on individual trees either directly derive a measure for wood density or produce rapid readings that allow a pre-selection in terms of wood stiffness. During harvesting, processor heads are able to measure log dimension and volume. With the integration of acoustic devices such as the processor head Hitman PH 330 (Fibre-gen Limited, Christchurch, New Zealand), new harvester heads now allow pre-sorting based on wood stiffness. Log assessment at road side, mill gate or log yards can also aim at wood property assessment, e.g. wood density and wood stiffness, using tools of similar testing approaches, such as stress waves, Eigen-frequency measurements, microwave or laser scattering (tracheid effect). Especially at mill gate, volumetric assessment and external log characterization by optical systems (laser cameras, etc.) already

gained certain importance. At this stage, high resolution x-ray based CT log scanning will play an increasingly important role. Technologies in front of the saw line can help to transfer the log specific quality information into value by orientation and positioning of logs for optimized break-down through optical cameras, simple x-ray sources for re-identification of already scanned logs and adapting sawing optimization. After break-down of the log further processing of semi- and end-products is accompanied by a set of NDT tools for wood quality assessment of sawn products. High-end solutions are multi-sensor technology solutions which combine light, laser, x-ray, vibration and mechanical testing.

The wood supply chain in middle Europe is characterized by a description of the resource, beginning at the stage of standing forest stands and following up the flow of the raw material along the forest and public roads to the (saw)mills where the first break-down into primary sawn products happens. Successful stake holders of the forest and wood industry branch need to have comprehensive information about the flowing resource roundwood as basis of their business. The focus lies on standing, transported and stacked volumes and their qualities related to a wide range of potential end-uses. Quality parameters of most interest are wood density, mechanical properties but also the optical appearance of surfaces of sawn products. Further more important is the factor time, which is essential in the first place for functioning delivery planning and steering as well as for a quality control along the delivery or stacking process. NDT-technologies represent very good options to fulfill the high expectations of forest owners, logging companies, transport enterprises and wood industry managers. It is the duty of scientists and the research institutes in strong partnership with technology developers to search for adapted technical solutions to strengthen the outlined processes for a successful forest wood-industry branch.

NDT assessment—options along the supply chain

Inventory the standing resource

For general inventory purposes, firstly the total standing volume and the volume differentiated by assortments is of main interest. Air-borne systems including modern UAV-technologies equipped with high resolution digital cameras can provide stand and tree data, specific crown parameters. Through modelling approaches it might be possible to derive first detailed information about branch distribution and allocation as well as branch sizes and their implications on inner wood structures.

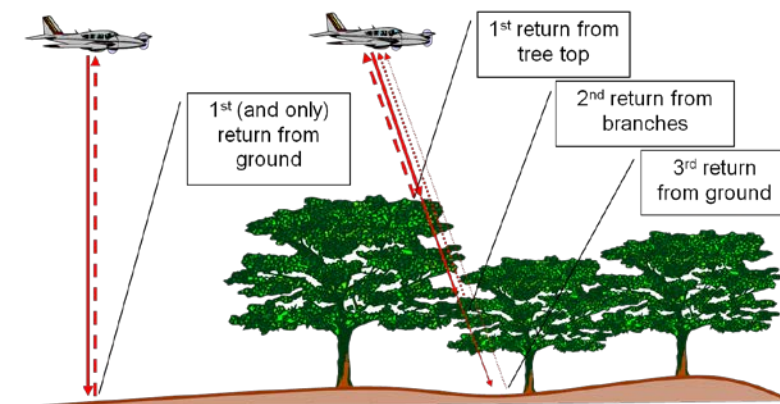


Figure 1—Laser scanning, crown dimensions and branch details can be measured as basis for further image processing (<http://www.wol.ugent.be/wp-content/uploads/2017/05/lidar-techniek.png>)

At stand level also terrestrial assessment systems e.g. t-LiDAR are available which give a first picture of dimension and branch sizes and number of the main stem up to the first part of the crown of trees to be cut.

The inner structure related to the physical properties resp. strength properties of the stem wood can be derived by tools like Hitman, Fakopp, Sylvatest Duo with which measurements are carried out at the lower trunk of a tree. Important support for strength properties is additional knowledge of stem wood density which can be assessed only for the basal area.

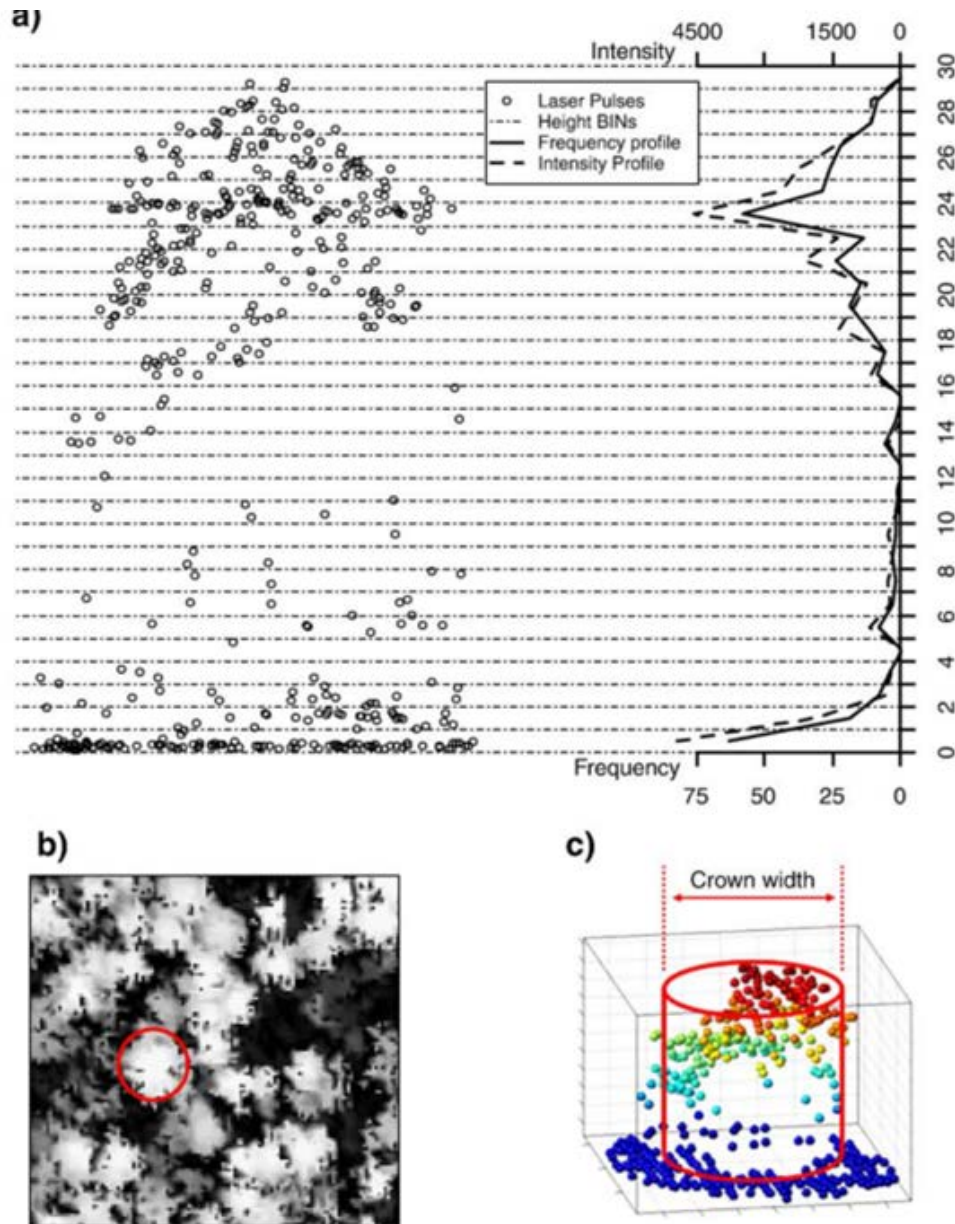


Figure 2—Measuring crown parameters from t-LiDAR method (Popescu et al. 2008)

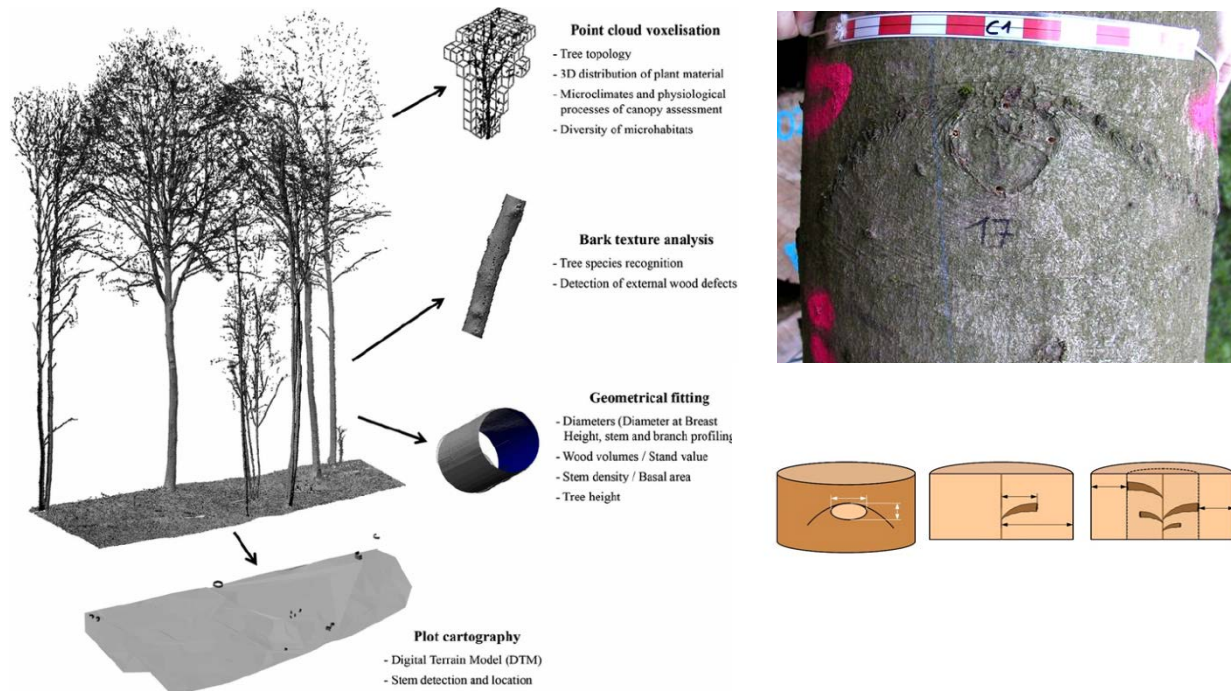


Figure 3—Clear-wood content in standing trees predicted from branch scar measurements with terrestrial LiDAR and verified with X-ray computed tomography (Staengle et al. 2014)

Assessments during harvesting, transport or stacking of stems

Next stage is after felling mostly done by modern harvester machines. During processing the felled tree including bucking into roundwood assortments the harvester head is able to measure stem dimensions already with high resolution. First installations of the acoustic tool Hitmann PH330 into the harvester head opens the view onto general physical parameters of the stem section processed. Such measurements allow already good estimations of MOE_{dyn} . Furthermore the bucked stem sections provided for the breakdown especially in softwood saw mills should be differentiated related to their strength properties based on e.g. Eigen-frequency-measurements to derive a more solid decision basis for further processing in the saw mill. At this point, the question arises where the most appropriate place for this assessment of stems would be.

Information demanded at mill gate/log yard

In most modern softwood mills and expectable also in bigger units of the hardwood industry the first step is a complete scan of the 3D-shape of each processed log. Widely spread techniques basing on laser scanning devices including adapted digital camera systems (see picture in Figure 4) which provide a detailed image whereas any surface anomaly can be identified. The data set of each stem can be further analyzed and specific volume calculation algorithms can be applied. But also stem quality parameters related to the stem form such as taper or sweep can be calculated automatically.

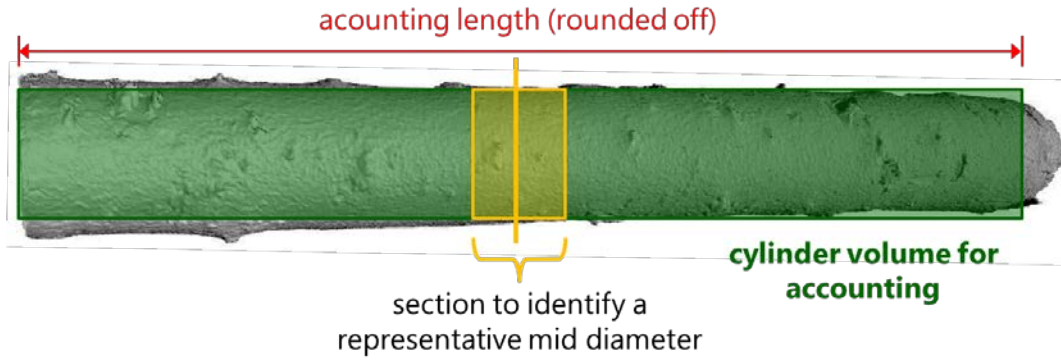


Figure 4— Methods for precise scaling and grading of saw logs using 3D-scanning systems (Sauter and Staudenmaier 2017)



Figure 5—Roundwood sawing optimisation according to X-ray based computed tomography; (Bruechert et al. 2017)

A wide range of further NDT assessment tools can be used at this stage of the process and the supply chain. A very important feature related to wood quality in general is wood density. Here microwave techniques are introduced and deliver already solid data of individual stem sections before sawing. Without claiming a complete list of NDT methods there is a last option to be mentioned for pre-sorting and for approaching the next step for sawing optimisation: CT scanning of logs. Meanwhile not only research units are installed and deliver individual precise and detailed images of the inner structure of a stem but also industry installations are running in five softwood mills with high speed worldwide. The technology allows to draw a picture of the density distribution across the stem as well as the positioning of most important quality relevant criterions like knots and their stage, rot, grain angle etc. For a breakdown simulation these information are used to be related to the aimed sawn products.

Conclusions

Depending on the stages, a wide range of NDT methods can be applied. Technologies for forest assessment are focused on tree dimension, volume, and first attempts to derive tree quality criterions such

as branch dimensions. Measurements rely on air-borne scanning systems with different resolutions. Technologies for individual tree assessment are terrestrial laser scanning by LiDAR systems for stem shape and knots. Other assessment tools for use on individual trees either directly derive a measure for wood density or produce rapid readings that allow a pre-selection in terms of wood stiffness. During harvesting, processor heads are able to measure log dimension and volume and allow pre-sorting based on wood stiffness. Log assessment at road side, mill gate or log yards can also aim on wood property assessment, e.g. wood density and wood stiffness, using tools of similar testing approaches, such as stress waves, Eigen-frequency measurements, microwave or laser scattering. Especially at mill gate, volumetric assessment and external log characterization by optical systems already gained certain importance. At this stage, high resolution x-ray based CT log scanning will play an increasingly important role. After breakdown of the log further processing of semi- and end-products is accompanied by a set of NDT tools for wood quality assessment of sawn products. High-end solutions are multi-sensor technology solutions which combine light, laser, x-ray, vibration and mechanical testing.

Acknowledgments

We thank our science partners from several common research projects. Special thank goes to our industry partner Microtec S.r.l. for strong research cooperation and providing some pictures of this publication. We thank all authors for their cooperation.

References

- Bruechert, F.; Baumgartner, R.; Laudon, N.; Breinig, L. and Sauter, U.H. 2017. Roundwood sawing optimisation based on x-ray based computed tomography. Proceedings, IUFRO Division V Conference, June 12-16 2017, Vancouver
- Popescu, S.C. and Kaiguang, Z. 2015. A voxel-based lidar method for estimating crown base height for deciduous and pine trees. Remote sensing of environment 112.3: 767-781.
- Staengle, S.; Bruechert, F.; Heikkila, A.; Usenius, T.; Usenius, A. and Sauter, U.H. 2015. Potentially increased sawmill yield from hardwoods using X-ray computed tomography for knot detection. Annals of Forest Science 72:57–65
- Staengle, S.; Bruechert, F.; Kretschmer, U.; Spiecker, H. and Sauter, U.H. 2014. Clear wood content in standing trees predicted from branch scar measurements with terrestrial LiDAR and verified with X-ray computed tomography. Can. J. For. Res. 44: 145–153
- Sauter, U.H. and Staudenmaier, J. 2017. Methods for precise scaling and grading of sawlogs using 3D-scanning system. Proceedings, IUFRO Division V Conference, June 12-16 2017, Vancouver

Dendrochronology—A Nondestructive Technique for Dating Historical String Musical Instruments

Voichita Bucur

Adjunct Professor, RMIT University, School of Science, Melbourne, Australia

Email: voichitabucur@yahoo.fr

Abstract

Since 1967, the historical musical instruments have been defined as objects belonging to the cultural heritage of humanity. Historical string instruments are mainly instruments of classical music belonging to the violin family – the violin, the viola, the cello, the double bass and also the guitars, the harps, the harpsichords and the pianos. These instruments have been made in Europe since the renaissance and the Baroque periods. Resonance spruce – *Picea abies* from the European Alps was the main material employed for the soundboard of these instruments. The authenticity of these instruments can be proved through the dendrochronological approach. Fourier transform near infrared spectroscopy informs about the geographic provenance of spruce used for the soundboards.

Keywords: dendrochronology, annual ring width, X ray, Fourier transform near infrared spectroscopy, historical string musical instruments, violin, double bass

Introduction

The document Carta di Cremona promulgated in 1967 defined the Old Italian musical instruments as objects belonging to the cultural heritage of humanity. These historical string instruments are mainly instruments for performing classical music since Renaissance and Baroque periods. Most of the instruments belong to the violin family – the violin, the viola, the cello, the double bass, etc. The guitars, the harps, the harpsichords and the pianos are also included in the group of historical string instruments. Since the 15th century old musical instruments have been made in Italy but also in several countries of Europe. Resonance spruce (*Picea abies*) from Alps was the main material employed for the soundboard of these instruments. The main problem for these instruments is related to their authenticity and to the methodology to prove it. It that follows we will discuss two non-destructive methods namely the dendrochronology for dating the wood and the Fourier transform near infrared spectroscopy for stating about the geographic provenance of spruce used for the soundboards of old string instruments.

Dendrochronology is a relatively new tool for dating old buildings or old historical musical instruments and is based on the analysis of the width and pattern of the annual rings of the soundboard. It is well known that spruce trees produce annual rings having a characteristic sequence determined by the climatic variations of the growing site. The sequence of the annual tree ring width can be superimposed exactly on the calendar year. The ring width could be small (less than 1 mm) or large (several mm) depending on the climatic conditions of the site in which the annual ring has been formed by tree metabolism. Figure 1 synthesises the principle of the dendrochronology for string musical instruments violin. For dating an instrument its floating chronology is measured on the instrument to be dated. Furthermore this chronology is compared with a master chronology. The overlapping time corresponds to the time life of the tree from which the soundboard was extracted.

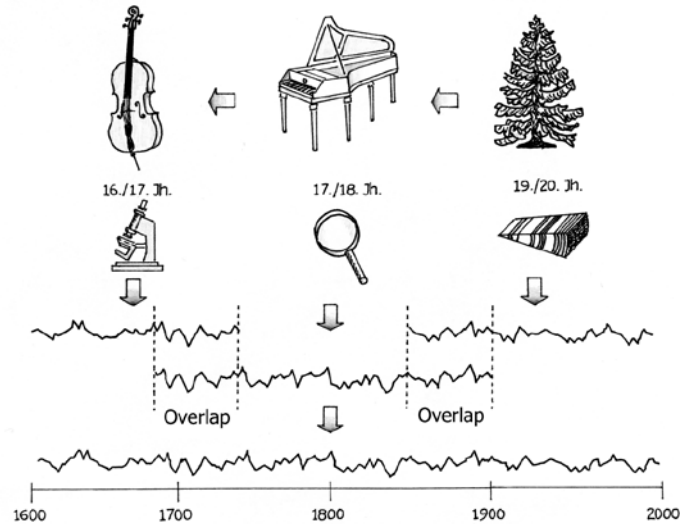


Figure 1—Principle of dendrochronology for musical instruments after Klein P. and Beuting M. (2007) Legend: Upper graph – floating chronology; Lower graph - Master chronology <http://www.orpheon.org/OldSite/Seiten/education/Dendrochronology.htm> access 1 December 2016

In the literature of wood science the first analysis of the annual ring width of the top of a violin was reported by Lottermoser and Mayer (1958) and referred to three Stravivari's violins and two Guarneri's violins. It was proved that the two constitutive parts of the soundboard of the violins had a symmetric structure with the same sequence of the annual ring width, measured with an optical microscope. Of course, the wood has not been dated because at that time the master chronologies of reference have been not yet been established. The geographic proximity of Cremona and Brescia to the Southern Alps suggested that Old Italian violin makers have been supplied with wood from this region. In the last decades of the 20th century master chronologies have been established for different geographic locations such as southern Italian Alps, Austrian Tyrol, and Bavarian Alps. As an example of dating a musical instrument with dendrochronological technique we referee to Klein et al. (1986). He superimposed the growth ring series measured on the soundboard of a violoncello made in 1892 by the violin maker Bisiach in Milan with the master chronology of Italian Alps. The concordance of data was confirmed and the age of the soundboard was demonstrated. On the other hand the dendrochronology is able to demonstrated that the two sides of the soundboard of a violin have been extracted from the same tree, as seen in **Fig. 2** in which is illustrated the variation of the width of the annual rings versus the chronological year for two controviolini made in 1791 and in 1793 by Valentino de Zorzi. These instruments belong to the collection of Cherubini Conservatory in Florence, Italy.

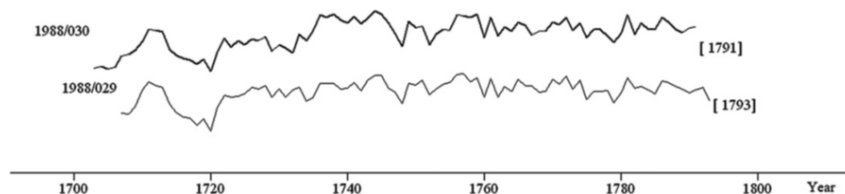


Figure 2—Width of the annual rings versus the chronological year for two controviolini made in 1791 and in 1793 by Valentino de Zorzi from the same tree (Bernabei et al. 2010, fig 4, p 198)

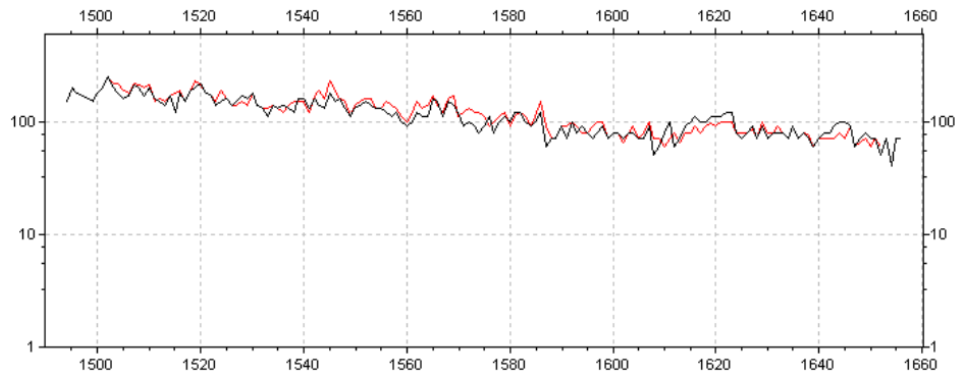


Figure 3 Superimposition of the time series of two violins made in Cremona, namely a Stradivari violin – the Sunrise, made in 1677 and an Amati violin 1673, made from the same tree. (Beuting 2009, fig 3, page 165)

Table 1—Dendrochronological data on some historical instruments (Klein et al.1989)

Instrument	Violinmaker	Manufactured date AD	Analysed rings number – bass side	Dendrochronological date – top, bass side AD	Difference (years)	Note
Viola da gamba	Vogel H Nuremberg	1563	64	1546	+37	Authentic
Violin	Stradivari	1713	72	1869	-156	False

Another interesting case is to see instruments made by different luthiers using wood from the same tree, as shown in **Fig 3**, with the superimposition of the time series of a Stradivari violin – the Sunrise, made in Cremona 1677 and an Amati violin made also in Cremona in 1673.

It is also possible to determine wood provenance of a soundboard of a violin made by an unknown master. This is the case of a violin made in Mirecourt, in France in 1846 with wood from Tyrol, as we will see later in the last Table of this article.

Instrument’s authenticity or instrument’s unauthenticity, can be demonstrated also with the dendrochronological analysis using X ray microdensitometric technique. Schweingruber (1983) demonstrated that a supposed Stradivari’s violin was not authentic, because the top of this violin had the annual ring microdensitometric profile ranging from 1894 to 1902. As we know, Stradivari lived in Cremona between 1644 and 1737. The science of Dendrochronology required a new notion– *terminus post quem* – which is the biological date of the youngest tree ring, or the oldest calendar year, that could be read on the soundboard. Logically, the authentic instruments have been made after this date. The manufactured data and the dendrological data of an authentic viola da gamba and that of falsely attributed Stradivari’s violin, are shown in **Table 1**.

The authenticity of a very famous double bass, known as Karr- Koussevitzky double bass was also submitted to the dendrochronologic methodology. The annual ring series of the soundboard was superimposed on the Alpine Obergurgl chronology – Tyrol Austria (**Fig. 4**). This instrument was acquired in France in the early years of the 1900s by the American conductor Serge Koussevitzky, as being made in 1611 by Amati brothers Antonio (1537-1607) and Girolamo (1551-1630). To obtain the annual ring width series of the soundboard of this instrument, measurements on 300 rings were performed with a microscope (0.01 mm precision) connected to a CDD camera. The latest chronological year observed was 1760 to which should be added the rings lost during processing, sawing and planing. It was noted that the tree was harvested probably after 1770 AD, and not during the life of Amati brothers. By analysing the organologic aspect of the instrument, Grissino-Mayer and Deweese (2005) stated that this splendid double bass was probably built by an unknown French master during the 19th century, using old wood from Tyrol.

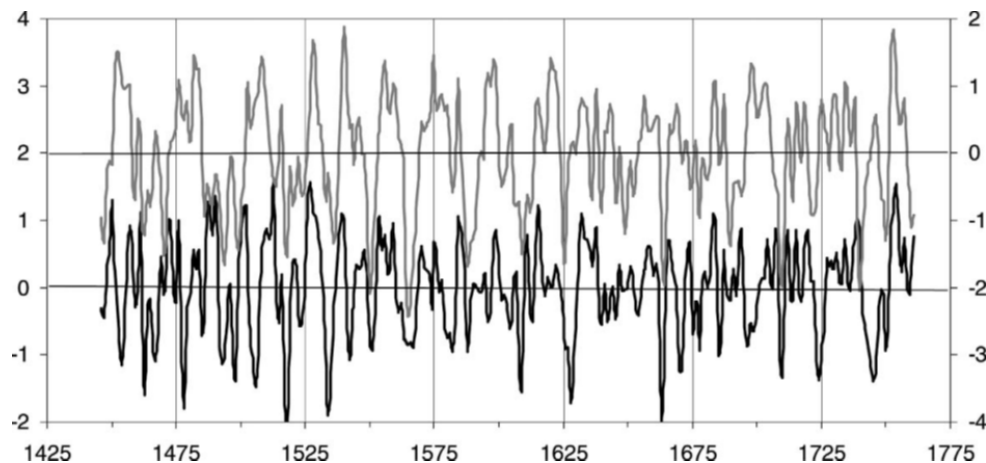


Figure 4—Superimposition of the Alpine Obergurgl chronology (upper) with the time series of the Karr- Koussevitzky double bass (lower) based on about 350 annual rings (Grissino-Mayer and Deweese 2005, fig 3, p. 82)

Another interesting question to answer is risen by the exact dendro-provenance of wood, or in other words from which forest the wood was harvested. [Corona \(1981\)](#) was the first to underline the links between the dendrochronology, the site chronology and the dendro-provenance of wood for a musical instrument from an Italian collection. He studied the annual ring width series of the viola called viola Bimbi – dated 1770 and belonging to the most famous collection of musical instruments in Florence – Italy. Bartolomeo Bimbi was a violin maker who worked in Sienna and made instruments for Medici’s Court in Florence. [Corona \(op.cit \)](#) compared the dendrochronological profile of the viola composed of 70 annual rings with two dendrochronological profiles found from two marriage chest, precisely dated and belonging to the noble family Zorzi from Ziano in Vall di Fiemme – Italy. The superposition of the annual ring width series of the viola and the series of the annual rings of the two chests was perfect. Then these three dendrochronological profiles have been compared with the Ötztal – Kerner 1975 – Master chronology for spruce and with the spruce Becker and Giertz 1970 chronology. The exact correspondence of curves allowed dating the wood for viola construction and allowed recognition of timber provenance - Val di Fiemme (Trentino, Italy) famous site for spruce resonance trees in Italy.

Wood provenance of Old Italian instruments

Resonance spruce trees (*Picea abies*) for Old Italian instruments were harvested in the forest of the region of Trentino, Italy. The exceptional quality of resonance wood extracted from the forest of Paneveggio was described and recognised by many authors ([Giordano 1974](#), [Dellagiacoma 2002](#), [Uzielli 2002](#)) and the well-known violinmakers starting with Amati and Stradivari. The management of this forest has a long tradition and the first historical record dates from 1007 AD. **Figure 5** shows the variation of the annual ring width in the trees harvested from the forest of Paneveggio in Trentino region during about three centuries, namely between 1680 AD and 1990 AD. Three plots have been studied, plot 1 and plot 2 were of natural origin and the oldest trees were over 400 years. The width of annual ring was between 1mm and 3.5 mm, with an average of about 2mm. Plot 3 included trees of 200 years and also younger trees of about 65 years old. The width of the annual ring was between 0.5mm and 2.5 mm, with an average about 1.5mm. It is noticeable that the annual width ring in 1700 AD was about 1mm, the same as the width of annual rings observed on Stradivari’s violin. The width of annual rings can be measured on increment cores using X ray densitometric analysis. Also, the width of the annual rings can be deduced from a synchrotron radiation microtomography of a violin as seen in **Fig 6**.

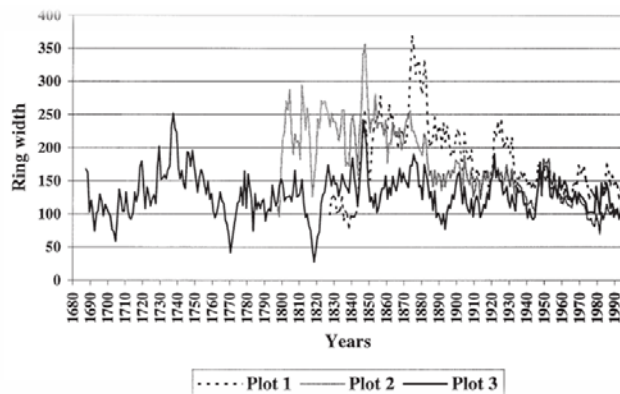


Figure 5—Variation of the annual ring width in the forest of Paneveggio during 310 years between 1680 AD and 1990 AD (Motta et al. 1999 fig. 8, p. 467)

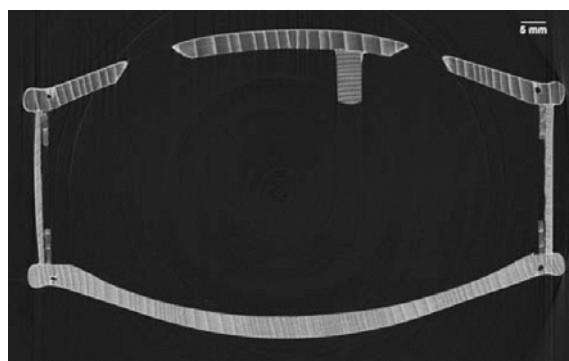


Figure 6—Image of a transverse section of a violin revealed with a synchrotron radiation microtomography in the middle bout at the level of *f*-holes. (Rigon et al. 2007, fig 2, p. 74)

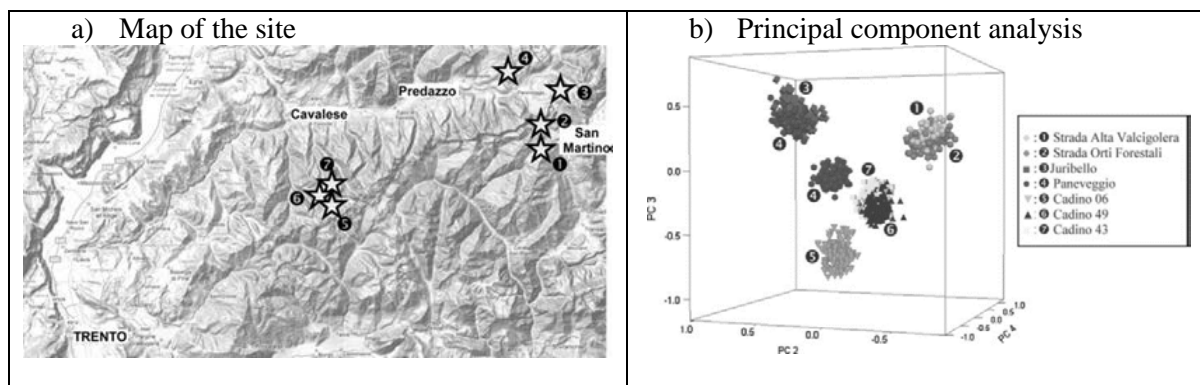


Figure 7—Differentiation of geographic origin of timber (*Picea abies*) in different forests in Trento- Italy, with principal component analysis on Fourier transform infrared spectra. Band 7500-5700 cm^{-1} and 5100 and 4500 cm^{-1} (Sandak et al. 2011, Fig 5, p 44)

The second non-destructive technique discussed in this paper is the Fourier transform near infrared spectroscopy which was developed during the last three decades of the 20th century, and which can be used to determine the site provenance of wood. This technique allows determination of many chemical components simultaneously on a wood sample without particular preparation of its surface. Based on the assumption that trees growing in various locations produce timber having different chemical composition, it was possible to study the spectra of spruce samples from Trentino- Italy forests. The spectral wave length was between 4000 and 7500 cm^{-1} . Principal component analysis clearly discriminated the origin of specimens (Sandak et al. 2011) as seen in **Fig. 7**.

Table 2—Annual ring width of resonance spruce wood grouped by provenance and deduced from master chronology (data from Bernabei and Bontadi 2011)

Parameters	Units	Italy Italian Alps	Italy Apennines	Switzerland	Austria Tyrol	Germany Bavaria
Mean value	1/100 mm	117	160	130	134	142
Standard deviation	1/100 mm	29	50	33	34	42
Coeff. of variation	%	25	50	25	25	30

Table 3—Master chronologies and dendro-date of some instruments made in different countries in Europe, showing the geographic origin of wood. *Test t* of confidence relating master chronology to annual ring series measured on the instrument (data from Bernabei and Bontadi 2011)

Nr.	Violins - Code of Instrument	Master chronology	Maker	Town of origin	Dendrodate Year - AD	Test t Significant value
1	2002/304	Siebenlist-Kerner (1984) Austria	F. Breton	Paris France	1698	8.8
2	1988/018	Siebenlist-Kerner (1984) Austria	Anonymous	Mirecourt France	1816	7.4
3	1988/237	Paneveggio Italien Alps	G. Gabbrielli	Florence Italy	1749	9.8
4	Bm901	Ital006 Cortina, Italy	I. Sderci	Florence Italy	1953	5.8
5	1988/017	Germ5 North Bavaria	J. Gagliano	Naples Italy	1765	7.7

However is worth mentioning that in various geographical region the resonance wood has a characteristic average annual ring width - such as 1.1 mm in the Italian Alps; 1.3 mm in Switzerland; 1.34 in Austrian Tyrol . Wood from Italian Apennines was used by the Tuscan violin makers, wood from Italian Alps was used by the violinmakers from Cremona, wood from Switzerland and Austria had been employed by the violinmakers in France, Italy and Great Britain as can be seen from **Table 2** for some of the instruments belonging to the collection of Cherubini Conservatorium in Florence.

Statistical analysis for dating musical instruments based on master chronologies and spatial correlation analysis

For dating a specific musical instrument, the corresponding pattern of growth rings series is compared with the reference master chronologies related to a geographic area, using the confidence statistical *test t*. Several examples are given in **Table 3** for some instruments made in Italy and France.

Conclusions

The process of dating historical musical instruments is based on the comparison between the annual ring width series built up from the soundboard of string instruments and the existing European master chronologies of resonance spruce (*Picea abies*). The annual ring width can be measured using an optical microscope connected with a camera, or in a more sophisticated way by using X ray microdensitometric technique, or with synchrotron radiation microtomography imaging. The geographical provenance of wood can be determined with Fourier transform infrared spectra. The techniques discussed illustrated the methodological approach for demonstrating the authenticity of period historical musical instruments. However historical musical instruments are art objects of very high monetary value, for example “Lady Blunt” Stradivarius violin was sold in 2011 for \$ 15.9

million. This aspect should be considered in the context of dendrochronology and the “economy of prestige”.

References

- Bernabei M, Bontadi J, Rossi-Rognoni G (2010) A dendrochronological investigation of stringed instruments from the collection of the Cherubini Conservatory in Florence. *J Cult. Herit.* 12, (2): 196-204
- Beuting M (2009) More than dating? Further information obtained by dendrochronology. In Vaiedelich S and Houssay A (eds.) *Proc. Dating the musical instruments*, 6 June 2009, Musée de la Musique, Paris: 159-165
- Bucur V (2016) *Handbook of materials for string musical instruments*. Chapter 14: 639-698, Springer International Publisher AG Switzerland
- Carta di Cremona (1967) Per una metodologia di salvaguardia e restauro dei beni liutai, a cura del Comitato per la Salvaguardia dei Beni Liutari Nazionali. CEL Cremona Italia 1987
- Corona E (1981) La viola Bimbi ha ‘ascendenze trentine’ ? *Natura Alpina* 32 : 27 – 29
- Dellagiacomina F (2002) Il legno di risonanza della foresta di Paneveggio. Aspetti di gestione forestale. In *Il legno di risonanza della Foresta di paneveggio. Tecnologia, Impiego, Valorizzazioune*. Ed Provincia Autonoma di Trento; Assessorato all Ambiente, Sport e Pari Opportunita, Servizio Parchi e Foreste Demaniali: Ufficio Foreste Demaniali di Cavalese e Primiero. Atti del Convegno. Predazzo 10- 11 settembre 1998 e ulteriori contribute: 123-130
- Giordano G (1974) *Technologie del legno*. Ed UTET Torino
- Grissino-Mayer HD, Deweese GG (2005) Tree-ring dating of the Karr-Koussevitzky double bass a case study in dendrochronology. *Tree Ring Res.* 61 (2): 77-86
- Klein P, Mehringer H, Bauch J (1989) Dendrochronological and wood biological investigations on string instruments. *Holzforschung* 40: 197-203
- Lottermoser W, Mayer J (1958) Über die Möglichkeit einer Dendrochronologie von altitalienischen Geigen. *Instrumentenbauzeitschrift* 12: 295-296
- Motta R, Nola P, Piussi P (1999) Structure and stand development in three subalpine Norway spruce (*Picea abies* L Karst.) stands in Paneveggio Trento Italy. *Glob. ecol. Biogeogr.* 8: 455-471
- Rigon L, Vallazza E, Arfelli F et al. (2010) Synchrotron-radiation microtomography for the non-destructive structural evaluation of bowed stringed instruments. *E-Preservation Science*, e-PS 7: 71-77
- Sandak A, Sandak J, Negri M (2011) Relationship between near-infrared spectra and the geographical provenance of timber. *Wood Sci. Techn.* 45: 35-48
- Schweingruber F H (1983) *Der Jahrring*. Verlag Paul Parey Hamburg, II
- Uzielli L (2002) Legno di risonanza. Legno con indentature. In *Il legno di risonanza della Foresta di paneveggio. Tecnologia, Impiego, Valorizzazioune*. Ed Provincia Autonoma di Trento: 39-47



Session 1

**In-Forest Wood
Property Assessment**

Partial Resistance Drilling to Assess Wood Density in Trees

Xiping Wang

USDA Forest Service, Forest Products Laboratory, Madison, Wisconsin, USA, xwang@fs.fed.us

Abstract

Increment core analysis has dominated research for more than half a century and has been used as a standard method for assessing basic wood density in forests, for determining biomass of ecosystems, and for investigating climate history through dendrochronological analysis. Comprehensive wood density models have been developed for commercially important species that use outer wood cores and knowledge of internal wood density distribution to fairly accurately predict the density of major tree components. With the development of SilviScan and near infrared spectroscopy instruments, more wood and fiber properties can be obtained from a single increment core sample, allowing comprehensive wood quality evaluation of plantation trees for genetic improvement, forest management, and optimal wood utilization. However, for many users or in many applications, increment core sampling and subsequent laboratory analysis are time-consuming and expensive. A rapid field-type nondestructive method is needed in various research programs and forest operations. This report provides an in-depth review of the traditional increment coring method and the more recent electronic resistance drilling technique for assessing wood density of trees. This report also proposes a new concept of partial resistance drilling for more efficient and economical collection of wood density data in the forest.

Keywords: amplitude, friction, increment core, Resistograph, resistance profile, wood density

Introduction

Density is one of the important wood characteristics of standing trees that affects the properties and performance of various wood products, such as sawn timber, reconstituted products, and pulp and paper (Gao et al. 2017). Wood density has been considered a quality trait in tree improvement programs because of its economic value and high degree of genetic control (Sprague et al. 1983); it is a fundamental component of biomass determinations in ecosystem studies and is a cornerstone of functional trait analysis in community ecology (Wiemann and Williamson 2013). Wood density is highly variable, particularly within and between individual trees in forests. The within-tree variation constitutes a major part of the overall variability and has been well-documented for some commercial species (Kandeel and Benseid 1969, Wiemann and Williamson 2014, Tian et al. 1995, Kimberley et al. 2015).

The traditional technique for determining wood density in standing trees is to extract increment cores from trees and measure their volume and mass of wood in a laboratory. Although this method is relatively easy and accurate, it is time-consuming and labor-intensive for wood quality surveys or genetic improvement programs that require extensive density analyses. Even so, since its invention in the mid-1800s (Pressler 1866), the increment borer has been the primary tool for “nondestructive” sampling of standing trees.

Another technique capable of providing highly accurate wood density measurement is x-ray densitometry. This technique also uses increment cores. Advantages of this technique are its ability to clearly obtain

wood density values in different biological zones and allow for densitometry comparisons between radii within the same tree, between trees on the same site, and between mean density values at different sites (Cown and Clement 1983, Eberhardt and Samuelson 2015). However, the x-ray method requires careful sample preparation and data analysis and can only be carried out in the laboratory. It does not satisfy the requirements for a rapid and economical evaluation of wood density in standing trees.

For the purpose of achieving rapid, reliable, and economical wood density measurements in standing trees without using increment borers, a field-type nondestructive method is needed in various research programs and forest operations. In a recent publication, Gao et al. (2017) reviewed world-wide research development in the use of several field nondestructive methods for rapid determination of wood density in trees and discussed pros and cons of each method for field applications. This report provides an in-depth analysis of the capability of increment borer and electronic resistance drilling tools and proposes a new concept of partial resistance drilling for more efficient and economical collection of wood density data in trees.

Increment coring

For many years, the increment borer has been used as a simple nondestructive tool to evaluate wood quality of forest resources. The tool was originally developed in Germany ca. 1855 (Pressler 1866) and has changed little since its original design (Grissino-Mayer 2003). Figure 1 shows an increment borer being used to extract a core sample from a standing tree at breast height. An increment core can provide a complete wood sample if it stretches from the pith to the bark and is only limited by the length of the borer and one's ability to extract an adequate core. Borer diameters range from 4 to 12 mm, with the larger diameters giving the best samples when larger quantities of wood are required (Jozsa 1988, Grissino-Mayer 2003, Williamson and Wiemann 2010). Larger diameter borers (12 mm) cause less compaction because the area to volume ratio of the wood sample is smaller, and larger samples are easier to measure. However, larger diameter borers require disproportionately greater expenditures of energy to extract cores. Therefore, limiting the depth of penetration to only that required to obtain an adequate sample is desirable. For most purposes, it is desirable to bore in a radial line to the pith. This is sometimes difficult because trees aren't perfectly round and human operation error may cause the core to be off center.



Figure 1. Increment borer being used to extract a core sample from a standing tree at breast height.

Reliable estimates of tree density are derived from cores that extend from bark to pith because they reveal the full extent of radial variation. Unfortunately, boring trees from bark to pith is often difficult and replete with problems. Some of the challenges encountered by foresters and dendrochronologists are (1) trees are too large for the borer to reach the pith; (2) the borer misses the pith, passing to the side of it; (3) borers are difficult to insert in trees with dense wood; and (4) borers are difficult to extract, for multiple reasons (Maeglin 1979, Jozsa 1988, Grissino-Mayer 2003).

Wiemann approximation

Given the problems of bark-to-pith boring, alternative partial sampling techniques have been developed for estimating tree density even when radial variation is substantial. Wiemann and Williamson (2012) suggested a novel approach, based on stem geometry, to sample only the wood that approximates the density of a whole disk. The concept is that, if a function describing the radial variation in density is known, then it can be used to determine the point along the radius at which the wood density equals the area-weighted density. In theory, the tree need only be bored to that point, termed the Wiemann approximation, to estimate density of the whole cross section. For radial changes that are linear, the point of approximation falls at two-thirds of the wood radius; that is, the wood density at two-thirds of the distance from pith to bark should equal the density of the whole disk (Wiemann and Williamson 2012). In application of this method, the point one-sixth of the diameter inward from the bark–xylem interface would be used to correspond to two-thirds of the distance from the pith outward. This method has been proven successful for trees with linear (or no) changes in density across the radius (Wiemann and Williamson 2012, 2013). The usefulness of the method for estimating wood density of a species is conditional on knowledge of the pattern of radial change in density and the degree of eccentricity in the species.

Outer wood density approach

Increment coring is by far the most widely used sampling technique to obtain wood density information in standing trees. Knowledge of within-tree patterns has allowed the use of outer wood values for stem selection in breeding programs and for preharvest assessments (Cown 2006, Kimberley et al. 2015). In New Zealand, extensive wood density surveys were carried out on radiata pine (*Pinus radiata* D. Don) resources by extracting partial cores at breast height. The survey results indicated a good relationship between outer wood density and whole-tree density. An empirical model called STANDQUA was developed in the mid 1990s that enabled within-tree patterns of radiata pine wood density to be estimated from breast-height core samples and the future log-level wood density to be predicted (Tian and Cown 1995, Tian et al. 1995). More recently, comprehensive wood density models were developed for radiata pine using an extensive wood density dataset (from breast-height increment cores and stem disks) collected during 50 years of research to predict within-tree, within-stand, and among-stand variation in wood density (Palmer et al. 2013, Kimberley et al. 2015). For instance, the breast-height wood density of radiata pine was found to show a monotonic increase with increasing ring number from the pith, with the rate of increase diminishing after approximately 20 rings from the pith (Fig. 2). Along a tree stem, whole-disk average density showed a sigmoidal pattern with relative height well-approximated by a cubic function (Fig. 3). These models can be used to predict the density of disks or logs cut from any position within a tree and can use measured outer wood density values to predict the density, by log height, for a particular stand. It can further be used in conjunction with outer wood density to predict wood density distributions by logs for stands of any specified geographic location and management regime (Kimberley et al. 2015). Many forest growers in New Zealand today routinely collect breast-height outer wood cores as part of their preharvest assessments.

Compared with the traditional destructive sampling method of cutting disks, the use of an increment borer to extract trunk tissue is considered an economically viable option to minimize the work load. In addition,

increment cores allow specific biological zones (for example, the inner 10 rings or the outer 10 rings) to be identified for study and ensure valid comparisons when properties vary with tree age. However, increment coring will always have potential to damage the trunks of the cored trees and incur some risk of negative impacts on tree health. For example, boring in a veneer quality black cherry tree will lower the value of the butt veneer log and is therefore considered destructive. Also, bore holes can be the entrance source for decay and disease (Hart and Wargo 1965). In addition, for many applications such as tree improvement programs and large-scale wood quality studies, in which potentially hundreds and even thousands of trees must be sampled for wood density information, increment coring is still time-consuming and expensive. A rapid field-type nondestructive method is becoming increasingly important for various research programs and forest operations.

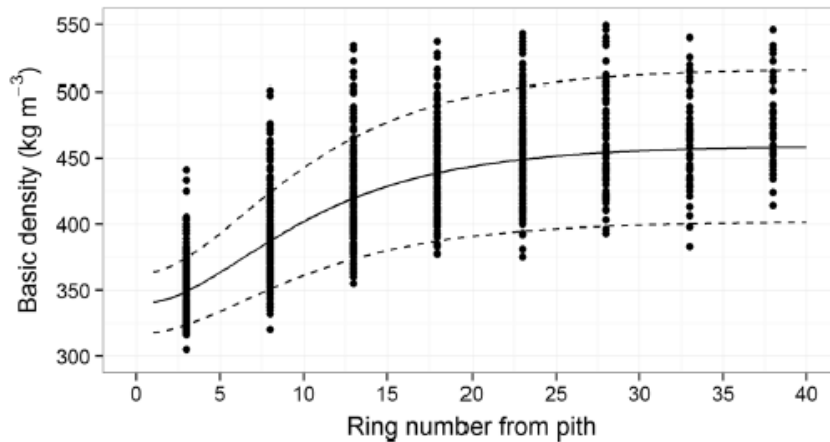


Figure 2. Pith-to-bark radial trend in breast-height wood density. Black dots correspond to mean densities by a five-ring group at each site. The black lines show density predicted by model 1 for an average site (middle solid line, $L = 0$) and for sites at the 5th and 95th percentiles (lower and upper dashed lines, $L = -34.6$ and $L = +34.6$, respectively) (Kimberley et al. 2015).

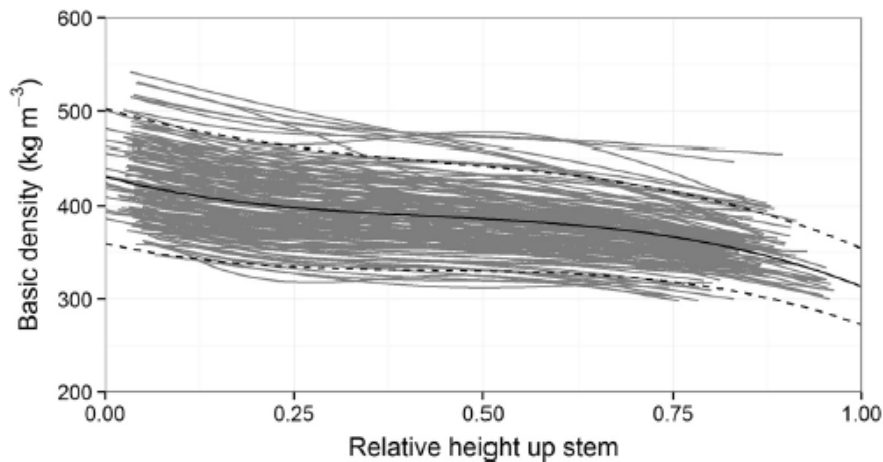


Figure 3. Variation in whole-disk density with relative height up the stem. The grey lines are smoothing curves fitted to the disk densities from each of 150 sites. The black lines show disk density predicted by model 3 for an average site (middle line, $L = 0$) and for sites at the 5th and 95th percentiles (lower and upper dashed lines, $L = -59.3$ and $L = +59.3$, respectively) (Kimberley et al. 2015).

Resistance drilling measurement

The resistance drilling tool is a mechanical drill system that measures the relative density profile as a rotating drill bit is driven into wood at a constant speed. Figure 4 shows the use of a resistance drill (Resistograph, Rinntech, Heidelberg, Germany) in a standing tree to obtain the relative resistance profile. The technique operates on the principle that drilling resistance (torque) is directly related to the density of the material being tested (Rinn 1988, 1989, 1990; Rinn et al. 1996). During the process of a drilling measurement, the relative drilling resistance, feeding force, and speed parameters can be measured continuously as a function of the drill bit position in the drilling path. A resistance drilling tool typically consists of a power drill unit, a small-diameter spade-type drill bit, and an electronic device that can be connected to the serial interface input of any standard personal computer. As the drill bit moves through the wood in a linear path, the penetration resistance along its path is measured and recorded. The pattern of change in relative resistance is recorded as a digital representation display.



Figure 4. Electronically regulated resistance drilling in a standing tree using a Resistograph tool (photo credit: Frank Rinn).

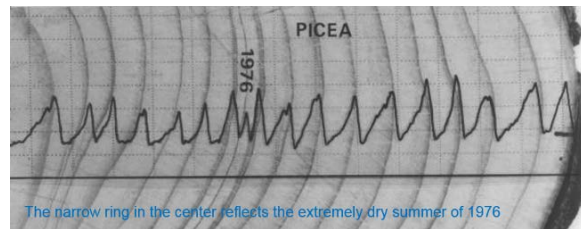


Figure 5. Resistance drilling profile obtained from a Norway spruce (*Picea abies*) revealing density variations inside tree rings (Rinn et al. 1996).
The narrow ring in the center reflects the extremely dry summer of 1976

Precision of resistance drilling profiles

A significant amount of research has been conducted to explore the use of resistance drilling measurements for various applications such as tree ring analysis, tree decay detection, and structural timber condition assessment. Rinn et al. (1996) demonstrated that Resistograph charts of coniferous and deciduous wood revealed tree ring variations. Figure 5 shows an example of a drilling profile obtained from Norway spruce (*Picea abies*) revealing density variations inside tree rings caused by earlywood and latewood zones. The extremely dry summer of 1976 can be identified by the corresponding narrow ring in the center. In the ideal case of drilling in the radial direction (perpendicular to the growth rings), the tree ring parameters in dry wood revealed by Resistograph charts showed excellent matches with those revealed by the x-ray density charts, both qualitatively and quantitatively (Rinn et al 1996). Chantre and Rozenberg (1997) compared Resistograph measurements with microdensitometry (MDM) on disks cut from 23-year-old Douglas-fir trees and found moderate to excellent correlations between profile

parameters (profile surface, profile energy, and mean density of the weighed profile) (r from 0.93 to 0.97). They concluded that the Resistograph appears to be better adapted to the evaluation of some whole-trunk parameters and is able to sum up in a single value one aspect of the standing tree global wood quality. Wang and Lin (2001) reported that the resistance drilling profile in *Taiwania* (*Taiwania cryptomerioides* Hayata) plantation wood revealed density variations inside tree rings caused by earlywood and latewood zones. The technique was also found useful in examining the effects of silvicultural treatments on density profiles and annual ring characteristics (Wang et al. 2003).

Wood density assessment

Research has quickly progressed to evaluate the potential of resistance drilling as an indirect method to measure density or specific gravity of dry wood. Some early studies demonstrated that there was a strong linear correlation between the mean drilling resistance and gross density of dry wood (Görlacher and Hättich 1990, Rinn et al. 1996). More recent studies on structural wood members also showed moderate to strong relationships between measured resistance values and wood density ($r^2 = 0.67$ reported by Ceraldi et al. 2001, $r^2 = 0.44$ reported by Zhang et al. 2009, $r^2 = 0.89$ reported by Park et al. 2006, $r^2 = 0.93$ reported by Bouffier et al. 2008, $r^2 = 0.62$ – 0.78 reported by Sharapov and Chernov 2014).

There has also been a growing interest in using the resistance drilling method for forest genetics field tests. In a tree genetic improvement program, Isik and Li (2003) evaluated the use of the Resistograph tool for rapid assessment of relative wood density of live loblolly pine trees in progeny trials. A total of 1,477 trees were sampled from 14 full-sib families of loblolly pine across the four test sites. They reported strong correlations among average drilling resistance values and wood density and strong genetic control at the family level. However, individual phenotypic correlations were found to be relatively weak. Similar results have also been reported by Gantz (2002), Charette et al. (2008), Gwaze and Stevenson (2008), and Eckard et al. (2010).

Friction factor

In a recent study, Oliveira et al. (2017) evaluated the use of resistance drilling for assessing wood specific gravity of young eucalyptus trees for pulpwood production. The genetic materials used consisted of fifty 34-month-old and fifty 62-month-old trees from *Eucalyptus grandis* Hill ex Maiden \times *Eucalyptus urophylla* ST Blake clonal plantations. It was found that drill penetration depth had a significant effect on the relationship between average resistance amplitude and specific gravity. They observed a clear trend of weakening correlation as the drill penetration depth increased (Fig. 6), which could be attributed to the increased friction acting on the drill shaft. When a needle drill bit cuts through wood, wood chips remain in the drilling channel causing friction on the rotating needle shaft (Rinn 2012). The spade-type needle drill bit used in resistance drilling measurements typically has a 3-mm-wide triangular shape cutting head, which is twice the diameter of the needle shaft (1.5 mm). The drill bit is designed to decrease the shaft friction during resistance drilling measurements. The shaft friction was reported to be minimal in drilling wood of softwood species (Rinn et al. 1996) but was found to be significant in drilling wood of some tropical species such as eucalyptus (Nutto and Biechele 2015, Oliveira et al. 2017).

Concept of partial resistance drilling

Recent studies indicated that the use of the resistance drilling method can potentially be extended into tree genetic improvement and wood quality survey programs in which hundreds or even thousands of trees must be sampled for wood density information. One of the key issues with the resistance drilling method is related to the internal friction as the drill bit cuts deep into the tree. Because of the increased friction acting on the drill shaft, the accuracy of the relative resistance measurement can be affected. As a consequence, the predictive power of the amplitude parameter obtained from a resistance profile can be substantially decreased, especially in trees of larger diameter and greater wood density.

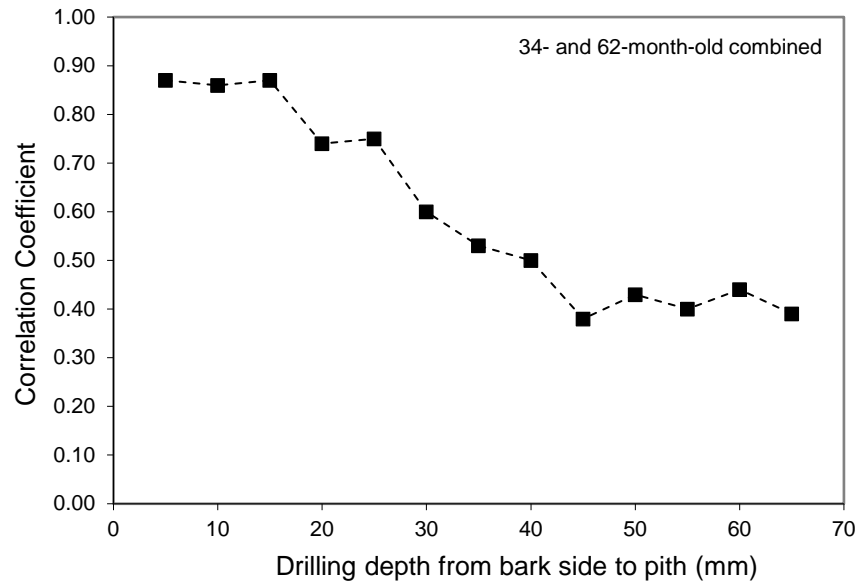


Figure 6. Correlation coefficient for the relationship between measured drilling resistance (expressed as amplitude in resistance profile) and specific gravity of 34- and 62-month-old *Eucalyptus grandis* × *Eucalyptus urophylla* trees as affected by the drilling depth (Oliveira et al. 2017).

A possible solution would be to conduct partial resistance drilling measurements on tree stems instead of drilling through the whole diameter, and assess the outer wood density of standing trees. If the outer wood density of a tree can be accurately determined through partial resistance drilling measurements, then the wood density models developed for the increment coring method can be used to predict the disk or whole-tree density using the outer wood density values. The validity of this partial resistance drilling approach needs to be tested in future research.

When selecting appropriate field nondestructive tools for determining wood density or specific gravity of standing trees, it is important that the solution must meet the needs of practicing foresters and reasonable estimates of average values with measurable errors will be more useful than expensive, highly technical procedures of greater accuracy. Although direct wood density measurements are often taken as the benchmark, wood density varies with stand age, site, silvicultural treatments, and genetics. A sound sampling strategy is critical in any wood density survey to ensure the validity of the method used. In general, the reasons for a nondestructive sampling procedure may include (1) assessing the wood quality of the forest resource available at a regional to a compartmental level; (2) examining the effects of site, climate, or silvicultural treatments on wood quality; and (3) assessing young trees for genetic improvement. For each of these reasons, different numbers of tree samples and sampling procedures will need to be carefully designed. A detailed discussion of nondestructive sampling methods can be found in Downes et al. (1997).

Conclusions

The basic increment core method has dominated research for more than half a century and has been used as a standard method for assessing wood quality of forest resources, determining biomass of ecosystems, and investigating climate history through dendrochronological analysis. Comprehensive wood density models have been developed for commercially important species that use outer wood cores and

knowledge of internal tree density distribution to fairly accurately predict the density of major tree components. With the development of SilviScan and near infrared spectroscopy instruments, more wood and fiber properties can be obtained from a single increment core sample, allowing comprehensive wood quality evaluation of plantation trees for genetic improvement, forest management, and optimal wood utilization. However, for many users or in many applications, increment core sampling and subsequent laboratory analysis are time-consuming and expensive. A more rapid field-type nondestructive method is needed in various research programs and forest operations.

The resistance drilling method has considerable advantages compared with the traditional increment coring method in terms of causing less damage to trees, faster data collection, and significantly less effort required for post data analysis. One factor that currently hinders the use of the resistance drilling tool for rapid wood density determination in trees is the internal friction encountered by the drill shaft as it cuts deeply into the tree stem. A partial resistance drilling approach coupled with knowledge of internal tree density distribution may offer an alternative to the widely used increment coring technique.

References

- Bouffier, L.; Charlot, C.; Raffin, A.; Rozenberg, P.; Kremer, A. 2008. Can wood density be efficiently selected at early stage in maritime pine (*Pinus pinaster Ait.*)? *Annals of Forest Science*. 65(1): 106-113.
- Ceraldi, C.; Mormone, V.; Ermolli, E.R. 2001. Resistographic inspection of ancient timber structures for the evaluation of mechanical characteristics. *Materials and Structures*. 34: 59-64.
- Chantre, G.; Rozenberg, P. 1997. Can drill resistance profiles (Resistograph) lead to within-profile and within-ring density parameters in Douglas-fir wood? In: Zhang, S.Y.; Gosselin, R.; Chauret, G., eds. Proc. of CTIA—International union of forestry research organizations (IUFRO) international wood quality workshop: Timber management toward wood quality and end-product value. Sainte-Foy, Quebec, Canada: Forintek Canada Corp: 41-47.
- Charette, P.; Lu, P.; Tang, F.; Zhang, S.Y. 2008. Evaluation of the resistograph for wood density estimate and the use of multi-trait selection index for genetic selection in jack pine. In: Simpson, J.D., ed. Proceedings of the 31st meeting of the Canadian Forest Genetics Association: adaptation and conservation in the era of forest tree genomics and environmental change. 25-28 August 2008, Quebec City, Quebec. Fredericton, N.B.: Natural Resources Canada, Canadian Forest Service: 88.
- Cown, D.J. 2006. Wood quality in standing timber—evolution of assessment methods in plantations. In: Kurjatko, S.; Kúdela, J.; Lagaña, R., eds. Proceedings of the 5th IUFRO symposium “Wood Structure and Properties ’06”. September 3-6, 2006, Sliac—Sielnica, Slovakia: 11-17.
- Cown, D.J.; Clement, B.C. 1983. A wood densitometer using direct scanning with x-ray. *Wood Science and Technology*. 17: 91-99.
- Downes, G.M.; Hudson, I.L.; Raymond, C.A.; Dean, G.H.; Michell, A.J.; Schimleck, L.R.; Evans, R.; Muneri, A. 1997. Sampling plantation eucalypts for wood and fibre properties. Melbourne, Australia: CSIRO.
- Eberhardt, T.L.; Samuelson, L.J. 2015. Collection of wood quality data by x-ray densitometry: a case study with three southern pines. *Wood Science and Technology*. 49: 739-753.

- Eckard, T.J.; Isik, F.; Bullock, B.; Li, B.; Gumpertz, M. 2010. Selection efficiency for solid wood traits in *Pinus taeda* using time-of-flight acoustic and micro-drill resistance methods. *Forest Science*. 56(3): 233-241.
- Gantz, C.H. 2002. Evaluating the efficiency of the Resistograph to estimate genetic parameters for wood density in two softwood and two hardwood species. MS thesis. Raleigh, NC: North Carolina State University. 88 p.
- Gao, S.; Wang, X.; Wiemann, M.C.; Brashaw, B.K.; Ross, R.J.; Wang, L. 2017. A critical analysis of methods for rapid and nondestructive determination of wood density in standing trees. *Annals of Forest Science*. 74: 27. DOI 10.1007/s13595-017-0623-4.
- Görlacher, R.; Hättich, R. 1990. Untersuchung von altem Konstruktionsholz: Die Bohrwiderstandsmessung. *Bauen mit Holz*. 92: 455-459.
- Grissino-Mayer, H.D. 2003. A manual and tutorial for the proper use of an increment borer. *Tree-Ring Research*. 59: 63-79.
- Gwaze, D.; Stevenson, A. 2008. Genetic variation of wood density and its relationship with drill resistance in shortleaf pine. *Southern Journal of Applied Forestry*. 32(3): 130-133.
- Hart, J.H.; Wargo, P.M. 1965. Increment borer wounds — penetration points for *Ceratocystis fagacearum*. *Journal of Forestry*. 63(1): 38-39.
- Isik, F.; Li, B. 2003. Rapid assessment of wood density of live trees using the Resistograph for selection in tree improvement programs. *Canadian Journal of Forestry Research*. 33: 2427-2435.
- Jozsa, L. 1988. Increment core sampling techniques for high quality cores. Special publication No. SP-30. Ottawa, Ontario, Canada: Forintek Canada Corporation. 26 p.
- Kandeel, E.S.A.E.; Benseid, D.W. 1969. Structure, density, and shrinkage variation within a silver maple tree. *Wood Science*. 1: 227-237.
- Kimberley, M.O.; Cown, D.J.; McKinley, R.B.; Moore, J.R.; Dowling, L.J. 2015. Modeling variation in wood density within and among trees in stands of New Zealand-grown radiata pine. *New Zealand Journal of Forestry Science*. 45: 22. doi: 10.1186/s40490-015-0053-8.
- Maeglin, R.R. 1979. Increment cores: how to collect, handle, and use them. Gen. Tech. Rep. FPL–GTR–25. Madison, WI: U.S. Department of Agriculture, Forest Service, Forest Products Laboratory. 18 p.
- Nutto, L.; Biechele, T. 2015. Drilling resistance measurement and the effect of shaft friction — using feed force information for improving decay identification on hard tropical wood. In: Ross, R.J.; Gonçalves, R.; Wang, X., eds. Proceedings of the 19th international nondestructive testing and evaluation of wood symposium. Gen. Tech. Rep. FPL–GTR–239. Madison, WI: U.S. Department of Agriculture, Forest Service, Forest Products Laboratory: 154-161.
- Oliveira, J.T.; Wang, X.; Vidaurre, G.B. 2017. Assessing specific gravity of young *eucalyptus* plantation trees using a resistance drilling technique. *Holzforschung*. 71(2):137-145.

- Palmer, D.J.; Kimberley, M.O.; Cown, D.J.; McKinley, R.B. 2013. Assessing prediction accuracy in a regression kriging surface of *Pinus radiata* outerwood density across New Zealand. *Forest Ecology and Management*. 308: 9-16.
- Park, C.Y.; Kim, S.J.; Lee, J.J. 2006. Evaluation of specific gravity in post member by drilling resistance test. *Mokchae Konghak*. 34(2): 1-9.
- Pressler, M.R. 1866. Der forstliche Zuwachsbohrer neuester Construction und dessen praktische Bedeutung und Anwendung für die forstliche Forschungs-, Taxations-, Pflege- und Nutzungs-Technik. *Tharander Jahrbuch*. 17, III: 113-209.
- Rinn, F. 1988. A new method for measuring tree-ring density parameters. Physics diploma thesis, Institute for Environmental Physics, Heidelberg University.
- Rinn, F. 2012. Basics of micro-resistance drilling for timber inspection. *Holztechnologie*. 53: 24-29.
- Rinn, F. 1990. Device for material testing, especially wood inspection by drill resistance measurements. German Patent 4122494.
- Rinn, F. 1989. Eine neue Bohrmethode zur Holzuntersuchung. *Holz-Zentralblatt*. 34: 529-530.
- Rinn, F.; Schweingruber, F.H.; Schar, E. 1996. Resistograph and x-ray density charts of wood comparative evaluation of drill resistance profiles and x-ray density charts of different wood species. *Holzforschung*. 50(4): 303-311.
- Sharapov, E.S.; Chernov, V.Y. 2014. Comparative analysis of wood density techniques determination with using x-ray and device for drilling resistance measurements. *Moscow State Forest University Bulletin - Lesnoy vestnik* 2(101): 89-95.
- Sprague, J.R.; Talbert, J.T.; Jett, J.B.; Bryant, R.L. 1983. Utility of the Pilodyn in selection for mature wood specific gravity in loblolly pine. *Forest Science*. 29(4): 696-701.
- Tian, X.; Cown, D.J. 1995. Modeling of wood properties in New Zealand. In: Klitscher, K.; Cown, D.J.; Donaldson, L., eds. *Wood quality workshop 95*. FRI bulletin 201. Rotorua, New Zealand: Forest Research Institute: 72-81.
- Tian, X.; Cown, D.J.; McConchie, D.L. 1995. Modeling of radiata pine wood properties. Part 2: wood density. *New Zealand Journal of Forestry Science*. 25(2): 214-230.
- Wang, S.Y.; Chiu, C.M.; Lin, C.J. 2003. Application of the drilling resistance method for annual ring characteristics: evaluation of Taiwan (*Taiwania cryptomerioides*) trees grown with different thinning and pruning treatments. *Journal of Wood Science*. 49: 116-124.
- Wang, S.Y.; Lin, C.J. 2001. Application of the drill resistance method for density boundary evaluation of earlywood and latewood of Taiwan (*Taiwania cryptomerioides* Hay.) plantation. *Taiwan Forest Science*. 16(3): 197-200.
- Wiemann, M.C.; Williamson, G.B. 2013. Biomass determination using wood specific gravity from increment cores. Gen. Tech. Rep. FPL-GTR-225. Madison, WI: U.S. Department of Agriculture, Forest Service, Forest Products Laboratory. 7 p.

Wiemann, M.C.; Williamson, G.B. 2012. Testing a novel method to approximate wood specific gravity of trees. *Forest Science*. 58: 577-591.

Wiemann, M.C.; Williamson, G.B. 2014. Wood specific gravity variation with height and its implications for biomass estimation. Res. Pap. FPL–RP–677. Madison, WI: U.S. Department of Agriculture, Forest Service, Forest Products Laboratory. 9 p.

Williamson, G.B.; Wiemann, M.C. 2010. Measuring wood specific gravity...correctly. *American Journal of Botany*. 97(3): 519-524.

Zhang, H.; Guo, Z.; Su, J. 2009. Application of a drill resistance technique for rapid determining wood density. *Progress of Machining Technology*. Key Engineering Materials. 407-408: 494-499.

Investigating Stress Wave Propagation Patterns in Standing Trees Using a Numerical Simulation Method

Fenglu Liu

School of Technology, Beijing Forestry University, Beijing, China, liufenglu39@126.com

Xiping Wang

USDA Forest Service Forest Products Laboratory, Madison, Wisconsin, USA, xwang@fs.fed.us

Fang Jiang

School of Technology, Beijing Forestry University, Beijing, China, jf0602@bjfu.edu.cn

Houjiang Zhang

School of Technology, Beijing Forestry University, Beijing, China, hjzhang6@bjfu.edu.cn

Abstract

In this paper, we examined the propagation patterns of longitudinal stress waves in standing trees through numerical simulation using a COMSOL Multiphysics® software. The simulation was based on wave propagation theory of solid medium with the assumption of orthotropic material for standing trees. Both two-dimensional and three-dimensional wave propagation patterns in virtual tree trunks were obtained and effects of tree diameter and propagation distance on wave velocity were investigated. Our simulation results indicate that the stress wave initially propagates in impact direction with a spherical wave front. As the wave continuously travels, the flow of stress wave energy gradually shifts toward longitudinal direction and its wave front gradually becomes flattened and close to perpendicular to the longitudinal axis, which implies that stress wave propagates as a dilatational wave in the early phase, then gradually changes to a quasi-plane wave. In a typical geometry model, the wave begins to travel as a quasi-one-dimensional wave when the diameter-to-distance ratio reaches 0.025. Both distance and tree diameter had an effect on the propagation patterns of stress wave. Travel distance was found to have no significant effect on wave velocity. Wave velocity generally increased as tree diameter increased.

Keywords: COMSOL Multiphysics software, diameter, orthotropic, stress wave, standing trees, wave front, wave velocity

Introduction

In recent years, stress wave technology has gained great attention in forest industry as a robust field method to assess wood stiffness and fibre properties in standing trees. However, the mechanism of a stress wave propagating in a tree trunk and how tree diameter, species, tree age, and environmental conditions affect wave propagation in a tree are still not well understood. Previous research have indicated that tree acoustic velocity measured using a time-of-flight (TOF) method was strongly correlated with log velocity measured using a resonance-based method, but tree velocity was found to be 7% to 36% higher than the corresponding log velocity. Some studies reported good relationships between tree diameter and stress wave velocity (or stiffness calculated from it) (Lasserre et al. 2004; 2005; Wang et al. 2003, 2004; Carter et al. 2005; Chauhan and Walker 2006). Others reported a weak or no correlation between tree diameter and acoustic velocity (Jerrymjr et al. 2009; Mora et al. 2009). There has been no reasonable and convincing explanations for the different relationships observed between tree diameter and tree velocity.

In this paper, we examined the propagation patterns of longitudinal stress waves in standing trees through numerical simulation using a COMSOL Multiphysics® software. The simulation was based on wave propagation theory of solid medium with the assumption of orthotropic material for standing trees. Both two-dimensional (2D) and three-dimensional (3D) wave propagation patterns in virtual tree trunks were obtained and effects of tree diameter and propagation distance on wave velocity were investigated.

Numerical Simulation of Stress Wave Propagation

A typical approach for *in situ* measurement of stress wave velocity in trees involves inserting two sensor probes (transmit probe and receiver probe) into the sapwood at about 45° to the trunk surface and introducing a stress wave impulse into the tree trunk through a mechanical impact (Figure 1) (Wang et al. 2000). The standing tree device, in fact, measures the time for the stress wave traveling from the transmit probe to the receiver probe. The stress wave velocity is subsequently calculated from the test span (L) between two sensor probes and the time of flight (TOF) data. The numerical computation was to simulate the wave propagation process and determine the patterns of stress wave wave front propagating from the transmit probe to the receiver probe.

Model geometry

For stands of 10 to 60 years old, the corresponding average diameter at breast height (DBH) of common Chinese larch (*Larix potaninii*) plantation trees generally ranges from 150 to 550 mm (Cheng 1985). Considering that the taper of the lower trunk of larch trees is typically small, for the efficiency of calculation in numerical simulation, the geometry models of standing trees were set to a series of cylindrical models with a length of 500 cm and a diameter of 20, 30, 40 and 50 cm. In addition, the wood mechanical properties in trees vary from pith to bark though they are normally considered as an orthotropic material. To facilitate the investigation of stress wave propagation in standing trees, we considered the following simplifications for the geometry models: 1) Considering a tree trunk as an orthotropic material; 2) Treating a tree trunk as a two-layer composite material that consists of heartwood and sapwood, with an orthotropic assumption for both of them; and 3) Assuming that the radius of heartwood accounts for half of the radius of the tree trunk, that is a 1:1 heartwood-to-sapwood ratio.

In the numerical simulations, we considered both 2D and 3D geometry models. The size parameters of the 3D geometry models are shown in Table 1. Taking model 2 as an example, the 3D geometry model constructed using COMSOL software is shown in Figure 2, where layer 1 is the heartwood and layer 2 is the sapwood.

Considering that 2D numerical simulation investigates the stress wave propagation patterns in longitudinal-radial plane of a standing tree, we set the longitudinal-radial plane of a tree trunk as the 2D geometric model, i.e. selected the longitudinal-radial plane of a 3D geometry model as the 2D geometry model, as shown in Figure 3, where layer 1 is the heartwood, layer 2 is the sapwood.

Material properties

A tree trunk was considered as an orthotropic cylinder, with longitudinal (L), radial (R), and tangential (T) directions as three principal axes (x, y, z) in Cartesian coordinates. Twelve elastic constants of heartwood and sapwood of green larch were determined through laboratory experiments in a previous study (Liu et al. 2015). The wood specimens used for determining the elastic constants were cut from three larch logs used for validation experiment. The average values of the elastic constants and green density for heartwood and sapwood are shown in Table 2 and Table 3, respectively.

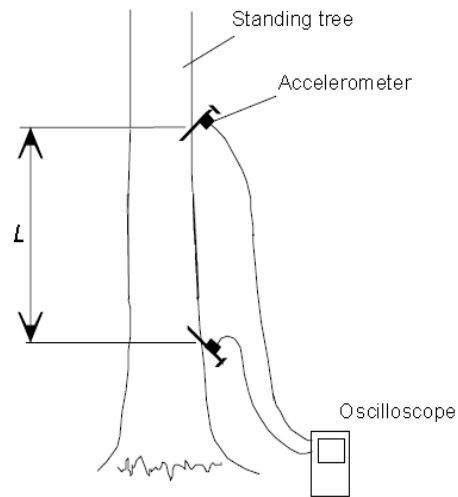


Figure 1—Schematic diagram of time-of-flight (TOF) stress wave measurement on standing trees (L =test span).

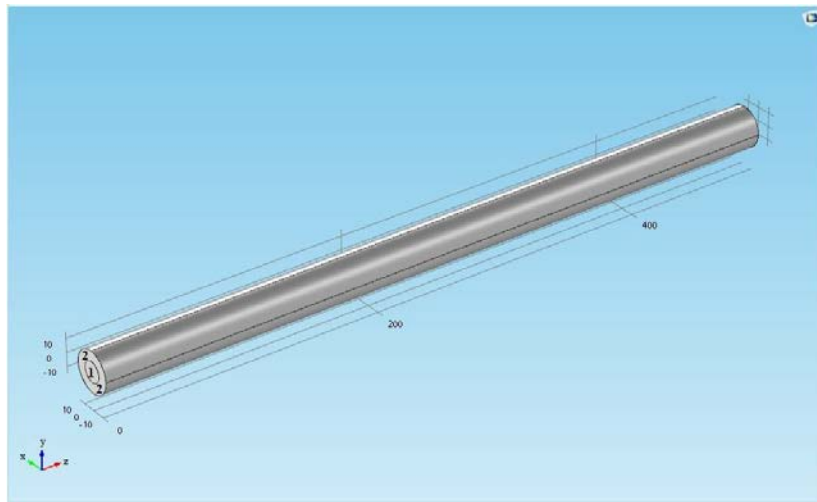


Figure 2—Three-dimensional geometry model constructed using COMSOL software (Model 2).

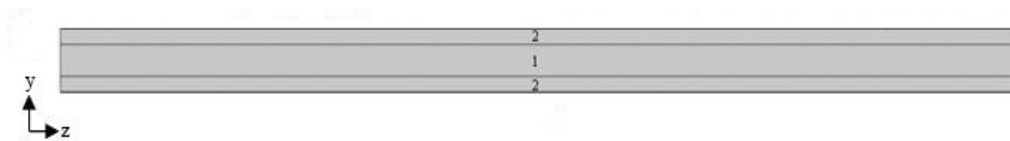


Figure 3—Two-dimensional geometry model constructed using COMSOL software (Model 2).

Table 1—Parameters of the 3D geometry models for Chinese larch.

Variable ^a	Model 1	Model 2	Model 3	Model 4
L (cm)	500	500	500	500
D (cm)	20	30	40	50
r (cm)	5	7.5	10	12.5
r_1 (cm)	5	7.5	10	12.5
r_2 (cm)	10	15	20	25

^a L , length of model; D , diameter of model; r , radius of layer 1; r_1 , inner radius of layer 2; r_2 , outer radius of layer 2

Table 2—Elastic constants and density of Chinese larch heartwood.

Modulus of elasticity (MPa) ^a		Modulus of rigidity (MPa) ^b		Poisson's ratio ^c		Density (Kg · m ⁻³)
E_L	6792.08	G_{RT}	414.58	ν_{RT}	0.76	500
E_T	282.27	G_{LR}	426.86	ν_{LR}	0.21	
E_R	342	G_{LT}	375.23	ν_{LT}	0.28	

^a E_L , longitudinal modulus of elasticity; E_T , tangential modulus of elasticity; E_R , radial modulus of elasticity

^b G_{RT} , shear modulus in R-T plane; G_{LR} , shear modulus in L-R plane; G_{LT} , shear modulus in L-T plane

^c ν_{LT} , Poisson's ratio of R-T direction; ν_{LR} , Poisson's ratio of L-R direction; ν_{RT} , Poisson's ratio of L-T direction

Table 3—Elastic constants and density of Chinese larch sapwood.

Modulus of elasticity (MPa)		Modulus of rigidity (MPa)		Poisson's ratio		Density (Kg · m ⁻³)
E_L	10137	G_{RT}	555.56	ν_{RT}	0.81	750
E_T	387.82	G_{LR}	430.05	ν_{LR}	0.26	
E_R	914.95	G_{LT}	445.78	ν_{LT}	0.36	

^a E_L , longitudinal modulus of elasticity; E_T , tangential modulus of elasticity; E_R , radial modulus of elasticity

^b G_{RT} , shear modulus in R-T plane; G_{LR} , shear modulus in L-R plane; G_{LT} , shear modulus in L-T plane

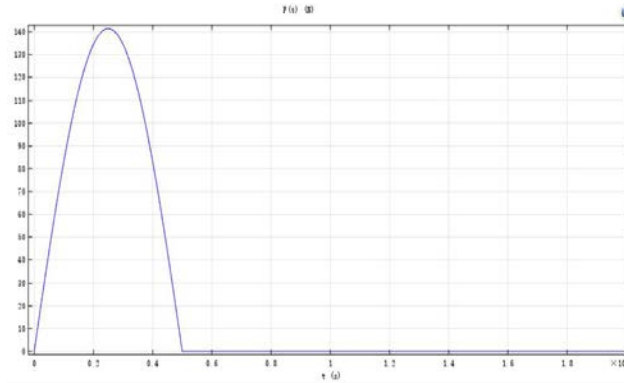
^c ν_{LT} , Poisson's ratio of R-T direction; ν_{LR} , Poisson's ratio of L-R direction; ν_{RT} , Poisson's ratio of L-T direction

Impulse load

Stress waves used in tree measurements are typically generated through a mechanical impact on the start transducer and this impact-induced stress wave has a very short duration. We used the following half-sine pulse function to express this impact force:

$$F(t) = \begin{cases} A \sin(2\pi ft), & t < (1/2f) \\ 0, & t \geq (1/2f) \end{cases} \quad (1)$$

Where A is the amplitude of the pulse and f is the frequency.

**Figure 4**—Function of half-sine pulse.

According to the actual pulse signals collected from a hammer impact in a laboratory testing, the amplitudes of the pulse signals were about 200 N. Because the start sensor probe is typically inserted into a tree trunk in a 45° angle with respect to the longitudinal axis, the impact force acting on the start sensor is also in a 45° angle to the longitudinal axis of the trunk. Based on the principle of vector decomposition, $F(t)$ can be decomposed into two orthogonal components: $F_y(t)$ and $F_z(t)$, and each component is 141.4 N. According to the frequency analysis of the actual impact signals, the frequency of the pulses was 1×10^4 (Hz). The function of a single pulse force component is shown in Figure 4.

Initial and boundary conditions

Since the particles of two-dimensional and three-dimensional models were in a static state prior to be subjected to a load, there was no initial displacement and initial velocity for each particle in the model. Consequently, the initial displacement and initial velocity of each particle in wood were set as zero. u is used to represent the particle displacement, the mathematical expressions of these two initial conditions are shown below:

$$\text{Initial displacement: } u_i = 0 \quad (i = x, y, z) \quad (2)$$

$$\text{Initial velocity: } \frac{\partial u_i}{\partial t} = 0 \quad (i = x, y, z) \quad (3)$$

The side surface of the models was set to have a free boundary condition (i.e. second boundary condition), which means that the compression waves and reflected waves coexist with the wave attenuation when the stress wave propagates to the boundaries. A low-reflection boundary condition (i.e. third boundary condition) was used for the end surface of the models, which implies that only the compression waves exist without any reflection wave or with a very small amount of reflected wave when the stress wave reaches the end surface of the model. The use of free boundary condition and low-reflection boundary could make the boundary condition of the models very close to the boundary condition of real standing trees. The mathematical expression of these two boundary conditions is shown as follows:

$$\text{Free boundary condition : } \left. \frac{\partial u}{\partial l} \right|_{(x^2+y^2=r_2^2, 0 \leq z \leq 500)} = 0 \quad (4)$$

$$\text{Low-reflection condition: } \sigma \cdot n = -\rho \cdot C_p \left(\frac{\partial u}{\partial t} \cdot n \right) \cdot n - \rho \cdot C_s \left(\frac{\partial u}{\partial t} \cdot t \right) \cdot t \quad (5)$$

Where l is the unit normal vector of boundary, r_2 is the large radius of the model (i.e. outer radius of layer 2), σ is the stress of particle, n and t are the unit normal vectors and unit tangent vectors of boundary, respectively, C_p is the longitudinal wave velocity, C_s is the shear wave velocity, ρ is the density of medium.

Meshing

For 2D models, the mesh was generated automatically with the triangular elements. Free meshing provided in COMSOL was used for the generation of mesh. The largest and smallest elements of 2D models were 1.25 cm and 0.0072 cm, respectively. Figure 5 shows the divided grids of the longitudinal-radial section in a virtual tree trunk, which corresponds to Model 2. The mesh has been refined at the region below the excitation source. A free time step for transient solver was selected as the initial step, 1e-9s, and the biggest step, 1e-4s. Output step of the result was 5e-6s and 1e-6s for calculating time step.

If the commonly used free meshing (i.e. the tetrahedral elements method) was employed for the 3D models, the number of meshes generated would be too huge due to its relatively large dimension, and then resulted in a surge in the computational complexity of the numerical simulation. Therefore, the swept method was applied for 3D models to get a reasonable number of grids. The largest and smallest elements of the end surface in 3D models were 1.4 cm and 0.004 cm, respectively. After the mesh of the end surface was finished, the swept method was used to extend the mesh to the entire 3D models. The total number of meshes obtained for 3D models was up to 44000. The divided grids of the 3D models was shown in Figure 6, which also corresponds to Model 2. A default free time step for transient solver was selected as initial step and biggest step. Calculated time step was 1e-6s and 5e-6 for output step of the results in the 3D models. After all the settings were completed, the COMSOL program was run to obtain simulation results.



Figure 5—Meshing of a 2D model (Model 2).

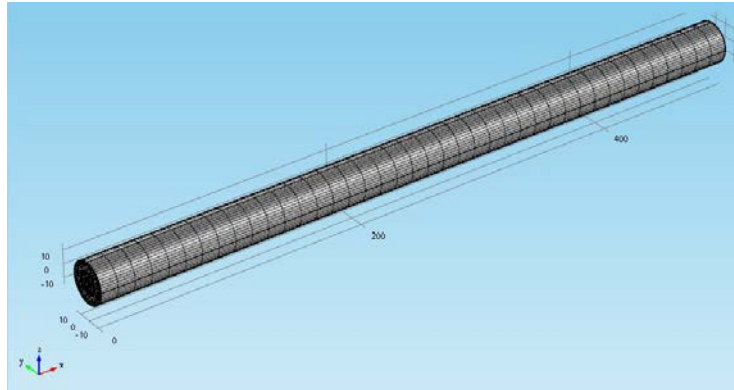


Figure 6—Meshing of a 3D model (Model 2).

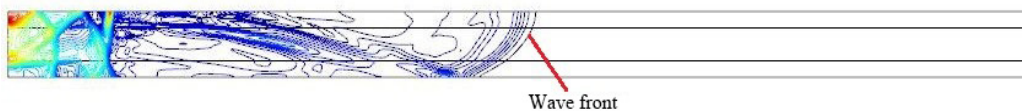


Figure 7—Contour map of total displacement in the longitudinal-radial (L-R) plane (Model 2, $t=700\mu\text{s}$).

Results and Discussion

Contour map of displacement

For each 2D tree trunk model, a contour map of displacement directly outputted from the post-processing of COMSOL Multiphysics software was obtained. Figure 7 shows a contour map of displacement obtained from Model 2 at the propagation time $t=700\mu\text{s}$. As it can be seen, each contour had different shapes and basically showed a progressive change between the contours except the denser parts at the left end of model. These variations in shape may be due to the reflected waves caused by the free boundary conditions of the upper and lower sides as well as the left end of the model. Actually, the forefront line along the wave propagation direction in displacement contour map for each time point was the wave front (shown as a curve in longitudinal-radial plane) generally defined as the boundary of stress wave disturbance zone and undisturbed area during the propagation. The study on stress wave propagation patterns in the tree trunk is exactly to explore the variation patterns of velocity and shapes of wave front in standing trees at different travel times.

2D wave front map

To visually display the propagation patterns of the impact-induced stress waves in a virtual tree trunk, a 2D wave front map was developed for each model by extracting the forefront contour lines from the displacement contour maps at various time points ($t=100, 200, 300, 400, 500, 600, 700, 800, 900, 1000, 1100, 1200, 1300\mu\text{s}$), as shown in Figure 8. This 2D wave front map is a cluster of leading contour lines where the travel time is same at any point of the line (iso-travel times), they represented therefore the wave fronts in a time sequence on the longitudinal-radial plane.

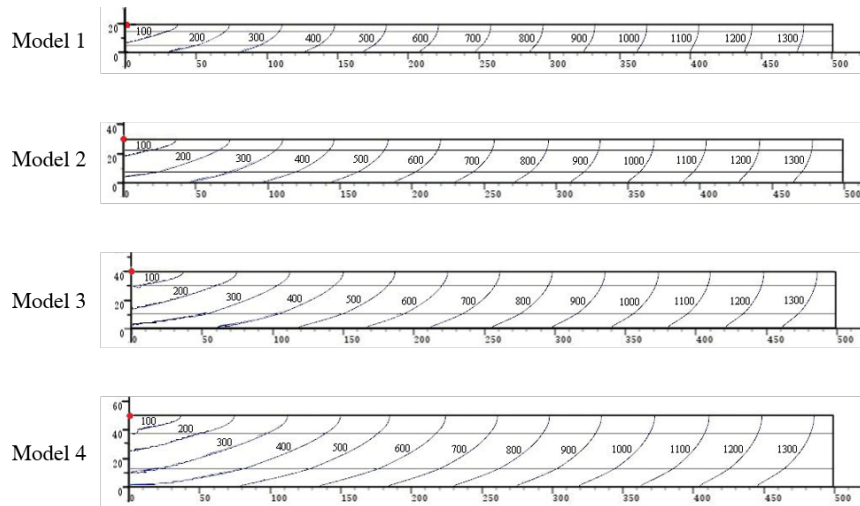


Figure 8—Two-dimensional simulation results of stress wave front (The numbers next to wave front lines were transmission time in microsecond; the red dot on the upper left of graph was the import source; horizontal and vertical axes were the length and diameter of tree trunk, respectively).

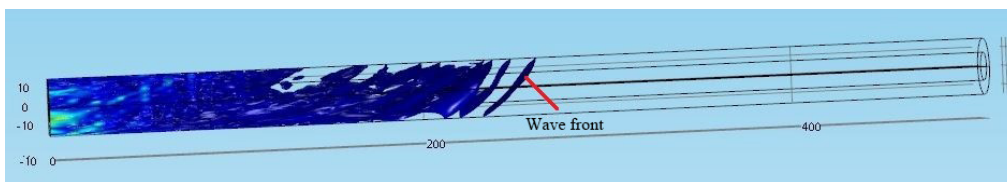


Figure 9—Contour surface map of total displacement of stress wave propagation in standing trees (Model 2, $t=700\ \mu\text{s}$).

It could be observed from Figure 8 that the wave front maps of all four 2D virtual tree models had the similar patterns: stress wave initially propagated in the impact direction with a spherical wave front bending towards the initiation point of the impact pulse; then propagation direction gradually shifted towards the longitudinal directions as the wave moved away from the energy source and its wave front gradually became flattened and close to perpendicular to the longitudinal axis, i.e. the wave front gradually transformed from a dilatational wave to a quasi-plane wave during the propagation. It was also found that the wave front curve near the import source was elongated and the tree diameter seems to have a positive impact on elongation effect. This can be attributed to, on the one hand, inertia introduced into the numerical simulation. The transverse dimension of the model, on the other hand, was not much smaller than wavelength and thus transverse inertia effect cannot be neglected. Wave dispersion phenomenon occurred in local area of the model under the effect of inertia and this phenomenon was strengthened as diameter increased. However, since the dispersion only worked within a limited space of the model, it does not affect the overall patterns of stress wave propagation in the tree trunk. Moreover, Figure 8 showed that the slope of wave front decreased more and more slowly as the tree diameter increased, that is, stress wave propagating in trunks need a longer time to transform from dilatational wave to one-dimensional plane wave. This indicated that diameter affected the propagation patterns of stress wave in standing trees.

Contour surface map of displacement

Similar to the displacement contour maps in 2D models, the contour surface maps of displacement in 3D models were generated from the software post-processing. The leading isosurface in displacement contour surface map just referred to the wave front described as the interface between disturbed region and undisturbed zone. A contour surface map for Model 2 at the propagation time $t=700\ \mu\text{s}$ was

presented in Figure 9. It can be seen that the isosurface at left end of the model was relatively dense, and there was a gradual change in the shape of each adjacent isosurface.

3D wave front map

Likewise, in order to visually display the propagation patterns of stress waves in a tree trunk, a 3D wave front map was constructed for each model by extracting the forefront isosurface of the displacement contour surface maps at various time points ($t=100, 200, 300, 400, 500, 600, 700, 800, 900, 1000, 1100, 1200, 1300\mu s$), as shown in Figure 10. Regardless of the difference in tree diameter, the stress wave firstly propagated in the impact direction with a tilted spherical surface bending towards the input point. Then the inclination of wave front gradually decreased as the propagation distance increased. Finally, the wave front gradually became near perpendicular to the longitudinal axis and thus transformed from a 3D wave to a quasi-plane wave. This result was consistent with that of 2D numerical simulation.

In addition, the dispersion phenomenon was found in the results of 3D simulation contributed to the introduction of transverse inertia and the relatively small lateral size of the model. It was also noted that the dispersion effect of the 3D numerical simulation was stronger than that of the 2D numerical simulation, which may be due to the fact that the dispersion effect was enhanced in space of the 3D model. Furthermore, it was equally found in the 3D numerical simulation that stress wave propagating in trunks needed a longer time to transform from a dilatational wave to a 1D plane wave as the tree diameter increases, which indicated that diameter has an impact on the propagation patterns of stress wave in standing trees. The results of the 2D and 3D numerical simulations were in agreement with the results obtained from the field stress wave experiments performed by Zhang et al. (2011).

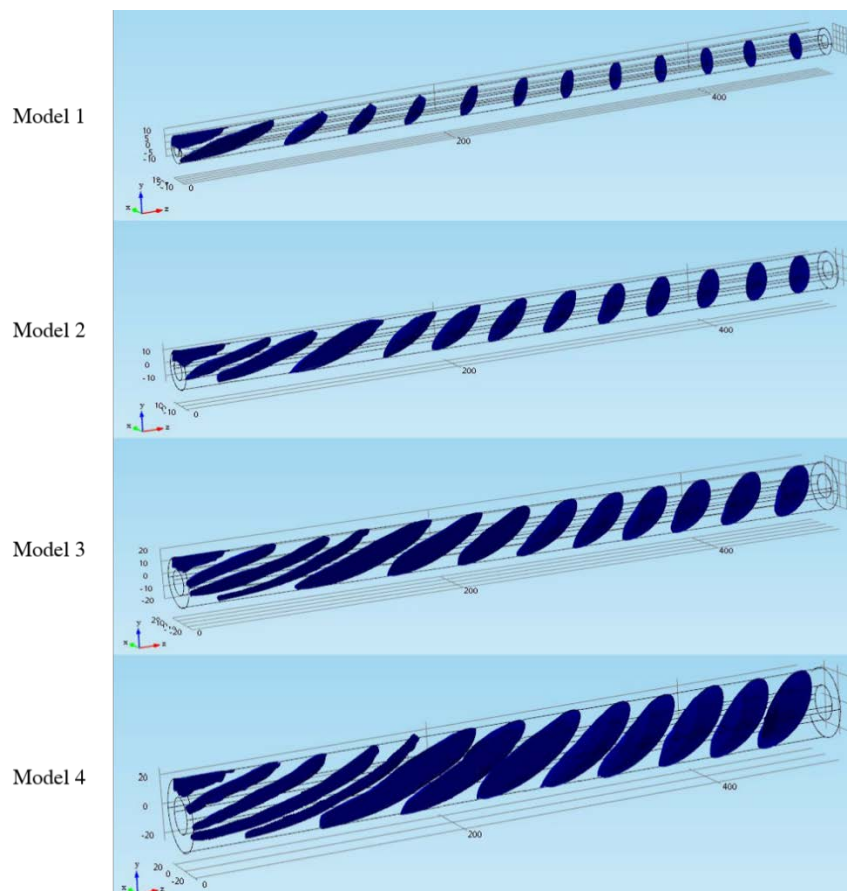


Figure 10—3D wave front maps showing propagation patterns of stress waves in tree trunks ($t=100, 200, 300, 400, 500, 600, 700, 800, 900, 1000, 1100, 1200, 1300\mu s$).

Effect of tree diameter and propagation distance on wave velocity

There have been very few studies looking into the effects of wave propagation distance and tree diameter on the wave velocity measured on trees. With respect to tree diameter, there were two distinct conclusions about the relationship between tree diameter and wave velocity. Some argued that tree diameter had no significant effect on the wave velocity measured on trees because of the poor relationships observed between them (Joe et al. 2004; Chauhan and Walker 2006; Raymond et al. 2008; Jerrymir et al. 2009). Others believed that tree diameter not only affected the propagation patterns of stress wave in trees, but also affected values of the measured wave velocity (Wang et al. 2000, 2007; Zhang et al. 2009).

To understand the relationships between tree diameter, propagation distance and wave velocity, the stress wave velocity in each tree model was calculated from the propagation distance (illustrated in Figure 11, $L=2$ m) divided by the corresponding propagation times derived from the two-dimensional simulations. Figure 12 shows the stress wave propagation time in relation to the propagation distance for each model. The regression analysis indicated an excellent linear relationship between wave propagation time and travel distance. The coefficients of determination (R^2) of the relationships were 0.999, 0.999, 0.999 and 0.998 for Model 1, Model 2, Model 3 and Model 4, respectively, which was consistent with the findings reported by Zhang et al. 2011. It seems clear that the propagation distance had little effect on wave velocity.

Figure 13 shows the relationship between wave velocity and tree diameter. Wave velocity generally increased as the tree diameter increased, particularly at 20 to 30 cm diameter range where wave velocity increased rapidly with the increase of diameter. However, when tree diameter exceeded 30 cm, the increase of wave velocity with increasing diameter became much less. It appears that the 30 cm could be a threshold of changing wave propagation pattern, thus resulting in two distinct wave velocity–tree diameter relationships.

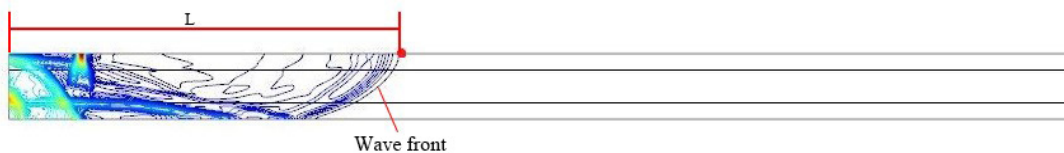


Figure 11—Wave propagation distance defined by the leading edge of the wavefront (Model 2).

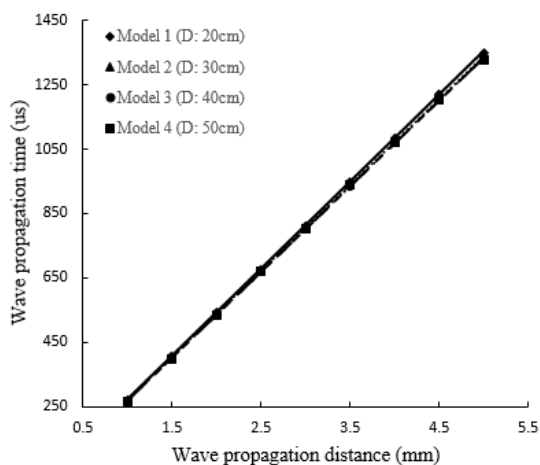


Figure 12—Relationship between wave propagation time and propagation distance.

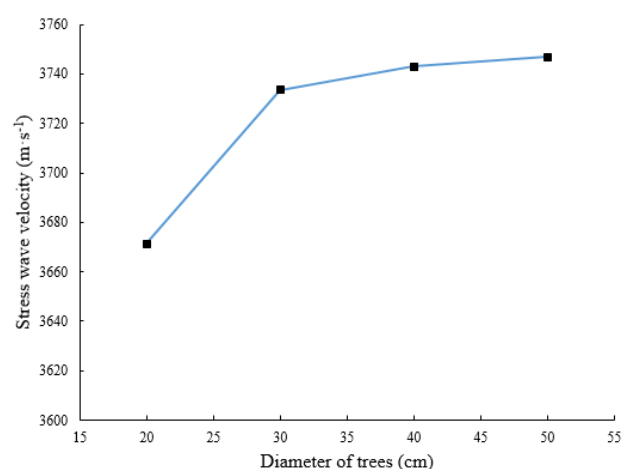


Figure 13—Relationship between wave velocity and tree diameter.

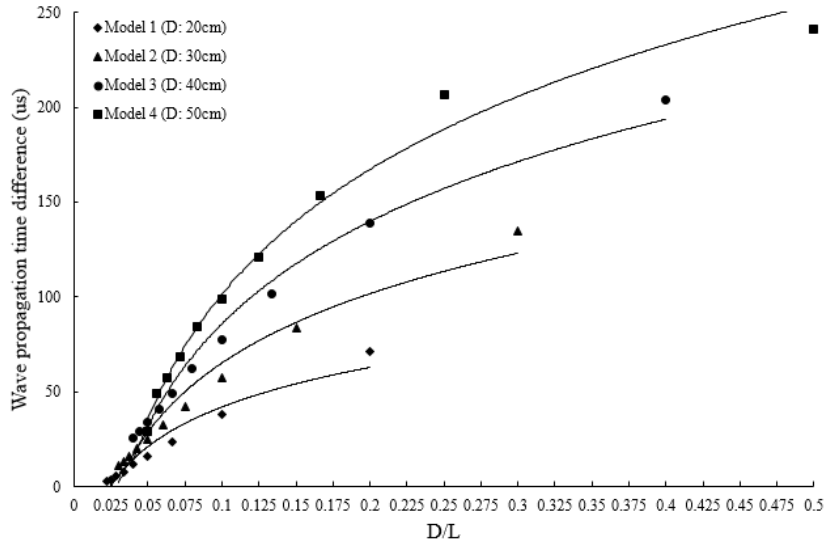


Figure 14—Wave propagation time difference in relation to diameter-distance ratio (D/L).

From the results of numerical simulation (Figure 8 and Figure 10), the shape of wave front is apparently related to tree diameter (D) and propagation distance (L). The wave front in the virtual tree trunk approached to a vertical line (in 2D model) or a plane (in 3D model) more quickly in small diameter models than in large diameter models. The shape of wave fronts in a tree trunk can be characterized by the TOF differences ($TOF_{max}-TOF_{min}$) in a tree cross-section. The TOF difference of “0” means a wave front having a vertical line or a vertical plane. Large TOF differences correspond to a wave front with big slope. From the simulation results, we found that the maximum TOF point was always located on the downside of the cross section, which is the travel path with the longest travel distance.

Figure 14 shows the relationships between the TOF difference in a cross section and the diameter to distance ratio (D/L). It is apparent that tree diameter and travel distance are two key factors that determine the characteristics of the wave fronts. As D/L approached to approximately 0.025, the wave fronts in four tree trunk models almost approached to a vertical line or vertical plane.

Conclusion

In this paper, COMSOL Multiphysics simulation software was used to investigate the two-dimensional and three-dimensional propagation patterns of stress wave in larch plantation trees and the relationships between tree diameter, travel distance and wave velocity. Based on the results of this study, the following conclusions can be drawn:

1. The two-dimensional wave propagation patterns in the longitudinal-radial plane of a tree trunk is basically in agreement with the three-dimensional wave propagation patterns in the trunk body: the stress wave initially traveled as a sloping curved line (2D) or spherical surface (3D) bending towards the input point in the impact direction; then the inclination of the wave front gradually decreased as the propagation distance increased; finally, wave front gradually became flattened and close to perpendicular to the longitudinal axis.
2. The wave dispersion effect was found in the results of 2D and 3D numerical simulations because of the transverse inertia and the relatively small transverse size of tree trunks. The wave front was thus locally elongated and flattened and this phenomenon was strengthened as

tree diameter increased. Dispersion effect in the three-dimensional numerical simulation was stronger than that in the two-dimensional numerical simulation because of the size effect.

3. The slope of stress wave front decreased slowly with increasing tree diameter, indicating that the diameter has a significant effect on the wave propagation patterns in the standing trees. Wave velocity increased as tree diameter increased.
4. No relationship was found between wave velocity and wave propagation distance.

Acknowledgment

This project was funded by the National Natural Science Foundation of China (Grant No. 31328005) and conducted under the cooperative research agreement between Beijing Forestry University, Beijing, China, and the USDA Forest Service, Forest Products Laboratory (FPL), Madison, WI.

References

- Carter P, Briggs D, Ross RJ, Wang X. (2005) Acoustic testing to enhance western forest values and meet customer wood quality needs. PNW-GTR-642, In: Harrington, CA, Schoenholtz SH, eds. Productivity of Western Forests: A Forest Products Focus. USDA Forest Service, Pacific Northwest Research Station, Portland, Oregon. pp 121-129.
- Chauhan SS, Walker JCF. (2006) Variation in acoustic velocity and density with age, and their interrelationships in radiata pine. *Forest Ecol Manag* 229: 388-394.
- Cheng J.Q. (1985) *Wood Science*[M]. Beijing: China Forestry Press, 1985.
- Jerrymjr, M., Lewis, J., Laurencer, S., Alexanderiii, C., Richardf, D. (2009) A comparison of sampling methods for a standing tree acoustic device. *Southern Journal of Applied Forestry*. 33(2): 62-68.
- Joe, B., Dickson, R., Raymond, C.A. (2004) Prediction of *Eucalyptus dunnii* and *Pinus radiata* timber stiffness using acoustics. RIRDC Publ. 04/013. 121 p.
- Lasserre J.P., Mason E., Watt M.S. (2004) The influence of initial stocking on corewood stiffness in a clonal experiment on 11-year-old *Pinus radiata* [D. Don]. *New Zeal. J. For. Sci.* 49:18–23.
- Lasserre, J.P., Mason, E.G., Watt, M.S. (2005) The effects of genotype and spacing on *Pinus radiata* [D. Don] corewood stiffness in an 11-year old experiment. *Forest Ecology and Management*. 205(1-3): 375–383.
- Liu F.L; Jiang F; Zhang J.Z.; Zhang H.J.; Wang X.P.; Yang Z. (2015) Twelve elastic constant values of larch forest. *Journal of Northwest Forestry University*. 30(6):227-231.
- Mora C.R., Schimleck L.R., Isik F., Mahon J.M., Clark A., Daniels R.F. (2009) Relationship between acoustic variables and different measures of stiffness in standing *Pinus taeda* trees. *Can J For Res*. 39(8):1421-1429.
- Raymond C.A., Joe B, Anderson DW, Watt DJ. (2008) Effect of thinning on relationships between three measures of wood stiffness in *Pinus radiata*: standing trees vs. logs vs. short clear specimens. *Can. J. For. Res.* 38: 2870-2879.
- Wang, X.P., Ross, R.J., Mccllellan, M., Barbour, R.J., Erickson, J.R., Forsman, J.W. (2000) Strength and stiffness assessment of standing trees using a nondestructive stress wave technique. Research Paper-Forest Products Laboratory, USDA Forest Service.
- Wang, X.P., Ross, R.J., Panches, J., Barbour, R.J., Forsman, J.W., Erickson, J.R. (2003) Evaluation of small-diameter timber for value-added manufacturing-a stress wave approach. In: *Proceedings, 2th*

International Precision Forestry Symposium, University of Washington College of Forest Resources, Seattle, Washington, June 15-17, 2003. pp. 91-96.

Wang, X.P., Ross, R.J., Brashaw, B.K., Panches J., Erickson, J.R., Forsman, J.W., Pellerin, R.F. (2004) Diameter effect on stress-wave evaluation of modulus of elasticity of logs. *Wood and Fiber Sci.* 36(3):368-377.

Wang X, Ross RJ, Carter P. (2007) Acoustic evaluation of wood quality in standing trees. Part I. Acoustic wave behaviour. *Wood and Fibre Science* 39(1):28-38.

Zhang, H.J., Wang, X.P., Ross, R.J. (2009) Stress wave propagation on standing trees: Part 1. Time-of-flight measurement and 2D stress wave contour maps. In: *Proceedings, 16th International Symposium on Nondestructive Testing and Evaluation of Wood*, Beijing Forestry University, Beijing, October 12-14, 2009. pp. 53-58.

Zhang H, Wang X, Su J. (2011) Experimental investigation of stress wave propagation in standing trees. *Holzforschung* 65(5):743-748.

Non-destructive Wood Quality Assessment Methods and Potential Application to Forest Inventory Assessments, Models and Forest Management

Mark Rudnicki*

Michigan Technological University, School of Forest Resources and Environmental Science, Houghton, MI, USA, mrudnick@mtu.edu

Yvette Dickinson

Michigan Technological University, School of Forest Resources and Environmental Science, Houghton, MI, USA, yldickin@mtu.edu

Xiping Wang

USDA Forest Service, Forest Products Laboratory, Madison, Wisconsin, USA, xwang@fs.fed.us

Robert Ross

USDA Forest Service, Forest Products Laboratory, Madison, Wisconsin, USA, rjross@fs.fed.us

* Corresponding author

Abstract

Wood production that can effectively meet the growing demand for wood will need to deliver more than increased volume. Technologies now exist for a more comprehensive and efficient non-destructive evaluation (NDE) of wood quality in the standing trees, which can allow for more value extraction by enabling highest best use for each individual tree. A systematic, large scale sampling of wood quality can also be used to drive modeling efforts to understand wood quality at the landscape scale and improve silviculture and forest management.

Keywords: Methods, modeling, forest inventory, forest management

Introduction

Background

To extract the highest value out of wood is vital to keeping local forest product markets competitive in a highly competitive global market. Using wood for highest potential requires an assessment of its quality traits at the start of the supply chain – the standing trees. The current value chain has historically focused on increasing volume, which has increased yields but also an unintended effect of lowering many wood quality attributes. In addition, the current chain tends to extract value at each link instead of working to create more value. Delivering the appropriate quality of wood poses serious challenges to the current value chain as customer requirements for specific wood quality attributes become more diverse. Accurate knowledge of wood quality is key for an optimal value chain to exist.

While there is certainly more opportunity in designing silvicultural prescriptions that include wood quality attributes, silviculture and the rest of the value chain ultimately depend on the ability to define and quantify wood quality attributes relevant to various end uses. A more comprehensive and efficient non-destructive evaluation (NDE) of wood quality in the standing trees can allow more value extraction from each tree by enabling sorting by quality as early as possible in the value chain. Furthermore, an improved understanding of the environmental factors that influence wood quality at the stand and site levels are important to understanding expectations of management actions on wood quality or the response of management to efficiently extract highest best use of the harvested wood.

The quality of standing trees has traditionally been assessed based on physical measurement (height, diameter, taper and sweep) and visual observation of surface characteristics (knots, wounds and other defects). A grade assigned to a standing tree using these techniques may be adequate if visual appearance is the primary concern, however this provides no information about the stiffness or strength of the wood produced. Using NDE to assess standing trees can provide attribute information about the plot which can be extended to the stand and landscape levels. Incorporating this information into a database will allow for easy access to population estimates of wood attributes. Understanding the attributes, such as stiffness, of a forest resource before harvesting may result in more efficient sorting and higher financial return (Gardiner and Moore 2014)

Nondestructive Evaluations

Nondestructive evaluation (NDE) techniques can be used to identify the physical and mechanical properties of a piece of material without altering its end-use capabilities. This information can then be used to make decisions regarding appropriate applications. Here we review a variety of nondestructive tests (NDT) that can be performed on a material with selection of the appropriate test dictated by the particular quality characteristic of interest (Ross 2015).

Resistance micro-drilling measures the resistance as a slender drill bit is driven into the tree stem at a constant rate. A resistance profile is produced and areas of decreased resistance may indicate areas of decay (Gao, Wang et al. 2012). Drilling at the exact location of the internal decay is necessary. A micro-drilling resistance tool typically consists of a power drill unit, a small-diameter drill bit, a paper chart recorder, and an electronic device that can be connected to the serial interface input of any standard personal computer. The diameter of the drill bit is typically very small, from 2 to 5 mm, so that any weakening effect of the drill hole on the wood cross section is negligible. The drill resistance RD is defined as

$$RD = T/\omega \quad (\text{Nm s/rad}) \quad (1)$$

Where T is drilling torque (Nm) and ω the angular speed (rad/s).

The use of acoustics and stress wave timers has been established as method applicable to forest products grading and the determination of bio-deterioration within standing trees (Wang and Carter 2015; Wang and Allison 2008). Single-path stress wave timing measured across the stem of a tree can be used to detect internal decay. Two accelerometers mounted on opposite sides of the tree are used to measure the time required for the sound wave to travel through the tree. The time-of-flight (TOF) of the sound waves through decayed wood are much greater than that for non-decayed wood. This method is dependent on tree species and temperature (Allison and Wang 2015). The transmission speed can then be compared to literature values to predict the extent of decay within the stem (Wang et al. 2004). A 30% increase in stress wave transmission time implies a 50% loss in strength and a 50% increase indicates severely decayed wood (Wang et al. 2004). High correlation has been found between acoustic velocity of standing trees and yield of structural grades of lumber (Amishev and Murphy 2008).

Acoustic time of flight measurements along the length of a log or standing tree stem can be used to predict the stiffness and strength of timber produced from that particular piece (Wang and Carter 2015). Probes are inserted through the bark into the sapwood with one sensor at approximately 50 cm above the ground and the second sensor 1.0 – 1.2 m above. A mechanical wave is introduced, typically by the use of a hammer, and the transmission time between the probes is recorded. The transmission time between probes, the distance between probes and the green density of the wood can be used to calculate the modulus of elasticity (MOE). MOE is calculated from the following equation

$$\text{MOE} = \rho V^2 \quad (2)$$

where V (m/s) is the acoustic velocity, ρ (kg/m^3) is the density of green wood. Even though this equation assumes a one-dimensional, homogenous, isotropic material it can be used if the length of the wave is larger than the lateral dimension of the object (Grabianowski et al. 2006)

Acoustic tomography uses multiple sensors around a tree to measure the stress wave time in multiple directions. The resulting tomogram produces a two-dimensional image of the stem determined by the transmission speed of the stress waves. This cross section can be used to assess the tree for internal decay (Allison and Wang 2015). The tomogram is a representation of the internal acoustic properties of the cross-section tested and may not reflect the actual internal conditions.

Large Scale Assessment

Tree morphology and wood anatomy, which are the basis of all wood properties, are controlled by genetics and environment. While many traits are known to be strongly heritable, environmental or growing conditions at the stand, landscape and even regional scales are also able to strongly affect wood properties.

Microenvironment is strongly influenced by stand density and knowledge of site factors can be important to understanding the stand level (or larger landscape level effects) on wood quality. Soil type, wind exposure, and climate level effects of mean temperature and precipitation can all effect wood formation and quality. For instance, strong wind loading is known to have a dramatic effect on wood properties and in steep terrain can have strongly localized effects. In coastal regions where strong winds are persistent, trees would be expected to produce higher density wood to resist failure.

Silvicultural efforts routinely alter the microenvironment by manipulating stand density. Some silvicultural practices not only increase the biomass production of trees but also might improve the quality of the wood in trees. Nakamura (1996) used ultrasonically induced waves to assess Todo-fir and larch trees and observed significant differences in acoustic velocities and acoustic-determined MOE for trees in forest stands at different locations and trees of different ages. Wang (1999) examined the effect of thinning treatments on both acoustic and static bending properties of young growth western hemlock and Sitka spruce trees obtained from seven sites in southeast Alaska. He found that trees with higher acoustic velocity and stiffness were mostly found in unthinned control stands and stands that received light thinning, whereas the lowest values were found in stands that received heavy and medium thinning. His work also indicates that time-of-flight acoustic technology may be used in the future to monitor wood property changes in trees and stands and to determine how environmental conditions and silvicultural innovations affect wood and fiber properties so that the most effective treatment can be selected for future plantations for desired fiber quality.

Salvaging merchantable wood from a widespread mortality event depends on a timely extraction of the wood before it deteriorates. With climate change there is an expectation that these events will continue to increase making improved utilization from salvage operations important. Understanding decay status,

rates and patterns of decay across a landscape is important to both increase wood recovery from stands and to guide silvicultural prescription for a restoration of forest health. Knowledge of recovered wood quality will also allow for improved utilization for high value products such as engineered cross-laminated timber panels.

Large-scale assessment of wood quality can be very useful for strategic forest management, and if accurately mapped, can show consistent existence of higher and lower areas of wood quality, which can in turn be utilized for highest value. To map wood quality gradients across a landscape or region requires an integration of many advanced tools and techniques such as GIS, remote sensing (passive sensors and/or active sensors such as LiDAR) (Pokharel et al. 2016) to assess both the detailed structure of the forest stand but also allow incorporation of larger scale terrain elements. Spatial analysis techniques can be used to combine spatially explicit factors with ground-truth data of intrinsic wood quality and produce maps that illustrate large-scale wood quality gradients. Hence accurate measures of wood quality across a landscape are critical to construct these maps and improve our understanding of factors that influence tree growth and wood quality. Efforts are already notably underway in New Zealand and Canada that have produced compelling maps of wood quality (Palmer 2013, Kimberley et al. 2016, Moore et al. 2014, Defo et al. 2015). If the Forest Inventory and Analysis program of the USDA Forest Service incorporated measures of wood density into their vast array of plots, it could enable unprecedented insight into drivers of wood quality and importantly the ability for industry to efficiently utilize wood for its highest and best use.

Conclusions

Portable and accurate wood quality assessment can now be done in the field where log handling and efficient value adding begins. However strategic forest management would benefit from a larger scale understanding of patterns of wood quality across the landscape or region. Adding wood quality assessment to existing forest monitoring plots would enable an empirically based scaling up which would also have benefits to those developing predictive models as factors influencing wood quality are complex.

Acknowledgments

Authors are grateful for the funding support from cooperative agreement 15-JV-11111133-076

References

Allison RB and Wang X (2015) Chapter 7: Nondestructive Testing in the Urban Forest. *Nondestructive Evaluation of Wood: Second Edition*, USDA Forest Service, Forest Products Laboratory: 77-86.

Amishev D, Murphy GE (2008) Preharvest Veneer Quality Evaluation of Douglas-fir Stands Using Time-of-Flight Acoustic Technique. *Wood and Fiber Science* 40(4): 587-598.

Defo M, Duchesne I, Stewart J (2015) A Review of the Current State of Wood Quality Modelling and Decision Support Systems in Canada INFORMATION REPORT FI-X-012 September 2015.

Gao S, Wang X, Brashaw B K, Ross R J, Wang LH (2012) Rapid assessment of wood density of standing trees with nondestructive methods - A review. 2012 International Conference on Biobase Material Science and Engineering (BMSE).

Gao S, Wang X, Wiemann MC, Brashaw BK, Ross RJ, Wang L (2017) A critical analysis of methods for rapid and nondestructive determination of wood density in standing trees. *Annals of Forest Science*, DOI 10.1007/s13595-017-0623-4.

Gardiner B, Moore J (2014) Creating the wood supply of the future, Challenges and Opportunities for the World's Forests in the 21st Century, 677-704, Springer, Netherlands.

Grabianowski M, Manley B, Walker JCF (2006) Acoustic measurements on standing trees, logs and green lumber. *Wood Science and Technology* 40(3): 205-216.

Kimberley MO, Cown DJ, McKinley RB, Moore JR, Dowling LJ (2015) Modelling variation in wood density within and among trees in stands of New Zealand-grown radiata pine. *New Zealand Journal of Forestry Science* 45:22

Moore JR, Cown DJ, McKinley RB (2014) Modelling microfibril angle variation in New Zealand-grown radiata pine. *New Zealand Journal of Forestry Science*, 44:25.

Nakamura N (1996) Measurement of the properties of standing trees with ultrasonics and mapping of the properties. University Forestry Research Rep. 96. Tokyo, Japan: Faculty of Agriculture, The University of Tokyo. P. 125-135.

Palmer DJ, Kimberley MO, Cown DJ, McKinley RB (2013) Assessing prediction accuracy in a regression kriging surface of outerwood density across New Zealand. *Forest Ecology and Management*, Volume 308, 2013, Pages 9-16.

Pokharel B, Groot A, Pitt DG, Woods M, Dech JP (2016) Predictive Modeling of Black Spruce (*Picea mariana* (Mill.) B.S.P.) Wood Density Using Stand Structure Variables Derived from Airborne LiDAR Data in Boreal Forests of Ontario. *Forests* (7) 311.

Ross RJ (2015) Nondestructive Evaluation of Wood. Second Edition. General Technical Report. FPL-GTR-238. Madison, WI: U.S. Department of Agriculture, Forest Service, Forest Products Laboratory: 167 p.

Wang X (1999) Stress wave-based nondestructive evaluation (NDE) methods for wood quality in standing trees. Ph.D. dissertation. Houghton, Michigan: Michigan Technological University. 187 p.

Wang X, Allison RB (2008) Decay Detection in Red Oak Trees Using a Combination of Visual Inspection, Acoustic Testing, and Resistance Microdrilling. *Arboriculture & Urban Forestry* 34(1): 1-4.

Wang X, Carter P (2015) Chapter 8: Acoustic Assessment of Wood Quality in Trees and Logs. *Nondestructive Evaluation of Wood: Second Edition*, USDA Forest Service, Forest Products Laboratory: 87-101.

Wang, X, Divos F, Pilon C, Brashaw BK, Ross RJ, Pellerin RF (2004) Assessment of Decay in Standing Timber Using Stress Wave Timing Nondestructive Evaluation Tools: A Guide for Use and Interpretation. Gen. Tech. Rep. FPL-GTR-147. Madison, WI: U.S. Department of Agriculture, Forest Service, Forest Products Laboratory. 12 p.

Multivariate Modeling of Acousto-Mechanical Response of 14-Year-Old Loblolly Pine (*Pinus taeda*) to Variation in Wood Chemistry, Microfibril Angle and Density

Charles Essien¹, Brian Via¹, Qingzheng Cheng¹, Thomas Gallagher¹, Timothy McDonald², Lori G. Eckhardt¹

1 School of Forestry & Wildlife Sciences, Auburn University, 602 Duncan Drive, Auburn, AL 36849, USA

2 Biosystems Engineering Department, Engineering Drive Auburn University Auburn, AL 36849.USA

Charles Essien Email: cze0017@auburn.edu ; Brian K.Via Email: brianvia@auburn.edu

Qingzheng Cheng Email: qzc0007@auburn.edu ; Thomas T Gallagher Email: gallatv@auburn.edu

Timothy Mcdonald Email : mcdonpt@auburn.edu; Lori G. Eckhardt Email: eckhalg@auburn.edu

Abstract

The polymeric angle and concentration within the S₂ layer of the softwood fiber cell wall are very critical for molecular and microscopic properties that influence strength, stiffness and acoustic velocity of wood at the macroscopic level. The main objective of this study was to elucidate the effect of cellulose, hemicellulose, lignin, microfibril angle (MFA) and density on acoustic velocity and material mechanical properties of 14 year old suppressed loblolly pine. Cellulose, hemicellulose and density are consistently the most important drivers of strength, stiffness and velocity. Cellulose and lignin are the highest and lowest contributor to velocity respectively with lignin acting as a sound wave dispersant while cellulose is the most important conductor of sound wave at the molecular level, while Hemicellulose acts as a special coupling agent between the these components. The polymeric constituents are thus important drivers of sound wave propagation at the molecular level while density played a subsequent role at the macroscale.

Keywords: microfibril angle, hemicelluloses, lignin, acoustic velocity

Introduction

Wood is a fibrous material made up of tubular cells that provide resistance to load bearing forces caused by tree weight and wind loading (Marra 1979). At the molecular level, wood is composed of cellulose, hemicellulose and lignin. Cellulose is the stiffest polymer in wood due to its high degree of polymerization, crystallinity, and linear orientation. Hemicellulose is a non-crystalline branched molecule composed of a linear backbone of galactoglucoman and glucoman, which is attached with side chains of pentose and hexose (Winandy and Rowell 2005). Winandy and Rowell (2005) stated that hemicellulose functions to connect the non-crystalline part of hydrophilic cellulose to the amorphous and hydrophobic lignin. Thus hemicellulose acts to transfer stress between cellulose and lignin. Lignin is a large hydrophobic tri-dimensional and highly branched phenolic molecule which binds and holds other

polymers together. It is also a stiffening agent for cellulose and provides resistance to compression forces (Winandy and Lebow 2001).

Researchers have hypothesized that these polymeric constituents influence the mechanical and acoustic properties of wood and wood products. Several polymeric cross sectional structural models exist to explain the morphology of this composite matrix, but most agree that the elementary fibrils of cellulose exhibit the least variation in dimension due to their high crystallinity, coupled with the interaction between the lignin and hemicellulose matrix. The hemicellulose matrix is sandwiched between lignin and the amorphous portion of the cellulose elementary fibrils and is thus defined as a coupling agent between cellulose and lignin (Winandy and Rowell 2005). The highly hydrophobic lignin polymer acts as a sheath around the hydrophilic cellulose and hemicellulose matrix. The lignin polymer is entangled in the xylan portion of the hemicellulose, while the glucomannan of hemicellulose is attached to the non-crystalline portion of the cellulose elementary fibrils (or microfibrils). Cellulose has been shown to significantly influence the elastic phase, when the load is applied nearly parallel to the cellulose plane, and thus is anticipated to impact modulus of elasticity (MOE) at the macroscale. Lignin and hemicellulose become dominant as the axis of the load is at an increased angle to the axis of the microfibrils. Strength is reduced by a factor of 10 at the nanoscale level for loads applied at a transverse angle to the fiber axis (Via et al. 2009). At the macroscopic level, softwoods are composed of 90% longitudinal fiber elements specialized for fluid conduction and mechanical strength. These fibers have multilayered cell walls consisting of one primary cell wall layer and three secondary layers (S₁, S₂, S₃). These layers are differentiated by the degree of orderliness and orientation of the crystalline portion of the cellulose. The S₂ layer is considered most important for the acoustic, or elastic, response of wood because it is located at the middle portion of the cell wall and accounts for 83% of the overall secondary cell wall (Gridl and Schoberl 2004).

The acoustic properties of live trees have been of significant interest in recent years because stems currently being harvested without any knowledge of the internal stiffness quality which affects the performance of the material. The velocity of acoustic waves propagating through the tissue of trees has been measured to estimate the stiffness of wood, but little is known about the influence of the polymeric constituents on acoustic velocity. It has been hypothesized that the acoustic response of wood varies as a function of wood chemistry, macro density, and the angle of the aggregate polymers. To date, only isolated examples exist where a study considered only one trait at a time, while the effect of all other traits that might influence velocity were assumed to be held constant.

Thus, the main objective of this study was to explore the effects of polymeric constituents, density, and microfibril angle (MFA) on the modulus of rupture (MOR), modulus of elasticity (MOE), and acoustic velocity of 14 year old suppressed loblolly pine.

Materials and Methods

Materials

The materials for this study were selected from a plantation of genetically improved families of loblolly pine (*P. taeda*), located at Brantley County near Nahunta, Georgia, USA (latitude 31°12'16''N and longitude 81°58'56''W). Eight trees were selected randomly from each family, with care taken to avoid trees with visible defects, such as leaning, forked stems, chlorotic needles, as well as other less significant growth defects. The diameters of the selected trees were measured at breast height and ranged from 8.8 to 12.6 cm with a mean of 10 cm.

Acoustic measurements

The selected trees were then harvested and bucked into 180 cm logs and 10 cm thick disks, alternately along the entire length, yielding 3 - 5 logs, depending on the length of the tree. All 34 logs obtained from

the 8 trees were used to determine log acoustics. The log acoustic velocity was determined while they were still green using a Director ST300 tool, the probes were positioned 120cm apart on the side of the log (Wang et al. 2001; Essien et al. 2016; Essien et al. 2017). Six readings per log were taken from the north and south aspects of the logs. The 180 cm logs were crosscut into two equal parts and four pair of disks, measuring 2 cm thick, were taken from the freshly cut surfaces, with 2 pairs taken from each piece. Three pairs were used to determine the moisture content and basic disk density (referred to as “disk density” in this study). The dimensions of the disk were taken to the nearest 0.025 mm using a digital caliper and weight was measured to the nearest 0.001 g. The remaining pair was used for the chemistry and MFA analysis.

Static MOE and MOR determination

Static MOE and modulus of rupture (MOR) were determined using the small clear specimens measuring 2.5 x 2.5 x 41cm (radial x tangential x longitudinal) prepared from the remaining log samples after the specimens were conditioned (at 65%RH, 23°C for three month) to approximately 12% equilibrium moisture content (EMC). Four outermost specimens (the first 2.5 cm sample obtained from each log without the bark material of the tree) from the north, south, east and west directions around the circumference of each log – totaling 136 specimens were used for the static bending tests following the protocols of ASTM D143 (ASTM D143 2007). The load was applied on the tangential-longitudinal face in a three-point configuration using a Z010 Zwick Roell Testing System (Zwick Roell, Kennesaw, GA, USA) at a loading rate of 1.3mm/min. The moisture content and outerwood density [referred to as outerwood density (ODW) in this study and it is the first 2.5 cm sample obtained without the bark material of the tree at test were determined following the protocols described in ASTM D143.

MFA determination

Strips measuring 1 cm in width were extracted through the pith of the pair of disk samples meant for the MFA measurement. One sample was prepared in the “south- north” direction while the other was in the “east-west” direction. Two thin sections of wood samples measuring 0.2mm were sliced from along the entire length of both 1cm strips per log – one along the north-south and the other east – west directions. The thin samples were macerated using equal volumes of hydrogen peroxide (30%) and glacial acetic acid at 80°C for 24 hours for thorough maceration (Essien 2011; Peter et al. 2003). Temporary slides were prepared from the macerated fibers and an MFA measured following the procedure described by Peter et al. (2003). The MFA measurements were performed on forty fibers selected from both the earlywood and latewood using Differential Interference Contrast (DIC) Microscope (Olympus BX53).

Chemistry

The remaining portion of the disks that were used for the MFA measurements were also used for chemistry; although the MFA measurements were extracted from subsamples of a smaller scale. The wood was ground to pass the 40-mesh screen sieve using a 3383L10 Wiley Mini Mill (Thomas Scientific, Swedesboro, NJ). Five grams of the ground sample were extracted with 150ml of acetone for six hours using a Soxhlet apparatus. The extractive free samples were then used to determine the lignin, cellulose and hemicellulose content according to the NREL/TP 510-42618. One-half grams of the air-dried extractive free sample was digested with 72% sulfuric acid and incubated in a water bath set at 30°C for two hours with intermittent stirring to ensure full and uniform hydrolysis. The solution was diluted with deionized water to a concentration of 4% and was then autoclaved at 121°C for one hour. The residue after hydrolysis was filtered and oven-dried to calculate the acid insoluble lignin (AIL). In order to account for the total lignin content in the specimens, UV- spectrophotometer was used to determine the acid soluble portion of the lignin. Portions of the filtrate were used to determine the Acid soluble lignin (ASL) using UV- spectrophotometer (Genesys 10-S Thermo Fisher Scientific, Madison, WI) set at the

absorbance wavelength of 240nm. The lignin content used in this study is the sum of the AIL and ASL. The remaining portion of the filtrate was used to determine the monosaccharide composition of the samples using High-Performance Liquid Chromatography (Shimadzu LC-20A) equipped with an Aminex 87 P column and differential refractive index detector, operated at 85°C for 35 minutes. The holocellulose, cellulose and hemicellulose contents of the samples were calculated using equations 1, 2 and 3 respectively (Acquah et al. 2015)

$$\text{Holocellulose} = \text{Glucan} + \text{Xylan} + \text{Arabinan} + \text{Mannan} \quad \text{Equation 1}$$

$$\text{Cellulose} = \text{Glucan} - \left(\frac{1}{3} * \text{Mannan}\right) \quad \text{Equation 2}$$

$$\text{Hemicellulose} = \text{Holocellulose} - \text{cellulose} \quad \text{Equation 3}$$

The actual moisture content of the air-dried extractive free samples used in this study were determined in order to calculate the dry weight of the samples used in the determination of the chemical composition of the samples and hence moisture was not included as weight during the computation of the cellulose, hemicelluloses and lignin. All experiments were performed in duplicate (Via et al. 2014). The data was analyzed using SAS (SAS, 2014)

Results and Discussion

Chemistry, MFA, density, velocity and mechanical properties

The descriptive statistics of the parameters studied are presented in Table 1. The influence of chemistry, MFA, and density on velocity, stiffness, and strength are presented in Table 2. Multiple linear regression analysis conducted reveals significant positive relationship between the response variables and cellulose, hemicelluloses and density (Table 2). On the other, MFA and lignin exhibit non-significant relationship with the entire response variables (Table 2). From Tables 2, cellulose, hemicellulose and density are required to estimate MOR, MOE, and velocity. The results from the indirect path analysis indicate a significant positive and negative relationship between the outerwood density versus cellulose and lignin respectively (Fig 1). Also, there were significant negative and positive relationships between the hemicellulose versus cellulose and lignin respectively (Fig 1). However the relationship between the predictors when disk density was used in the indirect path analysis indicates a non-significant relationship among the predictor variables except a significant negative relationship between cellulose and hemicellulose (Fig 2).

Density is the most influential predictor of MOR and MOE while cellulose is slightly important predictor of velocity than density (Table 2). The importance of hemicellulose and cellulose in predicting stiffness and strength confirmed several reports (Winandy and Rowell 2005; Via et al. 2009; Clausen and Kartel 2003). Via et al. (2009) reported that hemicellulose and cellulose associated wavelengths were very significant in predicting the strength and stiffness of 41 year old longleaf pine using principal component regression and near infrared reflectance (NIR) spectroscopy. Furthermore, Clausen and Kartal (2003) attributed the initial rapid loss of MOR (strength) to degradation of side chain sugars especially arabinose and xylose associated with hemicellulose when the wood is subjected to bio – deterioration.

Density, cellulose and hemicellulose are required for predicting velocity and MOE support the theoretical fact that the acoustic tools are capable of estimating the stiffness of wood. The major variables driving the wave propagation in order of importance are cellulose, density, and hemicellulose respectively. In softwoods, the S₂ layer which accounts for 80-86% of the cell wall and is composed of 32.7%, 18.4%,

and 9.1% for cellulose, hemicelluloses, and lignin respectively (Reiterer et al. 1999). Mark (1967) estimated the densities of the cell wall to be 1.5 g/cm³ for cellulose, 1.49g/cm³ for hemicellulose, and 1.4 g/cm³ for lignin. The higher proportion and density of cellulose and hemicellulose may be responsible for their respective importance in driving the propagation of acoustic waves at the molecular level. Stamm (1964) asserted that more than 60% of the cellulose appeared as crystalline which is much stiffer and stronger than the amorphous portion. The high crystallinity of the cellulose in the S₂ layer may be responsible for the sound conductance at the molecular level (Hori et al. 2002). Hori et al. (2002) found a positive correlation between the acoustic velocity and crystallinity of cellulose. From Models 1 and 2 (Table 2), hemicellulose is less important as compared with cellulose and density in the transmission of sound waves. At the molecular level, the hemicellulose, which is linked to the non-crystalline portion of the cellulose and lignin, functions as a coupling agent for effective distribution of stresses (Winandy and Rowell 2005) just as couplants such as silicone grease function in improving the transmission of sound waves during acoustics studies of wood (Hasegawa et al. 2011). It is therefore plausible that hemicellulose acts as a coupling agent for the lateral sound transmission between lignin and cellulose.

The velocity had a negative correlation with lignin. This negative coefficient is important because it supports the hypothesis that increased lignin slows the sound velocity.

It was hypothesized that lignin which has a highly branched tri-dimensional structure and hydrophobic in nature and hence may act as a sound dispersant or sink at the molecular level. Via et al. (2009) indicated that hemicellulose and lignin becomes very important when wood is loaded in the transverse direction. Similarly, when sound wave is transmitted in the transverse direction of wood, the less sound conductive hemicellulose and sound dispersant lignin become very important sound driver hence they can influence the magnitude of the incoming wave at the receiver probe. This observation explains the 2 and 3 times respective reduction in sound wave velocity in the radial and tangential directions as compared with sound propagation in the longitudinal direction as reported by Hasegawa et al. (2011). Lignin appeared to be non-significant predictor in the present study perhaps because the absorption of sound energy by lignin is passive compared to cellulose which acts as a conductor of sound resulting in a more direct influence on ToF. When lignin was investigated independently through the path analysis (Figure 1), it has a significant positive relation with hemicellulose. Notwithstanding however, since these polymeric constituents accounts for over 95% of the weight of southern pines (Via et al. 2009), their roles may overlap and therefore different constituent may assume critical influence contingent to the experimental methods, instrumentation and/or the statistical analytical procedure used.

The relationship between MFA and velocity, MOE and MOR are consistently non-significant as shown on Table 2 . This result is unexpected as it has been reported that a decrease in MFA will result in an increase in velocity because the sound wave travels through the axis of the cellulose along the MFA (Hasegawa et al. 2011). This unexpected result may be due to the sampling method used in the present study. Most studies investigating the effect of MFA on other wood properties optimize the range of MFA values through the use of matured wood (from 34 to 63 years) such that the MFA values cover wider range (Via et al. 2009; Hasegawa et al. 2011). In the present study, the random natural MFA range present in the 14 year old samples were used hence there was no intention of selecting a wide range of MFA to optimize its variance. The wood samples used for this study contained higher proportions of latewood which is not typical of 14 year old loblolly pine. The narrower range of MFA coupled with the higher density might have the potential to mask the importance of MFA on velocity, strength and stiffness as observed in this study.

Table 1 - Summary descriptive statistics of log velocity, chemistry and wood properties

	Mean	Standard deviation	Minimum	Maximum
Disk density (DD) (g/cm ³)	0.57	0.06	0.47	0.73
Outerwood density (OWD) (g/cm ³)	0.56	0.08	0.42	0.76
Modulus of elasticity (MoE) (GPa)	7.97	2.37	2.71	13.30
Modulus of rupture (MPa)	74.47	16.42	37.10	112.25
Cellulose (%)	42.01	2.30	38.46	48.15
Hemicelluloses (%)	23.84	3.55	16.86	29.91
Lignin (%)	27.39	0.99	25.20	29.39
log velocity (km/s)	4.44	0.44	3.40	5.18
MFA (°)	23.88	2.15	19.35	28.05

Table 2 - Full multiple linear regression models of chemistry, density and MFA for predicting MOR, MOE and velocity.

	MOR			MOE			Log velocity		
	Coefficient	SE	R ²	Coefficient	SE	R ²	Coefficient	SE	R ²
Model 1	74.47***	1.49	76.39	7.97***	0.23	72.9	4.44***	0.05	59.13
Cellulose	1.95 ^{ns}	1.74		0.84**	0.27		0.22***	0.06	
Hemicelluloses	5.18**	1.72		1.00***	0.26		0.14*	0.06	
Lignin	1.41 ^{ns}	1.67		0.17 ^{ns}	0.25		-0.04 ^{ns}	0.05	
OWD	13.6***	1.68		1.62***	0.26		0.21***	0.06	
MFA	-0.89 ^{ns}	1.54		-0.05 ^{ns}	0.23		0.08 ^{ns}	0.05	
Model 2	74.47***	2.06	54.4	7.97***	0.29	56.4	4.44***	0.05	60.04
Cellulose	6.94**	2.29		1.44***	0.32		0.30***	0.06	
Hemicelluloses	8.29**	2.38		1.37***	0.34		0.19**	0.06	
Lignin	-1.06 ^{ns}	2.23		-0.12 ^{ns}	0.31		-0.06 ^{ns}	0.06	
Disk density	9.99***	2.13		1.15***	0.31		0.20**	0.06	
MFA	-1.06 ^{ns}	2.21		-0.07 ^{ns}	0.30		0.07 ^{ns}	0.05	

*p<0.05, **p<0.01, ***p<0.001, ns not significant at p >0.05 DD= disk density OWD = outerwood density, MOE= modulus of elasticity, MOR= modulus of rupture

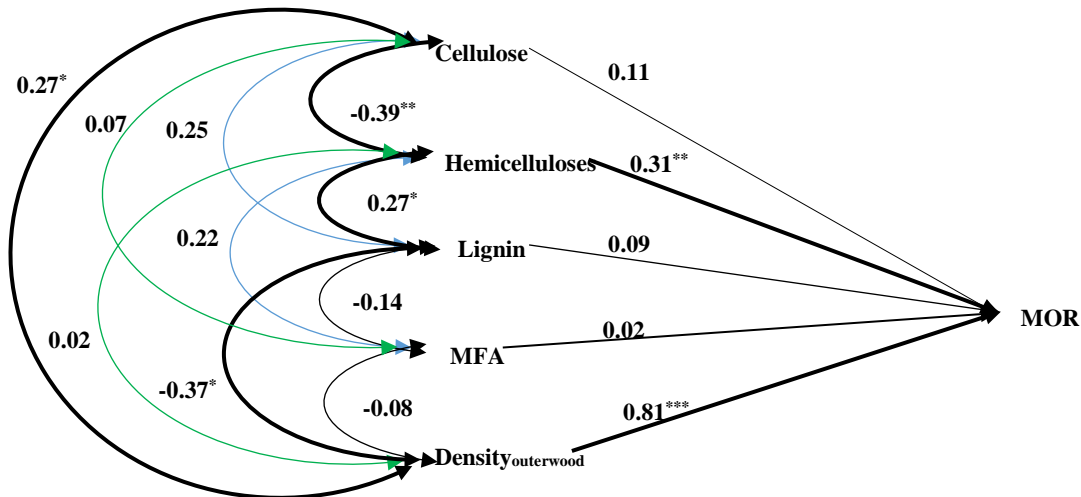


Fig 1 - Path analysis of the chemistry, MFA, outerwood density and MOR to examine the effect of outerwood density on the variables in the model. *p<0.1, **p<0.01, ***p<0.001 ns= nonsignificant at p>0.1

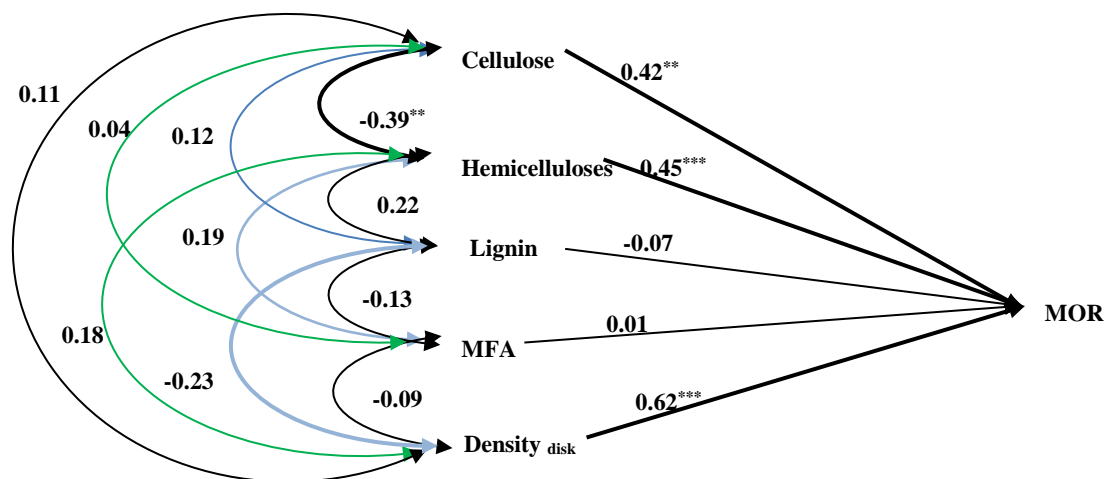


Fig 2 - Path analysis of the chemistry, MFA, disk density and MOR to examine the effect of disk density in the model * $p < 0.1$, ** $p < 0.01$, *** $p < 0.001$ ns= non-significant at $p > 0.1$

Conclusions

Acoustic velocity and mechanical properties of the suppressed loblolly pine wood were predicted using the cellulose, hemicellulose, lignin, MFA and density. Both the multiple linear regression and path analysis indicate that the same set of variables is responsible for predicting the stiffness and velocity. This result provides a molecular level evidence to confirm the capability of ToF acoustic tools to estimate stiffness. The results revealed that at the molecular level, cellulose is the most important molecular constituent responsible for the acoustic wave propagation; followed by the hemicelluloses; while lignin acts as a dispersant or sink, thereby reducing sound transmittance. Also the fact that the polymeric constituents and disk density explained higher proportion of variations in velocity than with outerwood density provides molecular level support that the ToF acoustic measurements on trees may rely on dilatational wave instead of the one-dimensional wave. It is possible that using matured trees may present a different picture which may further help us understand the theoretical operations of the acoustic tools.

References

Acquah, G.E., Via, B.K., Fasina, O., Eckhardt, L.G. 2015. Non-destructive prediction of the properties of Forest biomass for chemical and bioenergy application using near infrared spectroscopy. *Journal of Near infrared Spectroscopy* 23(2): 93 – 102

ASTM Standard D 143-94. 2007. Standard test methods for small clear specimens of timber. ASTM International, West Conshohocken, Pa. Available at www.astm.org [accessed 5 Jan. 2014].

Clausen, C.A., Kartal, S.N. 2003 Accelerated detection of brown-rot decay: Comparison of soil block test, chemical analysis, mechanical properties, and immunodetection. *Forest Products Journal* 53(11/12): 90-94

Essien, C., Cheng, Q., Via, B.K., Loewenstein, E.F., Wang, X. 2016. An Acoustic operations study for loblolly pine standing saw timber with different thinning history *BioResources* 11(3): 7512 – 7521

Essien C. 2011. Physical, Anatomical and Treatment characteristics of the wood of *Cola gigantea* and *Ficus sur*. Master of Philosophy Thesis, Faculty of Renewable Natural Resource - Kwame Nkrumah University of Science and Technology, Kumasi, Ghana. Pp 196

Essien, C., Via BK, Wang, X., Gallagher T, McDonald T, Eckhardt LG (2017) Multivariate Modeling of Acousto-mechanical Response of Fourteen Year Old Suppressed Loblolly Pine (*Pinus taeda*) to Variation in Wood Chemistry, Microfibril Angle, and Density Wood Sci Technol 51: 475 – 492.

Gindl W, Schoberl T (2004) The significance of elastic modulus of wood cell walls obtained from nanoindentation measurement. Composite Part A 35 (11):1345-1349

Hasegawa, M., Takata, M., Matsumura, J., Oda, K.2011. Effect of wood properties on within-tree variation in ultrasonic wave velocity in softwood. Ultrasonics 51 (3): 296-302

Hori,R., Müller, M., Watanabe, U., Lichtenegger, H., Frantzl, P., Sugiyama, J.2002.The importance of seasonal differences in the cellulose microfibril angle in softwoods in determining acoustic properties. Journal of Material Science 37 (20) :4279 – 4284

Mark, R.E.1967.Cell wall mechanics of tracheids. Yale University Press, New Haven & London.

Marra, G.1979. Overview of wood as material. Journal of Educational Modules for Materials Science and Engineering. 1(4): 699–710.

Peter, G.F., Benton, D.M., Bennett, K.2003.A simple direct method for measurement of microfibril angle in single fibres using differential interference contrast microscopy. J. Pulp and Paper Sci. 29: 274 - 280

Reiterer, A., Lichtenegger, H., Tschegg, S., Frantzl, P.1999.Experimental evidence of a mechanical function of cellulose microfibril angle in wood cell walls. Philosophical Magazine A 79(9): 2173-2184

Stamm, A.J.1964. Wood and cellulose science. The Ronald Press Co. New York.

Statistical Analysis Software (SAS) version 9.4 .2014. Cary, NC, USA

Via, B.K., So, C.L., Shupe, T.F., Groom, L.H., Wikaira, J.2009. Mechanical response of longleaf pine to variation in microfibril angle, chemistry associated wavelengths, density and radial position. Composites: Part A 40 (1):60-66

Via, B.K., Zhou, C., Acquah, G., Jiang, W., Eckhardt, L.2014. Near infrared calibration for wood chemistry: which chemometric technique is best for prediction and interpretation? Sensors 14 (8): 13532 - 13547

Wang, X., Ross, R.J., McClellan, M., Barbour, R. J., Erickson, J.R., Forsman, J.W., McGinnis, G.D.2001. Nondestructive evaluation of standing trees with a stress wave method. Wood & Fiber Science 33(4): 522-533

Winandy, J.E., Rowell, R.M.2005. Chemistry of wood strength In Handbook of chemistry and wood composite. CRC Press I.J.C. 305 - 343

Winandy, J.E., Lebow, P. K.2001. Modeling strength loss in wood by chemical composition Part1: An individual component model for southern pine. Wood and Fiber Science 33(2):239-254

Acoustic Technology—Enhanced Tools for Research and Operations

Peter Carter *

Chief Executive, Fibre-gen Limited, Christchurch, New Zealand, peter.carter@fibre-gen.com

Ciaran Doidge, InFact Limited, Christchurch, New Zealand. Ciaran.doidge@infact.co.nz

Abstract

Acoustic technologies are progressively being deployed in forestry and wood processing operations particularly where end wood product values are dependent upon stiffness. Hitman® technology has been developed to enable application of this technology in harsh operational environments, demanding robust ruggedised tools. Significant values are associated with stiffness in log supply for LVL veneer production and structural lumber manufacture. Measurement of acoustic speed allows this value to be captured through better decision-making, allocation of resource to highest value uses, and application of best processing methods dependent upon log-by-log measures. This paper reviews recent improvements of acoustic tools available for research and operational use to measure the stiffness of trees and logs in tree improvement, mid-rotation and pre-harvest inventory, harvesting and log-making, mill yard, and processing operations. It highlights technology improvements for easier use, improved precision, and better results.

Keywords: acoustic technology, Hitman®, stiffness, robust ruggedised tools, value, tree improvement, inventory, harvest, log making, bucking, mill yard, wood processing

Introduction

Background

Acoustic technology is increasingly being deployed in forestry and wood processing operations around the world, with greatest value where stiffness is an important property of end wood products. Field-rugged acoustic tool development and initial operational deployment began in New Zealand 18 years ago in response to demand from stiffness sensitive wood processors. Tools are used to measure the stiffness of trees and logs in tree improvement programs, mid-rotation and pre-harvest inventories, harvesting, log-



making, and mill yard and wood processing operations. The application of acoustic technology was summarised on a map of the world by participants at the 19th NDT symposium in Rio de Janeiro in 2015.

Research and operational application of acoustic technology has continued to expand around the world in response to diminishing supplies, transition to plantation grown forests, intensive silviculture, genetic improvement in growth rate rather than wood properties, and declining average age of harvest.

Targeted wood products include both LVL and machine stress graded structural sawn timber. Rugged field and processing site environments need robust, waterproof, rugged tools which keep on working in all weathers and take the knocks.



Engineered wood products

Where product values depend upon stiffness, measurement of acoustic speed enables better decision-making, allocation of resource to highest value uses, and application of best processing methods based on log-by-log measures. The most significant end product value propositions have been identified in engineered wood products including LVL, structural plywood, laminated beams, and structural lumber products.

Tools and technology

The range of tools and technology available has expanded to include hand tools for measuring standing trees in the forest, and for measuring logs on harvest sites, log yards, and processing operations.



Hitman® ST300



Hitman® HM200

Automated mechanized versions of these acoustic hand tools have been developed for harvest operations and wood processing sites.



Hitman® PH330



Hitman® LG640

It is envisaged that where possible, there will be opportunity dependent upon tool age for Hitman® hand tools to be upgraded from the current Hitman® ST300 to the new Hitman® ST330 specification, and from the current Hitman® HM200 to the new Hitman® HM220.

Hitman® standing tree tool improvements

While mechanised systems are subject to ongoing development and improvement and continue to gain acceptance in harvesting and wood processing operations, recent improvements have also been made to the hand tools in response to user feedback. The Hitman® ST300 will be superseded by the soon to be released Hitman® ST330 for measuring stiffness in standing trees. The new Hitman® ST330 implements a number of learnings from the PH330 processor head development program, including faster hitting,

better software and hardware filters, more repeatable results, and a number of usability improvements are planned.

Better productivity

No delay between ‘hits’ – now you can tap the probe in rapid succession, without waiting for each ‘tap’ to be processed – simply keep ‘tapping’ until you hear the ‘beep’

Better precision

Precision to the nearest 0.01km/sec simply by ‘tapping’ until this level is reached

Better options

Use your own mobile device (Windows, Android or Apple) with the Hitman® ST330 “app”

Hitman® ST300 study

A comparative study was undertaken in a radiata pine plantation near InFact Limited’s laboratory in Christchurch, New Zealand to compare the current Hitman® ST300 tool with the new improved Hitman® ST330 model.

Objectives

1. To determine the effectiveness of implementing the PH330 waveform filtering and sorting algorithm in the ST300 in a lab situation, and validation in a real world situation
2. To quantify the amount by which the PH330 time of flight (ToF) determination algorithm reduces ToF variation
3. Validate the improved time of flight measurements between the ST300 and ST330

Method

Required Tools

1. 2 x ST300 Rx tools with production settings (FW V5.00, Threshold = 500, Knee 1 = 8, Knee 2 = 35)
2. 2 x ST330 Rx tools with the PH330 algorithms installed and previously determined algorithm settings.
3. 1 x Tx s/n 0026.
4. 1 x HM200.
5. 1 x Panasonic Tough book field laptop and P121-010-ST Connect program to record the ToF measurements (Lab testing).
6. Testing hammer.
7. Tape measure.

Evaluation of ToF Variation (Lab Testing)

Log Selection

A single dry Radiata pine log was used to perform the lab testing. The log had been stored in the InFact workshop for approximately 12+ months.

Testing

The method used to carry out the testing in the lab was as follows:

1. Install the Rx probe holder 200 mm from the cut end and install the ST300 Rx probe (s/n 0120).
2. Install the Tx (s/n 0026) approximately 500 mm from the Rx probe holder.
3. Measure and record the face to face distance between the Tx and Rx probe using a tape measure. Record the distance displayed on the Rx probe.
4. Connect the ST300 to the P121-010-ST Connect program.
5. Ensure the algorithm settings are standard.
6. Perform 100 hit samples. For each set of hits, record the ToF measurements.
7. Leaving the Tx probe and Rx holder in place, remove the Rx probe and replace with a ST330 (s/n 0058) Rx probe running the ST330 algorithm (using the previously determined algorithm settings).
8. Repeat steps 2-6 for the ST330 tooling.
9. Start again from step 1 to achieve 3 sets of tests of 100 sequential hits for the ST300 and ST330 tooling.
10. Carry out steps 1-9 with the exception of steps 4 and 5 and instead record the velocity and ToF measurements from the readout on the Rx probe.

Evaluation of ToF Variation (Four Freshly Cut logs)

Log Selection

Two Radiata pine and two Douglas fir logs were sourced for testing. The properties of the test logs are given in the following Table.

	SED [mm]	LED [mm]	Length [mm]	Species
Log 1	320	370	2640	Radiata
Log 2	275	300	2590	Radiata
Log 3	290	345	2635	Douglas fir
Log 4	250	300	2595	Douglas fir

Algorithm Settings

For each log the output of the filtered accelerometer waveform data of 20 hits per log were recorded to determine suitable values for algorithm settings.

Testing

Each of the four logs was tested to determine the ToF at a probe spacing of 500 mm, 1000 mm and 1500 mm. The method used was as follows:

1. Install the Rx probe holder 200 mm from the cut end and install the ST300 Rx probe (s/n 0120).
2. Install the Tx (s/n 0026) approximately 500 mm from the Rx probe holder.
3. Measure and record the face to face distance between the Tx and Rx probe using a tape measure. Record the distance displayed on the Rx probe.
4. Use the STConnect software with the Toughbook to record 5 lots of 20 ToF measurements.
5. Repeat steps 3-4 for the ST330 (s/n 0058) tooling.
6. Repeat steps 2-5 for each distance of 500mm, 1000mm and 1500mm (note: Do not remove the Tx probe and Rx probe holder between tests with the ST300 and ST330 tooling).

7. Repeat steps 1-6 for each of the four test logs.

Results and Observations

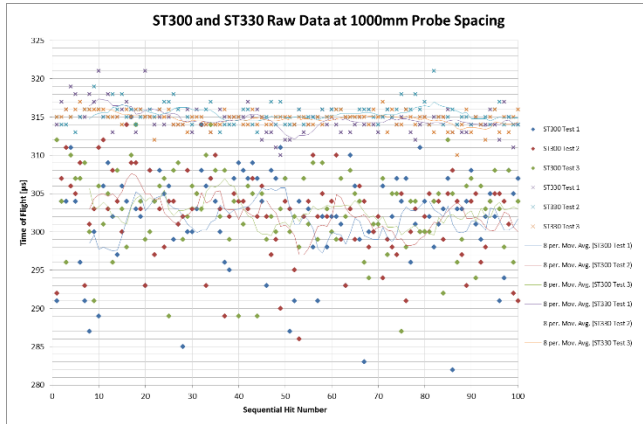
Evaluation of ToF Variation (Lab Testing)

To test the effectiveness of the ST330, three sets of tests of 100 sequential hits were carried out in the InFact workshop using both the ST300 and ST330. The time of flight for each hit was recorded using the P121-010-ST Connect monitoring program. Table 4 gives the average ToF and the standard deviation across the 100 hits of each test. Across all the tests the ST330 produced ToF data with a standard deviation of between 1 μs and 2 μs . The standard deviation of the ToF data using the ST300 was between 5 μs and 6 μs . This implied that the variance of the measurements using the ST300 was between 3 to 5 times larger than when using the ST330.

Table 1: Raw data

	ST300		ST330	
	Average ToF [μs]	Std. Dev [μs]	Average ToF [μs]	Std. Dev [μs]
Test 1	302	6	315	2
Test 2	302	6	315	1
Test 3	303	5	315	1

Figure 1: Raw data



The ST300 and ST330 were retested in the same manner as described in the method with the exception of taking the averaged ToF reading from the Rx display. Table 5 gives the average of ToF readings and the standard deviation across the 100 hits of each test. In all the tests, the ST330 produced ToF readings with a standard deviation of 1 μs . The standard deviation of the ToF readings using the ST300 was between 2 μs and 3 μs . This implied that the variance of the ST300 measurements was between 2 to 3 times larger than that of the ST330.

Table 2: Rx Readout data

	ST300		ST330	
	Average ToF [μs]	Std. Dev [μs]	Average ToF [μs]	Std. Dev [μs]
Test 1	251	2	262	1
Test 2	251	2	263	1
Test 3	255	3	262	1

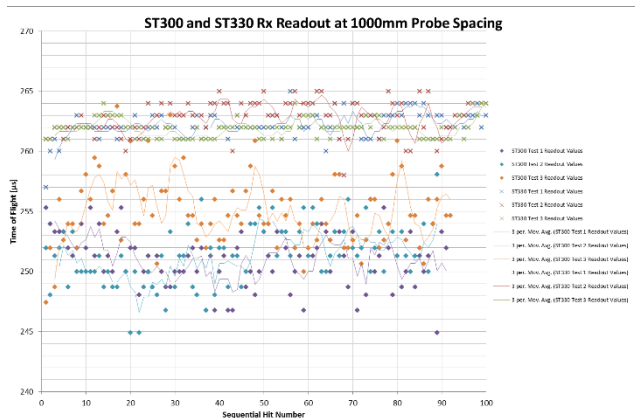


Figure 2: Data taken from Rx readout

Figure 3 shows how the ToF measurement’s cumulative standard error of the mean (SoM) decreased with an increase in number of hits. The ST300 SoM did not improve greatly after 90 to 100 hits whereas the ST330 SoM did not improve significantly after 30 hits. This implies that for testing, a sample of size of 90 to 100 hits would produce an average ToF result with a target standard error of 0.01km/s for both tools. It is also implied that for both the ST300 and ST330 tooling, after 90 sequential hits, the mean of each test would be less than 0.1 μ s away from the “real” ToF value of the test specimen. The SoM calculation method is described in the Appendix.

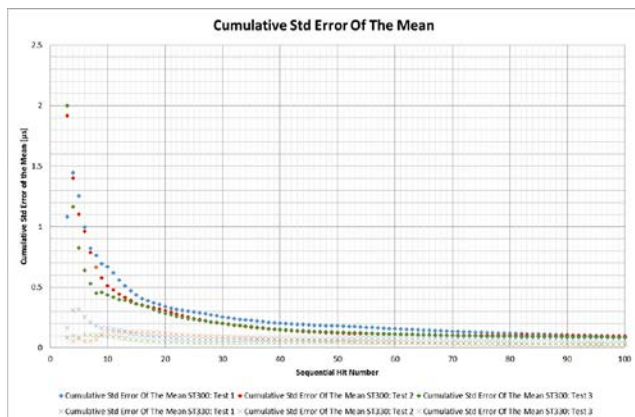


Figure 3: Cumulative Standard Error of the Mean

Assuming a test of 100 hits would be sufficiently close to the “real” ToF value of the test specimen, a two tailed t-test could be carried out to produce a ToF measurement within a pre-defined tolerance and a specified confidence interval (refer Appendix). If a 95% confidence level was chosen there would be confidence that the ToF value found after x number of hits would be plus or minus the tolerance level away from the sample mean in 95% of the tests.

Based on a 100 sample size and the cumulative standard deviation of the three tests carried out on the ST300 and ST330, Figure 4 shows that in order to report an average ToF measurement to an accuracy of $\pm 3 \mu$ s of the “real” ToF value with 95% confidence, at least 20 hits are required for the ST300 and at least 3 hits are required for the ST330. The minimum number of hits only applies to the individual test and therefore must be computed in real time. It should also be noted that an absolute minimum number of hits, for example 8, should be chosen to ensure the standard deviation was statistically significant. This method could be used as a way of determining the number of hits required to get to a pre-determined level of accuracy with 95% confidence, at which time the tool would signal the user to cease taking hit samples. Alternatively the confidence interval method could be used to estimate and display the standard error of the mean of the velocity measurements taken in real time such that the user would continue tapping until such time as an accuracy level determined by the user was met.

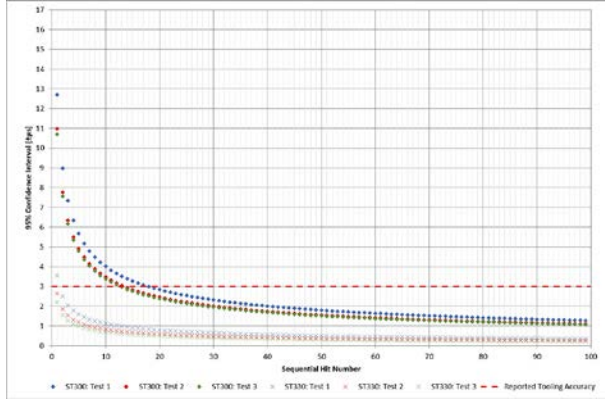


Figure 4: Number of hits required to meet a selected tooling accuracy

Evaluation of ToF Variation on Four Freshly Cut logs

Using the ST300 and ST330 tooling, ToF and wave velocity measurements of four freshly cut logs were taken at probe spacings of 500 mm, 1000 mm and 1500 mm. 5 lots of 20 ToF measurements were carried out at each distance for each tool. It was found that the variation in the ToF measurement in both species, was between 1.5 and 9 times larger for the ST300 than for the ST330 (refer Table 6 and Table 7). The variation in ToF measurements of the ST300 between the Radiata and Douglas fir logs was found to be approximately the same, with the largest difference in ToF of 1.5 between the species (refer Table 6). The variation in ToF measurements in the ST330 between Radiata and Douglas fir logs was found to be between 0 and 3 times greater (refer Table 7). Figure 5 shows the comparison of the ToF test results of the ST300 and ST330 tooling for both species of log.

The same testing process was carried out on a brass calibration bar to use as a datum, due to the homogenous material properties of brass. The average ToF and wave velocity measurements in brass for both toolings are also given in Table 6 and Table 7.

Table 6: ST300 Average ToF and Wave Velocity at Nominal Distances

ST300 Nominal Distance [mm]	Log 1 (Radiata)		Log 3 (Douglas fir)		Brass Calibration Bar	
	Average ToF [μs]	Standard Dev. [μs]	Average ToF [μs]	Standard Dev. [μs]	Average ToF [μs]	Standard Dev. [μs]
500	113	9	88	9	148	4
1000	241	6	201	4	287	0
1500	378	7	319	6	436	6
Nominal Distance [mm]	Average Velocity [km/s]	Standard Dev. [km/s]	Average Velocity [km/s]	Standard Dev. [km/s]	Average Velocity [km/s]	Standard Dev. [km/s]
	500	3.65	0.33	4.31	0.50	3.37
1000	3.63	0.09	4.36	0.09	3.48	0.08
1500	3.64	0.06	4.35	0.08	3.44	0.05

Table 3: ST330 Average ToF and Wave Velocity at Nominal Distances

ST330 Nominal Distance [mm]	Log 1 (Radiata)		Log 3 (Douglas fir)		Brass Calibration Bar	
	Average ToF [μs]	Standard Dev. [μs]	Average ToF [μs]	Standard Dev. [μs]	Average ToF [μs]	Standard Dev. [μs]

500	115	1	96	1	148	3
1000	257	3	214	1	291	3
1500	396	2	344	1	441	3
Nominal Distance [mm]	Average Velocity [km/s]	Standard Dev. [km/s]	Average Velocity [km/s]	Standard Dev. [km/s]	Average Velocity [km/s]	Standard Dev. [km/s]
500	3.51	0.02	3.90	0.04	3.38	0.06
1000	3.46	0.03	4.10	0.02	3.44	0.03
1500	3.47	0.01	4.01	0.01	3.40	0.02

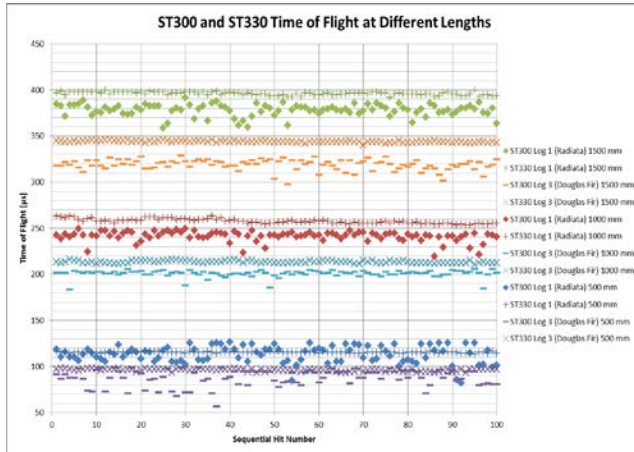


Figure 5: Comparison of ToF at Different Lengths

For each test length the face to face tooling distance, minus 150 mm for face to probe tip offset, was divided by the ToF measurement at that length to give the velocity of the acoustic wave (refer Table 6 and Table 7). This was carried out in order to normalise the ToF with respect to distance. Assuming that velocity is constant throughout the log's length and is not dependant on probe separation, the trend of velocity across the different probe distances should be horizontal.

Figure 6 and Figure 7 compare the acoustic wave velocity in a brass calibration bar, Radiata and Douglas fir, as measured by the ST300 and ST330 tooling respectively. The brass calibration bar was used as a datum as the material was considered to be homogenous throughout its length and has similar wave speed as seen in Radiata and Douglas fir. Figure 6 and Figure 7 show that the trend of velocity with respect with probe distance was found to be horizontal. This implies that the probe spacing had no effect on the wave velocity measurements.

Figure 6 shows that the variation in wave velocity of the ST300 was largest when the probe spacing was at 500 mm. However the ST330 did not show the same sensitivity, as the variation in velocity measurements were consistent at all distances on both log types (refer Figure 7). The ST330 velocity measurements at 500 mm showed the same or less variation than the ST300 at all probe distances. Error was introduced due to measurement and calibration uncertainties. The face to face measurement was carried out using a tape measure. It was assumed that the face to face distance could be measured to an accuracy of ± 5 mm. The calibration process reports a tooling accuracy of ± 3 μ s, which was used as a source of uncertainty. The relative uncertainty error from both sources was propagated to find the uncertainty error of the velocity measurements and is shown in Figure 6 and Figure 7 and also given in Table 8.

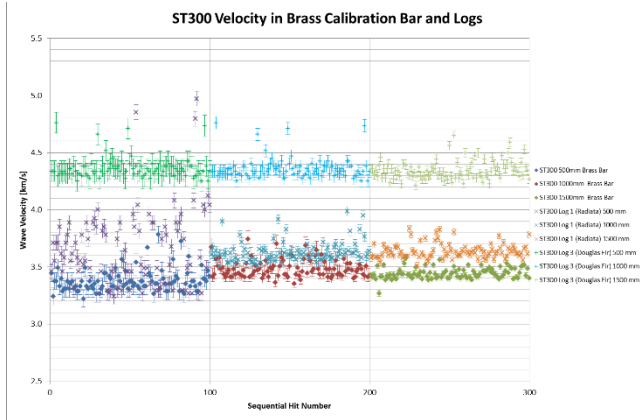


Figure 6: ST300 Comparison of Wave Velocity at Different Lengths*

*Note: Sequential Hit Number 0-100 are at a probe distance of 500 mm, 100-200 are at a probe distance of 1000 mm and 200-300 are at a probe distance of 1500 mm.

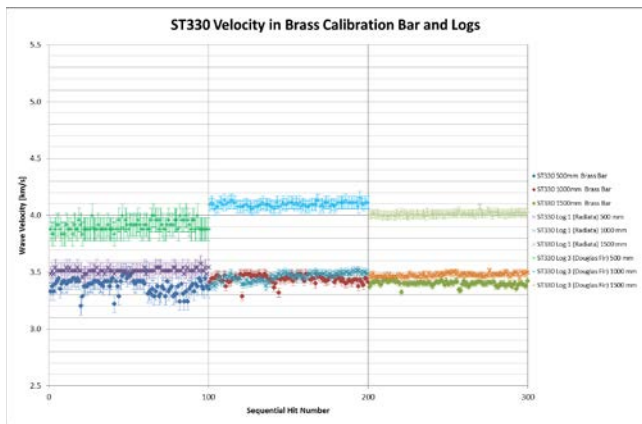


Figure 7: ST330 Comparison of Wave Velocity at Different Lengths*

*Note: Sequential Hit Number 0-100 are at a probe distance of 500 mm, 100-200 are at a probe distance of 1000 mm and 200-300 are at a probe distance of 1500 mm.

Table 4: Uncertainty Error in Wave Velocity Measurements

Nominal Distance [mm]	Brass Bar		Radiata		Douglas fir	
	ST300	ST330	ST300	ST330	ST300	ST330
	Error [±km/s]	Error [±km/s]	Error [±km/s]	Error [±km/s]	Error [±km/s]	Error [±km/s]
500	0.07	0.08	0.10	0.10	0.16	0.13
1000	0.04	0.04	0.05	0.04	0.07	0.06
1500	0.03	0.03	0.03	0.03	0.04	0.04

Conclusions

From lab testing it was found that the filtering and sorting algorithm used in the new model ST330 produced sequential time of flight (ToF) measurements with less variation when compared to the existing ST300.

From analysing the raw ToF data over 100 sequential hits the ST300 measurements were found to have a standard deviation between 5 μ s and 6 μ s for each test. The standard deviation for each test from the ST330 data was found to be between 1 μ s and 2 μ s. From the averaged ToF data taken from the Rx display the standard deviation across 100 sequential hits was found to be between 2 μ s and 3 μ s for each test using the ST300 and 1 μ s for each test with the ST330. The decrease in variance in sequential

measurements implied that the algorithm implemented in the ST330 improved the repeatability of the ST330 measurements when compared to the ST300. During testing no warm up behaviour was observed in either the ST300 or ST330 tooling.

The use of a confidence interval was proposed to determine when to stop taking hit samples either by allowing the user to choose the desired level of accuracy and cease taking hit samples when their chosen level was met or by pre-determining an accuracy level which when met the user would be informed by the tooling to stop taking hit samples.

The testing of four freshly cut logs at 500mm, 1000 mm and 1500mm probe spacing found that the variation in the ToF measurements was between 1.5 and 9 times larger for the ST300 than the ST330. The variance for the ST300 ToF measurements was between 6 μs and 9 μs in Radiata pine and between 4 μs and 9 μs in Douglas fir logs. The variance for the ST330 ToF measurements was between 1 μs and 3 μs in Radiata pine and 1 μs for all distances in Douglas fir. The results from the log testing further supported the result of the lab testing and validated the improvement of the filtering and sorting algorithm used in the ST330.

Due to the horizontal trend of the velocity measurements at various probe spacings, it was concluded that probe spacing had no effect on the wave velocity measurements.

Appendix

Standard error of the mean

The standard error of the mean (SoM) is calculated from a sample by taking the average of a successively growing subset of the ToF data, then taking the standard deviation of a successively growing subset of the averages found and dividing the cumulative standard deviations by the sample subset size. The equation is:

$$\sigma_s = \sqrt{\frac{\sum_{i=1}^n (x_i - \bar{x})^2}{n - 1}}$$

$$SoM = \frac{\sigma_s}{\sqrt{n}}$$

Where:

SoM cumulative standard error of the mean.

n is the subset sample size which grows with every recalculation (in this case hit) until the final SoM includes all ToF values in the sample.

σ_s is the cumulative standard deviation.

x is the ToF data.

\bar{x} is the subset ToF mean.

Confidence Interval

Table 5: Two tailed t-test

t Table		$t_{.90}$	$t_{.75}$	$t_{.50}$	$t_{.25}$	$t_{.10}$	$t_{.05}$	$t_{.025}$	$t_{.01}$	$t_{.005}$	$t_{.001}$	$t_{.0005}$
cum. prob	one-tail	0.50	0.25	0.20	0.15	0.10	0.05	0.025	0.01	0.005	0.001	0.0005
two-tails		1.00	0.50	0.40	0.30	0.20	0.10	0.05	0.02	0.01	0.002	0.001
df												
1	0.000	1.000	1.376	1.963	3.078	6.314	12.71	31.82	63.66	318.31	636.62	
2	0.000	0.816	1.061	1.386	1.886	2.920	4.303	6.965	9.925	22.327	31.599	
3	0.000	0.765	0.978	1.250	1.638	2.353	3.182	4.541	5.841	10.215	12.924	
4	0.000	0.741	0.941	1.190	1.533	2.132	2.776	3.747	4.604	7.173	8.610	
5	0.000	0.727	0.920	1.156	1.476	2.015	2.571	3.365	4.032	5.893	6.869	
6	0.000	0.718	0.906	1.134	1.440	1.943	2.447	3.143	3.707	5.208	5.959	
7	0.000	0.711	0.896	1.119	1.415	1.895	2.365	2.998	3.499	4.785	5.408	
8	0.000	0.706	0.889	1.108	1.397	1.860	2.306	2.896	3.355	4.501	5.041	
9	0.000	0.703	0.883	1.100	1.383	1.833	2.262	2.821	3.250	4.297	4.781	
10	0.000	0.700	0.879	1.093	1.372	1.812	2.228	2.764	3.169	4.144	4.587	
11	0.000	0.697	0.876	1.088	1.363	1.796	2.201	2.718	3.106	4.025	4.437	
12	0.000	0.695	0.873	1.083	1.356	1.782	2.179	2.681	3.055	3.930	4.318	
13	0.000	0.694	0.870	1.079	1.350	1.771	2.160	2.650	3.012	3.852	4.221	
14	0.000	0.692	0.868	1.076	1.345	1.761	2.145	2.624	2.977	3.787	4.140	
15	0.000	0.691	0.866	1.074	1.341	1.753	2.131	2.602	2.947	3.733	4.073	
16	0.000	0.690	0.865	1.071	1.337	1.746	2.120	2.583	2.921	3.686	4.015	
17	0.000	0.689	0.863	1.069	1.333	1.740	2.110	2.567	2.898	3.646	3.965	
18	0.000	0.688	0.862	1.067	1.330	1.734	2.101	2.552	2.878	3.610	3.922	
19	0.000	0.688	0.861	1.065	1.328	1.729	2.093	2.539	2.861	3.579	3.883	
20	0.000	0.687	0.860	1.064	1.325	1.725	2.086	2.528	2.845	3.552	3.850	
21	0.000	0.686	0.859	1.063	1.323	1.721	2.080	2.518	2.831	3.527	3.819	
22	0.000	0.686	0.858	1.061	1.321	1.717	2.074	2.508	2.819	3.505	3.792	
23	0.000	0.685	0.858	1.060	1.319	1.714	2.069	2.500	2.807	3.485	3.768	
24	0.000	0.685	0.857	1.059	1.318	1.711	2.064	2.492	2.797	3.467	3.745	
25	0.000	0.684	0.856	1.058	1.316	1.708	2.060	2.485	2.787	3.450	3.725	
26	0.000	0.684	0.856	1.058	1.315	1.706	2.056	2.479	2.779	3.435	3.707	
27	0.000	0.684	0.855	1.057	1.314	1.703	2.052	2.473	2.771	3.421	3.690	
28	0.000	0.683	0.855	1.056	1.313	1.701	2.048	2.467	2.763	3.408	3.674	
29	0.000	0.683	0.854	1.055	1.311	1.699	2.045	2.462	2.756	3.396	3.659	
30	0.000	0.683	0.854	1.055	1.310	1.697	2.042	2.457	2.750	3.385	3.646	
40	0.000	0.681	0.851	1.050	1.303	1.684	2.021	2.423	2.704	3.307	3.551	
60	0.000	0.679	0.848	1.045	1.296	1.671	2.000	2.390	2.660	3.232	3.460	
80	0.000	0.678	0.846	1.043	1.292	1.664	1.990	2.374	2.639	3.195	3.416	
100	0.000	0.677	0.845	1.042	1.290	1.660	1.984	2.364	2.626	3.174	3.390	
1000	0.000	0.675	0.842	1.037	1.282	1.646	1.962	2.330	2.581	3.098	3.300	
Z	0.000	0.674	0.842	1.036	1.282	1.645	1.960	2.326	2.576	3.090	3.291	
		0%	50%	60%	70%	80%	90%	95%	98%	99%	99.8%	99.9%
		Confidence Level										

Assuming the mean ToF of infinite hits will approximately equal to the ToF of the sampled tree, the $t_{0.95}$ value for an infinite set is:

$$t_{0.95} \text{ value} = 1.960$$

The confidence interval or error about the sample mean (\bar{x}) is:

$$\varepsilon_{0.95} = t_{0.95} \left(\frac{\sigma_s}{\sqrt{n}} \right)$$

Where: σ_s = Cumulative standard deviation of sample, n = number of samples or hits taken.

The error ($\pm \varepsilon_{0.95}$ [μs]) will mean you are confident that the mean of your sample data will be within $\pm \varepsilon_{0.95}$ [unit] of the “real” ToF value 95% of the time.

Velocity measurement display

After hitting has ceased and a certain length of time has passed the velocity measurement of the sample is to be displayed in the same way as the ToF measurements i.e. “ $v \pm E_{0.95}[\text{km/s}]$ ” for example “ $3.15 \pm 0.2 \text{ km/s}$ ”.

where:

$$v = \frac{D}{\bar{x}} \text{ is the velocity [km/s]}$$

\bar{x} is the average ToF of the hit data

$E_{0.95}$ is the error of the velocity measurement

The error of the velocity measurement will be propagated by:

$$E_{0.95} = v * \left(\frac{\varepsilon_{0.95}}{\bar{x}} \right)$$

Modified z-score method

The modified z-score method is a statistical technique developed by Iglewicz and Hoaglin (U.S Dept. of Commerce, 2013). The modified z-score of the data point is calculated at each hit. The method identifies potential outliers in the data by assessing whether the z-score value exceeds a threshold value (the value recommended by Iglewicz and Hoaglin is $t = 3.5$ however, this value can be changed to suit the typical ST330 ToF data). The formula for the modified z-score is as follows:

$$m_i = \frac{0.6745(x_i - \tilde{x})}{MAD}$$

Where:

x_i is the data value (i.e. ToF)

\tilde{x} is the median of the data subset

n is the data subset size

MAD is the median absolute deviation:

$$MAD = \frac{\sum_{i=1}^n |x_i - \tilde{x}|}{n}$$

If $|m_i| > t$ then the data point x_i may be a potential outlier.

It should be noted that the modified z-score has no significant effect in data sets with less the 6 data points. The larger the data set the more pronounced the effect of an outlier is and therefore the m_i value will be larger.

An explanation of the Modified z-score method can be found at:

<http://www.itl.nist.gov/div898/handbook/eda/section3/eda35h.htm>

References

Bekhta, P., Nimez, P., & Kucera, L. (2000). *The study of sound propagation in the wood-based composite materials*. Retrieved January 30, 2017, from Research Gate: https://www.researchgate.net/publication/267025160_The_study_of_sound_propagation_in_the_wood-based_composite_materials

The Engineering Toolbox. (n.d.). *Sound Speed of Solids*. Retrieved January 30, 2017, from The Engineering Toolbox: http://www.engineeringtoolbox.com/sound-speed-solids-d_713.html

U.S Dept. of Commerce. (2013, October 30). *Detection of Outliers*. Retrieved February 3, 2017, from Engineering Statistics Handbook: <http://www.itl.nist.gov/div898/handbook/eda/section3/eda35h.htm>

Nondestructive Evaluation of Hybrid Poplar Plantations

Türker Dündar

Faculty of Forestry, Istanbul University, Istanbul, Turkey, dundar@istanbul.edu.tr

Hüseyin Akkılıç

Faculty of Forestry, Istanbul University, Istanbul, Turkey, hakkilic@istanbul.edu.tr

Ümit Büyüksarı

Faculty of Forestry, Duzce University, Duzce, Turkey, umitbuyuksari@duzce.edu.tr

Abstract

We aimed to evaluate the hybrid poplar plantations from two growing sites by stress wave and fractometer nondestructive test techniques in order to determine the effects of growing site, clone differences and initial plant density on the wood quality of standing trees. The experiments were carried out on 11 years old and 12 years old stands in Ipsala and İzmit districts, respectively. These stands were consist of adjacent parts where five hybrid poplar clones, I-214 (*Populus nigra*×*P. deltoides*), I-45/51 (*P. nigra*×*P. deltoides*), I-77/51 (*P. deltoides*), S307 (*P. nigra*), and 89M (*P. nigra*) were planted with initial spacing of 2×2 m, 3×2 m, 3×3 m, and 4×3 m. Twenty five sample trees for every clones and initial spacing in two growing sites were measured to determine the wave velocity parallel to grain. A wood core in 5 mm diameter was extracted from the breast height of every trees with an increment borer for the bending fracture strength and compression strength. The results showed that there were no significant differences in stress wave velocities of the clones between the growing sites except I-77/51. However the bending fracture strength and the compression strength of poplar wood from Ipsala were slightly higher than Izmit. We found significant differences between the wave velocities of the trees from different clones. Similarly, the bending and the compression strengths obtained from the core samples by fractometer changed significantly between the clones. In general the lowest values were obtained from I-214 followed by I-45/51 and 89M at both growing sites. The highest values were observed in S307 and I-77/51. As for the plant density, we couldn't observed any comprehensible results in wave velocity and fractometer test.

Keywords: nondestructive test, stress wave, fractometer, poplar clones, plant density, growing site

Introduction

In Turkey, as well as all over the world, industrial plantations with fast growing species are of high priority to tackle the shortage of wood supply. Poplar (*Populus* spp.) represent the fastest growing trees in the temperate regions. Turkey is one of the major country for poplar plantations with an area of 125.000 ha which represents a remarkable increase in past two decades (FAO 2012). Planted poplar forests are primarily owned by the private sector (98% of total area) and are largely used for production purposes (≈80.000 ha for roundwood production). The registration and identification of poplar clones of different origins have continued in the experimental nurseries of the Poplar Research Institute, İzmit. Programs concerning the genetic modification of poplars continue to enhance resistance against pests, diseases and other stresses, namely drought or flooding, and to improve technical properties as well as growth and

yield. Breeding programs focus on black poplars (*Populus nigra* L.) as one of the main poplar species in the country. *P.x euramericana* “I-214”, *P.x euramericana* “I-45/51” and *P.deltoides* “Samsun” clones have been successfully planted in hybrid poplar plantations, which are composed of 75% “I-214” and “I-45/51” clones, and 25% “Samsun” clones, the latter being preferred in the Black Sea region due to its rapid growth (IPC 2012). In planted poplar forests, including highly productive poplar clones, growth rates are reported to range from 2.75 to 41 m³/ha/yr mean annual increment, on average 17 m³/ha/yr. Rotation periods are rather short and span in most cases 10 to 20 years for the production of industrial roundwood, and 2 to 30 years, on average 20 years, for the production of fuelwood and biomass (IPC 2012).

Poplar wood production continues to increase on or close to agricultural land. More than 80% of black poplar wood is utilized as roundwood for rural construction purposes and for the daily needs of the rural people. Additionally, poplar wood industries have developed, producing fiber boards and chip boards, furniture, packing material, particle boards, plywood, and matches, mainly from hybrid poplars (*P.x euramericana*). Turkey is one of the top producers of poplar wood with reported removals of 3.5 million m³ (IPC 2012).

As forest products companies are interested in hybrid poplar clones for the manufacture of a variety of products, the selected clones must meet the needs of the forest industry for diverse end uses. The physical and mechanical properties of hybrid poplar wood may show great variations depending on the growing site factors as well as the genetic differences between the clones. It is widely reported in the literature that significant variation in physical and chemical composition exists among hybrid poplar clones depending on the genetic makeup (Chantre 1995; Ivkovich, 1996; Matyas and Peszlen 1997; Hernández et al. 1998; Peszlen, 1998; Goyal et al 1999; DeBell et al 2002). Information on basic wood properties of poplar grown in short-rotation plantations and on opportunities to alter such properties through silvicultural practices and management decisions is limited. Reports on the relation of wood density or specific gravity to growth rate are inconsistent. Beaudoin et al. (1992) and Hernández et al. (1998) pointed out significant but weak negative correlations between wood density or mechanical properties and growth rate in *P. deltoides*×*nigra*. Peszlen (1998) found no effect of growth on specific gravity or mechanical wood properties of three poplar clones.

Significant efforts have been devoted to develop robust nondestructive evaluation (NDE) technologies capable of predicting the intrinsic wood properties of individual trees, stems, and logs, and to assess the value of stands and forests. Such technologies can help foresters make wise management decisions, grow higher quality wood, and lead to greater profitability for the forest industry. Acoustic technologies have been well established as material evaluation tools in the past several decades. Recent research developments on acoustic sensing technology offer further opportunities for wood manufacturers and forest owners to evaluate raw wood materials (standing trees, stems, and logs) for general wood quality and intrinsic wood properties. This provides strategic information that can help make economic and environmental management decisions on treatments for individual trees and forest stands, improve thinning and harvesting operations, and efficiently allocate timber resources for optimal utilization (Wang et al. 2007).

The aim of this study is to evaluate the hybrid poplar plantations from two growing sites by stress wave and fractometer nondestructive test techniques in order to determine the effects of clone differences and initial plant density on the wood quality of standing trees. Effect of growing site on the acoustic velocity and the strength of wood determined on the increment cores was also investigated.

Materials and Methods

Experimental stands

Two experimental poplar plantations planted by The Izmit Poplar Research Institute for research purposes in Ipsala and Izmit districts were selected as the sample sites. These plantations were composed of adjacent parts where five hybrid poplar clones that are I-214 (*Populus nigra*×*P. deltoides*), I-45/51 (*P. nigra*×*P. deltoides*), I-77/51 (*P. deltoides*), S307 (*P. nigra*), and 89M (*P. nigra*) were planted with initial spacing of 2×2 m, 3×2 m, 3×3 m, and 4×3 m. Figure 1 shows the plantation plan of the experimental sites. Each part of the stands had 25 poplar trees at the age of 11 in Ipsala and 12 in Izmit. Therefore, 500 trees from each growing site were sampled for the acoustic measurements and increment core tests.

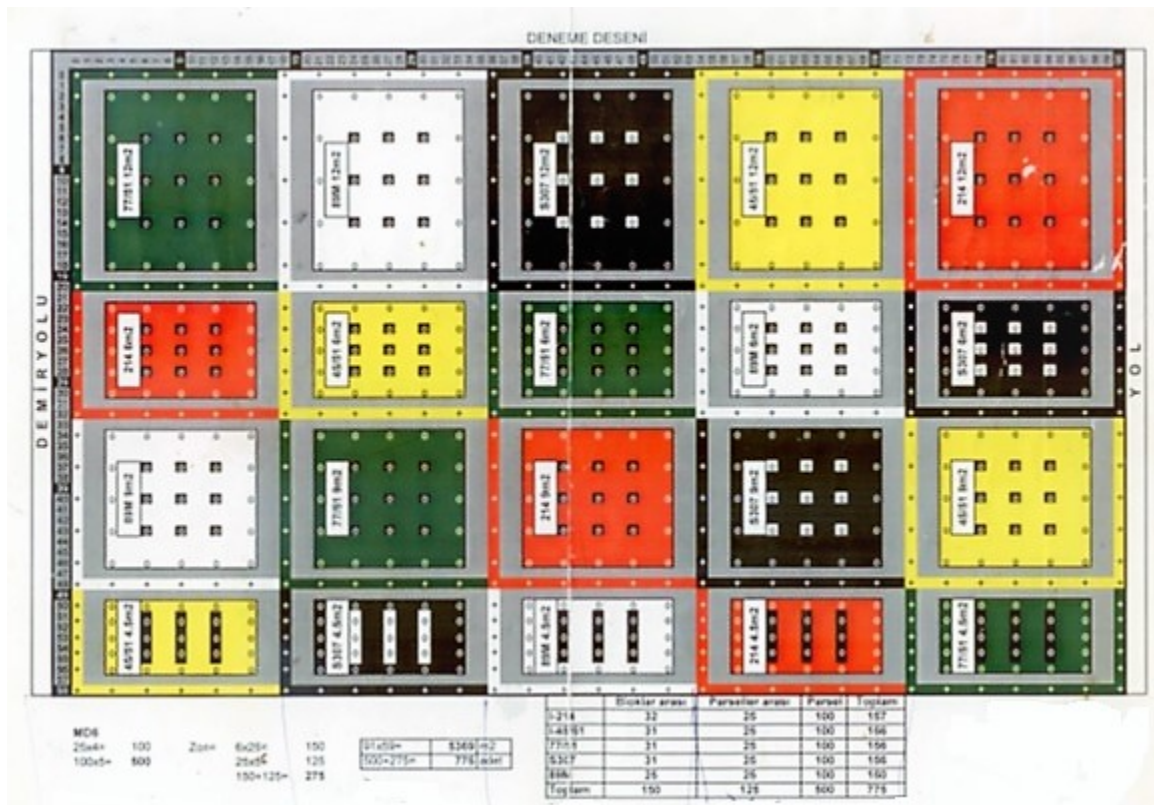


Figure 1— The plantation plan of the experimental sites.

Measurements on the standing trees

Time-of-flight (TOF) acoustic method was employed to determine the acoustic velocity of the standing poplar trees. The system includes two probes containing piezoelectric sensors (start sensor and stop sensor), a portable timer, and a hand-held hammer. The probes are inserted into the tree trunk (into sapwood) with an angle of less than 45° with the stem and aligned within a vertical plane on the same face. The lower probe is placed about 0.5-0.6 m above the ground. The distance between the lower and upper probes was 1 m (Figure 2). The acoustic energy is then directed into the tree trunk by hammer on the input probe. The resulting acoustic waves are detected by the sensors and transmitted to the timer and hence, time-of-flight was measured. After TOF measurement, acoustic velocities were calculate by

$$C_T = \frac{S}{TOF}$$

where C_T is tree acoustic velocity (m/s), and S is distance between the two probes (sensors) (m).

Tree measurements were taken from a randomly selected side of the tree trunk. Three readings were collected from each tree to derive average acoustic velocity. Diameter at breast height (DBH) of each tree was also measured.

Fractometer device developed by IML was used to determine the bending fracture strength and compression strength of the trees. This device breaks a radial increment core, 5 mm in diameter, under bending and compression loads. The bending angle, bending load at fracture and compression strength are determined. A wood core was extracted from the breast height of each tree trunk in a diameter of 5 mm with an increment borer. The wood cores were then placed in the corresponding clamping device, aligned according to its fibre direction, and loaded with bending and compression forces. The load is transmitted to the core sample by slowly and continuously pushing the two lever arms and it has to be increased until the wooden core fails or brakes. The maximum transmitted load equates to the failure load (Figure 3).

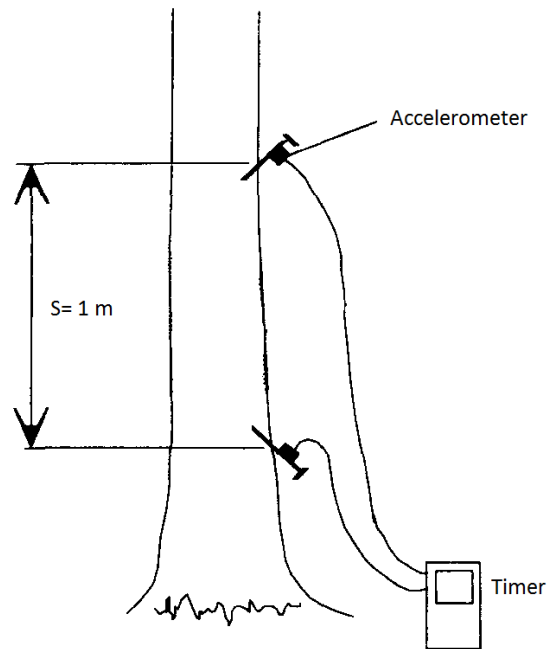


Figure 2— Experimental setup for acoustic measurements.



Figure 3— Experimental setup for radial bending (left) and compression parallel to grain (right) test on the increment cores.

Data analysis

Analysis of Variance (ANOVA) was used to determine the effect of clone differences and the planting density on the acoustic velocity of standing trees and the mechanical properties measured on the increment cores. Duncan test was applied to determine the homogeneity groups. In addition, t-test was applied to compare the poplar clones grown in Izmit and Ipsala.

Results and discussions

Table 1 shows the results of the acoustic velocity measurements of the poplar trees from Izmit district. The letters below the numbers indicate the homogeneity groups. The results showed that the acoustic velocity values of the trees changed significantly between the clones at a confidence level of 95% in Izmit district. The acoustic velocity of the I-214 and I-45/51 clones (*P. nigra*×*P. deltoides*) were found significantly lower than the I-77/51 (*P. deltoides*), S307 and 89M clones (*P. nigra*) at low planting densities (9 m² and 12 m²) where the latter clones were identical. However, when the planting density increased to 4.5 m² and 6 m² the differences between the clones have become insignificant except for S307 clone which had significantly higher velocity than the others. When the effect of planting density within the clones is examined, a significant decrease is seen in the velocities of I-214 and I-45/51 clones with the decreasing planting density to 9 m² and 12 m², while it was not found a comprehensible change in the velocity values depending on the planting density in the other clones. This finding also explains why I-214 and I-45/51 clones had significantly lower velocity values than others when planted sparsely while there were no remarkable difference between the clones when planted denser.

Table 1—Acoustic velocity measurements results for Izmit district

Clones	Planting density (m ²)			
	4.5	6	9	12
I-214	3861,8 (263,9) DE*	3784,2 (280,4) CD	3610,8 (251,1) B	3437,2 (228,1) A
I-45/51	3840,8 (338,8) DE	3646,8 (244,7) BC	3659,1 (271,7) BC	3538,2 (140,6) AB
I-77/51	3811,5 (296,8) CD	4123,4 (236,6) FGH	4162,0 (220,4) GH	4004,8 (198,2) EFG
S307	4198,3 (250,2) H	3991,4 (277,4) EF	4118,1 (175,9) FGH	3897,7 (192,5) DE
89M	3843,3 (248,7) DE	3775,6 (330,8) CD	3992,3 (235,3) EF	3844,3 (285,6) DE

*p<0,05

Table 2 shows the results of the acoustic velocity measurements gathered from Ipsala district. As in the Izmit plots, significant differences were found between the poplar clones in Ipsala plots. The acoustic velocity of the I-214 and I-45/51 clones (*P. nigra*×*P. deltoides*) were found significantly lower than the others while I-77/51 and S307 clones generally had the highest velocity values at all planting densities. When we examined the effect of planting density on the acoustic velocity, the results were a little bit confused. Nevertheless, it can be said with the exception of I-214 clone that the highest velocity values were obtained at the lowest planting space (4.5 m²) and inversely the lowest velocities were obtained at the highest planting space (12 m²).

Table 2—Acoustic velocity measurements results for Ipsala district

Clones	Planting density (m ²)			
	4.5	6	9	12
I-214	3763,4 (448,3) BC	3625,3 (193,5) B	3692,5 (242,9) B	3783,4 (257,4) BC
I-45/51	3891,1 (253,7) CD	3305,4 (220,8) A	3784,2 (267,1) BC	3454,3 (241,9) A
I-77/51	4242,1 (210,0) G	3770,8 (195,0) BC	3954,7 (240,2) D	3752,1 (169,1) BC
S307	4120,9 (193,8) EFG	4183,9 (142,9) FG	4018,2 (165,8) DE	3743,2 (207,5) BC
89M	4053,6 (344,7) DEF	3758,4 (321,9) BC	3906,4 (204,7) CD	3632,6 (165,3) B

*p<0,05

Table 3 and Table 4 show the results of radial bending strength and compression strength parallel to grain on the increment cores in Izmit district. As seen on the Tables, the lowest strength values in both bending and compression tests were determined in I-214 and I-45/51 clones which also had the lowest velocity values. However, when the planting space increase to 9 m² and 12 m², the bending strength of I-45/51 were significantly higher than I-214 and identical with the other clones. The strengt values obtained from I-77/51, S307, and 89M clones were relatively close to each other and generally placed in the same homogeneity group at all planting density. When we consider the planting density, even if some significant differences were observed, it can be conclude that the planting density had no comprehensible effect on the strength values determined on the increment cores.

Table 3—Radial bending strength results for Izmit district

Clones	Planting density (m ²)			
	4.5	6	9	12
I-214	6,60 (0,91) A	7,03 (0,46) AB	6,61 (0,61) A	7,63 (1,36) BCD
I-45/51	7,04 (0,69) AB	7,50 (1,28) BC	8,60 (0,83) FGH	8,38 (0,93) EFG
I-77/51	8,61 (0,98) FGH	9,14 (0,87) H	8,78 (0,76) FGH	8,91 (0,62) GH
S307	7,78 (0,78) CDE	8,26 (0,98) EFG	8,76 (0,91) FGH	8,63 (0,75) FGH
89M	7,38 (1,09) BC	8,46 (1,35) FG	8,17 (0,65) DEF	8,36 (1,30) EFG

*p<0,05

Table 4—Parallel compression strength test results for Izmit district

Clones	Planting density (m ²)			
	4.5	6	9	12
I-214	17,44 (1,60) AB	17,79 (1,41) BC	17,51 (1,22) AB	16,52 (2,08) A
I-45/51	17,64 (1,28) ABC	16,49 (1,27) A	18,79 (2,20) C	17,72 (1,39) BC
I-77/51	21,58 (1,86) EF	22,40 (1,61) F	21,61 (1,36) EF	22,02 (1,57) F
S307	22,58 (2,02) F	20,57 (1,67) DE	21,75 (1,57) EF	22,23 (1,71) F
89M	20,39 (1,93) D	21,72 (2,91) EF	21,48 (2,17) DEF	20,35 (2,35) D

*p<0,05

Table 5 and 6 show the results of radial bending strength and compression strength parallel to grain on the increment cores in Ipsala plots. It is clear from the tables that the lowest strength values in both bending and compression tests were determined in I-214 and I-45/51 clones at all planting spaces. The other clones were found close to each other and higher than I-214 and I-45/51 clones in terms of the strength values. As mentioned before similar trend was also observed in velocity values. Conflicting results were obtained about the effect of planting density on the strength values of hybrid poplars. Although the some significant differences were found between the planting densities, the results were not comprehensible. For instance, the compression strength of S307 clone tends to be low as the planting space increase, but we couldn't observed the same trend in radial bending. No significant differences were found between the compression strength of I-77/51 depending on the planting density. I-214 and I-45/51 clones reached the highest compression strength at 6 m² planting space, while I-77/51 and 89M clones reached the highest value at 9 m².

Table 5—Radial bending strength results for Ipsala district

Clones	Planting density (m ²)			
	4.5	6	9	12
I-214	8,93 (1,08) CDE	8,37 (0,92) ABC	8,07 (0,67) A	8,35 (0,95) ABC
I-45/51	8,85 (0,95) BCDE	8,65 (0,66) ABCD	8,19 (0,56) AB	8,66 (0,73) ABCD
I-77/51	10,13 (0,86) HIJ	9,39 (0,72) EFG	8,93 (1,14) CDE	9,98 (0,84) GHI
S307	10,67 (1,11) J	8,96 (0,59) CDE	9,56 (0,98) EFGHI	9,72 (0,76) FGHI
89M	9,45 (1,82) EFGH	9,23 (0,86) DEF	8,39 (1,14) ABC	10,21 (1,07) IJ

*p<0,05

Table 6—Parallel compression strength test results for Ipsala district

Clones	Planting density (m ²)			
	4.5	6	9	12
I-214	17,45 (0,96) A	19,27 (1,40) C	18,15 (1,74) ABC	17,07 (1,82) A
I-45/51	18,87 (1,19) BC	19,13 (1,60) C	17,99 (1,33) AB	18,94 (1,33) BC
I-77/51	22,74 (1,38) G	21,59 (1,49) EFG	22,67 (1,49) G	21,79 (1,41) FG
S307	22,47 (1,56) FG	22,33 (1,31) FG	21,40 (1,64) DEF	20,40 (1,14) D
89M	21,58 (1,28) EFG	20,62 (2,21) DE	22,51 (1,93) FG	21,36 (1,48) DEF

*p<0,05

Also the confusing results were observed when compared to the same clones in terms of the growing site. For example, for I-214 clone, according to t-test results, there was no significant difference between Izmit and Ipsala at 4.5 m², 6 m², and 9 m² spacing with regards the acoustic velocity while significant difference was found at 12 m². However, in I-77/51 clone, there were significant differences between Izmit and Ipsala at all planting density. Nevertheless, the velocity values obtained from two plots ranged from 3437 m/s to 4198 m/s for Izmit and ranged from 3305 m/s to 4242 m/s for Ipsala. Thus it can be say that the velocity values obtained from Izmit and Ipsala district were too close to each other. The same situation was true for radial bending and compression strength values.

When a general evaluation is made between the acoustic velocity and the bending and compression strength obtained from clones, it seem that the compression strength values were verified the acoustic velocity measurements where the values of I-214 and I-47/51 clones were significantly lower than the others while the other clones were close to each other. However, the same clear relation could not been observed between the velocity and radial bending strength.

Conclusions

The acoustic velocity values of the hybrid poplar trees changed significantly between the clones at a confidence level of 95% in both growing sites. In general, the acoustic velocity of the I-214 and I-45/51 clones were found significantly lower than the I-77/51 (*P. deltoides*), S307 and 89M clones (*P. nigra*). The same results were also obtained by the radial bending and parallel compression strength tests performed on the increment cores where the lowest strength values were determined again in I-214 and I-45/51 clones. Conflicting results were obtained about the effect of plant density on both the velocity and the strength values in both growing sites. We could not find a clear difference in velocity values or strength values of the poplar clones between Izmit and Ipsala growing sites. The parallel compression strength test performed on the increment core was more compatible with the acoustic measurements than the radial bending test.

Acknowledgments

“This work was supported by Scientific Research Projects Coordination Unit of Istanbul University. Project number BEK-2017-25531.

References

Beaudoin, M.; Hernandez, R.E.; Koubaa, A. [and others]. 1992. Interclonal, intraclonal and within-tree variation in wood density of poplar hybrid clones. *Wood and Fiber Science*. 24(2): 147-153.

Chantre, G. 1995. Variabilite clonale des caracteristiques technologiques chez le peuplier. *CR Acad Agric Fr*. 81 (3): 207-224.

DeBell, D.S.; Singleton, R.; Harrington, C.A. [and others]. 2002. Wood density and fiber length in young populus stems: relation to clon, age, growth rate, and pruning. *Wood and Fiber Science*. 34(4): 529-539.

FAO International Poplar Commission Report. 2012. Improving lives with poplars and willows, synthesis of country progress reports - activities related to poplar and willow cultivation and utilization-2008 through 2011.

Goyal, G.C.; Fisher, J.J.; Krohn, M.J. [and others]. 1999. Variability in pulping and fiber characteristics of hybrid poplar trees due to their genetic makeup, environmental factors and tree age. *Tappi Journal*. 82 (5): 141-147

Hernandez, R.E.; Koubaa, A.; Beaudoin, M. [and others]. 1998. Selected mechanical properties of fast-growing poplar hybrid clones. *Wood and Fiber Science*. 30(2): 138-147.

Ivkovich, M. 1996. Genetic variation of wood properties in Balsam Poplar (*Populus balsamifera* L.). *Silvae Genetica*. 45(2): 119-124.

Matyas, C.; Peszlen, I. 1997. Effect of age on selected wood quality traits of poplar clones. *Silvae Genetica*. 46(2-3): 64-72.

Peszlen, I. 1998. Variation in specific gravity and mechanical properties of poplar clones. *Drevarsky Vyskum*. 43(2): 1-17.

Wang, X.; Carter, P.; Ross, R.J. [and others]. 2007. Acoustic assessment of wood quality of raw forest materials – a path to increased profitability. *Forest Products Journal*. 57(5): 6-14.



Session 2

**Evaluation of
Structural Timber**

Experimental Study on Material Damping in Lumber Boards for CLT Panels

Alexander Opazo Vega*

Civil and Environmental Department, University of Bío-Bío, Concepcion, Chile, aopazove@ubiobio.cl

Franco Benedetti Leonelli

Civil and Environmental Department, University of Bío-Bío, Concepcion, Chile, fbenedet@ubiobio.cl

Sergio Alarcon Campos

Civil and Environmental Department, University of Bío-Bío, Concepcion, Chile, seralarc@alumnos.ubiobio.cl

* Corresponding author

Abstract

Cross laminated timber (CLT) is a multi-layer wooden panel that has received much attention in the last two years in Chile. Dimensional lumber is the main input material and it is desirable to know its material damping, specially for vibration performance assessment. The present study focuses on the evaluation of material damping in lumber board specimens with dimensions that are typical for CLT panels. Using the impact test method, 60 lumber boards made out of Radiata Pine were subjected to flexural vibrations. The tests involved different visual grades and lumber board orientations (edgewise and flatwise). A total of 240 material damping evaluations were performed, through Logarithmic Decrement and Circle Fit methods. The findings of this study suggest that lumber boards for CLT panels have low material damping ratios, with mean value of 0.72%. Lumber boards with lower visual grades have the highest damping ratios for edgewise vibration. On the other hand, both logarithmic decrement and circle fit methods are useful for estimating material damping ratios, with good accuracy. Finally, the exhaustive material damping database presented in this work may improve knowledge about damping mechanisms and vibration performance of CLT panels

Keywords: material damping, lumber boards, comfort properties, transverse vibration

Introduction

Cross laminated timber (CLT) is a multi-layer wooden panel that has received much attention in the last two years in Chile. Dimensional lumber is the main input material and it is desirable to know its material damping, especially for vibration performance assessment (Karacabeyli and Douglas, 2013).

Material damping is defined as internal friction by transformation of mechanical energy into heat during cyclic stress (Woodhouse, 1998; Ouis, 2002). When damping is close to resonance, it will have a large beneficial influence on the structural response since it decreases both the amplitude of steady-state oscillations as well as the duration of transient oscillations (Labonnote et al, 2013)

What is known about wood material damping is largely based on musical instruments studies (Fukada, 1950; Fukada, 1951; Ono and Norimoto, 1985; Nakao et al 1985; Foster, 1992; Bremaud et al, 2011). In

the last few years, much more information on material damping has become available for an acoustic use of timber (Obataya et al, 2000; Bucur, 2006; Spycher et al, 2008), or else concerning the mechanical pulping use of timber (Havino, 2009).

However, has been little discussion on the damping properties of timber elements for structural use. Some preliminary work was carried out in the early 1970s (Yeh et al, 1971). They reported material damping values on real-sized wood frames, by free flexural vibration tests. In a major advance in 2013, Labonnote et al provide new values for material damping of timber beams that are typical for common floor structures. They tested 22 timber beams, of two different types, in flexural vibrations through the impact test method. Their damping evaluations were performed for various configurations, which included different spans as well as orientations.

The present study focuses on the evaluation of material damping in lumber board specimens with dimensions that are typical for CLT panels. About sixty *Pinus Radiata* D.Don lumber boards (33x145x4900mm), with different visual and mechanical grades (INN, 2005), were tested in transverse vibration according ASTM D6874-12 standard (ASTM, 2012). A total of 240 material damping evaluations were performed, through logarithmic decrement and circle fit methods (Ewins, 2000; Brandt 2011). Due to the scarce quantification of damping properties for structural use, the intention of the present study is to provide new and reliable values for material damping of lumber boards that are typical for CLT panels.

Materials and Methods

Experimental Setup

A total of 60 *Pinus Radiata* D.Don lumber boards, with different visual grades, were tested in transverse vibration according ASTM D6874-12 standard. The nominal dimensions and properties are summarized in Table 1, and they represent typical dimensions in common lumber boards for Chilean CLT panels

Table 1— Nominal dimensions and properties of the tested lumber boards

Property	Lumber type 1	Lumber type 2	Lumber type 3
Visual grade (worst to better)	G2	G1	GS
Number of specimens	20	20	20
Length (mm)	4900	4900	4900
Cross section (mm x mm)	33x145	33x145	33x145
Mean density (kg/m ³)	479	488	513
Mean moisture content (%)	11	11	12
Mean modulus of elasticity (GPa)	10.52	12.00	13.11

Each lumber board was simply supported with a symmetric overhang. Supports used were constructed of either rigid steel tripods or sections of thick steel cylinders. Teflon sheets were added in between the timber beam, and the steel supports in order to minimize friction and other sources of structural damping. Unless otherwise stated, all boards were measured for 2 orientations: flatwise and edgewise, as shown in Figure 1.

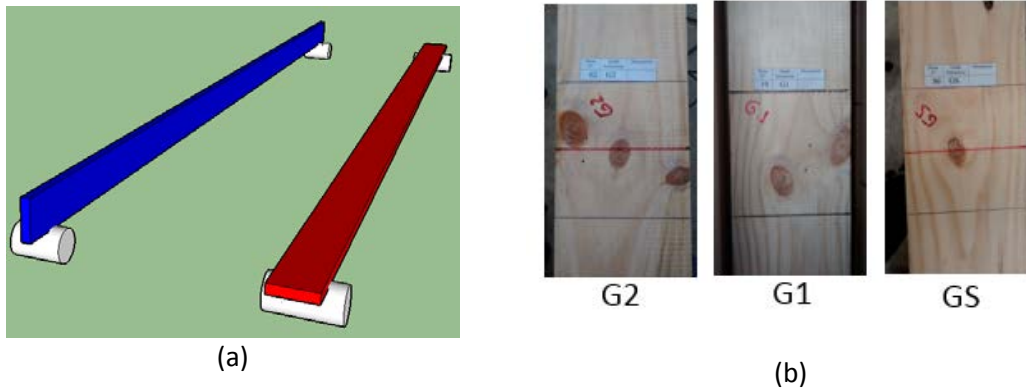


Figure 1—(a) Board orientations. (b) Example of visual grades of boards

Experimental evaluations of material damping ratios

A general-purpose modal analysis impact hammer was used to set the board into motion. A soft tip was employed in order to excite lower frequencies. Transient vibrations due to modal hammer impact were recorded by one industrial, ceramic shear, IMI accelerometer screwed into the board. The load and acceleration time series were then digitalized and processed by a compactDAQ system. The sampling frequency was fixed to 1652 Hz, and 10 s data were recorded for each impact. The experimental setup is displayed in Figure 2.

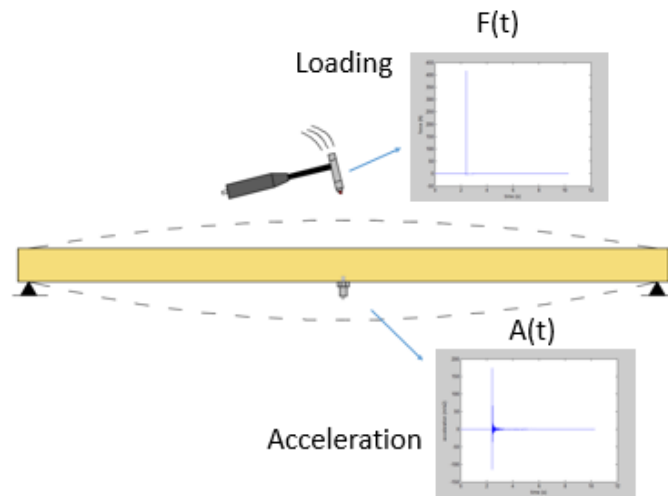


Figure 2— Experimental setup for material damping ratio evaluation

Logarithmic Decrement (LD) and Circle Fit (CF) methods were used for determining the fundamental frequency and damping ratios. LD uses the exponential regression line of the maximum amplitudes in the acceleration time history (Brandt, 2010), while CF uses the frequency response function between acceleration and force, through fast Fourier transformations (FFT) (Ewins, 2000). Figure 3 shows typical curves for both methods.

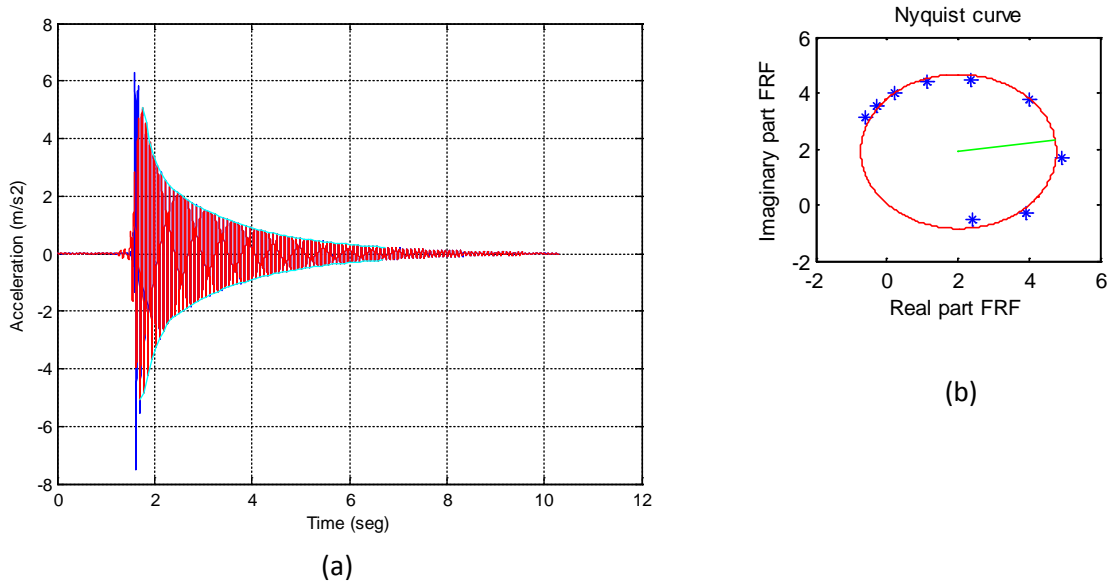


Figure 3— (a) Acceleration time history used for LD method. (b) Frequency response function used for CF method Experimental setup for material damping ratio evaluation

Results and Discussion

A total of 240 material damping evaluations were performed, through LD and CF methods, for edgewise (EW) and flatwise (FW) orientations. The mean value for material damping ratio was 0.72%, and significant difference was found between G2 and GS visual grades in FW orientation. On the other hand, no significant difference was observed between LD and CF methods, as shown in Figure 4.

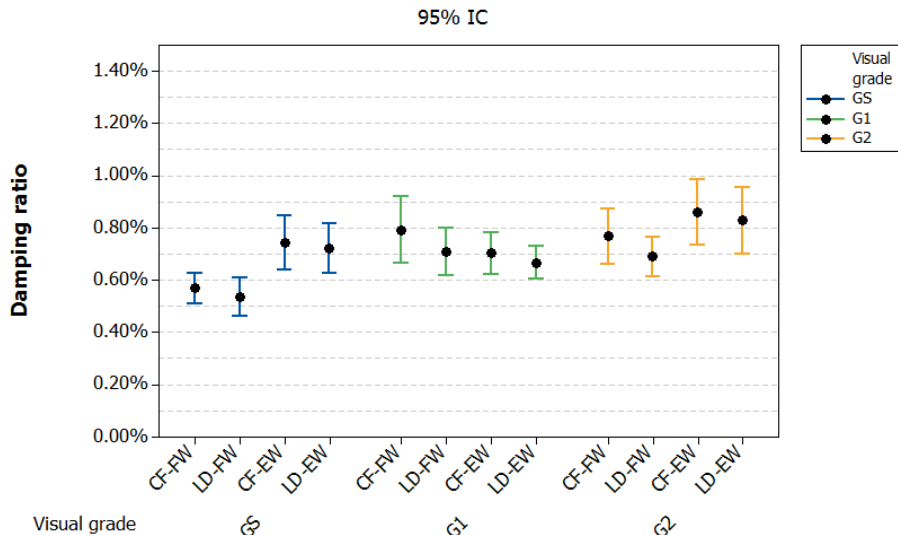


Figure 4— Confidence intervals (95%) for damping ratio evaluations

Conclusions

The findings of this study suggest that lumber boards for CLT panels have low material damping ratios, with mean value of 0.72%. Lumber boards with lower visual grades have the highest damping ratios for edgewise vibration. On the other hand, both logarithmic decrement and circle fit methods are useful for estimating material damping ratios, with good accuracy. Finally, the exhaustive material damping database presented in this work may improve knowledge about damping mechanisms and vibration performance of CLT panels.

Acknowledgments

This work was carried out within the framework of a DIUBB 151714 2/R research project and was partly sponsored by Civil and Environmental Engineering Department of Bio Bio University.

References

- ASTM D6874-12. 2012. Standard Test Methods for Nondestructive Evaluation of Wood-Based Flexural Members Using Transverse Vibration, ASTM International, West Conshohocken, PA.
- Brandt, A. 2011. Noise and Vibration Analysis: Signal Analysis and Experimental Procedures. John Wiley & Sons, Ltd.
- Bre´maud I, Gril J, Thibaut B. 2011. Anisotropy of wood vibrational properties: dependence on grain angle and review of literature data. *Wood Sci Technol* 45(4):735–754
- Bucur V. 2006. Acoustics of wood, 2nd edn. Springer, Berlin
- Ewins, D. J. 2000. Modal testing: theory, practice and application. Research Studies Press LTD., Baldock, Hertfordshire, England.
- Foster CG. 1992. Damping and poisson factor behaviour in timber considered as an orthotropic material: Part 1: the loss factor. *J Sound Vib* 158(3):405–425
- Fukada E. 1950. The vibrational properties of wood I. *J Phys Soc Jpn* 5:321–327
- Fukada E. 1951. The vibrational properties of wood II. *J Phys Soc Jpn* 6:417–421
- Havimo M. 2009. A literature-based study on the loss tangent of wood in connection with mechanical pulping. *Wood Sci Technol* 43(7):627–642
- INN. 2005. Norma Chilena Oficial Nch1207 of.2005, “Pino Radiata – Clasificación visual para uso estructural – Especificaciones de los grados de calidad”. Instituto Nacional de Normalización (INN).
- Karacabeyli, E. and Douglas, B. 2013. CLT Handbook Cross – Laminated Timber. US Edition.
- Labonnote, N., Rønquist, A., & Malo, K. A. 2013. Experimental evaluations of material damping in timber beams of structural dimensions. *Wood science and technology*, 47(5), 1033-1050.

Nakao T, Okano T, Asano I. 1985. Theoretical and experimental analysis of flexural vibration of the viscoelastic Timoshenko beam. *J Appl Mech* 52:728–731

Obataya E, Ono T, Norimoto M. 2000. Vibrational properties of wood along the grain. *J Mater Sci* 35:2993–3001

Ono T, Norimoto M. 1985. Anisotropy of dynamic young's modulus and internal friction in wood. *Jpn J Appl Phys* 1(24):960–964

Ouis D. 2002. On the frequency dependence of the modulus of elasticity of wood. *Wood Sci Technol* 36(4):335–346

Woodhouse J. 1998. Linear damping models for structural vibration. *J Sound Vib* 215(3):547–569

Yeh CT, Hartz BJ, Brown CB. 1971. Damping sources in wood structures. *J Sound Vib* 19(4):411–419

Effect of Visual Characteristics on Stiffness and Strength in Southern Pine No. 2 2 × 8 Lumber

Tâmara S. F. A. França

Department of Sustainable Bioproducts, Mississippi State University, Starkville, MS, USA,
tsf97@msstate.edu

Frederico J. N. França

Department of Sustainable Bioproducts, Mississippi State University, Starkville, MS, USA,
fn90@msstate.edu

R. Daniel Seale

Department of Sustainable Bioproducts, Mississippi State University, Starkville, MS, USA,
rds9@msstate.edu

Abstract

Southern pine is one of the most used softwood resource in the United States, which is commonly used in light frame construction. The use of wood as structural lumber requires a suitable method to ensure the strength and stiffness of the material. The majority of southern pine lumber is visually graded. Visual grading is based on the effect of growth characteristics have on the performance properties of structural lumber. Pith, number of rings per inch (RPI), and percentage of latewood (LW) are growth characteristics that can be visually identified, and its presence may indicates higher percentage of juvenile wood. The objective of this study was to evaluate the effect of pith (not included in the visual grading rules), RPI, and LW on specific gravity (SG), modulus of elasticity (MOE), and modulus of rupture (MOR). A total of 291 specimens of southern pine No. 2 2 × 8 lumber were used. Near half (54.7%) of the specimens tested contained pith, and averaged 4.5 RPI and 42.5 % latewood (LW) and met or exceeded the strength requirements for southern pine No. 2 grade. All growth characteristics (pith, RPI, and LW) had significant effect on SG, MOE, and MOR. However, the improvement in SG, MOE, and MOR yielded using RPI and LW as an indicator of stronger boards was higher than using pith.

Keywords: pith, rings per inch, percentage of latewood, mechanical properties

Introduction

The use of wood as structural lumber requires a precise grading method to ensure its strength and stiffness values (Blass and Frese 2004). There are two main methods of grading lumber; visual and mechanical grading systems. In the U.S., the most commonly used method is visual grading (Kretschmann and Hernandez 2006).

The visual grading system classifies lumber into grades based on characteristics of knots, wane, and warp which decrease lumber value and serviceability (Kimball and Lowery 1967). In addition to these characteristics, pith, annual rings and percent of latewood are growth characteristics that can also be used to classify lumber into different grades (Kretschmann 2010).

Visual grading was first developed in or around 1927 and it was based on lumber that contained a large percentage of mature wood from old-growth trees with a high percentage of clear wood. Juvenile wood

was not included in the visual grading system (Madsen and Nielsen 1992). To meet the demand for wood products, many landowners supply trees from managed plantations. The growth rate of southern pine is classified as fast-growing in plantations and the success of these plantations is largely due to an extensive silviculture program. Silviculture practices have significant positive impacts on the growth and yield of southern pines (Antony et al. 2015).

Any change in the growth of timber results changes in wood properties and consequently in the quality of wood products (Zobel and Van Buijtenen, 1989). Fast-grown plantations tend to be harvested in short age rotations which results in higher proportions of juvenile wood. Juvenile wood typically exhibits lower stiffness and strength and may not meet the performance requirements for dimension lumber (Larson et al. 2001; MacPeak et al. 1990; Kretschmann 2010).

A simple and fast way to identify lumber that contains high percent of juvenile wood is the presence of pith. However, this characteristic is not included in the visual grading rules (SPIB 2014). Many authors have reported that presence of pith can be an indicator of juvenile wood, which affects the density of the piece. In many cases, it is possible to identify the high strength pieces by eliminating those pieces that are low in density (Winandy and Boone 1988; Kretschmann and Bendtsen 1992; Tong et al. 2009; Dahlen et al, 2014). The objective of this study was to evaluate the effect of pith, number of rings per inch (RPI) and percentage of latewood (LW) on specific gravity, and bending strength and stiffness of commercially produced southern pine No. 2 2×8 lumber.

Material and Methods

A sample of southern pine visually graded weight by production per region was collected from 15 of the original 18 southern pine growth regions (Jones 1989) (Figure 1). A total of 291 pieces of 2×8 No. 2 grade structural lumber was collected. The lumber was grade stamped from either the Southern Pine Inspection Bureau (SPIB) or Timber Products Inspection (TP) grading agencies. The sampling mimicked the in-grade lumber sampling used to derive design values by SPIB. No. 2 grade lumber was selected because it accounts for the largest volume of southern pine produced. A certified grader from either SPIB or TP regraded all specimens to assure that the sample were actually No.2 grade.

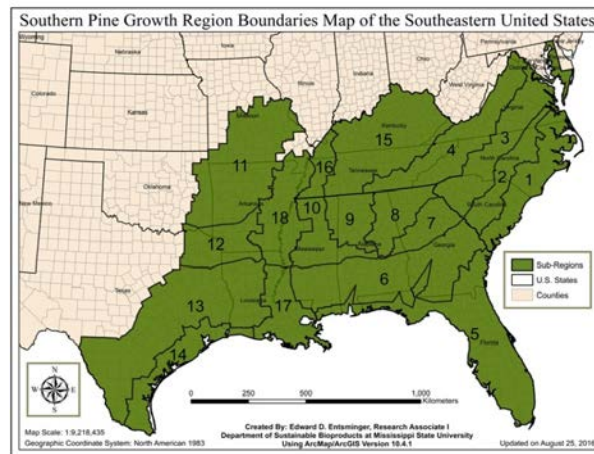


Figure 1. Map of southern pine growth regions of southern pine

The RPI and LW were measured at each end of each piece according SPIB (2014), and an average value for RPI and LW was calculated and recorded for each piece. All six faces of the specimens were inspected in order to evaluate the presence of pith. If pith appeared on either half of the length it was

considered as containing pith. The dimensions, weight, and moisture content (MC) of each specimen was recorded.

Edgewise bending tests were performed according to ASTM D 198 (2014c) via four-point loading on an Instron testing machine utilizing Bluehill 3 software, with a depth/span ratio of 17 to 1. The specimens were oriented randomly in the test fixture to better represent the actual in-service use. The rate of loading was in accordance with ASTM D 4761 (2014b). The deflection was measured by a deflectometer in the mid span to determine MOE. MOR was calculated from the maximum load.

The adjustments of each piece for MOE to standard loading conditions, were according to ASTM D 1990 (2014d), ASTM D 2915 (2014a), and Evans et al. (2001). Then, data was adjusted to 15% MC and adjusted to four-point uniform loading. The MOR of each specimen was adjusted to 15% MC according to ASTM D 1990 (2014d). The allowable design bending strength (F_b) for the sample was calculated using the nonparametric 5th percentile at a 75% confidence interval and divided by 2.1 safety and load duration factor according to ASTM D 2915 (2014a) and Evans et al. (2001). The results found in this research for MOE and F_b were compared to the new and prior design value (SBPIB 2013).

The statistical analyses and associated graphs were developed in SAS 9.4 (SAS Version 9.4, 2013) according to ASTM D 2915 (2014a). The mean, and coefficient of variation (COV) for RPI, LW, SG, MOE and MOR were calculated. Pith, RPI, and LW were divided into groups to evaluate their effects, if any, on mechanical properties. Pith was divided into groups, specimens containing no pith, and specimens containing pith.

The cut off point for RPI and LW groups followed SPIB rules. For souther pine lumber, No. 2 grade should have approximately 4 or more annual rings per inch on either end of the piece, or 1/3 average of summerwood. The two RPI groups were called upper RPI (specimens with RPI higher or equal to 4.0), and lower RPI (specimens with RPI lower than 4.0). The same was done for LW, upper LW group (specimens with LW higher or equal to 33.0%), and lower LW group (specimens LW lower than 33.0%). Statistically significant differences for SG, MOE and MOR between pith, RPI and LW groups were found using PROC GLM at $\alpha = 0.05$ level.

Results and Discussion

The summary statistics for pith, number of rings per inch, and percentage of latewood are shown in Table 1. Approximately, half (54.5 %) of the specimens contained pith, with an average of 4.5 RPI, and 42.5 % of latewood. The 2 × 8's specimens collected met the number of rings per inch, and percentage of latewood required for No. 2 grade southern pine lumber (SPIB 2014).

Table 1. Summary statistics for pith, number of rings per inch (RPI), percentage of latewood (LW), specific gravity (SG), modulus of elasticity (MOE), modulus of rupture (MOR) of No. 2 2 × 8 southern pine lumber

Overall	Mean	Median	COV
Pith (%)	54.7*	–	–
RPI	4.5	3.7	57.0
LW (%)	42.5	41.1	25.1

*Percentage of samples that contained pith

The effect of pith, number of rings per inch, and percentage of latewood on specific gravity, modulus of elasticity (MOE), modulus of rupture (MOR) are shown in Table 2. The SG, MOE and MOR mean values were 0.54, 10.5 GPa, and 39.0 MPa, respectively. The overall MOE yielded in this study exceeded the

new design value (9.7 GPa), and met the old design value (11.0 GPa) after rounding according to ASTM D1990 (2016).

Table 2. Effect of pith, number of rings per inch, and percentage of latewood on specific gravity (SG), modulus of elasticity (MOE), modulus of rupture (MOR) in No. 2 2×8 southern pine lumber

Variable	Overall	Presence of Pith		Rings per Inch		Percentage of Latewood	
		No Pith	Pith	≥ 4.0	< 4.0	≥ 33.0	< 33.0
SG	0.54 (10.0%)	0.55 (10.0%)	0.52 (9.0%)	0.57 (10.5%)	0.52 (8.3%)	0.55 (9.3%)	0.50 (7.8%)
MOE	10.6 ^a (20.6%)	10.9 ^a (19.4%)	10.0 ^b (21.1%)	12.0 ^a (18.3%)	10.0 ^b (19.1%)	11.0 ^a (19.3%)	9.2 ^b (18.4%)
MOR	39.0 (33.2%)	40.3 (36.1%)	37.1 (27.7%)	44.4 (36.2%)	36.8 (29.4%)	40.5 (33.6%)	34.6 (27.8%)

Coefficient of variation (shown in parenthesis)

*ns indicates no statistical difference at $\alpha = 0.05$ within groups

^aIndicates MOE value met 2011 design value (11.0 GPa) after rounding to nearest 0.7 GPa ASTM D1990 (2016)

^bIndicates MOE value met 2013 design value (9.7 GPa) after rounding to nearest 0.7 GPa ASTM D1990 (2016)

Specimens in the upper RPI yielded the higher MOE values (12.0 GPa), and exceeded the current (9.7 GPa) and previous (11.0 GPa) design value required for No. 2 grade southern pine lumber (SPIB 2014). Specimens in the upper LW (11.0 GPa) also exceeded the current design value and met the previous design value. The MOE yielded for lumber that contained pith (10.0 GPa), lumber with RPI lower than 4.0 (10.0 GPa), and lumber with LW lower than 33% (9.2 GPa) met the new design value only.

There was a significant effect of pith in SG, MOE, and MOR (Figure 2). The SG of specimens that contained pith was significantly higher than specimens that contained no pith, 0.55 vs 0.52, respectively. The MOE found for specimens that contained no pith were significantly higher than specimens with pith (10.9 vs 10.0 GPa). Same trend was found for MOR, where specimens with no pith were significantly higher than specimens with pith (40.3 vs 37.1 MPa). The results of this research were similar to the results reported by Dahlen et al. (2014), where specimens without pith were higher in SG (0.50 vs 0.44), MOE (11.9 vs 8.8 GPa), and MOR (53.4 vs 35.8 MPa) than specimens with pith.

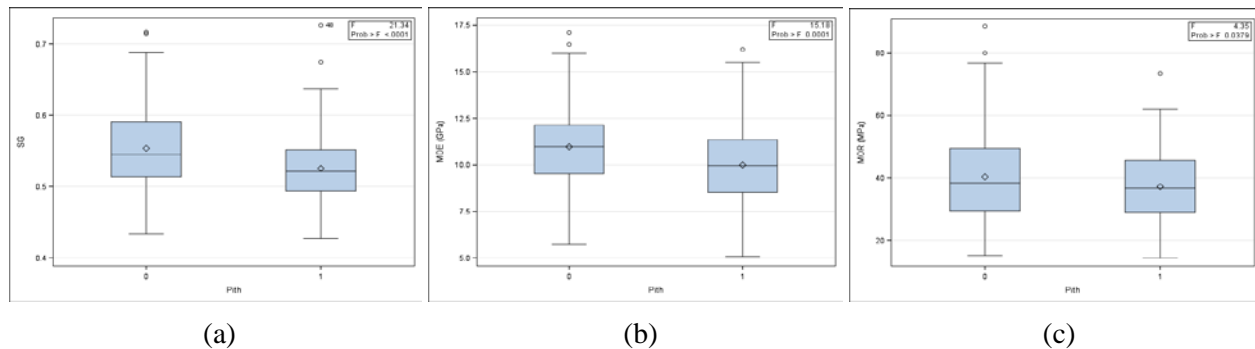


Figure 2. Boxplots of specimens contacting pith and containing no pith for (a) specific gravity; (b) modulus of elasticity (MOE); (c) modulus of rupture (MOR)

The RPI groups also had a significant effect on SG, and bending properties (Figure 3). The SG (0.57 vs 0.52), MOE (12.0 vs 10.0 GPa), and MOR (44.4 vs 36.8 MPa) of specimens that had RPI higher or equal to 4.0 were higher than specimens that had RPI lower than 4.0. For LW, specimens with LW equal or higher than 33% were significant higher in (0.55 vs 0.50), MOE (11.0 vs 9.2 GPa), and MOR (40.5 vs 34.6 MPa) (Figure 4).

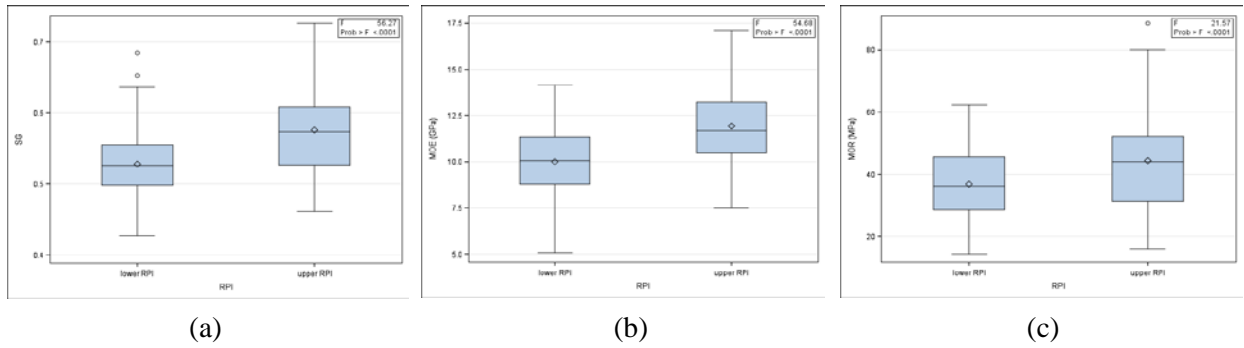


Figure 3. Boxplots of lumber in upper and lower classes of rings per inch for (a) modulus of elasticity (MOE); (b) and modulus of rupture (MOR) of No. 2 2 × 4 southern pine lumber

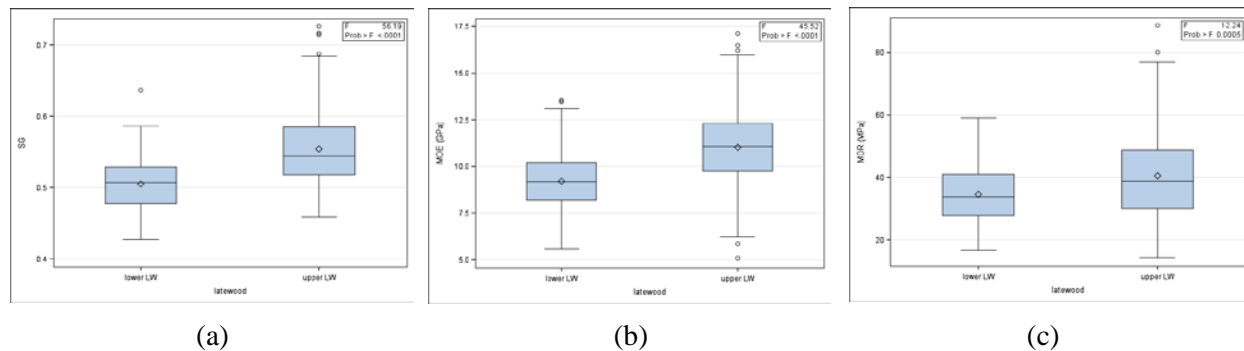


Figure 4. Boxplots of lumber in upper and lower classes of percentage of latewood for (a) modulus of elasticity (MOE); (b) and modulus of rupture (MOR) of No. 2 2 × 4 southern pine lumber

Table 3 shows the improvement in SG, MOE, and MOR of specimens that contained no pith, had upper RPI higher or equal to 4.0, and LW higher or equal to 33%, against specimen with pith, RPI lower than 4.0, and LW lower than 33%.

Table 3. Improvement of pith, number of rings per inch, and percentage of latewood on specific gravity, modulus of elasticity, modulus of rupture in No. 2 2 × 8 southern pine lumber

Variable	SG	MOE	MOR
Pith	5.5%	8.2%	8.0%
RPI	8.7%	16.6%	17.1%
LW	9.1%	16.3%	14.1%

The SG was the variable less influenced by pith, RPI, and LW (5.5%, 8.7%, and 9.1%, respectively). The highest improvement in MOE and MOR was observed between upper RPI and lower RPI groups (16.6% and 17.1%, respectively). For all growth characteristics evaluated, pith had the least percentage of improvement.

Many studies have been shown pith as an indicator of juvenile wood, which is the wood with lower strength and stiffness, and it could be used to improve the visual grading system. Kretschmann and Bendtsen (1992) found that specimens of 2 × 4 loblolly pine with pith were composed of at least 80% of juvenile wood. The authors also reported that pith could be used to improve the visual grading system. Dahlen et al. (2014) studying the effect of pith on SG, and mechanical properties in 2 × 4 southern pine

lumber, reported that lumber without pith was 14% greater SG, 35% greater MOE, and 49% greater MOR, which are higher than the results found in this study.

It appears that the difference on the effect of pith on 2 × 4s and 2 × 8s dues to the width of the specimens. Alexander (2014) observed a significant effect of pith on MOE, and an increase in MOR on specimens with pith when compared to the MOR of specimens with no pith (). The author reported that the increase in MOR may due to the effect of knots sizes rather than presence of pith. Future studies in different sizes and different growth characteristics (knot, slope of grain, wane) would be in order to improve the quality of visual grading system.

Conclusions

- Pith, number of rings per inch, and percentage of latewood had significant effect on specific gravity, and modulus of elasticity, and modulus of rupture
- Specimens that contained no pith, or RPI higher or equal to 4.0, and LW higher or equal to 33.0% LW yielded greater mean values of specific gravity, and bending properties
- Number of rings per inch and percentage of latewood yielded higher improvements in SG, MOE and MOR, than pith
- Pith appears to have less impact on 2 x 8s compared to 2 × 4s

Acknowledgments

The authors wish to acknowledge the support of U.S. Department of Agriculture (USDA), Research, Education, and Economics (REE), Agriculture Research Service (ARS), Administrative and Financial Management (AFM), Financial Management and Accounting Division (FMAD) Grants and Agreements Management Branch (GAMB), under Agreement No. 5B-0202-4-001. Any opinions, findings, conclusion, or recommendations expressed in this publication are those of the author(s) and do not necessarily reflect the view of the U.S. Department of Agriculture.” The authors acknowledge the support from USDA Forest Service Forest Products Laboratory (FPL) in Madison, Wisconsin, as a major contributor of technical assistance, advice, and guidance to this research.

References

AFPA. 2005. National design specification (NDS) for wood construction with commentary and supplement: Design values for wood construction 2005 edition. American Forest & Paper Association, Washington, DC.

Alexander, T. 2016. Investigation of a stress class system for No. 2 2 by 8 southern yellow pine. MS Thesis, Mississippi State University, Mississippi State, Mississippi. 135 p.

American Lumber Standards Committee – ALSC. 2014. American Lumber Standard Committee Board of Review: Board of Review Minutes. February 1, 2013. American Lumber Standards Committee, Germantown, MD.

American Society for Testing and Materials. 2014a. D 2915. Standard practice for sampling and data-analysis for structural wood and wood-based products.. ASTM International, West Conshohocken, PA.

American Society for Testing and Materials. 2014b. D 4761. Standard test methods for mechanical properties of lumber and wood-base structural material. ASTM International, West Conshohocken, PA.

American Society for Testing and Materials. 2014c. D 198. Standard test methods of static tests of lumber in structural sizes. ASTM International, West Conshohocken, PA.

American Society for Testing and Materials. 2014d. D 1990. Standard practice for establishing allowable properties for visually-graded dimension lumber from in-grade tests of full-size specimens. ASTM International, West Conshohocken, PA.

Antony, F.; Schimleck, L. R.; Daniels, R. F.; Clark III, A.; Borders, B. E.; Kane, M. B.; Burkhart, H. E. 2015. Whole-tree bark and wood properties of loblolly pine from intensively managed plantations. *Forest Science*. 61(1):55-66.

Bendtsen, B. A.; Ethington, R. L.; Galligan, W. L. 1972. Properties of major southern pines: Part II Structural properties and specific gravity. USDA Forest Service. Forest Products Laboratory. FPL-GTR-177. Madison, WI. 76 p.

Blass, H.; Frese, M. 2004. Combined visual and machine strength grading. *Holz Roh-Werkst* 62:325–334.

Dahlen, J.; Jones. P. D.; Seale, R. S.; Shmulsky, R. 2014. Bending strength and stiffness of wide dimension southern pine No. 2 lumber. *European Journal of Wood and Wood Products*. 72(6):759-768.

Doyle, D. V.; Markwardt, L. J. 1966. Properties of southern pine in relation to strength grading dimension lumber. USDA Forest Service. Forest Products Laboratory. FPL-64. Madison, WI. 62 p.

Evans, J. W.; Kretschmann, D. E.; Hatfield, C. A.; Green, D. W. 2001. Procedures for developing allowable properties for a single species under ASTM D1990 and computer programs useful for the calculation. USDA Forest Service. Forest Products Laboratory. FPL-GTR-126. 42 p.

Jones, E. 1989. Sampling procedures used in the in-grade lumber testing program. Pages: 11-14. In: DW Green, BE Shelley, and HP Vokey, eds. Proceedings of workshop sponsored by In-grade Testing Committee and Forest Products. Proceedings 47363. USDA Forest Service. Forest Products Laboratory. Madison, WI.

Kimball, K. E.; Lowery, D. P. 1967. Quality of studs dried by high and conventional temperature. *Forest Products Journal* 17(9):81-85.

Kretschmann, D. E.; Hernandez, R. 2006. Grading timber and glued structural members. In: Walker J. ed., *Primary Wood Processing* 2nd ed., pp. 339–390.

Kretschmann, D. E.; Bendtsen, B. A. 1992. Ultimate tensile stress and modulus of elasticity of fast-grown plantation loblolly pine lumber. *Wood and Fiber Science* 24(2):189-203.

Kretschmann, D. E.; Evans, J. W.; Brown, L. 2010. Stress Grades and Design Properties for Lumber, Round Timber and Ties. Pages 7-1-7-16. In: Ross RJ ed., *Wood Handbook*. USDA Forest Service. Forest Products Laboratory. FPL-GTR-190. Madison, WI.

Larson, P. R.; Kretschmann, D. E.; Clark III, A.; Isenbrands J. G. 2001. Juvenile wood formation and properties in southern pine. USDA Forest Service. Forest Products Laboratory. FPL-GTR-129. Madison, WI. 42 p.

MacPeak, M. D.; Burkhart, L. F.; Weldon, D. 1990. Comparison of grade, yield and mechanical properties of lumber produced from young fast-grown and older slow-grown planted slash pine. Forest Products Journal. 40(1):11-14.

Madsen, B.; Nielsen L. F. 1992. Structural Behavior of Timber. Timber Engineering Ltd., North Vancouver, British Columbia, Canada. 405 p.

SAS Institute. 2013. SAS® software, version 9.4. The SAS Institute Inc. Cary, NC.

Southern Pine Inspection Bureau – SPIB. 2014. Standard Grading Rules for Southern Pine Lumber. Southern Pine Inspection Bureau, Pensacola, FL.

Tong, Q-J.; Fleming, R. L.; Tanguay, F.; Zhang, S. Y. 2009. Wood and lumber properties from unthinned and precommercially thinned black spruce plantations. Wood and Fiber Science. 41(2):168-179.

Winandy, J. E.; Boone, R. S. 1988. The effects of CCA preservative treatment and redrying on the bending properties of 2 × 6 southern pine lumber. Wood and Fiber Science 20(3):350-364.

Zobel, B. J.; and Van Buijtenen, J. P. 1989. Wood Variation: Its Causes and Control. Berlin, Springer-Verlag, Heidelberg, DE. 418 p.

Sclerometric and Ultrasound Methods Applied to Timber Beams under Different Stress Levels

Nádia Veiga

Laboratory of Nondestructive Testing - LabEND, College of Agricultural Engineering - FEAGRI - University of Campinas - UNICAMP, Campinas, São Paulo, Brazil, nadiasveiga@gmail.com

Julio Soriano

LabEND, FEAGRI, UNICAMP, Campinas, São Paulo, Brazil, julio.soriano@feagri.unicamp.br

Davi Berling

LabEND, FEAGRI, UNICAMP, Campinas, São Paulo, Brazil, davi-berling@hotmail.com

Rafael Lorensani

LabEND, FEAGRI, UNICAMP, Campinas, São Paulo, Brazil, rafaelmansini@hotmail.com

Paulo Nunes

LabEND, FEAGRI, UNICAMP, Campinas, São Paulo, Brazil, paulo.nunes@feagri.unicamp.br

Abstract

Bending stress intensity on a structural element can influence the results of some non-destructive testing. Three beams with cross-section (50mm x 100mm) and span (2100mm) of *Apuleia leiocarpa* specie were submitted to the four-point bending test, with load intensity varying from 0% to 50% of the estimated rupture load. For each level, sclerometric impacts were applied at nine fixed points on each lateral face and, the ultrasonic wave propagation velocity was determined by these corresponding points. Statistical analysis showed that the results obtained by sclerometric test were equal. On the other hand, for stress levels, we obtained differences in the wave propagation velocity, implying non-homogeneity of the ultrasonic method results. The results of this research indicate that sclerometric method has a potential for estimating some properties independently of the stress level of beams in service.

Keywords: non-destructive testing, sclerometry, incremental loading.

Introduction

External forces applied to structural elements in service changes the internal stress state, which can affect the results of non-destructive testing, such as civil construction inspections. Research is necessary to understand how much the results of each method can be affected.

Presently, there are some studies to evaluate how the non-destructive methods are affected by stress intensity variations on wood structural elements. André *et al.* (2006) observed that it is possible to estimate wood stress level though the non-destructive method NIR (Near-infrared). For this, beams with cross-section 50.8mm x 50.8mm and span equal to 1016mm were submitted to four-point bending test, while NIR was applied between the load points, at tension and compression zones. They estimated tension and compression loads by NIR results and correlated this loads with applied loads, then they

obtained correlation coefficients greater than 0.96, proving that stress state changes the results of the non-destructive test used.

The wood's acoustoelasticity phenomenon, i.e., the relationship between state of stresses and waves propagation velocity through the material was evaluated by Gonçalves and Ormonde (2005). For this purpose, six pinus beams were submitted to flexural test with applied load in the middle of the span (three-point bending). During the application of loads varying from 10 to 50% of the rupture stress, ultrasonic wave velocity was obtained in the tangential direction to the fibers, i.e., the same direction of load application. The authors concluded that compression wave velocity decreases with the increase of the stress.

Ormonde *et al.* (2006) evaluated timber beams of Eucalyptus, measuring 60mm x 200mm x 6000mm and 100mm x 500mm x 1500mm, submitted to four-points bending test, and the ultrasound test was applied to the three wood orthogonal directions. They found correlation coefficients higher than 0.84 between the incremental tension and the ultrasonic velocity. They concluded that the results obtained from the normal direction to the grain were more influenced by bending load variation, therefore being the most recommended direction to evaluate the wood's acoustoelasticity.

In a recently study, Soriano *et al.* (2014) used the non-destructive sclerometric method to estimate wood density. For this, they used prismatic samples with 80mm x 200mm x 300mm extracted from beams of three Brazilian species. Sclerometric impacts were applied on radial, tangential and longitudinal anatomical directions of wood. They concluded that sclerometric indexes have correlation to wood density. Even if each direction needs an equation for estimating the density through sclerometric indexes, all anatomic directions showed correlation coefficients greater than 0.84 between sclerometric indexes and wood density. However, it is questioned if the results of this non-destructive method are affected by the stress intensity of beams.

In this context, this research aimed to evaluate if the increased stress in timber beams could produce some significant difference in sclerometric impact and ultrasonic velocity applied in the perpendicular direction of wood fibers.

Metodology

In this research were used three beams of garapa specie (*Apuleia leiocarpa*), with cross-section 50mm x 100mm and 2500mm of length. From one tip of each beam, a piece measuring 50mm was discarded, and another piece with 150mm was cut off to produce specimens for the compression parallel to grain testing. Thereby, each beam with 2300mm of length were used in four-point loading test as procedure described by American Society for Testing and Materials D198 (2014).

Four-point loading

The four-point loading test was applied as procedure of ASTM D198 (2014). Thus, the support points were placed with 2100mm span, and the distance between each support and load point was equal to 700mm (Figure 1).

To suppress the stress concentration influence on the loading points, the nearest 100mm from the load points were not used, resulting in a central region measuring 500mm for sclerometric and ultrasonic

testing (Figure 1). In this beam region, bending moment action is uniform and shear stress is zero, which is important for the purposes of this research.

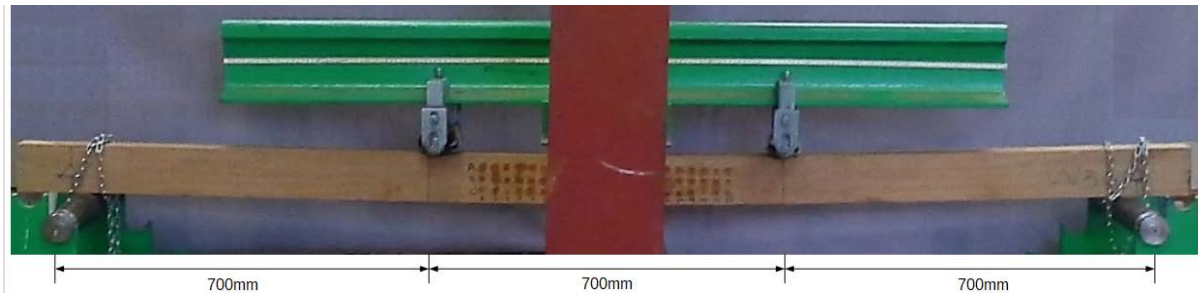


Figure 1. Four-point bending test and points for sclerometry and ultrasonography.

Points for sclerometric and ultrasonic testing

For sclerometry application, in the central span of the beam (500mm) a middle line and two other lines, 25mm distant from the top and bottom of the beam, were marked (Figure 2), as minimum value described by European Committee for Standardization BS EN 12504-2 (2012). Each line contained 21 points with equal stress zone: neutral line, compressive and tensile stress (Figure 3).

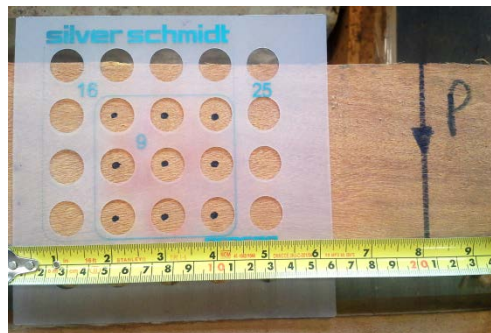


Figure 2. Points for sclerometric and ultrasonic tests

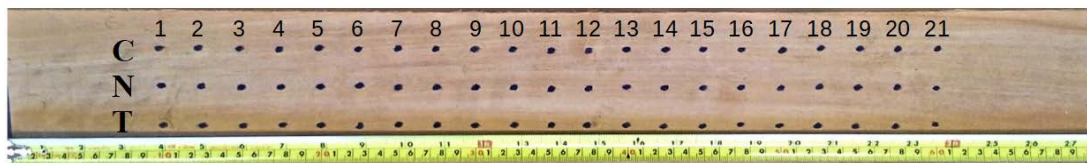


Figure 3. Beam marked at the compressive (C), neutral (N) and tensile (T) zones.

Load levels estimation

To evaluate the effects of varying load levels on sclerometry, seven load levels were preset accordingly to the fiber-parallel compression load. For this purpose, three specimens obtained from the beams with dimensions of 50mm x 50mm x 150mm were submitted to compressive test, as specified by Brazilian Association of Technical Standards ABNT NBR 7190 (1997). The lowest value of parallel compression strength was used for calculating the tensile strength (Eq. 1), that was used to estimation of the maximum load applied in the flexural test (Eq. 2).

$$f_{t0,est} = \frac{f_{c0}}{0.77} \quad (1)$$

where $f_{t0,est}$ is the estimated tensile strength (MPa), f_{c0} is the lower compressive strength parallel to the fiber obtained from the three samples for each beam (MPa)

Then, the maximum load to be applied on each beam was calculated by:

$$F_{max} = \frac{f_{t0,max} * I * 2}{\frac{L}{3} * \frac{h}{2}} \quad (2)$$

where F_{max} is the maximum flexural estimated load supported by beam (N), I is the beam's inertial moment (m^4), L is the span between the supports (m), h is the beam height cross-section (m)

Based on the maximum load (F_{max}), six intensity levels with 10%, 15%, 20%, 30%, 40% and 50% were calculated, that were applied on the beams at the four-point bending test (Table 1).

Concerning to the 0% level, only the weight of steel I-beam (equal to 1kN) were applied. The I-beam (Figure 1) was used to application of load in two points.

Table 1. Minimum fiber-parallel compressive strength (f_{c0}), estimated maximum load (F_{max}) and the load levels applied on the beams.

	Beam 1	Beam 2	Beam 3
f_{c0} (MPa)	78.44	66.86	70.65
F_{max} (kN)	23.92	20.25	21.87
0% (kN)	1.00	1.00	1.00
10% (kN)	2.39	2.02	2.19
15% (kN)	3.59	3.04	3.28
20% (kN)	4.78	4.05	4.37
30% (kN)	7.18	6.07	6.56
40% (kN)	9.57	8.10	8.75
50% (kN)	11.96	10.12	10.93

Sclerometric test

A Digital Silver Schmidt BN (PROCEQ, Switzerland) with 2.207J was used to apply sclerometric impacts. The equipment measures the rebound energy in relation to the energy from the impact applied against a plain surface. For each load level intensity in the bending test, the impacts were applied on three columns of points, in both faces of the beam. For each load level, a total of 18 sclerometric impacts were performed (Figure 4).



Figure 4. Sclerometric test.

Ultrasonography

On the same points of sclerometry application, the ultrasonography was performed, then, a total of nine ultrasonic wave velocity were obtained for each load level (Eq. 3). In each corresponding point, the ultrasonic test was applied before and during the flexural test. For this test, the equipment EPOCH 1000 (OLYMPUS NDT, EUA) and plane transducers of 1MHz were used (Figure 5).

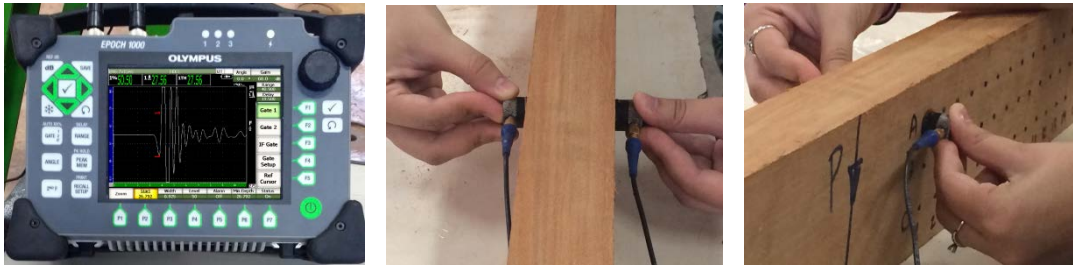


Figure 5. EPOCH 1000 (OLYMPUS NDT, EUA) and ultrasonic testing.

$$V = \frac{b}{t} \quad (3)$$

where V is the ultrasonic wave velocity (m/s); b is the cross-sectional width (m); t is the time obtained in the EPOCH 1000 (OLYMPUS NDT, EUA) (s)

The frequency of the transducers was chosen so that the piece thickness is comprised between 3 and 5 wavelengths, or more. Alves *et al.* (2013) evaluated cubic pieces of Garapa (*Apuleia leiocarpa*) measuring 150mm, at 12% moisture content, and obtained to the perpendicular direction of grain the wave velocity around $1,600\text{m}\cdot\text{s}^{-1}$. With this velocity and with the use of 1MHz transducers, by Equation 4, the wavelength results in approximately 1.6mm.

$$V = \lambda \cdot f \quad (4)$$

where V is the wave velocity ($\text{m}\cdot\text{s}^{-1}$); λ is the wavelength (m); f is the frequency of the transducers (Hz).

In the perpendicular to grain direction, the beams dimensions were approximately 50mm, ensuring at least 31 wavelengths through the material, according to the minimum number of ultrasound waves.

Statistical analysis

The normality of data was performed through skewness and kurtosis of the sclerometric impacts groups applied to each load level. Data were considered normal when skewness and kurtosis values were between -2 e 2 . If group normality is observed, the Tukey method can be applied for grouping creating.

Results

The statistical analysis showed that both sclerometry and ultrasonography data had a normal distribution, since skewness and kurtosis values varied between -2 and 2 , as presented in Table 2.

Table 2. Sclerometric indexes, wave velocity, and data normality.

	Load Level	Sclerometry				Ultrasonography			
		SI*	SDev**	Skewness	Kurtosis	WV*** (m/s)	SDev**	Skewness	Kurtosis
Beam 1	0%	22.9	6.4	0.33	-1.23	2094.1	34.9	-0.17	-1.93
	10%	23.3	6.3	0.57	-1.32	2055.3	28.3	0.60	-1.42
	15%	22.9	8.6	-0.86	1.45	2028.2	26.9	0.98	-0.48
	20%	23.0	5.3	0.71	-0.18	2011.5	20.6	0.73	-1.52
	30%	24.3	4.8	-0.23	-1.05	2027.5	30.3	0.76	1.61
	40%	23.2	4.5	0.83	1.72	2047.8	15.5	1.29	0.65
	50%	25.3	5.1	-0.14	-1.05	2051.4	19.6	0.00	-1.54
	Beam 2	0%	22.6	3.7	-0.64	0.44	2248.6	28.1	-0.08
10%		22.2	5.1	-0.04	0.18	2201.0	6.1	-0.77	-1.50
15%		20.7	5.4	-0.18	-1.16	2190.6	20.8	0.68	-0.88
20%		22.3	5.2	0.77	2.00	2181.6	26.8	-0.59	-0.02
30%		22.5	5.4	-0.09	-0.63	2188.6	23.9	-1.02	1.90
40%		21.9	5.3	-0.59	-0.77	2157.1	15.3	-0.91	0.33
50%		23.2	5.1	-0.53	-1.11	2165.3	26.1	-0.77	-0.11
Beam 3		0%	24.9	5.1	-0.23	-0.61	1919.2	13.1	-0.30
	10%	23.0	4.4	-0.38	-0.33	1901.7	17.9	0.29	-1.40
	15%	23.1	6.2	0.35	-0.66	1888.1	16.3	-0.51	-0.71
	20%	24.3	7.3	0.25	-1.48	1954.6	60.9	0.90	-0.60
	30%	23.4	5.9	0.13	-0.39	1923.4	36.0	0.20	-1.51
	40%	25.0	6.2	-0.45	-0.31	1946.6	68.4	0.68	-1.24
	50%	22.5	5.5	0.39	-0.08	1881.2	29.4	-0.81	-0.24

* SI = Sclerometric indexes, equivalent to the mean of 18 sclerometric impacts. ** Standard deviation

*** WV = Wave velocity, equivalent to the mean of nine wave velocities obtained by ultrasonography.

After verifying the normality of the sclerometrics and ultrasonic wave velocities results, the data from both methods were grouped through Tukey method at 95% confidence.

As the Tukey method denoted the same letter for all sclerometric data (Table 3), for each column, it is possible to conclude that the distinct load levels cannot be discerned for each one of the beams.

The non-differentiation of the sclerometric indexes results with the increase of bending load represent a useful information for some desired applications of the method. For example, when the sclerometric

method is used to estimate the density of the structural elements in service, the results are not dependent of the external loads applied.

Table 3. Sclerometry groupings.

Beam 1				Beam 2				Beam 3			
Load Level	NSI*	Mean	Group**	Load Level	NSI*	Mean	Group**	Load Level	NSI*	Mean	Group**
50%	18	25.3	A	50%	18	23.2	A	40%	18	25.0	A
30%	18	24.3	A	0%	18	22.6	A	0%	18	24.9	A
10%	18	23.3	A	30%	18	22.5	A	20%	18	24.3	A
40%	18	23.2	A	20%	18	22.3	A	30%	18	23.4	A
20%	18	23.0	A	10%	18	22.2	A	15%	18	23.1	A
15%	18	22.9	A	40%	18	21.9	A	10%	18	23.0	A
0%	18	22.9	A	15%	18	20.7	A	50%	18	22.5	A

* NSI = Number of sclerometric impacts

** Based on the LSD Tukey test with a 5.0% margin of error, there is no statistically significant difference between the values denoted by the same letter.

For ultrasonic results, as the Tukey method denoted different letters for distinct levels, it is possible to conclude that the distinct load levels cannot be discerned by ultrasound methods. The groupings are mixed, and it is not possible to discern the load level by the ultrasonic results, as occurred in the results of sclerometry.

However, it is estimated that the use of transducers with lower frequencies, the larger the wavelengths and the smaller the number of waves within the material would lead to more homogeneous groupings.

Table 4. Ultrasonography groupings.

Beam 1				Beam 2				Beam 3			
Load Level	NWV*	Mean	Group**	Load Level	NWV*	Mean	Group**	Load Level	NWV*	Mean	Group**
0%	9	2094.1	A	0%	9	2248.6	A	20%	9	1954.6	A
10%	9	2055.3	B	10%	8***	2201.0	B	40%	9	1946.6	A
50%	9	2051.4	B	15%	9	2190.6	BC	30%	9	1923.4	AB
40%	9	2047.8	BC	30%	9	2188.6	BCD	0%	9	1919.2	AB
15%	9	2028.2	BC	20%	9	2181.6	BCD	10%	9	1901.7	AB
30%	9	2027.5	BC	50%	9	2165.3	CD	15%	9	1888.1	B
20%	9	2011.5	C	40%	9	2157.1	D	50%	9	1881.2	B

* NWV = Number of wave velocity measurements. ** Based on the LSD Tukey test with a 5.0% margin of error, there is no statistically significant difference between the values denoted by the same letter. *** For this measurement, one of the wave velocity was discarded due to the presence of internal defects in the beam.

Conclusions

Based on the results obtained by sclerometric and ultrasound testing perpendicular to the wood fibers it was concluded that:

- The load level does not affect significantly the non-destructive sclerometric test results, showing the method's viability to evaluate wood structures on service, where loading is unknown.
- Ultrasonography was affected by the loading, however in a non-linear, unpredictable way. More research is needed to verify the relationship between load levels and ultrasonic wave velocity.

Acknowledgments

The authors acknowledge the support of the National Council of Technological and Scientific Development (CNPq) for the undergraduate research scholarship; to the Brazilian Federal Coordination for the Improvement of Higher Education Personnel (CAPES) for the PhD research scholarship; the Fund to Support Teaching, Research and Extension (FAPEX) and the Agricultural Engineering College (FEAGRI/UNICAMP) from the University of Campinas for the financial support.

References

Alves, R. C.; Martins, T.; Carrasco, E. V. M. 2013. Effect of density on wave propagation speed in seven tropical wood species. *Natural Resources*. 3(1): 6-13.

American Society for Testing and Materials. 2014. D198-14: Standard Test Methods of Static Tests of Lumber in Structural Sizes. West Conshohocken, PA: ASTM International. 27p.

André, N.; Labbé, N.; Rials, T. G.; Kelley, S. S. 2006. Assessment of wood load condition by Near Infrared (NIR) spectroscopy. *J. Mater. Sci.* 41(1): 1879–1886.

Brazilian Association of Technical Standards. 1997. ABNT NBR 7190: Design of wooden structures. Rio de Janeiro, RJ: ABNT - Associação Brasileira de Normas Técnicas. 107 p.

European Committee for Standardization. 2012. BS EN 12504-2: Testing concrete in structures - Part 2: Non-destructive testing-Determination of rebound number. London, UK: BSI Standards Limited. 14p.

Gonçalves, R.; Ormonde, P. Análise do estado de tensões na madeira utilizando ultra-som. 2005. In: Congresso Brasileiro de Engenharia Agrícola, 34. Anais. Canoas, Brazil: ULBRA. 1-4.

Ormonde, P. C.; Gonçalves, R.; Bartholomeu, A. 2006. O fenômeno acustoelástico na madeira de pinus e de eucalipto por meio de ultra-som. In: Seminário sobre a Aplicação de Ensaios não Destrutivos na Madeira e Materiais a Base de Madeira. Anais. Itatiba, Brazil: ABENDE, 1-7.

Soriano, J.; Veiga, N.S.; Martins, I.Z. 2015. Wood density estimation using the sclerometric method. *European Journal of Wood and Wood Products*. 73(6): 753-758.

Assessing Southern Pine 2x4's and 2x6's Lumber Quality Using Longitudinal and Transverse Vibration

Frederico J. N. França
fn90@msstate.edu

R. Daniel Seale
rds9@msstate.edu

Tâmara S. F. Amorim França
tsf97@msstate.edu

Department of Sustainable Bioproducts – Mississippi State University – Starkville, MS, USA

Abstract

The main procedure during the lumber grading process is the identification of the strength reducing characteristics that impact the modulus of rupture (MOR). Non-destructive evaluation technology can be used to identify higher-stiffness material. This study investigated the use of longitudinal and transverse vibration methods to evaluate the mechanical properties of 2x4 and 2x6 southern yellow pine lumber. A total of 1240 samples were conditioned to 12% equilibrium moisture content. All samples were first nondestructively tested using edgewise and flatwise transverse vibration equipment (Metriguard E-computer) and three different longitudinal vibration equipment (Fakopp Portable Lumber Grader, Director HM200 and Falcon A-grader) to obtain the vibration properties in the transverse and longitudinal methods. Dynamic modulus of elasticity (MOE) of each sample was calculated based on the fundamental wave equation. Static bending was subsequently conducted according to ASTM 198 (2012) and the speed of testing followed ASTM D4761 (ASTM, 2012). The results showed significant correlations between the properties determined by nondestructive techniques and the static MOE. No strong correlations were found for MOR because it is related to the ultimate strength of material, often associated with the existence of a localized defect (such as a knot) on the test specimen. This study indicates the nondestructive techniques can potentially be used to evaluate 2x4 and 2x6 southern pine lumber stiffness. The tools were suitable in this case.

Keywords: modulus of elasticity, transverse vibration, longitudinal vibration

Introduction

Wood is one of the main materials used in construction due to advantages when compared to materials, such as steel and concrete. It shows considerable mechanical strength being a light weight material that is easy to fasten, cut, and shape with relatively low cost tools compared to other materials. In addition, it is a sustainable, renewable and biodegradable bio-product; however, it needs to be classified for better use.

Ross et al. (1998) defines non-destructive assessment as the way to evaluate physical and mechanical properties of a piece of material without changing its characteristics. Non-destructive techniques, such as ultrasound, transverse vibration, longitudinal vibration, x-ray, and stress waves have been investigated, and have been adopted by industry because of their fast responses and high correlations (Brashaw et al., 2009).

According to Amishev and Murphy (2008), the modulus of elasticity (MOE) is one of the most important mechanical properties of wood since it is the indicator of load resistance most frequently used. The dynamic methods to characterize wood and other materials calculate the elastic modulus through the natural frequency of the specimen vibration and its geometric parameters. These methods have the advantage of being fast, using small samples, and being repeatable (Cossolino and Pereira, 2010).

As a building material, wood has many features which directly influence the quality of the chosen wood; therefore, a full knowledge of its structural potential is a necessity for its correct use in construction. Like other materials used in construction, the physical and mechanical properties of wood should be tested and then classified for structural use (Segundinho et al., 2012).

Since the 1960s, researchers from the forest products community have been developing non-destructive testing (NDT) tools for evaluating the quality of lumber products, especially with regard to mechanical grading (Divós and Tanaka, 2005). In the 1990's, Ross et al. (1991) developed personal computer software for making transverse vibration NDT tools available to a broader range of wood product manufacturers and users.

Predicting the MOE of lumber with longitudinal stress wave analysis has received considerable research efforts in recent years in terms of lumber grading or pre-sorting (Wang, 2013). The assessment of the quality of raw wood materials has become a crucial issue in the operational value chain as forestry and the wood processing industry which is increasingly under economic pressure to maximize its extracted value (Brashaw et al., 2009). New sensor technologies are improving the ability to determine with greater precision (Murphy, 2009).

The objectives of this study are to investigate the relationships between dynamic MOE and modulus elasticity, and compare the results to that of static bending MOE and MOR. For a better understanding of the relationships between dynamic and static evaluation methods, experimental tests on full size, in-grade lumber were conducted with four commercially available nondestructive tools.

Materials and Methods

To fully understand the relationships between dynamic and static lumber evaluation methods, experimental tests on 2x4 and 2x6 southern pine lumber were conducted with four commercially-available nondestructive tools. A total of 1240 pieces of No. 2 southern pine lumber were obtained from retail lumber yards in the southeastern U.S. The lumber was divided into two groups according to the cross section dimensions: 629 pieces of 2x4 ($38 \times 89 \text{ mm}^2$) and 611 pieces of 2x6 ($38 \times 140 \text{ mm}^2$). The average moisture content when tested was 11.4%, and the average air-dried density of was $557 \text{ kg}\cdot\text{m}^{-3}$.

First, the lumber was vibrated using a transverse vibration technique. Lumber specimens were simply supported flatwise as a beam spanning the entire length with a knife-edge support on one end and at the opposite end by a point support.

Each 2x4 was nondestructively examined using transverse vibration equipment. It can determine the MOE based on resonant vibration frequency and density using a Metriguard Model 340 Transverse Vibration E-Computer. The specimen was then set into vibration by gently tapping it near the center of the span. A load cell measured the frequency of vibration and board weight, and the E-Computer reached the transverse vibration frequency for each piece and calculated the dynamic MOE.

Using the same setup, vibration data was also collected using a portable device. The accelerometer (smartphone) was located in the middle of the lumber on the upside surface. Transversal vibration was initiated by impacting the middle part of the lumber. The signal collected by the smartphone app was a series of pulses with gradually decreasing (decaying) amplitude (Figure 1).

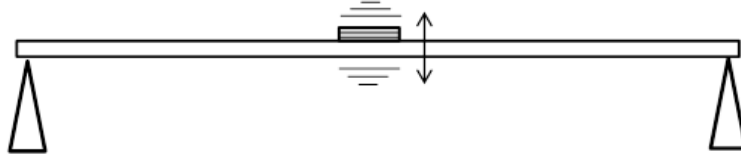


Figure 1 – Setup for frequency measurement using the portable device.

The application used worked as a vibration spectrum analyzer. It was written to emulate an oscilloscope based spectrum analyzer by recording the vibration of the material using the smartphone internal accelerometer. The app analyzed the vibratory motion. The parameter measured was resonant frequency (Fundamental frequency). It acquired the time series data, and performed a Fast Fourier Transformation (FFT) to produce frequency spectra, which allows the frequency analysis of the data.

The equation used to calculate the dynamic modulus of elasticity (MOE) was:

$$E_{tv} = \frac{f^2 W S^3}{K_d I g} \quad (1)$$

where E_{tv} is transverse vibration modulus of elasticity (Mpa), f is the frequency of oscillation (Hz), W is the weight of specimen (N), S is the span (m), K_d is the constant of free vibration of a simply supported beam, 2.47, I is specimen moment of inertia, $bd^3/12$ (m^4), b is width (m), d is depth (m), g is acceleration due to gravity ($9,807 \text{ m.s}^{-2}$).

For both procedures, the specimens were positioned such that an equal portion of the length overhung each support. The overhang adopted was 0.98 (span (l) to length (lt) ratio), as recommended by ASTM D 6874 (2012).

Longitudinal vibration measurement was conducted on each board to obtain the stress wave velocity using a Hitman (Director HM-200TM). A stress wave was initiated by a hammer impact on one end of the specimen. Stress wave propagation in the wood specimen was sensed by a piezoelectric transducer mounted on the same end of the sample. Stress wave velocity can be determined by Equation 2:

$$C = \frac{2.L}{\Delta t} \quad (2)$$

where C is stress wave velocity (m.s^{-1}), L is length of specimen (m), and Δt is time of flight (s).

The relation between acoustic velocity, density and wood stiffness is described by the fundamental wave equation (Bucur, 2003). The dynamic MOE of the specimens obtained by stress wave timer were determined using one-dimensional propagation waves, based on Equation 3.

$$E_{sw} = \rho . C^2 \quad (3)$$

where E_{sw} is dynamic modulus of elasticity, ρ is the density at 12% moisture content (kg.m^{-3}), and C is stress wave velocity (m.s^{-1}).

Results and Discussion

All statistical analyses were conducted using SAS 9.4 (SAS, 2013). Analysis of variance (ANOVA) was performed to characterize the differences within the specimens sampled by cross sections.

Statistical analyses of the static bending MOR and MOE values, dynamic MOE values obtained from NDT tools are listed in Table 1. There is a statistically significant difference ($\alpha=0.05$) between groups (2x4 and 2x6) only for MOR.

Table 1 - Static bending MOR and MOE values, dynamic MOE values obtained from NDT techniques

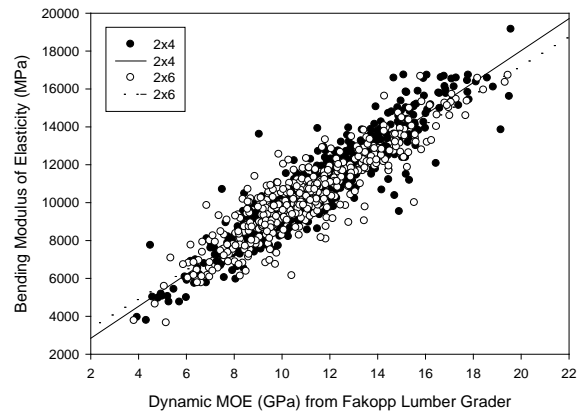
	Size	Mean	Median	Minimum	Maximum	STD	COV
MOR ^a (MPa)	2 × 4	55.39	53.76	10.89	121.35	20.76	37.5%
	2 × 6	45.88	44.66	7.70	99.25	17.93	39.1%
MOE ^b (MPa)	2 × 4	10855	10747	3616	19141	2798	25.8%
	2 × 6	10414	10252	3650	18270	2395	23.0%
dMOE _{FAK} ^c (GPa)	2 × 4	11.51	11.49	3.95	21.42	3.03	26.3%
	2 × 6	11.16	10.82	3.82	20.77	2.89	25.9%
dMOE _{DIR} ^d (GPa)	2 × 4	11.65	11.54	3.93	21.59	3.05	26.2%
	2 × 6	11.25	10.93	4.08	21.05	2.88	25.6%
dMOE _{FAL} ^e (GPa)	2 × 4	11.02	10.97	3.81	20.46	2.89	26.2%
	2 × 6	11.95	11.53	4.11	26.31	3.14	26.3%
dMOE _{EDGE} ^f (GPa)	2 × 4	11.61	11.50	4.26	20.80	2.93	25.2%
	2 × 6	11.19	10.90	4.17	20.30	2.67	23.9%
dMOE _{FLAT} ^g (GPa)	2 × 4	11.51	11.41	4.16	20.50	3.00	26.1%
	2 × 6	11.31	11.07	3.93	21.60	2.86	25.3%
^a Modulus of Rupture ^b Static bending MOE value ^c Longitudinal vibration MOE value from Fakopp lumber grader ^d Longitudinal vibration MOE value from Director HM200 ^e Longitudinal vibration MOE value from Falcon A-Grader ^f Edgewise transverse vibration MOE value ^g Flatwise transverse vibration MOE value							

Static bending MOR values ranged from 7.7 to 121.5 MPa. The average MOR value of all specimens is 55.4 MPa for 2x4 and 45.0 MPa for 2x6. Strength is greatly affected by the position of knots during destructive testing. For 2x4, the minimum, average and maximum MOE values are 3.62, 10.86 and 19.14 GPa respectively. For 2x6, the minimum, average and maximum MOE values are 3.65, 10.41 and 18.27 GPa respectively.

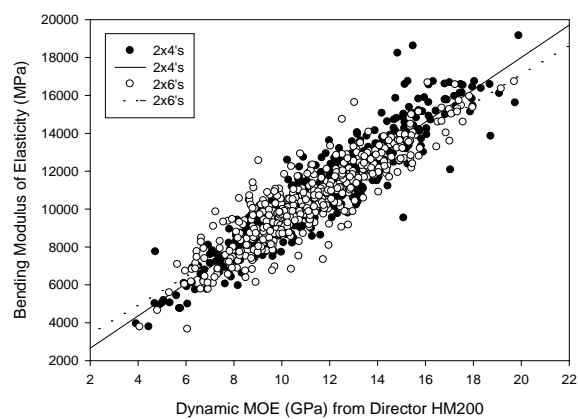
Doyle and Markwardt (1966) studying SYP dimensional lumber found MOE values ranging from 8.8 to 13.2 GPa. The dynamic MOE obtained with longitudinal vibration ranged between 5.3 and 18.4 GPa, with the average around 11.5 GPa for all three longitudinal vibration tools. The Falcon tool detected a greater range between low and high stiffness material. Applying

transverse vibration techniques, the dynamic MOE obtained ranged between 3.8 – 26.3 GPa, with the average being 10.0 GPa.

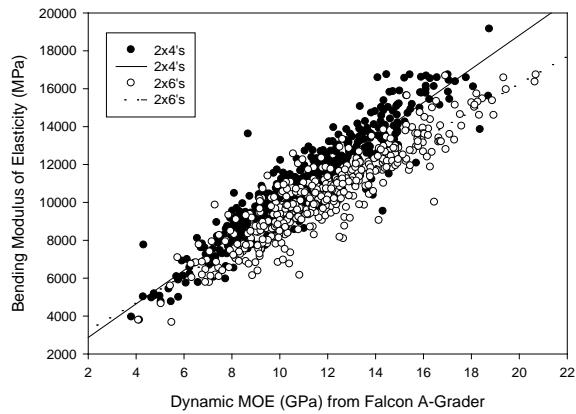
Mean trends in the relationship between dynamic MOE and bending MOE for the No.2 southern pine lumber are shown in Figure 2. Linear regression plots for each lumber size (2x4 and 2x6) for bending MOE versus dynamic MOE from (a) Fakopp Lumber Grader; (b) Director HM200; (c) Falcon A-Grader; (d) edgewise transverse vibration; (e) flatwise transverse vibration.



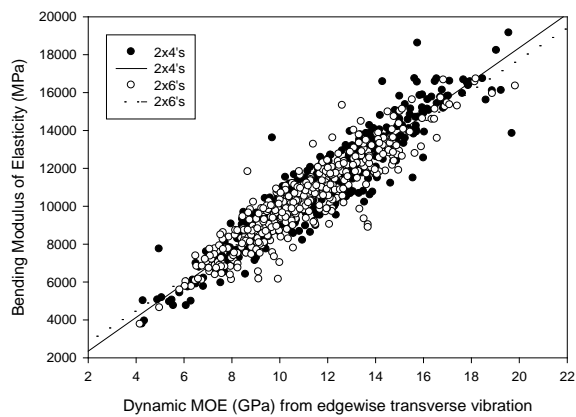
(a)



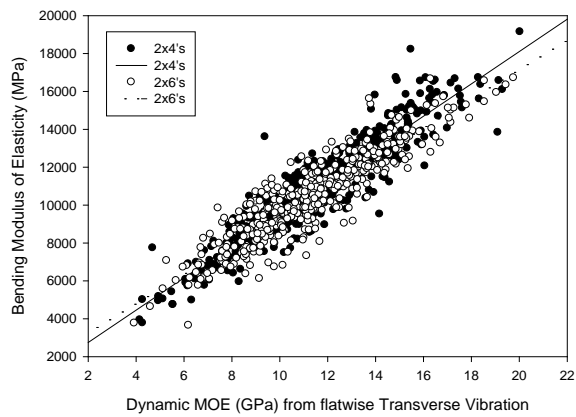
(b)



(c)



(d)



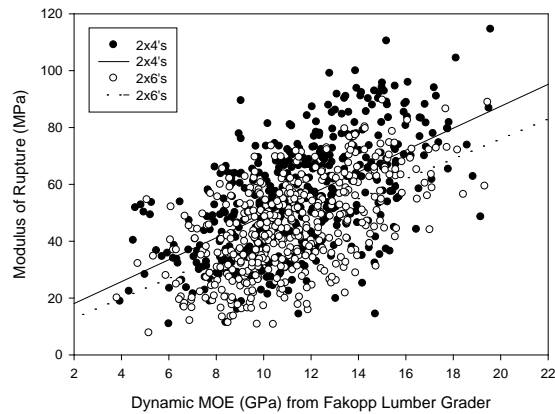
(e)

Figure 2 - Linear regression plots for each lumber size: bending modulus of elasticity versus dynamic MOE from (a) Fakopp Lumber Grader; (b) Director HM200; (c) Falcon A-Grader; (d) edgewise transverse vibration; (e) flatwise transverse vibration.

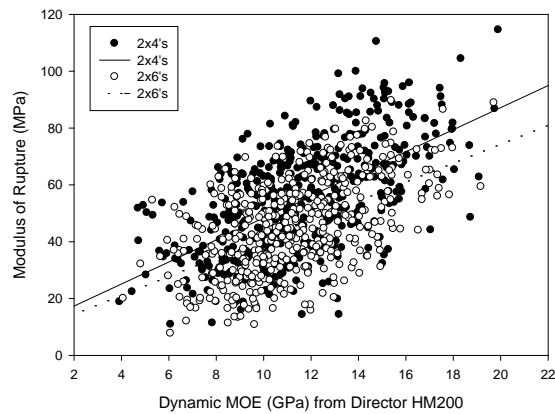
The results indicated significant correlations between the properties determined by nondestructive techniques and the static MOE (Table 2). Many studies with other softwood species and grades have already demonstrated the potential of these methods to estimate MOE (Ross et al., 1991; Divós & Tanaka, 1997).

Linear relationships between dynamic MOE and MOR were in general weak (Table 3.3). The low correlations are largely explained by (1) the presence of knots and other wood defects such as checks, splits and grain deviation present in SYP dimension lumber as well as by the fact that all lumber was in the same grade and (2) the NDT analysis was performed over the entire length of each piece but the static bending was performed over a 17:1 depth to span ratio that was randomly positioned in the testing machine. Inclusion of multiple grades would have provided specimens of both greater and lesser quality which would have most likely improved these correlations.

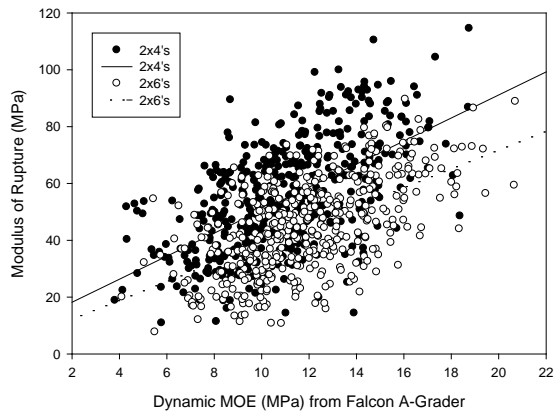
Mean trends in the relationship between dynamic MOE and bending MOR for the No.2 pine lumber are showed in Figure 3. Linear regression plots for each lumber size (2x4 and 2x6) for bending MOE versus dynamic MOE from (a) Fakopp Lumber Grader; (b) Director HM200; (c) Falcon A-Grader; (d) edgewise transverse vibration; (e) flatwise transverse vibration.



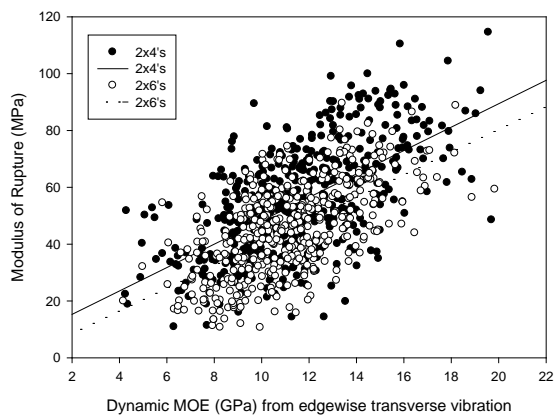
(a)



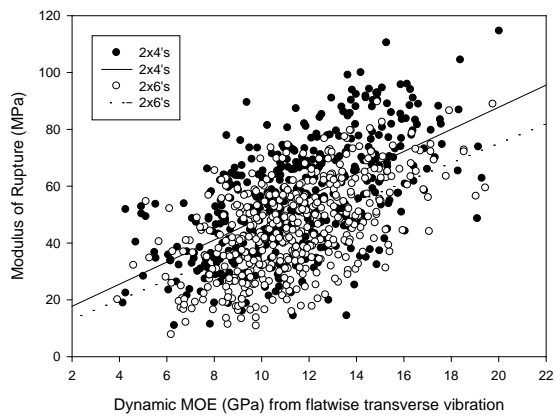
(b)



(c)



(d)



(e)

Figure 3 - Linear regression plots for each lumber size: modulus of rupture versus dynamic MOE from (a) Fakopp Lumber Grader; (b) Director HM200; (c) Falcon A-Grader; (d) edgewise transverse vibration; (e) flatwise transverse vibration.

The coefficients β_0 and β_1 are used in the generalized model static property = $\beta_0 + \beta_1 \cdot \text{dMOE}$. Results of linear regression analyses relating static bending MOE and dynamic MOE from different tools for 2x4 and 2x6 southern pine dimensional lumber are listed in Table 2.

Table 2 - Results of linear regression analyses relating static bending modulus of elasticity and dynamic MOE from different tools for 2x4 and 2x6 southern pine dimensional lumber

Size	Modulus of elasticity (MPa)					
	Tool	β_0	β_1	r^2	Standard error (u)	Durbin-Watson
2x4	FAK	0.6191	0.0010	0.8593	1.1368	2.0111
	DIR	0.6271	0.0010	0.8695	1.1011	1.9270
	FAL	0.5744	0.0001	0.8657	1.0615	1.9347
	EDGE	0.8718	0.0001	0.8909	0.9694	1.9200
	FLAT	0.7220	0.0001	0.8584	1.2781	1.9228
2x6	FAK	-0.3599	0.0011	0.8415	1.1511	1.7321
	DIR	-0.1130	0.0011	0.8236	1.2101	1.7043
	FAL	-0.3987	0.0012	0.8185	1.3384	1.7069
	EDGE	0.4563	0.0010	0.8543	1.0202	1.5220
	FLAT	0.0363	0.0011	0.8246	1.1968	1.6867

Results of linear regression analyses relating static bending MOR and dynamic MOE from different tools for 2x4 and 2x6 southern pine dimensional lumber are listed in Table 3.

Table 3 - Results of linear regression analyses relating static bending MOR and dynamic MOE from different tools for 2x4 and 2x6 southern pine lumber.

Size	Modulus of rupture (MPa)					
	Tool	β_0	β_1	r^2	Standard error (u)	Durbin-Watson
2x4	FAK	6.4932	0.0906	0.3855	2.3761	1.7436
	DIR	6.5668	0.0917	0.3905	2.3798	1.7365
	FAL	6.2118	0.0868	0.3878	2.2663	1.7271
	EDGE	6.5815	0.0908	0.4128	2.2487	1.7199
	FLAT	6.5631	0.0894	0.3818	2.3626	1.7276
2x6	FAK	6.4187	0.1034	0.4119	2.2172	1.6386
	DIR	6.6862	0.0994	0.3833	2.2625	1.6272
	FAL	6.8646	0.1108	0.4001	2.4319	1.6530
	EDGE	6.5997	0.1001	0.4512	1.9802	1.6686
	FLAT	6.6986	0.1006	0.3987	2.2163	1.5945

Table 4 summaries research conducted to examine the relationship between longitudinal vibration MOE and static bending (MOE and MOR) of structural lumber. The correlative relationships found in this study were comparable to those reported in the literature.

Table 4 - Summary of research conducted to examine the relationship between longitudinal vibration modulus of elasticity and static bending (modulus of elasticity and modulus of rupture) of structural lumber

Reference	Material	Correlation coefficient
Gerhards (1982)	Southern pine Knotty lumber Clear lumber	dMOE x MOE = 0.87 dMOE x MOE = 0.95
Porter et al. (1972)	Clear lumber	dMOE x MOE = 0.90-0.92
Shmulsky et al. (2006)	Southern pine dowels	dMOE x MOE = 0.81 dMOE x MOR = 0.42
Yang et al. (2015)	Southern pine dimensional lumber	dMOE x MOE = 0.92

Table 5 summaries research conducted to examine the relationship between free transverse vibration modulus of elasticity and static bending (modulus of elasticity and modulus of rupture) of structural lumber.

Table 5 - Summary of research conducted to examine the relationship between free transverse vibration MOE and static bending (MOE and MOR) of structural lumber

Reference	Dimensional Lumber Material	Reported properties	Correlation MOE x dynamic MOE
Pellerin (1965)	Douglas-fir	MOE, MOR	dMOE x MOE = 0.98 dMOE x MOR = 0.67-0.93
O'Halloran (1969)	Lodgepole pine	MOR, MOR	dMOE x MOE = 0.98 dMOE x MOR = 0.89
Ross et al. (1991)	Spruce-Pine-Fir	MOE	dMOE x MOE = 0.99
Wang et al. (1993)	Spruce-Pine-Fir	MOE	dMOE x MOE = 0.96-0.99
Yang et al. (2015)	Southern pine	MOE	dMOE x MOE = 0.95

Pellerin (1965) using free transverse vibration of Douglas-fir dimensional lumber found correlations between 0.67-0.93 for various lumber grades. O'Halloran (1972) studying lodgepole pine dimensional lumber with transverse vibration technique found coefficient of correlation equal 0.89. Green & McDonald (1993) using transverse vibration flatwise found correlation equal 0.58 for northern red oak lumber.

Carreira (2012) tested the transverse vibration method with *Eucalyptus* sp. logs in bending tests and concluded that this technique was not efficient to provide reliable estimates of the logs MOR. Vega et al. (2012) studying chestnut timber found r^2 between 0.10 to 0.17 using three different NDT methods (ultrasound, impact wave and longitudinal waves) concluding that dynamic variables are not adequate by themselves to estimate bending strength.

The quality of a strength grading system is determined by the ability of the tool and operator during measurement of the parameter to predict strength. This factor can be quantified by regression analysis (the obtained coefficient of determination, r^2). The measurement error of the predictor parameter is another factor and can be quantified by the coefficient of variation of the measurement error.

Another factor is the systems capability to sort-out pieces with different characteristics but consistently low strength. If the regression analysis is based on measurements made in the same conditions and the same apparatus that is used in the strength grading machine, the effect of the measurement error and coefficient of variation is already included in the r^2 value directly. If the measurements are made in laboratory conditions, the effect of measurement error should be considered separately, when evaluating the effectiveness of a certain strength grading system.

The differences of r^2 values among the tools were small and not considered as indication of superiority of a certain method compared to another due to reasons explained above. Furthermore, when considering the fitness of a strength grading system to a certain application, the evaluation of the prediction accuracy in terms of r^2 and coefficient of variation is not adequate alone. Obviously, the price of the system, its fitness to production line and target strength classes are other important factors.

Conclusions

- All tools tested are able to predict MOE. The differences between tools are minimum.
- Transverse vibration flatwise and longitudinal vibration MOE showed slightly lower correlation with static MOE compared to transverse vibration edgewise.

- Vibration methods were not reliable to predict MOR.
- Potentially, this study could have been improved by testing lumber specimens in both higher and lower grades and by testing the entire span of each piece consistent with the NDT analysis.
- Including additional grades, a greater range of stiffer/stronger pieces as well as less stiff/weaker pieces would have elongated the response data. The collective influence of the defects associated with each specimen perhaps interact and thus influence the stiffness to strength relationship.

Acknowledgments

The authors wish to acknowledge the support of U.S. Department of Agriculture (USDA), Research, Education, and Economics (REE), Agriculture Research Service (ARS), Administrative and Financial Management (AFM), Financial Management and Accounting Division (FMAD) Grants and Agreements Management Branch (GAMB), under Agreement No. 5B-0202-4-001. Any opinions, findings, conclusion, or recommendations expressed in this publication are those of the author(s) and do not necessarily reflect the view of the U.S. Department of Agriculture.” The authors acknowledge the support from USDA Forest Service Forest Products Laboratory (FPL) in Madison, Wisconsin, as a major contributor of technical assistance, advice, and guidance to this research.

References

American Society For Testing And Materials (2012) ASTM D – 198: Standard test methods of statics of lumber in structural sizes. Annual Book of ASTM Standards. West Conshohoken, PA.

American Society of Testing and Material (2009) ASTM E 1876: Standard Test Method for Dynamic Young’s Modulus, Shear Modulus, and Poisson’s Ratio by Impulse Excitation of Vibration. West Conshohocken, Pennsylvania, USA.

Amishev D, Murphy GE. 2008. In-forest assessment of veneer grade Douglas-fir logs based on acoustic measurement of wood stiffness. *For Prod J*, 58(11):42-47.

Brashaw BK, Bucur V, Divós F, Gonçalves R, Lu JX, Meder R, Pellerin RF, Potter S, Ross RJ, Wang X, Yin YF. 2009. Nondestructive testing and evaluation of wood: A worldwide research update. *For Prod J*, 59:7-14.

Carreira MR. 2012. Avaliação da Rigidez à Flexão de Toras de Madeira por meio de Vibração Transverse. 2012. Tese (Doutorado em Engenharia de Estruturas e Área de Concentração em Engenharia de Estruturas)–Escola de Engenharia de São Carlos, Universidade de São Paulo.

Cossolino LC, Pereira AHA. 2010. Informativo Técnico-Científico/ATCP Engenharia Física. Módulos elásticos: visão geral e métodos de caracterização. 2010. Available at: <<http://www.investagro.com.br>>. Access in: 4 Jan. 2016.

Divós F, Tanaka T. 1997. Lumber strength estimation by multiple regression. *Holzforschung* 51(5): 467-471.

Divós F, Tanaka T. 2005. Relation between Static and Dynamic Modulus of Elasticity of Wood, *Acta Silvatica et Lignatia Hungarica*, 1:105-110.

Doyle D V, Markwardt LJ. 1966. Properties of southern pine in relation to strength grading of dimension lumber. Res. Pap. FPL-RP-64. Madison, WI: U.S. Department of Agriculture, Forest Service, Forest Products Laboratory.

- Fakopp Enterprise Bt. 2005. Fast Fourier Vibration analyzer User's Guide. Fakopp Enterprise publication. Hungary.
- Gerhards CC. 1982. Longitudinal stress waves for lumbers stress grading: Factors affecting applications: State of art. *Forest Product Journal*. 32(20):20-25.
- Green DW and McDonald KA. 1993. Investigation of the mechanical properties of red oak 2 by 4's. *Wood and Fiber Sci*. 25(1): 35 – 45.
- O'Halloran MR. 1972. Nondestructive parameters of lodgepole pine dimension lumber. *For Prod J*, 22(2):44-51.
- Pellerin RF. 1965. A vibrational approach to nondestructive testing of structural lumber. . *For Prod J*, 15(3): 93 – 101.
- Porter AW, Kusec DJ, Olson SL. 1972. Digital computer for determining modulus of elasticity of structural lumber. WFPL Info. Rep. VP-X-99. Vancouver, BC: Department of Environment, Canadian Forest Service.
- Ross RJ, Geske EA, Larson GH, Murphy JF. 1991. Transverse Vibration Nondestructive Testing Using a Personal Computer. USDA Forest Service, Forest Products Laboratory RP-502. Madison, WI. 17 p.
- SAS Institute. 2013. SAS® software, version 9.4. The SAS Institute Inc. Cary, NC.
- Shmulsky R, Selae RD, Snow RD. 2006. Analysis of acoustic velocity as a predictor of stiffness and strength in 5-in-diameter pine dowels. *Forest Prod. J*. 56(9):52-55.
- Vega A, Guaita M, Dieste A, Majada J, Fernández I, Baño V. 2011. Evaluation of the influence of visual parameters on wave transmission velocity in sawn chestnut timber. In: 17th international nondestructive testing and evaluation of wood symposium. Sopron, Hungary.
- Wang X. 2013. Stress Wave E-Rating of Structural Timber—Size and Moisture Content Effects. In: *Proceedings: 18th International Nondestructive Testing and Evaluation of Wood Symposium*, Ross, R.J., Wang, X. (eds.) General Technical Report FPL-GTR-226, pp: 38-46, Madison, WI: U.S, Department of Agriculture, Forest Service, Forest Products Laboratory, USA.
- Wang Z, Ross RJ, Murphy JF. 1993. A comparison of several NDE techniques for determining the modulus of elasticity of lumber. *Wood Forestry Research*. 6(4): 86-88.
- Yang, BZ, Seale RD, Shmulsky R, Dahlen J, Wang X. 2015. Comparison of nondestructive testing methods for evaluating No. 2 southern pine lumber: Part A, Modulus of Elasticity. *Wood and Fiber Science*, Volume 47, Number 4, 2015; pp. 375-384.



Session 3

Evaluation of Engineered Wood Products

A Free Vibration Method for Evaluating the Mechanical Properties of Full-Size Oriented Strand Board

Lujing Zhou*

School of Technology, Beijing Forestry University, Beijing, China, Zhou_lu_jing@163.com

Xiping Wang

US Forest Service Forest Products Laboratory, Madison, WI, USA, xwang@fs.fed.us

Houjiang Zhang

School of Technology, Beijing Forestry University, Beijing, China, hjzhang6@bjfu.edu.cn

Robert J. Ross

US Forest Service Forest Products Laboratory, Madison, WI, USA, rjross@fs.fed.us

Cheng Guan

School of Technology, Beijing Forestry University, Beijing, China, 648911029@qq.com

Zhanguo Wei

College of Logistics & Transportation, Central-South University of Forestry and Technology, Changsha, Hunan, China, jackwzg007@163.com

* Corresponding author

Abstract

The flexural properties of wood composite panels are typically determined through static bending tests of half-size panels or small specimens cut from the full-size panels. In this study, we investigated the feasibility of using a free vibration method to directly evaluate the mechanical properties of full-size oriented strand board (OSB) without cutting the panels. The hypothesis is that the plate vibration theory with all free edges can be applied to a simple vibration test setup where the OSB panel is simply supported at the first nodal lines. To validate the test setup, we first conducted modal testing and free vibration test on 8 full-size OSB panels in 4 different thickness. Mode shapes and natural frequencies of the panels were determined and analyzed. In the second phase, 50 full-size OSB panels in different quality ranges and 5 different thicknesses were obtained and subjected to free vibration test using the vibration test setup. The panels were then cut into half-size and small specimens for determination of mechanical properties, including modulus of elasticity (in major and minor directions), shear modulus, internal bond, impact resistance, and Poisson's ratio. Our preliminary results indicate that, under the nodal-line support condition, the natural frequencies in the first 7 orders obtained from free vibration test showed an excellent agreement with the frequencies obtained from the modal analysis. The frequencies of 1st, 3rd, and 7th order obtained from vibration test were found to correspond to the vibration modes (2, 0), (2, 1), and (2, 2) respectively. The mechanical testing of the half panels and small specimens is currently underway. Further results will be reported later when the phase 2 is completed.

Keywords: Frequency, full-size panels, modulus of elasticity, oriented strand board, plate vibration, shear modulus, vibration mode

Introduction

Oriented strand board (OSB) is an engineered material that are suitable for load-bearing applications in construction. The most common uses are sheathing in walls, flooring, and roof decking. As an important structural component in a building system, OSB panels are required to meet certain mechanical performance standards to ensure the safety and integrity of the building system. Modulus of elasticity (MOE) (in both long and short axis) and in-plane shear modulus are important mechanical properties that determines the performance of an OSB panel under various loading conditions. A nondestructive method that can rapidly and accurately determine these properties in full-size panels will enable manufacturers to better control the manufacturing process and ensure the final products meeting the required specifications.

The most common method to determine MOE and shear modulus of a full-size OSB panel is to conduct static destructive tests on small specimens cut from different parts of a panel (ASTM 2006a). Based on the testing results of multiple small specimens, average property values are derived and assigned to a full-size panel. This is a costly and time-consuming process to OSB manufacturers. Research have been conducted to develop nondestructive methods to determine MOE of small OSB specimens with good results (Turk et al. 2008; Shyamasunder et al. 1993). However, very limited efforts have been made on developing nondestructive methods that can directly measure the mechanical properties of full-size OSB panels.

A simple method to calculate resonant frequencies and loss tangents were proposed by Nakao et al. (1985). They try to put forward this method to various shapes of plates. The plate was supported on four pieces of sponge rubber to simulate a completely free boundary condition. The experimental values were in good agreement with the theoretical values (Nakao et al. 1985). The testing system consisted of four pieces sponge rubber supported under a 300mm x 300mm wood plate, assumed a completely free boundary condition, and two microphones placed on the corner and the center part of the sample respectively to collect the displacement, a software based on the different deflection phases of both edges to identify the twist or bending modes to compute MOE automatically. The disadvantage of the system is that it was not able to determine the Poisson's ration (Sobue and Kitazumi 1991). To simultaneously determine the orthotropic elastic constants, the plywood panel was placed vertically with one long-edge supported by a V-cut rod and the other three edges were tapped with a small rubber ball, which was a simulated SFFF (simply supported-free-free-free) boundary condition. It was found that the modulus of elastic measured through vibration method were in a good agreement with those obtained by static bending and twisting tests. The higher modes of frequency was recommended for determining the shear moduli, in order to avoid the restriction of vibration at supported edge that affects the resonance frequencies in low vibration modes (Sobue and Katoh 1992).

The modulus of elasticity of a large specimen could be estimated by the cantilever torsional vibration principle (Lau and Tardif 1996). Based on the orthotropic plate vibrations and experimental modal analysis technique, a dynamic method for estimating the elastic properties of wood plane was proposed. The correlation coefficient between the dynamic and static bending testing showed that the proposed method was reliable. But there was a critical ratio of the plate length. When the ratio was lower than the critical value, the lower bending mode was (0, 2). As the increasing of the ratio and then higher than the critical value, the mode (2, 0) was the lower bending mode. It means that this method cannot be used when the ratio of the length closes to the critical value, which was the disadvantage of this method (Carfagni and Mannucci 1996). Bos and Casagrande (2003) developed a VibraPann system that can provide a good quality indicator for online control. Vertical cantilever vibration technique was used to determine the performance of chipboard and MDF-panels in large dimensions (Schulte et al. 1996). So far, a real online evaluation of wood composite panel performance system was not yet developed.

The objectives of this study were to determine the feasibility of using a free vibration method to directly evaluate the mechanical properties of full-size OSB panels without cutting the panels. The hypothesis is that the plate vibration theory with all free edges can be applied to a simple vibration test setup where the OSB panel is simply supported at the first nodal lines.

Plate vibration model with nodal-line supports

To simplify the vibration model, the OSB panels will be treated as an orthotropic thin-plate defined in a Cartesian coordinate system in a three dimensional space (Fig. 1). For an orthotropic thin plate, the differential equation for a flexural vibration can be expressed as follows,

$$D_1 \frac{\partial^4 u_3}{\partial x^4} + D_2 \frac{\partial^4 u_3}{\partial y^4} + 2(D_{12} + 2D_{66}) \frac{\partial^4 u_3}{\partial x^2 \partial y^2} + \rho h \frac{\partial^2 u_3}{\partial t^2} = 0 \quad (1)$$

$$D_1 = \frac{E_1 h^3}{12\mu}; D_2 = \frac{E_2 h^3}{12\mu}; D_{66} = \frac{G_{12} h^3}{12\mu}$$

$$D_{12} = \frac{\nu_{21} E_1 h^3}{12\mu} = \frac{\nu_{12} E_2 h^3}{12\mu}$$

$$\mu = 1 - \nu_{21} \nu_{12}$$

$$u_3 = X(x)Y(y) \quad (2)$$

Where D_1, D_2 are the flexural rigidities of the plate; D_{66} is the torsional rigidity; E_1 and E_2 are Young's modulus in x , and y directions; G_{12} is in-plane shear modulus; ν_{21}, ν_{12} are Poisson's ratios; u_3 is the displacement of the plate.

For a free-free plate, $X(x), Y(y)$ could be substituted with appropriate beam functions. According to the number of nodes, the integrals of characteristic beam function are different (Hearmon and Maradudin 1961). Appropriate solution to the differential equation 1 can be express as (Sobue and Katoh 1992):

$$f(i, j) = \frac{1}{2\pi} \sqrt{\frac{1}{\rho h}} \sqrt{D_1 \frac{\alpha_1(i, j)}{a^4} + D_2 \frac{\alpha_2(i, j)}{b^4} + 2D_{12} \frac{\alpha_3(i, j)}{a^2 b^2} + 4D_{66} \frac{\alpha_4(i, j)}{a^2 b^2}} \quad (3)$$

Where i denotes the number of nodal lines parallel to Y axis; j denotes the number of nodal lines parallel to X axis; f is frequency of the plate; a and b represent the length and width of the plate, respectively; h is the thickness; ρ is the density.

In this study, a simply support with two nodal-lines was chosen for vibration testing of full-size OSB panels because such support condition can be readily implemented in OSB production settings. For a plate with two nodal lines parallel to Y axis and zero nodal line parallel to X axis, equation 2 can be express as:

$$E_1 = \frac{4\pi^2 f^2(2,0) \rho a^4}{500.6} \times \frac{12(1-\nu_{21}\nu_{12})}{h^3} \quad (4)$$

When $i = 2$; and $j = 1$; equation 2 can be express as:

$$G_{12} = \left[4\pi^2 \rho h f^2(2,1) - \frac{E_1 h^3}{12(1-\nu_{21}\nu_{12})} \right] \times \frac{3a^2 b^2}{148.44 h^3} \quad (5)$$

When $i = 2$; and $j = 2$; equation 2 can be express as:

$$E_2 = \left[4\pi^2 \rho h f^2 (2,2) - \frac{E_1 h^3}{12(1-\nu_{21}\nu_{12})} \times \frac{500.6}{a^4} - \frac{61.5\pi^2}{8a^2 b^2} \times \frac{\nu_{21} E_1 h^3}{12(1-\nu_{21}\nu_{12})} - \frac{148.44\pi^2}{16a^2 b^2} G_{12} h^3 \right] \frac{3072(1-\nu_{21}\nu_{12}) b^4}{625\pi^5 h^3} \quad (6)$$

With the equations 3 to 5, moduli of elasticity in major and minor strength directions and in-plane shear modulus can be calculated when the geometry size (a , b , h), density (ρ), frequencies and the Poisson's ratios of a panel are given.

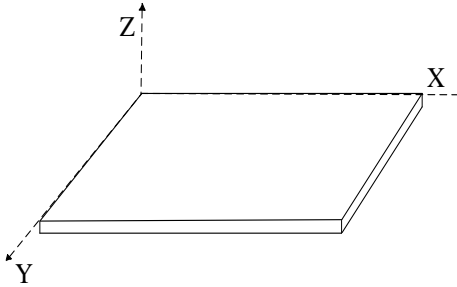


Figure 1—A full-size OSB panel modeled as a thin-plate in a Cartesian coordinate system.

Materials and methods

The laboratory experiments of this study included 3 parts: (1) Modal testing and analysis of full-size OSB panels with the nodal-line supports; (2) Free vibration test of full-size OSB with the nodal-line supports; (3) Determination of mechanical properties of the panels through destructive tests of multiple small specimens cut from the panels.

Modal testing and analysis

The supporting system designed for free vibration testing of full-size OSB panels is a simple support at two nodal lines (22.4% and 77.6% of the length) across the width. Experimental modal analysis was first performed to determine the modal parameters (modal or resonance frequency, mode damping, mode shape) of full-size OSB panels under this support condition. Figure 2 shows the experimental setup and grids of impact points for modal testing on a full-size OSB panel. The testing system is consisted of a multiple channel signal acquisition and analysis system (B&K 3560-C, Brüel and Kjær Copenhagen, Denmark), an accelerometer (type 4507-B-004, Brüel and Kjær Copenhagen, Denmark), an impact hammer (model 2302-10, Brüel and Kjær, Copenhagen, Denmark), a computer with data acquisition software (Pulse Software) and modal analysis software (ME'scope Software).

Eight 1.22 by 2.44 m commercial OSB panels of 4 different thickness (12, 15, 18, and 20 mm) were purchased and used in modal testing, 2 for each thickness. Each full-size OSB panel was simply supported on two rods, each located 22.4% from the short edge and fixed on a tri-stand. Modal testing was conducted with a single-point receiver coupled with multi-point excitation. The grids of impact points were marked on each panel as illustrated in Figure 2. The vibrational responses of the panel being tested were measured by an accelerometer attached to the corner, following the impacts at a series of locations as specified by the grid points. Modal analysis was then conducted based on a total of 60 measurements of the frequency response functions (FRFs) given by the relationship of the system's dynamic response and the excitation causing it (Carfagni and Mannucci 1996). Following modal testing, each panel was also subject to a free vibration test at the same support condition. The vibration responses were captured through a single laser sensor located beneath the panel at the mid-span. Natural frequencies of each panel were then determined through fast Fourier analysis (FFT) program.

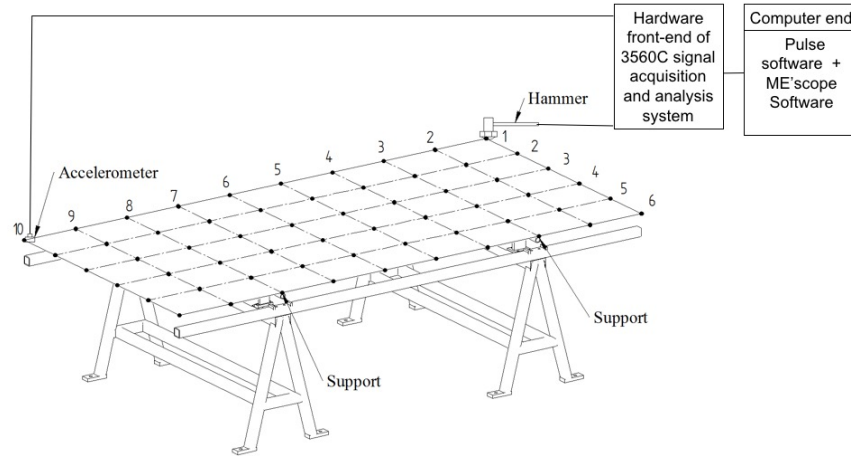
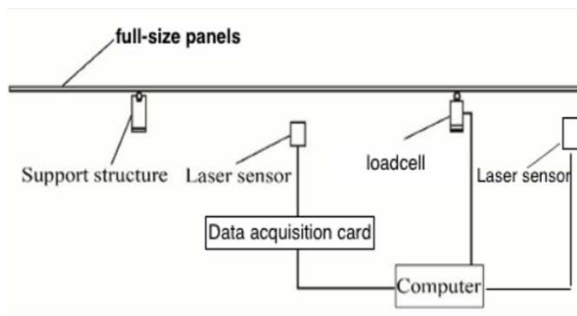


Figure 2—Experimental setup for modal testing of a full-size OSB panel.



(a)

(b)

Figure 3—Laboratory experimental setup for free vibration testing of full-size panels.

Free vibration test

Fifty 1.22 by 2.44 m full-size OSB panels of 5 thickness categories were obtained for free vibration test. Among the 50 panels, 26 panels were donated by two OSB manufacturers in the U.S., including 6 rejected panels (due to quality issues), and 24 panels were purchased from a local Home Depot store in Madison, Wisconsin, USA. These full-size panels constitute a matrix of 5 thickness groups (6, 11, 13, 15, and 18 mm), 10 panels for each group (Table 1). Upon receiving of the panels, they were stored in a conditioning room (21 °C and 50% relative humidity) for over 2 months waiting for the vibration test setup being built and ready for the full-size panel testing.

Figure 3 shows the schematic diagram of free vibration testing system and the testing apparatus constructed. The test system included a test frame with two steel rods attached on the frame, each at a nodal location and directly above the supports. Two load cells were installed under one of the bars to measure the weight of each panel. Two laser sensors were used to measure the vibrational responses of the panel, one located directly under the center of the panel and the other located at the corner of the panel, both were placed about 10 mm below the panel.

During vibration testing, a full-size OSB panel was first placed on the test frame and set to the test position by the stop levers installed on the steel beam. The weight of the panel was measured by two load cells. Then the panel was set into free vibration by impacting the center of the panel using an impact hammer. The laser sensors fed the vibration signals into the computer through a data acquisition card. A computer program was written and used for display and collect both the impact and response signals. Figure 4 shows the vibration testing of an OSB panel.

Table 1—1.22 by 2.44 m full size OSB panels obtained for free-vibration testing.

Category	Thickness (mm)	No. of panels	Material source		Note
			Manufactures ^a	Home Depot	
23/32	18	10	5	5	
19/32	15	10	10	0	2 rejected panels
1/2	13	10	1	9	1 rejected panel
7/16	11	10	10	0	3 panels rejected
1/4	6	10	0	10	

^a OSB panels donated by the manufacturers and purposely included some rejects.



Figure 4—Vibration test of a full-size OSB panel

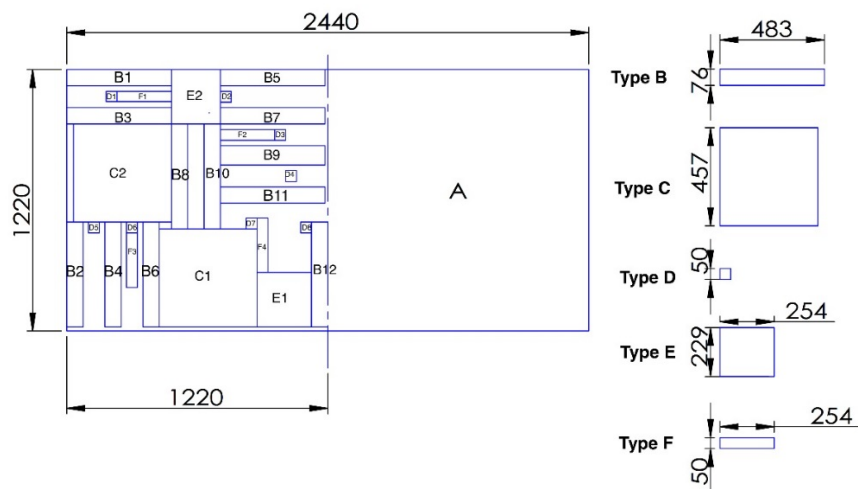


Figure 5—Diagram of cutting various small specimens from full-size panel for mechanical testing.

Determination of mechanical properties

Upon completion of vibration testing, 25 panels, 5 of each thickness group, were selected to cut into specimens of various sizes and conduct mechanical tests to determine the following properties of the panels: modulus of elasticity (in major and minor directions), shear modulus, internal bond, impact resistance, and Poisson's ratio. Figure 5 shows the specimen cutting diagram that resulted in six types of specimens: type A—half panel for pure moment test; type B—small flexure specimens for bending test; type C—small specimens for shear test; type D—small specimens for internal bond test; type E—small specimens for falling ball impact test; and type F—small specimens for Poisson ratios test. Detailed specimen information are shown in Table 2.

Modulus of elasticity

Modulus of elasticity of the type “A” (half panel) specimens will be determined based on ASTM D 3043, method C (ASTM 2006a).

Modulus of elasticity of the small flexure specimens (type B) in both major and minor strength directions will be determined through center point flexure test based on ASTM D 1037 (ASTM 2006b). A total of 12 small flexure specimens were cut from each panel, 6 along the main strength direction and 6 along the minor strength direction. These flexure specimens were named as type “B” as shown in Figure . The load-deflection curve will be recorded and used to calculate the MOE. Modulus of rupture (MOR) of the specimen will also be calculated by the maximum moment when the specimen breaks. The average MOE of 6 specimens in each direction will be treated as the MOE of the whole panel, in major and minor direction respectively.

Shear modulus

Shear modulus (G_{12}) of type C specimens will be determined based on ASTM D3044 (ASTM 2006c). A support jig is currently being built to load and observe the deflections along the diagonals as stipulated in the standard.

Internal bond

Internal bond, or tension perpendicular to surface, of type D specimens will be determined based on ASTM D1037 section 11 (ASTM 2006b). Loading blocks of aluminum alloy 50-mm square and 25 mm in thickness will be bonded with a suitable adhesive to the square faces of the specimens.

Falling ball impact

Falling ball impact test will be used to determine the impact resistance of the OSB panels from the kind of damage that occurs in service when struck by moving objects. Two type E specimens were obtained from each panel for this test. The test procedure will follow the ASTM D1037 section 21 (ASTM 2006b).

Poisson's ratios

Poisson ratios of OSB panels are key parameters that are needed in predicting the MOE in major and minor strength directions and shear modulus of OSB panels based on equations 4 to 6. However, this information is not available in existing literature. In this study, we will attempt to determine Poisson's ratios of the OSB panels through special experiments on type F specimens cut from selected panels. The experiments we used are similar to what Alan Sliker (1972) had done on solid wood specimens. The results of this experiment will provide realistic estimates of the Poisson's ratios of the OSB panels.

Table 2—Matrix of specimens and mechanical tests.

Mechanical tests	Specimen Type	Thickness (mm)	Length (mm)	Width (mm)	No. of specimens per panel	Total no. of specimens
Pure moment test (ASTM D 3043, method C)	A	18	1220	1220	1	5
		15	1220	1220	1	5
		13	1220	1220	1	5
		11	1220	1220	1	5
		6	1220	1220	1	5
Center-point flexure test (ASTM D 1037)	B	18	482	76	12	60
		15	432	76	12	60
		13	356	76	12	60
		11	330	76	12	60
		6	203	76	12	60
Shear test (ASTM D 3044)	C	18	457	457	2	10
		15	457	457	2	10
		13	457	457	2	10
		11	457	457	2	10
		6	203	203	2	10
Internal bond test (Tension perpendicular to surface) (ASTM D 1037)	D	18	51	51	8	40
		15	51	51	8	40
		13	51	51	8	40
		11	51	51	8	40
		6	51	51	8	40
Falling ball impact test (ASTM D 1037)	E	18	254	223	2	10
		15	254	223	2	10
		13	254	223	2	10
		11	254	223	2	10
		6	254	223	2	10
Poisson's ratios test	F	18	254	51	4	20
		15	254	51	4	20
		13	254	51	4	20
		11	254	51	4	20
		6	254	51	4	20

Results and discussion

Vibration modes of OSB panels

Based on the FRFs measured at 60 grid points on each panel, the vibration modes and frequencies of each tested panel were determined through modal analysis. As an example, Figure 6 shows the mode shapes of panel OSB15-2. It was observed that the mode shapes at the 1st and 2nd order were flexural along the length direction; the mode shapes at the 3rd, 4th, and 5th order were flexural along the length direction combined with torsion; and the mode shapes at the 6th and 7th order were flexural along both the length and width directions. These general observations about the mode shapes also apply to all other OSB panels tested. It was also observed that the OSB panels of 4 different thicknesses exhibited the same mode shape sequences in the experimental modal analysis. This observation is consistent with previous findings on medium density board and particleboard panels (Zhou et al. 2014).

Table 3 summarizes the specific modes identified for each panel. There were four cases where the exact modes were not very clear and hard to identify the exact nodal lines like the other modes. We speculate that these confused vibration modes could be caused by the warps occurred to those panels which resulted in an uneven supporting condition on the supporting rods. This implies that testing warped panels under the nodal-line support condition is a challenge. However, this may not be a problem if the vibration testing is conducted in a manufacturer facility when OSB panels are just coming out of the press with a very flat form.

The experimental mode shapes at the 1st, 3rd, 7th order were generally identified as the mode shapes (2, 0), (2, 1), and (2, 2) respectively, which are same as those for an OSB panel in completely free-edge support condition (Table 3). This can be explained by the fact that the nodal-line supports used for modal testing of full-size OSB panels coincided with the nodal lines of the panel in a completely free-edge support condition. It should be noted that exceptions were observed for OSB18-3 and OSB20-2 at the 3rd order and OSB 18-3 and OSB20-3 at the 7th order. The OSB panel 18-3 had a significant warp which affected the experimental mode shapes as we mentioned early. The mode shapes of other 3 cases could also be caused by the changes in supporting conditions resulted from the panel deformation, which could have been overlooked during the model testing.

The experimental modes identified at the 2nd, 4th, 5th, and 6th order were not in line with the same modes typically found in a completely free-edge condition. Apparently, due to the existence of two line supports, the nodal lines for these modes have shifted and resulted in these unique mode shapes.

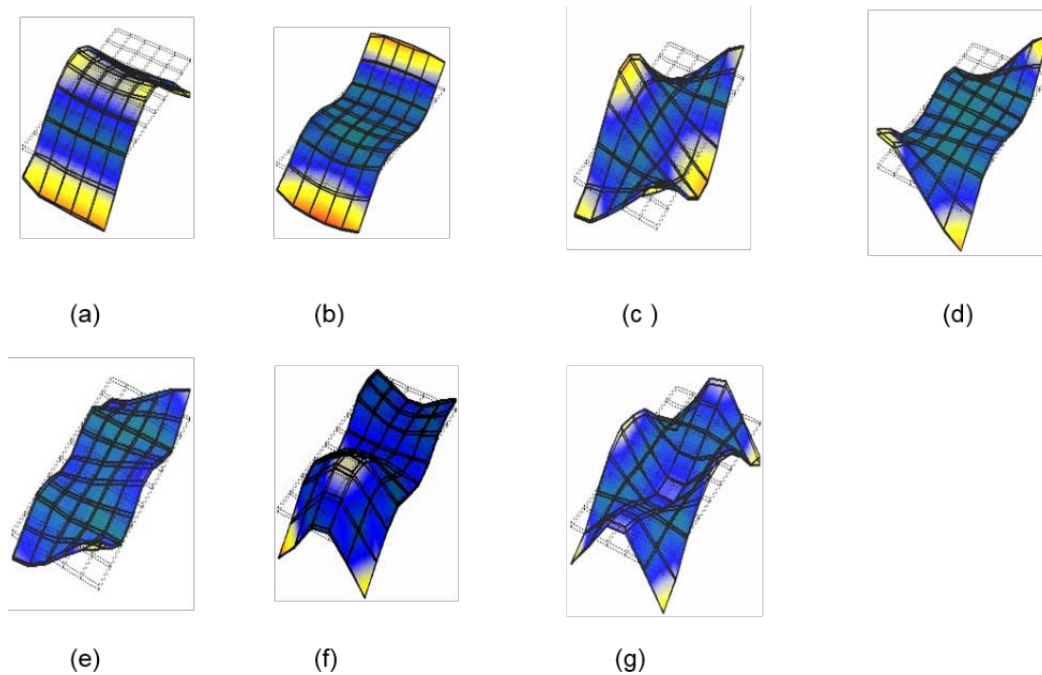


Figure 6—Mode shapes of OSB 15-2 identified through experimental modal analysis. (a) 1st mode (2, 0); (b) 2nd mode (3, 0); (c) 3rd mode (2, 1); (d) 4th mode (4, 0); (e) 5th mode (3, 1); (f) 6th mode (3, 1); (g) 7th mode (2, 2).

Table 3—Vibration modes of OSB panels identified in vibration testing under nodal-line supports.

Specimen No.	Thickness ^a (mm)	Vibration mode identified						
		1 st	2 nd	3 rd	4 th	5 th	6 th	7 th
OSB12-2	12	(2,0) ^b	(3,0)	(2,1) ^b	(4,1)	(3,2)	(2,2)	(2,2) ^b
OSB12-3	12	(2,0) ^b	(3,0)	(2,1) ^b	(3,1)	(4,1)	(4,1)	(2,2) ^b
OSB15-2	15	(2,0) ^b	(3,0)	(2,1) ^b	(4,0)	(3,1)	(2,2)	(2,2) ^b
OSB15-3	15	(2,0) ^b	(3,0)	(2,1) ^b	(3,1)	n/a ^c	(3,2)	(2,2) ^b
OSB18-2	18	(2,0) ^b	n/a ^c	(2,1) ^b	(3,1)	(1,2)	(4,2)	(2,2) ^b
OSB18-3	18	(2,0) ^b	(3,0)	n/a ^c	(2,1)	(4,1)	(0,2)	(3,2)
OSB20-2	20	(2,0) ^b	n/a ^c	(3,0)	(2,1)	(3,1)	(1,2)	(2,2) ^b
OSB20-3	20	(2,0) ^b	(3,0)	(2,1) ^b	(4,0)	(3,1)	(4,1)	(3,2)

^a Nominal thickness; ^b Same as the mode in a completely free-free condition; ^c Vibration mode was not clear and nodal lines cannot be identified.

The results of modal analysis indicate that vibration modes are affected by the support conditions. Under a simple two nodal-line support, the 1st, 3rd, and 7th order frequencies measured in a full-size panel correspond to the vibration modes (2, 0), (2, 1), and (2, 2) respectively. These frequency parameters can be used to predict the modulus of elasticity (MOE) of the panels using equations 3 and 5, and predict the shear modulus of the panels using equation 4.

Frequency comparison between modal analysis and free vibration test

The frequencies of the first 9 orders obtained from the experimental modal analysis and vibration testing are presented in Table 4. The difference between the frequency from vibration testing and the frequency from modal analysis was calculated for each order and shown as Δf . Figure 7 illustrates this frequency difference in relation to the frequency order. It is clear that two frequencies were very close within each order for the first 5 orders, with an absolute difference less than 1 Hz. The frequency difference began to increase at order 6. From there the difference got bigger when the order was further increased. The largest frequency discrepancy occurred at the 8th and 9th order, which could be due to the misidentification of the frequency orders. For example, in OSB12-2 panel, the 9th order from the modal analysis was actually closer to the 8th order from the vibration test, rather than the 9th order. It is possible that one frequency could have been missed in analyzing the response signal of the panel.

When we consider the frequencies of first seven orders, the frequency from vibration test showed a 1:1 linear relationship with the frequency from modal analysis ($R^2=0.99$) (Figure 8). This indicates that the vibration test system we proposed is a viable nondestructive testing system for obtaining the natural frequencies of OSB panels.

Table 4—Frequencies of the full-size OSB panels obtained from modal analysis and free vibration test.

Sample no.	Method	Frequency order								
		1	2	3	4	5	6	7	8	9
OSB 12-2	Modal test	6.99	13	15.7	17.4	25.2	33	36.2	41.4	56.4
	Vibration test	7.01	12.71	15.94	17.65	26.01	35.49	37.24	56.30	75.94
	Δf	0.02	-0.29	0.24	0.25	0.81	2.49	1.04	14.9	19.54
OSB 12-3	Modal test	7.49	11.1	15.3	17	21.5	26.3	34.3	38.1	43.4
	Vibration test	7.48	11.03	15.15	17.02	21.43	26.33	33.77	38.09	43.13
	Δf	-0.01	-0.07	-0.15	0.02	-0.07	0.03	-0.53	-0.01	-0.27
OSB 15-2	Modal test	9.3	16.2	20	22.8	25.5	28.4	39.8	43.4	48.9
	Vibration test	9.30	16.16	19.96	22.77	25.26	28.32	39.91	43.35	48.33
	Δf	0	-0.04	-0.04	-0.03	-0.24	-0.08	0.11	-0.05	-0.57
OSB 15-3	Modal test	8.79	14.8	17.6	19.5	20.7	26.5	29.8	38.9	41.1
	Vibration test	8.74	14.67	17.38	19.43	20.62	26.56	29.79	39.03	41.73
	Δf	-0.05	-0.13	-0.22	-0.07	-0.08	0.06	-0.01	0.13	0.63
OSB 18-2	Modal test	10.8	17.2	22.4	31.9	37.4	44.5	49.9	52.1	56.4
	Vibration test	10.90	17.17	22.97	32.22	37.43	44.54	48.38	49.66	51.71
	Δf	0.1	-0.03	0.57	0.32	0.03	0.04	-1.52	-2.44	-4.69
OSB 18-3	Modal test	11.2	13.9	15.7	19	23.1	23.7	32.5	38.2	49.3
	Vibration test	11.03	13.49	15.39	18.93	23.33	25.33	27.22	33.06	46.01
	Δf	-0.17	-0.41	-0.31	-0.07	0.23	1.63	-5.28	-5.14	-3.29
OSB 20-2	Modal test	12.1	15.4	20.7	26	35.9	47.2	54.9	58.7	64
	Vibration test	12.07	15.33	20.73	26.33	36.00	47.26	54.89	58.54	64.02
	Δf	-0.03	-0.07	0.03	0.33	0.1	0.06	-0.01	-0.16	0.02
OSB 20-3	Modal test	12.4	20.3	25.5	28.5	31	36.5	47.8	54.3	73.4
	Vibration test	12.36	20.25	25.45	28.28	30.98	36.56	47.69	54.33	73.03
	Δf	-0.04	-0.05	-0.05	-0.22	-0.02	0.06	-0.11	0.03	-0.37

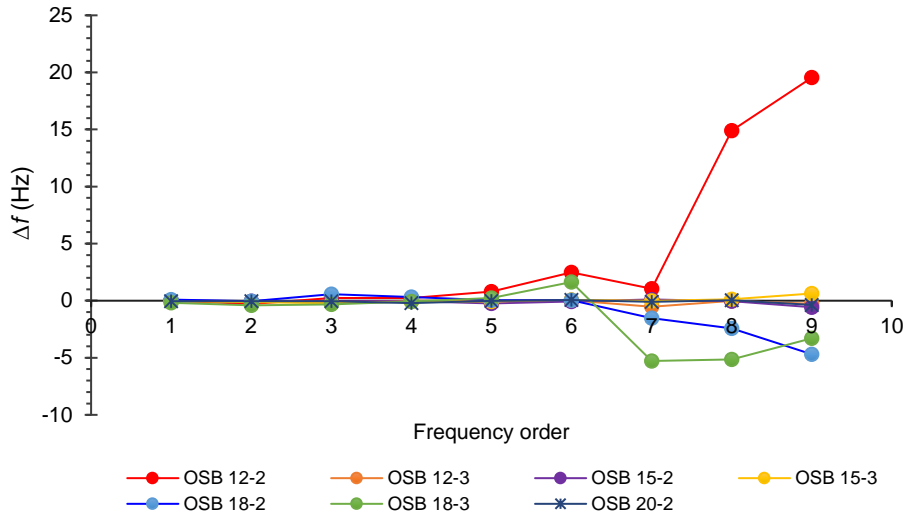


Figure 7— Difference between the frequency from vibration testing and the frequency from modal analysis.

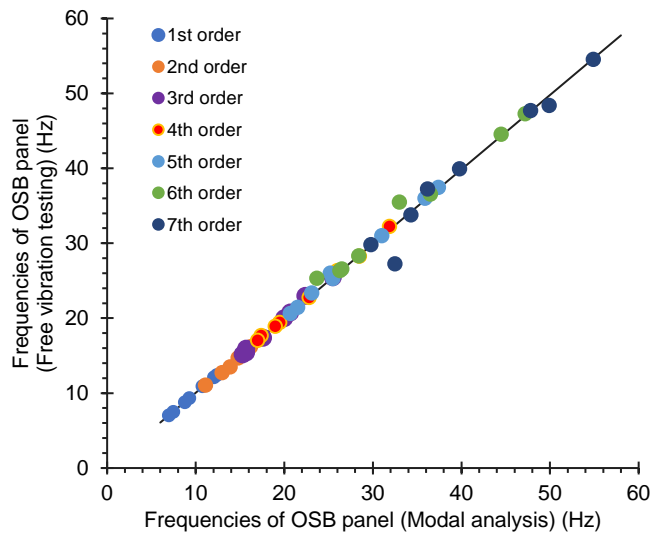


Figure 8—Relationship between frequency from vibration test and frequency from modal analysis.

Conclusions

The results of modal analysis indicated that vibration modes are affected by the support conditions. Under the two nodal-line support condition, the 1st, 3rd, and 7th order frequencies measured in a full-size panel correspond to the vibration modes (2, 0), (2, 1), and (2, 2) respectively. These frequency parameters can be used to predict the modulus of elasticity and shear modulus of the panels based on the equations derived from the plate vibration theory. The natural frequencies in the first 7 orders obtained from free vibration test showed an excellent agreement with the frequencies obtained from the modal analysis. This indicates that the vibration test system we proposed is a viable nondestructive testing system for measuring the natural frequencies of full-size OSB panels.

The vibration response signals of 50 full-size OSB panels are currently being analyzed to determine the natural frequencies in multiple orders. The mechanical testing of the half panels and small specimens is also underway now. Further paper will report the results on prediction of various mechanical properties of the OSB panels using the frequency and physical parameters.

Acknowledgement

This project was conducted through research cooperation between the USDA Forest Service Forest Products Laboratory (FPL) and Beijing Forestry University (BFU), Beijing, China. Ms. Lujing Zhou's research visit at FPL was supported by the China Scholarship Council and the Special Research Funds for Public Welfare (Grant No. 201304512) from State Forest Administration of China.

References

- ASTM. 2006a. D 3043. Standard test methods for structural panels in flexure. West Conshohocken, PA: American Society for Testing and Materials.
- ASTM. 2006b. D 1037. Standard test methods for evaluating properties of wood-base fiber and particle panel materials. West Conshohocken, PA: American Society for Testing and Materials.
- ASTM. 2006c. D 3044-94 (Reapproved 2006). Standard test method for shear modulus of wood-based structural panels. West Conshohocken, PA: American Society for Testing and Materials.
- Bos, F.; S. B. Casagrande. 2003. On-line non-destructive evaluation and control of wood-based panels by vibration analysis. *Journal of sound and vibration* 268(2): 403-412.
- Carfagni, M.; M. Mannucci. 1996. A simplified dynamic method based on experimental modal analysis for estimating the in-plane elastic properties of solid wood panels. *International symposium on nondestructive testing of wood*.
- Hearmon, R. F. S.; A. A. Maradudin. 1961. An introduction to applied anisotropic elasticity. *Physics Today* 14:48.
- Lau, P.; Y. Tardif. 1996. Evaluation of Moduli of Elasticity and Rigidity of Panel Products by Torsional-Bending Vibration. *Canadian Forest Service*.
- Zhou, L.; H. Zhang; C. Guan; X. Wang. 2014. Analysis of vibration modal testing for the full-size artificial board. *Journal of Multimedia* 9(6): 816-822.
- Nakao, T.; T. Okano; I. Asano. 1985. Vibrational properties of a wooden plate. *Mokuzai Gakkaishi* 31 (10): 793-800.
- Schulte, M.; A. Frühwald; F.-W. BRÖKER. 1996. Non-destructive testing of panel products by vibration technique. *International symposium on nondestructive testing of wood*.
- Shyamasunder, K.; B. Aswathanarayana; M. Naidu. 1993. Nondestructive evaluation of modulus of elasticity and modulus of rigidity of plywood by sonic methods. *Proceedings of the Ninth International Symposium on Nondestructive Testing of Wood*.

- Sliker, A. 1972. Measuring Poisson's ratios in wood. *Experimental Mechanics* 12 (5): 239-242.
- Sobue, N.; M. Kitazumi. 1991. Identification of power spectrum peaks of vibrating completely-free wood plates and moduli of elasticity measurements. *Mokuzai Gakkaishi* 37 (1): 9-15.
- Sobue, N.; A. Katoh. 1992. Simultaneous determination of orthotropic elastic constants of standard full-size plywoods by vibration method. *Mokuzai Gakkaishi* 38 (10): 895-902.
- Turk, C.; J. F. Hunt; D. J. Marr. 2008. Cantilever-beam dynamic modulus for wood composite products: Part 1 apparatus: Forest Products Laboratory, Forest Service, US Department of Agriculture.

Modal Testing and Theoretical Modal Analysis of Full-Size Medium Density Fiberboards Supported at Four Nodes

Cheng Guan

School of Technology, Beijing Forestry University, Beijing, China, 648911029@qq.com

Houjiang Zhang

School of Technology, Beijing Forestry University, Beijing, China, hjzhang6@bjfu.edu.cn

Lujing Zhou

School of Technology, Beijing Forestry University, Beijing, China, 229134038@qq.com

Xiping Wang

USDA Forest Service, Forest Products Laboratory, Madison, Wisconsin, USA, xwang@fs.fed.us

Abstract

In this study, modal parameters of full-size medium density fiberboard (MDF) panels supported at four nodes were analyzed for determining modulus of elasticity (E) in both major and minor axes as well as in-plane shear modulus of the panels using a vibration testing method. Modal testing was conducted on three full-size MDF panels of three different thicknesses (12, 15, 18 mm) to measure the natural frequencies and mode shapes of the first nine modes of vibration. Results of modal testing were compared with those obtained through theoretical modal analysis. A sensitivity analysis was then performed to identify sensitive modes for calculation of the modulus of elasticity (major axis: E_x and minor axis: E_y) and in-plane shear modulus (G_{xy}) of the panels. Mode shapes of the MDF panels from model testing were in agreement with the results from finite element analyses. A strong linear relationship was found between measured natural frequencies and calculated frequencies of the panels. The frequencies of modes (2, 0), (0, 2) and (2, 1) were determined as characteristic frequencies and used for calculation of E_x , E_y and G_{xy} of full-size MDF panels under four-node support condition. The results indicated that four-node support can be used in vibration testing to determine elastic properties of full-size MDF panels.

Keywords: modal testing, theoretical modal analysis, mode shape, natural frequency, panels, sensitivity analysis, vibration testing

Introduction

Medium density fiberboard (MDF), as one of the typical wood composite panels (WCPs), is widely used in furniture manufacture, packaging, decoration, building construction, musical instrument and other industrial sectors. Full-size MDF panels with a nominal size of 2440 mm \times 1220 mm (length \times width) are most universal in the production and sales. For full-size MDF panels, key mechanical characteristics such as modulus of elasticity (E) and in-plane shear modulus must be taken into consideration under different use conditions. Accurate measurement of these elastic properties for MDF panels is therefore of great importance to meet the requirements of different environments.

The application of non-destructive evaluation (NDE) methods, just like transverse vibration or longitudinal stress-wave, for elastic properties determination of WCPs has been studied for many years (Coppens 1988; Sobue et al. 1992; Schulte et al. 1996; Larsson 1997; Chi et al. 2006; Yoshihara 2011; Hunt et al. 2013; Mirbolouk et al. 2015; Guan et al. 2015; 2016a; 2016b; Zhou et al. 2016). Among these studies, property evaluation of small wood composite specimens through beam-vibrational method has been used with good success and a dynamic cantilever beam apparatus for elastic properties determination of small wood composite materials was presented by Hunt and Guan (2013; 2016a). However, non-destructive evaluation of full-size WCPs through panel-vibrational method was still in the research stage. A fundamental aspect of this method is to support a panel in a well-defined position, induce a vibration to the panel by a short impact and to measure the resonant frequencies. Knowing the resonant frequencies of different vibration modes and the boundary conditions, the elastic properties of the panel can be calculated, including the E in both major and minor axes and the in-plane shear modulus of the panel. Coppens (1988) was one of the first using this method to test the elastic constants of particleboards under the four sides completely free (FFFF) boundary condition by hanging them up on rubbers ties. A simultaneous measurement of elastic properties of full-size plywood with one edge simply supported and three edge free (SFFF) boundary condition by this vibration method was conducted by Sobue and Katoh (1992). The dynamic elastic properties of full-scale particleboard and MDF panels were tested using the same vibration technique in a vertical cantilever (CFFF) arrangement (Schulte et al. 1996). A laboratory testing apparatus was used to measure the dynamic MOE and dynamic viscoelasticity of full-size WCPs supported on their two nodal lines by a vibration testing way (Guan et al. 2015; 2016b). Based on a modal testing technique, Zhou et al. (2016) developed a NDE method for full-size engineered wood-based panels with a boundary condition, in which two opposite sides were simply supported and the other two sides were free (SFSF). In addition, finite element (FE) modelling was also used for estimation of elastic properties of full-size WCPs combined with NDE method. Larsson (1997) tested full-size oriented strand board modelled as thin orthotropic plate under FFFF boundary condition using modal analysis. These elastic constants were then estimated by minimizing the relative errors between experimental frequency and FE modelled values by an iteration process. It comes to a conclusion in all these works that there is a good correlation between elastic constants of full-size WCPs obtained by this panel-vibrational method and those measured by the traditional static method. However, due to poor operation, hitherto it seems the reported methods in these studies above are only applicable to conduct in the laboratory and not widely used for on-line property evaluation of full-size WCPs. Another conclusion can be also drawn from these studies that elastic properties of WCPs are closely associated with their vibration modal parameters. In order to determine elastic properties of full-size WCP, the key is to find out the vibration mode shapes required and measure the corresponding resonance frequencies of the panel under the given boundary condition.

In many cases, small MDF specimens are always regarded as being in-plane quasi-isotropic materials, which have nearly the same property values in the major and minor directions (Chi et al. 2006; Yoshihara 2011; Hunt et al. 2013; Guan et al. 2016b). However, full-size MDF panels can be modelled as orthotropic materials with non-uniform values in the major, minor and thickness directions in many studies (Schulte et al. 1996; Mirbolouk et al. 2015; Zhou et al. 2016). Zhang et al. (2015) also found that E along the major direction were 56% higher than that along the minor direction for a 20 mm thick full-size MDF panel using cantilever-beam bending. Thus full-size MDF panels were considered to be orthotropic materials in this study.

The objective of this presented study was to lay a foundation for determining elastic properties of full-size MDF panel by a vibration method for on-line non-destructive testing. The first nine modal parameters (natural frequency and mode shape) of the vibration of full-size MDF panel supported at four nodes with three different thicknesses were tested by experimental modal analysis. Results from experimental modal testing were compared with theoretical modal analysis by COMSOL Multiphysics® software (COMSOL Inc., Stockholm, Sweden). The sensitivity analysis was then performed to determine the sensitive modes

for calculation of E in both major and minor axes, as well as the in-plane shear modulus of full-size MDF panels with four nodes of support.

Relationship between modal parameters and elastic properties of full-size MDF panels

Full-size MDF panel is assumed for an orthotropic thin-plate modal. For a thin rectangular orthotropic plate, neglecting the effects of shear deformation and rotatory inertia, its governing differential equation for the transverse vibration is expressed as follows (Leissa 1969):

$$D_x \frac{\partial^4 \omega}{\partial x^4} + D_y \frac{\partial^4 \omega}{\partial y^4} + 2(D_1 + 2D_{xy}) \frac{\partial^4 \omega}{\partial x^2 \partial y^2} + \rho h \frac{\partial^2 \omega}{\partial t^2} = 0 \quad (1)$$

$$D_x = \frac{E_x h^3}{12(1 - \nu_{xy} \nu_{yx})} \quad (2)$$

$$D_y = \frac{E_y h^3}{12(1 - \nu_{xy} \nu_{yx})} \quad (3)$$

$$D_1 = D_x \nu_{yx} = D_y \nu_{xy} \quad (4)$$

$$D_{xy} = \frac{G_{xy} h^3}{12} \quad (5)$$

where D_x and D_y are the flexural rigidities along the major and minor directions of the plate, D_1 is the equivalent rigidity; D_{xy} is the torsional rigidity; ρ is the mass density of the plate; h is the thickness of the plate; ν_{xy} and ν_{yx} are the Poisson's ratios; and E_x , E_y , and G_{xy} are the E along the major and minor directions and in-plane shear modulus, respectively.

In this study, the four-node support is chosen for modal testing and analysis of full-size panels because vibration tests under such support conditions can be readily implemented for on-line non-destructive testing. The four-node support refers to a full-size panel being supported at four node points, the intersections of two nodal lines of mode (2, 0) and mode (0, 2). These four nodal lines are located at 22.4% and 77.6% of its length and width, respectively. This support can be regarded as a special FFFF boundary condition, therefore, the solution of Equation (1) is based on the Rayleigh method with one-term deformation expression for the specific modes presented by Hearmon (1961). The resonant frequencies for an orthotropic plate can be expressed as (Sobue et al. 1991):

$$f_{(m,n)} = \frac{1}{2\pi} \sqrt{\frac{1}{\rho h} \sqrt{D_x \frac{\alpha_1}{a^4} + D_y \frac{\alpha_2}{b^4} + 2D_1 \frac{\alpha_3}{a^2 b^2} + 4D_{xy} \frac{\alpha_4}{a^2 b^2}}} \quad (6)$$

where $f_{(m,n)}$ is the natural frequency of a specific mode (m, n); a and b are the length and width of the plate; (m, n) identifies the mode, where m and n represent the number of node lines including the simply supported sides in the minor and major directions of the plate, respectively; and $\alpha_{1(m,n)}$, $\alpha_{2(m,n)}$, $\alpha_{3(m,n)}$, and $\alpha_{4(m,n)}$ are the coefficients for each specific mode related to the boundary conditions. Four mode shapes are presented in Figure 1 and the corresponding coefficients α_k are given in Table 1 (Nakao et al. 1985).

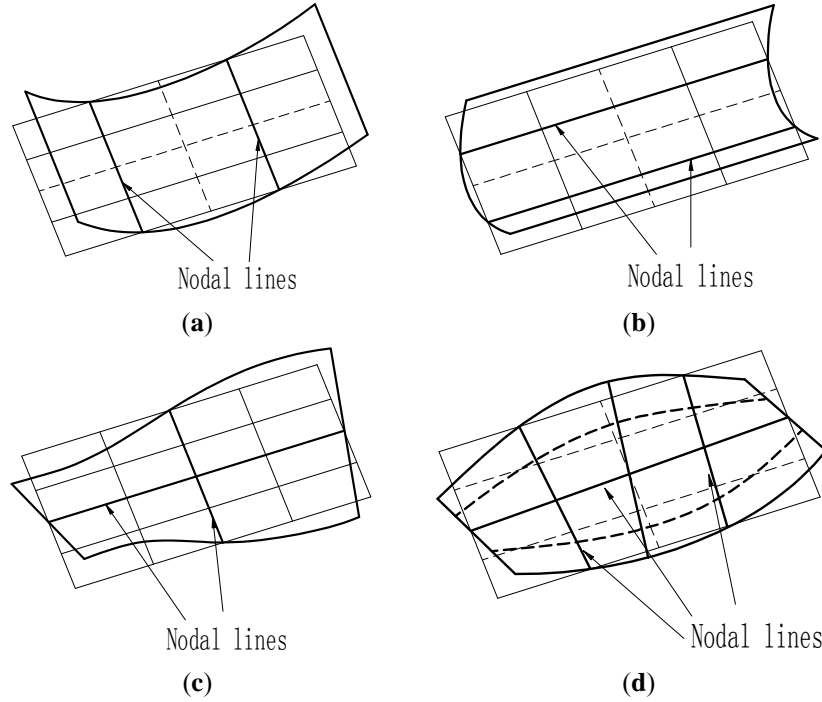


Figure 1-Four mode shapes. (a) Mode shape of mode (2, 0); (b) mode shape of mode (0, 2); (c) mode shape of mode (1, 1); and (d) mode shape of mode (2, 1).

Table 1-Corresponding coefficients for four mode shapes.

Mode		α_1	α_2	α_3	α_4
m	n				
2	0	500.6	0	0	0
0	2	0	500.6	0	0
1	1	0	0	0	144
2	1	500.6	0	0	593.76

Substituting Equations (2)–(5) into Equation (6), and considering the corresponding coefficients for four mode shapes shown in Table 1, the elastic properties E_x , E_y , and G_{xy} of a full-size MDF panel can be derived as follows:

$$E_x = \frac{48\pi^2 \rho a^4 (1 - \nu_{xy} \nu_{yx})}{500.6 h^2} f_{(2,0)}^2 \quad (7)$$

$$E_y = \frac{48\pi^2 \rho b^4 (1 - \nu_{xy} \nu_{yx})}{500.6 h^2} f_{(0,2)}^2 \quad (8)$$

$$G_{xy} = \frac{\pi^2 \rho a^2 b^2}{12 h^2} f_{(1,1)}^2 \quad (9)$$

$$G_{xy} = \frac{12 a^2}{593.76} \left(\frac{f_{(2,1)}^2 \pi^2 \rho b^2}{h^2} - \frac{500.6 E_x b^2}{48 a^4 (1 - \nu_{xy} \nu_{yx})} \right) \quad (10)$$

where $\nu_{xy} \nu_{yx}$ is substituted with 0.01 for most wood materials (Hearmon 1946).

When the panel geometry size (a , b , h) and density (ρ) are given, relationship between modal parameters and elastic properties of full-size MDF panels are obtained by taking these parameters to Eq. (7) - (10).

Materials and methods

Materials

Full-size MDF panels made of mixed species of both softwood and hardwood using urea-formaldehyde resin were provided by a local MDF manufacturer for this study. There were three different nominal thicknesses of 12, 15, 18 mm. The average moisture content of the panels was about 4%. The specifications of the samples are presented in Table 2.

Table 2-Specifications of full-size MDF panels tested.

Panel code	Panel sizes (thickness × width × length, mm)	Average density (kg/m ³)
MDF12	12.0 × 1220 × 2440	803
MDF15	15.0 × 1220 × 2440	723
MDF18	18.2 × 1220 × 2440	705

Experimental modal testing

Experimental modal testing is a technique for determining the modal parameters (modal or resonance frequency and mode shape) of a vibrating structure (Ewins 1986). The frequency response function (FRF) is generated by the relationship of the structure's dynamic response and the excitation causing it. Modal testing of the panels were conducted in a room with a relative humidity of $30 \pm 5\%$ and a temperature of 20 ± 2 °C. To obtain the mode shapes, a response (or excitation) reference point is set and the FRFs are measured at various points distributed on a preset grid. The mode shapes can then be reconstructed by means of the signs and magnitudes of the imaginary part of each measured resonance frequency.

Figure 2 shows the system diagram of modal testing and modal analysis for full-size MDF panels. The modal testing was performed using a Pulse signal collection and analysis system (type 3560-C, Brüel and Kjær, Copenhagen, Denmark). The vibrational response of the full-size MDF panel tested was measured by an accelerometer (type 4507-B-004, Brüel and Kjær, Copenhagen, Denmark), following the impact by an impulse hammer (model 2302-10, Brüel and Kjær, Copenhagen, Denmark). The signals were acquired and digitized via the chassis of this system. The modal parameters of the panels were obtained by some modal parameter identification methods using the post-processing software of this system.

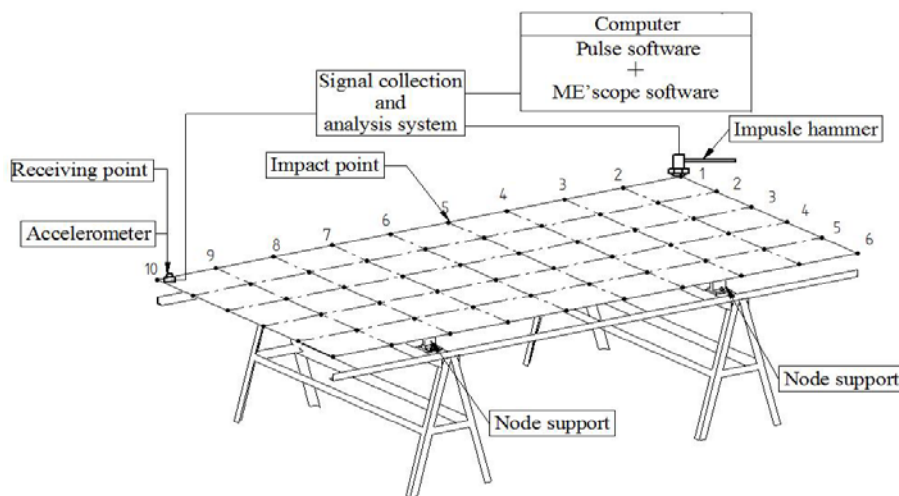


Figure 2-System diagram of modal testing and modal analysis for full-size MDF panels.

The supporting system designed for vibration testing of the panels is a four-node support as shown in Figure 2. In view of the reciprocity hypothesis satisfied between the excitation and response of the system, a single-point receiver coupled with multi-point excitation was adopted for the modal testing. For each panel under the four-node support, the receiver sensor is attached to the panel at a fixed position (plate corner), the panel is excited using an impulse hammer at a series of locations as specified by the grid points (Figure 2). In order to obtain ideal modal shapes, a total of 60 measurement points were selected and marked on each panel (5×9 grids).

During the modal testing, a full-size panel was symmetrically placed on the four-node support test bench. All of the measurement points on the panel were tapped successively to obtain the FRFs. To ensure the measurement accuracy and reduce random error, each measurement point was tested three times to obtain the average value of the FRFs. Then all the FRFs tested were imported into ME' scope software (Vibrant Technology Inc., Scotts Valley, USA) to carry through the modal parameter identification and mode shape simulation. The natural frequencies and mode shapes of the first nine vibration modes of the panel were obtained in this software.

Theoretical modal analysis

To further verify the modal parameters of the full-size MDF panel measured through the experimental modal testing, a theoretical modal analysis was conducted for each panel to obtain calculated frequencies and mode shapes of the first nine modes. Theoretical modal analysis is a modeling process that uses the FE method to discretize a vibrating structure, build a mathematical model about system eigenvalues, and solve the system eigenvalues and eigenvectors, namely modal frequencies and mode shapes of the structure (Guan et al. 2014). In this study, the COMSOL Multiphysics® software was used for theoretical modal analysis of the panels. Full-size MDF panels were modelled as a structural plate using plate element of the mixed interpolation of tensorial component (MITC) type, which can be used for analyzing both thin and thick plates. In this model, the major direction of the panel was set as X axis, the minor direction as Y axis and the thickness direction as Z axis. Since full-size panels were regarded as orthotropic materials, the model for each panel was established based on the input parameters including two E (E_x and E_y), three shear modulus (G_{xy} , G_{yz} , G_{xz}), one Poisson's ratio (ν_{xy}), density (ρ), and geometry size (a , b , h). Among them, E_x and E_y can be initially estimated based on the natural frequencies of modes (2, 0) and (0, 2) obtained in the above experimental modal testing according to Equations (7) and (8), respectively. The in-plane shear modulus G_{xy} was initially estimated using the natural frequency of mode (1, 1) obtained in the experimental modal testing according to Equation (9). Out-of-plane shear moduli G_{yz} and G_{xz} were determined by conducting three-point bending test on small MDF specimens cut from the full-size panels at different short spans (Divos et al. 1998; Yoshihara et al. 1998). Previous studies showed that the Poisson's ratio of a panel had a very small influence on the natural frequencies (Schulte et al. 1996; Larsson 1997; Sobue et al. 1991). Hence, the value of the Poisson ratio from the literature data was used in this study (Ganev et al. 2005).

In addition of density and geometry size (Table 2), other input parameters are shown in Table 3. Grid division methods had a very small effect on the result of the FE analysis for the plate model, and the model was conveniently meshed using free triangular meshing in the software. In order to ensure the numerical accuracy of the FE analysis, an initial and a smaller element mesh were used to obtain calculated frequencies, respectively. Through convergence analysis between calculated frequencies, a fit element mesh was chosen with the modal meshed with the largest element of 24.4 mm and the smallest element of 0.005 mm. According to the supporting system of the panel, the degree of freedom of four nodes on the Z axis was restricted in the model.

Table 3-Input parameters of the full-size MDF panels used in theoretical modal analysis.

Panel Code	MOE (GPa)		Shear Modulus (GPa)			Poisson's Ratio
	E_x	E_y	G_{xy}	G_{yz}	G_{xz}	
MDF12	4.09	4.22	1.99	0.12	0.13	0.3
MDF15	3.28	3.39	1.60	0.16	0.21	
MDF18	3.10	3.66	1.55	0.17	0.17	

Table 4-Initial calculated frequencies of full-size MDF panels in theoretical modal analysis.

Panel Code	Initial Calculated Frequencies (Hz)								
	1	2	3	4	5	6	7	8	9
MDF12	4.70	8.85	13.67	14.77	16.98	18.43	19.83	23.53	33.09
MDF15	5.53	10.42	16.14	17.44	20.08	21.83	23.37	27.76	39.09
MDF18	6.63	12.48	19.48	20.86	24.22	26.33	30.02	34.97	48.23

Since there were no closed-form solutions for the rectangular plate with FFFF direction condition, and the Rayleigh method applied for the calculation of Equation (1) was an approximate numerical method, the estimation of E_x , E_y , and G_{xy} , as three main input parameters, need to be refined. Those initially-estimated three elastic constants were updated according to the following equations [4]:

$$\left| \frac{f_{(2,0)}^{FE} - f_{(2,0)}^{EM}}{f_{(2,0)}^{EM}} \right| > 0.01 \Rightarrow E_x(N+1) = E_x(N) \left(\frac{f_{(2,0)}^{EM}}{f_{(2,0)}^{FE}} \right)^2 \quad (11)$$

$$\left| \frac{f_{(0,2)}^{FE} - f_{(0,2)}^{EM}}{f_{(0,2)}^{EM}} \right| > 0.01 \Rightarrow E_y(N+1) = E_y(N) \left(\frac{f_{(0,2)}^{EM}}{f_{(0,2)}^{FE}} \right)^2 \quad (12)$$

$$\left| \frac{f_{(1,1)}^{FE} - f_{(1,1)}^{EM}}{f_{(1,1)}^{EM}} \right| > 0.01 \Rightarrow G_{xy}(N+1) = G_{xy}(N) \left(\frac{f_{(1,1)}^{EM}}{f_{(1,1)}^{FE}} \right)^2 \quad (13)$$

Where N is number of iterations; f_{FE} represents the calculated frequency obtained by the FE method; and f_{EM} represents the experimental frequency obtained in the experimental modal testing. The experimental frequencies for modes (2, 0), (1, 1), and (0, 2) were compared with the corresponding initial calculated frequencies (Table 4). The initial estimates of $E_x(1)$, $E_y(1)$, and $G_{xy}(1)$ were updated according to Equations (11)–(13), respectively. The updated $E_x(2)$, $E_y(2)$, and $G_{xy}(2)$ were then used as new input parameters for another FE analysis. New frequencies were calculated next and were compared with the corresponding experimental ones again. Iteration step number one was then implemented. It was found that it was often effective to have three iterations.

Sensitivity analysis

Theoretically, any three natural frequencies can be used to calculate the three elastic constants (E_x , E_y , and G_{xy}) of the panel under a FFFF boundary condition according to Equation (6). For a specific boundary condition, however, some modes may be more sensitive to the variation of some elastic constants than others; therefore, the identification of the most sensitive modes for calculation was needed. One approach of sensitivity analysis is to change 10% of each elastic constant in a FE model and check the relative frequency differences (Larsson 1997; Antunes et al. 2008). Based on this approach, the sensitivity (Δ) can be defined as the frequency change as a specific elastic constant change:

$$\Delta = \frac{|f_{(m,n)}[\text{inc}] - f_{(m,n)}[\text{ref}]|}{f_{(m,n)}[\text{ref}]} \times 100\% \quad (13)$$

Where $f_{(m,n)}[\text{inc}]$ represents the calculated frequency of mode (m, n) when the input specific elastic constant in the FE model increases 10%, and $f_{(m,n)}[\text{ref}]$ represents the reference frequency. After three iterations in the above theoretical modal analysis, the calculated frequencies obtained were used as reference frequency values. Likewise, these input elastic constants for calculating reference frequencies were chosen as reference values of specific elastic constants, shown in Table 5. At first, the constant E_x was increased by 10% from its reference value and a new FM calculation was performed. Relative deviations between $f_{(m,n)}[\text{inc}]$ and $f_{(m,n)}[\text{ref}]$ of the first nine modes of vibration were calculated. Similar calculations were performed for E_y and G_{xy} . Scatterplots were used to indicate results of sensitivity analysis for full-size MDF panels tested.

Table 5-Reference values of moduli of elasticity E_x , E_y , and in-plane shear modulus G_{xy} .

Panel Code	Elastic Constants (GPa)		
	E_x	E_y	G_{xy}
MDF12	4.09	3.92	1.55
MDF15	3.28	3.14	1.24
MDF18	3.10	3.37	1.22

Results and discussion

Comparison between mode shapes of full-size MDF panels

The first nine mode shapes of MDF12 obtained from the experimental and theoretical modal analysis are shown in Figures 3 and 4, respectively. It can be seen from these figures that the same order for MDF12 shows the same mode shape obtained in the experimental and theoretical modal analysis: the mode shape at the first, second, and fourth order is flexural along the length direction; the mode shape at the third and sixth order is flexural along the length direction combined with torsion; the mode shapes at the seventh, eighth, and ninth order are flexural along the width direction, flexural along the width direction combined with torsion, and flexural along the length direction combined with flexural along the width direction, respectively; it is noted that the mode shape at the fifth order is made up of torsion consisted of the left and right part of two nodal lines along the width direction and nearly static part between two nodal lines along the width direction, thus the mode shape at the fifth order can be considered as torsion in mode (1, 1) neglecting the static part between two nodal lines along the width direction. In addition, the first nine order mode shapes for MDF15 and MDF18 obey the same rule in the experimental and theoretical modal analysis. For the first nine mode shapes of full-size MDF panels of three thicknesses, the same order shows the same mode shape in the experimental and theoretical modal analysis, which verifies the feasibility of these two modal analyses.

Comparison between resonance frequencies of full-size MDF panels

The first nine natural frequencies of full-size MDF panels with three different thicknesses in the experimental and theoretical modal analysis are given in Table 6. The calculated frequencies are the values obtained after three iterations in the theoretical modal analysis. The relative deviation (Diff) between the experimental frequency and calculated frequency are also given in Table 6. It can be seen from the table that the experimental frequencies at the first nine modes are in good agreement with the

calculated frequencies and the Diffs between all the frequencies are within 6% for all of the panels; the Diffs between the frequencies at the first, fifth and seventh order are within 1% after three iterations.

Figure 5 shows the relationship between the experimental frequencies and calculated frequencies in the first nine modes for the full-size MDF panels. There is a strong linear relationship between the experimental frequencies and calculated frequencies of all of the panels. This indicates that the vibration modal parameters of full-size MDF panels obtained through experimental modal analysis are valid.

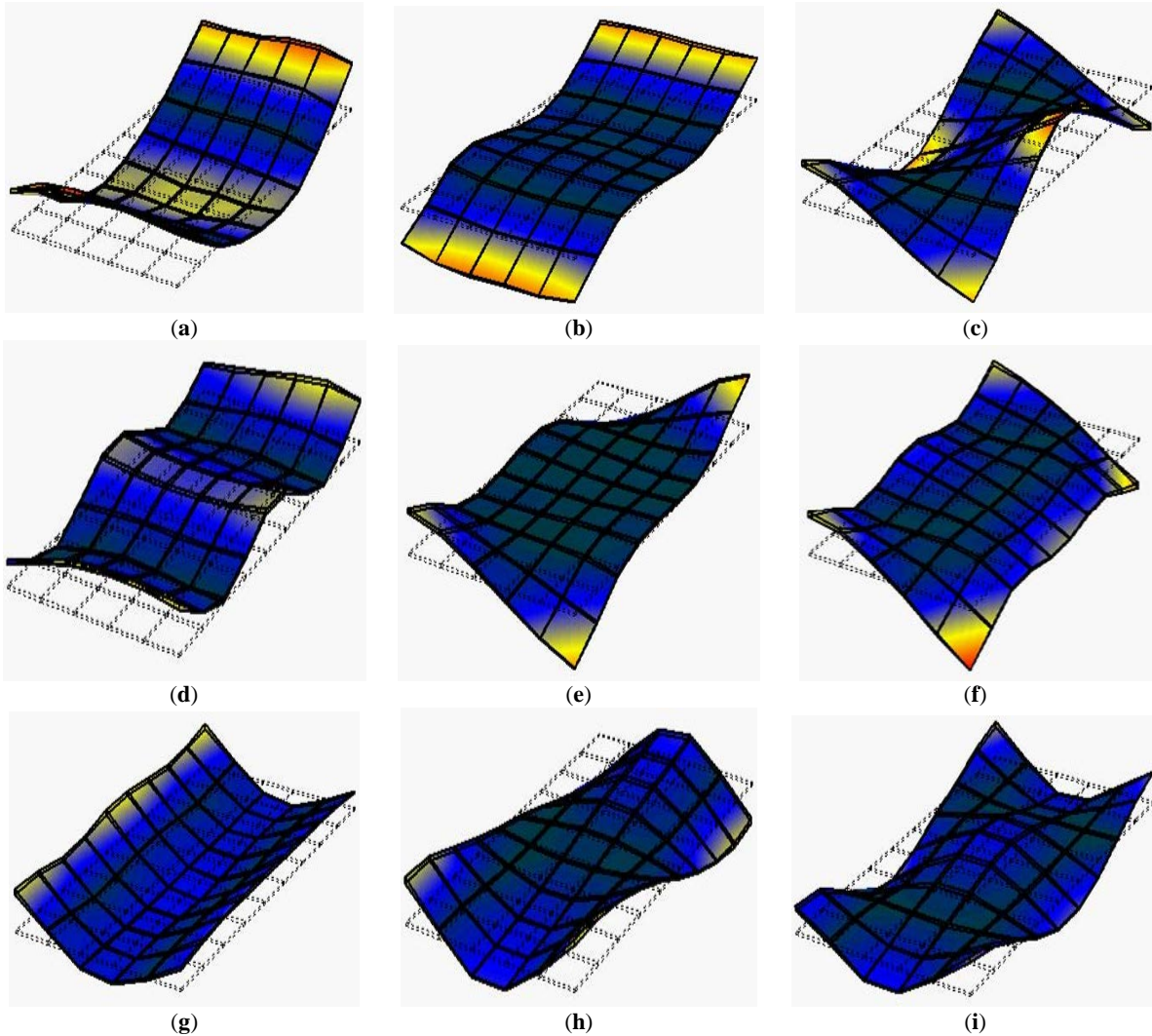


Figure 3-The first nine mode shapes of MDF12 obtained through experimental modal analysis. (a) Mode shape of the first mode (2, 0); (b) mode shape of the second mode (3, 0); (c) mode shape of the third mode (2, 1); (d) mode shape of the fourth mode (4, 0); (e) mode shape of the fifth mode (1, 1); (f) mode shape of the sixth mode (4, 1); (g) mode shape of the seventh mode (0, 2); (h) mode shape of the eighth mode (1, 2); and (i) mode shape of the ninth mode (2, 2).

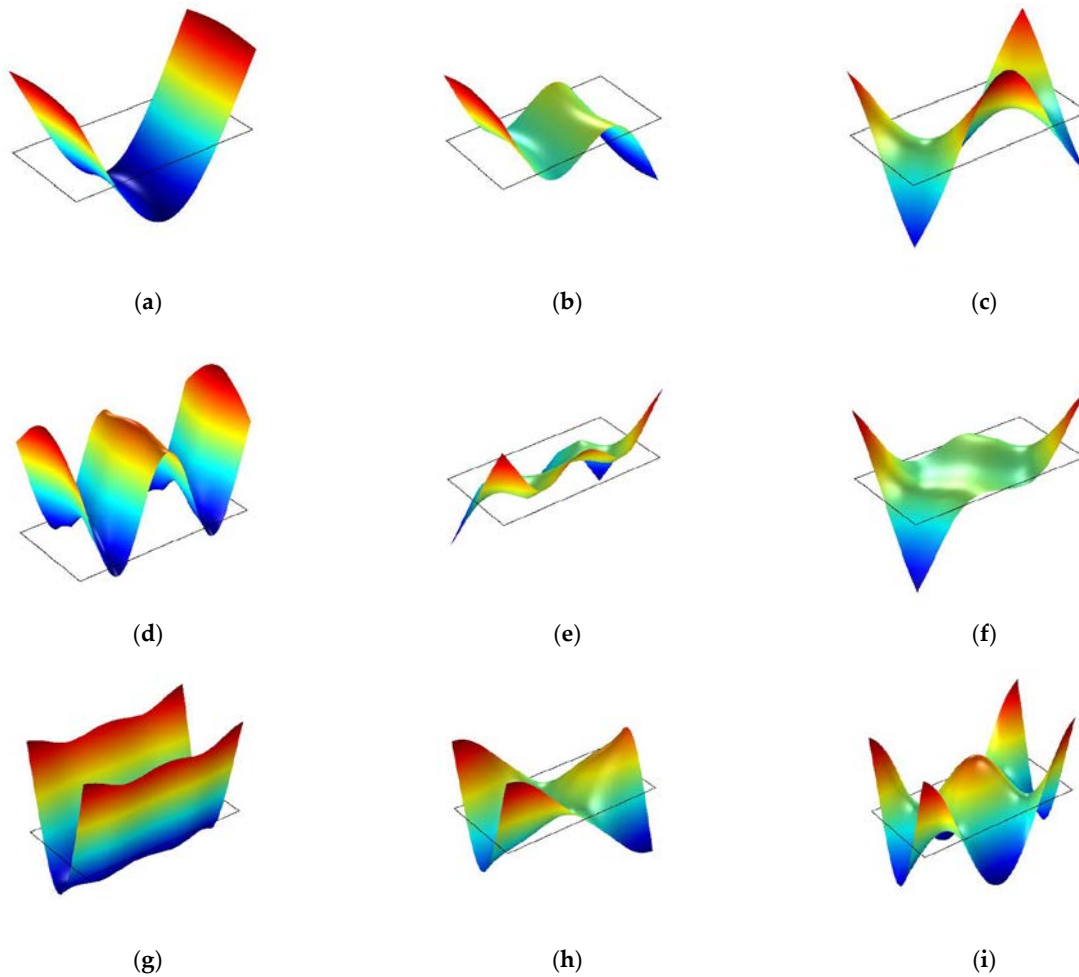


Figure 4—The first nine mode shapes of MDF12 obtained through theoretical modal analysis. (a) Mode shape of the first mode (2, 0); (b) mode shape of the second mode (3, 0); (c) mode shape of the third mode (2, 1); (d) mode shape of the fourth mode (4, 0); (e) mode shape of the fifth mode (1, 1); (f) mode shape of the sixth mode (4, 1); (g) mode shape of the seventh mode (0, 2); (h) mode shape of the eighth mode (1, 2); and (i) mode shape of the ninth mode (2, 2).

Table 6—The first nine natural frequencies of the full-size MDF panels obtained through the experimental and theoretical modal analysis ^a.

Order	Panel Code								
	MDF12			MDF15			MDF18		
	EF (Hz)	CF (Hz)	Diff (%)	EF (Hz)	CF (Hz)	Diff (%)	EF (Hz)	CF (Hz)	Diff (%)
1	4.70	4.70	0.05	5.53	5.53	0.04	6.62	6.62	0.01
2	8.67	8.81	1.64	10.20	10.38	1.77	12.20	12.43	1.85
3	12.50	12.42	0.66	14.80	14.62	1.23	17.70	17.75	0.26
4	14.20	14.67	3.31	16.70	17.32	3.69	20.10	20.72	3.08
5	15.60	15.67	0.47	18.40	18.49	0.47	22.30	22.40	0.47
6	16.90	17.52	3.66	19.70	20.72	5.16	24.30	25.05	3.07
7	19.10	19.05	0.28	22.50	22.44	0.28	28.80	28.70	0.34
8	22.30	22.11	0.84	26.20	26.05	0.57	33.20	32.86	1.03
9	30.70	30.45	0.81	36.40	35.88	1.43	45.30	44.48	1.81

^a EF—experimental frequencies; CF—calculated frequencies.

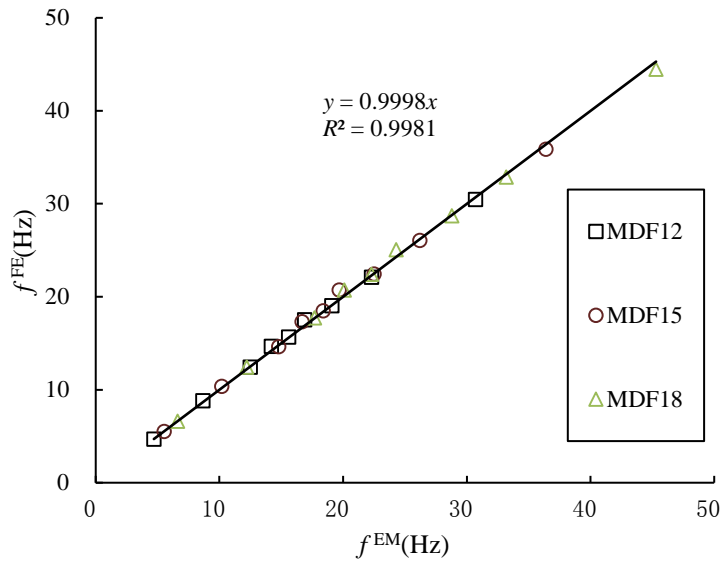
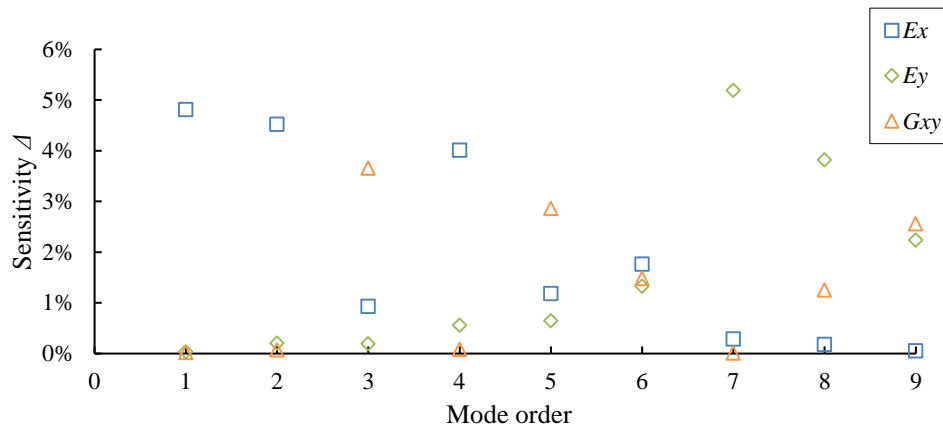


Figure 5-The relationship between the experimental frequencies and calculated frequencies of the full-size MDF panels in three different thicknesses.

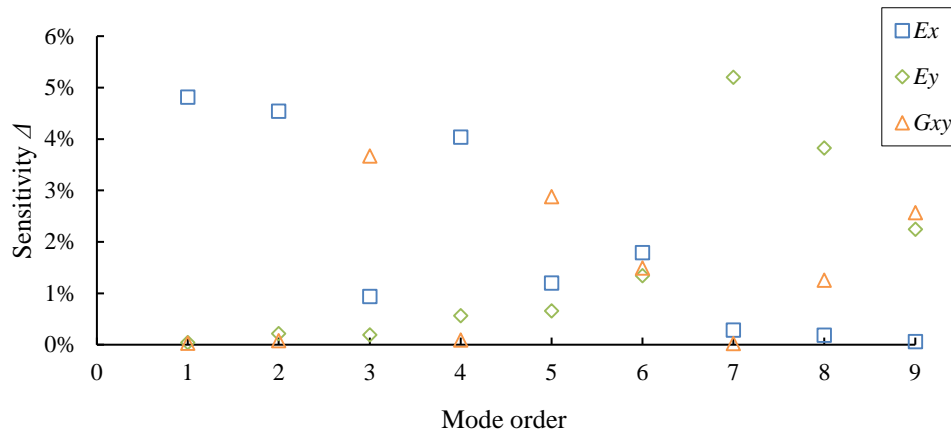
Results analysis of sensitivity analysis for full-size MDF panels

Results of sensitivity analysis for the modal parameters of full-size MDF panels are shown in Figures 6. It can be seen from the figures that the frequencies of the first, second, and fourth orders, namely modes (2, 0), (3, 0), and (4, 0), are most sensitive to the change in E_x ; frequencies of the third, fifth and ninth orders, namely modes (2, 1), (1, 1), and (2, 2), are most sensitive to the change in G_{xy} ; frequencies of the seventh and eighth orders, namely modes (0, 2) and (1, 2), are most sensitive to the change in E_y ; frequency of the sixth order mode (4, 1) has nearly the same sensitivities to the changes in E_x , E_y , and G_{xy} . The results also indicate that the full-size MDF panels with different thicknesses show the same results, indicating that the panel thickness has no effect on the sensitivities of the mode's frequency with respect to changes in E_x , E_y , and G_{xy} .

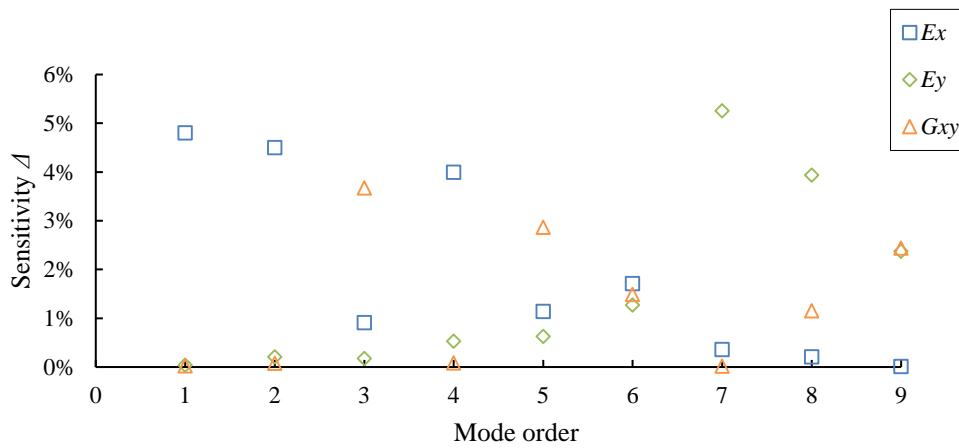
In addition, the boundary condition of a full-size MDF panels under the four-node support can be considered completely free on four sides. However, in fact, the six vibration modes (2,0), (2,1), (1,1), (0, 2), (1,2), and (2, 2) of the full-size MDF panels tested remain free when the other three modes (3, 0),(4, 0), and (4, 1) are attenuated (the four supports are not placed on the nodes for these three modes (Hearmon 1966)). Therefore, the corresponding frequencies of modes (3, 0) (4, 0), and (4, 1) are not suitable for calculating the elastic constants of full-size MDF panels supported on four nodes according to Equation (6). In summary, the sensitive modes for calculating E_x and E_y of full-size MDF panels are (2, 0) and (0 or 1, 2), and the sensitive modes for calculating G_{xy} are (2, 1), (1, 1), and (2, 2). In view of the strongest sensitivity and the convenience of the frequency testing, the frequencies of modes (2, 0), (0, 2), and (2, 1) are preferred in calculating E_x , E_y , and G_{xy} of full-size MDF panels based on Equations (7), (8), and (10), respectively.



(a)



(b)



(c)

Figure 6-Results of sensitivity analysis for full-size MDF panels with three different thicknesses. (a) MDF12; (b) MDF15; and (c) MDF18.

Conclusions

In this study, the natural frequencies and mode shapes of the first nine vibration modes for full-size MDF panels supported at four nodes were determined using experimental modal analysis. Modal parameters of the panels obtained from experimental modal testing were compared with the results of theoretical modal analysis. Sensitivity analysis was performed to identify the vibration modes that are most sensitive to the changes in elastic constants. Based on the results and analysis, we concluded the following:

- (1) Mode shapes of the full-size MDF panels obtained from modal testing are in good agreement with those obtained from theoretical modal analyses. A strong linear relationship exists between the measured natural frequencies and the calculated frequencies of the panels.
- (2) The frequencies of modes (2, 0), (0, 2), and (2, 1) of full-size MDF panels under the four-node support condition are identified as the characteristic frequencies for determining moduli of elasticity in major and minor directions and the in-plane shear modulus of the panels. Panel thickness has no effect on the sensitivity of the frequencies in terms of elastic property prediction.
- (3) The results of this study indicate that a free vibration system under four-node support has a good potential to be used for evaluating the elastic properties of full-size MDF panels.

Acknowledgements

The authors greatly thank the State Forest Administration of China through the Special Research Funds for Public Welfare (Grant No. 201304512) for funding this project.

References

- Antunes, F.; Ramalho, A.; Ferreira, J.A.M. [and others]. 2008. Determination of elastic properties by resonant technique: A sensitivity analysis. *Journal of Testing & Evaluation*. 36(1): 89–99.
- Chi, D.R.; Tong, X.; Lin, X.Q. 2006. Dynamic detection for Yong's modules and bend strength of fiberboard. *Wood Processing Machinery*. 17(5):14–17.
- Coppens, H. 1988. Quality control of particleboards by means of their oscillation behavior. In *Proceedings of the FESYP Technical Conference, Munich, Germany*: 143-165.
- Divos, F.; Tanaka, T.; Nagao, H. [and others]. 1998. Determination of shear modulus on construction size timber. *Wood Science & Technology*. 32(6):393–402.
- Ewins, D.J. 1986. *Modal Testing: Theory and Practice*. Research Studies Press Limited: Letchworth, UK.
- Ganev, S.; Gendron, G.; Cloutier, A. [and others]. 2005. Mechanical properties of MDF as a function of density and moisture content. *Wood & Fiber Science*. 37(2): 314–326.
- Guan, C.; Zhang, H.J.; Hunt, J.F. [and others]. 2016a. Determining shear modulus of thin wood composite materials using a cantilever beam vibration method. *Construction & Building Materials*. 121:285–289.
- Guan, C.; Zhang, H.J.; Hunt, J.F. [and others]. 2016b. Measurement of dynamic viscoelasticity of full-size wood composite panels using a vibration testing method. *BioResources*. 11(2): 4593–4604.

- Guan, C.; Zhang, H.J.; Zhou, L.J. [and others].2015. Dynamic determination of modulus of elasticity of full-size wood composite panels using a vibration method. *Construction & Building Materials*. 100: 201-206.
- Guan, C.; Zhou, L.J.; Zhang, H.J. [and others].2014. Vibration modal analysis of the full-sized medium density fiberboard. *Applied Mechanics and Materials*.620: 268–273.
- Hearmon, R.F.S. 1946. The fundamental frequency of vibration of rectangular wood and plywood plates. *Proceedings of the Physical Society*. 58(1): 78–92.
- Hearmon, R.F.S. 1966. Vibration testing of wood. *Forest Products Journal*. 16(8):29–40.
- Hearmon, R.F.S.1961. *An Introduction to Applied Anisotropic Elasticity*. Oxford University Press: Oxford, UK.
- Hunt, J.F.; Zhang, H.J.; Guo, Z.R. [and others]. 2013. Cantilever beam static and dynamic response comparison with mid-point bending for thin MDF composite panels. *BioResources*. 8(1): 115–129.
- Larsson, D. 1997. Using modal analysis for estimation of anisotropic material constants. *Journal of Engineering Mechanics*. 123(3): 222-229.
- Leissa, A.W. 1969. *Vibration of Plates*. Ohio State University: Columbus, OH, USA.
- Mirbolouk, P.; Roohnia, M. 2015. Evaluation of dynamic modulus of elasticity of medium density fiberboard panel from longitudinal vibration tests on specimens. *BioResources*. 10(1): 613–621.
- Nakao, T.; Okano, T.; Asano, I. 1985. Vibrational properties of a wooden plate. *Mokuzai Gakkaishi*. 31(10): 793–800.
- Schulte, M.; Frühwald, A.; Bröker, F.W. 1996. Non-destructive testing of panel products by vibration technique. In *Proceedings of the 10th International Symposium on Nondestructive Testing of Wood*, Lausanne, Switzerland: 259-268.
- Sobue, N.; Katoh, A. 1992. Simultaneous determination of orthotropic elastic constants of standard full-size plywoods by vibration method. *Mokuzai Gakkaishi*. 38(10): 895–902.
- Sobue, N.; Kitazumi, M. 1991. Identification of power spectrum peaks of vibrating completely-free wood plates and moduli of elasticity measurements. *Mokuzai Gakkaishi*. 37(1): 9–15.
- Yoshihara, H. 2011. Measurement of the Young's modulus and shear modulus of in-plane quasi-isotropic medium-density fiberboard by flexural vibration. *BioResources*. 6(4): 4871–4885.
- Yoshihara, H.; Kubojima, Y.; Nagaoka, K. [and others].1998. Measurement of the shear modulus of wood by static bending tests. *Journal of Wood Science*. 44(1): 15–20.
- Zhang, H.J.; Hunt, J.F.; Zhou, L.J. 2015. Comparison of wood composite properties using cantilever-beam bending. *BioResources*. 10(2):3070–3078.
- Zhou, J.H.; Chui, Y.H.; Gong, M. [and others].2016. Simultaneous measurement of elastic constants of full-size engineered wood-based panels by modal testing. *Holzforschung*. 70(7): 673–682.

Determination of Mechanical Properties of Wood Based Materials using Modal Updating

Torben Marhenke

Leibniz Universität Hannover, Institute of Dynamics and Vibration Research, Hannover, Germany, marhenke@ids.uni-hannover.de

Jens Twiefel

Leibniz Universität Hannover, Institute of Dynamics and Vibration Research, Hannover, Germany, twiefel@ids.uni-hannover.de

Jörg Hasener

Fagus-GreCon Greten GmbH & Co. KG, Alfeld, Germany, joerg.hasener@grecon.de

Jörg Wallaschek

Leibniz Universität Hannover, Institute of Dynamics and Vibration Research, Hannover, Germany, wallaschek@ids.uni-hannover.de

Abstract

A current research topic of wood based materials is the determination of the elastic material parameters. There are hardly any complete material parameter sets for wood based materials available in current literature. One possible method, described in detail in this paper, is modal updating, in which the mechanical characteristic values of a simulation model are adjusted until the modal parameters between measurement and simulation match. For this purpose, an experimental modal analysis is performed and the material parameters of a subsequent numerical simulation are optimized until the difference between numerical and experimental eigenvectors and values has fallen below a certain threshold. The parameter set, which represents the smallest deviation, provides an approximation for the characteristic values of the real wood structure. The main advantage of this method is that it is non-destructive and no special sample bodies are needed. Additionally, only one test setup is necessary to determine the values.

Keywords: mechanical properties, wood based material, model updating, material characterization

Introduction

Despite the longstanding use of wood based materials, there is a lack of engineering knowledge about the mechanical behavior of wood based materials. The anisotropic fiber structure and the associated complex material properties pose major challenges in the characterization of the orthotropic material parameters. New insights from the research of structure-property relationships over the last decades show possibilities to make use of structural anisotropy.

Already in 1931 Goens worked on the identification of the elastic modulus of beams (Goens, 1931). His approach approximates the elasticity module from the beam theory according to Timoshenko by solving the differential equations for the bending vibration of free bars. Hearmon applied Goens' method for the investigation of the shear effect and the rotary inertia on the free bending oscillation of wooden beams (Hearmon, 1958).

Ohlsson and Perstorper explored the elastic properties of wood by means of dynamic tests (Ohlsson and Perstorper, 1992). The modal properties of a wooden beam are determined through experimental experiments. Investigations on beams have made initial assessments of the elasticity and shear modulus of wood. Due to the beam geometry it was possible to identify two independent material parameters (Larsson, 1997). Dynamic tests on anisotropic plates, on the other hand, allow for the determination of additional material characteristics. Taking into account the anisotropic properties, Hearmon investigated the vibrational frequencies of wood panels (Hearmon, 1946). The elastic modulus in the x and y plane directions (E_x , E_y) as well as the shear modulus in the plane (G_{xy}), were determined for various wood materials. Albers carried out a further mechanical investigation on wood based panels (Albers, 1970). Beech veneers and particle boards were used as sample materials. The aim was to investigate the anisotropic material properties of wood materials, which have not yet been thoroughly investigated. Numerous experiments studying elastic parameters have been carried out for this purpose. Kruse dealt with the determination of the mechanical properties of wood panels using a non-contact method involving ultrasound (Kruse, 1997).

In 1987, Deobald and Gibson were among the first to deal with the determination of orthotropic material parameters via a vibration analysis. They modeled modes of vibrations of orthotropic plates using the Rayleigh-Ritz method. The result was the determination of four of the nine elastic material properties (Deobald and Gibson, 1988). Larsson determined the elastic properties of thin orthotropic oriented structural board (OSB) on the basis of the experimental modal analysis. The results are limited to the plate plane, so that only five of the nine elastic parameters could be determined (Larsson, 1997). Grimsel (1999) defined all nine elastic material parameters of a beech timber wood panel with the same method.

It becomes clear that there some approaches for identifying the elastic material parameters especially of timber wood. In this paper a method of the inverse identification of all nine parameters for wood based materials by model updating will be presented. Due to the inhomogeneous structure and the high attenuation of these materials, there was currently no method to reliably determine all nine parameters of these substances. In addition, the stability of the process was examined for the first time and the uncertainties resulting from external influences are investigated. Also the parameters of samples of identical base material but of different size were determined and compared with each other.

At the beginning, the mechanical properties of wood based materials are described and the method of model updating is presented. The different steps of the updating process are explained in more detail below and applied to the inverse parameter identification for wood based materials. Following influences on the eigenfrequencies and the uncertainty of the method are investigated. Finally, the results are compared with reference values from the literature.

Materials and Methods

Materials

For this study, two different wood based materials were used; particle and medium density fiber boards (MDF). The boards have different bulk densities (between 470 and 750 kg/m³) and thicknesses (between 6 and 35 mm). The size of the plates varies between 200 mm x 300 mm and up to 600 mm x 800 mm. An orthotropic material model is used to describe the mechanical behavior. Orthotropy is a combination of orthogonal and anisotropic and describes directional properties of material with three orthogonal symmetry planes (Lekhnitskiĭ, 1963). The elastic properties in the three main cutting directions have different values (Dunky and Niemz, 2002). In the three symmetry planes, the mechanical properties are completely independent from one another (Stephen and Edward, 1971). With respect to these coordinates, there are no couplings between normal and shear strains. This results in the following relationship in the main directions:

$$\varepsilon_{ii} = \frac{1}{E_i} \sigma_{ii} - \frac{\nu_{ji}}{E_j} \sigma_{jj} - \frac{\nu_{ki}}{E_k} \sigma_{kk} \quad (1)$$

$$\varepsilon_{ij} = \frac{1}{G_{ij}} \sigma_{ij} \quad (2)$$

where ε_{ii} is normal strain, E is Young's modulus, σ_{ii} is normal stress, ν is Poisson's ratio, ε_{ij} is shear strain, G_{ij} is shear modulus and σ_{ij} is shear stress.

If the material is loaded outside these axes of symmetry, stress-strain couplings occur. The three main directions of the orthotropy result in twelve material constants for the formulation of the elasticity law (Lekhnitskiĭ, 1963). These are three moduli of elasticity, three shear moduli, and six transverse contraction numbers. Only three transverse contraction numbers are linearly independent because of the symmetry conditions. For this reason, wood based materials can be mechanically described by nine independent parameters. (Dunky and Niemz, 2002).

Methods

The model updating method is used to determine all nine material parameters required for the complete description of wood materials as an orthogonal material. Model updating is a method for matching results from an experimental and numerical modal analysis (Figure 1).

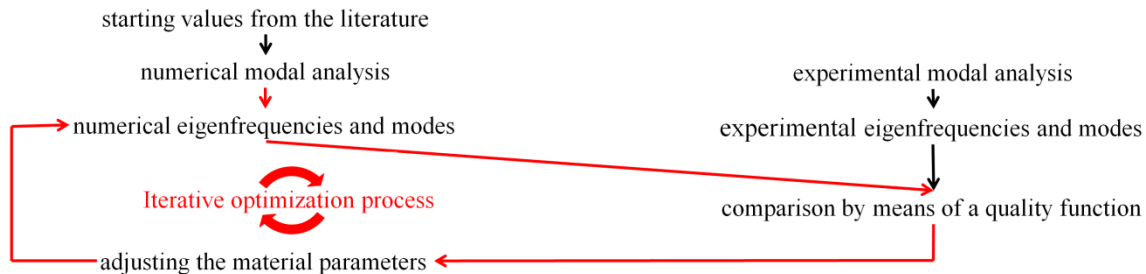


Figure 1—Model updating process to match measurement and simulation

Normally model updating is used to validate a numerical model of a structure by taking the results of the experiment as a reference (Gladwell et al., 1995). In this paper, a numerical representation of the real structure is also needed. The method is used to determine the mechanical characteristic values of the examined wood based material samples by means of an inverse identification.

The results of the experimental modal analysis will deviate from the real properties by measuring inaccuracies from the environment, the operating state or disturbance variables. Nevertheless, it is generally assumed that the experimental results represent a good approximation of the real structural properties and can be used to calibrate the simulation (Ribeiro et al., 2012). In order to ensure a realistic representation of the dynamic properties using the numerical model, validation from the experimentally obtained results is required. The measurements and results of the experimental modal analysis are used as a reference to adjust the dynamic properties of the model. The experiment and simulation are matched by means of defined quality functions (Marwala, 2010). The result of the quality function (residual) provides the target value to be minimized in the optimization.

The relationship between residuals (the errors between analytic and experimental values) and the input parameters, which are the material parameters in the case of the inverse parameter determination, is

generally described by non-linear functions. So it is a non-linear minimization problem which must be iteratively solved. In the case of iterative methods, the input parameters of the numerical model are gradually adjusted. In each step the residue is determined (Heylen et al., 1998). By changing the input parameters for the simulation, the target function is minimized until the residuals are below a certain threshold. The material parameters used in the optimization step with the smallest residue represent a good approximation of reality and are the result of the inverse parameter identification. The individual steps of the model updating (Figure 1) are described in detail below.

Experimental Modal Analysis

Experimental modal analysis is a common method used to determine the eigenfrequencies and eigenvalues of real structures (Hagedorn and Otterbein, 1987). This makes it possible to detect the dynamic properties of the structure and thus to calculate its modal parameters on the basis of the measured response vibrations of a system. The eigenvectors and eigenvalues are determined by a direct measurement of the free oscillations of the system. For this purpose, the system is excited to vibrate and the vibration response is recorded (Hagedorn and Otterbein, 1987). Each measuring point at which the response is recorded corresponds to a degree of freedom n . Theoretically, two measuring points are sufficient to carry out the experimental modal analysis. The experiment must be repeated $n-1$ times to get the vibrations of all n degrees of freedom. As the number of sensors increases, the experiment has to be carried out less frequently. When using n sensors, it is sufficient to carry out the experiment once. However, more sensors mean a higher additional weight application to the structure to be examined and can thus influence the results. The oscillation excitation of the structure is often carried out by means of a modal hammer, alternatively other forms of stimulation such as a sinusoidal signal can also be used (Maia and de Silva 1997; Schwarz and Richardson, 1999). The modal hammer stimulates the body with a pulse-like hit (Avitabile, 2001). Both the force of the pulse in the hammer tip and the resulting dynamic displacement of the body at defined points are measured by measurement techniques (Schwarz and Richardson, 1999). It is not important whether the path $x(t)$, the velocity $\dot{x}(t)$ or the acceleration $\ddot{x}(t)$ is measured since these can easily be converted into one another. Identification of the modal parameters always follows the assumption of an idealized linear model:

$$M\ddot{x} + D\dot{x} + Cx = f(t) \quad (3)$$

For the tests 64 uniformly distributed measuring points on the plates were defined. The measurement consists of 16 measurement series. In each series the vibration was measured at four positions at the same time. In the following series acceleration sensors were put at the next measuring point. The excitation was always at the same position. This method is called "Roving sensor" (16 series with 4 sensors equal 64 degree of freedom). The mean value of five measurements was determined in each measurement series. From the examination of optimal storage, it has been found that acoustic foam shows the best repeat accuracy and the smallest deviation with different positioning. Tested in different positions, the amounts of wax needed to fix the accelerometers and excitation energies have shown a standard deviation of only 0.9 %. For this reason, the influence of the inaccuracy of the experimental modal analysis can almost be ignored. The result of the experimental modal analysis is a universal file, which contains the geometry data of the plates, the measuring points as well as the eigenmodes and frequencies.

Numerical Modal Analysis

The numerical modal analysis of the wood based board is carried out using a simulation. The model is created in the simulation software ANSYS. In ANSYS, a parametric and orthotropic model is created so that an adaptation of the material parameters in the model updating process can be performed automatically. The geometric data for the numerical mapping of the board are taken from the universal

file. By meshing the body, additional net points are generated at the position where the oscillation was experimentally recorded. After performing the numerical modal analysis, the numeric eigenmodes and frequencies at these positions are exported in a text file.

Determination of the quality function

The eigenfrequencies and eigenmodes are used for the calibration of the model. In the process of model updating, the numerical and experimental eigenmodes as well as the corresponding eigenfrequencies are paired together (Brehm et al., 2010). This is an important step, as the eigenmodes of the simulation can be interchanged with those of the experiment. It is also possible that the numerical model represents modes which were not detected in the experiment. All further results are dependent on the eigenmodes being correctly assigned. In order to compare the modes of the experiment with those from the simulation, the Model Assurance Criterion (MAC) is a widely accepted method. The MAC forms the scalar product between the normalized eigenvectors of the simulation $\psi_{i,num}$ and the experiment $\psi_{i,exp}$ and determines the consistency of the eigenmodes (Allemang and Brown, 1982).

$$(MAC)_{ij} = \frac{(\psi_{i,exp}^T \psi_{j,num})^2}{(\psi_{i,exp}^T \psi_{i,exp})(\psi_{j,num}^T \psi_{j,num})} \quad (4)$$

Target functions are defined in order to determine deviations between the numerical model and the experimental results. The correlation of the MAC serves as a secondary condition in order to compare equivalent modes only. The target function usually contains the difference of the eigenfrequencies and the MAC values. From the literature, various target functions for model updating are known. One of these target functions is described by Ribeiro et al. and was used for the calibration of a railway arch bridge model (Ribeiro et al., 2012). The first part refers to the eigenfrequencies ω_i^{EXP} and ω_i^{NUM} , while the second part considers the MAC values between the corresponding modes. The two components of the function can be arbitrarily weighted by the factors α and β . Optimization has shown that the combination of $\alpha = 0.2$ and $\beta = 0.8$ is a suitable choice for the inverse parameter determination.

$$q = \alpha \sum_{i=1}^n \frac{|\omega_i^{EXP} - \omega_i^{NUM}|}{\omega_i^{EXP}} + \beta \sum_{i=1}^n |MAC_{ii} - 1| \quad (5)$$

Optimization

The aim of the model updating process is to generate the highest possible correlation between the experimental and analytical results while maintaining the physical significance of the updated parameters by minimizing the quality function q . The material parameters, which are to be determined within the scope of the optimization by inverse parameter identification, serve as correcting variables. Optimization is based on target functions and the difference between the eigenfrequencies and MAC values of the experimental and numerical modal analysis. In order to investigate the influence of the material parameters on the different eigenfrequencies and eigenmodes, a sensitivity analysis is carried out before optimization. This provides an understanding of the relationships between the frequencies, modes and material parameters. Starting from the material values given in the literature, a design space of about 50% of the initial values is defined. The design space is the area that is examined in the sensitivity analysis and represents the limits of the individual parameters in the optimization. The design space is examined using 200 discrete designs of the numerical model within the defined range. Each design represents a different, complete parameter set of the material properties. To determine the design samples, deterministic or

stochastic approaches can be used. The present work uses the stochastic Advanced Latin Hypercube sampling (Huntington and Lyrintzis, 1998). Figure 2 shows the dependence of the quality function for a 19 mm particleboard on the material parameters. The highest correlation is found for the elasticity modules in the x- and y-directions and the shear modulus G_{xy} .

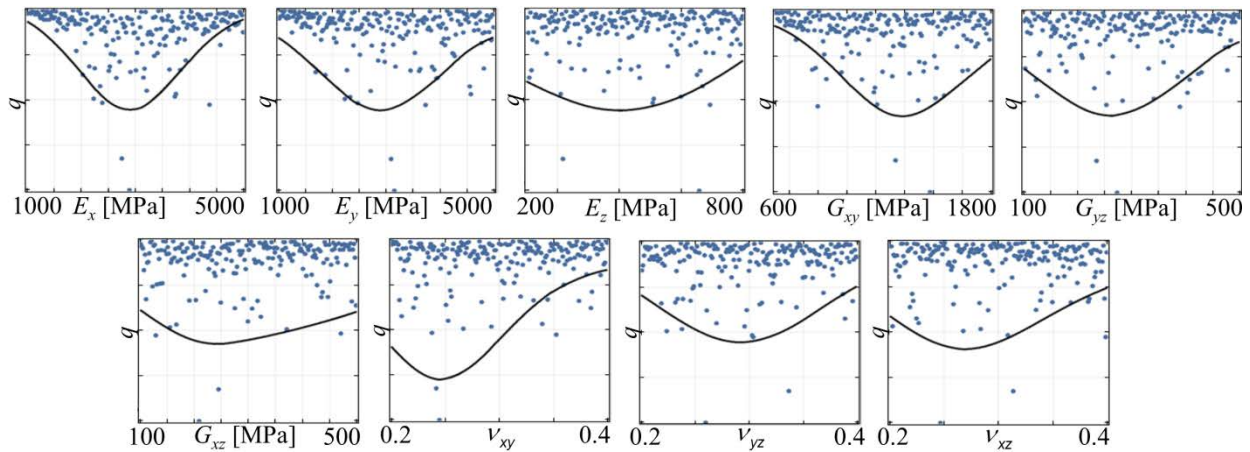


Figure 2— Result of the sensitivity analysis, relationship between material parameters and quality function

However, the remaining six material parameters show a recognizable minimum of the target function. After the sensitivity analysis, the optimization is carried out. Based on the target function, the numerical model is optimized with respect to the experimental results in order to identify the material parameters. The optimization is carried out in two stages with two different optimization strategies. Initially, a pre-optimization is carried out on the basis of response surfaces out of the sensitivity analysis. The optimal design is determined based on this metamodel. Since the required information from the sensitivity analysis is already available, this optimization is very fast and has a low computational intensity. The quality depends on the quality of the metamodel. Afterwards the final optimization is calculated by additional numerical simulations. The results of the pre-optimization are used as starting designs. In contrast to pre-optimization, the numerical modal analysis has to be solved and the calculations are very complex and time-intensive. The parameter set with the smallest residual obtained in the optimization is the best approximation of the real structure.

Results and Discussion

The results of the updating process are presented using the examples of a 12 and 19 mm particle board (p.b.) and a 16 mm MDF board. For the 19 mm p.b., additional results from the analysis of the plate size as well as a comparison to literature values are explained. For the 16 mm p.b. and 19 mm MDF board, 14 eigenfrequencies were identified in the experimental modal analysis. The numerical model maps all frequencies very well. The percentage deviations for the p.b. are on average only 0.29 % and 0.41 % for the MDF. The maximum deviation occurs with 0.58% for the tenth eigenfrequency and with 1.06% for the fourteenth mode (Figure 3 a).

Figure 3b shows the comparison between the eignfrequencies and the MAC values as well as a visualization of the eigenmodes for a 12 mm p.b.. It becomes clear that a high degree of matching could be achieved between the measurement and the numerical simulation.

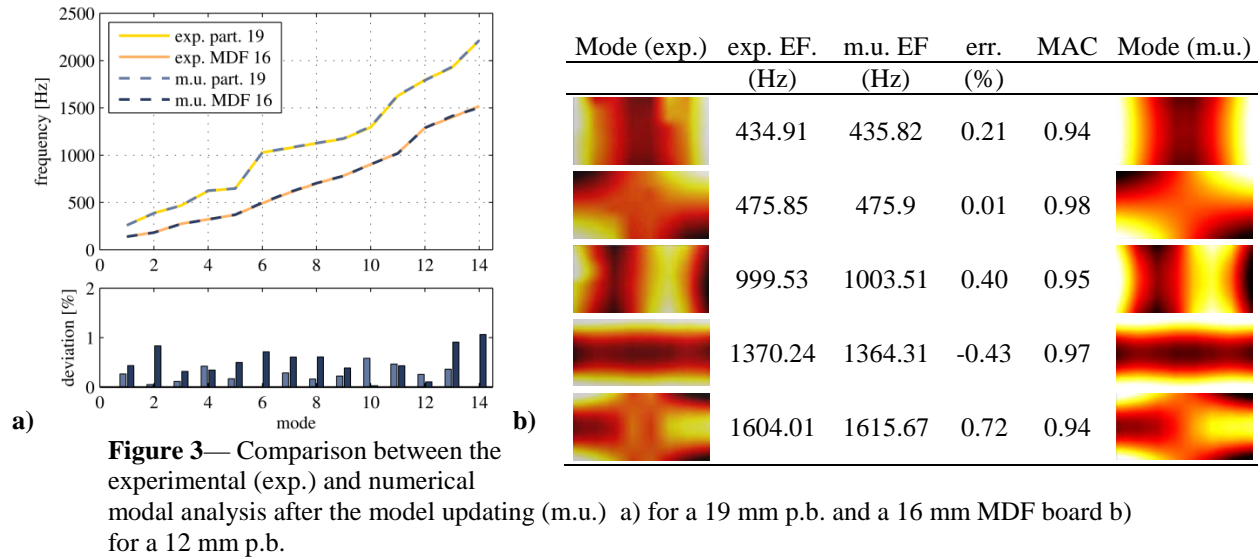


Table 1— Different board sizes, identical base material

Parameter	Model Updating			Literature Albers [1970]
	300 x 194 mm ²	320 x 300 mm ²	400 x 485 mm ²	
E_x [MPa]	2779	2728	2719	2636
E_y [MPa]	3201	3266	3279	3103
E_z [MPa]	480	462	496	206
G_{xy} [MPa]	274	269	273	228
G_{yz} [MPa]	253	250	247	211
G_{xz} [MPa]	1478	1455	1512	1153
ν_{xy}	0.269	0.265	0.275	0.22
ν_{yz}	0.282	0.276	0.284	0.25
ν_{xz}	0.274	0.273	0.279	0.24

Table 1 shows an investigation with differently sized plate dimensions for the 19 mm p.b.. The inversely determined material parameters show an average deviation of 2.2% with the maximum difference being 7.2%. In view of the inhomogeneity of a p.b., these values are very low and show good reproducibility of the process. In addition to this, it becomes clear that non-linear effects, which could be caused by plate sizes of different sizes, are so small that their influence is hardly noticeable.

Compared to the parameter set known from Albers for a 19 mm p.b., a good agreement is also shown. Only the modulus of elasticity in the z-direction and the shear modulus G_{xz}

show an increased deviation. The deviations can be explained by development in the bonding and production of p.b..

Conclusions

In the paper has been shown for the first time that it is possible to determine the complete parameter set for the description of wood based materials as an orthotropic material by using the model updating method. It was also found that the uncertainties that arise during the experimental modal analysis are so small that their deviations can be neglected. In order to demonstrate the reproducibility of the method, plates of different sizes were examined and an updating procedure was carried out for each. The comparison of these results shows deviations with a mean value of 2.2% and a maximum value of less than 10%. In addition, a good agreement with values from the literature was shown.

References

- Albers, K., 1970. Querdehnungs- und Gleitzahlen sowie Schub- und Scherfestigkeiten von Holzwerkstoffen. Dissertation, Karlsruhe.
- Allemang, R.J., Brown, D.L., 1982. A correlation coefficient for modal vector analysis. Proceedings of the 1st International Modal Analysis Conference (IMAC), SEM, Orlando.
- Avitabile, P., 2001. Experimental modal analysis. *Sound and vibration* 35 (1), 20–31.
- Brehm, M., Zabel, V., Bucher, C., 2010. An automatic mode pairing strategy using an enhanced modal assurance criterion based on modal strain energies. *Journal of Sound and Vibration* 329 (25), 5375–5392.
- Deobald, L.R., Gibson, R.F., 1988. Determination of elastic constants of orthotropic plates by a modal analysis/Rayleigh-Ritz technique. *Journal of Sound and Vibration* 124 (2), 269–283.
- Dunky, M., Niemz, P., 2002. *Holzwerkstoffe und Leime*. Springer Berlin Heidelberg, Berlin, Heidelberg.
- Goens, E., 1931. Über die Bestimmung des Elastizitätsmoduls von Stäben mit Hilfe von Biegungsschwingungen. *Annalen der Physik* 403 (6), 649–678.
- Grimsel, M., 1999. *Mechanisches Verhalten von Holz: Struktur- und Parameteridentifikation eines anisotropen Werkstoffes*. Dissertation, Technische Universität Dresden.
- Hagedorn, P., Otterbein, S., 1987. *Technische Schwingungslehre*. Springer Berlin Heidelberg, Berlin, Heidelberg.
- Hearmon, R.F., 1946. The fundamental frequency of vibration of rectangular wood and plywood plates. *Proceedings of the Physical Society* 58 (1), 78.
- Hearmon, R.F., 1958. The influence of shear and rotatory inertia on the free flexural vibration of wooden beams. *British Journal of Applied Physics* 9 (10), 381.
- Heylen, W., Lammens, S., Sas, P., 1998. *Modal analysis theory and testing*, 2nd ed. Katholieke Universiteit Leuven, Faculty of Engineering.
- Huntington, D.E., Lyrinzis, C.S., 1998. Improvements to and limitations of Latin hypercube sampling. *Probabilistic Engineering Mechanics* 13 (4), 245–253.
- Kruse, K., 1997. *Entwicklung eines Verfahrens der berührungslosen Ermittlung von Schallgeschwindigkeiten*. Dissertation, Technische Universität Hamburg.
- Larsson, D., 1997. Using Modal Analysis for Estimation of Anisotropic Material Constants. *Journal of Engineering Mechanics*.
- Lekhnitskiĭ, S.G., 1963. *Theory of elasticity of an anisotropic elastic body*. Holden-day.
- Maia, N.M.M., e Silva, Júlio Martins Montalvao, 1997. *Theoretical and experimental modal analysis*. Research Studies Press.

- Ohlsson, S., Perstorper, M., 1992. Elastic wood properties from dynamic tests and computer modeling. *Journal of Structural Engineering* 118 (10), 2677–2690.
- Ribeiro, D., Calçada, R., Delgado, R., Brehm, M., Zabel, V., 2012. Finite element model updating of a bowstring-arch railway bridge based on experimental modal parameters. *Engineering Structures* 40, 413–435.
- Schwarz, B.J., Richardson, M.H., 1999. Experimental modal analysis. *CSI Reliability week* 35 (1), 1–12.
- Sipple, J.D., Sanayei, M., 2013. Finite element model updating using frequency response functions and numerical sensitivities. *Struct. Control Health Monit.* 365 (2).
- Stephen, W.T., Edward, M.W., 1971. A General Theory of Strength for Anisotropic Materials. *Journal of Composite Materials* 5 (1), 58–80.



Session 4

**Urban Tree Defect
Assessment and
Risk Analysis I**

Reliability and Applicability of Nondestructive Testing Instruments for Risk Assessment of Urban Trees

Xi Wu

School of IoT Engineering, Jiangnan University, Wuxi, Jiangsu, China,
7161905006@vip.jiangnan.edu.cn

Guanghai Li

School of IoT Engineering, Jiangnan University, Wuxi, Jiangsu, China, ghli@jiangnan.edu.edu
Institution of Jiangsu High Technology Research Key Laboratory for Wireless Sensor Networks, Nanjing, Jiangsu, China, ghli@jiangnan.edu.edu

Zhi Jiao

School of IoT Engineering, Jiangnan University, Wuxi, Jiangsu, China, wcjzjz@163.com

Abstract

Nondestructive testing technology such as stress wave, radar wave and micro-drilling resistance has been applied for evaluating the internal condition of live trees for many years. The main purpose of this paper is to analyze and evaluate the reliability and applicability of various instruments. A method was proposed to estimate the defective area of tomography by extracting the pixels of defective region. The experiments were finished in Yangzhou Slender West Lake Park, China. Not only the live trees were assessed, but also three kinds of logs were chosen as samples to evaluate the accuracy of different equipments. The experimental results showed that, the acoustic tomography and the resistance curve can accurately reflect the position and degree of decay within the live trees, and accord with each other well. In addition, it was found that the accuracy of radar scanner TRUTM system was lower than the other two instruments.

Key words: Nondestructive testing; Risk assessment; Tomography; Live trees

Introduction

The destruction, fragmentation and death of trees caused by the deterioration of the natural environment directly lead to damage to the ecological balance and the loss of national heritage, and the nondestructive testing and evaluation of live trees have drawn more and more attention from both research and industrial fields. To increase the reliability of the inspection and decide the extent and location of any internal decay, it would be practical to conduct multiple measurements in different orientations at one cross-section of trees with different equipments. At present, stress wave testing, resistance micro-drilling and penetrate ground radar have been applied in nondestructive testing and evaluation of live trees for a long time.

Xiping Wang et al. (2004) proposed the principles of stress wave nondestructive testing, and measurement techniques for stress wave nondestructive testing. This guide was prepared to assist field foresters in the use of stress wave timing instruments to locate and define areas of decay in standing timber. Lina Karilinasari et al. (2016) combined traditional visual assessment with tomography to evaluate the sound wave velocity change from green to dry conditions in agarwood and tomographic images associated with changes in the moisture content. Guanghai Li et al. (2016) proposed a stress velocity model in longitudinal-radial plane and proved a relationship between wave velocity and

measurement angle. Andre´s Arciniegas et al. (2014) discussed the effect of various parameters when using tomography techniques and gave a general conclusion to future signal-processing work in the acoustic and ultrasonic tomography of standing trees.

Jana Jezova et al. (2016) investigated particularities of tree trunks' radar images, considering the circumferential data acquisition geometry, as a function of the radar configuration and trunk section structures. Their experimental results showed satisfactorily the internal inhomogeneity and the information will be useful for future tomographic reconstruction. Li Guo et al. (2013) recently reviewed the principle and application of GPR, and discussed its potentials, constraints, possible solutions, and future outlooks. Because GPR root detection is highly site specific, Yeung Shan Wing et al. (2016) provided a local reference for GPR performance for the detection of main roots. Their findings demonstrate that the 900 MHz GPR is applicable in Hong Kong for the detection of main roots.

Micro-drilling resistance testing is an assessment method to measure borehole resistance. Pokorny Jill et al. (2003) explained how to record the resistance by penetrometer when the probe was drilling into a trunk by rotating at a high constant velocity. Similar to PICUS, the test results are affected by the physical properties and the chemical properties of the environment and the material too. Fikret Isik and Bailian Li (2003) suggested that the Resistograph® could be used reliably and efficiently to assess relative wood density of live trees for selection in tree improvement programs. The efficiency of using the Resistograph® as a means of indirect selection for improvement of wood density was 87% at the family level.

To detect the internal defects of live trees accurately, people often use multiple nondestructive testing tools. Ningsie Indahsuary et al. (2014) evaluated the reliability of sonic tomography (PICUS) to detect agar wood within *Microcarpa Baill.* Xiping Wang and R. Bruce Allison (2008) demonstrated the effectiveness of a trunk detection using a combination of visual inspection, acoustic test and resistance micro-drilling. Michal Kloibera et al. (2016) assessed the suitability and sensitivity of selecting acoustic devices used on detection, the results obtained indicate that it was not possible to fully rely on in situ acoustic methods for inspection of defects in wooden elements of historical structures, and therefore they should be combined with visual inspection and some other instrumental methods.

Nevertheless, the detection results with different instruments sometimes generate different conclusions, which may lead to deviation from the actual situation of the trees. The main purpose of this paper is to analyze and evaluate the applicability and reliability of various instruments.

Materials and Methods

The NDT experiments were conducted in the Slender West Lake Park, Yangzhou City, China. 157 ancient live trees aged from 90 to 300 years were chosen as testing samples, covering 32 species including Cypress, Maple, Ginkgo and so on. In addition, three logs were detected for assessing the accuracy of Resistograph®.

To ensure accuracy of NDT in operation, cross-sections at different heights were examined carefully, and PICUS (Argus Electronic GmbH), TRU (Tree Radar Company), and 4452-P Resistograph® (Rinntech, Inc.) were applied in this NDT. We assessed the trees' health condition with two steps. Firstly, acoustic wave and radar wave tests were utilized to distinguish trees which had serious cavity, crack or large decay. Then, micro-drilling testing was applied to evaluate the defect severity precisely for the defective trees.

Based on acoustic wave theory, internal health conditions of each standing trees trunk were mapped to image by tomography of PICUS. The imaging data was collected by sensors evenly deployed around the tree cross-section. In general, the more sensors PICUS used around circumference, the higher quality image could be displayed. However, less sensors could be used for those trees with small trunk such as *Buxus sinica*. As shown in Fig. 1(a), PICUS testing based on acoustic wave required plunging nails on the cross-section under test, which would result in damage to the tree trunk slightly. Afterwards, TRU would be used to scan around the cross-section from the same beginning position as that of PICUS testing, which is shown in Fig. 1(b). It is helpful to compare between different testing results of different equipments. Based on the results of PICUS and TRU, F400S Resistograph® was further applied to assess the internal defect level of live trees. It is essential to perpendicularly plunge the probe to the bark before test as shown in Fig. 1(c), and to connect the starting point with the ending point of resistance curve of each path, which is convenient to decide the defective region. Several stress wave paths should be detected by Resistograph® tool to evaluate the testing results of PICUS and TRU.



Figure 1—This figure caption is Field testing environment of three equipments, (a) is the experimental environment of PICUS, (b) is the experimental environment of TRU, (c) is the experimental environment of Resistograph®.

To assess the reliability of the equipment by comparing of the actual image and the mathematic tomography, three performance parameters were proposed in this paper. First, the defect rate (*DR*) refers to the proportion of the defective parts in the processing images. Second, the error rate (*ER*) refers to the deviation between the two *DR* of actual imaging and of automatic imaging. Finally, the gather rate (*GR*) means the difference between the *DR* values of two different instruments.

In order to ensure the feature extraction more accurately with clear boundary, the defective area was extracted manually. As shown in Fig. 2(b), though there were slight errors around the image edge, the deviation on the edge of decay area was small enough so that it can be negligible. The interested region in Fig. 2(a) was mapped into white area in Fig. 2(b).

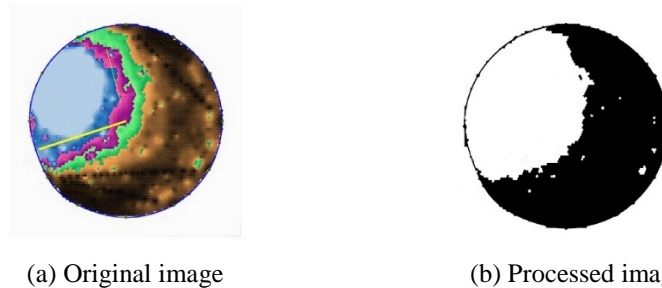


Figure 2—This figure caption is Comparison between processed image and primary image, (a) is the original image imaged by PICUS, (b) is the image after image processing.

Finally, after the edge were accurately extracted, the parameters *Rate* which represent the area of interested region can be calculated as follows.

$$Rate = \frac{Num_w}{Num_w + Num_b} \quad (1)$$

Here, Num_w denotes amount of white pixel points, and the Num_b represents the number of black pixel points.

Results

Accuracy of Resistograph®

To evaluate the accuracy of Resistograph® tool, micro-drilling testing experiments on three log samples along different paths marked by black color as shown in Fig. 3(a) were finished. For example, the resistance value of red interval of path 2 shown in Fig. 3(b) reflected the existence of cavity. For each path of same samples, the comparison between actual defective length and that computed from the resistance curve was showed in Table 1. The mean error was about 3 mm and the ER was about 3.36%. So, we used the testing results of micro-drilling instrument as references to evaluate the accuracy of the other two equipments.

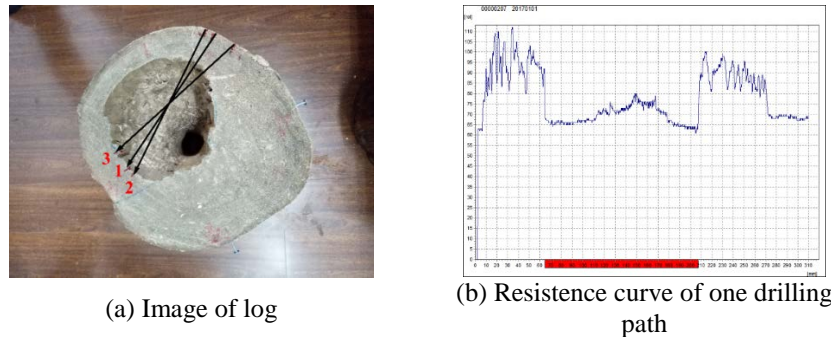


Figure 3—This figure caption is Experiments on log at different directions, (a) is one image of three experimental logs, imaged by PICUS, (b) is Resistance curve of one drilling path.

Table 1—Comparison of deteriorate length between actual paths and dilling paths

Sample	Actual	Resistograph®	Error length	ER
	(mm)	(mm)	(mm)	(%)
1	166	168	2	1.20
2	162	160	2	1.23
3	164	167	3	1.83
4	69	73	4	5.80
5	65	64	1	1.54
6	63	68	5	7.94
7	90	94	4	4.44
8	95	93	2	2.10
9	97	93	4	4.12

The table title is Comparison of deteriorate length between actual paths and drilling paths.

Accuracy of PICUS and TRU

Among these 157 trees, only 5 trees were suitable to take the micro drilling tests. After the stress wave testing by PICUS, micro-drilling testing along the stress wave paths was carried out. After computing the

defective length of the drilling curve and that of the tomography of PICUS for the same path, the decay length ratio were calculated shown in Figure 4. From Fig.4, it can be seen that the decay length gotten from the resistance curve is often longer than that calculated from stress wave tomography. In other words, the PICUS has lower accuracy than Resistograph®.

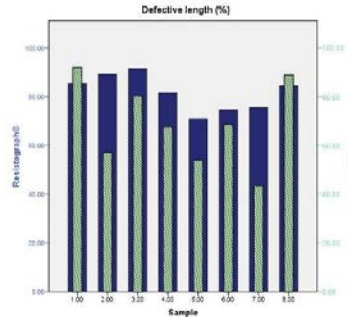


Figure 4—This figure caption is Ratio of decay length between Resistograph® and PICUS, the green bars represent the ratio of deteriorate length on experimental paths of PICUS, the blue bars represent the ratio of deteriorate length on drilling paths.

There were 60 live trees assessed by TRU. Dramatically, some results of TRU had opposite results to PICUS. Except for 11 data sets of TRU which were collected from defective trees, the rest data consisting of radius and *DR* were shown in Fig. 5(a). The decay range on images of TRU and PICUS reflects opposite results on the same cross-section displayed by Fig.6. Fig. 6 illustrated that those trees which were decided to be healthy by PICUS had negative conclusions by TRU. The *GR* of this kind of deviation was not beyond 25% shown in Fig. 5(b). It explained that TRU had error on determining trees' health condition whether the internal decay existed or not.

There were 11 data sets measured from defective trees by PICUS and TRU. For example, Fig. 7 showed the tomographic images of the same height from ground of No. 100 Mulberry tree generated by PICUS and TRU. Fig. 7 (a) indicated that the defective area located at the top right of the cross-section, but Fig. 7(b) showed the defective area was in the center of cross-section. These results indicated that TRU has lower accuracy than PICUS in evaluating the internal condition of live trees. Moreover, TRU uses only one color representing the internal defects, which limits the ability of defect classification. A correspondence of radius and *GR* were found by observing and analyzing these data from Fig. 11(a). Fig.5 shows the relation between *DR* and radius of cross-section of tree. It can be seen that the radius of each cross-section has impact on the imaging process of TRU. Actually, the *DR* value rises with the increasing of the radius.

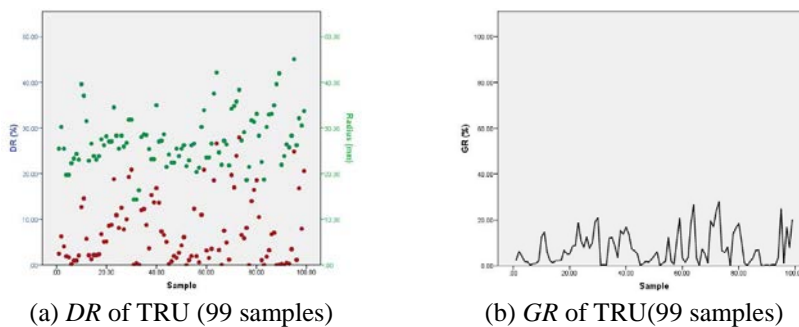


Figure 5—This figure caption is *DR* and *GR* of 99 samples on TRU, (a) is the image of *DR* and radius of 99 samples on TRU, (b) is a line chart of the *GR* of TRU on 99 samples.

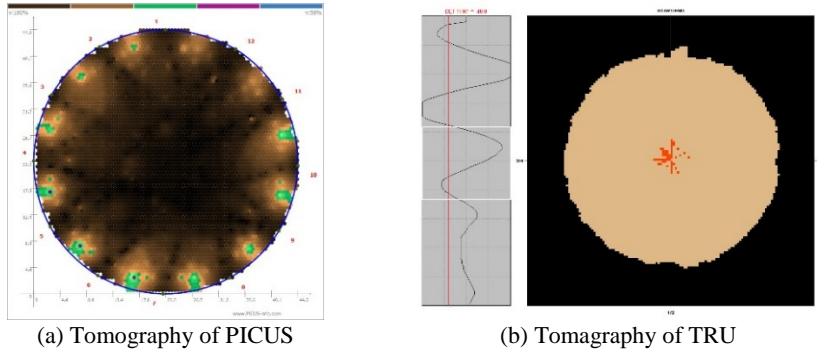


Figure 6—This figure caption is Comparison of results of one same cross-section by TRU and PICUS, (a) is the tomography of one cross-section by PICUS, (b) is the tomography of one cross-section by TRU.

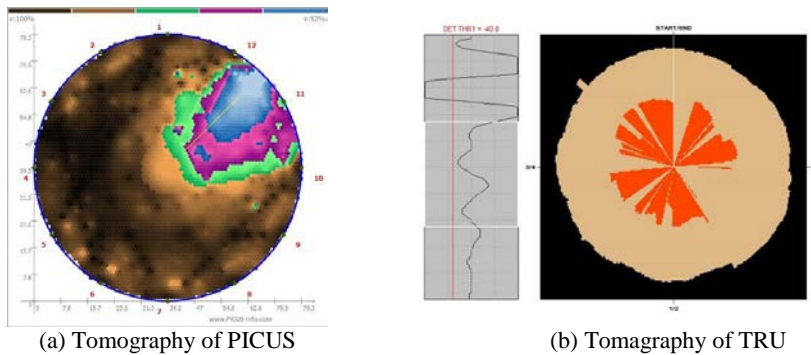


Figure 7—This figure caption is Tomographies Comparison between PICUS and TRU, (a) is the tomography of one cross-section by PICUS, (b) is the tomography of one cross-section by TRU.

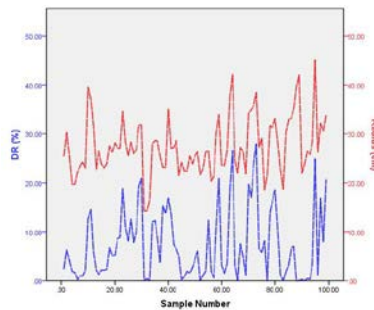


Figure 8—This figure caption is Relation between *GR* and radius, the red line chart represents the radius of 99 samples, the blue line chart represents the *DR* of TRU on samples.

Special cases

During the test, some limitations affected the use of testing equipment. Firstly, the radius of the tree trunk determines the amount of sensors and the reality of imaging. TRU has relatively strict limitation on radius, and it is required that the tree trunk's diameter should be more than 20cm to run the imaging software. For example, a poplar tree with diameter about 15cm was unsuitable to test by TRU, but it can be tested by PICUS. In addition, the TRU's drilling depth should not exceed 45cm. Secondly, the hardness of wood limits the effect of micro-drilling testing. For example, we found that smog or fire may rise when the cypress trees with high hardness under micro-drilling test as showed in Fig. 9.



Figure 9—This figure caption is Resistograph® experiment with smog, smog rised by micro-drilling testing.

Conclusions

This study demonstrated the effectiveness of using a combination of multiple equipments to detect the location and size of internal defects of a tree trunk. We proposed a method of edge detection and feature extraction to calculate the performance parameters (*DR*, *ER*, *GR*), and make quantitative analysis. It was found that the results of stress wave testing and micro-drilling resistance testing were more accurate than radar scanning. Furthermore, we put forward a comprehensive assessment on three testing instruments (PICUS, TRU, Resistograph®) to estimate the applicability of each equipment for risk evaluation of live trees. Each instrument has respective advantages and disadvantages. It is suggested that the stress wave testing can be applied at first for evaluation of live trees, and then radar scanning can be used as an auxiliary step. Once the internal defects are found by stress wave or radar testing, the micro-drilling resistance testing may be used to decide the severity of defects.

Acknowledgments

This study was supported in part by the National Natural Science Foundation of China (Grant No. 61472368), Key Research and Development Project of Jiangsu Province (Grant No. BE2016627), Jiangsu Innovation Project of Postgraduate Training (Grant No. SJLX16_0499) and the Fundamental Research Funds for the Central Universities (Grant No. RP51635B).

Reference

- Andre´s, A.; Flavio, P.; Loi`c, B. [and others]. 2014. Literature review of acoustic and ultrasonic tomography in standing trees. *Trees*. 28(6): 1559-1567.
- Fikret, I.; Bailian, L. 2003. Rapid assessment of wood density of live trees using the Resistograph for selection in tree improvement programs. *Canadian Journal of Forest Research*. 33(12): 2426-2435.
- Guanghai, L.; Xiang, W.; Xiaocheng, D. [and others]. 2016. Stress wave velocity patterns in the longitudinal–radial plane of trees for defect diagnosis. *Computers and Electronics in Agriculture*. 124(C): 23-28.
- Li, G.; Jin, C.; Xihong, C. [and others]. 2013. Application of ground penetrating radar for coarse root detection and quantification: a review. *Plant and Soil*. 362(1-2): 1-23.
- Ningsie, I.; Lina, K.; Dodi, N. [and others]. 2014. Reliability of sonic tomography to detect agarwood in *Aquilaria microcarpa* Baill. *Indian Academy of Wood Science*. 11(1): 65-71.
- Jana, J.; Laurence, M.; Sébastien, L. 2016. Ground-penetrating radar for observing tree trunks and other cylindrical objects. *Construction and Building Materials*. 123: 214-225.

Lina, K.; Nadya, P; Maman, T. [and others]. 2016. Moisture content effect on sound wave velocity and acoustic tomograms in agarwood. *Turkish Journal of Agriculture and Forestry*. 40: 696-704.

Michal, K.; Ladislav, R.; Jaroslav, H. [and others]. 2016. Comparative evaluation of acoustic techniques for detection of damages in historical wood. *Journal of Cultural Heritage*. 20: 622-631.

Pokorny, J. 2003. *Urban Tree Risks Management: A Community Guide to Program Design and Implementation*. NA-TP-03-03. USDA Forest Service, Northeastern Area, State and Private Forestry, St. Paul, MN. 194 pp.

Xiping, W.; Ferenc, D.; Crystal, P. [and others]. 2004. Assessment of decay in standing timber using stress wave timing nondestructive evaluation tools—A guide for use and interpretation. General Technical Report FPL –GTR–147. S. Department of Agriculture, Forest Service, Forest Products Laboratory, Madison, WI, p 12.

Xiping, W.; R. Bruce, A. 2008. Decay Detection in Red Oak Trees Using a Combination of Visual Inspection, Acoustic Testing, and Resistance Microdrilling. *Arboriculture & Urban Forestry*. 34(1): 1-4.

Yeung, S.W.; Yan,W.M.; Hau, C.H.B. 2016. Performance of ground penetrating radar in root detection and its application in root diameter estimation under controlled conditions. *Science China Earth Sciences*. 59(1): 145-155.

Dynamic Tree Trunk Stability Evaluation

Ferenc Divos

Professor, Institute of Physics and Electronics, University of Sopron, Hungary.
divos.ferenc@uni-sopron.hu

Balázs Major

PhD student, Institute of Physics and Electronics, University of Sopron, Hungary.
balazs.major@gastudent.nyme.hu

Abstract

The weather and other biotic factors can cause serious defects and damages in urban trees. The urban tree inspections are very important methods to preserve as much tree as we can, and maintains safety on the streets and public parks.

The goal of the research was to modify the conventional pulling test to a more realistic dynamic test by changing the static pulling device to the realistic wind load. We measured the deformation of the tree trunk by high sensitivity displacement sensor and wind velocity. The displacement sensor resolution is 260 nm. About 50 trees were investigated with two displacement sensors. The applied anemometer is a ball type anemometer, sampling rate is 1Hz. We measured not only the wind velocity but the wind direction as well. Distance between anemometer and tree was less than 500m. We found linear relationship between the tree trunk deformation and wind pressure. The wind pressure is calculated using the wind speed and air density. The results are the critical wind pressure and tree trunk safety factor.

Keywords: wind pressure, tree trunk deformation, dynamic loading, tree trunk, safety factor, torque

Introduction

The stability of urban trees is a key question that affects everyone. Diseased and unstable urban trees pose much risk for everyone, and are a serious liability for municipalities in case of an accident. Tree stability and safety assessment is therefore of the utmost importance. In the meantime, it tends to be much neglected in many areas.

At present, the most accepted method for evaluating the safety and stability of trees is the pulling test. It involves applying a bending load on the trunk via a cable attached to the tree. The method can be used either to assess the uprooting stability of the tree (by measuring the inclination at the bottom of the trunk), or to establish the risk of trunk breakage (through measuring the bending stresses using extensometers attached to the trunk). Both of these methods are introduced here briefly.

Pulling test for trunk safety evaluation

When trees sway in the wind, the trunk of the tree bends. If the wind load is severe, excessive bending may lead to permanent damage, or even the breakage of the tree trunk, even if the roots are strong enough to

hold. This is especially true if the trunk is diseased, hollow, or otherwise damaged. The trunk safety test is designed to assess the safety of the tree in this respect.

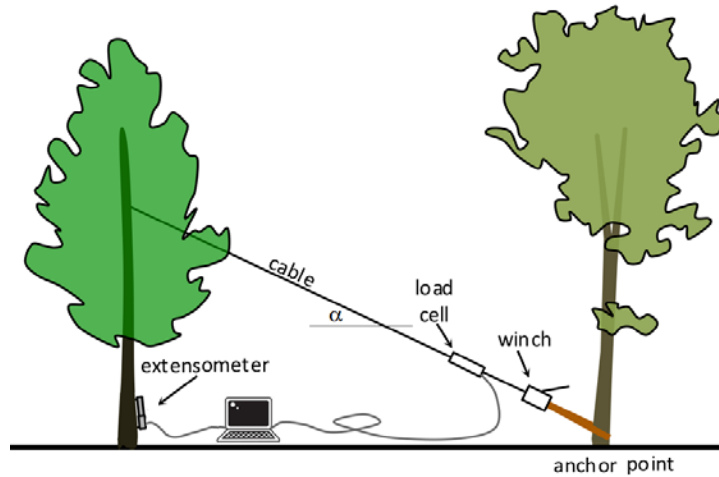


Figure 1. The pulling test setup for tree trunk safety assessment.

Trunk safety assessment is a technique very similar to uprooting safety evaluation, except, in this case, instead of inclination, we measure the deformation of the tree trunk. During the pulling test, the trunk bends. Bending causes both compaction and elongation in the trunk, on the side nearest to and farthest from the cable, respectively. By measuring the extent of this deformation on either or both sides, it is possible to predict the safety of the tree against trunk damage.

The testing procedure is much the same as in the case of uprooting safety determination, but in this case an extensometer is used on the compression or the tension side (or possibly both sides) of the trunk, instead of an inclinometer. The load and deformation data are collected analyzed by a computer software.

Trunk safety is determined based on the so-called linear elastic limit. When trees bend, up to a point, their deformation is linear. More importantly, this deformation is not permanent, and, up to this point, there is no permanent damage to the trunk. This safe limit of relative deformation is called the linear elastic limit (*EL*).

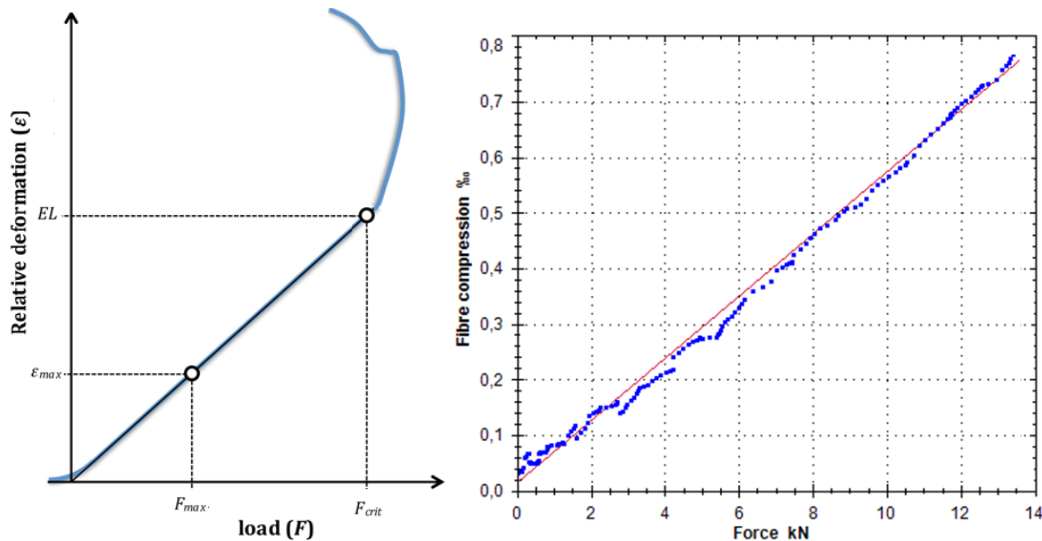


Figure 2. The load-deformation curve. The elastic limit (*EL*) is shown on the left and the measured points of a real pulling test (blue) with the linear trend line (pink) on the right.

The linear elastic limit is a constant that depends on the tree species. The deformation induced by the pulling test (ϵ_{max}) stays well below the *EL*. Based on the measured load and deformation data, it is possible to extrapolate to the critical load (F_{crit}) that would be required to reach the *EL*. Once we have the critical load, the Safety Factor calculation is given by the following formula:

$$M_{crit} = F_{crit} h \cos(\alpha), \quad (1)$$

where h is the height at which the rope is attached to the tree, α is the angle of the rope, see figure 1. The torque acting on the tree at a certain wind velocity is calculated using the following equation:

$$M_{wind} = A \frac{\rho}{2} v^2 c_w h_{cr}, \quad (2)$$

where: A - crown surface area,
 ρ - air density,
 v - wind velocity
 c_w - aerodynamic drag factor
 h_{cr} - the height of the crown center point

The drag factor is a constant that is different for each wood species, determined by Wessoly and Erb (1998). Comparing M_{wind} to M_{crit} , we can calculate the so-called Safety Factor (SF) that indicates the tree trunk stability:

$$SF = \frac{M_{crit}}{M_{wind}}, \quad (3)$$

If this value is above 1.5, the tree is safe, while a SF below 1 signals high risk. In-between these two values, there is in a grey zone, a moderate risk of tree trunk failure.

Turning the static pulling test into a dynamic test

Converting the static pulling test to a dynamic test is necessary, because the wind load is a dynamic load, (James 2014). Our idea is to replace static pulling with the dynamic load created by the wind. For this approach, we need a high sensitivity extensometer, because, at moderate wind speeds, the tree trunk deformation is rather small. Figure 3 shows the applied setup. Because the wind direction is unknown, we use two extensometers at the same height, but at a 90 degrees angle around the tree trunk center, see bottom left in figure 3. Instead of force, we determine the wind pressure:

$$p_{wind} = 0,5 \rho_{air} V^2 \quad (4)$$

where ρ_{air} is the air density and V the wind speed. Wind speed is measured using a high sampling rate (1Hz) ball type TX20 anemometer. Data are recorded by a data logger and stored on an SD card together with the time provided by GPS.

The extensometer is and LVDT (Linear variable Differential Transformer) type sensor. The resolution is 260 nm, working range is 15 mm. Even at minor (2 km/h) wind speeds we are able to detect the tree trunk deformation. For easy mounting, the extensometers we adopted a quick mounting house – developed by Dr. Ludek Praus, Mendel University, Brno, Czech Republic. Figure 3 shows the quick mounting house of the LVDT sensor. The benefit of this device is that setup is really quick, takes less than 1 minute. The procedure includes driving 2 screws into the tree to hold the LVDT, and opening the device head. The base length – the distance between the two screws – is 235 mm.

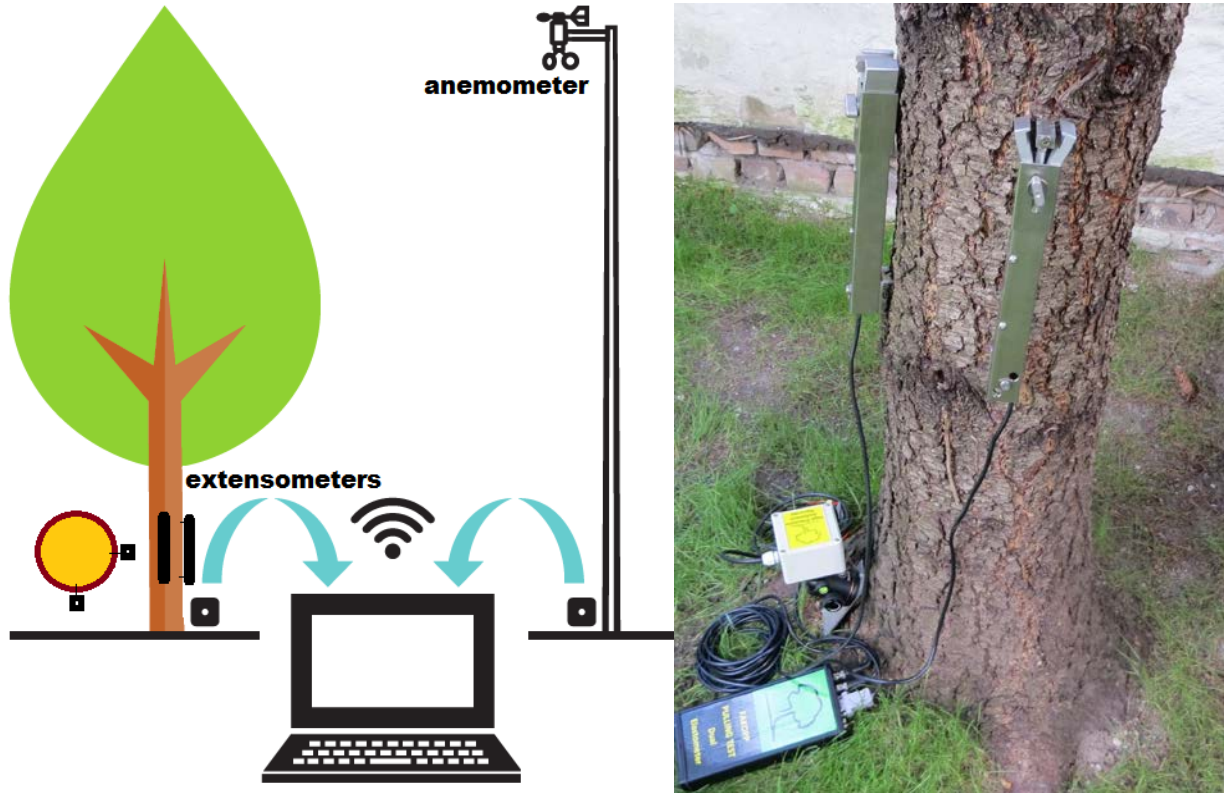


Figure 3. The applied setup for dynamic tree trunk evaluation.

The frequency of the tree trunk deformation measurement is 10 Hz. Data are recorded by a data logger and stored on an SD card along with the time provided by GPS. Time data is used to synchronize the wind and deformation data. The data collection period was typically 2 hours or longer. The data evaluation process is, as follows:

- Wind and extensometer data synchronization,
- Taring of extensometer 1 and extensometer 2,
- Determination of the tree trunk deformation using the Pythagorean theorem, based on extensometer 1 and 2 data.
- Segmentation of measured data into 5-minute intervals. A 5-minute data set includes 300 wind and 2 x 3000 extension readings.
- Statistical evaluation of each segment, resulting in one data-pair representing wind and deformation.
- Plotting the deformation versus wind pressure; determination of the slope of the trend line, see figure 4.
- Calculation of the critical wind pressure (p_{crit}) using the elastic limit (EL).
- Safety factor calculation using the formula below:

$$SF = \frac{M_{crit}}{M_{wind}} = \frac{p_{crit} A_{crown} h_{cr} c_w}{p_{wind} A_{crown} h_{cr} c_w} = \frac{p_{crit}}{p_{wind}} \quad (5)$$

where p_{wind} is the highest expected wind pressure of the given area. It is higher at sea shore and hill top and lower in a valley. In Hungary, most places we use 33 m/s as maximum wind speed and 667 Pa as wind pressure.

The beauty of the dynamic tree trunk test compared to the static pulling test is no crown surface area (A_{crown}), no crown center height (h_{cr}) and no aerodynamic drag factor (c_w) is necessary for the safety factor (SF) calculation.

Figure 4 shows the relationship between wind pressure and deformation based on actual experimental data of *Picea abies* and *Sequoiadendron gigantea* trees. The data set is one of the best among 42 tests. Some scatter is still present. The reason is the chaotic relationship between the wind pressure and the tree's response. The correlation coefficient between wind pressure and tree trunk deformation is around 0.8 – 0.9.

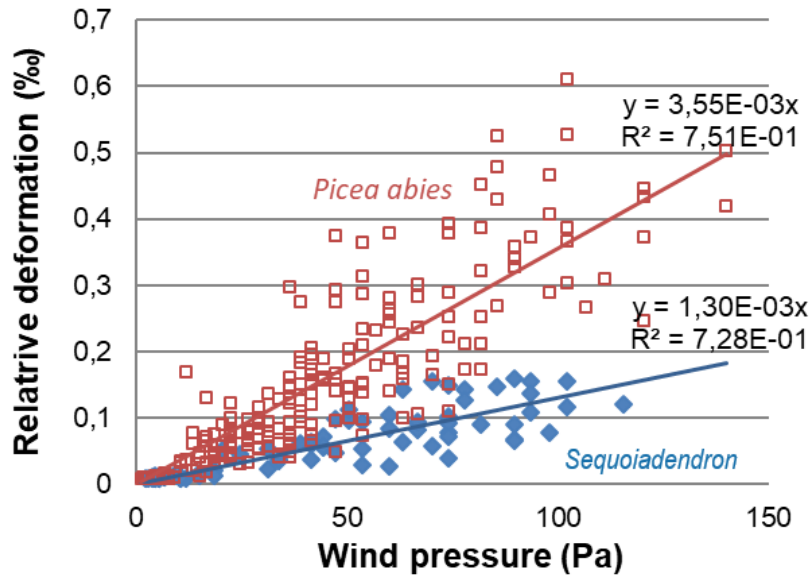


Figure 4.: The relationship between tree trunk deformation and wind pressure

The calculated safety factor of *Picea abies* and *Sequoiadendron giganteum* trees are 0,97 and 4,6 respectively. The reference wind speed is 33 m/s, the reference wind pressure is 667 Pa. The calculation of the safety factor according to the equation 5 is shown in table 1.

Tree	slope (fig. 4.) (‰/Pa)	Elastic limit (‰)	Critical wind pressure (Pa)	Safety factor
<i>Picea abies</i>	0,00355	2,3	648	0,97
<i>Sequoiadendron giganteum</i>	0,00130	4,0	3077	4,61

Table 1. The calculation of the safety factor

Conclusion

We have tested 42 trees and found good correlation between tree trunk deformation and wind pressure. Our experiments indicate the capabilities of this technique of turning the static pulling test into a more realistic dynamic test. The method's major benefit is that no crown surface area, no crown center height, and no aerodynamic drag factor is necessary in safety factor calculation for the safety factor calculation. The limitation is that the technique is feasible only in windy conditions.

Acknowledgments

This article was made in frame of the „EFOP-3.6.1-16-2016-00018 – Improving the role of research+development+innovation in the higher education through institutional developments assisting intelligent specialization in Sopron and Szombathely”.

Instruments were developed and supplied by the FAKOPP enterprise.

References

Kenneth R. James, et al.: Tree Biomechanics Literature Review: Dynamics, Arboriculture & Urban Forestry 2014. 40(1):1–15-v

Wessolly, L., and M. Erb 1998. Handbuch der Baumstatik und Baumkontrolle. Patzer Verlag, Berlin, Germany.

Quantitative Detection of Internal Decay Degree for Standing Trees Based on Three NDT Methods- Electric Resistance Tomography, Stress Wave Imaging and Resistograph Techniques

Xiaoquan Yue

College of Transportation and Civil Engineering, Fujian Agriculture and Forestry University, Fuzhou Fujian China, yxqzrh@foxmail.com

Lihai Wang*

College of Engineering and Technology, Northeast Forestry University, Harbin Heilongjiang, China, lihaiwang@yahoo.com

Xiaowen Ge

College of Engineering and Technology, Northeast Forestry University, Harbin Heilongjiang, China, gexiaowen2013@126.com

Xinglong Wang

College of Engineering and Technology, Northeast Forestry University, Harbin Heilongjiang, China, 823390979@qq.com

Abstract

An investigation about the accuracy of different NDT methods was carried out in the Experiment Forest of Northeast Forestry University in Harbin City, Heilongjiang Province. 100 cross-sections of *Fraxinus mandshurica* and *Populus simonii* standing trees were tested by four methods: Electric Resistance Tomography (ERT), Stress Wave Tomography (SWT), Resistograph and estimation weight loss ratios of wooden increment cores. Taking wood core samples as research objects, testing results of three other kinds of NDT methods were compared. E_s determined by estimating weight loss ratios of wooden cores was regarded as the truth value of degree of decay. Results showed that three NDT methods were able to make different degree estimation for the degree of decay. ERT can show better diagnosis than the other two for incipient decay of standing trees, while SWT can be significantly used in the middle stage of decay testing, and Resistograph can be used in the different stages of decay.

Keywords: weight loss rate; electric resistance tomography; velocity of stress wave; wood core resistance loss; decay degree

Introduction

In recent years, several decay detecting techniques, such as Electric Resistance Tomography, Stress Wave Imaging and Resistograph, are employed to survey and detect the internal decay for standing trees. Practical application shows that each detecting technique has its own merit and demerit; therefore, it is necessary to make comparisons on those techniques in order to find out the appropriate technique matched with specific condition of standing trees in the forest field.

Electric Resistance Tomography (ERT) is convenient to use for wood defect inspection since it has been developed only in recent years in our country. It has been proved the possible of the ERT's application to wood defect inspection more early abroad (Jacobs, 1998). Combined with sonic computerized tomography and EIT (Electric Impedance Tomography), ERT was used to detect and quantify the internal decay for standing trees (Brazee, 2011). Measured resistance value, ERT could be employed to analyze the moisture distribution and movement in the tree trunk, and then two-dimensional resistively image could be acquired by means of inversion calculation, so that the effect done by rainfall and diurnal variations on moisture variation could be known (Xu su, 2006; Wu Huqiao, 2008; Zhou Quyou, 2009).

Stress Wave is widely used in fields of wood detecting due to its ability to inspect the mechanical properties and internal flaw. Referred to Stress Wave Tomography (SWT), Xu Huadong et al. (2010) made study of the application and propagation rules of stress wave by detecting 40 *Salix matsuyama*, and he offered the assessment of *Salix matsuyama*'s safe condition. Wang Lihai et al. (2007) indicated that sensors had influence to the fitting degree and error rate of the Stress Wave image, and pointed out that it is needed at least 12 sensors to make the image fitting degree approach 90% and the error rate reduce to 0.1. Ge Xiaowen et al. (2014) demonstrated that the relation between stress wave and resistance value is significance by using Stress Wave and Resistograph technology to detect the inner decay of *Salix Matsudana* using.

Resistograph technology is mainly employed to inspect standing trees, timber bridges and wood structure (Huang Rongfeng, 2007; Sun Tianyong, 2013; Sun Tianyong, 2014). Resistance graph is the most commonly used method for the structure security evaluation because of its good efficiency to detect the wood internal defects.

The goals of this study were to detect the decay of standing trees trunks and to describe the decay degree quantitatively on the base of field and indoor test. In order to investigate the accuracy of different NDT methods, cross-sections of standing trees were tested by four methods: Electric Resistance Tomography, Stress Wave Tomography, and Resistograph and estimation weight loss ratios of wooden increment cores. Taking wood core samples as research objects, testing results of three other kinds of NDT methods were compared to find out the appropriate technique matched with specific condition of standing trees in the forest field.

Materials and methods

2.1 Research area

The research area lies in Experiment Forest of Northeast Forestry University in Harbin City, Heilongjiang Province. This area is located longitude 126°37' E, latitude 45°43' N, is about 140 meter above sea level, slope of 5degrees, covers 43.95 hectares. It is the warm temperate zone half moist monsoon climatic region, with an average annual temperature of 3.6 degree, the highest temperature in July is 36.4 degree and the lowest temperature is -38.1 degree. There is an average of the frost-free period 600 millimeters a year of rain in this area. By afforestation on the spot between the early 1950s and the late 1960s, there have been 18 species there which was divided in 46 sample plots, with a kind of tree in each sample spot.

2.2 Experiment material and equipment

In July 2015, in the experimental field, we chose the trees that had internal decay defects by visually checking from cavities in the trunk, withered leaves, and corrupt bark and so on. Then, we selected 25(15 decayed, 10 healthy) *Fraxinus mandshurica* standing trees and 25(15 decayed, 10 healthy) *Populus simonii* standing trees, and all selected trees were 50-60 years. The DBH of *Fraxinus mandshurica* standing trees was 20~38cm, the DBH of *Populus simonii* standing trees was 30~50cm.

The instruments employed were mainly as followed: PICUS Tree Tronic electric resistance tomography system of Argus Company from Germany , Arbotom stress wave tomography system of RINNTECH Company form Germany, needle Resistograph of FrankRinnIML Company from Germany , Wood core drill made in Sweden and 101–3A Electric Heating air-blowing Drier of Teste Company from Tianjing.

2.3 Test Methods

Two sections were tested of each tree: one section was 30cm from the ground, and another was 100cm from the ground. Firstly, ERT and SWT were employed to tested two highly sections of each tree. Both of them were adopted 12 sensors equidistant arranged around the trunk, and were tested on the same measure points. In order to be analyzed conveniently, the first sensor was arranged in the south of the tree and the others were fixed up according to clockwise. The testing result of ERT and SWT were two-dimensional resistively image (Bao Zhengyu, 2013) and two-dimensional stress wave image (Wang Chaozhi,2006; Lin Wenshu,2005; Wang Lihai , 2008). Secondly, two directions of each section were tested by Resistograph: one section was from south to north and another was from east to west along radical direction, and the result was a resistance curve graph. After Resistograph detection, wooden core was got out by Wood growth cone drill near the detecting point of Resistograph, and was immediately took back to laboratory. When a wooden core was decayed, we would get out a healthy wooden core nearby for comparison (Xu Kaihong, 2004; Li Wenbing, 2008.). Finally, the weight loss rate of wooden core was calculated in laboratory. After weighing, the wooden cores were dried at 70°C to a constant weight and weighed again. Weight per unit length of healthy wooden core (m_j') was calculated as

$$m_j' = \frac{m_j}{L_1} \quad (1)$$

Where m_j' is the weight per unit length of healthy wooden core, m_j is the weight of health wooden core got out nearby the decayed wooden core, and L_1 is the length of healthy wooden core. The estimated weight of decayed wooden core circumstanced healthy (m_f') was calculated as

$$m_f' = m_j' \times L_0 \quad (2)$$

Where m_f' is the estimated weight of decayed wooden core circumstanced healthy, m_j' is the weight per unit length of healthy wooden core, and L_0 is the length of decayed wooden core. The weight loss rate of wooden core(E_s) was calculated as

$$E_s = \frac{m_f' - m_f}{m_f'} \times 100\% \quad (3)$$

Where E_s is the weight loss rate of wooden, m_f' is the estimated weight of decayed wooden core circumstanced healthy, m_f is the actual weight the decayed wooden core.

2.4 Statistical Analyses

2.4.1 Statistical Analyses of ERT

To quantitatively assess the tomograms of sample trees, all corresponding electrical resistances (ERs) at each pixel of the tomogram were further calculated by the tomogram's visualization and inversion,

and ER maps of the cross-sections were displayed using Matlab software. The ERT and schematic of the corresponding ER map grids are shown in Figs. 1-2. The decayed degree detected by ERT (E_d) was calculated as

$$E_d = \frac{R_0 - R_d}{R_0} \times 100\% \quad (4)$$

Where E_d is the decayed degree by ERT, R_0 is the average ER value of the detected direction in the same healthy tree species cross-sections, in Ω ; R_d is the average ER value of the detected direction in a decayed cross-section, in Ω .

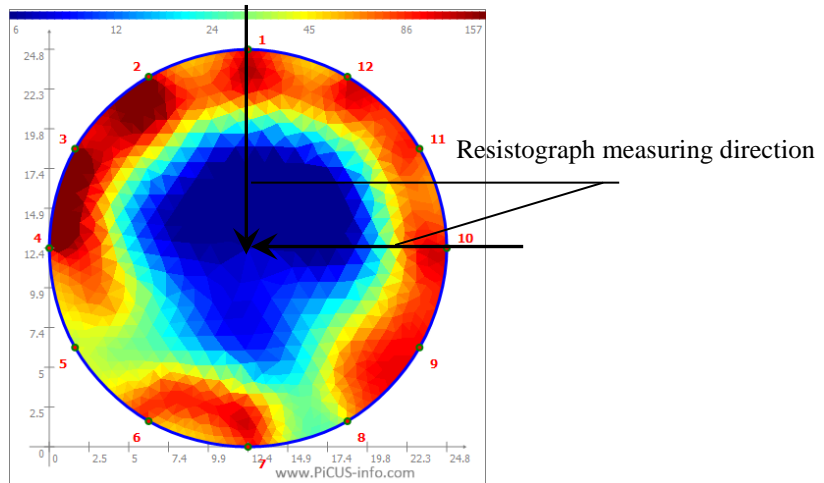
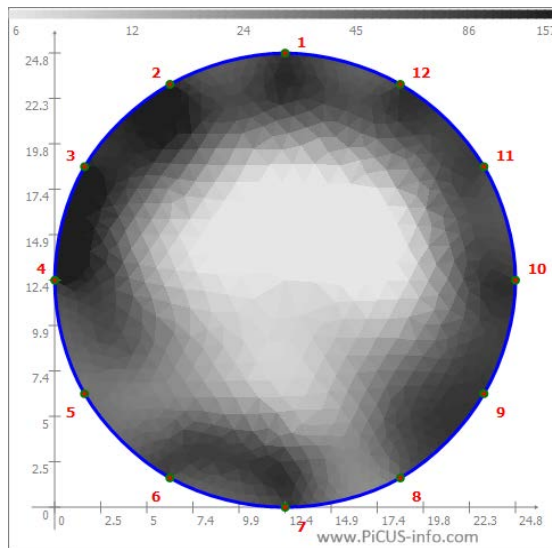


Fig.1 Resistance distribution of cross- section



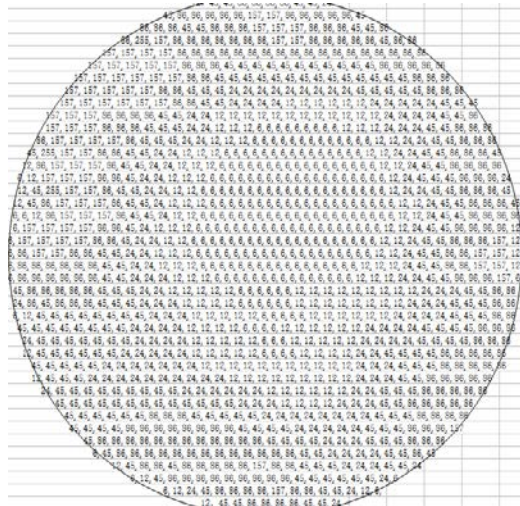


Fig.2 Grey-scale map and corresponding value of resistance distribution

2.4.2 Statistical Analyses of SWT

The velocity distribution of stress wave about cross-section is shown in Fig.3. The Stress Wave velocity distribution was dealt with as ER maps, and the decayed degree detected by SWT (E_y) was calculated as

$$E_y = \frac{V_j - V_f}{V_j} \times 100\% \quad (5)$$

Where E_y is the decayed degree detected by SWT, V_j is the average velocity of stress wave in the same healthy tree species cross-sections, m/s; V_f is the average velocity of stress wave of the detected direction in a decayed cross-section, m/s.

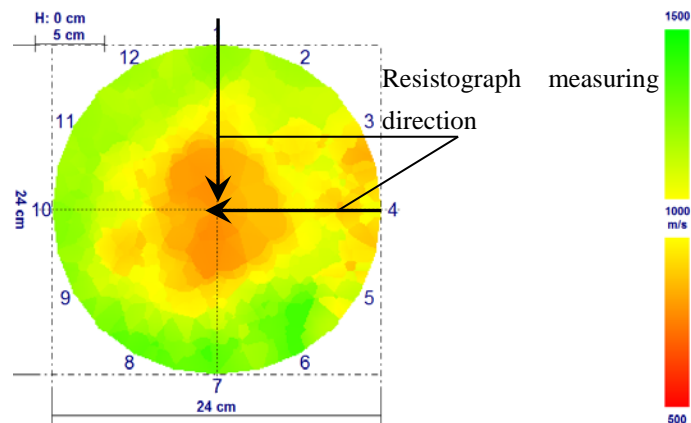


Fig.3 The velocity distribution of stress wave about cross-section

2.4.3 Statistical Analyses of Resistograph

The resistance curve of cross-section by Resistograph is shown in the Fig. 4, with the depth drilled into the wood on the horizontal axis and the resistance of Resistograph on the vertical one. The Physical and mechanical property of wood, such as hardness and density, influence the resistance (Huang Rongfeng, 2008; An Yuan, 2008.), while the wood is decayed, its mechanical strength and density will reduce , therefore the resistance tested by Resistograph will also decrease. The area of ABCD in the Resistance curve on the Fig.4 indicates that the cross-section is decayed. The decayed degree (E) signified on the Resistance curve was calculated as

$$E = \frac{L}{D} \times \frac{H + h}{2} \quad (6)$$

Where E is the decayed degree signified on the resistance curve, L is the length of decline curve on the t horizontal axis, H is the length of left decline curve on the on the vertical axis, h is the length of right decline curve on the on the vertical axis, D is the diameter of the tested cross section. The decayed degree (E) of each resistance curves could be calculated according to formula (6), the maximum value of all E values was as E_{max} , then the decayed degree tested by Resistograph(E_z) was calculated as formula (7)

$$E_z = \frac{E}{E_{max}} \times 100\% \quad (7)$$

Where E_z is a percentage between 0% and 100%.

3. Result

Based on former calculation and analysis, the decayed degree determined by the weight loss rate of wood core regarded as the truth value of the decayed degree (E_s), the decayed degree tested by ERT (E_d), the decayed degree tested by SWT (E_y) and the decayed degree tested by Resistograph (E_z) were statistically analyzed (Table.1).

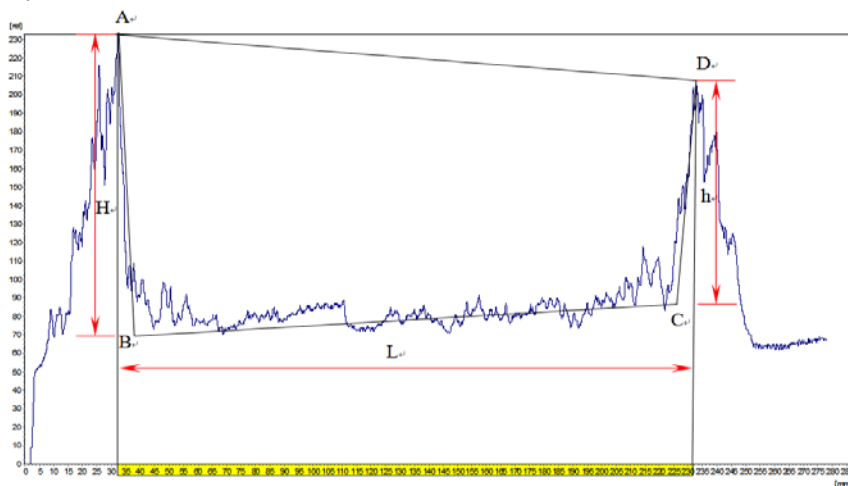


Fig.4 Resistance curve of cross-section by Resistograph

Tab. 1 Statistics of Various test results

decayed degree (%)	category	average value	maximum value	minimum value	standard deviation	skewness	kurtosis	normality test
$E_s < 30$	E_d	22.82	55.80	2.30	14.83	0.49	-0.70	followed the normal distribution
	E_y	24.46	63.90	0.00	17.26	0.79	-0.13	followed the normal distribution
	E_z	25.30	79.20	0.00	18.52	0.60	0.06	followed the normal distribution
$30 \leq E_s \leq 50$	E_d	35.51	58.00	14.20	9.78	0.06	-0.21	followed the normal distribution
	E_y	45.50	76.00	19.50	10.04	0.51	0.16	followed the normal distribution
	E_z	42.92	69.10	25.70	10.24	0.71	-0.14	followed the normal distribution
$E_s > 50$	E_d	51.71	66.00	25.60	14.29	-0.14	0.65	followed the normal distribution
	E_y	73.21	91.00	41.20	17.22	-0.88	-0.45	followed the normal distribution
	E_z	73.94	92.70	55.90	12.68	0.01	0.16	followed the normal distribution

3.1 The relation between E_d and E_s

SPSS software was used to conduct the regression analysis between E_d and E_s and the analysis results are shown as following:

The correlation coefficient (R) between E_d and E_s is 0.7188 ($P < 0.01$), and the regression equation is

$$E_d = 0.6659E_s + 11.852 \quad (8)$$

When E_s was divided into three parts as $E_s < 30\%$, $30\% \leq E_s < 50\%$ and $E_s \geq 50\%$, some difference were explored. When $E_s < 30\%$, The correlation coefficient (R) between E_d and E_s is 0.8230 ($P < 0.01$), and the regression equation is

$$E_d = 1.3033E_s + 4.2855 \quad (9)$$

When $30\% \leq E_s < 50\%$, the correlation coefficient (R) between E_d and E_s is 0.2602 ($P < 0.01$), and the regression equation is

$$E_d = 0.75769E_s + 13.427 \quad (10)$$

When $E_s \geq 50\%$, the correlation coefficient (R) between E_d and E_s is 0.5522 ($P < 0.01$), and the regression equation is

$$E_d = 1.3622E_s - 30.292 \quad (11)$$

The results are shown in Figs.5.

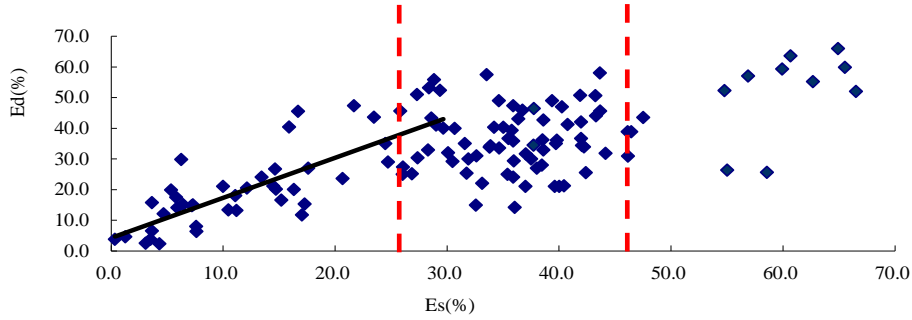


Fig. 5 Relationship between result of measuring resistance E_d and the truth value of degree of decay E_s

3.2 The relation between E_y and E_s

SPSS software was also used to conduct the regression analysis between E_y and E_s and the analysis results are shown as following:

The correlation coefficient (R) between E_y and E_s is 0.799 ($P < 0.01$), and the regression equation is

$$E_y = 0.9993E_s + 7.5369 \quad (12)$$

When $E_s < 30\%$, The correlation coefficient (R) between E_y and E_s is 0.632 ($P < 0.01$), and the regression equation is

$$E_y = 1.2501E_s + 5.9497 \quad (13)$$

When $30\% \leq E_s < 50\%$, the correlation coefficient (R) between E_y and E_s is 0.658 ($P < 0.01$), and the regression equation is

$$E_y = 1.086E_s + 1.268 \quad (14)$$

When $E_s \geq 50\%$, the correlation coefficient (R) between E_y and E_s is 0.791 ($P < 0.01$), and the regression equation is

$$E_y = 2.011E_s - 47.8 \quad (15)$$

The results are shown in Figs.6.

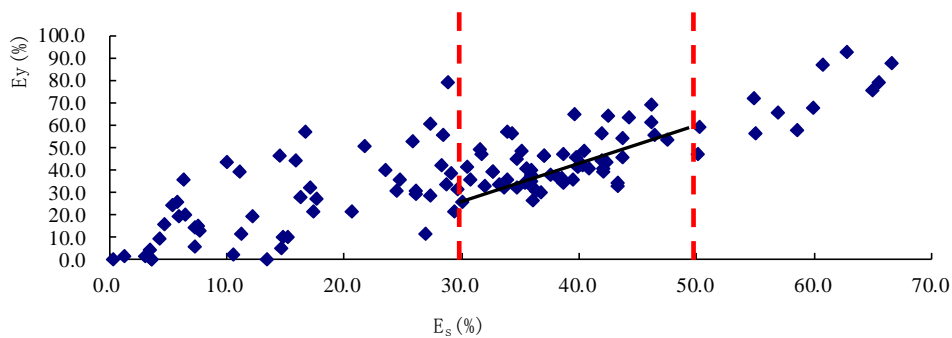


Fig. 6 Relationship between result of Stress Wave E_y and the truth value of degree of decay E_s

3.3 The relation between E_z and E_s

SPSS software was also used to conduct the regression analysis between E_z and E_s and the analysis results are shown as following:

The correlation coefficient (R) between E_z and E_s is 0.829 ($P<0.01$), and the regression equation is

$$E_z=1.08E_s+5.317 \quad (16)$$

When $E_s < 30\%$, The correlation coefficient (R) between E_z and E_s is 0.711 ($P<0.01$), and the regression equation is

$$E_z=1.311E_s+2.538 \quad (17)$$

When $30\% \leq E_s < 50\%$, the correlation coefficient (R) between E_z and E_s is 0.58 ($P<0.01$), and the regression equation is

$$E_z=1.184E_s-2.398 \quad (18)$$

When $E_s \geq 50\%$, the correlation coefficient (R) between E_z and E_s is 0.914 ($P<0.01$), and the regression equation is

$$E_z=4.177E_s-182.63 \quad (19)$$

The results are shown in Figs.7.

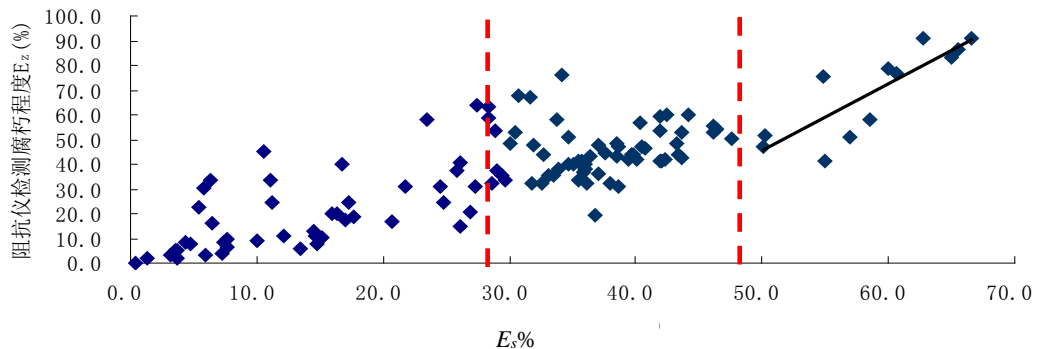


Fig. 7 Relationship between result of Resistance E_z and the truth value of degree of decay E_s

4 Discussion

4.1 Analysis of the relation between E_d and E_s

Once the wood is infected by wood-destroying fungi, decay and disintegration could appear with the wood cell wall's decomposing. Wood stain and decay will enable water content to increase because of the growth of hyphae, than ions will be released from wood cells. Research showed that many metal ions such as potassium ions, calcium ions, manganese ions and magnesium ions in rotten wood would increase with the wood decaying. While compared in the healthy wood, in the decayed wood, the electrical resistance would decrease obviously with increasing the concentration of cation (Houston D R.,1971). The decayed degree detected by ERT (E_d) mainly reflects water content ratio and metal ions increase of the decayed area of the standing tree. The decayed degree determined by the weight loss rate of wood (E_s) mainly reflects the wood weight loss rate which is closely related to decay

distribution range, wood structural damage and mechanical strength. Both E_d and E_s reflect the wood decayed degree. In this study, when $E_s < 30\%$, there is significant correlation between E_d and E_s , and the correlation coefficient is the highest (Yang Zhong, 2005). Therefore, ERT can show better diagnosis than the other two methods for incipient decay of standing tree. If wood decay be detected as early as possible, it could be prevented and treated as soon as possible.

4.2 Analysis of the relation between E_y and E_s

When Cellulose, hemicelluloses and lignin of wood are corroded by wood-rotting fungi, density of wood will reduce accordingly and the internal hole defects of wood will appear. When stress wave travel in the defective wood, it will spread along edges around the defective area, travel path will be from straight line to curve, time of propagation will increase and velocity will be decrease (Xu Huadong, 2014). The decayed degree detected by SWT (E_y) mainly reflects the size of the internal indication of standing trees, while the weight loss rate of wood is also closely related to decay distribution range, wood structural damage and mechanical strength. There exist a correlation between E_y and E_s , because both methods can indicate the decayed degree of standing trees. In this study, when $30\% \leq E_s < 50\%$, there is a significant correlation between E_y and E_s , and the correlation coefficient is the highest among three methods, in other words, in this decayed degree, SWT is better than other two methods.

4.3 Analysis of the relation between E_z and E_s

Decay leads to the decrease of the wood density and strength, therefore the decayed degree tested by Resistograph (E_z) mainly reflect the distribution ratio of decay area in the standing trees and decline proportion of the mechanical strength (Huang Rongfeng, 2007), while the weight loss rate of wood is also closely related to decay distribution range, wood structural damage and mechanical strength. Both E_z and E_s embody decayed degree and have a strong correlation in theory. In this study, when $E_s > 50\%$, there is a significant correlation between E_z and E_s , and the correlation coefficient is the highest among three methods, in other words, Resistograph is better in the later stage of decay testing than other two methods.

4.4 Compare of Three NDT Methods

Overall, E_z fitted E_s better than E_d and E_y . The reasons for this are likely as follows: electrical resistance value of standing trees is affected by many factors such as ambient humidity, temperature, moisture content, decayed degree, growing season and measuring position and so on, moreover, it is easy to misjudge for the sensitivity of resistance testing (Wang Lihai, 2001; Just A, 1998) The detection results of SWT are affected by cross-section shape, defect types, decayed degree and number of sensors (Bao Zhengyu, 2013; Liu Zexu, 2014). While for Resistograph, resistance is closely related to wood mechanical strength and is difficultly influenced by other factors as well as the weight loss ratio of wood.

For different decayed degrees, in three methods, when $E_s < 30\%$, E_d had a relatively high fitting degree with E_s . when $30\% \leq E_s < 50\%$, E_y had a relatively high fitting degree with E_s , and when $E_s > 50\%$, E_z had a relatively high fitting degree with E_s . The result was connected with decay process of timber. During incipient decay, wood quality and facade looked unchanged; however, chemical component had changed a lot. Chi Yujie indicated that wood destroying fungi breed because of extension and spreading of hypha, when as fungus invaded and settled down into wood cells, and then they secreted several enzymes to decompose cellulose, hemicellulose and lignin as fuel (Chi Yujie, 2002). Electrical resistance of wood is mainly related with moisture and metal ions content, so ERT was more exact during incipient decay. Once decomposition of fungi began to stabilize, variation of electrical resistance became to flatten (Chi Yujie, 2002.). For SWT, during incipient decay, SWT was notoriously inaccurate as there have been not cavitations. Then SWT was more accurate. As there

were holes slowly with the decay grew worse (Li Jian, 2002). Some research has showed that stress wave could travel around the holes when it met holes, then propagation of stress wave would lengthen and the travel time of stress wave would increase. According to the calculation method of stress wave, the velocity change of stress wave could reflect the decayed degree (Xu Huadong, 2014). For Resistograph, once wood is decayed, the density and strength of wood will decrease, so the result tested by Resistograph can be relatively accurate, no matter what decayed degree (Zhang Houjiang, 2011). Studies have shown that the more decay serious, the more result of Resistograph decline obviously.

5 Conclusions

The purpose of this study was to compare three NDT methods to find out the appropriate technique matched with specific condition of standing trees in the forest field. 100 cross-sections of standing trees were tested by three NDT methods: Electric Resistance Tomography, Stress Wave Tomography and Resistograph and estimation weight loss ratios of wooden increment cores. The results showed as following:

- (1) Positive correlation was shown obviously between the result decayed degrees detected by ERT (E_d) and truth-value of the decayed degree (E_s), and when $E_s < 30\%$, E_d had the highest correlation coefficient ($R=0.823$, $P<0.01$) with E_s among the three methods.
- (2) Positive correlation was shown obviously between the result decayed degrees detected by SWT (E_y) and truth-value of the decayed degree (E_s), and when $30\% \leq E_s < 50\%$, E_y had the highest correlation coefficient ($R=0.658$, $P<0.01$) with E_s among the three methods.
- (3) Positive correlation was shown obviously between the result decayed degrees detected by Resistograph (E_z) and truth-value of the decayed degree (E_s), and when $E_s > 50\%$, E_z had the highest correlation coefficient ($R=0.914$, $P<0.01$) with E_s among the three methods.
- (4) All three of the NDT methods, ERT, SWT and Resistograph could represent the weight loss rate of wood which was the index for expressing decayed degree. Therefore, all three NDT methods can detect the decay of standing trees effectively in some certain range.
- (5) ERT, SWT and Resistograph had distinctive features and advantages. ERT can show better diagnosis than the other two for incipient decay ($E_s < 30\%$) of standing trees, while SWT can significantly used in the middle stage of decay ($30\% \leq E_s < 50\%$) testing, and Resistograph revealed the most accurate result in the later stage of decay detecting can be used in the different stages of decay, but Resistograph can cause micro-damage of standing trees. Therefore, it is suggested that each technique can be employed in the practical internal decay testing for standing trees according to the decay stage and operational conditions.

Acknowledgements

The authors gratefully acknowledge the State Bureau of Forestry 948 Project (2014-4-78), Science and Technology Project of Fujian Educational Bureau (JA15155) and National Natural Science Foundation of China (31300474) for funding this project. All research partners in these projects are thanked for their cooperation and collaboration.

References

- Just A, Jacobs F. 1998. Elektrische Widerstandstomographie zur Untersuchung des Gesundheitszustandes von Bäumen; VII. Seminar, Hochauflösende Geoelektrik, Universität Leipzig, Institut für Geophysik und Geologie.
- Nicholas J. Brazeo, Robert E. Marra, Lothar Göcke, Phillip Van Wassenaeer. 2011. Non-destructive assessment of internal decay in three hardwood species of northeastern North America using sonic and electrical impedance tomography [J]. *Forestry*, 84 (1): 33-39.

- Xu Su, Zhou Quyou, Liu Hanle. 2006. Application of ERT method in monitoring tree water movement. *Journal of Guilin University of Technology*, 26(3): 347-352.
- Wu Huaqiao, Zhou Quyou, Liu Hanle. 2008. Temporal and spatial monitoring of water distribution and migration in a tree trunk using electrical receptivity tomography. *Progress Geophysice*, 23(4):1310-1316.
- Zhou Quyou, Liu Hanle, Tang Mingjie. 2009. Application of electrical resistivity tomography in studying water uptake process in tree trunk. *Chinese Journal of Ecology*, 28(2): 350-356.
- Xu Huadong, Wang Lihai, You Xiangfei. 2010. Analysis of Stress Wave Propagation in Hankow Willow Standing Trees and Stability Assessment. *Scientia Silvae Sinicae*, 46(08):145-150.
- Wang Lihai, Xu Huadong, Zhou Cilin. 2007. Effect of sensor quantity on measurement accuracy of log inner defects defects by using stress wave. *Journal of Forestry Research*, 18 (03):221-225+251.
- Ge Xiaowen, Wang Lihai, Sun Tianyong, et al. 2014. Quantitative detection of *Salix matsudana* inner decay based on stress wave and resistograph techniques. *China Forestry Science and Technology*, 28(5): 87-91.
- Huang Rongfeng, Wang Xiaohuang, Li Hua, et al. 2007. Quantitative analysis on the detected results by resistograph on inside wood decay of ancient architecture. *Journal of Beijing Forestry University*, 29(06): 167-171.
- Sun Tianyong, Wang Lihai, Sun Molong. 2013. Correlations between standing trees trunk decay degree and soil physical-chemical properties in Korean pine- broadleaved mixed forest in Xiao Xing'an Mountains of Northeast China. *Chinese Journal of Applied Ecology*, 24(07): 1837-1842.
- Sun Tianyong, Wang Lihai, Xu Huadong, et al. 2014. Effects of soil chemical properties on trunk decay of Korean pine standing trees in Xiao Xing'an Mountains of northeastern China. *Journal of Beijing Forestry University*, 36(02):30-37.
- Bao Zhengyu, Wang Lihai. 2013. Application of Electrical Resistance Testing Method in Detection of Decay in Standing Trees. *Forest Engineering*, 29 (6): 47-51.
- Wang Chaozhi, Zhang Houjiang. 2006. The Research Progress in Wood and Standing Tree Based on Stress Wave Method. *Forestry Machinery & Woodworking Equipment*, 34 (3) :9-13.
- Lin Wenshu, Yang Huimin, Wang Lihai. 2005. Comparative Study on Ultrasonic and Stress Wave for Nondestructive Test of Wood Defects. *Forestry Science & Technology*, 30(2):39-41.
- Wang Lihai, Xu Huadong, Run Zaixing, et al. 2008. Effects of Sensor Quantity and Planar Distribution on Testing Results of Log Defects Based on Stress Wave. *Scientia Silvae Sinicae*, 44(05):115-121.
- Xu Kaihong. 2004. Theory and Technology of Detecting Inner-defects in wood with A Probing Drill Device. PhD Thesis, Northeast Forestry University, Harbin, China.
- Li Wenbing. 2008. 15th International Symposium on Nondestructive Testing of Wood. *International Academic Developments*, (4): 41-42.
- An Yuan, Ying Yafang, Jiang Xiaomei, et al. 2008. Inspection of Decay Distribution in Wood Column by Stress Wave and Resistograph Techniques. *Journal of Building Materials*, 11(4): 457-463.
- Houston D R. 1971. Discoloration and decay in red maple and yellow birch. *Forest Sci*, 17:402-406.

Yang Zhong. 2005. Modeling Slash Pine Plantation Wood Properties and Decay Using Near Infrared Spectroscopy. PhD Thesis, Chinese Academy of Forestry.

Xu Huadong, Xu Guoqi, Wang Lihai, et al. 2014. Construction of Stress Wave Time Isolines on Log Cross Section and Analysis of Its Effect Factors. *Scientia Silvae Sinicae*, 50(4):95-100.

Wang Lihai, Yang Xuechun, Xu Kaihong. 2001. The present situation and advance in development of wood non-destructive testing techniques. *Forest Engineering*, 17(6): 1-3.

Bao Zhengyu, Di Xianghui, Wang Lihai. 2013. Effects of Moisture Content on Propagation Velocity of Stress Wave in *Abies Fabric* Standing Trees in Xiaoxing'anling Nature Forest. *China Forestry Science and Technology*, 38(1): 22-24.

Liu Zexu, Di Xianghui, Wang Lihai, et al. 2014. Effect of Different Detection Angle on Propagation Velocity of Stress Wave in Health Standing Trees. *Journal of Northeast Forestry University*, 42(4): 105-108.

Chi Yujie. 2002. Wood decay and wood decay fungi. Science Press, Beijing.

Li Jian. 2002. Wood Science. Higher Education Press, Beijing.

Xu Huadong, Xu Guoqi, Wang Lihai, et al. 2014. Construction of Stress Wave Time Isolines on Log Cross Section and Analysis of Its Effect Factors. *Scientia Silvae Sinicae*, 50(4):95-100.

Zhang Houjiang, Zhu Lei, Sun Yanliang, et al. 2011. Determining main mechanical properties of ancient architectural timber. *Journal of Beijing Forestry University*, 33(05): 126-129.

Ultrasonic Tomography in Logs of Urban Trees with Different Levels and Types of Hollows

Raquel Gonçalves

Professor, Coordinator of the Laboratory of Nondestructive Testing – LabEND, School of Agricultural Engineering - FEAGRI - University of Campinas - UNICAMP, Brazil – E-mail: Raquel@agr.unicamp.br

Mariana Nagle dos Reis

Master student, Laboratory of Nondestructive Testing – LabEND, School of Agricultural Engineering - FEAGRI - University of Campinas - UNICAMP, Brazil – E-mail: ma.nagle.reis@gmail.com

Danilo Profeta Ziller

Graduation student, Laboratory of Nondestructive Testing – LabEND, School of Agricultural Engineering - FEAGRI - University of Campinas - UNICAMP, Brazil – E-mail: danilo_ziller94@gmail.com

Stella Stopa Assis Palma

Master student, Laboratory of Nondestructive Testing – LabEND, School of Agricultural Engineering - FEAGRI - University of Campinas - UNICAMP, Brazil – E-mail: ssapalma@gmail.com

Mar Ainhoa Basterrechea

M.Sc. in Forestry Engineering. Department of Forest and Environmental Engineering and Management, MONTES (School of Forest Engineering and Natural Resources), Universidad Politécnica de Madrid, Spain. mar.ainhoaba@gmail.com

Abstract

The correct interpretation of the acoustic tomographic images can help to obtain precise and safe diagnosis about the risk of falling of a tree, especially in urban areas where there is a risk against life and urban equipment. The objective of this research was to analyze, qualitatively and quantitatively, the results of ultrasound tomography with different levels and types of hollows in urban tree disks. Tests were carried out on 6 disks from 4 different tree species, three of which with natural decays and three with artificial holes. In general, hollowed areas present greater than 70% velocity reduction and, the identification of hollowed area using this velocity loss allows to obtain less than 10% error comparing with the area obtained using the mask. In general, the ultrasonic tomography images were adequate to provide important information for the tree risk assessment.

Keywords: ultrasound, image pattern, hollowed wood

Introduction

Different types of deterioration can cause changes in the wood's structure. The mechanical wave propagation is mainly affected by differences in elastic properties (Bucur 2006). In wood deterioration by termites or other xylophagous insects, the wood presents galleries in its interior, but the surrounding material is generally intact. Weiler et al. (2013) showed statistically significant variations of modulus of elasticity (MOE) and rupture (MOR) when termite deterioration was between 20% and 100%.

The association of fungal attack, followed by termites, may be responsible for the existence of hollowed areas in trees. In these cases (galleries and hollows) the wave propagation will suffer deviations and consequent velocity reduction. Deviations occur because mechanical waves seek the material medium to propagate (Weiller et al. 2013, Secco et al. 2012, Najafi et al. 2009, Lin et al. 2008, Bucur 2006, Wang et al. 2007, Wang et al. 2004). Thus, if deteriorations or cavities in the wood reduce the velocity of wave propagation, the variations can be used as changes identifiers in the material.

In order to obtain a scan in the inspected element, a measurement mesh (Divos and Szalai, 2002), called diffraction (Example in Fig. 1a) is used. Through this mesh it is possible to obtain measurement routes, whose quantity depends on the number of sensors used. In order to facilitate visualization, velocity variations are associated with colors and, through interpolation software (Du et al. 2015, Feng et al., 2014, Zeng et al., 2013), images are constructed (Example in Fig. 1b). This procedure is called acoustic tomography. The quality of the image is affected by the interpolation process used, but the accuracy of the results, especially in the case of ultrasound, also suffers interference from the power of the equipment and the quality of the data obtained in the field.

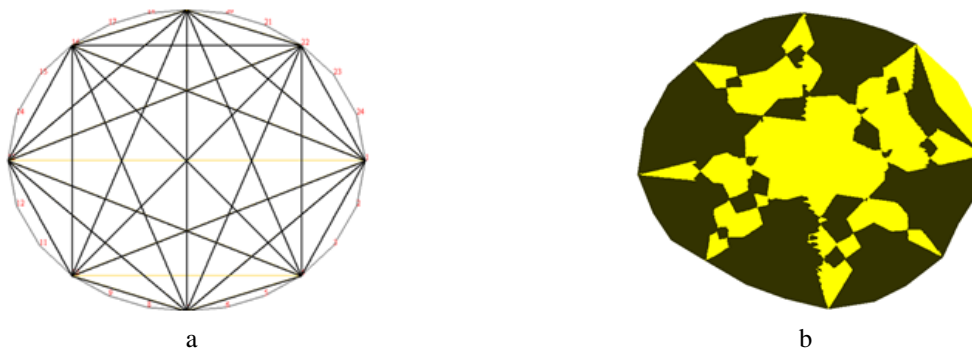


Fig. 1 Example of measurement mesh (a) and tomography image generated (b)

There are several commercial acoustic tomography equipment's on the market, mainly using propagation of stress waves (called sonic tomographs). Pereira et al. (2007) concluded that acoustic tomography is a developing technique and, therefore, lacking in studies. The same conclusion was presented by the USDA (2014), which discusses acoustic tomography in one of its chapters, presenting examples of tomographic images produced using commercial tomographs, but indicating that the greatest limitation of the method is still the interpretation of the tomographic image.

Considering the aspects mentioned, the objective of this research was to evaluate, qualitative and quantitatively, the results of ultrasound tomography using equipment and software developed in our research group, in face of different types and levels of hollows in urban trees.

Materials and Methods

The wood samples used in this study were taken from trunks of trees of the species: *Centrolobium sp*, *Liquidambar styraciflua* and *Copaifera sp*. In order to carry out the ultrasonic tests, disks with a minimum of 200 mm height were cut from those trunks.

The ultrasound tests were performed using the diffraction mesh (Fig. 1a) in which 8 measurement points were adopted for all species. The measuring points were approximately equidistant and positioned at the middle height of the disk. As used in the standing tree tests, at each measurement point, 3 mm holes were drilled for the introduction of the transducer tip with the use of a drill, to ensure coupling of the transducer to the wood and not to the bark.

The tests performed on each diffraction mesh measurement route (Fig. 1a) were done using conventional ultrasound equipment developed by the research group in partnership with a technology-based company (USLab, Agricef, Brazil) and longitudinal 45-kHz frequency transducers. In order to obtain the tomography image, the software (*ImageWood 2.0*), also developed in the research group, was used.

After the ultrasound tests, the disks were cut at the height where the measurements were taken and the disk surface was polished to be analyzed and photographed in detail. The species presented different conditions of deterioration and the deteriorated zones were determined only macroscopically through a detailed visual analysis of its surfaces.

The generated photographs were used to obtain representative mask of the deteriorated zone, using the free software *ImageJ*. This mask was used to calculate the percentage of deteriorated area.

The tomographic images were generated in two ways. In the first one, 6 velocity bands were used, based on the maximum velocity (V_{MAX}) obtained in the disk (*red* : V_{MIN} to 20% V_{MAX} , *orange* 20-30% of V_{MAX} , *yellow* 30-50% of V_{MAX} , *green* 50-70% of V_{MAX} , *blue* 70-80% of V_{MAX} and *black* 80-100% of V_{MAX}). According to a USDA publication (2014), a 50% reduction in wave propagation velocity means that the region presents severe deterioration, so the second procedure was done considering only two colors: *brown* for zones with velocities above 50% of V_{MAX} and *yellow* for zones with velocities below 50% of V_{MAX} , which were considered as areas with severe deterioration. These two-color images were used to determine the percentage of impaired area inferred by tomography, also using the free *ImageJ* software.

The images generated in different colors by the ultrasound tomography were visually compared with the photographs obtained from the surface. In addition to this visual analysis, the percentage of deteriorated area, inferred by tomographic images with two colors, was compared with the percentage of deteriorated area obtained from the photograph of the disks surface (mask).

Results and Discussion

The visual analysis of the treated surfaces allowed detailing the deteriorated zones in the disks of the different species: *Centrolobium sp* had a large hollow caused by termite attack; *Liquidambar styraciflua* had a lateral crack from the pith to the bark caused by drying process and *Copaifera sp* had large hollow caused by termites. In the surroundings of these hollows there is indication of deterioration by fungi.

The images of the disks of the species *Centrolobium sp* and *Copaifera sp* (Fig.2a, 2c) are those with red and orange colors, which represent zones with speeds lower than 30% of V_{MAX} (or velocity loss greater than 70%). These disks are the ones that have great hollowed regions. Thus, although the image does not represent the shape and exact size of the deteriorated region, the tomographic image was efficient to assess the falling risk of these two specimens, as it identified advanced deterioration inside the specimen, which would be enough to indicate the risk involved.

In the *Liquidambar styraciflua* disk (Fig. 2b) there's also a small region with the orange color located at the edge, representing reduction of 70% to 80% of the velocity. This region corresponds to the zone of greater opening of the crack in the disk. The rest of the image of this disk shows a zone with a velocity loss between 30% and 50% (green), which is on the same side of the crack and most of the area with velocity losses below 20% (black). The tomographic image analysis would not adequately identify the size and position of the crack. The ability to detect defects using wave propagation is associated with the relationship between wavelength (λ) and defect size (Bucur 2006). In general, the detection sensitivity is about $\lambda/2$ (Bucur 2006). In the case of the *Liquidambar styraciflua* specimen, the maximum velocity (integral area) was 2000 m.s⁻¹, so $\lambda \cong 44$ mm. Thus, defect detection of the order of 22 mm is expected to be possible. The largest aperture of the crack, located at the edge of the

disk and detected in the tomographic image (Fig. 2c) is 25 mm, consistent with the theoretical aspects of this test.

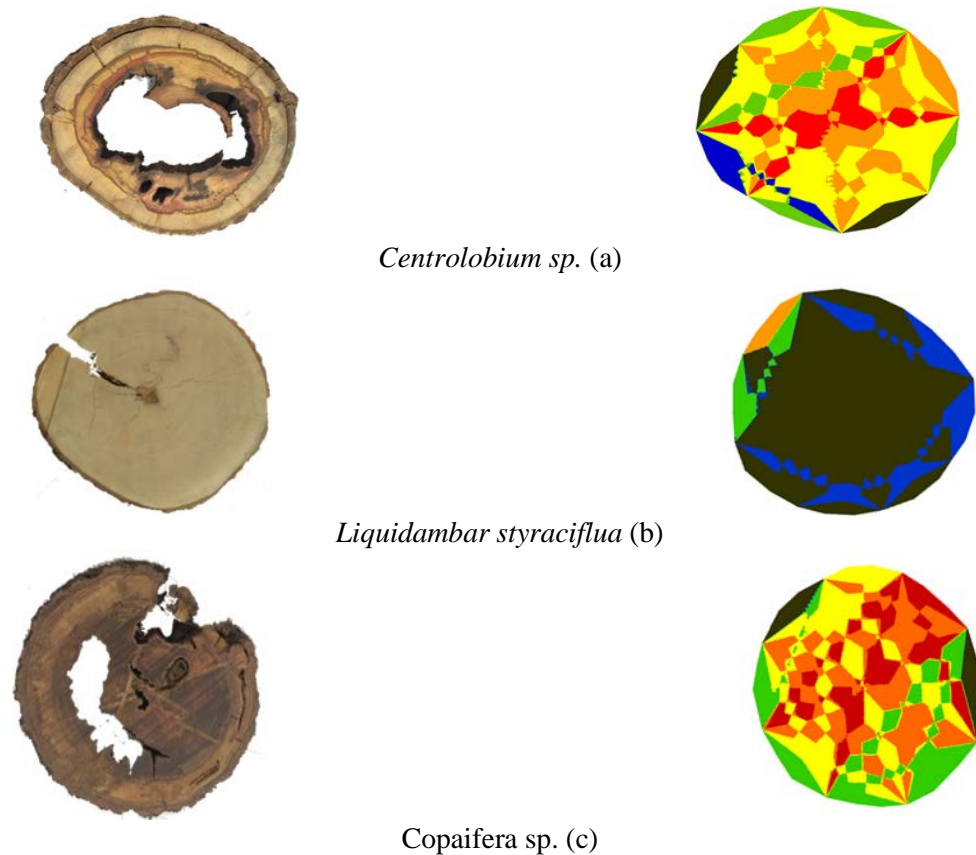


Fig. 2: Photographs of the surfaces of the disks from the different species and images of its ultrasonic tomography

Legend as a function of maximum velocity (V_{MAX}): *red* : V_{MIN} to 20% V_{MAX} , *orange* 20-30% of V_{MAX} , *yellow* 30-50% of V_{MAX} , *green* 50-70% of V_{MAX} , *blue* 70-80% of V_{MAX} and *black* 80-100% of V_{MAX}

At the *Centrolobium sp* and *Copaifera sp* disks, containing hollows, the percentage of deteriorated area (Table 1), obtained using *ImageJ* (Fig. 2), was approximately 30% lower than the percentage of deterioration area inferred by the tomographic image (Table 1) constructed with two colors (Fig. 3). This is due to the fact that there are large decreases in the minimum velocity (Trinca et al., 2015), which in this case were higher than 70%. Considering that in the tomographic images with two colors (Fig. 3), the velocities range adopted is that corresponding to a loss of 50% of the velocity (yellow), the area of this zone also covered regions not affected only by the hollow .

Table 1. Percentage of deteriorated area using the photograph of the disks surfaces; percentage of deteriorated area using ultrasound tomography and difference between these two percentages

Species	Deteriorated area (%)		
	Surface photography	Tomographic image*	Difference (%)
<i>Centrolobium sp</i>	48,09	78,34	-30,25
<i>Copaifera sp</i>	43,46	73,70	-30,24
<i>Liquidambar styraciflua</i>	1,83	2,29	-0,46

* Areas of the image representing a velocity loss superior to 50%

Applying the expected velocity variations to zones with hollows and with deterioration caused by fungi (Trinca et al., 2015), new tomographic images were constructed with two colors (Fig. 3). For the disks with hollows (*Centrolobium sp* and *Copaifera sp*), yellow represents areas with 70% velocity loss (Fig. 3a, 3c). The purpose of this evaluation was to study the velocity losses associated with hollows. Using the same procedure to calculate deteriorated areas (mask and tomographic image), it is verifiable that the difference between the hollowed areas (*Centrolobium sp* and *Copaifera sp* species) provided by the ultrasonic tomography is close to the actually affected areas (Table 2).

Table 2 Percentage of deteriorated area using the photograph of the disks surfaces and the image of ultrasonic tomography, and difference between these two percentages

Species	Deteriorated area (%)		
	Surface photograph	Tomographic image	Difference (%)
<i>Centrolobium sp</i>	48,09	38,74*	9,35
<i>Copaifera sp</i>	43,46	45,50*	-2,04

* Areas of the image representing velocities losses exceeding 70%

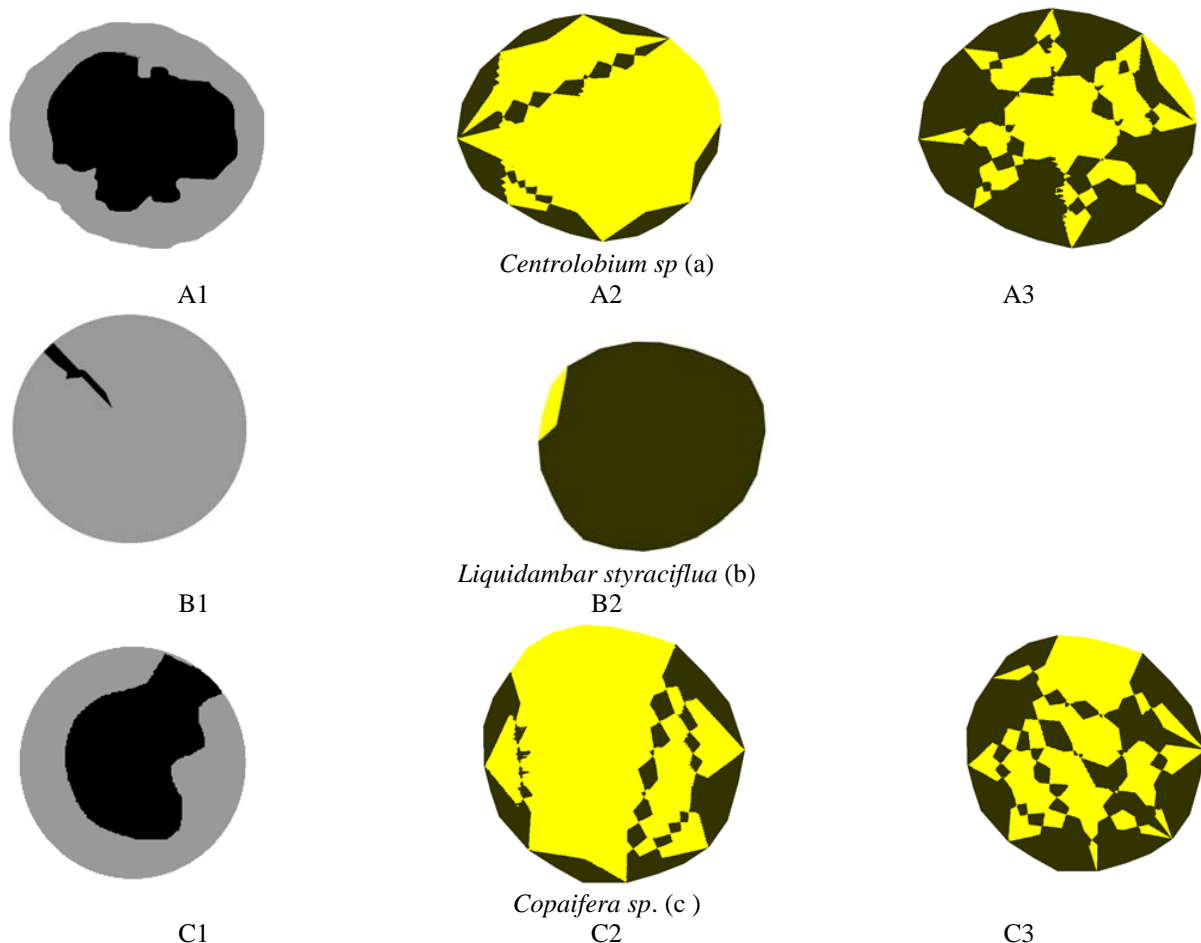


Figure 3 Masks representative of the deteriorated zones based on the surface pictures (A1, B1, and C1) and ultrasonic tomography images considering two situations. Situation 1: *yellow*: velocity losses greater than 50% and *brown*: velocity losses less than 50% (A2, B2, C2). Situation 2: disks with hollow - *yellow*: velocity losses greater than 70% and *brown*: velocity losses of less than 70% (A3, C3)

The tomography image generated with different colors (Fig. 2) is a little more confusing for a layman, but conceptually allows better differentiation of velocity variation levels, and consequently the

location of the zones with greatest loss in wood stiffness, regardless deterioration type. Using only to colors to construct the images (above and below 50% loss of speed) the amplified hollowed region is shown (Table 1). However, the visualization is clearer and represents an important tool for falling tree risk assessment purposes, since it allows inferring the existence of zones with great loss of stiffness.

Conclusions

Ultrasound tomography images are adequate to provide important information for falling tree risk assessment. The identification of the percentages of hollowed areas had errors of less than 10% when regions with a velocity loss greater than 70% are considered and overestimate 30% of such zones when velocity losses greater than 50% are considered. The identification of cracks depends on the relationship between their size and the transducers frequency; there was coherence in the detection of the zone where the crack had the largest aperture.

Acknowledgments

The authors would like to thank the National Council for Scientific and Technological Development (CNPQ) for the scholarships and Sao Paulo Research Foundation (FAPESP) - Proc. 2015/05692-3 - for the research funding. They also thank the Environment Department of UNICAMP for donating the logs used in the tests.

References

- BATISTA, F.; GONÇALVES, R.; CERRI, D.G.P.; SECCO, C.B., (2010) Reprodução da condição interna de peças de madeira através de imagens representativas da propagação de ondas, XXVIII Congresso Nacional de Ensaio Não Destrutivo e Inspeção - 14a. Conferencia Internacional sobre Evaluacion de Integridad y Extension de Vida de Equipos Industriales, Vol. 1, pp.1-12, Santos, SP, BRASIL
- BATISTA, F.A.F; GONÇALVES, R.; CERRI, D.G.P.; SECCO, C.B. (2009) Reprodução da condição interna de peças de madeira através de imagens representativas da propagação de ondas. *Madeira: Arquitetura e Engenharia*, v.10 (25), p 23-32
- BUCUR, V. (2006) *Acoustics of wood*. 2nd ed. New York: Springer-Verlag, 393p
- DIVOS, F.; SZALAI, L. (2002) Tree evaluation by acoustic tomography. In: *Proceedings of the 13th International symposium on nondestructive testing of wood*; 2002 August 19. 21; Berkeley, CA. Madison, WI: Forest Products Society: 251.256
- DU, X. et al. (2015) Stress Wave Tomography of Wood Internal Defects using Ellipse-Based Spatial Interpolation and Velocity Compensation. *BioResources*, v. 10, n. 3, p. 3948-3962
- FENG, H. et al. (2014) Tomographic image reconstruction using an interpolation method for tree decay detection. *BioResources*, v. 9, n. 2, p. 3248-3263
- LIN, C.J.; KAO, Y.; LIN, T et al (2008) Application of ultrasonic tomographic technique for detecting defects in standing trees. *International Biodeterioration & Biodegradation*, 62, p.434-441
- NAJAFI, S. K.; SHALBAFAN, A.; EBRAHIMI, G. (2009) Internal decay assessment in standing beech trees using ultrasonic velocity measurement, *Eur. J. Forest Res.* 128, 345-350
- PEREIRA, L.C., FILHO, D.F.S., TOMAZELLO, M., COUTO, H.T.Z., MOREIRA, J.M.M.A.P., POLIZEL, J.L. (2007) Tomografia de impulso para avaliação do interior do lenho de árvores. *Revista da sociedade brasileira de arborização urbana*, Volume 2, Número 2

SECCO, C. B.; GONÇALVES, R.; CERRI, D. G.; VASQUES, E.C.; BATISTA, F. (2012) Behavior of ultrasonic wave propagation in presence of holes on wood. *Cerne (UFLA)*, v. 18, p. 12-16

TRINCA, A.J., GUERRA, M.R., GONÇALVES, R. (2015) Velocity variation in wood as a function of defects, In: *International Nondestructive Testing and Evaluation of Wood Symposium*, v.19. Rio de Janeiro, Brasil, p. 593 – 599

UNITED STATES DEPARTMENT OF AGRICULTURE (USDA), (2014) *Wood and Timber Assessment Manual*. Forest Products Laboratory, Madison, WI, 2ed. 94p.

WANG, X.; CARTER, P.; ROSS, R.J.; BRASHAW, B.K.. (2007) Acoustic assessment of wood quality of raw forest materials – a path to increased profitability. *Forest Products Journal*, Madison, v.57, n.5, p.6-14

WANG, X; ROSS, R. J.; BRASHAW, B. K.; VERHEY, S. A.; FORSMAN, J. W.; ERICKSON, J. R. (2004) Flexural properties of laminated veneer lumber manufactured from ultrasonically rated red maple veneer. *USDA/FS/FPL Research Note FPL-RN-0288*. 5p

WEILER, M.; MISSIO, A.L.; GATTO, D.A.; GUTHS, W.G. (2013) Nondestructive Evaluation of Wood Decayed by Xylophagous Organisms, *Materials Research*: 16(5): 1203-1208

ZENG, L. et al. (2013) Interference resisting design for guided wave tomography. *Smart Materials and Structures*, v. 22, n. 5, p. 055017

Figura 1 Exemplo de malha de medição (a) e de imagem de tomografia gerada (b)

Association of Ultrasonic Tomography and Drilling Resistance in Decay Evaluation of Trees

Mariana Nagle dos Reis

Master student, Laboratory of Nondestructive Testing – LabEND, School of Agricultural Engineering - FEAGRI - University of Campinas - UNICAMP, Brazil – E-mail: ma.nagle.reis@gmail.com

Stella Stopa Assis Palma

Master student, Laboratory of Nondestructive Testing – LabEND, School of Agricultural Engineering - FEAGRI - University of Campinas - UNICAMP, Brazil – E-mail:ssapalma@gmail.com

Danilo Profeta Ziller

Graduation student, Laboratory of Nondestructive Testing – LabEND, School of Agricultural Engineering - FEAGRI - University of Campinas - UNICAMP, Brazil – E-mail:danilo_ziller94@gmail.com

Raquel Gonçalves

Professor, Coordinator of the Laboratory of Nondestructive Testing – LabEND, School of Agricultural Engineering - FEAGRI - University of Campinas - UNICAMP, Brazil – E-mail: raquel@agr.unicamp.br

Miguel Esteban

Department of Forest and Environmental Engineering and Management, MONTES (School of Forest Engineering and Natural Resources), Universidad Politécnica de Madrid, Spain. E-mail: miguel.esteban@upm.es

Guillermo Íñiguez-González

Department of Forest and Environmental Engineering and Management, MONTES (School of Forest Engineering and Natural Resources), Universidad Politécnica de Madrid, Spain. E-mail: guillermo.iniguez@upm.es

Mar Ainhoa Basterrechea

M.Sc. in Forestry Engineering. Department of Forest and Environmental Engineering and Management, MONTES (School of Forest Engineering and Natural Resources), Universidad Politécnica de Madrid, Spain. mar.ainhoaba@gmail.com

Abstract

Both tomography and drilling resistance have shown great potential to be used, in association with visual analysis, in tree inspections, but both have limitations inherent to any technology. Therefore, the objective of this research was to evaluate the association of the nondestructive tools - ultrasound tomography and drilling resistance – to identify internal conditions of trees. The results showed that the tomography is sufficient to predict the condition of a region with severe and extensive deterioration. However, can fail if it is necessary to have more precise information about size and location of the deteriorated zone. The drilling resistance gives very efficient diagnoses of areas with hollows. However, in trees with different levels of deterioration a calibration is necessary to have clear information. The tree diagnosis are more precise and safe with the association of both technologies.

Keywords: ultrasonic tomography, drilling resistance, deterioration of wood, tree risk assessment

Introduction

The urban forestry has great social, aesthetic, cultural and educational relevance, as well as significant climatic and environmental aspects. However, lack of urban forest planning and environmental conditions can lead to the declining of trees, with significant changes in size, shape and position relative to the axis. These conditions make trees more susceptible to pathological problems that can lead to its fall. In addition, trees are living organisms and as such have a life cycle that involves the onset of growth, juvenile stage, adulthood and natural death. Therefore, its correct maintenance is extremely important for the safety of the population and integrity of urban equipment and public goods. All these aspects bring the necessity of more studies involving the subsidies for the use of effective methodologies and economically feasible inspection tools (Martinez and Diaz 2016, Rollo et al. 2013).

Visual inspection, already practiced in several parts of the world, is a very important tool, since it allows the identification of pathologies with low cost and is very useful to be the starting point of the tree evaluation (Wang and Allison 2008, Mattheck 2007, Kennard et al. 1996). On the other hand, besides being highly dependent on the inspector's experience, it may not include the identification of internal anomalies indicative of fragility or instabilities of the trunk (Martinez and Diaz 2016, Rollo et al. 2013). In many cases it is necessary, to infer tree risk, associate visual analysis with technologies capable of inferring and monitoring the internal condition of the tree.

Tomography using sonic methods has been used to evaluate the internal condition of trees in several countries, mainly as an auxiliary tool to the falling tree risk assessment. There are several commercial acoustic tomography equipment on the market, mainly using propagation of stress waves (sonic tomographs). Other techniques are also used to generate tomographic images with adequate results (Nicolotti et al. 2003). Due to the need for a better understanding of the meaning of the generated image, as well as its reach in terms of accuracy, there is still a lot of research in the area showing a still lack of knowledge (Pereira 2007) and space to scientific contribution, highlighting the image interpretation (USDA 2014) and improvements in algorithmic of interpolation to image construction (Du et al. 2015).

Likewise, drilling resistance has been recognized as a technique that shows good results in inspections of trees and structures, although in a much-localized way (Rollo et al. 2013). Considering that the equipment measures the resistance offering to drill, it is also expected that its results can be correlated with material strength losses due to deterioration. Studies have been developed to evaluate the correlation between the amplitude of the drilling resistance obtained by the equipment and the strength of the wood or its effectiveness in detection of decay in timber members (Brashaw et al. 2011; Tannert et al. 2013, Rinn 2012), on logs (Nutto & Biechele 2015) or on trees (Johnstone et al. 2010; Wang et al. 2008).

Both tomography and drilling resistance have shown great potential to be used in tree inspections, but both have limitations, which is inherent in any technology. Rollo et al. (2013) obtained very good correlations between results from impulse tomography and drilling resistance using logs from sound wood. For decayed wood Wang & Allison (2008) analyzed the results of a trunk inspection combining visual, single-path stress wave testing, sonic tomography and drilling resistance using a trunk of red oak (*Quercus rubra*).

The objective of this research was to evaluate the association of ultrasonic tomography and drilling resistance to inspect the internal conditions of trunks with different types of decay.

Methodology

The sampling used in this research was composed of trunks collected from three species: *Centrolobium sp.*, *Tabebuia ochracea*, *Liquidambar styraciflua* and *Platanus sp.* These species are widely found in the urban forestry from São Paulo state, Brazil. From these trunks were removed 4 discs approximately 200 mm thick.

Ultrasound tests were performed using the diffraction mesh proposed by Divos and Szalai (2002). At the mean height of each disc, 8 equidistant points were marked in the perimeter, in which 3 mm holes were drilled through the bark region, to coupling the exponential faces of the 45-kHz-frequency longitudinal transducers. The tests were performed with conventional ultrasound equipment (UsLab, Agricef, Brazil), developed by the research group in partnership with a spin-off company. In the diffraction mesh, each of the points is connected to the other 7, configuring 28 measurement paths, in which are obtained the wave propagation times. In order to obtain the tomography image, we used a software (*ImageWood 2.0*) also developed in the research group. The images were generated using 6 velocity ranges, adopted according to the maximum velocity (V_{MAX}) obtained in each disc (*red* : V_{MIN} to 20% V_{MAX} , *orange* 20-30% of V_{MAX} , *yellow* 30-50% of V_{MAX} , *green* 50-70% of V_{MAX} , *blue* 70-80% of V_{MAX} and *black* 80-100% of V_{MAX}).

After the ultrasonic tests, the measurements of drilling resistance (IML F400 Resistograph, Germany) were carried out in the perpendicular to the grain direction, on the same radial measurement routes used for the ultrasonic tests. For the tests the discs were fixed to a concrete table. The drilling resistance equipment used in the tests allows the choice of different feed rates (from 15 cm / min to 200 cm / min) and needle rotation (1500 rpm to 5000 rpm). These adjustments are usually made in function of density of the wood as well as its level of deterioration. Therefore, speeds used in each species took these aspects into consideration. From the tests, 48 drilling resistance amplitude graphs were obtained according to the different routes.

After the ultrasonic and drilling resistance tests, the discs were sawn at the exact height where the measurements were taken and the surface of the new discs obtained was sanded to be macroscopically analyzed and digitally photographed. From the macroscopic visual analysis, it was verified that the discs presented different conditions and degrees of deterioration.

Results and Discussion

The ultrasonic images were generated and associated with the drilling resistance graph (Figure – 1). Previous studies by the research group (Trinca et al. 2015) allowed to conclude that images as arrow forms represent interferences produced by the interpolation algorithm used by *ImageWood 2.0* software. Therefore, these areas (with arrow forms) should not be considered in the interpretation of the tomographic images.

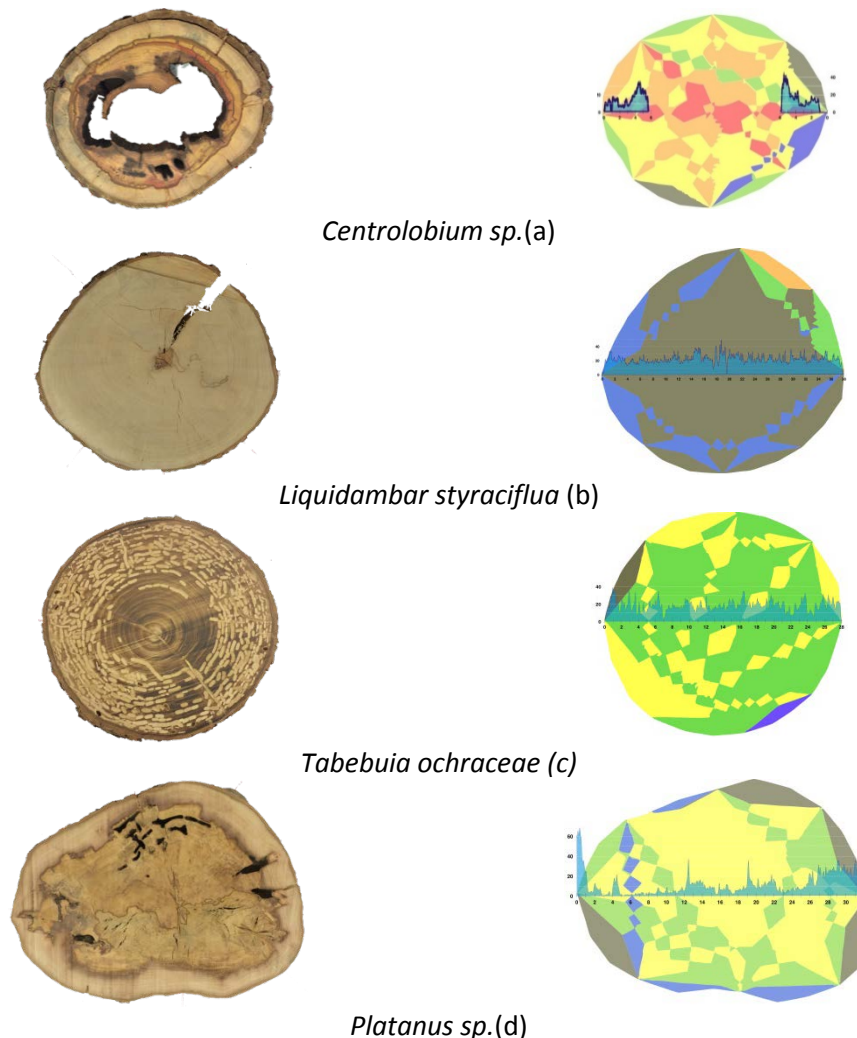


Figure 1 - Comparative images of the digital pictures of the discs and the superposition of the ultrasound tomographic images to the drilling resistance amplitude graphics

Legend: percentages of maximum velocity (V_{MAX}): *red* : V_{MIN} to 20% V_{MAX} , *orange* 20-30% of V_{MAX} , *yellow* 30-50% of V_{MAX} , *green* 50-70% of V_{MAX} , *blue* 70-80% of V_{MAX} and *black* 80-100% of V_{MAX} .

The *Centrolobium sp.* disc (Fig.1a) present the colors red and orange on its images, representing zones with velocities lower than 30% of the maximum velocity obtained in these discs. In the case of the *Centrolobium sp.* disc, the use of the drilling resistance equipment made it possible to verify that the area delimited by velocities with less than 30% of the maximum velocity obtained on disc was effectively a hollow, once the amplitude was zero in that region in all measurement routes (Example in Figure 2a). The zones in yellow presented amplitudes around 20%. Near the zone with more severe deterioration, represented by zero amplitude, there is an amplitude increase to 40% (Figure 2a). Thus, for this disc, the association of drilling resistance to the tomographic image allowed us to identify and delimit, more precisely, the hollow dimension (regions with zero amplitude). In the case of a tree inspection, this result, repeated in different highs would assist in a decision making for the suppression.

In the *Liquidambar styraciflua* disc (Fig.1b) the crack is apparent and can, therefore, be detected visually. This disc is being used in this discussion to simulate the situation of a defect of smaller proportions than

the two previously analyzed. In addition, in the previous situation, mainly for the *Copaifera sp.*, the wood around the hollow was also deteriorated, while in the *Liquidambar styraciflua* disc the wood is sound. In the tomographic image of the *Liquidambar styraciflua* disc appears a small region, located in the upper right border, represented by orange color, indicative of reduction of 70% to 80% of the velocity. This region corresponds to the zone of greater opening of the crack in the disc. Thus, the tomographic image did not allow seeing the depth of the crack, indicating only reduction of speed in the border. Eliminating from the analysis the images in arrows form (interferences) the interpretation of the tomography would be that the disc has only a stiffness loss in the upper right border (zones in orange and uninterrupted green in Figure 3). This behavior of the tomographic image is related to the limitation given by the relation between the wavelength and the size of the defect evaluated (Bucur, 2006). Since the wavelength is affected by the frequency of the transducer used in the test and by the propagation velocity of the wave in the medium, the defects visible for the test conditions of this research would be around 20 mm. The drilling resistance test in *Liquidambar styraciflua* disc did not identified the crack, since no measurement route passed through it. This result is a good example of a localized test problem, such as the drilling resistance test. The average amplitude of the drilling resistance in different measurement routes was around 20%. Considering that the wood is sound, it is verified that the numerical value of the percentage of drilling resistance cannot be used directly or alone to interpret the condition of strength or stiffness, since, for example, amplitudes of 20% in *Centrolobium sp.* disc were obtained in deteriorated areas. The *Liquidambar styraciflua* has lower density than *Centrolobium sp.* affecting the drilling resistance. So, more important than the level of drilling resistance amplitude is the homogeneity of the graphic (example in Figure 3), indicating sound wood.

The image of the *Tabebuia ochracea* disc (Fig 1c) shows, for the most part, ranges of velocities in green and yellow, indicating velocity reductions from 30% to 50% (green zone) and from 50% to 70% (yellow zone). Eliminating from the image the yellow arrow forms within the green zone, the interpretation of the tomography would be that a large part of the disc has velocity losses from 30% to 50%, which, indicates zones with more than 50% loss in strength (USDA 2014). Large yellow areas are observed at the edges of this image (Figure 4), indicating a reduction in velocity superior to 50% (USDA 2014), with severe deterioration. As there are no red or orange areas in the image, the interpretation of the tomography would not lead to infer the existence of hollowed areas. The association of the tomography with the drilling resistance test in *Tabebuia ochracea* disc would confirm the absence of hollows, since there was no zero-amplitude registered in any of the graphic routes (Example in Figure 4). The average amplitude of drilling resistance on the different routes was 20%, therefore equal to the one obtained in *Liquidambar styraciflua* disc.

The *Liquidambar styraciflua* disc presented velocity losses from 0 to 20%, while for *Tabebuia ochracea* between 30% and 50%. The amplitude graph in this disc was not as regular as in the *Liquidambar styraciflua* disc, but the interpretation of this isolated result would be not evident, indicating the importance of the two methods association. The high density of *Tabebuia ochracea* play a very important hole in the drilling resistance amplitude. Isolated, the drilling resistance test would indicate that the disc is in good condition; however, the diagnosis of the ultrasound inspection infers a considerable loss of velocity, evidencing, in the case of a tree inspection, a possible risk. The visual analysis shows that the piece is almost completely taken up of cavities and that, at the extremities, more severe attack of the *Coleoptera* insects, compatible with the loss of velocity shown in the tomographic image.

The image generated by ultrasonic tomography of *Platanus sp.* (Fig. 5) indicates severe deterioration in practically all its extension, since it shows a large area in yellow (velocity reduction between 50% and 70%). The green strings would be eliminated from the interpretation, because it is considered as interpolation interferences. The absence of red and orange areas in the image would lead to infer that the piece had no areas with holes. The association of the drilling resistance amplitude would indicate the loss of stiffness inside of the disc, once the graphic is quite irregular, with large and continuous zones with

very low amplitudes (5 to 10%). According to USDA (2014) drilling resistance from 5 to 15% indicate moderate decay level but, in this case, the graph irregularity would indicate wood more decayed. The drilling resistance test also did not show any hollowed areas. So, the interpretation of the inspection using the association of both methods would allow to infer that the wood, although without any hole, present moderate to severe decay, therefore subject to risk.

Conclusions

The results shows that the association of ultrasound tomography and drilling resistance allows improving the quality of the diagnosis, since both techniques are suitable for inspection, but both have limitations. Ultrasound tomography allows a global analysis of velocity variation, which is related to the deterioration and wood stiffness loss. The drilling resistance allows very efficient diagnostics of areas with hollows. In wood severely and extensively decayed ultrasound tomography shows clearly results and the diagnosis using only this tool would already indicate the high risk. However, in zones with moderately or with insipient decay the ultrasound tomography can generate important doubts. So, in these cases, the association with the drilling resistance is essential to ensure the safety of the diagnosis, showing more precisely the size and the location of the decayed zones.

Acknowledgments

The authors would like to thank the National Council for Scientific and Technological Development (CNPQ) for the scholarships and Sao Paulo Research Foundation (FAPESP) - Proc. 2015/05692-3 - for the research funding. They also thank the Environment Department of UNICAMP for donating the logs used in the tests and to PD Instruments Company for lending the equipment used in tests of drilling resistance.

Reference list

- BRASHAW, B. K.; VATALARO, R.; ROSS, R. J.; WANG, X.; SCHMIEDING, S.; OKSTAD, W. (2011) Historic Log Cabin structural condition assessment and rehabilitation – A case study. In: International nondestructive testing and evaluation of wood symposium, 17, Hungria. Anais... Hungria: University of West Hungary, v.2, p. 505-512
- BUCUR, V. (2006) Acoustics of wood. 2nd ed. New York: Springer-Verlag, 393p
- DIVOS, F.; SZALAI, L. (2002) Tree evaluation by acoustic tomography. In: Proceedings of the 13th International symposium on nondestructive testing of wood; 2002 August 19. 21; Berkeley, CA. Madison, WI: Forest Products Society: 251.256
- DU, X. et al. (2015) Stress Wave Tomography of Wood Internal Defects using Ellipse-Based Spatial Interpolation and Velocity Compensation. BioResources, v. 10, n. 3, p. 3948-3962
- JOHNSTONE, D.; MOORE, G.; TAUSZ, M.; NICOLAS, M. (2010) The Measurement of Wood Decay in Landscape Trees, Arboriculture & Urban Forestry, 36(3), p. 121-127
- MARTÍNEZ P C, DÍAZ M I I (2016). El riesgo del Arbolado Urbano – Contexto, concepto y evaluación. Ediciones Mundi-Prensa, Madrid, Espanha, 465p.

MATTHECK C. (2007). Field Guide for Visual Tree Assessment. Forschungszentrum Karlsruhe GmbH. Alemanha, 170p.

NICOLOTTI, G.; SOCCO, L. V.; MARTINIS, R.; GODIO, A.; SAMBUELLI, L. (2003) Application and comparison of three tomographic techniques for detection of decay in trees. Journal of Arboriculture, Champaign, v. 29, n. 2, p. 66-78

NUTTO, L.; BIECHELE, T. (2015) Drilling resistance measurement and the effect of shaft friction – using feed force information for improving decay identification on hard tropical wood. In: International nondestructive testing and evaluation of wood symposium, 19 Anais... Brasil, Rio de Janeiro, p. 156-160

PEREIRA, L.C., FILHO, D.F.S., TOMAZELLO, M., COUTO, H.T.Z., MOREIRA, J.M.M.A.P., POLIZEL, J.L. (2007) Tomografia de impulso para avaliação do interior do lenho de árvores. Revista da sociedade brasileira de arborização urbana, Volume 2, Número 2

ROLLO, M.A; SOAVE Jr, F.; ANGELO, M.; Viana, M.; ROLLO, S.C.P.; COUTO, L.Z.; THADEU, H.; SILVA FILHO, D.F. Comparação entre leituras de resistógrafo e imagens tomográficas na avaliação interna de troncos de árvores. CERNE, vol. 19, n. 2, abril-junho, pp. 331-337, 2013, Universidade Federal de Lavras. Lavras, Brasil

TANNERT, T.; ANTHONY, R.W.; KASAL, B.; KLOIBER, M.; PIAZZA, M.; RIGGIO, M.; RINN, F.; WIDMANN, R.; YAMAGUCHI, N. (2013): In situ assessment of structural timber using semi-destructive techniques. Materials and Structures DOI 10.1617/s11527-013-0094-5. July 2013

TRINCA, A.J., GUERRA, M.R., GONÇALVES, R. (2015) Velocity variation in wood as a function of defects, In: International Nondestructive Testing and Evaluation of Wood Symposium, v.19. Rio de Janeiro, Brasil, p. 593 – 599

UNITED STATES DEPARTMENT OF AGRICULTURE (USDA), (2014) Wood and Timber Assessment Manual. Forest Products Laboratory, Madison, WI, 2ed. 94p

WANG, X.; ALLISON, R.B. (2008) Decay Detection in Red Oak Trees Using a Combination of Visual Inspection, Acoustic Testing, and Resistance Microdrilling. Arboriculture & Urban Forestry, 34(1), p. 1-4

Interference of Pith, Knots and Interpolation System in Ultrasonic Tomography Images

Stella Stopa Assis Palma

Master student, Laboratory of Nondestructive Testing – LabEND, School of Agricultural Engineering - FEAGRI - University of Campinas - UNICAMP, Brazil

E-mail: ssapalma@gmail.com

Raquel Gonçalves *

Professor, Laboratory of Nondestructive Testing – LabEND, School of Agricultural Engineering - FEAGRI - University of Campinas - UNICAMP, Brazil –

E-mail: raquel@agr.unicamp.br

Alex Julio Trinca

PhD, Post-doctoral researcher, Laboratory of Nondestructive Testing – LabEND, School of Agricultural Engineering - FEAGRI - University of Campinas - UNICAMP, Brazil

E-mail: ajtrinca@mx.com.br

Cândida Pereira da Costa

PhD, Post-doctoral researcher, Laboratory of Nondestructive Testing - LabEND, School of Agricultural Engineering - FEAGRI - University of Campinas - UNICAMP, Brazil

E-mail: candidapcosta@gmail.com

Guilherme A. Martins

Graduation student, Laboratory of Nondestructive Testing – LabEND, School of Agricultural Engineering - FEAGRI - University of Campinas - UNICAMP, Brazil

E-mail: guimartins93@gmail.com

* Corresponding author

Abstract.

The internal conditions of trees can be evaluated by ultrasonic tomography techniques using images generated by velocities ranges associated with colors. These velocities are affected by the stiffness and anatomical properties of the material. The aim of this research was to evaluate the interference caused by the presence of knots, different positions of the pith and by the interpolation system used in the software adopted to generate the tomography. For the test were used 44 disks of *Pinus* sp. The results indicate that, although the velocities in knots are higher than on clean wood, and in compression wood higher than opposite wood, in general, the interference on image is very low. In all images, there are zones of arrows forms caused by the interpolation system (Inverse distance square). However, none of the conditions caused severe interference in the image.

Keywords: ultrasonic tomography, nondestructive testing, tree inspection.

Introduction

In urban centers, the fall of tree is a great concern of the public administration, because they cause serious accidents and economic losses. Acoustic tomography applied on trees, with the objective of analyzing the presence of anomalies or deteriorations, is based on the generation of images produced using different colors representing velocity bands obtained in the material under inspection.

There are several types of flaws (hollows, cracks or zones attacked by fungi and termites) or singularities (knots, resin bags, displaced pith) that can occur in trees. All these defects and singularities affect, on less or greater degree, the anatomical structure of the material and, as a consequence, may affect the velocity of wave propagation.

Knots have an anatomical structure distinct of the normal wood, being more rigid. However, they cause interruption of the fibers (hardwoods) or tracheid (conifers), leading to a deviation of the grain (Furiati 1981). Considering that the velocity of acoustic waves in the wood is higher in the grain direction, because it is a path that facilitates the propagation, it is expected that deviations or slopes in this path cause a velocity reduction. In addition, the knots can reduce locally the mechanical properties of the wood, since they form discontinuities, besides being points of tension concentration. The reductions of the wood strength due to knots depend on its positions in the piece of the wood, as well as on its size and type, but this reduction may reach to 43% (Haygreen and Bower 1995).

Trinca et al (2013) isolated knots and perform ultrasonic tests. Their results show that the average velocity in the isolated element was 118% higher than the velocity in normal wood. Considering that the literature indicates that there is a reduction of wood properties (including acoustic properties) when knots are present in wood, it is inferred that this reduction is a function of grain deviations and local discontinuities. Therefore, the magnitude of the reduction of the velocity of propagation of ultrasound waves in pieces with knots will be a function of the relation between the volume of the knots and the healthy wood that surrounds it.

Puccini et al. (2002) estimated the influence of knots, pith and fiber deviation on the longitudinal velocity of ultrasound wave propagation parallel to the grain. The results indicated that the velocity variation was highly significant in the models involving, as independent variable, the presence of knots, pith and grain deviation. The multiple correlation analysis lead to the conclusion that the reduction of the ultrasonic wave velocity was most related to the presence of knots. The same conclusion was obtained by Sandoz (1989), which indicated the knot as the biggest influence on the wave propagation velocity parallel to the grain. In the case of woods with knots, the longitudinal velocity was 85% of the velocity in woods without the singularity (Puccini 2002).

The pith is a portion resulting from the vertical growth of the plant and has an anatomical structure differentiated from the wood trunk (Bodig and Jayne 1993). Puccini (2002) analyzed the influence of the presence of piths on the ultrasound wave propagation. He used specimens with different proportions of pith and concluded that the longitudinal velocity through pith was 89% of the velocity in wood. Trinca et al (2013) also analyzed isolated pith elements, having concluded that the velocity of ultrasound wave propagation through pith was 55% of the velocity in the wood.

Other aspects that have influence on tomography images is the interpolation system used to calculate velocities of wave propagation outside the measurement routes. It is necessary to assigned velocities for the entire section under inspection. According to Bucur (2010) there are several types of algorithms that can be used to form images using data obtained by the ultrasound method.

A relatively simple interpolator used in certain image generation programs is the inverse distance square (IDS) method. The IDS are an interpolator model that operates by multiplying the values of the observations by the inverse of their respective distances from a reference point. Results obtained by Trinca and Gonçalves (2014) using IDS interpolations to construct tomography images show interferences in the images produced. These interferences are displayed as "strings" with arrow shapes, and must be known in order to interpret the image appropriately. Interferences from the interpolation methods, recognized and assimilated by the researchers, do not produce errors of interpretation if there is a standard allowing differentiate interferences from effective results (Bucur 2010).

Objective

The objective of this paper was to characterize the interference of the displaced pith, knots and inverse distance square (IDS) method used as interpolation system in ultrasonic tomography images. This evaluation is important because trees generally have these singularities and it is necessary to know if such singularities have the potential to affect the identification of deteriorations.

Methodology

For the construction and evaluation of the tomography images, we used data from ultrasound tests collected in other researches of the group, using *Pinus* sp. Two discs (named a and b) were cut from each wood log. The discs were evaluated in detail and 44 were chosen so that sampling was composed of discs with approximately centered pith and apparently normal wood (Figure 1a), with approximately centered pith and presence of knots (Figure 1b) and with a displaced pith (Figure 1c). The discs with displaced wood have a zone of reaction wood, which can be recognized as the zone darker and with more distant growth rings (Figure 1c).

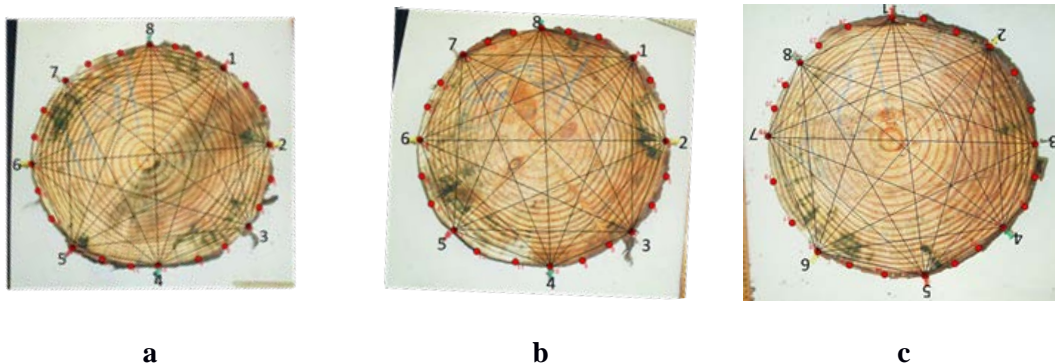


Figure 1—Example of disk with approximately centered pith and apparently normal wood (a), with approximately centered pith and knots (b) and with displaced pith (c)

During the tests, the contour coordinates of the disk (Figure 1, red points on the contour) and the coordinates of the measurement points were designed (Figure 1, points numbered from 1 to 8). In Figure 1 it is also possible to visualize the mesh that represents the measurement routes, called the diffraction mesh. For each point of measurement of the diffraction mesh, the propagation times of the ultrasound waves were determined.

The data of ultrasound measurement in the diffraction grid (Figure 1) generate 64 time values of wave propagation. Thus, the first step of the research was to organize the data in spreadsheets with a suitable format to be inserted in the software *Image Wood 2.0*.

In order to obtain the spreadsheet named "Contour", it was used a software developed by the research group. Using it, we could obtain the coordinates X, Y (Figure 1 - red dots) of the contour points. To obtain the spreadsheet named "Time", the data were organized such that the coordinates of the initial points (X_i , Y_i) and final points (X_f , Y_f) corresponded to the routes of measurements in the diffraction grid (Figure 1 - lines connecting the points numbered from 1 to 8), and the time of wave propagation obtained in the ultrasound test on each of these routes.

The time of wave propagation in each measurement route is obtained by keeping the transducer emitting the ultrasound wave at one point, while the transducer that picks up the ultrasound wave is positioned at the other 7 points of the grid, generating the measurement routes. This procedure is repeated until the transducer that emits the ultrasound signal passes through the 8 points of the grid. With this procedure there are repeated measurement routes, such as 1-2 and 2-1; 1-3 and 3-1, and so on. This procedure is important for the process, but the software does not allow two different time values for the same route. Thus, for these points, it was necessary to average the propagation times measured. For each line, one has the coordinates of the initial point (where is located the transducer that emits the signal) and of the final point (where is located the transducer that receives the ultrasound signal) and the average time of measurement obtained. This procedure was performed for measurements on 44 disks, thus generating 44 spreadsheets "Contour" and 44 spreadsheets "Time".

The image generated by the software uses colors associated with the velocities ranges adopted. The software computes the minimum (V_{MIN}) and maximum (V_{MAX}) velocities obtained on the disks, on the different measurement routes. The software allows automated adoption of velocity ranges associated with colors or manual one. The automatic form uses the difference between the maximum and minimum velocity and divides at equal intervals, depending on the number of bands that one wants. This procedure is simpler, but in the case of this project, which aims to analyze patterns of images, it would be not appropriate. Thus, it was adopted 6 velocity bands, always associated with a percentage of the maximum velocity obtained on the disk. This procedure was done to compare the images on the different disks. The standard established was:

1. V_{MIN} up to 20% of V_{MAX} : red
2. from 20% to 30% of V_{MAX} : pink
3. from 30% to 50% of V_{MAX} : yellow
4. from 50% to 70% of V_{MAX} : green
5. from 70% to 80% of V_{MAX} : orange
6. from 80% up to V_{MAX} : brown

In this way, it was possible to compare the images generated by the software with the photos taken from each disk, and to analyze the behavior of the wave velocity range in the different conditions adopted in this project. Regarding the interference of the interpolation system used by the software (IDS), the analysis was done to confirm the previous pattern already obtained by the research group. This pattern indicates that arrow-shaped images formed on the tomography represent interferences of the interpolation system and should be neglected in the interpretation of the images.

Results and Discussion

The wood is a heterogeneous material, constituted of different anatomical elements and with characteristics of growth influenced by environmental factors. If the velocity of wave propagation reflects the conditions of the material, it is not expected that the disk image will exhibit only one color, represented by a single velocity range. In addition, the wood is considered orthotropic, and the propagation velocities of the waves vary according to these directions. In the measurement routes (Figure 1) it can be verified that there are radial routes (passing through the centered pith) and tangential routes (tangential to the growth rings). From the theoretical bases of wave

propagation, it is known that the radial velocity is greater than the tangential ones, even if the wood is completely sound. This behavior reinforces that homogeneity of velocities is not expected in wood.

The *Pinus* sp. specie is very susceptible to fungi attack. Considering that the logs were removed immediately after cut, the moisture content of the disk was very high. The disks were kept in plastic bags for the test to be carried out in the saturated condition, but there was a proliferation of fungi, which in the visual analysis are stains, which do not cause damage in wood structure. After tests this condition was confirmed.

The evaluation of the disks was performed considering the three different initial conditions proposed for the research - normal condition (pith approximately centered and wood apparently in good condition); pith approximately centered and presence of knots and displaced pith with presence of compression wood. In addition, it was also evaluated the interference by the interpolation system (IDS).

Disks with pith approximately centered and without knots

The disks under normal conditions (pith approximately centered and wood visually normal, except for the fungus issue) generally presented most of the cross-sectional area in the brown and orange colors, indicating that velocity ranged from 70% to 100% of the maximum velocity (Figure 2). In some disks under normal conditions appeared the colors green (50% to 70% of the maximum velocity) and yellow (30 to 50% of the maximum velocity), generally associated with external routs (Figure 2). The external routes are tangential and with greater angle in relation to the radial one (lower velocities). The colors pink, yellow and green also appeared in arrow-shaped images (Figure 2), which were identified as interferences of the interpolation system(IDS).

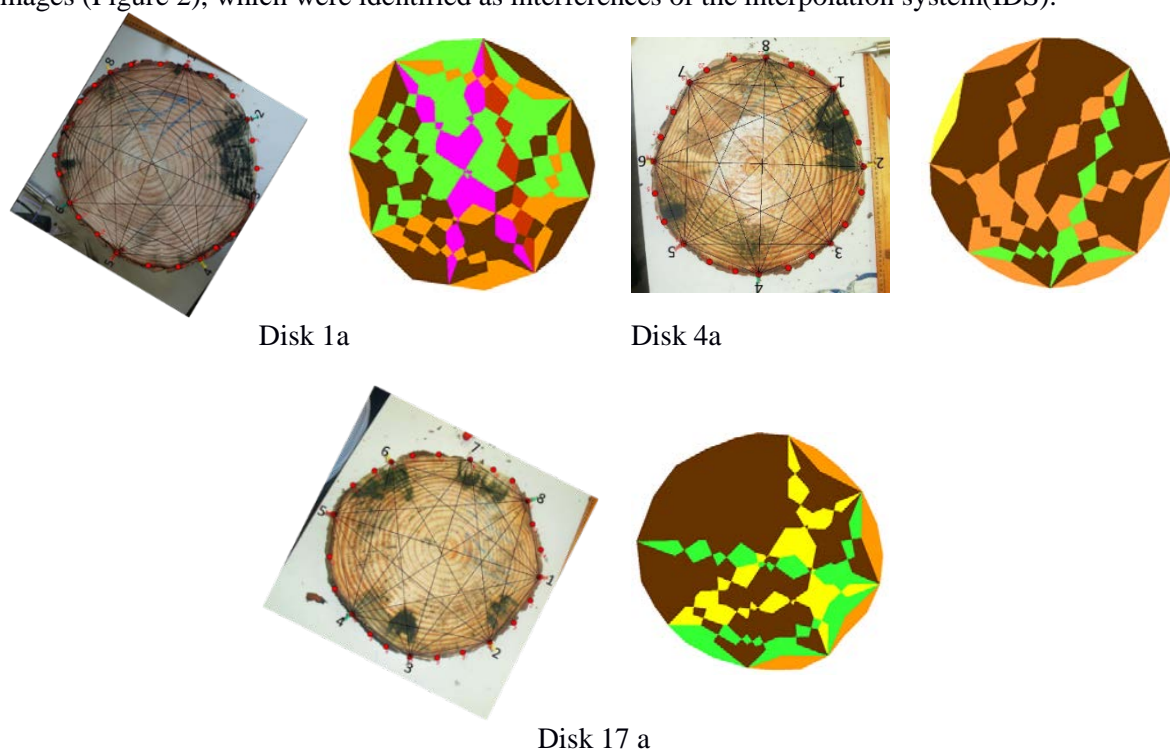


Figure 2—Samples of disks under normal conditions (pith centered and without knots) and their respective images of ultrasound tomography

Legend: V_{MIN} up to 20% of V_{MAX} : red; from 20% to 30% of V_{MAX} : pink; from 30% to 50% of V_{MAX} : yellow; from 50% to 70% of V_{MAX} : green; from 70% to 80% of V_{MAX} : orange; from 80% up to V_{MAX} : brown

Disks with pith approximately centered and with knots

In the disks with approximately centered pith and presence of knots we observed the occurrence of more regions in brown colors (Figure 3) than in disks with similar situation in terms of pith (approximately centered) but without knots (Figure 2). The disk 16b (Figure 3), for example, has 3 knots around the pith, but the image shows the inner part of the disk with high velocity (brown color). The same occurs on disk 22a (Figure 3), although with more interference (pink, green and yellow arrows) but with a large brown surface. The area formed by the crossing of arrow-shaped cords seems to coincide, in some cases, with the knot region (Disk 4b, 22a and 18b in Figure 3). The disks with knots present more images in cording shapes (theoretically interferences of the measurement system) than in the other analyzed situations. This behavior can be a consequence of the fact that the knot is a localized singularity and thus reflecting more the interferences.

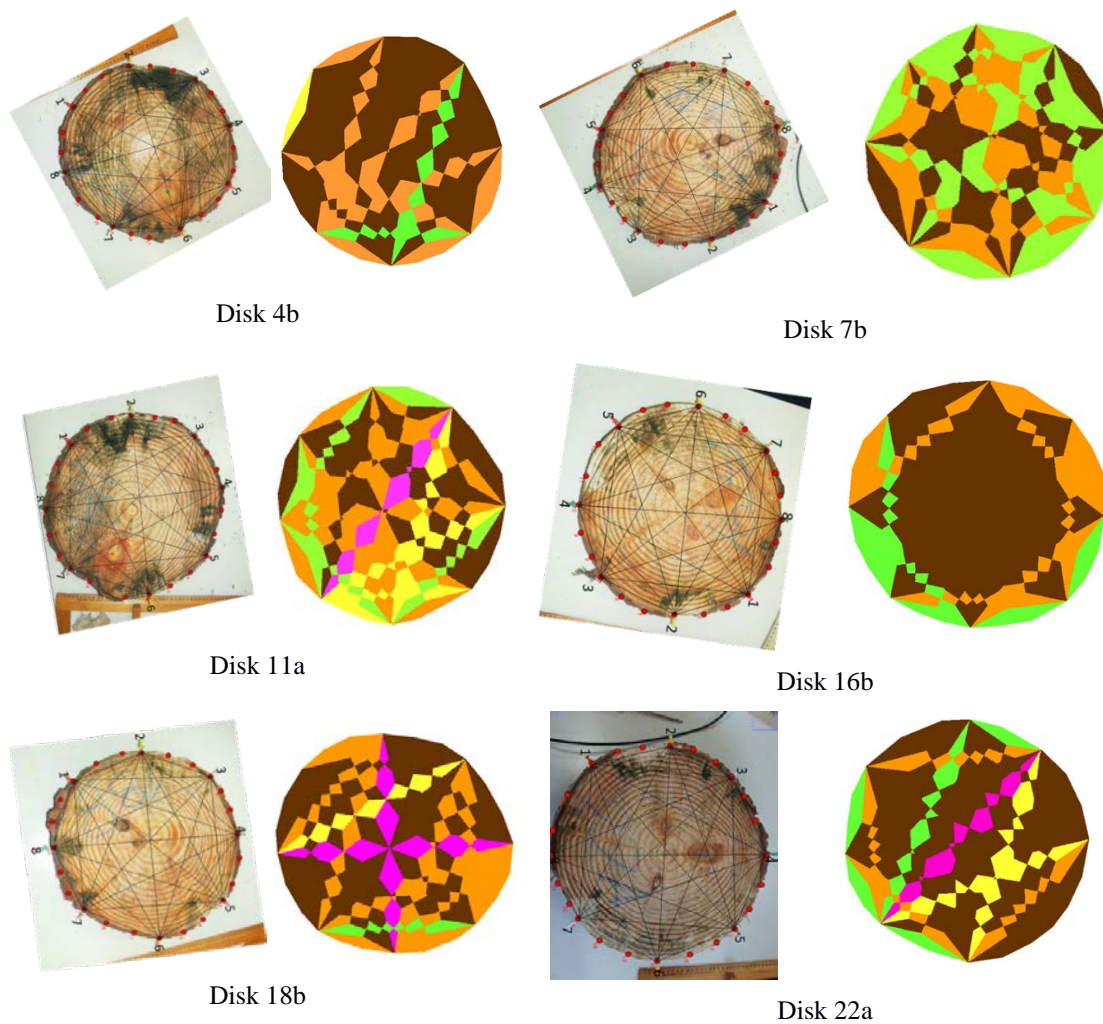


Figure 3—Samples of disks with approximately centered pith and their respective ultrasound tomography images

Legend: V_{MIN} up to 20% of V_{MAX} : red; from 20% to 30% of V_{MAX} : pink; from 30% to 50% of V_{MAX} : yellow; from 50% to 70% of V_{MAX} : green; from 70% to 80% of V_{MAX} : orange; from 80% up to V_{MAX} : brown

Disks with displaced pith

Disks with displaced pith have more green regions (velocity losses of 30% to 50%) than disks with pith approximately centered and without knots. It is also possible to verify fewer cords representing interferences of the interpolation system. The images of many disks seem not to be affected by the displaced pith, since they present in a large part of the section the colors brown and orange. The image of the disk 18a (Figure 4) presented lower overall velocities (green zones) and a well localized yellow region, more like a knot's effect pattern than reaction wood. More detailed evaluation made latter shows little differences between compression and opposite wood, with velocities little high in compression zone.

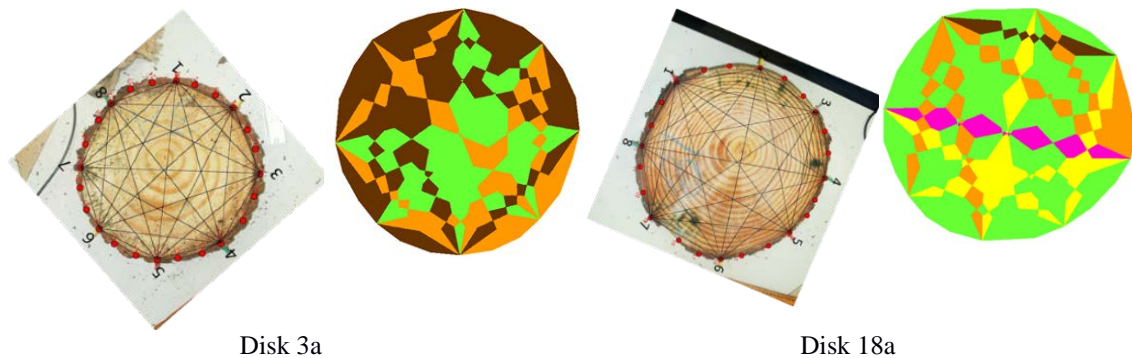


Figure 4— Samples of disks with approximately centered pith and their respective ultrasound tomography images

Legend: V_{MIN} up to 20% of V_{MAX} : red; from 20% to 30% of V_{MAX} : pink; from 30% to 50% of V_{MAX} : yellow; from 50% to 70% of V_{MAX} : green; from 70% to 80% of V_{MAX} : orange; from 80% up to V_{MAX} : brown

Conclusions

Considering the heterogeneous and orthotropic nature of the wood, velocity variations are normal, even in pieces with approximately centered pith and normal wood. For the pine wood studied in this research, it was observed that, in general, the images of the disks under normal conditions (pith approximately centered and without apparent knots) presented representative colors of velocities ranging from 70% to 100% of the maximum velocity (orange and brown).

In the disks with displaced pith, although many disks presented the same color level of disks with centered pith (orange and brown), color representative of velocities ranging from 50% to 70% of maximum velocity (green) occurred more frequently than in disks with centered pith. Velocities are little high in compression zone than in opposite zone.

The disks present velocities little higher in zones with presence of knots. The image pattern in these disks was the one that presented more arrow-shaped cords, which represents interference of the inverse distance square (IDS) method to interpolate velocities. It is possible that this pattern (cords in the form of arrows) is related to the peculiarity of the knot, which is a localized singularity.

Acknowledgments

The authors are grateful to FAPESP (Proc. 2015/05692-3) for the financial support and MEC/CAPES and CNPq for granting scholarships to the Master and undergraduate students.

References list

Bodig, J.; Jayne, B. A. Mechanics of wood and wood composites. 2ed Malabar, Flórida: Krieger, 1993.

Bucur, V. Acoustic emission activity induced by delamination and fracture of wood structure. *Delamination in Wood, Wood Products and Wood-Based Composites*. Springer, Netherlands, 2010.

Furiati, M. Classificação estrutural de peças de madeira. 1981. Tese de Doutorado. Dissertação.

Haygreen, J. G.; Bowyer, J. L. Forest products and wood science and introduction. 2. ed. Ames: Iowa State University Press. 500. 1989.

Puccini, C. T. Avaliação de aspectos de qualidade da madeira utilizando o ultra-som. 2002. 139f. 2002. Tese de Doutorado. Tese (Doutorado em Engenharia Agrícola)-Universidade Estadual de Campinas, Campinas.

Sandoz, J. L. Grading of construction timber by ultrasound. *Wood Science and Technology*, v. 23, n. 1, p. 95-108, 1989.

Trinca, A. J.; Gonçalves, R.; Agustino, D. M.; Van Dijk, R. Interference of Pith in Ultrasonic Tomography. In: 18th Symp. Nondestructive Testing of Wood, Vol. 1. Sept. Madison, USA. 2013.

Trinca, A. J.; Gonçalves, R.; Linhares, C. S. F. Ultrasonic Tomography in Detecting Knots. In: 18th Symp. Nondestructive Testing of Wood, Vol. 1. Sept. Madison, USA. 2013.

Trinca, A. J.; Gonçalves, R. Imagem da Estrutura Interna da Árvore Utilizando Ultrassom. Relatório Científico. Campinas – SP, 2014.



Session 5

**Condition Assessment
and Evaluation of
Wood Structures I**

Structural Condition Assessment of a Historic Tower

Robert J. Ross, Forest Products Laboratory, USDA Forest Service, Madison, WI, USA, rjross@fs.fed.us

Xiping Wang, Forest Products Laboratory, USDA Forest Service, Madison, WI, USA, xwang@fs.fed.us

C. Adam Senalik, Forest Products Laboratory, USDA Forest Service, Madison, WI, USA,
<mailto:christopherasenalik@fs.fed.us>

R. Bruce Allison, Allison Tree Care, Madison, WI, USA, rbruceallison@tds.net

Lujing Zhou, Graduate Research Assistant, Beijing Forestry University, Beijing, China,
lujingzhou6@gmail.com

Abstract

This paper presents the use of several nondestructive evaluation techniques in the structural condition assessment of a historic timber viewing tower. Visual, laser, mechanical probing, and acoustic techniques were used to evaluate the structural integrity of a timber viewing tower.

Keywords: timber, tower, visual, lasers, probing, acoustic, condition assessment

Density-based Evaluation Method of Degraded Timber for ISO13822

Nobuyoshi Yamaguchi

Department of Building Materials and Components, Building Research Institute, Tsukuba, Ibaraki-Pref., Japan, yamaguch@kenken.go.jp

Abstract

Timber structures degrade biologically, and need assessment for those preservation and renovation. ISO 13822 Annex E proposes the concept of ‘time-dependent reliability’, which needs quantitative evaluation based on mechanical properties of timbers. Density is significant property which correlated with mechanical properties of timber approximately. For the estimation of timber density, assessment method using screw withdrawals with short thread was developed. ‘Normalized Withdrawal Resistance (NWR)’ was proposed to estimate timber density from withdrawals. Relationship between NWR and density of timber was analyzed, and regression equations were obtained. ‘Benchmark Method’ and ‘Nominal Value Method’ to distinguish sound timber and degraded timber were proposed. In order to develop method to predict mechanical properties of degraded timber, relationship between weight loss and residual percentage of mechanical properties of degraded timbers are analyzed, and ‘density-based degradation model of timbers’ is proposed.

Keywords: screw, density, mechanical, properties, decay

Introduction

Timber structures from old heritages to modern CLT buildings were constructed. These existing old and new timber structures need assessment for the preservation of cultural values and economic efficiency. Standards and regulations for the assessment of existing structures have been prepared. Assessment of existing structures was described in ISO 13822 ‘Bases for design of structures’ (ISO. 2010). Annex E of the standard proposes concept of ‘Time-Dependent Reliability’ for the stochastic evaluation of degraded structures. Figure 1 indicates the concept of ‘time-dependent reliability’ of the Annex E. Degrading curve in Figure 1 represents that resistant performance of structures degrades with time. Initial safety factor

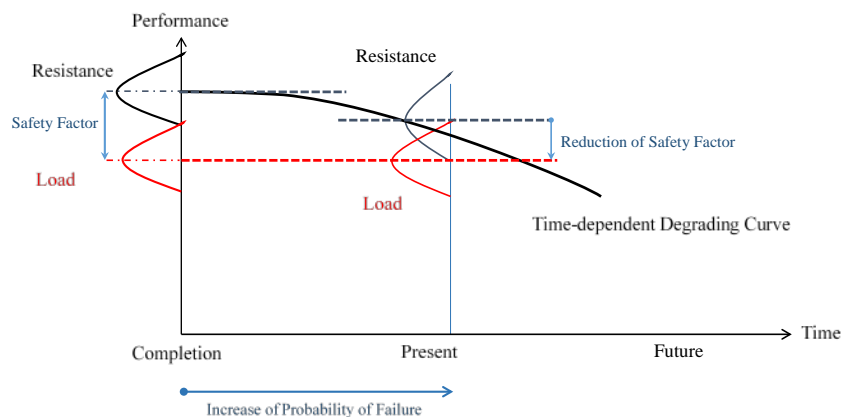


Figure 1 – ‘Time-Dependent Reliability’ of ISO 13822 Annex E

reduces gradually, and probability of structural failure increases with time. Degradation of existing timber structures is expected to be quantified and evaluated stochastically in ISO13822. Technical committee TC215-AST ‘Assessment of Structural Timber’ was established 2005 in RILEM to summarize in situ NDT/SDT methods (Kasal et al. 2011). COST Action FP1101 ‘Assessment, Reinforcement and Monitoring of Timber Structures’ was established to support the safety and serviceability of existing structures (Machado et al. 2015). Research committee ‘Assessment method of Existing Timber structures (AET)’ has been established 2015 in the Architectural Institute of Japan (AIJ) to prepare guidelines of the assessment of timber structures. Author had been developing assessment method using screw withdrawals from 2006 (Yamaguchi 2013), (Yamaguchi et al. 2015). Objective of this paper is to propose evaluation method which predicts mechanical properties of degraded timber using densities estimated by screw withdrawals or other methods.

Estimation of Timber Densities using Screw Withdrawals

Screw Withdrawals

Standards such as ‘Eurocode 5’ describe method to calculate withdrawal resistance of wood screws (CEN, 2008). These methods use timber density, diameter and penetration length of wood screws, which means withdrawal resistances are correlated with the timber densities. Screw withdrawal is a practical method for the estimation of timber densities.

Probe

Author developed probe manufactured from threaded-rod with short thread which meet with the standard (ISO261, 724). The probe has 3.87mm diameter and 12.87mm length thread, which was shown in Figure 2 and Photo 1. This probe needs pre-drilled holes with 3mm diameter bored in timber. The probe is screwed into the pre-drilled holes and the thread is set at the target depth.

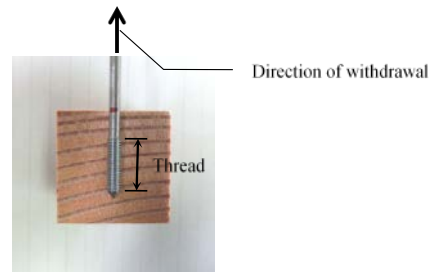


Figure 2 – Probe **Photo 1 – Thread Screwed into Timber**

Normalized Withdrawal Resistance

Withdrawal resistance is equivalent to shear strength on the cylindrical shear plane around the thread diameter of the probe shown in Figure 3. Normalized withdrawal resistance (NWR) is resistance normalized with cylindrical shear plane around the thread diameter, which is defined by Equation 1. Because NWR does not include the effect of dimensions of threads, NWR is correlated with timber density better than withdrawals.

$${}_N W_R = \frac{W_R}{R_t \times \pi \times l} \quad (1)$$

where ${}_N W_R$ is Normalized withdrawal resistance (N/mm²), W_R is Withdrawal resistance (N), R_t is Diameter of threads (peak to peak, mm), π is Circular constant, l is Length of probethread (mm).

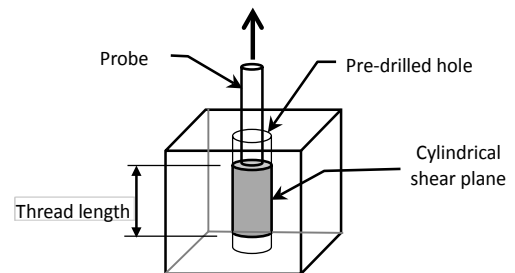


Figure 3 – Cylindrical Shear Plane around Thread Diameter

Density Estimation of Sound Timber from Screw Withdrawals

Relationships between density D and normalized withdrawal resistance ${}_N W_R$ (R or T directions) of three timber species of Sugi (*Cyptomeria Japonica*), Hinoki (*Chamaecyparis obtusa*) and Douglas-Fir (*Pseudotsuga menziesli*) are shown in Figure 4. A regression equation between D and ${}_N W_R$ are shown in Equation (2). Square of coefficients of correlation (R^2) between density D and ${}_N W_R$ was 0.923. (Yamaguchi, 2013)

$$D = 0.032 \times {}_N W_R + 0.1745 \quad (2)$$

where ${}_N W_R$ is Normalized withdrawal resistance (N/mm²) and D is Timber density (g/cm³).

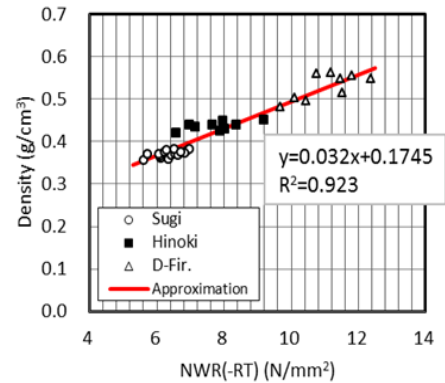


Figure 4 –Density Estimated from NWR

Evaluation of Timber using Screw Withdrawals in Situ

‘Benchmark Method’ to Distinguish Degraded Timber

Sound timber is used as benchmark that must be same timber species as object timber. The benchmark timber should have average properties of timber species of the object timber. In case the benchmark timber is not used, measurements are applied for sound area and degraded area of the object timber. ‘Benchmark Method’ using screw withdrawals compares withdrawal resistances of sound timber/area and degraded timber/area, and provide ratio of withdrawal resistances between sound and degraded timbers.

‘Nominal Value Method’ for In situ Assessment

Strength Class in EN338 describes mechanical properties and densities of ‘lumber’ (CEN. 2009), and ‘Industrial Wood Handbook Japan (IWHJ)’ also describes those of ‘clear wood’ (FFPRI. 2004). These values which are described in the EN338 and the Handbook could be regarded as nominal values.

Evaluation of Lumbers Classified in EN338 Strength Class

Nominal densities and probe withdrawals of lumbers classified in EN338 strength class (CEN. 2009) are

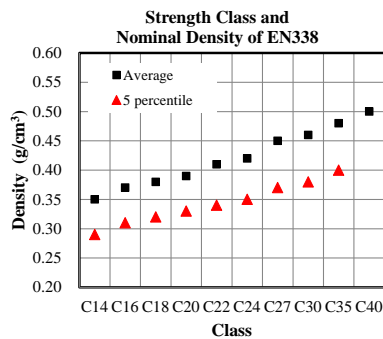


Figure 5 –Nominal Densities of Strength Classes of EN338

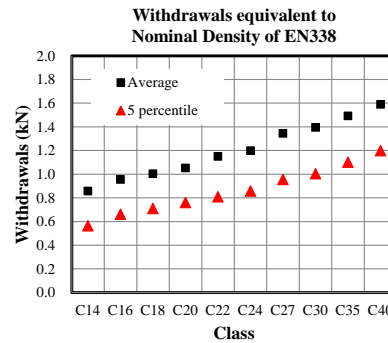


Figure 6 – Probe Withdrawals of Strength Classes equivalent to Nominal Densities of EN338

shown in Figure 5 and Figure 6, respectively. The probe withdrawals are equivalent to the nominal densities, which are calculated from Equation 1 and Equation 2. Square and triangle marks in Figure 5 and Figure 6 indicate relationship between *Average* and *5 percentile* nominal densities and equivalent probe withdrawals of those. These probe withdrawals W_R are used in situ for the density-based assessment of lumbers classified by EN338. ‘*Average*’ or ‘*5 percentile*’ marks plotted in Figure 6 could be used as criteria to distinguish degradation of timber in situ. (Yamaguchi. 2015)

Evaluation of Clear Wood listed in Industrial Wood Handbook Japan

Nominal densities (FFPRI. 2004) and calculated probe withdrawals of clear wood are indicated in Figure 7 and Figure 8. The probe withdrawals are equivalent to the nominal densities, which are calculated using Equation 1 and Equation 2. Diamond, square and triangle marks indicate nominal *Upper*, *Average* and *Lower* densities of the clear wood in Figure 7, and *Upper*, *Average* and *Lower* probe withdrawals of the clear wood respectively in Figure 8. ‘*Ave.*’ or ‘*Lower*’ marks plotted in Figure 8 could be used as criteria to distinguish degradation of timber in situ. (Yamaguchi. 2015)

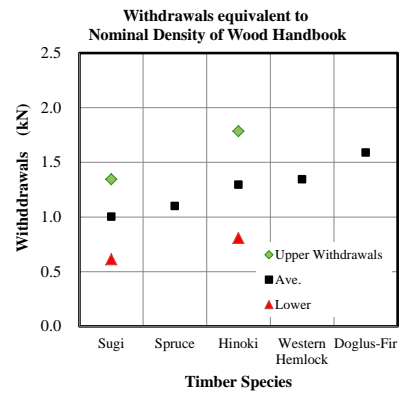
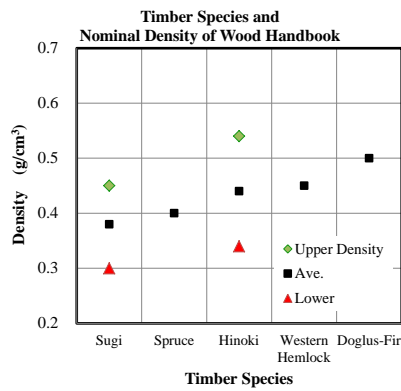


Figure 7– Nominal Densities of Timber Species **Figure 8** – Probe Withdrawals Equivalent to Nominal Densities

Relationship between Mechanical Properties and Densities

Mechanical Properties of EN338 Strength Classes

Mechanical properties and densities of EN338 strength classes are listed in EN338 (CEN. 2009). These mechanical properties and densities could be regarded as nominal values of lumber and shown in Figure 9, Figure 10, Figure 11 and Figure 12. These mechanical properties are correlated with those densities. Regression equations of those are summarized in Equation 3, Equation 4, Equation 5 and Equation 6.

$$E = 43.797 \times D - 7.9386 \quad (3)$$

$$f_b = 166.47 \times D - 45.486 \quad (4)$$

$$f_c = 66.385 \times D - 7.2481 \quad (5)$$

$$f_s = 13.668 \times D - 3.1944 \quad (6)$$

Where E kN/mm² is MOE, f_b N/mm² is bending strength, f_c N/mm² is compression strength, f_s N/mm² is shear strength and D g/cm³ is density of lumber.

Mechanical Properties of Clear Wood listed in Industrial Wood Handbook Japan

Mechanical properties and densities of clear wood are listed in IWHJ (FFPRI. 2004). These properties and densities are average values and regarded as nominal values, which shown in Figure 9, Figure 10,

Figure 11 and Figure 12. These properties are correlated with those densities. Regression equations of these are summarized in Equation 7, Equation 8, Equation 9 and Equation 10.

$$E' = 25.329 \times D - 2.1464 \quad (7)$$

$$f_b' = 172.7 \times D - 3.7253 \quad (8)$$

$$f_c' = 98.684 \times D - 5.1645 \quad (9)$$

$$f_s' = 21.711 \times D - 2.2862 \quad (10)$$

where E' kN/mm² is MOE, f_b' N/mm² is bending strength, f_c' N/mm² is compression strength, f_s' N/mm² is shear strength and D g/cm³ is density of 'clear wood'

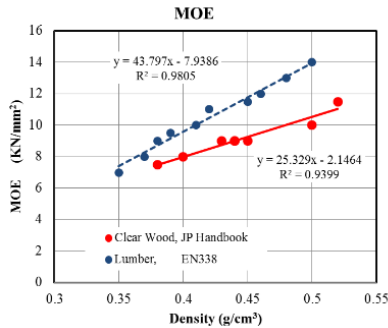


Figure 9 – MOE and Density

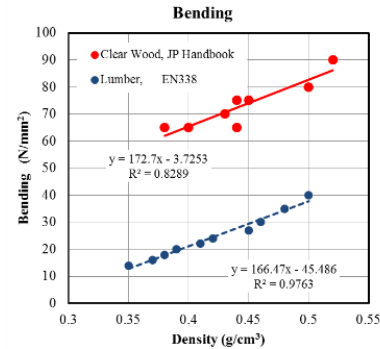


Figure 10 – Bending and Density

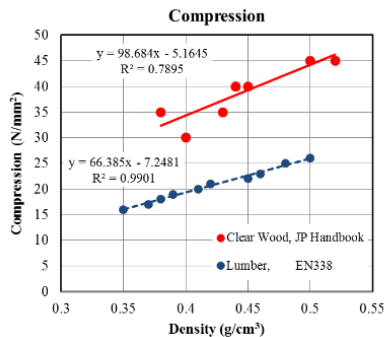


Figure 11 – Compression and Density

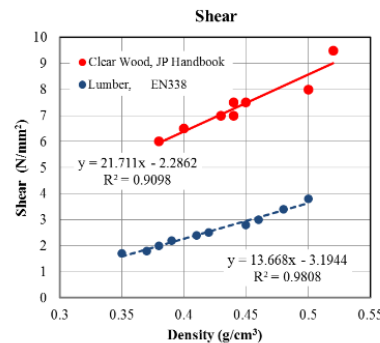


Figure 12 – Shear and Density

Prediction of Mechanical Properties of Sound Timber

Prediction of Mechanical Properties of Sound Timber using Estimated Density

MOE, bending, compression and shear strengths of sound 'lumber' are predicted by Equation 3, Equation 4, Equation 5 and Equation 6 using densities D . MOE, bending, compression and shear strengths of sound 'clear wood' are predicted by Equation 7, Equation 8, Equation 9 and Equation 10 using densities D . These densities are estimated from screw withdrawals, etc.

Prediction of Mechanical Properties of Degraded Timber

Weight loss and Residual Mechanical Properties of Timber Decayed by Fungi

Mechanical properties of degraded timber had been studied. Stalnaker summarized information on resistance to decay of timbers, and proposed approximate residual percentage of mechanical properties of decayed softwood in early stage of decay 5 to 10% weight loss (Stalnaker et al. 1997). Mizumoto composed deterioration test of Japanese red pine (*Pinus densiflora*) sap wood decayed by *Gloeophyllum*

trabeum which causes brown-rot fungi, and reported residual mechanical properties during deterioration (Mizumoto 1966). Residual bending strengths of Sugi (*Cryptomeria japonica*) decayed by brown-rot and white-rot fungi were reported by Imamura (Imamura et al. 1987). Table 1 summarizes residual mechanical properties in early stage of decayed timber proposed and reported by them. Bending, compression and shear strengths listed in Table 1 are parallel to the grain. Table 1 shows that bending is mostly affected by decay and brown-rot fungi affect for the deterioration of timber more than white-rot fungi. Figure 13 shows degradation curves of bending strengths reported by Mizumoto and Imamura. Approximations are applied for the results by Imamura. Degradation curve reported by Mizumoto is between the degradation curves of brown-rot and white-rot reported by Imamura. Deterioration by fungi is affected by many factors related to materials and environmental conditions. Much additional research is expected. These weight losses are replaced to density reductions assuming those timber volumes are constant during deterioration.

Table 1 – Weight Loss and Residual Mechanical Properties of Timber Decayed by Fungi

	Imamura White-rot	Mizumoto Brown-rot	Stalnaker	Imamura Brown-rot
Weight Loss	10%	10%	5-10%	10%
Bending	65%	50%	30%	25%
Compression		50%	55%	
Shear		80%	80%	

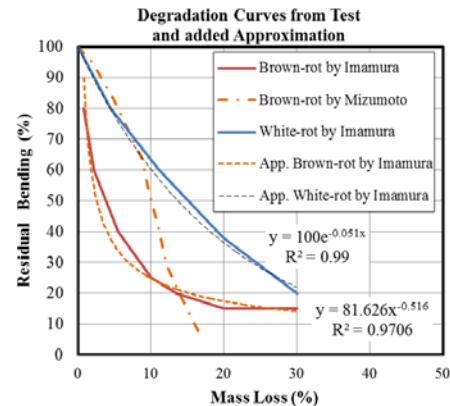


Figure 13 – Residual Percentage of Bending Strength Decayed by Fungi (Mizumoto 1966, Imamura et al. 1987)

Prediction of Mechanical Properties of Degraded Timber

Mechanical Properties of Sound and Degraded Timber

Density-based degradation model of timbers with MP-S and MP-D lines are proposed. MP-S line reveals relationship between mechanical properties and density of pre-degrade sound timber/point, which is indicated by *dotted line* in Figure 14. MP-D line reveals relationship between mechanical properties and

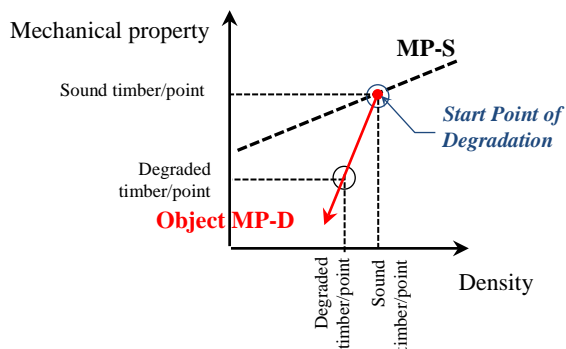


Figure 14 – Density-based Degradation Model of Timbers

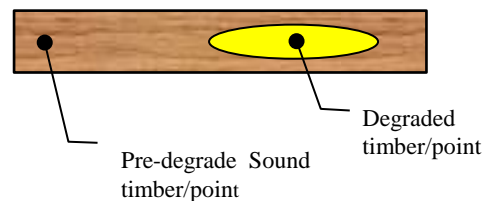


Figure 15 – Sound and Degraded Timber/Point allocated in Object Timber

degraded timber/point, which is indicated by *solid line* in Figure 14. There are two types of mechanical properties of ‘lumber’ or ‘clear wood’, and one of those must be chosen for the prediction. MP-S line is drawn by one of Equation 3, 4, 5 and 6 in case of ‘lumber’, and also that is drawn by one of Equation 7, 8, 9 and 10 in case of ‘clear wood’. MP-D line correlated with degraded timber is drawn using residual

percentages of properties and weight-loss obtained from experimental results or proposals such as Table 1. Because timber always starts to degrade from sound, MP-D line is drawn from a point on MP-S line downwardly and the point is given the name of ‘*Start point of degradation*’. The point is correlated with the density of pre-degrade sound timber. Figure 15 shows the measuring points of densities in pre-degrade sound and degraded timber/area allocated on object timber. The pre-degrade sound or degraded points must be chosen in pre-degrade sound or degraded areas on the object timber. Object MP-D line is drawn from the ‘*Start point of degradation*’ correlated with the density of pre-degrade sound timber/point in the object timber. The mechanical properties at sound timber/point are obtained from the MP-S line using density at sound timber/point. The mechanical properties of degraded timber/point are obtained from the Object MP-D line using the two densities at pre-degrade sound and degraded timber/point.

Prediction of Mechanical Properties using Density-based Degradation Model

Bending MP-S line of ‘clear wood’ calculated by Equation 8 is drawn using *dotted-line* in Figure 16, for example. Bending MP-D lines are drawn using *solid-lines* in Figure 16. Bending MP-D lines are drawn based on residual percentage of ‘bending strength’ proposed by Stalnaker shown in Table 1. Sample MP-D lines are drawn as measures from ‘*Start point of degradation*’ relating to the sound timber densities of 0.38, 0.4, 0.44, 0.48 and 0.52. ‘*Object MP-D line*’ are required to be added parallel to the sample MP-D lines with estimated density of pre-degrade sound and decayed timber/point of the object. Residual mechanical property of the degraded object timber is obtained using the ‘*Object MP-D line*’. In Figure 16, two declining *thin dotted curves* are plotted beside the sample MP-D lines for comparison, the curves reveal degradation of timber by brown-rot and white-rot fungi by Imamura shown in Figure 13. MP-D lines proposed by Stalnaker are allocated between the two *thin dotted curves* based on the experiments by Imamura.

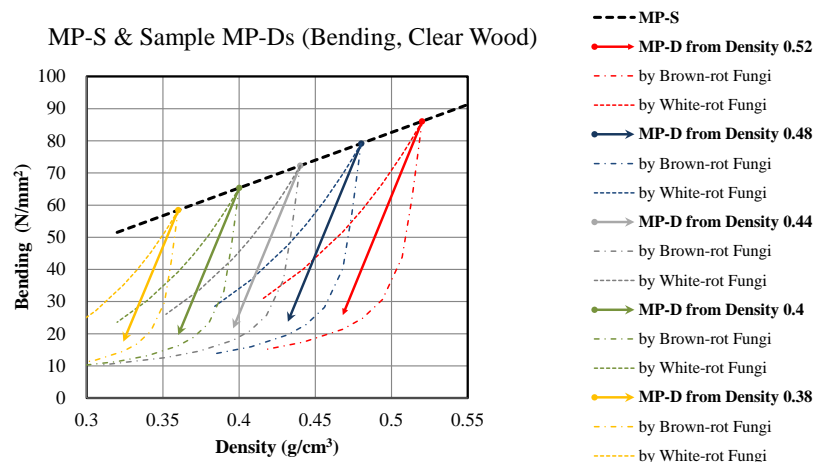


Figure 16 – Prediction of Bending using Density-based Degradation Model (*Clear Wood*)

Procedures to Predict Properties of Degraded Timber

- 1) Densities of sound timber/point and degraded timber/point of the object are estimated by screw withdrawals or other.
- 2) Choose between two types of timber properties ‘clear wood’ or ‘lumber’ for the prediction of mechanical properties.
- 3) Choose type of mechanical properties from MOE, bending, compression and shear strengths.
- 4) Draw MP-S line using Equation 3 to 10.
- 5) Plot a ‘*Start point of degradation*’ on the MP-S line, which is correspond to the density of pre-degrade sound timber/point of the object.
- 6) Draw ‘*Object MP-D*’ line which are drawn from the ‘*Start point of degradation*’ downwardly. The object MP-D line should be parallel to the sample MP-D lines. These samples could use residual percentage proposed by Stalnaker or other.
- 7) Find mechanical properties on the ‘*object MP-D line*’ correspond to the estimated density of the decayed object timber/point.

Conclusions

For the assessment of existing timber structures, probes for the screw withdrawals, 'Normalized Withdrawal Resistance' for the estimation of timber density, 'Benchmark Method' and 'Nominal Value Method' for the evaluation of timber degradation were proposed. Equations to predict mechanical properties of sound 'clear wood' and 'lumber' were proposed. The MP-D was proposed to predict mechanical properties of degraded timber, and these procedures were summarized. For more reliable predictions of degraded timber, additional research is expected.

Acknowledgments

This research was supported by Building Research Institute Japan. Contributions of Masao Nakajima (Kanto Gakuin Univ.) and members of AET-Committee AIJ are greatly appreciated. Gratitude is addressed to Hirofumi Sakuma (CBL) and Bohumil Kasal, Jose Sapporiti Machardo, Thomas Tannert, Mariapaola Riggio (RILEM TC 215-AST, COST Action FP1101).

References

- CEN. 2008. *Axially loaded screws*. Eurocode 5. EN1995-1-1:2004+A1:2008
- CEN. 2009. *Structural timber – Streng Classes*, EN338
- FFPRI. 2004, *Industrial Wood Handbook Japan*, Forest and Forest Product Research Institute Japan, Maruzen
- Imamura Y., Takahashi M. *Report of the Grant-in-Aid for Scientific Research(KAKENHI)* by Ministry of Education Japan, 75/1987
- ISO. 2010. *Bases for design of structures – Assessment of existing structures*, ISO 13822 Second edition. International Standard Organization, 2010-08-01
- Kasal B.; Tannert T. 2011. *In Situ Assessment of Structural Timber*, RILEM State of the Art Reports Volume 7, Springer
- Machado J. S.; Riggio M.; Descamp T. 2015. *Combined Use of NDT/SDT Methods for the Assessment of Structural Timber Members*, State of the art report COST Action FP1101, UMONS
- Mizumoto S. 1966, *The Effect of Decay caused by Gloeophyllum trabeum on the Strength Properties of Japanese Red Pine Sap-wood*, Mokuzai Gakkaishi (Journal of the Japan Wood Research Society) 48(1), 7-11, 1966-01-25
- Stalnaker J. J.; Harris E. C. 1997. *Structural Design in Wood*, Second Edition, Kluwer Academic publishers
- Yamaguchi N. 2013. *Distribution of Shear Strengths in Wood Estimated from Normalized Withdrawal Resistances of Probes*, Proceedings of the 18th International Nondestructive Testing and Evaluation of Wood Symposium, Madison, USA
- Yamaguchi N.; Nakao M. 2015. *In-situ Assessment Method for Timbers based on Shear Strengths Predicted with Screw Withdrawals*. Proceedings of 3rd International Conference on Structural Health Assessment of Timber Structures. Wroclaw, Poland

Procedural Considerations for the Assessment of Mechanical Properties in Existing Timber Structures

Francisco Arriaga

Department of Forest and Environmental Engineering and Management, MONTES (School of Forest Engineering and Natural Environment), Universidad Politécnica de Madrid, Spain, ORCID: 0000-0001-5535-0786, francisco.arriaga@upm.es

Guillermo Íñiguez-González

Department of Forest and Environmental Engineering and Management, MONTES (School of Forest Engineering and Natural Environment), Universidad Politécnica de Madrid, Spain, ORCID: 0000-0003-2917-842X, guillermo.iniguez@upm.es

Daniel F. Llana

Department of Forest and Environmental Engineering and Management, MONTES (School of Forest Engineering and Natural Environment), Universidad Politécnica de Madrid, Spain, ORCID: 0000-0001-7758-9456, danielllana@gmail.com

Ignacio Bobadilla

Department of Forest and Environmental Engineering and Management, MONTES (School of Forest Engineering and Natural Environment), Universidad Politécnica de Madrid, Spain, ORCID: 0000-0002-4627-3130, i.bobadilla@upm.es

Miguel Esteban

Department of Forest and Environmental Engineering and Management, MONTES (School of Forest Engineering and Natural Environment), Universidad Politécnica de Madrid, Spain, ORCID: 0000-0003-3364-9044, miguel.esteban@upm.es

Abstract

This document presents the preliminary ideas of a draft procedure for the assessment of existing timber structures. The estimation of the mechanical properties in existing timber structures is usually based on visual stress grading and non-destructive techniques. Both techniques have some important peculiarities respecting their application to the grading of new sawn timber. A procedure should be defined for the different tasks involved in inspection and evaluation. The irregular cross-section geometry in old timber structures requires some specific considerations. Visual grading is very limited by problems with access, and non-destructive techniques help to complete the information. The most frequent nondestructive parameters are estimation of density and determination of wave transmission velocity. Different options and questions are proposed to create a more consistent and practical evaluation procedure.

Keywords: assessment, dynamic modulus of elasticity, existing timber structures, mechanical properties, non-destructive methods

Introduction

Since the beginning of this century there has been increasing interest in the rehabilitation and conservation of existing buildings. While these are mainly of historical and artistic

importance, general buildings are also involved. Several relevant documents focus on timber structures. The 12th general assembly in Mexico in 1999 of the International Council of Monuments and Sites (ICOMOS) adopted the worldwide recognized document “Principles for the preservation of historic timber structures” (ICOMOS, 1999). This is a short document with fifteen items covering inspection, monitoring-maintenance, intervention, repair- replacement, historic forests and contemporary technologies. Some of the specialists involved in ICOMOS have published papers on the conservation of timber structures. One example is the Norwegian ecological conservation approach for historic timber structures (Larsen and Marstein 2000). More recently, an interesting Italian view was based on an extensive compilation and study of real cases of timber structure failures (Tampone, 2016).

The work of the COST Action IE0601 “Wood Science for Conservation of Cultural Heritage” (WoodCultHer) must also be mentioned. This was developed in 2007-2008 within the framework of the European Cooperation in Science and Technology (COST Actions). The Task Group “Assessment of Timber Structures” generated a document titled “Guidelines for On-Site Assessment of Historic Timber Structures” and gave rise to an interesting publication with the same title (Cruz et al., 2010). It was drafted as a pre-normative document and is currently being developed within the European Committee for Standardization, Technical Committee 346 “Conservation of Cultural Heritage” (CEN/TC 346) by its Working Group 10 “Historic Timber Structures”. This project for a European Standard will be adopted in 2018.

The conservation of timber structures requires verification of their safety, and this involves a survey, estimation of mechanical properties and verification of their load capacity. This paper covers the first phase of the complete process of timber structure assessment (inspection).

Data collection at inspection

Definition of homogeneous batches and species identification

The preliminary inspection of structures should centre on checking which structural types and geometrical characteristics (cross-section size and length) and species of wood are present, as well as quality characteristics and date of construction. Each different type (batches) should be considered as independent, giving rise to specific estimation of their mechanical properties.

It is in principle necessary to identify the species used in a structure to determine its mechanical properties. In Spain only a few species can generally be found in old timber structures. For coniferous species: Scots pine (*Pinus sylvestris* L.), lario pine (*Pinus nigra* ssp. *salzmannii* (Dunal) Franco) and maritime pine (*Pinus pinaster* Ait. ssp. *mesogeensis* Fieschi&Gaussen) are the main home-grown species. It must be noted that the wood of Scots pine and lario pine cannot be differentiated, even by microscopic sample analysis. Furthermore, in some buildings it is possible to find a mix of these coniferous species (maritime and Scots or lario pine). Less frequently, Southern yellow pine (*Pinus echinata* Mill, *elliottii* Engelm, *palustris* Mill., *taeda* L.) can be found in some buildings, mainly in the North of Spain. The hardwood species used are: European oak (*Quercus robur* L., *Quercus petraea* (Matt.) Liebl.) and sweet chestnut (*Castanea sativa* Mill.) in the North of Spain, together with poplar (*Populus alba* L., *Populus nigra* L.).

Geometry

The load-carrying capacity of a timber piece depends on the mechanical properties of the material (strength and modulus of elasticity) and on its cross-section dimensions. Nowadays, the cross-section of timber pieces in a homogenous batch in the structure has a regular shape and little dimensional variation, so it can be considered to be practically constant. However, the cross-section of timber pieces in older structures is not generally a regular rectangular shape. As a consequence of this, timber pieces vary widely in cross-section in the same type of members (joists, rafters, etc.) and even along the same member. It is therefore not a simple task to measure cross-section dimensions, and the measurement method will affect the final results.

Measurement methods: the most common practical method for measuring the cross-section dimensions of a piece is by using a tape measure attached to the face or edge of the cross-section and trying, in the case of waney, to ensure that the measurement corresponds to the whole cross-section, Figure 1 (direct method). Another option, which seems more regular in procedure, is to use a caliper to measure the distance between two parallel faces, attaching one of the jaws of the apparatus on the flattest face, figure 1 (caliper method) and the other parallel jaw where it makes contact with the cross-section. In the example of figure 1 it is observed that the measurements taken by both methods vary by ± 5 mm, and this value would increase if the section were more irregular. This small variation in the dimensions results, for this example, in a 6% variation of the cross-section area, 12% of the section modulus and 18% of the moment of inertia. The effect of this on bearing capacity has a certain relevance and is not negligible.

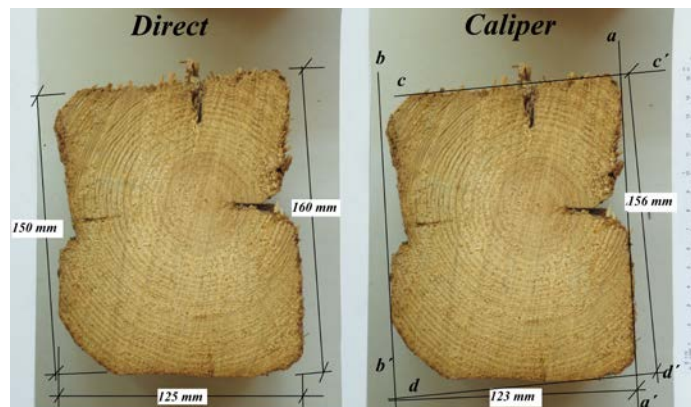


Figure 1—Different measurement methods: direct (left) and caliper (right).

The effect of notches on faces: the cross-sections of certain timber joists in existing structures have face notches to offer better support for the filling material between joists. In practice, the dimensions of cross-sections are measured as the circumscribed rectangle. The properties of the cross-section (area, moment of inertia and section modulus) obtained are therefore slightly larger than the actual ones. As an example, Figure 2 shows a cross-section with typical notched faces where the differences between moment of inertia and the section modulus of the rectangle and the actual cross-section are less than 3%. The repercussion on load bearing capacity in this case is negligible.

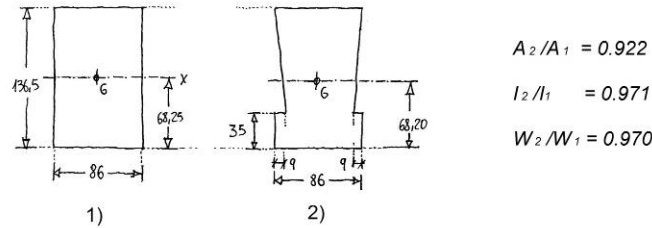


Figure 2—Face notch effect on cross-section properties (A: cross-section area, I: moment of inertia and W: section modulus; 1: rectangle and 2: notched cross-section).

Cross-section variability: a large variation in the dimensions of the same batch is often found. Table 1 shows the geometrical properties of several batches of recent timber from mechanical characterization tests of large cross-section pieces (Íñiguez 2007). The cross-section dimension variation coefficients are less than 2% and for the moment of inertia they stand at just over 3%. However, the same table shows the geometrical properties of four batches of timber pieces from existing and old buildings (approximately 1776 -1900) in which the cross-section dimensions variation coefficient reaches mean values from approximately 6% to 9%. This coefficient rises to 16% for the section modulus and to 21% for the moment of inertia.

Table 1. Coefficients of variation of cross-section dimensions and geometrical properties of new sawn timber pieces and in solid timber pieces from old structures.

Species	Date	N	Average Cross-section b x h (mm)	CoV (%)				
				b	h	A	W	I
1		80	149x199	0.5	0.5	0.9	1.3	1.8
		75	147x246	1	0.7	1.3	1.8	2.3
2	2007	60	142x190	1.9	1.3	2.3	3.2	4.4
		60	191x246	2.2	1.2	2.3	3.0	3.9
3		60	144x196	1.2	0.9	1.4	2.2	3.1
		60	195x247	1.1	0.9	1.7	2.4	3.2
Average values				1.3	0.9	1.7	2.3	3.1
2-3	1900	14	118x161	9.0	6.0	13.0	17.9	22.9
2-3-4	1861	20	126x181	5.4	4.7	6.9	10.5	14.8
2-3	1780	28	142x197	8.1	7.6	13.0	19.6	26.6
2-3	1776	63	140x175	8.9	5.3	11.3	15.2	19.7
Average values				7.9	5.9	11.1	15.8	21.0

Species: 1 Radiata pine, 2 Scots pine, 3 laricio pine, 4 maritime pine

Date: approx. year of the timber or the building in case of existing structure

N: numb. pieces; b: width, h: depth; A: cross-sectional area; W: section modulus; I: moment of inertia

Assignment of the cross-section size in a homogeneous batch: as was mentioned above, even in a homogeneous batch (i.e. one with similar geometric characteristics and material quality) there will be variations in dimensions and quality between the pieces. Structural systems with members repeated at short intervals (i.e. joists and rafters) and supporting the load through other constructive elements with enough capacity to redistribute the load according to their stiffness, have a better structural behavior. This effect is the load sharing effect considered by Eurocode 5 (EN 1995-1-1 2004), and may justify the consideration of a common average section size for the whole system. A proposal for the assignment of the section size of a batch is outlined below. The cross-section size of a piece (width and depth) should be taken as the mean value from at least two cross-sections of the central third of the length of the piece. The cross-section size for the batch will be taken as the mean value of the cross-section pieces.

Visual strength grading

The visual strength grading standards of timber are intended for applications to pieces produced in a sawmill, in order to classify them into groups with different mechanical properties. In this process a small part of the material is always rejected for structural use because it does not meet the lower grade requirements. When these types of grading procedures are applied to old timber pieces in existing structures some drawbacks arise. Firstly, the most frequent result is that pieces in the same batch are assigned to different grades defined by the standard, including a group of rejected pieces. Normally, if the complete grading standard criteria are applied, the percentage rejected will be too high. However, it is neither possible to discard rejected pieces in an existing structure, and nor would this make any sense. Secondly, in existing structures it is not always possible to access all four faces of a piece, so that visual classification is incomplete.

Furthermore, some of the singularities of timber pieces (defects) that are considered in timber grading have little relevance in the case of existing structures. Fissures and cracks, which are more present in large cross-section pieces, do not imply a significant loss of load carrying capacity (Esteban et al. 2010). Similarly, the effect of waness, which are also very frequent in ancient and large cross-section pieces, is generally considered to be only a loss of section area, without reducing strength (Arriaga et al. 2007, Esteban et al. 2010). The most relevant defects in classification will therefore be knots and the slope of grain. Some experimental studies propose grading based solely on these two parameters (Arriaga et al., 2005). The Italian grading standard UNI 11119:2004 is probably the only one that specifically includes a procedure for timber grading in existing structures. It proposes a grading system with three grades (I, II and III) and its main grading parameters are knot, fiber deviation, wane and fissure. The effect of waness is limited to loss of piece cross-section area, and fissures are permitted provided they do not pass completely through the piece.

To summarize, although visual timber grading in existing structures is a procedure that can help estimate their mechanical properties, it needs to take into account nuances such as those proposed in the standard discussed above.

Moisture content

The measurement of timber moisture content in the inspection of a structure has two main objectives. The first is to locate areas with particularly high moisture content, since the presence of fungal attack or some insect attacks, such as subterranean termite infestation, are closely related to high moisture content. The second objective is to adjust the data registered by nondestructive methods in temporary abnormal moisture content situations, in order to correct it to dry (or standard) conditions.

If nondestructive techniques are used to grade new timber, the estimated mechanical properties must be referred to standard hydrothermal conditions. These conditions correspond to $65\pm 5\%$ air relative humidity and $20\pm 2^\circ\text{C}$ temperature according to Eurocode 5 (EN 1995-1-1:2004) for timber structural design, and they correspond approximately to an equilibrium moisture content of 12% in coniferous wood. However, when estimating the mechanical properties of timber in existing structures and moisture content is stabilized at the average equilibrium moisture content conditions, it is not necessary to correct to 12%. The estimated mechanical properties will therefore be directly applicable to service conditions.

Nondestructive measurements for density estimation

Density is a physical property strongly related to mechanical properties, and it is defined as the relationship between mass and volume. Three different methods have been used to determine the density in the nondestructive testing research field: a) Small clear specimens in the form of rectangular prisms having a cross-section of not less than 20 mm by 20 mm and a minimum length

along the grain of 20 mm, according to standard ISO 13061-2:2014. This method is generally used to determine the density of the material in particular areas of the wooden piece or tree, as density varies depending on position in the tree (juvenile or mature wood, sapwood or heartwood, etc.). It is very precise but also varies widely in a single piece of timber; b) Local density of structural timber, with a specimen obtained as a slice of the full cross-section of the piece, free from knots and resin pockets, according to standard EN 408; and c) overall density obtained as the ratio between the mass and volume of the whole piece. This is used for structural timber when it is not possible to obtain a slice specimen as this would imply the destruction of the piece.

Table 2 shows the density values of several batches of large cross-section sawn timber of four coniferous species (*Pinus sylvestris* L. – Scots pine, *Pinus nigra* A. – Laricio pine, *Pinus pinaster* A. – Maritime pine, and *Pinus radiata* D. – Radiata pine) of several sizes. The global density is 2.5% greater than average local density, and the coefficient of variation for the overall (global) density is slightly lower than it is for average local density.

Table 2. Densities of four Spanish-sourced coniferous species referred to 12% moisture content in structural large cross-section pieces and small clear specimens.

Species	Size bxh (mm) - L (m)	Number pieces	Global density, ρ_G mean-CoV (kg/m ³ - %)	Local density, ρ_L mean-CoV (kg/m ³ - %)	Ratio ρ_G / ρ_L	Small clear specimen kg/m ³
Scots p.	200x250-4.7	60 ¹⁾	531-10.4	511-10.5	1.039	500-520-540 ⁴⁾
	150x200-5.2	60 ¹⁾	507-8.3	496-9.4	1.022	
	100x150-4.0	25 ²⁾	511-5.7	499-8.3	1.024	
Laricio p.	200x250-5.0	60 ¹⁾	589-11.4	592-14.9	0.995	510-540-550 ⁴⁾
	150x200-4.0	60 ¹⁾	598-10.3	586-13.4	1.021	
	100x150-4.0	25 ²⁾	578-6.7	559-9.8	1.034	
Maritime p.	100x150-4.0	25 ²⁾	569-5.6	546-4.7	1.042	530-540-550 ⁴⁾
	150x250-5.6	75 ¹⁾	506-7.5	493-8.7	1.026	
Radiata p.	150x200-4.5	80 ¹⁾	493-8.4	475-9.8	1.038	420-470-500 ⁴⁾ 500 ⁵⁾
	100x150-4.0	25 ²⁾	503-10.0	498-10.8	1.010	
	80x120-2.5	150 ³⁾	515-11.1	501-11.6	1.028	
mean values:			8.7	10.2	1.025	

b, h, L width, depth and length
¹⁾ Íñiguez 2007; ²⁾ Llana 2016; ³⁾ Montón 2012; ⁴⁾ EN 350:2016; ⁵⁾ Vignote 1984

The standard error and the coefficient of determination differences between the mechanical modulus of elasticity and the dynamic one obtained with global and local density are negligible. Both values can therefore be used interchangeably in predictions.

Although many semi-destructive methods can be used to estimate the density of wood pieces, the most practical for in situ use are the following: a) Probes such as the Pilodyn 6J Forest device (Proceq, Switzerland). It measures the penetration depth of a 2.5-mm-diameter steel needle, which is shot into the wood with constant energy (6 J). Another recent probe device is the “Woodpecker” wood sclerometer; a sharp needle is introduced by constant energy strokes and the depth correlates with wood density; b) The screw withdrawal force meter is a test device designed specifically to record the maximum load required to extract a screw previously inserted into the timber. The most frequently used device is the portable Screw Withdrawal Resistance Meter (SWRM), designed by Fakopp (Hungary); c) The wood extractor is a new device for in-situ density estimation of timber pieces, based on weighing the residue generated by conventional drilling (Martínez et al. 2017); and d) Taking cylindrical cores by drilling from the pieces, with a diameter from 8 to 16 mm and a length of 30 to 50 mm to measure density directly. The effect of the resulting hole in the piece is smaller than that of a knot, although it is greater than that of the other devices (Íñiguez-González et al. 2015).

In any case, for practical application it will be necessary to answer the following questions: a) How many pieces should be measured?; b) How many cross-sections should be measured in each piece?; and, c) How many points should be measured in a cross-section?.

Nondestructive measurements for modulus of elasticity estimation

The modulus of elasticity can be determined from the density of the material and the propagation wave velocity according to the following equation:

$$E_d = \rho \cdot v^2 \quad (1)$$

where E_d is the dynamic modulus of elasticity, v is the wave propagation velocity and ρ is the density. This equation is valid when the dimensions of the cross-section are small in comparison with the length of the piece (one-dimensional wave theory).

Density can be estimated in-situ by means of one of the semi-destructive techniques described above. Velocity can be determined from time-of-flight measurements using a stress wave method. Low frequency (in the audible range) stress waves are often used; high frequency ultrasonic waves (above the audible range, >20000 Hz) are also used. Stress waves generate long wavelengths with the advantage that they can travel long distances. On the other hand, ultrasonic waves have short wavelengths that have higher attenuation and travel shorter distances.

Some of the instruments used the most often for time-of-flight measurements based on ultrasonic waves are the Sylvatest Duo (CBS-CBT, France-Switzerland) with conical 22 kHz sensors and the USLab (Agricef, Campinas, Brazil) with sensors from 20 to 90 kHz and piezoelectric sensor induced excitation. The most widely-used sonic stress wave instrument is the MicroSecond Timer (MST) (Fakopp Enterprise, Sopron, Hungary) in which excitation is hammer induced.

Two different ways to in-situ measure time-of-flight can be used: Surface measurements, with both sensors placed on the same edge or on the same face; and crossed measurements with a sensor placed on one face and the other one on the opposite face. In the latter case, two measurement points should be considered for each face, located at thirds of the specimen depth (Arriaga et al. 2017). Sensor orientation should be at an angle equal to or slightly less than 45° with respect to the timber surface. It is recommended to measure time-of-flight over distance of at least 2.5-3 m to avoid the measurement error (time lag) observed when distances are shorter. If time-of-flight is not adjusted to account for time lag, the error in calculating velocity would be around 11% in 1-m pieces and 3% in 4-m distances. These errors are magnified when the square velocity is used to obtain the dynamic modulus of elasticity in order to predict structural properties (Llana et al. 2016).

Conclusions

This work is a preliminary analysis and reflective study of previous experimental results, and it is only about the survey phase. Although it is therefore not possible to draw conclusions yet, some ideas are pointed out. It is essential to maintain a practical approach in the elaboration of an inspection protocol for existing structures, so that proposals are realistic and, as far as possible, generalizable.

This first phase of the work on inspection will be continued by the phases of estimating the mechanical properties of timber, and final evaluation of structural load bearing capacity. Its validity should be verified by applying it to actual cases of existing structure evaluation. It is then that it will be possible to really draw the conclusions of this work.

Acknowledgments

Ministerio de Economía y Competitividad, España, Programa Estatal I + D, 2013–2016 (Ministry of Economy and Competitiveness, Spain, State Plan, Research and Development), Proy.: BIA2014-55089-P.

References

Arriaga, F., Esteban, M. and Relea, E. 2005. Evaluation of the load carrying capacity of large cross section coniferous timber in standing structures. *Materiales de Construcción (mater construcc)*. Vol. 55, nº 280, 43-52.

Arriaga, F., Esteban, M., Argüelles, R., Bobadilla, I. and Íñiguez, G. 2007. The effect of wanes on the bending strength of solid timber beams. *Materiales de Construcción (mater construcc)*. Vol. 57, nº 288, 61-76.

Arriaga, F., Llana, D.F., Esteban, M., Íñiguez-Gonzalez, G. 2017. Influence of length and sensor positioning on acoustic time-of-flight (ToF) measurement in structural timber. *Holzforschung*. Published online. DOI: 10.1515/hf-2016-0214

Cruz, H., Yeomans, D., Tsakanika, E., Macchioni, N., Jorissen, A., Touza, T., Mannucci, M., and Lourenço, P.B. 2015. Guidelines for On-Site Assessment of Historic Timber Structures. *International Journal of Architectural Heritage*, 9: 277–289. DOI: 10.1080/15583058.2013.774070.

EN 1995-1-1:2004+AC:2006+A1:2008+A2:2014. Eurocode 5. Design of timber structures. Part 1-1: General. Common rules and rules for buildings. European Committee for Standardization.

Ente Nazionale Italiano di Unificazione [Italian Organization for Standardization] (UNI). 2004. UNI 11119: Cultural heritage–wooden artefacts–load-bearing structures. On-site inspections for the diagnosis of timber members [English version, original in Italian]. Milan, Italy: UNI.

Esteban, M., Arriaga, F., Íñiguez, G., Bobadilla, I. and Mateo, R. (2010). The effect of fissures on the strength of structural timber. *Materiales de Construcción. Mater. Construcc.*, Vol. 60, 299, 115-132. DOI: 10.3989/mc.2010.48208

European Standard (2010 + A1:2012) EN 408. Timber structures. Structural timber and glued laminated timber. Determination of some physical and mechanical properties. European Committee for Standardization (CEN), Brussels, Belgium.

European Standard 2016 EN 350. Durability of wood and wood-based products. Testing and classification of the durability to biological agent of wood and wood-based materials. European Committee for Standardization CEN), Brussels, Belgium.

International Council of Monuments and Sites (ICOMOS). 1999. Principles for the preservation of historic timber structures.

Íñiguez G. 2007. Clasificación mediante técnicas no destructivas y evaluación de las propiedades mecánicas de la madera aserrada de coníferas de gran escuadría para uso estructural (Grading by non destructive techniques and assessment of the mechanical

properties of large cross section coniferous sawn timber for structural use) [Doctoral thesis]. Universidad Politécnica de Madrid, ETS de Ingenieros de Montes; p. 223. PDF file: <http://oa.upm.es/415>.

Íñiguez-González, G., Montón, J., Arriaga, F., Segué, E. 2015. In-situ assessment of structural timber density using non-destructive and semi-destructive testing. *BioResources* 10(2): 2256-2265.

ISO 13061-2:2014+A1. Physical and mechanical properties of wood. Test methods for small clear wood specimens. Part 2: Determination of density for physical and mechanical tests.

Larsen, K.E., Marstein, N. 2000. Conservation of Historic Timber Structures. An ecological approach. Butterworth-Heinemann Series in Conservation and Museology, Woburn, MA, USA. Open archive at ICOMOS, 2016.

Llana, D.F. 2016. Influencia de factores físicos y geométricos en la clasificación estructural de la madera mediante técnicas no destructivas [The influence of physical and geometrical factors on timber stress-grading by non-destructive techniques]. Doctoral thesis. Universidad Politécnica de Madrid, ETSI Montes, Forestal y del Medio Natural. 412 p. DOI and pdf file: <https://doi.org/10.20868/UPM.thesis.43696>

Llana, D.F., Íñiguez-González, G., Arriaga, F., Wang, X. 2016. Time-of-flight adjustment procedure on for acoustic measurements in structural timber. *BioResources* 11(2): 3303-3317.

Martínez, R.D., Calvo, J., Arriaga, F. and Bobadilla, I. 2017. In situ density estimation of timber pieces by drilling residue analysis. *European Journal of Wood and Wood Products*, in press.

Montón, J. 2012. Clasificación estructural de la madera de *Pinus radiata* D. Don procedente de Cataluña mediante métodos no destructivos y su aplicabilidad en la diagnosis estructural, (Structural grading of *Pinus radiata* D. Don timber from Catalonia using nondestructive methods and their applicability in structural diagnosis). Doctoral thesis, Universitat Politècnica de Catalunya. Escola Tècnica Superior D'Arquitectura de Barcelona, pp. 160-309. <http://hdl.handle.net/10803/96423>, Accessed 04/11/2014.

Tampone, G. 2016. Atlas of the failures of timber structures. Nardini Editores, Firenze, Italy.

Vignote, S. 1984. Características físico-mecánicas del pino insignis y su influencia con la edad y el crecimiento (Physical and mechanical properties of *Pinus insignis* and the influence of age and rate of growth). Ph.D. thesis, Universidad Politécnica de Madrid, ETS de Ingenieros de Montes, Madrid, Spain.

The background of the slide features a large, leafless tree with a complex, branching structure, set against a soft, hazy, yellowish-green background that suggests a misty or foggy day. The tree is positioned on the right side of the frame, with its branches extending towards the center. The overall atmosphere is calm and natural.

Session 6

**Wood Material
Characterization I**

Moisture-Dependent Elastic Characteristics of Wood by Means of Ultrasonic Waves and Mechanical Test

Peter Niemz

Bern University of Applied Science, Solothurnstrasse 102, POB 6096, CH-2500 Biel 5, Switzerland, mail: peter.niemz@bfh.ch

Eidgenössische Technische Hochschule Zürich, Institute for Building Materials, Stefano-Franscini-Platz 3, CH 8093 Zürich, HIF E 29.2. Switzerland

mail:niemzp@retired.ethz.ch

Erik V. Bachtiar

Eidgenössische Technische Hochschule Zürich, Institute for Building Materials, Stefano-Franscini-Platz 3, CH 8093 Zürich, HIF E 29.1, Switzerland, mail: berik.ethz.ch

Abstract: In this study, two types of hardwood Walnut (*Juglans regia* L.) and Cherry (*Prunus avium* L.) are tested using both ultrasonic and mechanical testing methods. These species frequently appear in cultural heritage objects in museums (e.g. musical instruments, furniture). In analyzing the ultrasound data, the elastic moduli can only be accurately estimated from stiffness data if the Poisson ratios are available. Three data evaluation techniques which differ in the way to incorporate the Poisson's ratios (full-stiffness-inversion, simplified uncorrected, and simplified corrected) are used to estimate the elastic moduli from the ultrasonic results. The full-stiffness-inversion method, which requires four specimen types, gives the best estimation for the elastic moduli. The simplified uncorrected method requires only one specimen type, but leads to an overestimation of elastic moduli. The corrected method, that based on the Poisson ratios obtained from mechanical tests, only partially reduces the overestimation for L Young's modulus.

Keywords: ultrasonic test, mechanical test, moisture-dependent elastic and shear properties, Poisson's ratios, Walnut (*Juglans regia* L.), Cherry (*Prunus avium* L.)

1 Introduction

In engineering, elastic material parameters are essential inputs to advanced material models. However, the availability of elastic material parameters in the case of wood is often very limited. It is mainly due to the enormous amount of species, each with own characteristics as well as due to its natural complexity. The material properties of wood are different in the three orthogonal material directions: longitudinal (L), radial (R) and tangential (T). Consequently, a considerable experimental effort is required to estimate the elastic parameters of only one particular wood species.

Various experimental methods have been developed to support the characterization of wood properties using the mechanical test as the standard (Hörig, 1935; Keunecke et al, 2008; Ozyhar et al., 2012). The mechanical test allows direct and accurate measurement of all elastic properties: Young's moduli (E), shear moduli (G) and Poisson's ratios (μ). However, the test is a destructive test, which limits its applicability. In a case of assessing standing constructions or cultural objects, the non-destructive tests are more suitable. The non-destructive testing of choice for wood elastic

properties, which has been developed over the last decades, is ultrasonic testing (Bucur and Archer, 1984; Goncalves et al, 2011; Ozyhar et al, 2013). Despite its reliability of estimating E in the principal axes (L, R, and T) and G on the material planes (LR, LT and RT), its applicability estimating ν is uncertain. Since the ultrasonic method is based on the inversion of the stiffness data, E and μ values are partially related. Therefore, the uncertainty of μ questioned the accuracy of E.

Both ultrasonic and mechanical testing methods of two types of hardwood walnut (*Juglans regia* L.) and cherry (*Prunus avium* L.).

2 Material and Methods

Material and Method

The measurements in this study were performed for walnut (*Juglans regia* L.) and cherry (*Prunus avium* L.) wood growth in the Caucasus region. The average wood densities (ρ) were 670 kg/m³ and 575 kg/m³ respectively and were measured in normal climatic conditions with a temperature of 20°C and an RH of 65%. The specimens were small clear wood without any natural growth characteristics such as reaction wood or knots.

Based on Hooke's law, the relation between stress and strain for an orthotropic material presented under Voigt's notation is

$$[\varepsilon] = [S] \cdot [\sigma]$$

$$\begin{bmatrix} \varepsilon_{LL} \\ \varepsilon_{RR} \\ \varepsilon_{TT} \\ 2\varepsilon_{RT} \\ 2\varepsilon_{TL} \\ 2\varepsilon_{LR} \end{bmatrix} = \begin{bmatrix} \frac{1}{E_L} & \frac{-\nu_{RL}}{E_R} & \frac{-\nu_{TL}}{E_T} & 0 & 0 & 0 \\ \frac{-\nu_{LR}}{E_L} & \frac{1}{E_R} & \frac{-\nu_{TR}}{E_T} & 0 & 0 & 0 \\ \frac{-\nu_{LT}}{E_L} & \frac{-\nu_{RT}}{E_R} & \frac{1}{E_T} & 0 & 0 & 0 \\ 0 & 0 & 0 & 1 & 0 & 0 \\ 0 & 0 & 0 & 0 & 1 & 0 \\ 0 & 0 & 0 & 0 & 0 & 1 \end{bmatrix} \cdot \begin{bmatrix} \sigma_{LL} \\ \sigma_{RR} \\ \sigma_{TT} \\ \sigma_{RT} \\ \sigma_{TL} \\ \sigma_{LR} \end{bmatrix} \quad (1)$$

where, [S] is the compliance tensor, $[\sigma]$ and $[\varepsilon]$ are stress and strain tensor respectively.

Under Voigt's notation, they become matrixes and vectors as shown previously. E_i is the Young's modulus along axis i . G_{ij} is the shear modulus, which load is in direction j working on the plane which normal is in direction i . ν_{ij} is the Poisson's ratio that corresponds to a passive contraction in direction j when an extension is applied in direction i . Due to the material symmetry, the [S] matrix is symmetric, which leads to $\frac{\nu_{RL}}{E_R} = \frac{\nu_{LR}}{E_L}$, $\frac{\nu_{TL}}{E_T} = \frac{\nu_{LT}}{E_L}$ and $\frac{\nu_{RT}}{E_R} = \frac{\nu_{TR}}{E_T}$. Therefore, the orthotropic constitutive equation

incorporates nine independent elastic constants comprised of three Young's moduli, three Poisson's ratios and three shear moduli. In the mechanical test, all elastic parameters are directly obtained as test results. In the ultrasonic test, however, ultrasound waves propagating through the material provide the stiffness matrix [C], which needs to be inverted to calculate $[S] = [C]^{-1}$ and furthermore used to obtain the elastic parameter.

Mechanical Test

Compression and Tension Tests

The specimens used for the test were dog-bone shaped specimens. They were prepared for three different loading direction L, R and T. Specimens with similar dimensions have been successfully tested to determine the E and ν of yew and spruce wood (Keunecke et al. 2008) and beech wood (Hering et al. 2012; Ozyhar et al. 2013a). The specimens were acclimatized at 50%, 65%, 85% and 95% RH and a constant temperature 20°C for at least two months before the tests. For each RH level, loading direction and wood species, 10-15 specimens were prepared.

Compression (CT) and tension (TT) test were performed using a Universal Testing Machine (Zwick Roell Z100, Zwick Germany) equipped with a 100 kN load cell. A 50 N predefined initial force was set with a displacement rate of 5 mm/min and used as a starting point for the measurement. The tests were continued under a displacement-controlled rate of 1 mm/min to achieve failure within 90(±30)s (Keunecke et al. 2008). For the measurement of strain a speckle pattern was applied with a airbrush gun. The strain evaluation was performed using the digital image correlation (DIC) technique. Based on these set of pictures, the surface strains were calculated with a commercial two-dimensional digital image correlation software (VIC 2D, Correlated Solution). This method was explained in Keunecke et al. (2008).

Arcan Tests

Arcan test (AT) was performed to determine the shear moduli (G) mechanically. The specimens used for arcan test were 130 mm long and 50 mm wide boards with notches. They were prepared in six different load axes direction (RT, TR, TL, LT, LR and RL). The tests were performed in standard climatic conditions (65% RH, 20°C). 10-15 samples were prepared for each loading direction and wood species.

Ultrasonic Test

The ultrasonic test is a non-destructive testing techniques based on the propagation of ultrasonic waves in a material. Two types of wave are used, longitudinal wave and shear/ transverse wave. To determine all independent components of the $[C]$ matrix at least three longitudinal, three shear wave velocities propagating along the principal axes and three shear wave velocities measured at a suitable angle on the principal axes (quasi-shear wave) are needed (Bucur 2006). In this study, the selected angle for the quasi-shear wave is $\alpha=45^\circ$ with respect to principal direction. The notation for the wave velocities is shown in Table 1.

Table 1 Notation for the ultrasound propagation velocities (Ashman et al. 1984)

Wave velocities ^a	Explanation
V_{ii}	Wave velocity of longitudinal wave propagating in the i direction and the particle motion (direction of polarization) in the same direction
V_{ij}	Wave velocity of shear wave propagating in the i direction and the particle motion in the perpendicular j direction
$V_{ij/ij}$	Wave velocity of quasi-shear wave with propagation along $n = \left(\frac{1}{\sqrt{2}} \quad \frac{1}{\sqrt{2}}\right)^T$ ($\alpha= 45^\circ$ angle between the i and j directions) and particle motion on the $i - j$ plane

^a $i, j \in L, R, T$

To carry the ultrasonic test (UT), four different types of cuboid specimens, corresponding to specific material planes (Figure 1) were used. Each specimen type was manufactured in 3 different edge lengths (16, 13 and 10 mm). They were further acclimatized at RH 50%, 65%, 85%, 95% and a constant temperature of 20°C. Approximately 10-15 specimens were prepared for each type, dimension, wood species and RH level. The ultrasonic test was performed in the climate room where the samples had been stored. The test was carried out using the Epoch XT flaw detector (complies to EN-12668-110 (2010)) with a through-transmission technique. A transmitter transducer (Olympus A133S with a diameter of 12 mm for longitudinal waves and Staveley S-0104 with diameter of 12.7 mm for transversal waves) sends ultrasound waves from one surface of the specimen and a separate receiver detects the first arrival of waves (time of flight) on the opposite surface.

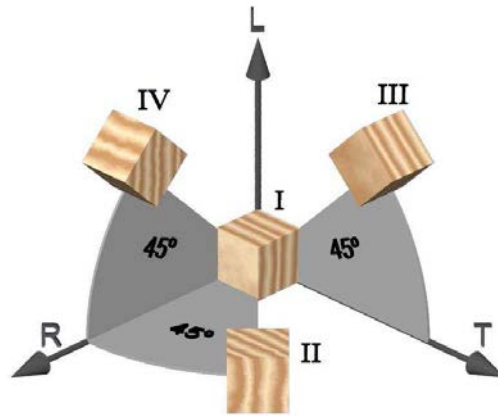


Figure 1 Specimen types for ultrasound velocity measurement. Each type was produced in three different edge length: 16, 13 and 10 mm

The selected longitudinal and shear waves frequency were 2.27 MHz and 1 MHz respectively, which lead to wavelength of 0.5-2.5 mm. The selected wavelength must be smaller than specimen dimension to avoid guided wave effects and larger than wood microstructure to capture macroscopic material behaviour (Bucur 2006; Zaoui 2002). Moreover, this selected range of frequency (1 MHz or higher) has been successfully attempted in several previous studies for other wood species (Bucur and Archer 1984; Gonçalves et al. 2011; Ozyhar et al. 2013b).

Table 2 Equation to calculate the stiffness components from the ultrasound wave velocities

Specimen type	Wave velocities ^a	Explanation
I	V_{LL}	$c_{11} = \rho V_{LL}^2$
	V_{RR}	$c_{22} = \rho V_{RR}^2$
	V_{TT}	$c_{33} = \rho V_{TT}^2$
	V_{RT}/V_{TR}	$c_{44} = (\rho V_{RT}^2 + \rho V_{TR}^2)/2$
	V_{TL}/V_{LT}	$c_{55} = (\rho V_{TL}^2 + \rho V_{LT}^2)/2$
	V_{LR}/V_{RL}	$c_{66} = (\rho V_{LR}^2 + \rho V_{RL}^2)/2$
II	$V_{RT/RT}^a$	$c_{23} = \sqrt{(c_{22} + c_{44} - 2\rho V_{RT/RT}^2)(c_{33} + c_{44} - 2\rho V_{RT/RT}^2)} - c_{44}$
III	$V_{TL/TL}^a$	$c_{31} = \sqrt{(c_{11} + c_{55} - 2\rho V_{TL/TL}^2)(c_{33} + c_{55} - 2\rho V_{TL/TL}^2)} - c_{55}$
IV	$V_{LR/LR}^a$	$c_{12} = \sqrt{(c_{11} + c_{66} - 2\rho V_{LR/LR}^2)(c_{22} + c_{66} - 2\rho V_{LR/LR}^2)} - c_{66}$

$i, j \in L, R, T$

In this experimental test, the flight time of three longitudinal, six shear waves and three quasi-shear waves propagating on each specimen dimension were recorded for each specimen thickness. The velocities were determined by linear regression between the measured times and the specimens thicknesses. Then, the resulting velocities were used to estimate the elastic constants.

Three different data evaluation techniques were used to evaluate the ultrasound results. The first data evaluation technique, **full-stiffness-inversion** (UT-FSI, see tab. 2), is the method that has been implemented in the previous studies (Bucur and Archer 1984; Kriz and Stinchcomb 1979; Ozyhar et al. 2013b). To estimate the Young's moduli, this technique requires the whole set of the wave velocities. Each component of stiffness matrix $[C]$ is calculated using the equations in Table 2. Then, the $[S]$ matrix is calculated by inverting the $[C]$ matrix, from which the whole set of E , G and ν are obtained with Eq. (1). The second data evaluation technique, **simplified, uncorrected** (UT-SU), is a simplified version of ultrasound data analysis, which only requires the wave velocities from specimens type I (see eq.2). This method significantly increases the time efficiency of the ultrasonic test. However, the main diagonal terms of the stiffness matrix are assumed equal to E and G . The calculation of G , which is independent of ν , is not influenced by this assumption. However, it leads to an over estimation of E (Ozyhar et al. 2013b).

$$\begin{aligned} E_i &\approx c_{ii} = \rho V_{ii}^2 && \text{for all } i \in 1, 2, 3 \\ G_{ij} &= G_{ji} = c_{(9-i-j)(9-i-j)} = (\rho V_{ij}^2 + \rho V_{ji}^2) / 2 && \text{for all } i, j \in 1, 2, 3 \text{ and } i \neq j \end{aligned} \quad (2)$$

To avoid the overestimation of the E , a third data evaluation technique, **simplified, corrected** (UT-SC, see eq.3), is proposed. A parametric inversion of the $[S]$ matrix is performed to obtain analytical expressions of the axial stiffness c_{ii} in function of the E and ν . By operating Eq. (1), exact expressions for the first three diagonal terms of the $[S]$ matrix are obtained. Each stiffness component is equal to an E in the corresponding direction multiplied by a certain correction factor (k_i) which is a function of the ν (Eq. (3)). With assumptions that the nominal values of the ν are known (e.g. from literature data (LD), from selected mechanical or other ultrasound tests) and their variations among different specimens of the same species introduce a negligible impact on the E calculations, these correction factors can be calculated. By using this method, an accurate E estimation can be performed even though only specimens of type I are available during the ultrasonic measurement.

$$\begin{aligned} c_{11} &= E_L \cdot k_L = E_L \cdot \frac{1 - \nu_{RT} \nu_{TR}}{1 - \nu_{LR} \nu_{RL} - \nu_{RT} \nu_{TR} - \nu_{TL} \nu_{LT} - \nu_{LR} \nu_{RT} \nu_{TL} - \nu_{RL} \nu_{LT} \nu_{TR}} \\ c_{22} &= E_R \cdot k_R = E_R \cdot \frac{1 - \nu_{TL} \nu_{LT}}{1 - \nu_{LR} \nu_{RL} - \nu_{RT} \nu_{TR} - \nu_{TL} \nu_{LT} - \nu_{LR} \nu_{RT} \nu_{TL} - \nu_{RL} \nu_{LT} \nu_{TR}} \\ c_{33} &= E_T \cdot k_T = E_T \cdot \frac{1 - \nu_{LR} \nu_{RL}}{1 - \nu_{LR} \nu_{RL} - \nu_{RT} \nu_{TR} - \nu_{TL} \nu_{LT} - \nu_{LR} \nu_{RT} \nu_{TL} - \nu_{RL} \nu_{LT} \nu_{TR}} \end{aligned} \quad (3)$$

3. Results and Discussion

The results obtained with the three different evaluation techniques are presented in Table 3. However, due to the low availability of supported reference studies for Walnut and Cherry wood, the correction factor cannot be optimally applied. A full set of material parameters can only be found for Walnut (Keylwerth 1951) but only for a specific moisture condition. These data were used together with mechanical test results for comparison. For the validation purposes, correction factors (k) based on the ν of UT-FSI method were also calculated and presented in Table 3. The cross-validations were made

by multiplying E of the UT-FSI with k in the corresponding direction. Since Eq. (3) is formally equivalent to the inversion of the $[C]$ matrix, the results are equal to the component of $[C]$ matrix in the same direction, which is none other than E of the simplified uncorrected (UT-SU) technique.

Table 3 Data evaluation results of Walnut (*Juglans regia* L.) and Cherry (*Prunus avium* L.) at different moisture content u

Experimental Data	u (%)	ρ (kg/m^3)	Elasticity Moduli (MPa) (CoV(%))			Shear Moduli (MPa) (CoV(%))			Poisson's Ratio(-) (CoV(%))						
			E_L	E_R	E_T	G_{RT}	G_{LT}	G_{LR}	ν_{RL}	ν_{LR}	ν_{TL}	ν_{LT}	ν_{TR}	ν_{RT}	
Walnut															
Mechanical	Compression (CT)	7.2	642	12849(9.19)	1227(6.08)	1091(7.35)				0.043(27.5)	0.288(6.26)	0.035(15.8)	0.180(16.3)	0.316(11.4)	0.519(4.50)
		9.2	693	10721(9.21)	1149(4.82)	1083(3.02)				0.035(20.5)	0.290(8.99)	0.032(14.5)	0.193(21.5)	0.297(1.88)	0.524(1.84)
		12.5	647	10217(7.76)	968(4.13)	908(4.96)				0.033(6.18)	0.240(17.2)	0.036(10.1)	0.131(46.6)	0.352(6.61)	0.543(3.49)
	15.1	671	6793(21.2)	907(10.4)	873(2.89)				0.067(15.3)	0.201(22.4)	0.059(8.94)	0.083(48.8)	0.340(2.97)	0.559(3.27)	
	Tension (TT)	7.2	642	13621(8.07)	1467(5.74)	1284(5.66)				0.075(19.0)	0.230(16.1)	0.062(8.69)	0.125(33.6)	0.333(6.34)	0.513(4.40)
		9.2	693	11253(4.85)	1352(2.72)	1260(3.45)				0.060(7.67)	0.260(9.83)	0.065(7.43)	0.129(15.4)	0.340(2.28)	0.541(2.32)
12.5		647	11094(8.90)	1170(4.85)	1124(3.95)				0.053(15.6)	0.250(14.0)	0.060(11.0)	0.125(25.5)	0.394(6.68)	0.590(2.51)	
15.1	671	9708(20.1)	1056(7.64)	1028(3.68)				0.066(12.3)	0.274(18.3)	0.057(6.86)	0.115(45.8)	0.363(1.72)	0.579(3.30)		
Arcan (AT)	10.0	561				194(2.55)	868(7.10)	1020(3.45)							
Ultrasound full stiffness inversion (UT-FSI)															
	7.2	635	11598	1518	746	395	1222	1813	0.061	0.469	0.075	1.173	0.460	0.936	
	9.2	647	11190	1377	682	264	995	1389	0.055	0.448	0.079	1.298	0.437	0.883	
	12.5	628	10906	1151	489	218	863	1173	0.109	1.035	0.012	0.268	0.416	0.978	
15.1	677	10021	1007	408	208	861	1095	0.094	0.934	0.021	0.525	0.435	1.072		
Cherry															
Mechanical	Compression (CT)	8.4	559	8947(10.3)	1634(7.47)	930(10.5)				0.059(16.3)	0.289(10.7)	0.046(16.6)	0.291(22.6)	0.344(2.26)	0.715(3.18)
		10.7	589	8707(10.7)	1505(8.39)	720(13.2)				0.055(5.17)	0.257(13.6)	0.042(9.41)	0.242(14.9)	0.321(4.34)	0.734(2.64)
		14.2	565	8627(7.77)	1307(8.89)	717(4.77)				0.057(7.16)	0.292(9.88)	0.048(16.2)	0.263(11.6)	0.321(2.78)	0.768(4.20)
	16.3	562	6808(12.4)	1079(5.07)	610(19.1)				0.057(5.87)	0.179(15.6)	0.036(22.8)	0.141(22.3)	0.348(4.21)	0.828(2.17)	
	Tension (TT)	8.4	559	9826(8.71)	1830(5.25)	1069(9.43)				0.091(10.0)	0.300(4.57)	0.067(4.41)	0.266(24.1)	0.360(2.60)	0.736(2.61)
		10.7	589	9709(9.02)	1609(17.2)	885(11.7)				0.088(4.28)	0.303(16.9)	0.064(9.98)	0.271(15.2)	0.350(3.73)	0.775(0.99)
14.2		565	9396(9.76)	1502(7.42)	864(4.28)				0.083(7.64)	0.310(12.6)	0.060(14.4)	0.259(15.6)	0.372(4.30)	0.825(1.80)	
16.3	562	8592(8.76)	1280(3.94)	825(12.9)				0.075(5.88)	0.306(14.6)	0.055(19.7)	0.258(14.1)	0.407(4.97)	0.877(2.29)		
Arcan (AT)	10.0	554				218(3.90)	782(4.35)	1188(4.95)							
Ultrasound full stiffness inversion (UT-FSI)															
	8.4	579	9489	1489	884	239	1050	1230	0.163	1.041	0.027	0.289	0.446	0.752	
	10.7	560	8238	1384	644	228	895	1112	0.141	0.838	0.059	0.755	0.372	0.798	
	14.2	556	7496	1233	509	209	802	956	0.117	0.711	0.066	0.966	0.372	0.900	
16.3	592	7309	1229	475	202	711	950	0.116	0.689	0.052	0.807	0.375	0.971		

Table 3 Data evaluation results of Walnut (*Juglans regia* L.) and Cherry (*Prunus avium* L.) at 20°C/ RH 65%

Experimental Data	u (%)	ρ (kg/m^3)	Elasticity Moduli (MPa)			Shear Moduli (MPa)			Poisson's Ratio(-)						Correction factors(-)				
			E_L	E_R	E_T	G_{RT}	G_{LT}	G_{LR}	ν_{RL}	ν_{LR}	ν_{TL}	ν_{LT}	ν_{TR}	ν_{RT}	k_L	k_R	k_T		
Walnut																			
Mechanical	Compression (CT)		9.2	693	10721	1149	1083				0.035	0.290	0.032	0.193	0.297	0.524			
	Tension (TT)		9.2	693	11253	1352	1260				0.060	0.260	0.065	0.123	0.340	0.541			
	Arcan (AT)		10.0	561				194	868	1020									
Literature Data (LD ^a)		11.0	590	11416	1214	641	234	714	980	0.052	0.490	0.036	0.636	0.375	0.710				
Ultrasound(UT)	UT-FSI (Tab.2)		9.2	647	11190	1377	682	264	995	1389	0.055	0.448	0.079	1.298	0.437	0.883	1.447	2.113	2.296
	UT-SU (Eq.2)		9.2	647	16189	2910	1565	264	995	1389	0.000	0.000	0.000	0.000	0.000	0.000	1.000	1.000	1.000
	UT-SC (CT) (Eq.3)		9.2	647 - 693	15745	2403	1298	264	995	1389	0.035	0.290	0.032	0.193	0.297	0.524	1.028	1.211	1.206
	UT-SC (TT) (Eq.3)		9.2	647 - 693	15482	2290	1241	264	995	1389	0.060	0.260	0.065	0.123	0.340	0.541	1.046	1.271	1.261
	UT-SC (LD ^a) (Eq.3)		9.2 - 11.0	590 - 647	14578	1967	1061	264	995	1389	0.052	0.490	0.036	0.636	0.375	0.710	1.111	1.479	1.475
^a Ozyhar et al (2013)																			
Cherry																			
Mechanical	Compression (CT)		10.7	589	8707	1505	720				0.055	0.257	0.042	0.242	0.321	0.734			
	Tension (TT)		10.7	589	9709	1609	885				0.088	0.303	0.064	0.271	0.350	0.775			
	Arcan (AT)		10.0	554				218	782	1188									
Ultrasound(UT)	UT-FSI (Tab.2)		10.7	560	8238	1384	644	228	895	1112	0.141	0.838	0.059	0.755	0.372	0.798	1.523	2.068	1.909
	UT-SU (Eq.2)		10.7	560	12542	2862	1230	228	895	1112	0.000	0.000	0.000	0.000	0.000	0.000	1.000	1.000	1.000
	UT-SC (CT) (Eq.3)		10.7	560 - 589	11943	2104	908	228	895	1112	0.055	0.257	0.042	0.242	0.321	0.734	1.050	1.360	1.355
	UT-SC (TT) (Eq.3)		10.7	560 - 589	11382	1926	836	228	895	1112	0.088	0.303	0.064	0.271	0.350	0.775	1.102	1.485	1.472

Moreover, the Poisson's ratio (ν) calculated based on the full stiffness inversion (UT-FSI) method show inconsistent results. It is expected due to the combination of the wood inhomogeneity and the ill-posed problem arise from the inversion of stiffness matrix $[C]$. The combination of multiple specimens used during the ultrasonic measurement leads to an averaged material properties. Since the specimens

introduce with its own natural inhomogeneity, their properties may slightly vary. While for E and G this problem is negligible, it is clearly pronounced in the resulted ν . Moreover I case of the ill-posed problem, a typical variation of 0.5-2% in the ultrasonic velocities leads to large errors up to 30% in the resulted ν after the stiffness inversion. For E and G , this variation arises only up to 5%, hence they are mostly unaffected.

4. Conclusions

The change of moisture influences the elastic parameters of walnut and cherry wood. A high moisture level (u) leads to lower Young's (E) and shear moduli (G). Based on the mechanical test results of walnut wood, EL were in average decreased by 679 MPa in compression and 423 MPa in tension for every percent increase in the u . For the Poisson's ratios (ν), however, no clear trend of moisture influence can be observed. The UT-FSI method requires the measurement of multiple specimen types (type I, II, III and IV). The simplified method of E as equivalent to the diagonal terms of the stiffness matrix, requires only the ultrasound measurement of specimens type I, which greatly improves the time-efficiency of the test by reducing the number of samples to one fourth. However, it leads to an overestimation, e.g. for walnut wood with u 9.2%-11.0%, the overestimation $\Delta EL=47\%$, $\Delta ER=133\%$ and $\Delta ER=34\%$. The exact correction factors for the simplified method based on nominal ν obtained from mechanical tests or literature can alleviate the overcompensation. In most cases, it gave the better agreement with the mechanical test results (e.g. ΔET of walnut and cherry wood; ΔEL and ΔER of beech wood). In other exceptional cases (e.g. ΔEL , ΔER of walnut and cherry wood), the UT-FSI although providing inaccurate Poisson's ratios, still gave the best estimation (for walnut wood the ΔEL of UT-FSI =2% while the ΔEL of UT-SC (LD) =32%). This trend is also observed in the ultrasonic Beech results from Ozyhar et al (2013).

Acknowledgments This study was founded through the Swiss National Foundation (SNF) project no. 147672

5. References

- Ashman RB, Cowin SC, van Buskirk WC, Rice JC (1984) A continuous wave technique for the measurement of elastic properties of cortical bone. *Journal of Biomechanics* 17:349-361
- Bodig J, Jayne B (1993) *Mechanics of Wood and Wood Composites*. Krieger Publishing Company,
- Bucur V (2006) *Acoustic of Wood*. Springer Series in Wood Science. Springer,
- Bucur V, Archer R (1984) Elastic constants for wood by an ultrasonic method *Wood Science and Technology* 18:255-265
- EN-12668-110 (2010) Non-destructive testing - characterization and verification of ultrasonic examination equipment - part 1: instruments.
- Gonçalves R, Trinca AJ, Cerri DGP (2011) Comparison of elastic constants of wood determined by ultrasonic wave propagation and static compression testing. *Wood Fiber and Science* 43:64-75
- Hering S, Keunecke D, Niemz P (2012) Moisture-dependent orthotropic elasticity of beech wood. *Wood Science and Technology* 46:927-938
- Hörig H (1935) Anwendung der Elastizitätstheorie anisotroper Körper auf Messungen an Holz. *Ingenieur-Archiv* 6:8-14
- Keunecke D, Hering S, Niemz P (2008) Three-dimensional elastic behaviour of common yew and norway spruce. *Wood Science and Technology* 42:633-647
- Keylwerth R (1951) The anisotropic elasticity of wood and plywood (Die anisotrope Elastizität des Holzes und der Lagenhölzer). Verlag des Vereins Deutscher Ingenieure VDI-Forschungsheft 430
- Kriz RD, Stinchcomb WW (1979) Elastic moduli of transversely isotropic graphite fibers and their composites. *Experimental Mechanics* 19:41-49

- Ozyhar T, Hering S, Niemz P (2013a) Moisture-dependent orthotropic tension-compression asymmetry of wood. *Holzforschung* 67:395-404
- Ozyhar T, Hering S, Sanabria S, Niemz P (2013b) Determining moisture-dependent elastic characteristics of beech wood by means of ultrasonic waves. *Wood Science and Technology* 47:329-341
- R. Gonçalves AJT, D.G.P. Cerri (2011) Comparison of elastic constants of wood determined by ultrasonic wave propagation and static compression testing *Wood Fiber and Science* 43:64-75
- Stamer J, Sieglerschmidt H (1933) Elastische Formänderung der Hölzer. *Z Ver Dtsch Ing* 77:503-505
- T. Ozyhar SH, P. Niemz (2012) Moisture-dependent elastic and strength anisotropy of european beech wood in tension. *Journal of Materials Science* 47:6141-6150
- T. Ozyhar SH, S. J. Sanabria, P. Niemz (2013) Determining moisture-dependent elastic characteristics of beech wood by means of ultrasonic waves. *Wood Science and Technology* 47:329-341
- Ting TCT, Chen T (2005) Poisson's ratio for anisotropic elastic materials can have no bounds. *The Quarterly Journal of Mechanics and Applied Mathematics* 58:73-82
- V. Bucur RA (1984) Elastic constants for wood by an ultrasonic method *Wood Science and Technology* 18:255-265
- Zaoui A (2002) Continuum Micromechanics: Survey *Journal of Engineering Mechanics* 128:808-816

Correction Factors in the Determination of Moduli of Elasticity of Orthotropic Material Using Ultrasonic Longitudinal Wave Propagation Method

Bambang Suryoatmono

Department of Civil Engineering, Parahyangan Catholic University, Bandung, West Java, Indonesia, suryoatm@unpar.ac.id

Abstract

In an orthotropic material such as wood, there are nine independent coefficients in the constitutive matrix, namely six diagonal coefficients and three off-diagonal coefficients. In order to determine the moduli of elasticity of the material accurately, one needs to establish not only the diagonal coefficients but also the off-diagonal coefficients. For simplification, many researches assume that the moduli of elasticity are the same as the first three diagonal coefficients so that the off-diagonal coefficients do not have to be evaluated. In this paper, a statistical based method is developed to establish modulus of elasticity in any one principle axis of wood that uses correction factor that represents the influence of all other elastic properties. The method is developed using known elastic properties of many wood species. By using the correction factors proposed in the method, moduli of elasticity of an orthotropic material can be established easily and more accurately.

Keywords: ultrasonic longitudinal wave propagation method, correction factor, modulus of elasticity, orthotropic material

Introduction

Orthotropic Material

In analyzing structural behavior of wood, especially using finite element method, wood is frequently assumed as orthotropic material. The three mutually perpendicular principal directions of the material are longitudinal (L), radial (R), and tangential (T), as seen in Figure 1. The longitudinal axis coincides with the fiber direction of the material. By doing so, there are three perpendicular planes of symmetry, namely L-R, L-T, and R-T planes. With respect to these three axes, the strain components $\{\varepsilon\}$ can be expressed in the stress components by $\{\varepsilon\} = [S]\{\sigma\}$ where $[S]$ is the compliance matrix of the material. The relationship is as follows

$$\begin{Bmatrix} \varepsilon_L \\ \varepsilon_R \\ \varepsilon_T \\ \gamma_{LR} \\ \gamma_{LT} \\ \gamma_{RT} \end{Bmatrix} = \begin{bmatrix} \frac{1}{E_L} & -\frac{\mu_{RL}}{E_R} & -\frac{\mu_{TL}}{E_T} & 0 & 0 & 0 \\ -\frac{\mu_{LR}}{E_L} & \frac{1}{E_R} & -\frac{\mu_{TR}}{E_T} & 0 & 0 & 0 \\ -\frac{\mu_{LT}}{E_L} & -\frac{\mu_{RT}}{E_R} & \frac{1}{E_T} & 0 & 0 & 0 \\ 0 & 0 & 0 & \frac{1}{G_{LR}} & 0 & 0 \\ 0 & 0 & 0 & 0 & \frac{1}{G_{LT}} & 0 \\ 0 & 0 & 0 & 0 & 0 & \frac{1}{G_{RT}} \end{bmatrix} \begin{Bmatrix} \sigma_L \\ \sigma_R \\ \sigma_T \\ \tau_{LR} \\ \tau_{LT} \\ \tau_{RT} \end{Bmatrix} \quad (1)$$

where E_L, E_R, E_T , are moduli of elasticity, μ_{ij} are Poisson's ratios, and G_{ij} are shear moduli in i - j planes (Sadd 2009). Poisson's ratio μ_{ij} is defined by $-\varepsilon_j/\varepsilon_i$ for a stress in the i direction. Because the compliance matrix is symmetric, only nine elastic constants are independent and hence Poisson's ratio $\mu_{ij} = \mu_{ji}E_i/E_j$ for $i, j = L, R$, and T .

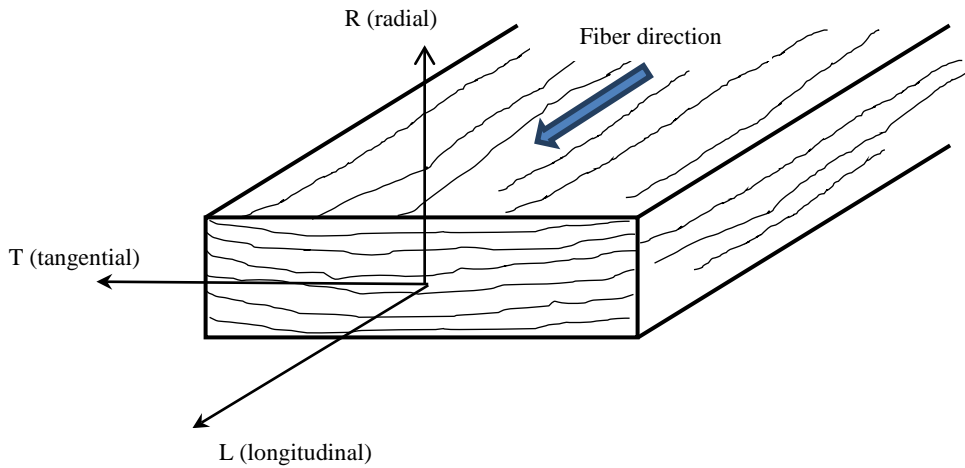


Figure 1—Three principal axes of wood assuming wood as orthotropic material

The inverse relationship of Eq. (1) is as follows

$$\begin{Bmatrix} \sigma_L \\ \sigma_R \\ \sigma_T \\ \tau_{LR} \\ \tau_{LT} \\ \tau_{RT} \end{Bmatrix} = \begin{bmatrix} C_{11} & C_{12} & C_{13} & 0 & 0 & 0 \\ C_{21} & C_{22} & C_{23} & 0 & 0 & 0 \\ C_{31} & C_{32} & C_{33} & 0 & 0 & 0 \\ 0 & 0 & 0 & C_{44} & 0 & 0 \\ 0 & 0 & 0 & 0 & C_{55} & 0 \\ 0 & 0 & 0 & 0 & 0 & C_{66} \end{bmatrix} \begin{Bmatrix} \varepsilon_L \\ \varepsilon_R \\ \varepsilon_T \\ \gamma_{LR} \\ \gamma_{LT} \\ \gamma_{RT} \end{Bmatrix} \quad (2)$$

or, in the condensed form, $\{\sigma\} = [C]\{\varepsilon\}$, where $[C] = [S]^{-1}$ is the constitutive matrix of the material. Because the compliance matrix is symmetric, then its inverse, the constitutive matrix, is also symmetric. While the diagonal components of the compliance matrix can be expressed in a simple form of elastic

constants, it is not the case for the constitutive matrix. The first three diagonal components of the constitutive matrix are

$$C_{11} = \frac{E_L^2 E_R - E_L^2 E_T \mu_{RT}^2}{E_L E_R - E_R^2 \mu_{LR}^2 - 2E_T E_R \mu_{RT} \mu_{LR} \mu_{LT} - E_T E_R \mu_{LT}^2 - E_L E_T \mu_{RT}^2} \quad (3)$$

$$C_{22} = \frac{E_R^2 E_L - E_R^2 E_T \mu_{LT}^2}{E_L E_R - E_R^2 \mu_{LR}^2 - 2E_T E_R \mu_{RT} \mu_{LR} \mu_{LT} - E_T E_R \mu_{LT}^2 - E_L E_T \mu_{RT}^2} \quad (4)$$

$$C_{33} = \frac{E_L E_R E_T - E_R^2 E_T \mu_{LR}^2}{E_L E_R - E_R^2 \mu_{LR}^2 - 2E_T E_R \mu_{RT} \mu_{LR} \mu_{LT} - E_T E_R \mu_{LT}^2 - E_L E_T \mu_{RT}^2} \quad (5)$$

As seen in Equations (3), (4), and (5), each of the first three diagonal components of the constitutive matrix depends on six elastic properties of the material, namely E_L , E_R , E_T , μ_{LR} , μ_{LT} , and μ_{RT} . If all Poisson's ratios are zero, then the first three diagonal components of the constitutive matrix are the same as moduli of elasticity, i.e. $C_{11} = E_L$, $C_{22} = E_R$, and $C_{33} = E_T$. Furthermore, if all moduli of elasticity are the same ($= E$) and all Poisson's ratios are the same ($= \mu$), then Equations (3), (4), and (5) reduce to the equation for isotropic material, i.e. $C_{11} = C_{22} = C_{33} = E(1 - \mu^2)/(1 - 3\mu^2 - 2\mu^3) = E(1 - \mu)/[(1 + \mu)(1 - 2\mu)]$.

Ultrasonic longitudinal wave

Ultrasonic longitudinal wave propagation method has long been used in many material including wood. The purpose of using the method is mainly to establish the mechanical properties of the material non destructively. Figure 2 shows an example of the use of ultrasonic longitudinal wave propagation method to obtain longitudinal modulus of elasticity of wood. In this method, the traveling velocity of the wave is measured. If the density of the material is denoted as ρ , it can be proven (Bucur 2006) that the wave travels in the longitudinal direction of the material such that

$$C_{11} = \rho V_L^2 \quad (6)$$

where V_L is the wave speed in the longitudinal direction. Similarly, if the ultrasonic longitudinal wave propagates in the radial and tangential directions, then $C_{22} = \rho V_R^2$ and $C_{33} = \rho V_T^2$, respectively.

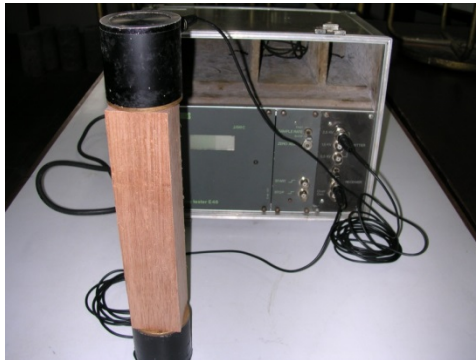


Figure 2— Measuring ultrasonic wave velocity in longitudinal direction of a wood specimen using Portable Ultrasonic Nondestructive Digital Indicating Tester (Pundit).

As seen in Equations (3), (4), and (5), measuring wave velocities in each of the principal directions of the material is not sufficient in order to obtain all nine independent elastic properties. One possible way is by combining those measurements with measuring velocities of quasi longitudinal (QL) wave in three

different out of principal directions, and measuring velocities of transverse shear wave in each of the three material symmetry planes. Although it is not straightforward, these nine measurements result in nine equations that have to be solved simultaneously to obtain all nine elastic properties of the material (Bucur 2006). The disadvantage of this method is that if one of the material properties needs to be established, for example longitudinal modulus of elasticity, then nine measurements are needed. In the following, this problem is addressed so that only one measurement is needed to obtain one modulus of elasticity,

Correction factors

Development of the factors

Most researchers, for example Ross et.al. (2004) and Iniguez and Bobadilla (2008), assume that by using ultrasonic longitudinal wave propagation method, moduli of elasticity can be computed using

$$E_i = \rho V_i^2 \quad (7)$$

where i = longitudinal, radial, and transversal. This is the same as assuming that $C_{11} = E_L$, $C_{22} = E_R$, and $C_{33} = E_T$. From Equations (3), (4), (5), and (6) this is clearly not true unless all Poisson's ratios are zero. In the method described below, moduli of elasticity using Eq. (7) is corrected using correction factors k_i such that

$$E_i = k_i \rho V_i^2 \quad (8)$$

to reflect the difference between moduli of elasticity (E_L , E_R , and E_T) and the first three diagonal components of the constitutive matrix (C_{11} , C_{22} , and C_{33}). The correction factors k_i is the ratio between moduli of elasticity E_i and the diagonal components of the constitutive matrix C_{ii} , i.e.

$$k_L = \frac{E_L}{C_{11}} \quad (9)$$

$$k_R = \frac{E_R}{C_{22}} \quad (10)$$

$$k_T = \frac{E_T}{C_{33}} \quad (11)$$

As seen in Equations (9), (10), and (11), the correction factors depend on all six elastic properties (three moduli of elasticity and three Poisson's ratios) of the material, and hence vary from one species to another. As an approximation, the average values from 28 species as seen in Table 1 can be utilized. The first eleven species are hardwoods and the rest are softwoods. All six elastic properties in the table are from USDA (2010). As suggested in USDA (2010), the longitudinal modulus of elasticity E_L is approximated by multiplying static bending modulus of elasticity, E_{sb} , by a factor of 1.10. The diagonal components of constitutive matrix C_{11} , C_{22} , and C_{33} in the table are computed using Equations (3), (4), and (5). Finally, the correction factors k_L , k_R , and k_T are computed using Equations (9), (10), and (11). Table 1 is an extension and an updated values of similar table found in Tjondro and Suryoatmono (2008).

Table 1 - Ratios between moduli of elasticity and diagonal components of constitutive matrix (k_L , k_R , and k_T) of 28 species with known elastic properties.

No Species	E_L MPa	E_R MPa	E_T MPa	μ_{LR}	μ_{LT}	μ_{RT}	C_{11} MPa	C_{22} MPa	C_{33} MPa	k_L	k_R	k_T
1 Ash, white	13200	1650	1056	0.371	0.440	0.684	14227	2499	1597	0.93	0.66	0.66
2 Basswood	11110	733	300	0.364	0.406	0.912	11466	1142	465	0.97	0.64	0.64
3 Birch, yellow	15290	1193	765	0.426	0.451	0.697	16176	1814	1158	0.95	0.66	0.66
4 Cherry, black	11330	2243	974	0.392	0.428	0.695	12367	3050	1305	0.92	0.74	0.75
5 Cottonwood, eastern	10340	858	486	0.344	0.420	0.875	10918	1587	897	0.95	0.54	0.54
6 Maple, sugar	13860	1836	901	0.424	0.476	0.774	15120	2795	1359	0.92	0.66	0.66
7 Maple, red	12430	1740	833	0.434	0.509	0.762	13686	2607	1236	0.91	0.67	0.67
8 Oak, red	12430	1914	1019	0.350	0.448	0.560	13219	2404	1277	0.94	0.80	0.80
9 Oak, white	7810	1273	562	0.369	0.428	0.682	8344	1689	739	0.94	0.75	0.76
10 Sweetgum	12430	1429	622	0.495	0.632	0.718	13675	1986	856	0.91	0.72	0.73
11 Yellow-poplar	11990	1103	516	0.318	0.392	0.703	12367	1470	685	0.97	0.75	0.75
12 Baldcypress	10890	915	425	0.338	0.326	0.411	11098	1007	465	0.98	0.91	0.91
13 Cedar, northern white	6050	1107	490	0.337	0.340	0.458	6319	1263	553	0.96	0.88	0.89
14 Cedar, western red	8470	686	466	0.378	0.296	0.484	8701	834	563	0.97	0.82	0.83
15 Douglas-fir	14740	1002	737	0.292	0.449	0.390	15097	1144	845	0.98	0.88	0.87
16 Fir, subalpine	9790	999	382	0.341	0.332	0.437	10006	1096	416	0.98	0.91	0.92
17 Hemlock, western	12430	721	385	0.485	0.423	0.442	12784	823	436	0.97	0.88	0.88
18 Larch, western	14190	1121	922	0.355	0.276	0.389	14519	1304	1067	0.98	0.86	0.86
19 Pine, Loblolly	13530	1529	1055	0.328	0.292	0.382	13909	1736	1192	0.97	0.88	0.89
20 Pine, Lodgepole	10120	1032	688	0.316	0.347	0.469	10430	1236	823	0.97	0.83	0.84
21 Pine, Longleaf	15070	1537	829	0.332	0.365	0.384	15468	1701	914	0.97	0.90	0.91
22 Pine, Ponderosa	9790	1194	813	0.337	0.400	0.426	10217	1403	954	0.96	0.85	0.85
23 Pine, Red	12320	1084	542	0.347	0.315	0.408	12579	1202	597	0.98	0.90	0.91
24 Pine, Slash	15070	1115	678	0.392	0.444	0.447	15552	1298	788	0.97	0.86	0.86
25 Pine, Sugar	9020	1182	785	0.356	0.349	0.428	9411	1389	917	0.96	0.85	0.86
26 Pine, Western white	11110	867	422	0.329	0.344	0.410	11313	957	464	0.98	0.91	0.91
27 Redwood	10120	880	901	0.360	0.346	0.373	10489	1053	1076	0.96	0.84	0.84
28 Spruce, Sitka	11880	927	511	0.372	0.467	0.435	12245	1056	581	0.97	0.88	0.88
									Avg.	0.96	0.80	0.80
									Std.Dev.	0.02	0.10	0.10

Discussions

As seen in Table 1, the average correction factor for longitudinal modulus of elasticity, k_L , is 0.96 with standard deviation of 0.02. This means that the coefficient of variation (c.o.v.) of k_L is only 2.43%. As seen in Figure 3, the spread of correction factors for moduli of elasticity perpendicular to the grain (radial and tangential) are larger than the spread of correction factors for modulus of elasticity parallel to the

grain. However, the coefficient of variations of k_R and k_T are only 12.87%. and 12.83%, respectively. These small values of coefficient of variations indicate that the correction factors are sufficiently accurate.

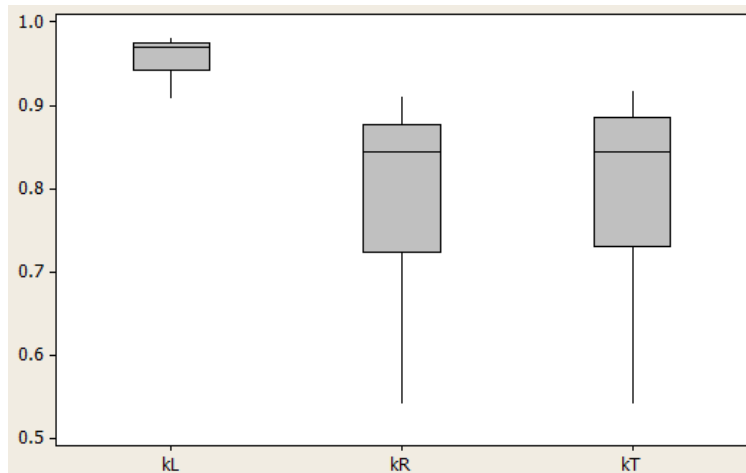


Figure 3— Boxplots of correction factors k_L , k_R , and k_T of 28 species with known material properties.

It is interesting to note that the species groups (hardwoods and softwoods) do not influence the correction factors significantly. Both groups show the same trends of correction factors, namely 0.96 for modulus of elasticity parallel to the grain and 0.80 for modulus of elasticity perpendicular to the grain.

Further investigation into Table 1 show another interesting result. Species with the smallest and largest longitudinal moduli of elasticity (Cedar, northern white and Birch, yellow) have nearly the same correction factors, namely 0.96 and 0.95, respectively. This, once again, proves that k_L of 0.96 is accurate enough.

Conclusions

A simple statistical based and relatively accurate method has been developed to estimate the moduli of elasticity of both hardwood and softwood using ultrasonic longitudinal wave. To estimate the longitudinal modulus of elasticity, the widely accepted formula in the form of the material density times the square of velocity in the longitudinal direction needs to be reduced by four percent to include the effects of all elastic properties on the predicted longitudinal modulus of elasticity. To estimate the radial and tangential moduli of elasticity, the reduction is twenty percent. It should be noted, however, that the method was developed using the average values of known mechanical properties of 28 species of hardwoods and softwoods. Therefore, there is a possibility that the reduction percentage differs from the above mentioned values.

Acknowledgments

The author wish to acknowledge the Faculty of Engineering, Parahyangan Catholic University for the financial support.

References

Bucur, V. 2006. Acoustics of Wood. 2nd Ed. Springer, New York.

Iniguez, G.; Bobadilla, I. 2008. Influence of Specimen Length on Ultrasound Wave Velocity. Proceedings of the 15th International Symposium on Nondestructive Testing of Wood. Forest Products Society. Madison, WI. 155-159

Ross, R.J. et.al. 2004. Yield and ultrasonic modulus of elasticity of red maple veneer. Forest Products Journal. 54 (12): 220-225.

Sadd, M.H. 2009. Elasticity: Theory, Applications, and Numerics. 2nd Ed. Academic Press. Burlington, MA. Chapter 11.

Tjondro, A.; Suryatmono, B. 2008. The effects of specimen dimensions on the accuracy of the determination of moduli of elasticity using ultrasonic longitudinal wave propagation method. Proceedings of 15th International Symposium on Nondestructive Testing of Wood. Forest Products Society. Madison, WI. 181-186.

U.S. Department of Agriculture, Forest Service. 2010. Wood Handbook: Wood as an Engineering Material.

Young Modulus Determination of Turkish Red Pine Wood by Destructive and Nondestructive Test Methods

Tuğba Yılmaz Aydın*

Department of Forest Industrial Engineering, Suleyman Demirel University, Isparta, Turkey,
tugbayilmaz@sdu.edu.tr

Murat Aydın

Department of Material and Material Processing, Suleyman Demirel University, Isparta, Turkey,
murataydin@sdu.edu.tr

*Corresponding author

Abstract

In this study, compression properties in L direction of Turkish red pine (*Pinus brutia* Ten.) which exposed to heat from 120 to 210°C temperature were investigated by destructive and non-destructive test methods. Test specimens, 20x20x60mm of sizes, exposed to four different temperature (120, 150, 180 and 210°C) for three different duration (2, 5 and 8hours) at atmospheric environment. Test specimens conditioned for 8 weeks at 20±1°C and 65%Rh after the heat treatment and then tests were carried out. Control specimens used for all temperature groups. Non-destructive tests were carried out by measuring of time of flight values using an ultrasonic flaw detector. Wave velocities (length/time) and E_{dyn} values were calculated from the time results obtained by ultrasound device. Compression tests were carried out using a bi-axial extensometer. Stress-strain curves obtained from compression test were used to calculate Young moduli. Results show that coefficient of determination between dynamic modulus of elasticity and static modulus of elasticity is high (R^2 : 0.94-0.82). As a result, it can be said that compression properties of Turkish red pine wood can be well predicted by using ultrasonic test method.

Keywords: Turkish red pine, young modulus, non-destructive testing, ultrasound

Introduction

Measured properties of wood material depend on some parameters such as its structure, environmental conditions, and life history of tree, and test method. These factors are especially valid for mechanical properties. It's known that lots of factor effect mechanical properties of wood. And especially moisture content (MC) and temperature, which are environmental factors, are important factors that affect wood properties. Gerhards (1982) reported that decrease of MC and temperature cause increase on mechanic properties.

Static and dynamic methods can be performed to determine mechanic properties. Elasticity modulus can be determined using compression or tension tests and is generally termed as Young's modulus. Static bending and dynamic impact strengths are two of the most effected mechanic properties from higher temperatures. Decrease depends on wood type or species and process conditions. According to Esteves and Pereira (2009) elasticity modulus shows increase at initial stages and soft processes but decrease intensive and long processes.

Material properties can be determined by static (destructive) and dynamic (non-destructive) tests. One of the main differences between these two methods is that material properties are irreversibly altered and in general tested material would not be usable anymore after the static tests but it is usable when dynamic tests are performed because almost no changes occur while performing the tests - hence, called non-destructive. That's why non-destructive tests methods are preferable for lots of applications such as cultural heritages for example wooden building. To protect cultural heritages static tests could not be performed on these structures to determine whether they are healthy or not. At this stage, importance of non-destructive test methods arises. Structures are safe when all the members are in good condition. And, structures are safe when the members behave in the limits of elastic region under real conditions. Young's modulus (E_L , E_R , E_T), shear modulus (G_{LR} , G_{LT} , G_{RT}) and Poisson's ratio (μ_{LR} , μ_{RL} , μ_{RT} , μ_{TR} , μ_{LT} , μ_{TL}) are elastic constants of wood and they determine elastic behavior of wood material.

Non-destructive testing let us know that structures or critical members of any structure and mechanic parts of systems safely function and provide cost-effective testing too. Also, invisible discontinuities in a material can be determined quite easily and quickly by NDT technics while DT may not be capable to find it. Visual inspection is one of the oldest NDT technic and still in use. Besides, optical inspection, radiography, ultrasonic, acoustic, liquid penetrant, magnetic particle and etc. are some of the modern NDT techniques. Ultrasonic is one of the most common used NDT technic. Hearmon (1965) was one of the first researchers that encourage the use of ultrasonic wave technic for elastic characterization of wood. From this date on, lots of researchers, Goncalves et al. (2011; 2014), Ozyhar et al. (2013), Kohlhauser and Hellmich (2012), Longo et al. (2012), El Mouridi et al. (2011) and Dahmen et al. (2010) were some of them, used this technic to predict some properties of wood species. Ultrasonic method can cause obtaining overestimated results. And, Dackermann et al. (2016) reported that dynamic test result is 20% greater than static test results for shear modulus determination of *Eucalyptus Maculate* and *Eucalyptus Microcorys*. Bucur (2006) ultrasonic test results of elastic parameters tests are higher than static test results.

The aim of this study was to investigate effects of high temperature on Young's modulus in L direction of Turkish red pine (*Pinus brutia* Ten) wood. To perform this aim, Young's modulus were determined by both destructive (compression test) and non-destructive (ultrasonic) ways. And, results were compared to suggest whether an ultrasonic measurement is capable to predict Young's modulus closely or not.

Material and Method

Turkish red pine (*Pinus brutia* Ten.) is one of the main commercial softwood species grown in Turkey. Turkish red pines were harvested from stand in Bucak forest region of Burdur city which is located at Mediterranean region of Turkey. Trees with straight trunk were approximately 60 years old and have average 45cm diameters. Logs were sawn into slabs and air dried to EMC. And then 22x65mm laths were obtained from these slabs' sapwood sections.

Laths were conditioned at 120, 150, 180, and 210°C temperature and 2, 5, and 8 hours in a drying oven (Nüve, FN 500, Ankara, Turkey) works in atmospheric environment. Each temperature and duration groups have their own control group and they were matched-up while cutting the laths.

20x20x60mm compression specimens were prepared after all groups, expect control ones, exposed to temperature for dedicated durations. All the samples were acclimatized at 20±1°C and %65RH for almost two months before testing.

Turkish Standard, TS 2472, used to calculate sample densities. Densities calculated by stereo-metric method that uses sample volume and mass values.

Non-destructive measurements were done by ultrasonic test technique. Two contact transducers, (A133S-RM, Olympus, Panametrics NDT, USA) that propagate 2.25 MHz longitudinal sound waves, attached to EPOCH 650 ultrasonic flaw detector (compliance with EN12668-1 2010) to measure time of flight (ToF) values. Ultrasonic sound velocities (USV) were calculated using ToF values with velocity time equation. Dynamic Young's modulus (E_{dyn}) was calculated using obtained USV with equation 1.

$$E_{dyn} = \rho V^2 10^6 \quad (1)$$

where E_{dyn} , is elasticity modulus (N/mm²), ρ , is sample density (kg/m³), and V, is ultrasonic sound propagation velocity (m/s).

Universal Test Machine (UTM, Mares, İstanbul, Turkey), 5 ton capacity, was used to perform compression tests with 6mm/min. loading speed. Stress and strain values while loading were obtained using Bi-axial extensometer (Epsilon, U.S.A.). Obtained stress and strain curves were used to calculate Young's modulus using equation 2.

$$E_i = \frac{\Delta\sigma_i}{\Delta\varepsilon_i} = \frac{\sigma_{i,2} - \sigma_{i,1}}{\varepsilon_{i,2} - \varepsilon_{i,1}} \quad i \in R \quad (2)$$

where E_i ; is Young modulus (N/mm²), σ , is stress values and ε , is strain values.

Obtained static and dynamic Young's modulus values were compared and presented using graphs.

Results and Discussion

Average density, calculated sound velocities, E_{dyn} and Young's modulus values of Turkish red pine in L direction are summarized in Table 1. Densities were affected by temperature as is seen in Table 1. In general, density values decreased while temperature and exposure duration increased. Untreated density determined as 0.50 g/cm³ while treated (210°C for 8 hours) one decreased up to 0.45 g/cm³. Untreated density of Turkish red pine wood reported as 0.53 g/cm³ by Ateş et al. (2009).

Table 1 - Density, Sound Velocity, E_{dyn} , and Young's modulus values in L direction of Turkish red pine wood

Temp. °C	Hour	Density (g/cm ³)	Velocity (m/s)		E_{dyn} (N/mm ²)		Young's Modulus (N/mm ²)	
			Mean	Cov	Mean	Cov	Mean	Cov
120	Control	0.49	5196.82	3.60	13464.68	6.99	8709.47	10.22
	2	0.49	5406.02	6.97	14455.38	7.33	9088.00	11.77
	5	0.49	5520.32	5.81	15009.34	5.58	9403.00	9.69
	8	0.48	5493.12	7.64	14829.50	4.38	9470.00	8.60
150	Control	0.50	4967.10	5.57	12482.05	4.40	8430.81	9.90
	2	0.49	5321.01	10.0	13950.08	7.18	9144.77	10.30
	5	0.48	5235.04	3.36	13624.09	6.54	9622.26	8.67
	8	0.48	4961.87	3.88	12074.37	7.50	9044.05	9.97
180	Control	0.49	5135.86	2.95	13175.01	5.36	8468.52	8.33
	2	0.48	5065.92	3.46	12424.46	6.75	8384.68	11.23
	5	0.46	5032.96	5.37	11794.86	10.11	7984.69	11.47
	8	0.45	4978.10	6.57	11555.93	9.79	7866.42	12.47
210	Control	0.50	5258.92	4.16	13929.56	6.65	8655.24	7.81
	2	0.47	5156.28	4.20	12526.28	7.96	7985.21	11.31
	5	0.46	5005.15	4.87	11781.79	9.02	7678.90	12.54
	8	0.45	4846.78	3.05	10843.19	7.01	7358.61	8.97

*cov = coefficient of variation (%)

Effect of temperature and duration on E_{dyn} in L direction is seen in Figure 1 and it is clearly seen that each temperature levels and exposure durations have effects on E_{dyn} values. E_{dyn} increased at lower and softer treatment such as 120°C for 2 and 5 hours duration but decreased a little for 8 hours exposure duration. Treatment at 150°C for 2 hours increased E_{dyn} but then decreased a bit for 5 hours and became lower than control value for 8 hours duration. E_{dyn} nearly linearly decreased at 180 and 210°C temperature treatment for all durations. Maximum increase and decrease (-22%) obtained at 120°C for 5 hours exposure duration and at 210°C for 8 hours exposure duration, respectively. Invisible micro cracks maybe occur while treatment and could affect E_{dyn} values obtained both from static and dynamic test. Beside this, some parameters such as polarization, transducer surface contact problem, used medium, measurement parameters such as selected frequency and etc. could affect the results. Llana et al. (2014) reported that a few factors, such as aforementioned, should be taken into consideration while performing non-destructive tests.

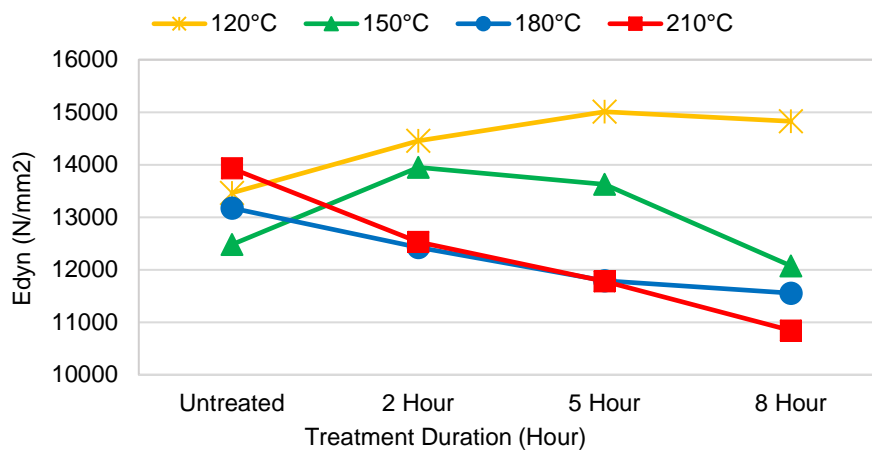


Figure 1- Effects of temperature and exposure duration on E_{dyn}

Sound velocities through L direction of Turkish red pine wood are seen in Figure 2. As it is seen in Figure 2, a significant relation between temperature and velocity was not observed. Also there is not an agreement between researchers about relation between density and sound velocity. This is because, a weak negative relation was observed by Güntekin et al. (2015), a positive relation was observed by Oliveira and Sales (2006) and Baradit and Niemz (2012), and no relation was observed by Oliveira et al. (2002), Ilic (2003) and Teles et al. (2011).

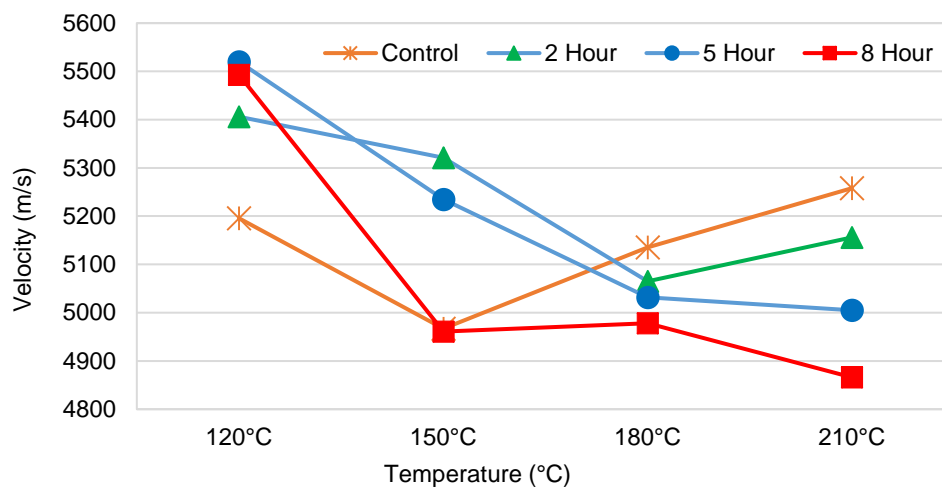


Figure 2 - Calculated L direction velocities of temperature and duration groups

Effects of temperature and exposure duration on Young's modulus are presented in Figure 3. Young's modulus increased for all exposure duration at 120°C treatment but reached maximum (8.75%) after 8 hours treatment. Young's modulus increased up to 14.13% for 5 hours exposure at 150°C and then decreased a bit below of 2 hours treatment point. But Young's modulus gradually decreased through exposure durations of 180 and 210°C treatments. Maximum decrease percentages were 7.11% and 14.98% for 180 and 210°C treatments, respectively. It's clear that some improvement on Young's modulus in L direction can be achieved up to 180°C treatment except at 150°C for 8 hours. But higher temperature and longer durations cause decreases. Young's modulus values' coefficient of variations varied between 7.81 to 12.54%.

Windeisen et al. (2008) and Taghiyari et al. (2012) reported that thermal modification slightly increased compressive stress values of poplar, beech and ash wood through L direction. This increase maybe occurs due to increase of crystallinity index of cellulose. Esteves ve Pereira (2009) stated that elasticity modulus in bending increases when short duration and low temperature heat treatment performed but decreases when long duration and high temperature heat treatment performed.

Kubojima et al. (1998) observed that Young's modulus of Sitka spruce in L and R directions increased at the beginning (first two hours) of treatment for 120, 160 and 200°C temperature groups but became constant for further durations. On the other hand, Schaffer (1970) reported that elasticity modulus dramatically affected by temperature over 225°C. According to Kubojima et al. (2000) Young's modulus increased at the beginning of heat treatment but later on decreased.

Reasons of changes on mechanic properties were reviewed by Boonstra et al. (2007) and it's mentioned that poly condensation reaction of lignin which cause inclined chord has effects essentially through longitudinal direction. And, lower equilibrium moisture content (EMC) can positively affect mechanic properties of heat treated wood but this effect unfortunately can be disabled by the degradation of chemical compounds. Also, translation of hemicellulose to volatile compounds due to degradation and vaporization of extractives are assumed as some of the essential reasons of decrease on density.

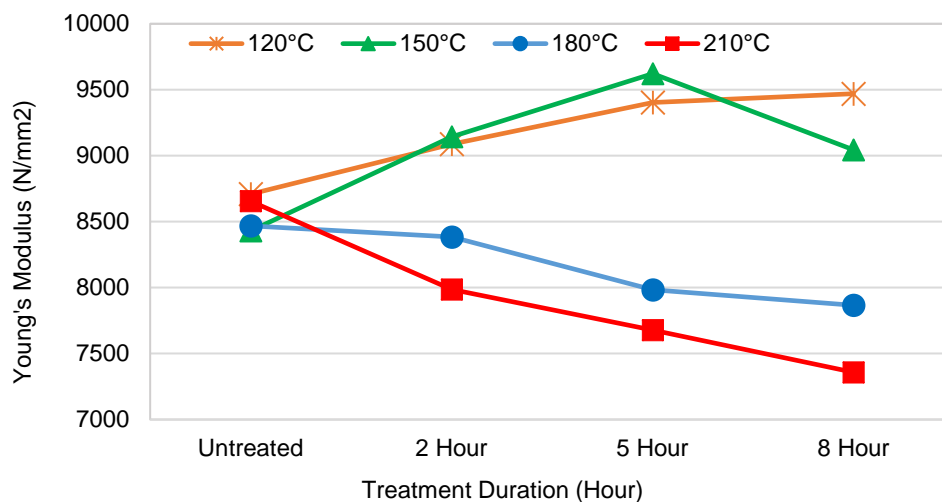


Figure 3 – Effects of temperature and duration on Young's modulus

Correlation between E_{dyn} and Young's Modulus is presented in Figure 4 and results pointed out that there is a strong relation between them. Best correlation (R^2 : 0.94) obtained between 120°C control and 180°C 8 hours groups. Minimum correlation (R^2 : 0.82) calculated between 150°C 5 hours and 210°C 8 hours groups.

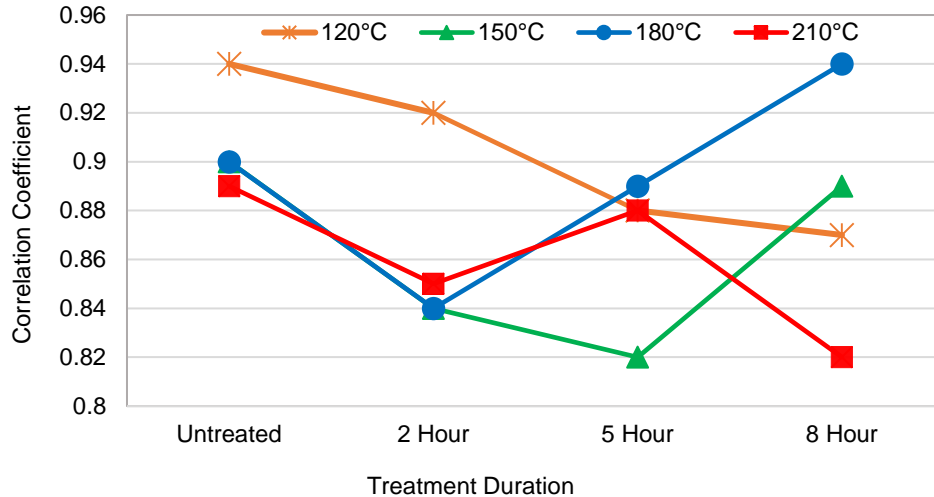


Figure 4 - Correlation between the E_{dyn} and Young's Modulus

Conclusion

It's found that temperature and exposure duration have either positive or negative effects according to treatment set-ups. Lower temperatures such as 120 and 150°C provides some incensement on Young's modulus for shorter durations but decrease observed when durations get longer. This increase may be related to low equilibrium moisture content. Up to 14.98% decrease on Young's modulus observed when temperature ad treatment duration were 210°C and 8 hours, respectively.

E_{dyn} values predicted more than Young's modulus that obtained by static test. Up to 22% decrease calculated from E_{dyn} values while temperature rose to 180 or 210°C temperature.

Very high correlation (0.82 to 0.94) is presented between Young's modulus ve E_{dyn} and results suggested that ultrasonic measurement can be used to comprehensibly predict Young's modulus.

References

- Ateş, S.; Akyildiz, M.H.; Ozdemir, H., 2009. Effects of heat treatment on Calabrian pine (*Pinus Brutia* Ten.) Wood. *Bioresources*. 4(3): 1032-1043.
- Baradit, E.; Niemz, P. 2012. Elastic constants of some native Chilean wood species using ultrasound techniques. *Wood Res*. 7(3): 497-504.
- Boonstra, M.; Van Acker, J.; Tjeerdsma, B. [and others]. 2007. Strength properties of thermally modified Softwoods and its relation to polymeric structural wood constituents. *Annals of Forest Science*. 64: 679-690.
- Bucur, V. 2006. *Acoustics of wood*. Berlin, Germany: Springer Verlag.
- Dackermann, U.; Elsener, R.; Li, J. [and others]. 2016. A comparative study of using static and ultrasonic material testing methods to determine the anisotropic material properties of wood, *Construction and Building Materials*. 102: 963-976.
- Dahmen, S.; Ketata, H.; Ben Ghazlen, M.H. [and others]. 2010. Elastic constants measurement of anisotropic Olivier wood plates using air-coupled transducers generated Lamb wave and ultrasonic bulk wave. *Ultrasonics*. 50: 502-507.

El Mouridi, M.; Laurent, T.; Brancheriau, L. [and others]. 2011. Searching for material symmetries in the burr wood of thuja by a direct contact ultrasonic method on spherical samples. *Maderas Ciencia y tecnología*. 13(3): 285-296.

EN 12668-1. 2010. Non-destructive testing - Characterization and verification of ultrasonic examination equipment - Part 1: Instruments, European Standards.

Esteves, B.M.; Pereira, H.M. 2009. Wood modification by heat treatment: A review. *BioResources*. 4(1): 370-404.

Gerhards, C.C. 1982. Effect of moisture content and temperature on the mechanical properties of wood: An analysis of immediate effects. *Wood and Fiber Science*. 14(1): 4-36.

Goncalves, R.; Trinca, A.J.; Cerri, D.G.P. 2011. Comparison of elastic constants of wood determined by ultrasonic wave propagation and static compression testing. *Wood Fiber Sci*. 43: 64-75.

Goncalves, R.; Trinca, A.J.; Pellis, B.P. 2014. Elastic constants of wood determined by ultrasound using three geometries of specimens. *Wood Sci Technol*. 48: 269–287

Güntekin, E.; Yılmaz Aydın, T.; Niemz, P. 2015. Prediction of compression properties in three orthotropic directions for some important Turkish wood species using ultrasound. *BioResources*. 10(4): 7252-7262.

Hearmon, R.F.S. 1965. The assessment of wood properties by vibrations and high frequency acoustic waves, in: symposium on nondestructive testing of wood. Pullman, WA: Washington State University. pp. 49-66.

Ilic, J. 2003. Dynamic MOE of 55 species using small wood beams. *Holz als Roh-und Werkstoff*. 61(3): 167-172.

Kohlhauser, C.; Hellmich, C. 2012. Determination of Poisson's ratios in isotropic, transversely isotropic, and orthotropic materials by means of combined ultrasonic-mechanical testing of normal stiffnesses: application to metals and wood. *Eur J Mech A-Solid*. 33: 82-98.

Kubojima, Y.; Okano, T.; Ohta, M. 1998. Vibrational properties of Sitka spruce heat-treated in Nitrogen gas. *Journal of Wood Science*. 44: 73-77.

Kubojima, Y.; Okano, T.; Ohta, M. 2000. Bending strength and toughness of heat-treated wood. *Journal of Wood Science*,.46: 8-15.

Llana, D.F.; Iñiguez-Gonzalez, G.; Arriaga, F. [and other]. 2014. Influence of temperature and moisture content on non-destructive measurements in Scots pine wood. *Wood Research*. 59 (5): 769-780.

Longo, R.; Delaunay, T.; Laux, D. [and others]. 2012. Wood elastic characterization from a single sample by resonant ultrasound spectroscopy. *Ultrasonics*. 52: 971-974.

Oliveira, F.G.R.; Campos, J.A.O.; Sales, A. 2002. Ultrasonic measurements in Brazilian hardwood. *Materials Research*. 5(1): 51-55.

Oliveira, F.G.R.; Sales, A. 2006. Relationship between density and ultrasonic velocity in Brazilian tropical woods. *Bioresource Technology*. 97(2006): 2443-2446.

Ozyhar, T.; Hering, S.; Sanabria, S.J. [and others]. 2013. Determining moisture-dependent elastic characteristics of beech wood by means of ultrasonic waves. *Wood Sci. Technol*. 47(2): 329-341

Schaffer, E.L. 1970. Elevated temperature effect on the longitudinal mechanical properties of wood. Madison, WI, USA: University of Wisconsin, Dep. Eng. Mech., Ph.D. Thesis.

Taghiyari, H.R.; Enayati, A.; Gholamiyan, H. 2012. Effects of nano silver impregnation on brittleness, physical and mechanical properties of heat treated hardwoods. *Wood Science and Technology*. 47(3): 467-480.

Teles, F.T.; Del Menezzi, C.S.; De Souza, F. [and others]. 2011. Nondestructive evaluation of a tropical hardwood: Interrelationship between methods and physical-acoustical variables. *Ciência da Madeira*. 2(1): 1-14.

TS 2472, 2005. Wood- Determination of density for physical and mechanical tests. Ankara, Turkey: Turkish Standard Institute,.

Windeisen, E.; Bachle, H.; Zimmer, B. [and others]. 2008. Relations between chemical changes and mechanical properties of thermally treated wood. *Holzforschung*. 63(6): 773-778.

Shear Modulus Determination of Black Pine Wood Using Ultrasound

Murat Aydın*

Dept. of Material and Material Processing, Suleyman Demirel University, Isparta, Turkey,
murataydin@sdu.edu.tr

Hasan Hüseyin Ciritcioğlu

Department of Woodworking Industrial Engineering, Duzce University, Duzce, Turkey,
hhciritci@gmail.com

Tuğba Yılmaz Aydın

Department of Forest Industrial Engineering, Suleyman Demirel University, Isparta, Turkey,
tugbayilmaz@sdu.edu.tr

*Corresponding author

Abstract

Shear Modulus is one of the properties of materials which determines elastic behavior of materials under loading or real conditions. Mechanic properties of wood material can be divided into two; elastic and strength properties. Shear modulus determination is a complex and difficult issue due to obtained impure values contains not only shear properties but also other values according to the used techniques. Recent developments in non-destructive testing allow us roughly determine shear modulus by using RF waves. In this study, shear modulus (G_{LR} or C_{66} , G_{LT} or C_{55} , G_{RT} or C_{44}) of Black Pine (*Pinus nigra* Arnold.) wood determined by using NDT test method. EPOCH 650 ultrasonic flaw detector and Panametrics-NDT™ V153 shear wave transducers used to carry out measurements. Olympus shear wave gel medium used to minimize the noise of transmitted and received radio frequency which propagates at 1Mhz. 65x65x65mm 20 Polyhedral samples cut from planks and then conditioned at conditioning chamber that set up 20 ± 1 C° and 65%Rh. Shear modulus in LR, LT and RT planes were calculated respectively. Determined shear modulus values of Black pine wood can be used for advanced engineering analysis of models by using computational software such as CATIA®.

Keywords: black pine, shear modulus, elastic constants, non-destructive testing

Introduction

Elastic behavior of wood can be explained by Young's modulus (E_L , E_R , E_T), shear modulus (G_{LR} , G_{LT} , G_{RT}) and Poisson's ratio (μ_{LR} , μ_{RL} , μ_{RT} , μ_{TR} , μ_{LT} , μ_{TL}). These parameters are not fully determined for some wood species and it's not easy to determine these parameters accurately especially for shear modulus. Bachtiar et al. (2017) reported that elastic parameters of wood are necessary for advanced modeling but these are often very limited. To design or built a safe and strong enough model or structure, stress-strain relation of material through the elastic region must be known. This relation, of course with other necessary parameters, lets us to conduct some analysis such as Finite Element. But input parameters vary according to material properties of model such as isotropic, anisotropic and orthotropic. According to Sadd (2014) wood is assumed as anisotropic material due to its different elastic moduli in three essential directions. Even if wood is technically anisotropic, it is usually modeled as transversely isotropic material (Miller 2001). Only five elastic constants are enough when wood modeled as isotropic and Young's modulus and Poisson ratios are one of them. But wood

should be modeled as anisotropic, especially orthotropic (2 or 3 dimensional) material to conduct real-like analysis and Shear modulus are required when wood modeled as anisotropic or orthotropic.

In literature, generally Modulus of Elasticity and Poisson's ratio on three directions determined but less known about shear modulus. Also, less data available about shear modulus of black pine (*Pinus nigra* Arnold). This softwood species is one of the most common and important commercial tree species in Turkey. From this point of view, this study tried to determine shear modulus of black pine wood using nondestructive test method.

Materials and Methods

In this study, Black pine (*Pinus nigra* Arnold.) wood, trees were harvested from Sutculer stand in Isparta which is located of the Southwest of Turkey, were used to carry out tests. Black pine logs sawn to radial and tangential planks. They were dried in open air for several months. MC values of planks were measured week by week using RAM DT 129 industrial wide range digital wood timber moisture and temperature meter. They were planed by Unimat (Michael Weinig AG, Germany) planning machine when they reached equilibrium moisture content (EMC). Then, small and defects free clear samples were cut from as outer part as these sapwood planks. First, 65x65x65mm cubic samples were prepared for density measurements of the specimens. The average wood density was measured in normal climatic conditions at 20 ± 1 C° and 65%Rh and determined as 540 kg/m³. Then, 26 surface polyhedral samples were prepared for ultrasonic measurement. As known from the literature (Goncalves et al. 2014; Vazquez et al. 2015), this sample geometry lets us carry out all tests both for principal axes and off axes (45°) on one sample. It can be said that this may provide more accurate data due to all the measurements is obtained on one sample.

Polyhedral samples were acclimatized at 65%Rh and a constant temperature of 20 ± 1 C°. Approx. 6-8 weeks later samples were ready to conduct tests. Stereo-metric method, based on volume and mass measurement of the sample, was used to determine samples densities. Each loading direction derivable from only one 26 surface Polyhedral specimen and thus 20 specimens were prepared.

Orthotropic elastic behavior of wood can be explained using Hooke's three dimensional law of elasticity which is expressed by its compliance matrix (Güntekin and Yılmaz Aydın 2016). And Shear modulus can be estimated dynamically using terms of Compliance matrix (G_{RL} or C_{66} , G_{LT} or C_{55} , G_{RT} or C_{44}) or stiffness matrix $[S]$ ($1/G_{23}$, $1/G_{13}$ and $1/G_{12}$) which is inverse of compliance matrix $[C]$ seen in equation 1.

$$[C] = \begin{bmatrix} C_{11} & C_{12} & C_{13} & 0 & 0 & 0 \\ C_{12} & C_{22} & C_{23} & 0 & 0 & 0 \\ C_{13} & C_{23} & C_{33} & 0 & 0 & 0 \\ 0 & 0 & 0 & C_{44} & 0 & 0 \\ 0 & 0 & 0 & 0 & C_{55} & 0 \\ 0 & 0 & 0 & 0 & 0 & C_{66} \end{bmatrix} \quad [S] = \begin{bmatrix} \frac{1}{E_1} & -\frac{\nu_{21}}{E_2} & -\frac{\nu_{31}}{E_3} & 0 & 0 & 0 \\ -\frac{\nu_{12}}{E_1} & \frac{1}{E_2} & -\frac{\nu_{32}}{E_3} & 0 & 0 & 0 \\ -\frac{\nu_{13}}{E_1} & -\frac{\nu_{23}}{E_2} & \frac{1}{E_3} & 0 & 0 & 0 \\ 0 & 0 & 0 & \frac{1}{G_{23}} & 0 & 0 \\ 0 & 0 & 0 & 0 & \frac{1}{G_{13}} & 0 \\ 0 & 0 & 0 & 0 & 0 & \frac{1}{G_{12}} \end{bmatrix} \quad (1)$$

where G_{ij} are the shear modulus (Bodig and Jayne 1993).

Using these matrixes, Shear moduli terms (G_{ij} or C_{ij}) of main diagonal were defined using following equations:

$$C_{44} = C_{RT} = \rho ((V_{RT} + V_{TR}) / 2)^2 10^{-6} \quad (2)$$

$$C_{55} = C_{LT} = \rho ((V_{LT} + V_{TL}) / 2)^2 10^{-6} \quad (3)$$

$$C_{66} = C_{RL} = \rho ((V_{RL} + V_{LR}) / 2)^2 10^{-6} \quad (4)$$

where G_{ij} or C_{ij} are terms of the main diagonal in the matrix or Shear modulus (N/mm²), ρ is the density of the wood (kg/m³), and V_{α} or V_{ij} is the wave velocity in the α direction (m/s).

Six shear wave velocities (V_{LR} , V_{LT} , V_{RL} , V_{RT} , V_{TL} and V_{TR}), along the principles axes of anisotropy, were measured by EPOCH 650 ultrasonic flaw detector (compliance with EN12668-1 (2010)) with using Panametrics-NDTTM V153 shear wave transducers. Olympus shear wave gel (Chemtrec, Waltham, USA) medium used to minimize the noise of transmitted and received radio frequency which propagates at 1 MHz. Also this ensured coupling of specimens and transducers while measurements performed. Transducers are pressured to specimens by a small pressure applied by hand. The tests were performed under standard climatic conditions (65%Rh, 20±1 C°).

1MHz or higher frequencies used for several previous studies to determine wood species parameters (Bucur and Archer 1984; Ozyhar et al. 2013; Goncalves et al. 2011). Because of this reason shear transducers that propagate 1MHz frequency chosen.

Results and Discussion

Average density and moisture content (MC) of the samples which acclimatized at 65% RH and a constant temperature of 20±1 C° conditions were 540 kg/m³ and 12,6% respectively.

Average density of specimens and distance between transducers through the L, R and T directions of measurements performed are presented in Table 1. Güntekin and Yılmaz Aydın (2016) determined average density of Black pine as 530 kg/m³ after same acclimatization conditions. This little difference may be occurred due to growing conditions of tree and or sampling from the slabs and laths. In literature, there is no agreement on density effects the measurements. According to Brandner et al. (2007) density, positively affects shear modulus while MC, temperature and loading direction negatively affect shear modulus of wood. Oliveira and Sales (2006) and Baradit and Niemz (2012) observed positive relation between density and sound velocity but Oliveira et al. (2002), Ilic (2003) and Teles et al. (2011) couldn't observe either positive or negative.

Table 1-Average density of samples and distance between transducers

	Density (kg/m ³)	Distance between transducers (mm)		
		L	R	T
Average	540.96	64.39	64.35	64.24
Std. Dev.	13.77	0.11	0.15	0.18
CoV*	2.54	0.17	0.23	0.28

*Coefficient of variation

Average ultrasound propagation velocities measured by NDT method are presented in Table 2. Values shown in parenthesis are the ratio between V_{LR} , V_{LT} and V_{RT} and calculated as 2.48, 2.13 and 1. All measured velocities are in the range that Bucur (2006) reported. Güntekin and Yılmaz Aydın (2016) measured V_{LT} lower then this range. This difference may be occurred due to used contact gel and or annual ring angle or slope of grain, micro-fibril angle, invisible inner faults of material, transducers orientation, plane parallelism, and measuring parameters. According to Ilic (2003) and Krauss and Kudela (2011) micro-fibril angle is one of the main factor that effect the wave propagation speed. Gerhards (1982) and Beall (2002) suggested that grain angle plays important role on propagation speed. In this study, original Olympus gel used to ensure the surface contact and minimize the noise. This may made contributions on measurements.

Table 2-Average ultrasonic wave velocities

	Wave Velocities (m/s)		
	V_{LR}	V_{LT}	V_{RT}
Average	1374.91 (2.48)	1181.45 (2.13)	554.13 (1)
Std. Dev.	83.39	45.82	32.71
CoV*	6.06	3.88	5.90
Softwoods (Bucur 2006)	1050-1630	1030-1660	298-600

*Coefficient of variation

By using velocities shown in Table 2, shear modulus in *LR*, *LT* and *RT* planes were determined as 1025.78, 755.36 and 166.34 N/mm², respectively as seen in Table 3. Values in parenthesis are ratios between G_{RT} , G_{LT} and G_{LR} . There are different ratios between G_{RT} , G_{LT} and G_{LR} in literature. Dackermann et al. (2016) reported 1/1.8/2.1 and 1/1.5/1.9 for *Eucalyptus Maculate* and *Eucalyptus Microcorys*, respectively. Bergman et al. (2010) reported this ratio as 1/3.3/4.6 for *Fraxinus americana*, *Tilia americana*, *Betula alleghaniensis*, *Prunus serotina*, *Populus deltoides*, *Acer saccharum*, *Acer rubrum*, *Liquidambar styraciflua*, *Juglans nigra* and *Liriodendron tulipifera*. For hardwood species this ratios reported as 1/2.5/3.25 (Scheer 1986). But maximum ratios were reported by Bodig and Jayne (1982) as 1/9.4/10 both for soft and hardwood species.

Bending of cell wall causes obtaining very low shear modulus values than other direction in static test (Gillis 1972) and annual rings act as a barrier for wave propagation in dynamic test (Dackerman et al. 2016). This may explain the wave propagation velocities through the principle axes of wood and according to Gillis (1972) sequence of shear modulus is $G_{LR} \approx G_{LT} > G_{RT}$. But according to Hearmon and Barkas (1941), Bodig and Goodman (1973), and Neumann (1988) Shear stiffness of wood in *LR* and *LT* planes is third or fourth times higher than in *RT* plane. And from this point of view, pith rays reduce the longitudinal shear stiffness and they may play the essential role obtaining the higher G_{LR} than G_{LT} (Brabec et al. 2017).

Table 3-Calculated shear modulus values and ratios between them.

	Shear Modulus (N/mm ²)		
	G_{RT}	G_{LT}	G_{LR}
Average	166.34 (1)	755.36 (4.54)	1025.78 (6.17)
Std. Dev.	14.92	39.03	108.16
CoV*	8.97	5.17	10.54

*Coefficient of variation

According to Koponen et al. (1991) G_{LR} , G_{LT} and G_{RT} values are between 500-1750, 510-830 and 23-85 MPa for softwoods, respectively. Hearmon (1948), Haines, (1979), and Ghelmeziu and Beldie (1972) reported shear modulus of hardwood and softwood species but they differ each other. This situation can be expressed by difficulty and complexity of shear modulus determination. Only G_{RT} (166N/mm²) is agreeing with the results of Guntekin and Yilmaz Aydın (2016). They found 159 (-4.4%), 527 (-43%), and 743 (-38%) N/mm² for G_{RT} , G_{LT} , and G_{LR} , respectively.

Hering et al (2012) and Bucur and Archer (1984) reported 1,50 and 1,43 G_{LR}/G_{LT} ratio, respectively, for beech (*Fagus sylvatica* L.) wood determined using ultrasonic wave. Guntekin et al. (2016a) calculated 1,39 and 2,06 G_{LR}/G_{LT} and G_{LT}/G_{RT} ratios for beech wood determined using ultrasonic wave, respectively. Also they reported 1,14 and 3,43 G_{LR}/G_{LT} and G_{LT}/G_{RT} ratios for oak wood, respectively. According to Bachtiar et al. (2017) G_{LR}/G_{LT} and G_{LT}/G_{RT} ratios calculated using ultrasonic measurement values are 1,4 and 3,77 for Walnut and 1,24 and 3,92 for Cherry wood, respectively. Guntekin et al. (2016b) noted 1,35 and 3,62 G_{LR}/G_{LT} and G_{LT}/G_{RT} ratios for Calabrian pine wood determined using ultrasonic wave, respectively. Also they reported 1,17 and 3,1 G_{LR}/G_{LT}

and G_{LT}/G_{RT} ratios for Cedar wood, respectively. In this study G_{LR}/G_{LT} and G_{LT}/G_{RT} ratios were calculated as 1.35 and 4.54, respectively.

Natural inhomogeneity and ill-posed problems arises from the inversion of stiffness matrix (Bachtiar et al. 2017) can cause over estimation by ultrasonic measurements. According to Bachtiar et al. (2017) influence of these problems is negligible for determination of E and G . It is suspected measurements are overestimated due to wood in-homogeneities, extractive level, annual ring and fiber orientation or angle, slope of grain, wave propagation uncertainties, geometry, ill-posed problem of the stiffness matrix and etc. But it is capable of estimating G with sufficient accuracy (Bachtiar et al. 2017).

Conclusion

Results of NDT tests are differ according to conducted methods and used material and its' properties such as shape, dimension, slope of grain, direction and etc. (Güntekin and Yılmaz Aydın, 2016). Wood material can present different properties at all due to each tree has unique properties by means of growing location and conditions.

Determination of shear modulus is complex and difficult for wood material but from results presented in this study, it can be said that ultrasonic method is capable to estimate shear modulus of wood by non-destructive way.

Elastic constants of wood such as shear modulus are important parameter for analysis such as Finite Element to design safer wooden structures. Obtained shear modulus values can be used as input parameters for analysis and contribute literature too.

Acknowledgement

This study is a part of 2016.07.01.501 project which supported by Duzce University Scientific Research Projects Coordinatorship.

References

- Bachtiar, E.V.; Sanabria, S.J.; Mitting, J.P. [and others]. 2017. Moisture-dependent elastic characteristics of walnut and cherry wood by means of mechanical and ultrasonic test incorporating three different ultrasound data evaluation techniques. *Wood Sci Technol.* 51: 47-67
- Baradit, E.; Niemz, P. 2012. Elastic constants of some native Chilean wood species using ultrasound techniques. *Wood Research.* 57(3): 497-504.
- Beall, F.C. 2002. Overview of the use of ultrasonic technologies in research on wood properties. *Wood Sci. Technol.* 36(3):197-212.
- Bergman, R.; Cai, Z.; Carll, C.G. [and others]. 2010. *Wood handbook - Wood as an engineering material.* Madison, WI: U.S. Department of Agriculture, Forest Service, Forest Products Laboratory.
- Bodig, J.; Goodman, J.R. 1973. Prediction of elastic parameters of wood. *Wood Sci.* 5: 249-264.
- Bodig, J.; Jayne, B.A. 1982. *Mechanics of wood and wood composites.* NY: Van Nostrand Reinhold Company Inc.
- Bodig, J.; Jayne, B.A. 1993. *Mechanics of wood and wood composites.* Malabar, FL: Krieger Publishing Company.

- Brabec, M.; Lagana, R.; Milch, J. [and others]. 2017. Utilization of digital image correlation in determining of both longitudinal shear moduli of wood at single torsion test. *Wood Sci, Technol.* 51: 29-45.
- Brandner, R.; Gehri, E.; Bogensperger, T. [and others]. 2007. Determination of modulus of shear and elasticity of glued laminated timber and related examinations. CIB W 18-40-12-2, Bled, Slovenia.
- Bucur, V. 2006. *Acoustics of wood*. Berlin, Germany: Springer Verlag.
- Bucur, V.; Archer, R. 1984. Elastic constants for wood by an ultrasonic method. *Wood Sci Technol.* 18(4): 255–265
- Dackermann, U.; Elsener, R.; Li, J. [and others]. 2016. A comparative study of using static and ultrasonic material testing methods to determine the anisotropic material properties of wood, *Construction and Building Materials.* 102: 963-976.
- EN 12668-1. 2010. Non-destructive testing - Characterization and verification of ultrasonic examination equipment - Part 1: Instruments, European Standards.
- Gerhards. C.C. 1982. Longitudinal stress waves for lumber stress grading: factors affecting applications. *Forest Prod. J.* 32(2): 20-25.
- Ghelmeziu, N.; Beldie, I.P. 1972. On the characteristics of resonance spruce wood. *Catgut Acoust Soc Newsl.* 17: 10-16.
- Gillis, P.P. 1972. Orthotropic elastic constants of wood. *Wood Science and Technology.* 6: 138-156.
- Goncalves, R.; Trinca, A.J.; Cerri, D.G.P. 2011. Comparison of elastic constants of wood determined by ultrasonic wave propagation and static compression testing. *Wood Fiber Sci.* 43: 64-75.
- Goncalves, R.; Trinca, A.J.; Pellis, B.P. 2014. Elastic constants of wood determined by ultrasound using three geometries of specimens. *Wood Sci Technol.* 48: 269–287
- Güntekin, E.; Yılmaz Aydın, T. 2016. Determination of elastic constants for Anatolian Black pine wood using ultrasound. *World Conference on Timber Engineering, 22-25 August, Vienna.*
- Güntekin, E.; Yılmaz Aydın, T.; Aydın, M. 2016a. Elastic constants of oriental beech (*Fagus orientalis* L.) and sessile oak (*Quercus petraea*), 2nd International Furniture Congress, 13-15 October, Muğla, Turkey.
- Güntekin, E.; Yılmaz Aydın, T.; Aydın, M. 2016b. Elastic constants of Calabrian pine and cedar, *International Forestry Symposium, 07-10 December, Kastamonu, Turkey.*
- Haines, D. 1979. On musical instrument wood. *Catgut Acoust Soc Newsl*, 1(31): 23-32
- Hearmon, R.F.S. 1948. *The elasticity of wood and plywood*. Forest Products Research Special Rep 7. H.M. Stationery Office, London, England; Department of Science and Industry Research.
- Hearmon, R.F.S.; Barkas, W.W. 1941. The effect of grain direction on Young's moduli and rigidity moduli of beech and Sitka spruce. *Proc Physc Soc.* 53: 674-680.
- Hering, S.; Keunecke, D.; Niemz, P. 2012. Moisture-dependent orthotropic elasticity of beech wood. *Wood Sci Technol.* 46: 927-938.

- Ilic, J. 2003. Dynamic MoE of 55 species using small wood beams. *Holz als Roh und Werkstoff*. 61: 167-172.
- Koponen, S.; Toratti, T.; Kanerva, P. 1991. Modelling elastic and shrinkage properties of wood based on cell structure. *Wood. Sci. Technol.* 25: 25-32.
- Krauss, A.; Kúdela, J. 2011. Ultrasonic wave propagation and Young's modulus of elasticity along the grain of Scots pine wood (*Pinus Sylvestris* L.) varying with distance from the pith. *Wood Research*. 56(4): 479- 488.
- Miller, P.H. 2001. EN 380 Notes on wood and timber as a marine material. <https://www.usna.edu/Users/naome/phmiller/courses/EN380docs/wood.doc> [Access Date: 28 March 2017].
- Neumann, A.J. 1988. Identification and evaluation of the elastic properties of solid wood depending on the moisture and anisotropy. Dresden, Germany: Dresden Technical University. M.S. thesis.
- Oliveira, F.G.R.; Sales, A. 2006. Relationship between density and ultrasonic velocity in Brazilian tropical woods. *Bioresource Technology*. 97: 2443-2446.
- Oliveira, F.G.R.; de Campos, J.A.O.; Pletz, E. [and others]. 2002. Nondestructive evaluation of wood using ultrasonic technique. *Maderas. Ciencia y tecnologia*, 4(2): 133-139.
- Ozyhar, T.; Hering, S.; Sanabria, S.J. [and others]. 2013. Determining moisture-dependent elastic characteristics of beech wood by means of ultrasonic waves. *Wood Sci. Technol.* 47(2): 329-341.
- Sadd, M.H. 2014. *Elasticity, theory, applications, and numerics*, NY, USA: Elsevier.
- Scheer, C. 1986. *Holzbau-Taschenbuch, Band 1.8. Auflage ed.* Berlin, Germany: Ernst and Sohn.
- Teles, F.T.; Del Menezzi, C.S.; de Souza, F. [and others]. 2011. Nondestructive evaluation of a tropical hardwood: Interrelationship between methods and physical-acoustical variables. *Ciência da Madeira*. 02(01): 01-14.
- Vazquez, C.; Goncalves, R.; Bertoldo, C. [and others]. M. 2015. Determination of the mechanical properties of *Castanea sativa* Mill. using ultrasonic wave propagation and comparison with static compression and bending methods. *Wood Sci Technol.* 49: 607-622.

Physical and Mechanical Characterization of Roots

Nina M. O. Cavalcanti*

Master student, Laboratory of Nondestructive Testing – LabEND, School of Agricultural Engineering - FEAGRI - University of Campinas - UNICAMP, Brazil

E-mail: nina.ocavalcanti@gmail.com

Cinthy Bertoldo

Professor, Laboratory of Nondestructive Testing - LabEND, School of Agricultural Engineering - FEAGRI - University of Campinas – UNICAMP, Brazil. E-mail: cinthya.bertoldo@feagri.unicamp.br

João Pedro O. Ferreira

Undergraduate student, Laboratory of Nondestructive Testing – LabEND, School of Agricultural Engineering - FEAGRI - University of Campinas - UNICAMP, Brazil

E-mail: j146639@dac.unicamp.br

Raquel Gonçalves

Professor, Laboratory of Nondestructive Testing – LabEND, School of Agricultural Engineering - FEAGRI - University of Campinas - UNICAMP, Brazil –

E-mail: raquel@agr.unicamp.br

* Corresponding author

Abstract

Urban forestry is extremely beneficial to the population of a city, but the weakening of individual trees, due to human interference and poor planning can lead to accidents. It makes biomechanical analyzes involving risk of falling an important assessment. Roots are organs for anchoring and balance the trees, but there are few studies that includes the wood properties of this part of the tree. The purpose of this study was to present the methodology and preliminary results of physical and acoustic characterization of wood from roots. The research was conducted in roots of six species, in which it was determined the basic density and the velocity of ultrasound wave propagation. It was verified that the methodology was able to characterize physical (basic density) and acoustically (longitudinal and radial velocities) the wood from roots and the results point to important contributions in inspections aiming analyses risk of falling through biomechanical studies.

Key words: nondestructive inspection, urban trees, ultrasound.

Introduction

The urban arboriculture provides many benefits to the population in cities, even though some irregularities exist (Silva Filho et al., 2002). One example of problems is the weakening of individuals trees because of human interferences, mostly cause by the lack of maintenance and inappropriate management. These actions can compromise tree's functional structure leading it to be more susceptible to accidents (Pereira et al., 2011).

In order to make possible using technology in tree inspections as acoustic tomography for example, it is necessary to know the physical and acoustical proprieties of wood of the whole tree, including

branches, trunk and roots. This knowledge will allow the correct interpretation of the generated images and also the appropriate use of the results in tree risk analyses using biomechanical.

However, properties of species used in urban zones rarely are available because most of urban tree species are not of interest to the civil construction, furniture and forestry sectors. Besides, even to those species of interest to some industrial sectors, the proprieties are known, in general, in equilibrium moisture content (around 12%) and not in green condition, which is the condition of a living tree.

Additionally, despite the high percentage of tree fall due to root blown-over, if some property are available or will be obtained, these properties are always from trunk and not from roots. Therefore, despite the fact that roots are fundamental organs for anchorage and stability of trees, scientific researches aiming determine the proprieties of wood from this organ are still scarce, evidencing a lack in this area of studies.

Objectives

Considering the discussed aspects, the objective of this study was to propose a methodology to obtain physical and acoustical parameters of wood from roots and present preliminary results of the application of this methodology.

Material and Methods

During a micro-bursts occurred in Campinas city on June 5, 2016, greater than 100 km/h winds provoked the broken and fall of a lot of trees. Mostly of fallen trees had their root system exposed, allowing the roots collection. There was collected samples of 6 different tree species: Tamboril (*Enterolobium contortisiliquum* (Vell.) Hauman; ingá (*Inga cf sessilis* (Vell.) Mart; Mogno (*cf Swietenia macrophylla* King); Pau d'álho (*Galesia cf integrifolia* (Spreng.) Harms; Ipê rosa (*cf Handroanthus pentaphylla*(L.) Hemsl and Aroeira salsa (*Schinus molle* L.).

The specimens collected in roots were taken after the trunk flare, where roots are submitted to higher stresses resulting from branches and trunk bending (Figure 1).



Figure 1 – Removal of root specimens.

The specimens were stored in a humid chamber to maintain the green condition until the tests. The specimens were measured to obtain the length (L) and the biggest (D) and smallest diameter (d). After measurements, the specimens were submitted to the wave propagation tests, to determine the time of wave propagation (t). The wave propagation tests were made with ultrasound (USLab, Agricef, Brazil) and 45-kHz frequency transducers with exponential tips.

The ultrasound tests were carried out in two ways: direct and indirect. The direct tests were made in longitudinal (Figure 2a) and radial directions (Figure 2b), coupling the transducers on opposite and parallel faces. The indirect tests were made with both transducers (emitter and receiver) positioned at the same surface and at 45° (Figure 2c) and distanced (L_s) from each other. Each test was repeated three times and the average of the times of wave propagation were used.

To calculate the basic density, a small cylinder was removed from each root sample with an increment borer (Figure 2d). Cylinder's volume was measured on the saturated condition (V_{sat}). After drying in an oven until reached the anhydrous condition, the cylinder was weighed again to obtain the dry mass (m₀).

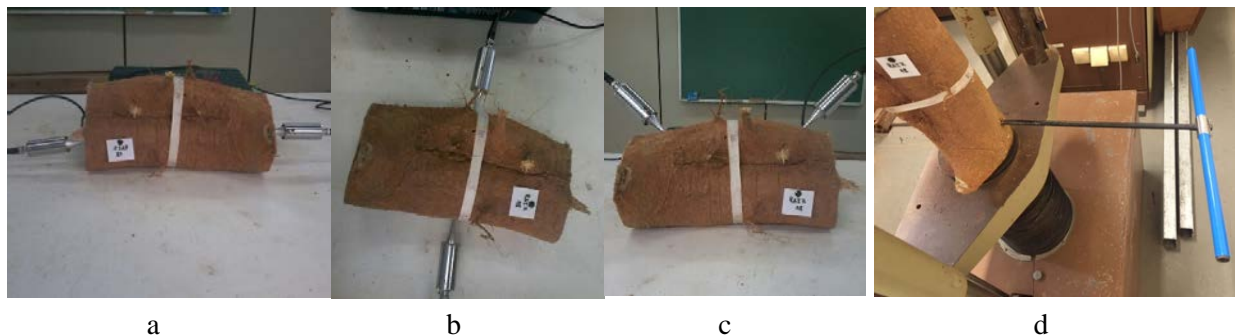


Figure 2 – Direct ultrasound test in longitudinal (a) and radial (b) directions; indirect ultrasound test (c) and withdrawal of a cylinder with increment borer (d)

With the results of ultrasound wave propagation time in all different measurements conditions and with the traveled distances, was possible to calculate the longitudinal direct velocities ($V_L = t_l/L$); radial considering the smaller diameter ($V_{Rd} = d/t_d$); radial considering the bigger diameter ($V_{RD} = D/V_D$) and the longitudinal indirect velocity ($V_S = L_S/t_S$). With the results of the dry mass and the volume on a saturated condition, the basic density was calculated ($\rho_{bas} = m_0/V_{sat}$). The longitudinal direct velocity and basic density was also used to calculate de stiffness coefficient ($C_{LL} = \rho_{bas} V_{LL}^2$). The stiffness coefficient is calculated with apparent density (in general at equilibrium moisture content), but as we are using green condition we decide use basic density.

Results

Velocities had variation among species (Table 1) indicating that its wood have stiffness variation, as showed by the great variation of the stiffness coefficient among species (Table 1). This result show the importance of knowledge properties of roots to use in biomechanical analyses. Ipê Rosa present the greatest stiffness coefficient (5396 MPa) while Aroeira Salsa the smallest (1848 MPa). This difference in stiffness certainly will reflect in differences in capacity to resist hard winds.

Statistical analysis shows that radial velocities considering the smaller and bigger diameter has no differences (Table 1) and are smaller than Longitudinal velocities obtained directly or indirectly

(Figure 3). This result indicates that in field tests the measurement can be conducted on the possible or convenient radial position and that indirect measurement can be used, as the direct is not possible in field conditions.

Table - 1 Average velocities measured directly in longitudinal direction (V_L) and in radial direction on smaller (V_{Rd}) and bigger diameter (V_{RD}) and average velocity in indirect measurement (V_S); basic density (ρ_{bas}) and stiffness coefficient (C_{LL}) of roots.

Species	V_L	V_S	V_{RD}	V_{Rd}	ρ_{bas}	C_{LL}
Tamboril	2896	2649	1446	1435	300	2516
Ingá	2916	2941	1829	1874	450	3826
Mogno	3317	3831	1494	1533	290	3191
Pau d' alho 1	2680	2491	1352	1373	380	2729
Ipê rosa	3502	3931	2155	2232	440	5396
Aroeira salsa 1	2235	2105	1648	1657	370	1848
Average among species*	2924 (15.5%)	2991 (24.8%)	1654 (18.0%)	1684 (19.1%)	372 (18.1%)	3251 (38.2%)
Velocity variation among species	57%	87%	59%	63%	55%	192%

*values in parenthesis are the coefficient of variation

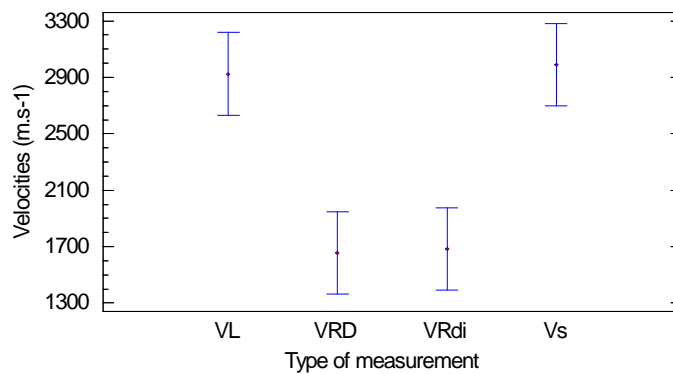


Figure 3. Means velocity plot considering the types of measurement

Legend: velocity in direct measurement in longitudinal (V_L) and in radial direction on smaller (V_{Rd}) and bigger diameter (V_{RD}) and in indirect measurement (V_S)

There are a statistic correlation between velocities obtained in direct and indirect measurements (Figure 4) that is also an important result considering the practical point of view because in field the inspections only can be done on the indirect way.

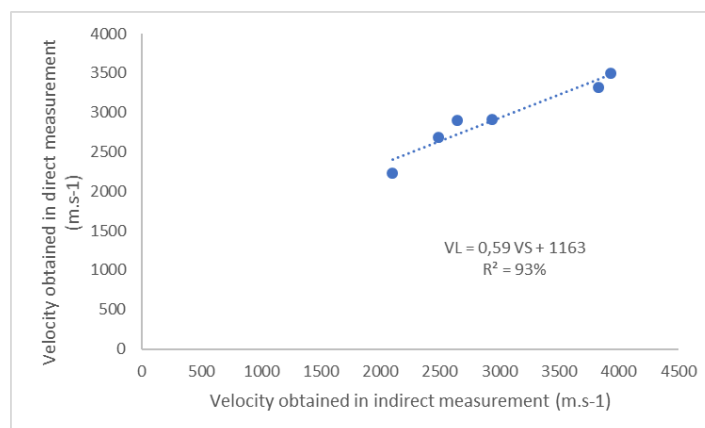


Figure - 4 Correlation between longitudinal velocities obtained direct (V_L) and indirect (V_S)

Conclusions

Even though these are preliminary results, it is verified the viability of the methodology to determine the physical and acoustical properties of wood from roots. The results allows verify that there are variation among velocities and stiffness between roots from different species. Velocities obtained directly in radial direction are statistically equivalent in greater or smaller diameter and longitudinal velocities obtained indirectly was equivalent to that obtained indirectly validating the indirect tests possible in field conditions. The indirect velocities can also be correlated with direct velocities in longitudinal directions.

The next challenge is obtaining the complete characterization (obtaining the 12 elastic constants) of wood from roots using ultrasound technology and also obtaining some static parameters (modulus of elasticity and Poisson ratio) in compression test using root samples.

Acknowledgments

The authors are grateful to FAPESP (Proc. 2015/05692-3) for the financial support and MEC/CAPES and CNPq for granting scholarships to the Master and undergraduate students.

References

- PEREIRA, P. H.; TOPANOTTI, L. R.; DALLACORT, S.; DA MOTA, C. J. BRUN, G. K.; SILVA, R. T. L. Estudo de caso do risco de queda de árvores urbanas em via pública na cidade de Dois Vizinhos-PR. *Synergismus scyentifica*, Dois Vizinhos, v.6 (1), 2011.
- SILVA FILHO, D. F.; PIZETTA, U. C.; DE ALMEIDA, J. B. S. A.; PIVETTA, K. F. L.; FERRAUDO, A. S. Banco de dados relacional para cadastro, avaliação e manejo da arborização urbana em vias públicas. **Revista Árvore**, Viçosa, v.26 (5), p.629-642, 2002.

Determination of Compression Properties in Radial Direction of Oriental Beech Exposed to Temperature Using Ultrasound and Static Tests

Tuğba Yılmaz Aydın*

Department of Forest Industrial Engineering, Suleyman Demirel University, Isparta, Turkey,
tugbayilmaz@sdu.edu.tr

Murat Aydın

Department of Material and Material Processing, Suleyman Demirel University, Isparta, Turkey,
murataydin@sdu.edu.tr

*Corresponding author

Abstract

Due to its orthotropic nature wood has different mechanic properties through all principle axes. In this study compression properties of Oriental beech (*Fagus orientalis* Lipsky.) in R direction were determined both destructive and non-destructive methods. Study conducted at four different temperature levels (120, 150, 180 and 210°C) and duration of 2, 5 and 8 hours in atmospheric condition. Nüve FN500 (Ankara, Turkey) was used to conduct heat treatment. Each temperature level has its control groups consist of at least 15 samples. After exposure period, all the samples were acclimatized at 65% Rh and a constant temperature of $20\pm 1^\circ\text{C}$ for at least two months. And then test were performed. 20x20x60 mm samples were used for compression test (CT). Strain values which occurred while testing were obtained using bi-axial extensometer and static Young Modulus was calculated using obtained stress-strain curves. Wave velocities and consequently *Edyn* were calculated with time of flight values which were obtained using ultrasonic flaw detector. Results presented in this study show that coefficient of determination between static modulus of elasticity and dynamic modulus of elasticity varied between 0,84 to 0,94. As a conclusion, it can be said that compression properties of wood, exposed to temperature, in R direction can be well estimated using ultrasonic method.

Keywords: Oriental beech, young modulus, ultrasound, radial direction

Introduction

Wood structure and mechanical properties of wood must be known to utilize wood as a structural building material. Wood has a complex and hierarchical structure. And this complexity strongly affects its mechanical behavior (Ozyhar 2013). In general and technically wood is an-isotropic material and in furtherance Sadd (2014) noted that it is an-isotropic because of it has different elastic moduli in three principal directions (L, R and T). And it can be said that there is a lack of knowledge about mechanical properties of wood especially for R and T directions due to insufficient experimental studies. This study aims to contribute the literature by putting forward some properties of Oriental beech (*Fagus orientalis* Lipsky.) for R direction.

Generally, some mechanical properties of wood decrease while material exposed to temperature or heated and increase while exposed to lower temperature or cooled. Mechanic properties have nearly linear relationship with temperature if the moisture content is constant and temperature is under 150°C (Kretschmann 2010). From this point of view this study focused on four different temperature (120, 150, 180 and 210°C) and a control group to identify the effects of temperature on R direction properties.

Non-destructive evaluation (NDE) is used to determine material properties and let users to make correct decision about usage and maintenance of material (Pellerin and Ross 2002). Performing a non-destructive test is easier than a destructive one but some parameters can affect and alter the results while evaluation is in progress and this important point must be taken into consideration to conduct a non-destructive test (NDT) (Llana et al. 2014).

There are lots of ways to perform a NDT to determine properties of materials such as metals, plastics, ceramics, and natural composites such as wood. It can be used to detect and identify cracks, delamination, decays, knots, internal faults and etc. without destructing the material. Visual inspection is the oldest NDT technic and in use. It causes a loss of time and requires labor force but also has high error ratio. Microscopy, radiography, liquid penetrant inspection, ultrasonic, and acoustic are some of the commonly used modern NDT techniques. Ultrasonic technic is performed for lots of applications (Wang et al. 2004) and according to Esteban et al. (2009) it is advantageous than the other techniques. But ultrasonic technic has some limitations such as transmission of the sound waves through the material. Therefore tested material must be suitable for sound transmission. In this sense, wood material is not easy as other materials that have homogeny structure due to its orthotropic nature.

Elastic properties are important for designing structural wooden members. These properties can be determined both destructive and non-destructive ways. But, use of non-destructive test methods to determine some properties of wood increases day by day.

Studies concerns with elastic properties through L direction of wood material that exposed to temperature are common in literature but studies that concern with perpendiculars (R and T directions) are limited. Extensive characterization of elastic properties related with temperature still inadequate for lots of species and lack for Oriental beech (*Fagus orientalis* Lipsky.). This study tried to find out effects of temperature on Young's modulus values in R direction of Oriental beech wood by performing compression test and ultrasonic test.

Material and Method

Oriental beech (*Fagus orientalis* Lipsky.) trees, approx. 140 years old and average 50cm diameter, were harvested from Devrek forest zone that located in Black sea region of Turkey. Logs were sawn into lumber and then radial and tangential planks were obtained from them. 22x65mm laths were cut using these planks.

Air-dried radial laths were conditioned at 120, 150, 180, and 210°C temperature and 2, 5, and 8 hours in a drying oven (Nüve, FN 500, Ankara, Turkey). After this treatment, 20x20x60mm compression specimens were prepared. Control groups were not exposed to any temperature and all the samples were acclimatized at 20±1°C and %65RH for around two months before testing.

Densities of samples were determined according to TS 2472 using stereo-metric method which uses sample volume and mass values.

Olympus EPOCH 650 ultrasonic flaw detector used to perform non-destructive test. Time of flight (ToF) values was obtained by A133S-RM contact transducers using 2.25MHz frequency. This transducer has longitudinal wave propagation. Ultrasonic sound velocities (USV) were calculated using ToF values with velocity time equation. Dynamic Young's modulus (E_{dyn}) was calculated using these USV with equation 1.

$$E_{dyn} = \rho V^2 10^6 \quad (1)$$

where E_{dyn} , is elasticity modulus (N/mm²), ρ , is sample density (kg/m³), and V, is ultrasonic sound propagation velocity (m/s).

Compression tests were conducted using 5 ton capacity universal test machine (UTM, Mares, Istanbul, Turkey). Loading speed was 6mm/min. Bi-axial extensometer (Epsilon, U.S.A.) was used to obtain stress and strain values and Young's modulus calculated using these values. Young's modulus was calculated using equation 2.

$$E_i = \frac{\Delta\sigma_i}{\Delta\varepsilon_i} = \frac{\sigma_{i,2} - \sigma_{i,1}}{\varepsilon_{i,2} - \varepsilon_{i,1}} \quad i \in R \quad (2)$$

where E_i is Young modulus (N/mm²), σ , is stress values and ε , is strain values.

Results and Discussion

Average density, sound velocity (V), E_{dyn} and Young's modulus values of beech wood in R direction are presented in Table 1. As seen in table, in general, density decreased while temperature and duration increased. Density of the control groups was between 0.70-0.69 g/cm³ and but decreased up to 0.65 g/cm³ by increase of temperature and exposure duration. Maximum decrease occurred at 210 °C temperature and 8 hours exposure conditions. Efe and Çağatay (2011) reported the density of untreated oriental beech wood as 0.71 g/cm³.

Temperature and duration effect on Young's modulus (E_R) of oriental beech wood in R direction is seen in Figure 1. Young's modulus values were increased up to 9.25% and 4.97% at 120°C and 150°C temperature for 8 and 5 hours exposure durations respectively but decreased at 150°C temperature for 8 hours exposure duration. In contrast with 120°C and 150°C groups, Young's modulus (E_R) values were decreased up to 8.86% and 18.35% at 180°C and 210°C temperature treatment for all durations respectively. According to Holecek et al. (2017) an increment on elasticity modulus occurred firstly by the increase of temperature but then decrease observed for heat treated Spruce wood.

Boonstra et al. (2007) stated that lower equilibrium moisture content (EMC) can positively affect mechanic properties of heat treated wood but this effect unfortunately can be disabled by the degradation of chemical compounds. Degradation of hemicellulose, while temperature and exposure duration increases, is supposed to be the main reason of decrease on mechanic properties (Boonstra et al. 2007). According to Hillis (1984) weakest heat resistant wood polymer is hemicellulose. Hemicellulose which is in S1 and S3 layers has significant effects on mechanic properties in R direction of wood. Cellulose micro-fibrils are mostly related with mechanic properties in L direction (Bergander and Salen, 2002). Also, Esteves and Pereira (2009) stated that micro cracks which occurs while heat treatment can effect mechanic properties.

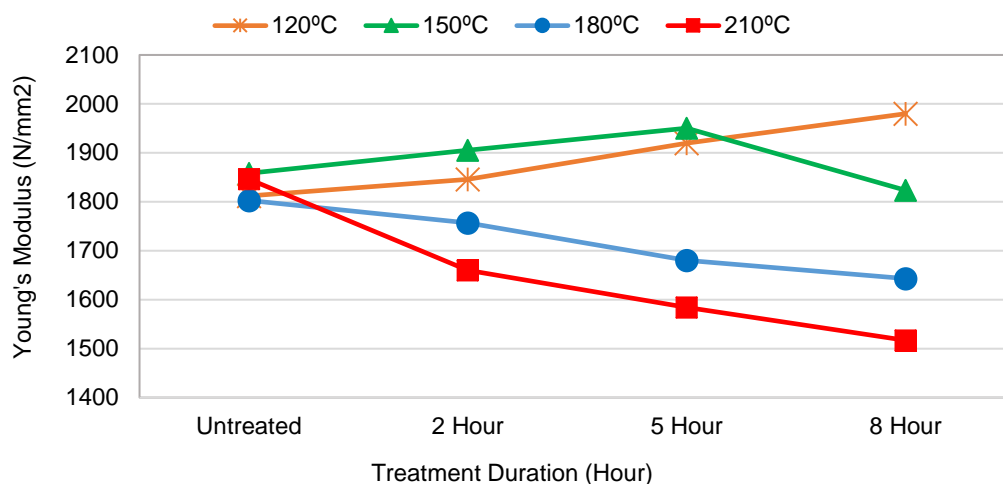


Figure 1 - Effect of temperature and exposure duration on Young's modulus in R direction

Temperature and exposure duration effect on E_{dyn} in R direction is seen in Figure 2. It is seen that all temperature and duration levels have effects on E_{dyn} . A little increase observed at 120°C temperature. A significant increase observed for 2 and 5 hours treatment at 150°C and then decrease observed for 8 hours exposure duration but not till control values. Nearly linear decrease observed for 180 and 210°C temperature treatment for all exposure durations except 180°C and 8 hours.

Density decreased while temperature increased. A significant relation between sound velocity and density not observed. There is a contradiction about whether sound velocity is related with wood material density or not when literature reviewed. Oliveira and Sales (2006) and Baradit and Niemz (2012) stated that there is positive relation between density and velocity but Oliveira et al. (2002), Ilic (2003) and Teles et al. (2011) reported no relation between them.

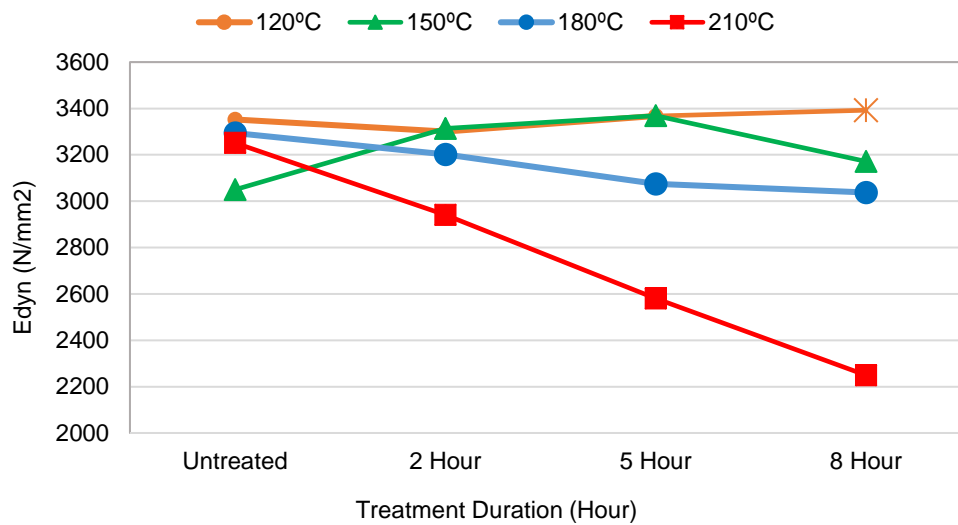


Figure 2 - Effect of temperature and exposure duration on E_{dyn} in R direction

Table 1- Density, Sound Velocity, E_{dyn} , and Young’s modulus values in R direction of beech wood

Temp. °C	Hour	Density (g/cm ³)	Velocity (m/s)		E_{dyn} (N/mm ²)		Young’s modulus (N/mm ²)	
			Mean	Cov	Mean	Cov	Mean	Cov
120	Control	0.70	2165.97	2.29	3353.01	4.38	1812	8.84
	2	0.69	2185.85	5.77	3300.43	7.49	1846	8.36
	5	0.69	2208.11	3.54	3367.27	5.73	1920	10.65
	8	0.69	2207.47	4.01	3392.47	5.72	1980	7.76
150	Control	0.69	2176.79	2.75	3049.79	6.67	1858.12	8.43
	2	0.68	2205.98	6.38	3313.23	7.83	1905.28	6.92
	5	0.68	2225.79	2.83	3368.99	4.61	1950.44	8.76
	8	0.67	2175.18	3.55	3171.56	4.13	1823.46	9.62
180	Control	0.69	2135.58	5.53	3293.81	8.57	1802.73	7.94
	2	0.68	2175.03	2.25	3201.69	4.43	1757.18	8.16
	5	0.67	2138.27	4.66	3074.31	6.95	1680.45	9.91
	8	0.67	2125.88	3.40	3037.52	6.67	1643.08	11.64
210	Control	0.70	2137.05	2.09	3251.12	4.64	1846.24	8.40
	2	0.68	2079.18	3.15	2940.63	6.10	1660.14	9.36
	5	0.67	1960.31	7.34	2580.01	8.18	1584.45	9.02
	8	0.65	1855.08	4.25	2249.34	8.09	1516.90	13.18

*cov = coefficient of variation (%)

Correlation (R^2) between E_{dyn} and Young’s modulus values is seen in Figure 3 and it is seen that there is a very strong relation between them. Best correlation (R^2 : 0.94) seen between control groups of 150

and 210°C temperature. Weakest correlation (R^2 : 0.84) seen between 180 and 210°C temperature and 2 and 8 hours exposure durations, respectively.

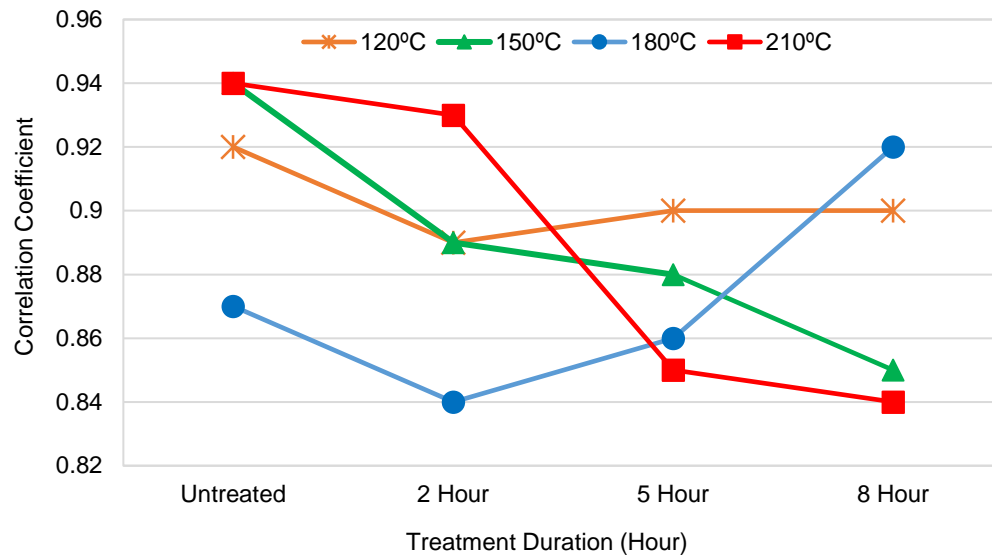


Figure 3 - Correlation between the E_{dyn} and Young's modulus

Conclusion

It is seen that temperature and exposure duration have effects on Young's modulus and E_{dyn} in R direction. In general, lower temperature (120 and 150°C) treatment caused some increase on Young's modulus values but following temperature levels (180 and 210°C) caused decrease on Young's modulus values. Also increase of exposure duration caused decrease on Young's modulus values.

Ultrasonic test results matched well with static results and thus it can be said that ultrasonic test method can be used to predict R direction Young's modulus values of wood material.

Very high correlations (0.84 to 0.94) were observed between Young's modulus and E_{dyn} values.

References

- Baradit, E.; Niemz, P. 2012. Elastic constants of some native Chilean wood species using ultrasound techniques. *Wood Res.* 7(3): 497-504.
- Bergander, A.; Salmen, L. 2002. Cell wall properties and their effects on the mechanical properties of fibers. *Journal of Materials Science.* 37: 151-156.
- Boonstra, M.; Van Acker, J.; Tjeerdsma, B.; [and others]. 2007. Strength properties of thermally modified Softwoods and its relation to polymeric structural wood constituents. *Annals of Forest Science*, 64: 679-690.
- Efe, H.; Çağatay, K. 2011. Determination of some physical and mechanical properties of various wood materials. *Journal of Polytechnic.* 14(1): 55-61.
- Esteban, L.G.; Fernandez, F.G.; De Palacios, P. 2009. MOE prediction in *Abies pinsapo* Boiss. timber: Application of an artificial neural network using nondestructive testing. *Comput. Struct.* 87(2009): 1360-1365.

- Esteves, B.M.; Pereira, H.M. 2009. Wood Modification by Heat Treatment: A Review. *BioResources*. 4(1): 370-404.
- Hillis, W.E. 1984. High-temperature and chemical effects on wood stability. Part 1. General considerations. *Wood Science and Technology*. 18: 281-293.
- Holeček, T.; Gašparík, M.; Lagaňa, R. [and others]. 2017. Measuring the Modulus of Elasticity of thermally treated Spruce wood using the ultrasound and resonance methods. *BioResources*. 12(1): 819-838.
- Ilic, J. 2003. Dynamic MOE of 55 species using small wood beams. *Holz als Roh-und Werkstoff*. 61(3): 167-172.
- Kretschmann, D.E. 2010. Wood handbook, wood as engineering material. Gen. Tech. Rep. FPL-GTR-190. Madison, WI: U.S. Department of Agriculture, Forest Service, Forest Products Laboratory.
- Llana, D.F.; Iñiguez-Gonzalez, G.; Arriaga, F. [and other]. 2014. Influence of temperature and moisture content on non-destructive measurements in Scots pine wood. *Wood Research*. 59 (5): 769-780.
- Oliveira, F.G.R.; Campos, J.A.O.; Sales, A. 2002. Ultrasonic measurements in Brazilian hardwood. *Materials Research*. 5(1): 51-55.
- Oliveira, F.G.R.; Sales, A. 2006. Relationship between density and ultrasonic velocity in Brazilian tropical woods. *Bioresource Technology*. 97(2006): 2443-2446.
- Ozyhar, T. 2013. Moisture and time-dependent orthotropic mechanical characterization of Beech Wood. Zurich, Switzerland: Swiss Federal Institute of Technology. 150 p. Ph.D. Thesis.
- Pellerin, R.F.; Ross, R.J. 2002. *Nondestructive evaluation of wood*. Madison, WI: Forest Products Society.
- Sadd, M.H. 2014. *Elasticity, theory, applications, and numerics*, NY, USA: Elsevier.
- Teles, F.T.; Del Menezzi, C.S.; De Souza, F. [and others]. 2011. Nondestructive evaluation of a tropical hardwood: Interrelationship between methods and physical-acoustical variables. *Ciência da Madeira*. 2(1): 1-14.
- TS 2472, 2005. *Wood- Determination of density for physical and mechanical tests*. Ankara, Turkey: Turkish Standard Institute.
- Wang, X.; Divos, F.; Pilon, C. [and others]. 2004. Assessment of decay in standing timber using stress wave timing nondestructive evaluation tools. Tech. Rep. 147. Madison, WI : U.S. Department of Agriculture, Forest Products Laboratory.



Session 7

**Urban Tree Defect
Assessment and
Risk Analysis II**

Development of Bioacoustic Nondestructive Testing Instruments for Early Detection of Bark Beetle Infestation

Richard Bruce Allison

Forest and Wildlife Ecology Department, University of Wisconsin-Madison

Abstract

Damage to trees from bark beetle attack presents an economic and aesthetic cost affecting forest crops and urban forest landscapes. Bioacoustic sensors have been used to nondestructively test for insect activity in wood and standing trees. Advancing technology and electronic component cost reductions for acoustic emission monitoring sensors provide the opportunity to develop tools to eavesdrop on the sounds generated by bark beetles hidden within trees.

Keywords: Bark beetle detection, bioacoustic sensors, nondestructive testing

Damage to trees from bark beetle attack presents an economic and aesthetic cost affecting forest crops and urban forest landscapes. In many cases early detection offers the option of therapeutic treatments. Though concealed from view under the tree bark, the sounds generated by larvae feeding, insect movement and stridulation provide telltale indications of bark beetle presence. Acoustic emission (AE) as defined by Eitzen and Wadley (1984) of the National Bureau of Standards is “the transient mechanical waves spontaneously generated by abrupt localized changes of strain within a body” They continue, “the surface motion due to an AE source contains information about both the location and characteristics of the source.” Various sensors have been used for many years in industry to gather AE information. In the biological sciences, researchers have examined acoustic emissions from sources as varied as birds, marine life, mammals and insects. This area of study is bioacoustics. Bioacoustic sensors have been used to nondestructively test for insect activity in wood and standing trees. Advancing technology and electronic component cost reductions for acoustic emission monitoring sensors provide the opportunity to develop tools to eavesdrop on the very low amplitude sounds generated by bark beetles hidden within trees.

In a review of advances in insect acoustic detection and monitoring, Mankin (2011) points out that insect predators and parasitoids have always been eavesdropping on insect communications, feeding and movement sounds and vibrations to locate prey and hosts. Articles as early as 1909 (Main 1909) have been published on acoustic detection of termites and many since (Fujii et al. 1990; Lemaster et al. 1997; Mankin et al. 2002; Yanase et al. 1998, 2000). Several researchers have recently focused on the use of bioacoustic sensors for early detection of the red palm weevil (Hetzroni et al. 2016; Hussein et al. 2010; Mukhtar et al. 2011; Dosunmu et al. 2014, Potamitis et al. 2008), an invasive from Southeast Asia attacking the historically important date palm in the Middle East. Other insects have been the subject of bioacoustic researchers (Cross and Thomas 1978; Haack et al. 1988; Mankin et al. 2008; Mankin 2011; Osbrink 2013; Siriwardena et al. 2010) including serious bark beetle pests of pine bark beetle (Hofstetter et al 2014) and emerald ash borer (McCullough 2016). When the Asian long horn beetle attacked trees in Central Park,

New York City, the USDA through Oak Ridge Laboratories developed piezoelectric sensor instruments as detection tools (Smith and Poland 2001). Mankin in his review states that even though the understanding of insect acoustical and vibrational communication has advanced the development and adoption of simple to use monitoring tools has lagged in part for the following reasons:

1. “limited understanding of acoustic signal attenuation across various substrates,”
2. “difficulties in interpreting weak insect signals in environments with high background noise,”
3. “limited knowledge of the behaviors of the cryptic targeted species that produce the signals”
4. “the small market for insect detection instrumentation.”

Attenuation is the gradual loss of signal magnitude as a wave moves through a substrate. This is caused by absorption of the signal within the substrate, reflections at interfaces or dilution as the wave passes into a larger volume area. Within a wood substrate reflection is a significant factor when the signal moves across the wood fiber versus along the wood fiber. The attenuation coefficient, the rate of signal decay per unit distance, is approximately 2-5 times greater along the wood fiber than across it (Lemaster et al. 1997; Yanase et al. 2000). Wood has a low attenuation coefficient and thus is a good substrate for acoustic detection of insect activity. The area of detection, known as the active space, is greater in low frequency sounds than ultrasound (greater than 20KHz). Scheffrahn et al. (1993) detected termite high frequency sounds in an active space up to 2.2 m in wood. Mankin et al. (2011) detected some of the louder low frequency sounds of the red palm weevil over 4 m below the insects.

Of equal significance to the gathering of acoustic signals is the interpretation of the signal. Signal analysis requires not only being able to identify the unique insect sound but also differentiating the sound of the insects from background noise. Trained listeners can identify specific insect sounds but automated processing using software to sift through multiple sounds looking for the programmed specified wave characteristics is available as is newer voice recognition software (Chesmore and Schofield 2010; Pinhas et al. 2008; Potamis 2009; Watanabe et al. 2016)

The understanding of the behavior of certain bark beetles, specifically emerald ash borer and pine bark beetles, has increased significantly as a result of the intense research conducted in response to the unprecedented damage being done to the western forest crop and the urban forest landscape. It is not an exaggeration to say that the outbreak of pine bark beetles in the Western United States is the greatest in recorded fossil history and the invasion of Emerald Ash Borer in the Midwest United States rivals Dutch elm disease in the cost and disruption to the urban forest. Hofstetter et al (2014) propose acoustic methods to not only detect pine bark beetles but also use sounds imitating insect communication to dissuade insect infestation within forests (Aflitto and Hofstetter 2014). Professor Deborah McCullough at Michigan State University is actively researching acoustic detection and deterrence methods for Emerald Ash Borer (McCullough 2016). Increase in the global distribution of wood products has also stimulated an interest in the effective use of acoustic monitoring by national border regulators to avoid the importation of wood damaging insects (Brandstetter and Hubner 2015; Chesmore 2008; Schofield and Chesmore 2008).

The current small market available to developers of bioacoustic sensing instruments has not deterred some scientists from a thorough investigation into optimum sensor instruments (Scheffrahn et al 1993; Fiala et al. 2014; Hyvernaud et al. 1996; Mankin et al. 1996; Zahid et al. 2012; Rach et al. 2012; Wiest et al. 1996). Liu (2017) in a recent review of available technologies describes various instruments used as acoustic sensors. Accelerometers and

piezoelectric sensors characterize vibration by measuring the acceleration of the substrates on which they are attached. Accelerometers can sense impact or vibration in one, two or three axes. Martin et al. (2013) using an accelerometer (MEMS MMA 7361, Fujitsu, Japan) was able to detect small larvae in palm trees. Piezoelectric sensors are composed of piezoelectric crystals having the ability to convert mechanical stress into an electric charge. By compressing or pulling the crystal charges are built up on opposite faces generating a current that can be measured between the faces. Sound waves or vibration is thus measured by a transform from acoustic signal to an electric signal (Janshoff et al. 2007). Kuroda (2012) observes that even physiological activity within the tree such as xylem embolism can be monitored by acoustic emission.

Microphones provide impact acoustic (IA) measurement of an acoustic signal (sound) striking a material like a metal plate or membrane. They can either be in contact with the substrate of interest or in non-contact. Mankin et al. (2011) observes that microphones do not interface well with wood or other solid materials and that accelerometers or piezoelectric generate superior results.

Another method of measuring vibration coming from insect activity in wood is the laser Doppler vibrometer (LDV). It has proved highly sensitive with the advantage of non-contact measurements (Zorovic and Cokl 2015). The cost however makes it currently prohibitive for common field applications. An inquiry to Polytec, Inc. USA, the manufacturer of the LDV (PVD-100) used in the Zorovic experiment, revealed a retail price of \$40, 000 and a weekly rental of \$1,500.

Two bioacoustic sensing instruments were developed with the assistance of an acoustic engineer in the University of Wisconsin School of Computer and Electrical Engineering. The first consists of an electret microphone and enclosed metal probe, specially designed amplifier that can drive headphones. The second has a uniaxial accelerometer (MEMS) attached to a scratch awl to be lightly hammered into the white wood, and a similar amplifier that can drive a headphone. The microphone has a frequency response range equal to the human hearing range of 20 Hz to 20 KHz. The accelerometer has a more limited frequency response range of 1 Hz to 2.5 KHz. Tests were conducted in August on ash trees in Madison, WI infested with Emerald Ash Borer. Both instruments were able to detect the pulsed clicking sound of the mandibles as the larvae were feeding below the bark.

These instruments were developed building on ideas from published research papers and consist of low cost components making them economical and available for general use by tree care professionals and scientists. Further development efforts are required on these instruments to provide recording and signal analysis making one or both of them adequate for field use in detection of a variety of bark beetles and other wood infesting insects.

References

- Aflitto, N.C., Hofstetter, R.W. 2014. Use of acoustics to deter bark beetles from entering tree material. *Pest Management Science* 70 (12), pp. 1808-1814.
- Brandstetter, M.; Huebner, S. 2015. Bioacoustics – a method to detect wood-boring insect. *Waldwissen* author translation of article in *Fortschutz aktuell*; 60-61; 31-36.
- Chesmore, D. and J. Schofield. 2010. Acoustic detection of regulated pests in hardwood

materials. EPPO/OEPP Bulletin 40:46-51.

Chesmore, D. 2008. Automated bioacoustic identification of insects for phytosanitary and ecological application. In: Frommolt K.H., Bardeli R. and Clasen M (Eds.) Computational Bioacoustics for Assessing Biodiversity. BfN-scripts Nr. 234:59-72.

Cross, D. J. and R. S. Thomas. 1978. An acoustic amplifier and activity integrator for laboratory studies on wood borer. *Laboratory Practice* 27: 567-569.

Dosunmu, O.G., Herrick, N.J., Haseeb, M., Hix, R.L., Mankin, R.W. 2014. Acoustic detectability of *rhynchophorus cruentatus* (Coleoptera: Dryophthoridae). *Florida Entomologist* 97 (2): 431-438.

Eitzen, D. G and Wadley, H.N.G., 1984. Acoustic emission: establishing the fundamentals. *Journal of Research of the National Bureau of Standards*. Vol. 89. No. 1, January-February 1984.

Fiala, P., Friedl, M., Cap, M., Konas, P., Smira, P., Naswetrova, A. 2014. Nondestructive method for detection wood-destroying insects. *Progress in Electromagnetics Research Symposium*, pp. 1642-1646.

Fujii, Y., M. Noguchi, Y. Imamura, and M. Tokoro. 1990. Using acoustic emission monitoring to detect termite activity in wood. *Forest Products J.* 40: 34-36.

Haack, R. A, R. W. Blank, F. T. Fink, and w: J Mattson. 1988. Ultrasonic acoustical emissions from sapwood of eastern white pine, northern red oak, red maple, and paper birch: implications for bark- and wood-feeding insects. *Fla. Entomol.* 71: 427-440.

Hetzroni, A.; Soroker, V.; Cohen, Y. 2016. Toward practical acoustic red palm weevil detection. *Computers and electronics in agriculture* 124 (); 100-106.

Hofstetter, RW; Dunn, DD; McGuire, R; Potter, KA. Using acoustic technology to reduce bark beetle reproduction. *Pest management science* 2014; 70 (1): 24-27

Hussein, w: B., M. A. Hussein, and T. Becker. 2010. Detection of the red palm weevil, *Rhynchophorus ferrugineus* using its bioacoustics features. *Bioacoustics* 19: 177-194.

Hyvernaud, M., Wiest, F., Serment, M.M., Angulo, M., Winkel, O. 1996. Make ready for a detection system for insect attack by acoustic method. *International Research Group on Wood Preservation, IRG/WP/96-10183*.

Janshoff, A., Steinem, C., Cooper, M.A. *Piezoelectric Sensors*. Berlin, Germany: Springer. ISBN 9783540365679.

Kuroda, K. 2012. Monitoring of xylem embolism and dysfunction by the acoustic emission technique in *Pinus thunbergii* inoculated with the pine wood nematode *Bursaphelenchus xylophilus*. *Journal of Forest Research* 17 (1): 58-64.

Lemaster, R. L., F. C. Beall, and V. R Lewis. 1997. Detection of termites with acoustic emission. *Forest Products Journal* 47(2): 75-79.

Liu, Huajian, Sang-Heon Lee, JV Chahl. 2017. A review of recent sensing technologies to detect

invertebrates on crops. *Precision Agric* 18:635-666.

Main, F. 1909. La destruction des fourmis blanches. *J. Agric. Tropicale* 101: 350.

Mankin, R.W., W.L. Osbrink, F. Oi, and J. B. Anderson. 2002. Acoustic detection of termite infestations in urban trees. *J. Econ. Entomol.* 95: 981-988.

Mankin, R. W., Shuman, D., and Coffelt, J. A. 1996. Noise shielding of acoustic devices for insect detection. *J. Econ. Entomol.* 89: 1301-1308.

Mankin, R. W., M. T. Smith, J. M. Tropp, E. B. Atkinson, and D. Y. Jong. 2008. Detection of *Anoplophora glabripennis* (Coleoptera: Cerambycidae) larvae in different host trees and tissues by automated analyses of sound-impulse frequency and temporal patterns. *J. Econ. Entomol.* 101: 838-849.

Mankin, R.W., Hagstrum, D.W., Smith, M. T., Roda, A. L., Kairo, M.T.K. 2011. Perspective and promise: a century of insect acoustic detection and monitoring. *American Entomologist*, vol. 57, number 1.

Mankin, R.W. 2011. Eavesdropping on coconut rhinoceros beetles, red palm weevils, Asian longhorned beetles, and other invasive travelers. *Proceedings of Meetings on Acoustics*, 14, art. no. 010001, 8 p.

Martin, R.W., Juliet, V., Sankaranarayanan, P., Gopal, A. Rajkumar, I. 2013. Wireless implementation of mems accelerometer to detect red palm weevil on palms. *IEEE International Conference on Advanced Electric Systems* (pp.248-252).

McCullough, Deborah. 2016. Personal email on Emerald Ash Borer research done at Michigan State University, East Lansing, MI.

Mukhtar, M; Rasool, KG; Parrella, MP; Sheikh, QI; Pain, A; Lopez-Llorca, LV; Aldryhim, YN; Mankin, RW; Aldawood, AS. 2011. New initiatives for management of red palm weevil threats to historical Arabian date palms. *Florida Entomologist* 94 (4): 733-736.

Osbrink, W.; Cornelius, M. 2013. Utility of acoustical detection of *Coptotermes formosanus* (Isoptera: Rhinotermitidae). *Sociobiology* 60 (1): 69-76.

Pinhas, J., V. Soroker, A. Hetzroni, A. Mizrach, M. Teicher, and J. Goldberger. 2008. Automatic acoustic detection of the red palm weevil. *Computers and Electronics in Agriculture* 63: 131-139.

Potamitis, I.; Fakotakis, N.; Ganchev, T. 2008. Automatic bioacoustic detection of *rhynchophorus ferrugineus*. *European signal processing conference*.

Potamitis, I., T. Ganchev, and D. Kontodimas. 2009. On automatic bioacoustics detection of pests: the cases of *Rhynchophorus ferrugineus* and *Sitophilus oryzae*. *J. Econ. Entomol.* 102: 1681-1690.

Rach, Miguel Martinez, Gomis, H.M., Granado, O.L., Malumbres, M.P., Campoy, A.M., Martin, J.J.S. 2013. On the design of a bioacoustic sensor for the early detection of the red palm weevil. *Sensors* 13, 1706-1729.

- Scheffrahn, R.H., W.P. Robbins, P. Busey, N.V.Su, and R.K. Mueller. 1993. Evaluation of a novel, hand-held, acoustic emissions detector to monitor termites (Isoptera: Kalotermitidae, Rhinotermitidae) in wood. *J. Econ. Entomol.* 86: 1720-1729.
- Schofield, J., Chesmore, D. 2008. Automated acoustic identification of beetle larvae in imported goods using time domain analysis. *Proceedings - European Conference on Noise Control*, pp. 5929-5934.
- Siriwardena, K.A.P., Fernando, L.C.P., Nanyakkara, N., Perera, K.F.G., Kumara, A.D.N.T. Portable acoustic device for detection of coconut palms infested by *Rynchophorus ferrugineus* (Coleoptera: Curculionidae) 2010. *Crop Protection* 29(2010) 25-29.
- Smith, Cyrus M. and Therese Poland. 2001. Asian longhorned beetle acoustic detector user's manual. Internal document prepared by Oak Ridge National Laboratory, Instrumentation and Controls Division and USDA Forest Service, North Central Research Station
- Watanabe, H.; Yanase, Y.; Fujii, Y. 2016. Relationship between the movements of the mouthparts of the bamboo powder-post beetle *Dinoderus minutus* and the generation of acoustic emission. *Journal of Wood Science* 62 (1): 85-92
- Wiest, F. ; Serment, M. M. ; Angulo, M. ; Winkel, O. 1996. Make ready of a detection system for insect attack by acoustical method. Document - International Research Group on Wood Preservation Issue: IRG/WP/96-10183, Pages: 8 pp.
- Yanase, Y., Y. Fujii, S. Okumura, and Y. Imamura. 1998. Detection of AE generated by the feeding activity of termites using PVDF (*polyvinylidene fluoride*) film. *Forest Products Journal* 48(7): 43-46.
- Yanase, Y., Y. Fujii, S. Okumura, and T. Yoshimura. 2000. Plate-type waveguides for detecting acoustic emissions generated by termite attacks. *J. Wood Sci.* 46: 243-247.
- Zorović, M., Čokl, A. 2015. Laser vibrometry as a diagnostic tool for detecting wood-boring beetle larvae. *Journal of Pest Science* 88 (1): 107-112.
- Zahid, I; Grgurinovic, C.; Zaman, T.; De Keyzer, R.; Cayzer, L. 2012. Assessment of technologies and dogs for detecting insect pests in timber and forest products. *Scandinavian Journal of Forest Research* 27 (5): 492-502.

Dynamic Root Stability Assessment — Basics and Practical Examples

Laszlo Bejo

Associate Professor, Institute of Wood Based Products and Technologies, University of Sopron, Hungary.
bejo.laszlo@uni-sopron.hu

Ferenc Divos

Professor, Institute of Physics and Electronics, University of Sopron, Hungary. divos@fakopp.hu

Shadabeh Fathi

Doctorate Student, Institute of Wood Based Products and Technologies, University of Sopron, Hungary.
shadabeh.fathi@gmail.com

Abstract

Currently, the only accepted method for root stability evaluation is the pulling test, where force is applied to a rope fixed in the tree crown, while the inclination and the applied load is measured. This method has several limitations, including uncertainties in safety factor calculation, heavy equipment and strenuous testing, as well as the contradiction of modeling the dynamic effect through static loading. This paper introduces a dynamic root evaluation technique, where force exerted by the wind is used directly for testing.

The movement of trees in the wind is governed by deterministic chaos, i.e. there is no immediate relationship between wind speed and tree inclination. However, a statistical method, whereby inclination and wind speed is evaluated over longer periods of time, yields a reasonably good relationship. This study introduces theoretical underpinnings of the method, and shows its reliability through some practical examples.

Keywords: wind pressure, tree inclination, dynamic loading, uprooting, safety factor, deterministic chaos

Introduction

Many factors influence the root collar inclination due to wind load, including species, crown area, age, pruning, site conditions, climate and seasonal factors. The biomechanics of the trees' response to wind have been studied extensively (Baker and Bell 1992, James et al. 2006 Moore and Maguire, 2008). An excellent literature review by James et al. (2014) summarizes research activity in dynamic tree evaluation. These models rely on physical models or finite element modeling and account for many of the above factors. However, taking all of these factors in consideration is not possible from a practical point of view. This work focuses on uprooting safety, based on load and inclination measurements only, similar to the accepted pulling method.

The dynamic tree evaluation method is available and commercialized by Argus Electronics (TMS, 2015). The method is based on the tree root collar inclination measurement. The measured inclination is compared with inclination measured on other trees. The tree which shows higher inclination is considered weak. Details of this technique can be seen in Argus Electronics publications.

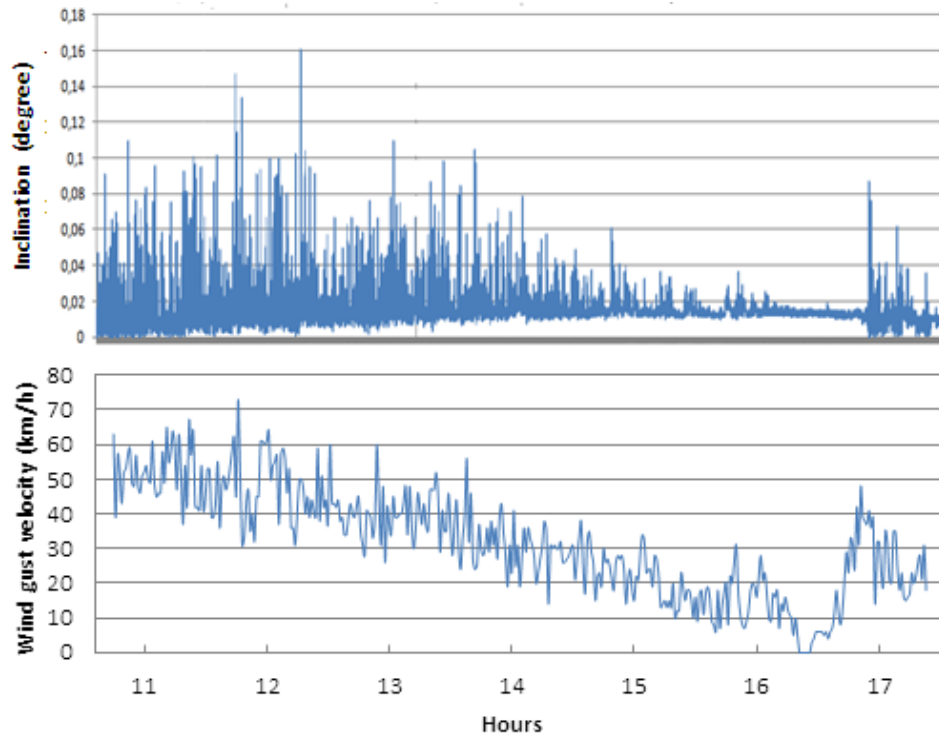


Figure 1— Simultaneous inclination and wind velocity data showing no immediate correlation between the two factors.

Based on literature data and on our own experience, there is no direct and immediate relationship between wind load and trunk inclination (**Figure 1**). Tree inclination is often minimal during high wind gusts, while extreme trunk movement sometimes occurs later, in a relative lull. The reason for this is that leaves, twigs, branches and trunk form a very complex system, not unlike a damped multiple pendulum. The behavior of such systems is extremely sensitive to the initial boundary conditions, and is virtually impossible to predict long term. This type of behavior is called chaotic motion, and multiple pendulums are also dubbed chaotic pendulums for this reason.

The branches and the trunk constitute a nonlinear vibrating system. Forced vibrations are induced by dynamic wind load, and the relationship between the tree trunk inclination and wind load is nonlinear. The same is true in static pulling tests, where nonlinear material characteristics are observed.

Unfortunately, this type of nonlinear and chaotic system is virtually impossible to model by deterministic methods. However, chaotic systems may be studied using statistical methods (Strogatz 2014). In the long run the system will realize all possible states, and the averages of the parameters over a certain period provide meaningful information. Therefore, in our study, the relationship between averages of wind load and trunk inclination data over various periods of time was investigated.

The goals of the research were, as follows:

- to investigate the possibility of using statistical methods for finding a relationship between wind load and tree inclination
- to develop a practical uprooting safety determination method based on wind loading
- to verify the applicability of the method based on practical experience

Theoretical considerations

According to the established safety determination technique (described by Wessoly and Orb, 1998) the uprooting safety of a tree is expressed by the so-called safety factor, which is calculated, as follows:

$$SF = \frac{M_{crit}}{M_{wind}}, \quad (1)$$

where M_{crit} is the torque required for uprooting the tree, and M_{wind} is the torque exerted by the wind on the base of the tree, at a given wind velocity. M_{crit} is usually estimated based on the results of a static pulling test, where a load is exerted on the tree via a cable until a safe 0.25 degrees of inclination is reached. M_{crit} is estimated based on the load-inclination curve, which follows a special second order tangential relationship, which is extrapolated to determine the maximum torque.

For a given wind velocity, M_{wind} is calculated using the following formula:

$$M_{wind} = Ap_w c_w h_{cr}, \quad (2)$$

where: A – crown area (estimated by the safety expert)

p_w – wind pressure ($\rho/2 v^2$)

c_w – experimental drag factor (Wesolly and Orb 1998)

h_{cr} – crown centerpoint height (estimated by the safety expert)

The interpretation of the safety factor is fairly straightforward. A SF below one means that a wind velocity corresponding to M_{wind} is likely to uproot the tree. Trees with SF above 1.5 are considered safe, and in-between these two values there is a region of uncertainty.

Unfortunately, some uncertainty is involved in the above calculation. Crown area and crown centerpoint height is subject to estimation errors, not to mention that in some instances (e.g. in diseased trees), the crown may be less than contiguous. The drag factors used for the estimation, determined for several species by Wesolly and Orb (1998), are shown to be reliable by practical experience, but within-species variation may also affect their values. Last, but not least, trees tend to behave erratically in actual wind load conditions, and their safety may not be correctly determined by static loading.

As mentioned before, there is no immediate relationship between momentary wind conditions and tree collar inclination, due to the complicated architecture of leaves, twigs branches and tree trunk that makes it impossible to create a deterministic model of tree movement in the wind. However, using a statistical approach and considering the tree movement and wind load over longer periods of time may yield an acceptably good relationship between these two factors. In that case, M_{crit} could be calculated from actual wind load data, rather than the static loading curve, and (1) can be expressed, as follows:

$$SF = \frac{M_{crit}}{M_{wind}} = \frac{Ap_{crit}c_w h_{cr}}{Ap_w c_w h_{cr}} = \frac{p_{crit}}{p_w}, \quad (3)$$

where p_{crit} is the maximum wind pressure that the tree can withstand with out uprooting, and is determined from the wind pressure-inclination curve analogously to M_{crit} in the static pulling test. This method does not require crown area and centerpoint height estimation or the drag factor, which eliminates much of the uncertainty in the traditional method. Also, the determining p_{crit} from actual wind load data is likely to provide a better estimate than the M_{crit} value originating from static testing

Materials and methods

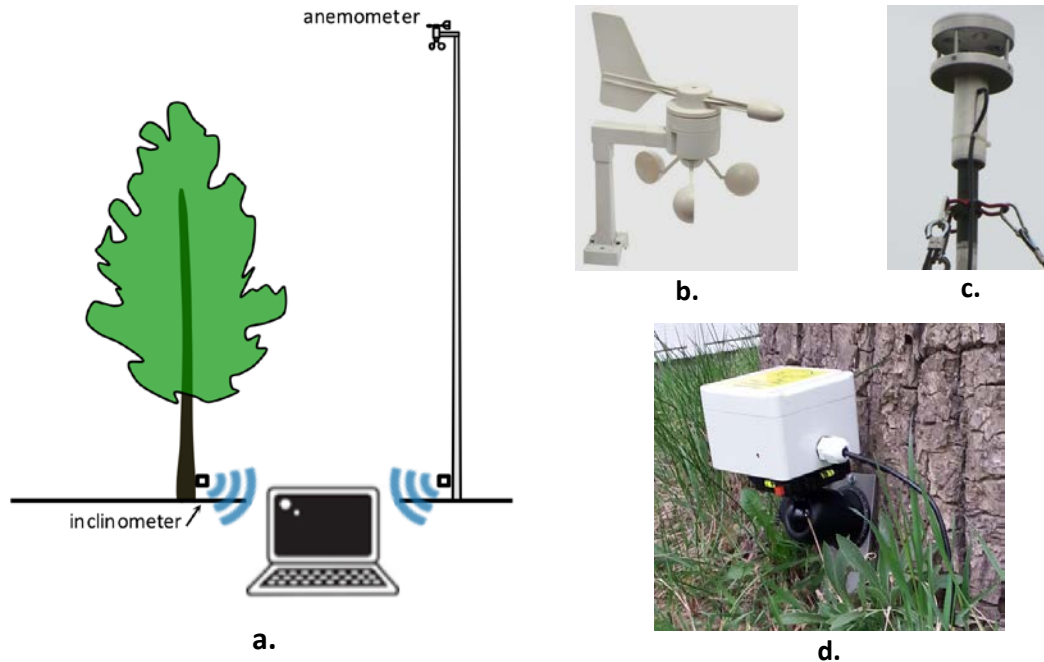


Figure 2—a: Measurement setup, b: Cup type anemometer, c: Ultrasonic anemometer, d: Dual-axis inclinometer

Dynamic uprooting safety evaluation tests were carried out using the authors' own measurement setup (**Figure 2**). A cup type anemometers or an ultrasonic anemometer was used for wind velocity measurements, both with 1 second sampling rates. The anemometers were always positioned several meters above the tops of trees or nearby buildings, where their interference was negligible. Both instruments worked equally well for dynamic root evaluation. The anemometers were equipped with a data logger and a precise GPS-based clock.

Inclination sensors used in the experiments had to be sensitive enough to pick up inclination at very low wind speeds (10 – 30 km/h). The instrument has a bubble type biaxial inclinometer, with a sampling frequency of 10 Hz and a resolution of 0.001 degree. The inclinometer is equipped with a data logger and GPS timer (also provides location data if needed), for precise synchronization of wind pressure and inclination data. Precise time data is stored together with measured data. A mounting palate with 3 pins and a ball head were used to attach the inclinometer at the bottom of the tree trunk. The inclinometer's operating range is ± 2 degrees. Fine position tuning of the inclinometer was possible by the photo ball head, but software tare was also applied. A single screw secured the mounting plate to the tree collar. The injury caused by the screw is minor and not harmful for the tree. After finishing data collection, we removed the screw. Data collection periods varied between 1 hour and 2 days.

Each time the weather conditions were suitable (wind gust velocities higher than 20 km/h), wind speed and inclination data was collected. A total of 25 trees of various species (Magnolia, Pinus, Picea, Larix, Quercus, Fagus, Acer, Ginko, and Betulus spp.) were evaluated over a 4 month period, in 6 different locations in Hungary, Italy and Slovakia. The distance between the anemometer and the trees varied between 15 m and 5.6 km.

Since, at the given rate, almost 80 thousand data points are collected every hour, evaluation by spreadsheet software was too slow for our purposes. An evaluation software dedicated for wind and inclination data analysis was created by the FAKOPP company. The main steps of the evaluation are:

- software tare on inclination data
- determination of the total inclination from “X” and “Y” values,
- wind pressure calculation from wind velocity and air density ($P_{wind} = \rho/2 V^2$)
- pairing wind pressure and inclination data
- selecting averaging time window and averaging.
- fitting the tangent function to the measured points.
- calculation of the critical wind pressure.

Typical averaging time was 5 minutes, i.e. 300 velocity data points and 3000 inclination data points collected in that time window was averaged to create a single data pair. This significantly reduced number of data points used to analyze the correlation between wind pressure and inclination.

Evaluation and results

Typical results and reliability of estimation

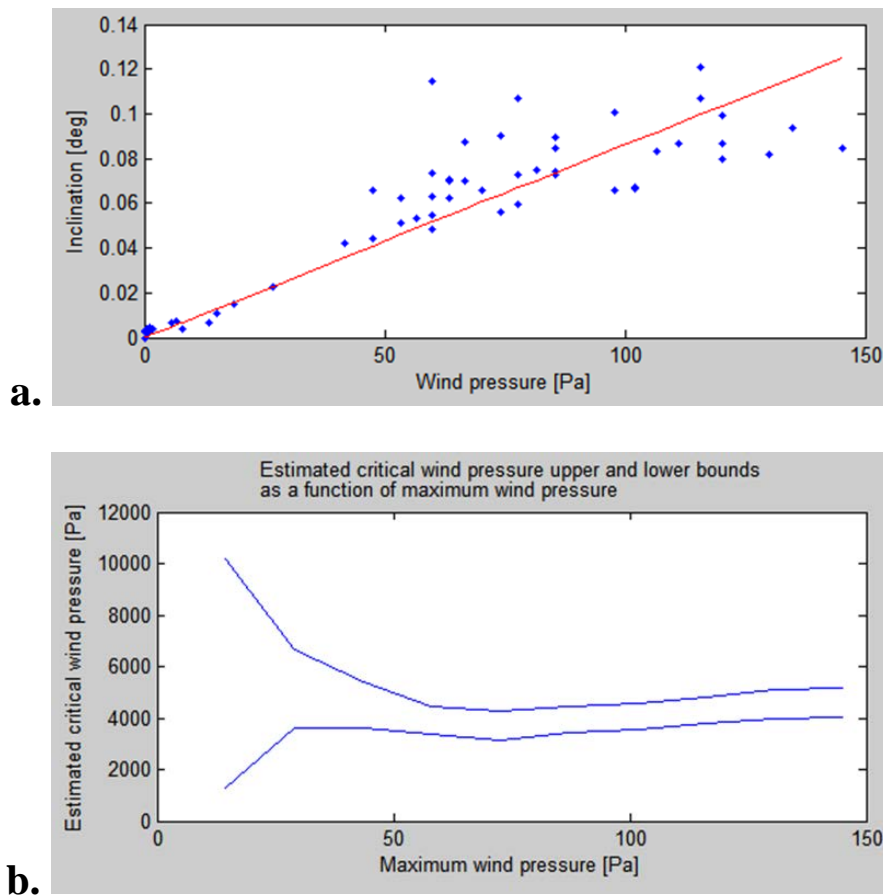


Figure 3— a: Relationship between wind pressure and inclination. **b:** The upper and lower margin of estimated critical wind speed as the function of the maximum wind pressure.

Figure 3a shows a typical DRE test result of a Norway spruce tree. In this test, the data collection took 4 hours, with a 5 minute averaging time window, and a distance between anemometer and tree was 5 km. The highest wind gust velocity during the whole data set was 56 km/h. In this case, the correlation coefficient was 0.86. The estimated critical wind pressure – that would uproot the tree – is 4220 +/-650 Pa. This was determined by similar methods as used in the pulling test (extrapolating a tangent curve fitted to the inclination-force graph). This allows for the safety factor evaluation for a given wind speed. Based on a highest anticipated wind gust velocity of 120 km/h, (a wind pressure of 667 Pa), the uprooting safety factor is $4220/667=6.3$, means tree root structure is safe.

The correlation coefficients we found throughout our examination were in the range of 0.78 and 0.97, based on 25 trees, depending on the distance between anemometer and tree location.

To determine the minimum wind gust velocity, where the DRE test would provide applicable results, the critical wind pressure at various maximum wind pressures was examined. Using the same data set as above, we used partial data set that included only the data up to a given wind pressure value. Taking the maximum measured wind pressure as 100% we calculated the critical wind pressure for the ranges of 0-100%, 0-90%, 0-80%, etc. The calculated critical wind pressure's upper and lower boundary (statistical confidence interval) is plotted as the function of the maximum wind pressure in **Figure 3b**. At low wind pressures, the error becomes high. Above 30 Pa (roughly 25 km/h wind velocity) critical wind pressure prediction is reliable.

The effect of averaging window size and tree-to-anemometer distance

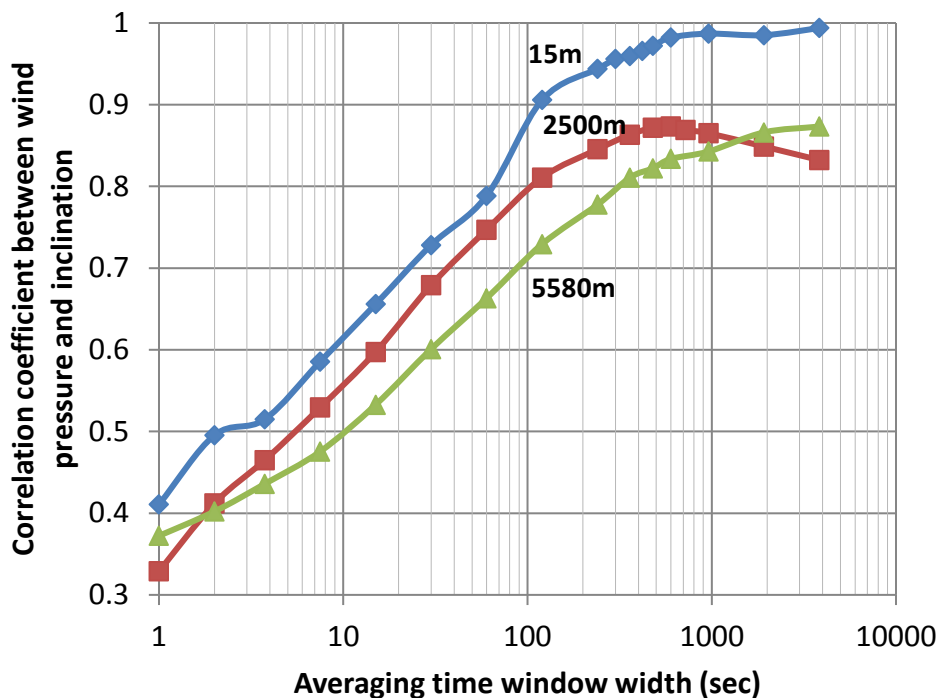


Figure 4— The correlation coefficient between the wind pressure and inclination as a function of statistical window size for three specimens of varying tree-to anemometer distances (as indicated)

Figure 4 shows the effect of averaging window size on the correlation coefficient between wind pressure and inclination, at three different tree-to-anemometer distances. An averaging window of 1s (i.e. using the data without averaging) results in a very low correlation coefficient of 0.3-0.4. Increasing the window size leads to improving correlations, but also requires longer data collection periods for acquiring a sufficient number of data points.

Figure 4 also demonstrates the effect of tree-to-anemometer distance. Larger distances result in lower correlation coefficients. Using larger statistical window sizes (and increased testing periods) can compensate for this problem. It is best to position the anemometer as close to the tree as possible, but acceptable correlation (above 0.8) is achievable if the distance is no larger than 5 km. One anemometer can serve a 5 km radius area.

Reproducibility and practical application

We have tested the reproducibility of DRE. In strong winds (70 km/h velocity), the obtained safety factor was 1.9 +/- 0.1. Given the same tree a month later, when wind velocity was 34 km/h, the measured safety factor was 1.6 +/- 0.3.

We have successfully tested the DRE technique in controlling tree pruning of *Prunus armeniaca*. Strong pruning, around 50% crone area loss resulted increase in safety factor from 3.4 to 6.7. Similar results were found in *Prunus domestica*. The effect of wind direction was tested as well. In typical wind direction (NW) the safety factor was 20% higher compared to measuring in a SW wind.

Finally, a week maple tree's case demonstrated the practical applicability of the new method in a dramatic way. The dynamic test showed this tree to be in danger of uprooting (SF<1 for wind speeds in excess of 70 km/h.) Static pulling tests showed similar results. Finally, the tree was uprooted in relatively windy weather, at 63 km/h wind speed.

Advantages and disadvantages

The advantages and disadvantages of the proposed dynamic root evaluation method over the conventional pulling test method are summarized, as follows:

- The pulling test is an accepted test method, but it requires an anchor point and the application of high loads. Manual input of crown area and the aerodynamic drag factor is necessary for safety factor calculation. The pulling test is possible only in low wind speeds below 25 km/h. The test procedure is slow, tedious and uses static loading.
- The Dynamic Root Evaluation technique is a new technique, not yet established for uprooting safety evaluation. It is fast, requires no crown area or aerodynamic drag factor, and the applied load is realistic, dynamic. The major limitation is that the required wind gust velocity is 25 km/h or higher. Testing periods are similar or higher than those of the static testing, but the method allows simultaneous assessment of several trees (with little additional cost in terms of equipment or time), and the operator does not need to be present during data collection.

Summary and conclusions

Traditional, static testing for tree uprooting safety determination methods have several disadvantages. Using actual wind measurements have several advantages, but there is no immediate relationship between wind pressure and. The statistical approach proposed in this article offers a viable method for correlating wind pressure and tree inclination. The conclusions of our study are, as follows:

- The statistical approach of averaging wind pressure and inclination data, respectively, over an approx. 5-10 min interval yields reasonably good correlation between these parameters, above 25 km/h wind velocity.
- A method was proposed whereby the critical wind pressure is calculated from the pressure-inclination curves the same way as M_{\max} in the traditional pulling test, and is compared to reference wind pressure values to calculate the safety factor.
- According to preliminary experience, the results are repeatable, comparable to pulling test SF determination results, and correctly indicate the effect of tree crown pruning.
- Tree-to-anemometer distances are negatively correlated to the reliability of the method, but sufficient accuracy is possible at distances up to 5 km.

Further investigations will follow to provide further proof for the reliability of the new method, as well as to extend its applications in various real-life scenarios.

Acknowledgments

This article was made in frame of the „EFOP-3.6.1-16-2016-00018 – Improving the role of research+development+innovation in the higher education through institutional developments assisting intelligent specialization in Sopron and Szombathely”.

Instruments were developed and supplied by the FAKOPP enterprise.

References

- Baker, C.J., and H.J. Bell. 1992. Aerodynamics of urban trees. *Journal of Wind Engineering and Industrial Aerodynamics* 44:2655–2666.
- Hanns-Christof Spatz, Benoit Theckes: Oscillation damping in trees, *Plant Science*, Volume 207, June 2013, Pages 66–71
- TMS – Tree Motion Sensors, <http://www.argus-electronic.de/en/tree-inspection-technology/products/tms-tree-motion-sensors>, Date: June 27, 2016
- James, Kent.R., N. Haritos, and P.K. Addes. 2006. Mechanical stability of trees under dynamic loads. *American Journal of Botany* 93(10):1361–1369.
- Kenneth R. James, et al.: *Tree Biomechanics Literature Review: Dynamics, Arboriculture & Urban Forestry* 2014. 40(1):1–15-v
- Moore, J.R., and D.A. Maguire. 2008. Simulating the dynamic behavior of Douglas-fir trees under applied loads by the finite element method. *Tree Physiology* 28:75–83
- Strogatz, S. H. 2014. *Nonlinear Dynamics and Chaos: With Applications to Physics, Biology, Chemistry, and Engineering*. Westview Press. 500 pp. ISBN: 0813349117, 9780813349114
- Wessolly, L., and M. Erb 1998. *Handbuch der Baumstatik und Baumkontrolle*. Patzer Verlag, Berlin, Germany.



Session 8

**Condition Assessment
and Evaluation of
Wood Structures II**

Evaluation of the Old Timber Members of a Masonry Building by Using Ultrasonic Test Together with Destructive Test Methods

Gülru Koca *

Department of Interior Architecture-Faculty of Fine Arts, Işık University, Istanbul, Turkey, gulru.koca@isikun.edu.tr

Türker Dündar

Forest Industry Engineering-Faculty of Forestry, Istanbul University, Istanbul, Turkey, dundar@istanbul.edu.tr

Nusret As

Forest Industry Engineering-Faculty of Forestry, Istanbul University, Istanbul, Turkey, nusretas@istanbul.edu.tr

Abstract

This research is part of the assessment of the structural timber members of an existing old building. An experimental campaign on the mechanical characterization of historic timber members using combined non-destructive test (NDT) and destructive (DT) methods were carried out in order to determine the correlations between the test results. In particular, fir (*abies cilicica*), spruce (*picea abies*) and chestnut (*castanea sativa*) wood were evaluated. Ultrasonic stress wave test was carried out as non-destructive method. Modulus of elasticity in bending and bending strength tests were carried out as destructive tests. The evaluation show that, the coefficients of determination varied according to species and strong correlations were obtained for softwoods (fir and spruce). About 57-73% of the strength properties could be explained by dynamic modulus of elasticity (MoE_D) for fir and spruce specimens. However, the coefficient of correlations for chestnut were relatively weak, which can be explained by the small number of specimens and also the heterogeneous structure of hardwoods. Based on the correlations between the acoustic measurements and the strength properties of structural members, we can conclude that the acoustic NDTs can be used efficiently in the in-situ assessment of the timber buildings' safety and residual structural capacity for fir and spruce. However, further investigations are needed with larger sample sizes for chestnut wood.

Keywords: Non-destructive methods, wood structures, destructive tests, fir wood, chestnut wood, spruce wood

Introduction

The assessment of old timber buildings has gained importance in recent years, due to the large heritage of the old cities which needs to be preserved. In order to determine the type of intervention, the residual structural capacity and condition of buildings has to be surveyed (Calderoni 2010). Consequently, the number of evaluation techniques has increased and the requirement for reliable assessment methods became crucial. In existing old structures this evaluation cannot be carried out by destructive methods, which can cause the loss of structural integrity. Visual inspection together with non-destructive methods are the most used diagnosis techniques in the assessment of safety and residual structural capacity of the buildings (Machado and Palma 2011; Morales et al. 2014). Visual inspection is the oldest non-destructive method which does not require any special tool and depend on the assignment of defects and decays of wood. However this method can sometimes be misleading due to the knowledge of the specialist. Visual inspection has to be applied by experts in order to prevent failures which could lead large-scale replacement of building members. Also, other non-destructive

methods (NDT) has to be carried out together with visual inspection to increase the reliability of survey (Calderoni 2010; Feio and Machado 2015; Faggiano et al. 2011).

NDTs are applied with special tools and techniques to get information about the internal structure of wood and the level of deterioration. Ultrasonic stress wave is one of the most used NDT in the evaluation of timber building members. This technique depends on the acoustic properties of the material and is applied in two different ways; direct and indirect replacement of two sensors (Sousa 2013). In direct method the sensors are placed in line with each other at the ends of the building member. Nevertheless, in existing buildings direct method is usually inapplicable due to most of the members are covered up or have inaccessible ends. For this reason the sensors are placed to the surfaces of the members, which is called indirect method. After the placement of sensors the transmission time of the stress wave is measured to determine the wave transmission velocity. The dynamic modulus of elasticity can also be calculated by using transmission velocity and density of the specimen. In particular, it can be mentioned that longer transmission times generally implies defects or deteriorations in ultrasonic stress wave technique.

Although NDTs are widely used in the evaluation of timber members because of their simplicity and cheapness, experimental data from different species are needed in order to reduce the uncertainty of non-destructive tests. Therefore, destructive tests are carried out together with NDTs to increase the efficiency of these techniques and obtain additional correlations with the strength properties of wood. Correlations between non-destructive and destructive tests of different species have been studied in previous researches. Strong correlations were obtained for most of the structural wood species.

In this context, an experimental campaign including non-destructive and destructive tests was carried out to evaluate the strength properties of structural timber members of an old building. Ultrasonic stress wave tests were performed as NDTs while modulus of elasticity in bending and bending strength parallel to grain tests were carried out as destructive tests. The objective of this research is to provide reliable NDT-DT correlations between strength properties of timber based on statistical analysis.

Materials and methods

Testing material

Test specimens were extracted from different parts of a typical old building in Istanbul, Kadıköy, built up at the beginning of 20th century (Figure 1). The floors, interior walls and stairs of the building are constructed from timber members supported by two masonry walls. At the top floor load-bearing walls and roof are also constructed from timber.



Figure 1 – Facade from 80's

In particular, 35 structural elements from fir (*abies cilicica*), spruce (*picea abies*) and chestnut (*castanea sativa*) wood were extracted from the building. Initially the specimens were visually inspected and then they were sawn into small specimens. After being sawn into small sizes they were evaluated with non-destructive and destructive tests.

Method and equipment

Non-destructive and destructive tests were carried out in order to obtain correlations between strength parameters. Before the experiments the specimens were sawn with a minimum length of 16 times the height of the section as mentioned in the related EN standards. Visual inspection (V), determination of density (D), determination of moisture content (MC) and ultrasonic tests (U) have been carried out as non-destructive tests. Bending strength (B) and modulus of elasticity (MoE_s) tests were carried out as destructive tests.

Table 1 – The experimental stage, dimensions and specimen numbers

	Specimen	Number	Size
Roof	Ridgepole	8	40×40×640
	Roof board	70	15×15×250
	Rafter	24	40×40×640
Wall	Stud	19	30×30×495
	Nogging	8	40×40×640
	Diagonal brace	4	40×40×640
Floor	Flooring	80	20×20×330
	Floor beam	24	40×40×640

The presence of natural defects, sawing defects and biological attacks of the specimens were identified by visual inspection. Before measurement of density, the specimens were conditioned in a climatic room at constant temperature (20±2°C) and humidity (65±5%). The average density was determined as recommended by EN 408 for a moisture content of 12% by measuring the mass (m) and volume (V) of the specimens with the formula;

$$\rho_{12} = m/V \text{ (kg/m}^3\text{)} \quad (1)$$

The moisture content of the specimens was measured in accordance with EN 13183-1 standard. The specimens were oven-dried and weighed before and after the oven drying period. Then the moisture content were determined according to the formula;

$$MC = (m_H - m_O) / m_O \times 100 \quad (2)$$

Here m_H is the initial mass and m_O is the oven-dried mass.

Ultrasonic test

Ultrasonic wave transmission time was measured by using Sylvatest Duo equipment, with conical probes at 22 kHz. The equipment emits a wave from transmitter sensor to the receiver sensor and determines the average time of flight (ToF) obtained from 5 consecutive readings for each measurement. Measurements were performed with direct method by placing sensors at the ends of each specimen (Figure 2). Wave velocity was determined according to the equation;

$$V = L/ToF \text{ (m/s)} \quad (3)$$

where L is the length of the specimen and ToF is time of flight.

The dynamic modulus of elasticity (MoE_D) was determined by using velocity (V) and density (ρ) of the specimen with the equation;

$$\text{MoE}_D = V^2 \times \rho \text{ (N/mm}^2\text{)} \quad (4)$$



Figure 2 – Direct ultrasonic stress wave measurement

Bending strength and MoE_S in bending

The bending strength of timber pieces were determined by three-point bending test using Lloyd LS100 Universal test machine. The applied force has been transferred to the specimen by steel devices and the deflection has been measured at the middle of the specimen by steel transducers which are located both on the loading device and on the specimen (Figure 3).

The modulus of elasticity in bending was determined by the test machine already described. By loading the specimen at a constant rate; the minimum load, maximum load and deformation of the specimens were measured. The modulus of elasticity in bending (MoE_S) is determined by the given formula;

$$E_w = \frac{\Delta P}{\Delta f} \frac{l^3}{4bh^3} \text{ (N/mm}^2\text{)} \quad (3)$$

Here, ΔP is the increase of load in Newtons, Δf is the increase of deformation, l is span, b is width and h is depth of the specimen in millimeters.



Figure 3 – Bending strength test

Results and discussion

According to test results it can be mentioned that; although the building was approximately a hundred years old, the building members were considerably preserved due to its constant moisture amount and continuous residential and commercial use.

As the results of visual inspection, the specimens were affected by some defects such as checks, cracks and insect attacks. Nevertheless mechanical deformation was not observed on any specimen. The moisture content of all specimens has been measured between 10-12%, in line with a healthy wood specimen's moisture content in normal ambient conditions. The arithmetic mean values of non-destructive tests are presented in Table 2. According to the obtained results the densities are mostly appropriate with the literature values. However, wall and floor specimens of fir have lower densities.

The wave velocity values of chestnut specimens are in good accordance with other research results (Lourenço et al. 2007). The average values of ultrasonic wave velocity differ between the specimen groups of softwood tree species (fir, spruce) and most of the groups have appropriate values with the literature stated for softwoods. Wall specimens of fir again have lower values than the other specimen groups (USDA 2015).

Table 2 – The experimental results of non-destructive tests

Member	Specie	Density	Wave velocity parallel to grain
		ρ (kg/m ³)	V (m/s)
Roof	Fir	426.40 (57.50)	6050.75 (621.05)
Wall	Fir	402.32 (16.89)	5083.23 (529.50)
	Chestnut	569.79 (40.13)	4879.53 (300.60)
Floor	Fir	411.93 (34.70)	5680.15 (199.24)
	Spruce	482.90 (66.60)	5596.17 (438.17)

The results of destructive tests are given in Table 3 in terms of arithmetic mean values. The values given between brackets are the standard deviation results. According to the test results; the wall specimens of fir wood have low strength values, while roof and floor specimens are in accordance with the literature (Calderoni et al. 2006; Korkut 2008; Feio et al. 2004; Sousa 2013). The bending strength and MoE_s values for chestnut and spruce wood are again in good accordance with the literature and other research results (Bozkurt and Göker 1996; Korkut 2008; Berkel 1970; Sousa 2013).

Table 3 – The experimental results of destructive tests

Member	Specie	Bending	
		Bending strength (MOR)	Modulus of elasticity
		f_b (N/mm ²)	MoE _s (N/mm ²)
Roof	Fir	66.84 (21.39)	10009.86 (3050.91)
Wall	Fir	46.20 (11.15)	6294.41 (906.25)
	Chestnut	65.84 (13.12)	8643.58 (1314.05)
Floor	Fir	54.17 (12.17)	8277.08 (1298.81)
	Spruce	67.25 (17.67)	9973.12 (2180.84)

As a conclusion most of the specimens have values in accordance with the literature. However, both the density and strength values of the wall specimens of fir are lower than the literature values given for new fir wood.

Correlations between destructive (DT) and non-destructive tests (NDT)

The results of non-destructive and destructive tests were statistically analyzed by means of linear regressions, using SPSS program. The importance of regression is evaluated by the coefficient of determination (R²). The coefficients of determination, as result of regression analysis between destructive and non-destructive tests, and the equations are given in Table 4.

Table 4. Coefficient of determination (R^2) of regression analysis between non-destructive and destructive test results

Property	Fir		Spruce		Chestnut
	R^2	Equation	R^2	Equation	R^2
V -MoEs	0.73	MoEs=4.2946×V-15374	0.63	MoEs =4.0683×V-12906	0.53
MoED - MoEs	0.71	MoEs=0.6212×MoED+279.7	0.73	MoEs=0.5448×MoED+903.56	0.32
V -fb	0.55	fb=0.0225×V-69.45	0.61	fb=0.0333×V-119.79	0.30
MoED -fb	0.57	fb=0.0037×MoED+6.4658	0.68	fb=0.004×MoED+2.3918	0.21

The efficiency of the regressions differed by species type. The coefficient of correlation values were high for softwoods (fir and spruce) but lower correlations were obtained for chestnut. Fir and spruce have very similar performance and coefficient of correlation results.

The dynamic modulus of elasticity (MoED) is a good predictor for softwoods. About 57-73% of the strength properties can be explained by dynamic modulus of elasticity (MoED), while 43-73% of the strength properties can be explained by velocity. However, although chestnut have high strength values, there was only one reasonable coefficient of correlation value obtained between destructive and non-destructive tests.

Conclusion

This article aims to assess the mechanical properties of different wood species by using destructive and non-destructive tests. According to the results obtained from destructive tests, all of the species had good strength properties, and softwoods (fir and spruce) have similar strength properties. However, the wall specimens for fir have lower strength properties than the other groups.

Linear regressions were proposed for strength properties of wood specimens by using ultrasonic stress wave method together with destructive tests. The efficiency of regressions were high for softwoods (fir and spruce) but lower correlations were obtained for chestnut. Dynamic modulus of elasticity was a better predictor of strength properties, while velocity is also a good predictor for fir and spruce. About 57-73% of the strength properties can be explained by dynamic modulus of elasticity (MoED) and 55-73% of the strength properties can be explained by velocity for softwoods. For chestnut, the values of the coefficient of determination were relatively low. The only reasonable result was between velocity and modulus of elasticity ($R^2=0.53$). This was probably caused by the small number of specimens and from the heterogeneous structure of hardwoods.

As a conclusion, ultrasonic tests can be recommended for the evaluation of softwoods due to the good coefficients of determination obtained. Although good strength properties were obtained for chestnut wood, it cannot be easily evaluated by this technique. However, further investigations are needed with large sample sizes of chestnut wood.

References

- Berkel A. 1970. Ağaç malzeme teknolojisi. Kurtulmuş Publications. Istanbul.
- Bozkurt Y.A., Göker Y. 1996. Fiziksel ve mekanik ağaç teknolojisi ders kitabı, İ.U. Publications, Istanbul.
- BS EN 408: 2010+A1: 2012. Timber structures. Structural timber and glued laminated timber. Determination of some physical and mechanical properties.

Calderoni C.; Matteis G.; Giubileo C.; Mazzolani F.M. 2010. Experimental correlations between destructive and non-destructive tests on ancient timber elements. *Engineering Structures*. 32(2): 442-448.

EN 13183-1: 2002. Moisture content of a piece of sawn timber. Determination by oven dry method.

Faggiano B.; Grippa M.R.; Marzo A.; Mazzolani F.M. 2011. Experimental study for non-destructive mechanical evaluation of ancient chestnut timber. *Journal of Civil Structural Health Monitoring*. 1(3): 103-112.

Feio A.; Machado J.S. 2015. In-situ assessment of timber structural members: Combining information from visual strength grading and NDT/SDT methods-A review. *Construction and Building Materials*. 101(2): 1157-1165.

Feio A.; Machado J.S.; Lourenço P.B. 2004. Compressive behavior and NDT correlations for chestnut wood. *Proceedings of International Seminar on Structural Analysis of Historical Constructions*, Padova, 2004.

Korkut S. 2008. The effects of heat treatment on some technological properties in Uludağ fir (*Abies bornmuelleriana* Mattf.) wood. *Building and Environment*. 43(4): 422-428.

Lourenço P.B.; Feio A.O.; Machado J.S. 2007. Chestnut wood in compression perpendicular to the grain: Non-destructive correlations for test results in new and old wood. *Construction and Building Materials*. 21(8): 1617-1627.

Machado J.S.; Palma P. 2011. Non-destructive evaluation of the bending behavior of in-service pine timber structural elements. *Materials and Structures*. 44(5): 901-910.

Morales Conde J.; Rodriguez Liñan C.; Rubio de Hita P. 2014. Use of Ultrasound as a non-destructive evaluation technique for sustainable interventions on wooden structures. *Building and Environment*. 82: 247-257.

Nondestructive Evaluation of Wood, USDA, 2015.

Sousa H. 2013. Methodology for safety evaluation of existing timber elements. University of Minho, Portugal. PhD thesis.

Assessing Ability of Ground-Penetrating Radar to Detect Internal Moisture and Fungal Decay in Douglas-Fir Beams

C. Adam Senalik

USDA Forest Service, Forest Products Laboratory, Madison, Wisconsin, USA,
christopherasenalik@fs.fed.us

James P. Wacker

USDA Forest Service, Forest Products Laboratory, Madison, Wisconsin, USA, jwacker@fs.fed.us

Xiping Wang

USDA Forest Service, Forest Products Laboratory, Madison, Wisconsin, USA, xwang@fs.fed.us

Brunela Pollastrelli Rodrigues

Southwest Bahia State University-Estrada Bem Querer, Vitoria da Conquista, Brazil,
brunelafloresta@yahoo.com.br

Frank Jalinoos

United States Department of Transportation, Federal Highway Administration, Office of Infrastructure R&D, McLean, Virginia, USA, Frank.Jalinoos@dot.gov

Abstract

This report describes the testing plan and preliminary results in an ongoing project to assess the efficacy of using ground-penetrating radar (GPR) to detect internal moisture and fungal decay within Douglas-fir beams. Initially, the test beams were assessed using a variety of physical, mechanical, and nondestructive evaluation (NDE) test methods including micro-resistance drilling, Janka hardness, stress wave transmission, and GPR. After initial baseline assessment, test beams were inoculated with brown-rot fungus, *Fomitopsis pinicola*, and exposed to just above-ground conditions 22 miles (35.4 km) north of Gulfport, Mississippi, USA. Test beam specimens were inspected in the field at 6, 12, and 17 months of exposure using GPR, moisture measurements, and stress wave transmission. Select specimens were removed from the field during each site visit and returned to USDA Forest Service, Forest Products Laboratory, where the NDE tests were repeated. In addition, computer tomography (CT) scans were taken of a subset of the returned specimens. Finally, destructive Janka hardness testing provided insight into mechanical property change during exposure. The GPR scans were compared with the NDE, CT scans, and hardness results. It was found that the GPR scan was sensitive to the presence of internal moisture, which will be useful in locating areas of potential decay.

Keywords: ground-penetrating radar, fungus, brown-rot, Douglas-fir, sawn timber, glulam, weather exposure

Introduction

The 2014 Federal Highway Administration (FHWA) National Bridge Inventory indicates there are more than 40,000 wood or timber roadway bridges in the United States (USDOT 2014). To ensure continued safe usage of these bridges, regular maintenance and inspection is necessary. There are many well-known and reliable wood inspection techniques such as stress wave measurement, transverse vibration, and resistance drilling to name a few (Ross 2015). Many of the techniques require point by point inspection, which makes a comprehensive evaluation of the entire bridge structure a time-consuming undertaking as well as a safety risk because of limited access and passing traffic. Several techniques require specialized equipment that is too bulky to be moved into the field. As processing speed and computing power increases, so does the availability of advanced, field-ready tools that can process large amounts of data in sufficiently short times, which makes their use during routine inspections feasible.

Ground-penetrating radar (GPR) is a tool used for a variety of inspection purposes including concrete and masonry structures, paved and unpaved roads, ground imaging, archeological sites, and ice-covered areas to name a few examples. Currently available commercial GPR units are simple to use and provide near instantaneous and easily interpreted inspection data. Until recently, the use of GPR on wood and wood structures was a little-explored area.

Muller (2003) found that GPR was a reliable method for locating internal defects such as piping and rot in timber girders as large as 16.7 in. (425 mm) in diameter. The GPR results in that study closely correlated to the defects located using test microdrilling and post inspection cutting of the examined wood girders.

Rodriguez-Abad et al. (2011) examined 7.9- by 3-in. (200- by 75-mm) timbers of maritime pine (*Pinus pinaster* Ait.) and showed that signal amplitude, propagation velocity, and spectral composition varied significantly between propagation directions parallel to grain as opposed to those perpendicular to grain. No significant differences were noticed between propagation directions that were parallel to the radial axis and those parallel to the tangential axis. Martínez-Sala et al. (2013) presented similar findings and expanded the study to examine the variation in parameters previously listed with respect to 12 species commonly used for commercialized sawn timber in Spain. It was found that, for all examined species, longitudinal versus transverse dielectric wood behavior was clearly identifiable.

Riggio et al. (2014) gives brief overviews of several nondestructive wood inspection techniques including GPR. Advantages and disadvantages of GPR are listed, and a frequency range of 1.5 to 2.5 GHz is recommended for wood inspection. Mai et al. (2014) showed that dielectric permittivity was affected by moisture content of the wood, fiber direction, and wood density. A subsequent study found that GPR provided the possibility of estimating wood dielectric permittivity. As a result, GPR was assessed as a promising technique for moisture evaluation and early stage diagnosis of timber structures (Mai et al. 2015).

Hans et al. (2015a, 2015b) explored the use of GPR to determine the moisture content (MC) of frozen and thawed logs. In that study, it was found that a partial least square (PLS) regression between the signal amplitude and MC led to robust models that had greater accuracy when attempting to estimate MC from the GPR signal. A related study examined the use of propagation velocity (PV) to measure MC. Although the PLS method yielded a more accurate prediction of MC, the PV method covered a larger wood volume than the PLS method and was more easily transferable among GPR equipment with the same center frequency (Hans et al. 2015c).

A major concern with any wood inspection tool is its ability to detect internal decay. Internal decay is often found in areas of elevated internal moisture. In this project, the efficacy of using GPR to detect

internal moisture and fungal decay within Douglas-fir beams is examined. This report is an update of Senalik et al. (2016) in which the research project was described but included no data from the test specimens.

Research study

The goal of these research efforts is to find fast, reliable nondestructive inspection technique(s) for covered timber bridges. Ideally, the technique(s) will require access to only one side of the inspected object, detect moisture pockets, detect voids, require minimal setup time, collect data quickly, provide instantaneous results in a manner easily interpreted at the inspection site, and penetrate through asphalt to underlying wood. Several techniques were initially evaluated by several industry representatives in a laboratory setting. All industry representatives tested the same specimens in a blind study. Techniques used were GPR, microwave, impact echo, ultrasound, and shear wave tomography. GPR was the inspection technique that best satisfied the criteria and therefore was selected for further in-depth investigation. The entire selection process is described in Wacker et al. (2016).

Objectives and field test setup

The objective of the research study was to assess the ability of GPR to detect internal decay and moisture in wood beams with cross-sectional sizes representative of those used in covered timber bridges. Douglas-fir specimens of varying degree of internal decay activity were created through fungal inoculation and are undergoing field exposure across a range of time from 6 to 48 months. At regular 6-month intervals throughout the decaying process, the specimens were examined using a variety of nondestructive techniques including GPR. At the conclusion of the study, bench marks for measuring efficacy of GPR for detecting internal pockets of fungal decay will be created through visual assessments, NDE evaluation, CT imaging, and hardness profile mapping of cut-away cross sections of the specimen interiors.

Material and methods

Douglas-fir specimens with internal decay were created from sawn timber and glulam beams with cross-sectional sizes representative of those used in covered timber bridges. Figure 1 shows the total number of specimens as well as the months of exposure. Four specimen cross-sectional sizes were selected for the study: 5.125- by 9-in. (130- by 229-mm) glulams, 5.125- by 7.5-in. (130- by 191-mm) glulams, 3.5- by 5.5-in. (89- by 140-mm) sawn timbers, and 3.5- by 7.25-in. (89- by 184-mm) sawn timbers. Six 11-ft (3.4-m) or longer beams of each cross-sectional size were selected and cut into four 32-in. (0.8-m) specimens for a total of 96 specimens (4 cross sections \times 6 beams per cross section \times 4 specimens per beam). There were three duplicates of each cross section for each time interval of testing. The cutting of each beam yielded remnants, which were used for initial cross-sectional hardness testing.

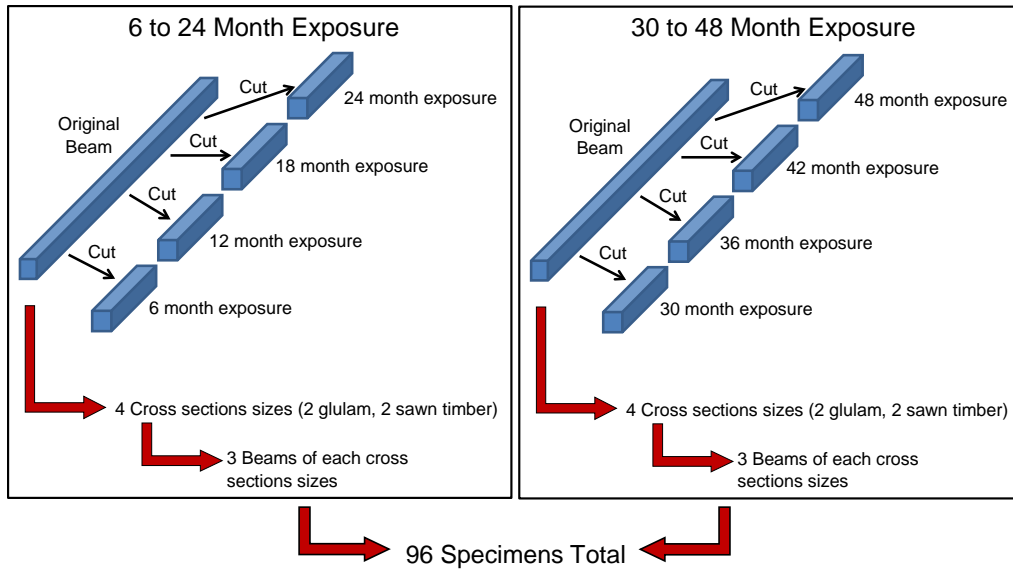


Figure 1. Number of specimens and months of exposure (12 specimens for each exposure subgroup).

Partial-depth circular holes were drilled into each specimen to serve as fungal growth cavities as shown in Figure 2a. The holes were nominally 1 in. (25 mm) diameter and 3 in. (76 mm) deep. The holes were located on the ends and top of each specimen. The hole on the end was centered at the midheight and midwidth of the specimen cross section and drilled parallel to the longitudinal axis. The holes on top were centered midwidth. Figure 2b shows holes drilled into six-laminate glulam specimens.

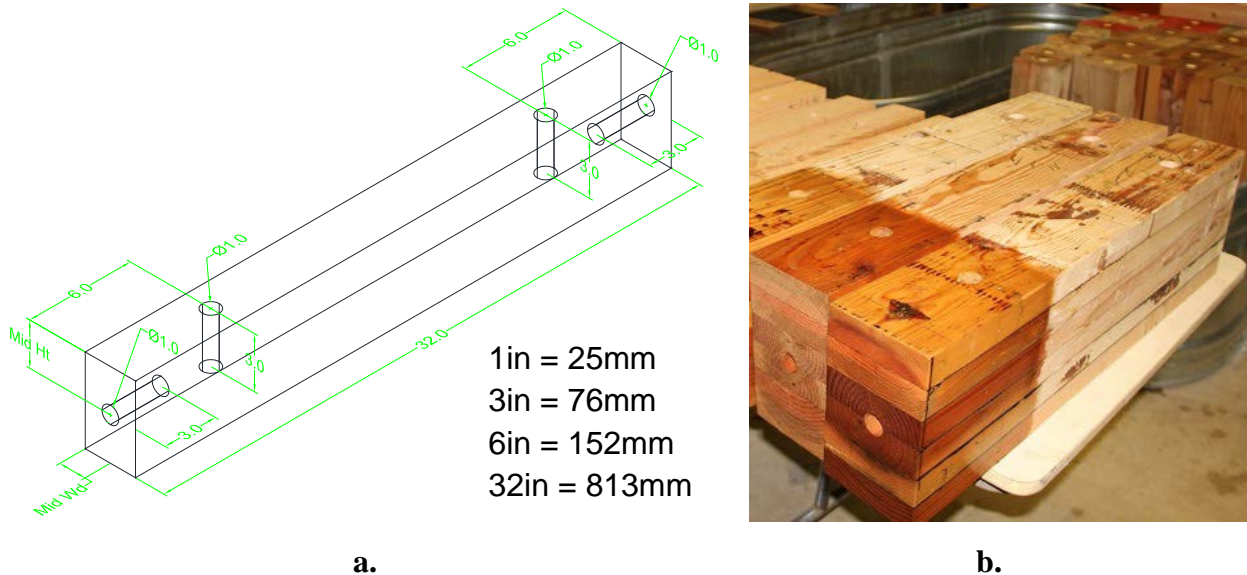


Figure 2. Fungal cavity holes in specimens: (a) locations of the drilled holes (units shown are inches); (b) holes drilled in a six-laminate glulam.

Initial baseline data were collected on the specimens. The baseline data provided the control against which post-exposure data were compared. Data collected included mass, MC, stress wave transmission time, microresistance drilling, GPR scanning, and Janka hardness. MC was collected using a Delmhorst R-2000 electrical resistance moisture meter with two 3-in. (76-mm) insulated probes from Delmhorst

Instrument Company (Towaco, New Jersey, USA). Stress wave time was measured using the Fakopp Microsecond Timber from Fakopp Enterprises (Agfalva, Hungary). Microresistance drilling was performed on selected specimens using the PD 400 Resistograph from IML Wood Testing Systems (Moultonborough, New Hampshire, USA). Several GPR scans were taken of each specimen using a SIR 4000 GPR data acquisition system (Geophysical Survey Systems, Inc., Salem, New Hampshire, USA) with a 2.0-GHz palm antenna. The center frequency of the palm antenna was 2.0 GHz, but the frequencies emitted and received ranged between 500 MHz and 4 GHz. During post-collection data analysis, narrower frequency ranges were explored to determine what, if any, frequency range was particularly sensitive to the presence of brown-rot. The data acquisition system and antenna were purchased from Geophysical Survey Systems, Inc. A 2-in.- (51-mm) thick piece was cut from each beam remnant, and Janka hardness tests were performed using an Instron 5587 testing machine (Instron, Norwood, Massachusetts, USA). Measurements were taken across the cross section (parallel to grain) as shown in Figure 3; however, additional measurements were taken on the sides of each specimen (perpendicular to grain). It was assumed that beams were sufficiently consistent that the hardness profile obtained from the Janka tests of the remnant was representative of the hardness profiles of all specimens cut from that beam.



Figure 3. Janka hardness testing: (a) sawn timber remnant undergoing Janka hardness test; (b) hardness test impressions across glulam remnant cross section.

After initial data collection, one end of each specimen was placed in a water tank for 14 days. The water was sufficiently deep to cover the holes drilled near the ends of the specimens by no less than 2 in. (51 mm). At the end of the soaking period, the specimens were removed and wet sawdust previously inoculated with *Fomitopsis pinicola*, a brown-rot fungus capable of attacking Douglas-fir, was placed in each hole that had been below water level (Fig. 4). The soaking supplied water to the wood that the brown-rot would have used to establish itself and promote fungal growth. The holes were then sealed with cork stoppers. The specimens were then placed back into the soaking tanks with the opposite end below water level. After 14 days, the process was repeated with the holes on the opposite end of the specimen.

The inoculated specimens were shipped to the USDA Forest Service, Harrison Experimental Forest (HEF), approximately 22 miles (35.4 km) north of Gulfport, Mississippi, USA. The site was chosen as an ideal location to promote fungal growth because of its warm climate, high yearly rainfall, and high average relative humidity. Local temperature and precipitation data were recorded by a weather station at HEF. A field site was cleared down to soil level. Surrounding trees provided shade during most of the day

other than midday when the sun was directly overhead; otherwise, sun–shade was not a controlled variable. Two layers of ultraviolet resistant, 8 mil black landscaping plastic were placed on the ground to prevent plant growth under the specimens. The specimens were raised off the ground approximately 7 in. (178 mm) using treated wood blocks to prevent external decay caused by ground contact. Once in place, each inoculated specimen was scanned with the GPR unit to provide a baseline against which post-exposure scans were compared. Black plastic covers were then placed over each specimen. The covers were approximately 18 in. (457 mm) long to protect the area of the beam between the two inoculated holes. The covers minimized rain contact with the middle portion of the beam, lowering the possibility that surface decay developed in that region and increasing the likelihood that when decay occurred within the center region, it grew internally from the fungal cavities rather than from the external surface. Small holes approximately 0.25 in. (6 mm) wide were drilled through each cork to allow moisture to enter the fungal cavities. The specimens were installed in the field on January 12th, 2016. Specimen placement as well as specimen scanning using the GPR tool is shown in Figure 5.



Figure 4. Inoculating specimens with *Fomitopsis pinicola*, brown-rot.



Figure 5. Specimens as positioned on site, and GPR scanning of specimens.

In 6-month intervals, USDA Forest Service, Forest Products Laboratory (FPL), researchers have returned to the test site for data collection. The return dates were July 2016 (6 months), January 2017 (12 months), and June 2017 (17 months). A limited pilot study conducted by FPL using Douglas-fir beams inoculated in a manner similar to those in this report showed that noticeable fungal growth could begin within 6 months in favorable conditions. Data collection included GPR scanning, MC readings, stress wave transmission time, and a visual assessment of the specimen condition. In addition, 12 predetermined specimens (three of each cross section) were retrieved during each site visit and returned to FPL. The retrieved specimens were reconditioned to 12% MC and then cut into 2-in. (51-mm) pieces along the length and perpendicular to the longitudinal axis. Janka hardness tests were performed across the cross section to obtain a hardness profile, which was compared with the original hardness profile for each beam as an indicator of the extent of fungal decay within each specimen (Green et al. 2006).

The process will be repeated until the final 12 specimens are retrieved after 48 months of exposure. The interval testing and the range of exposure times should increase the likelihood that data will be collected on specimens with internal decay ranging in severity from incipient, in which the wood is not perceptibly impaired, to advanced, in which the destruction is readily recognized (Ross 2010). At the conclusion of those 48 months, it is expected that the body of collected data will include GPR scans, NDE data, and hardness profiles for each of the four cross-section types from a period of 0 to 48 months in 6-month increments.

Results

To date, there were four site visits: at 0 months (when the specimens were initially placed), 6 months, 12 months, and 17 months. MC measurements taken on a random selection of the specimens at the site during each visit showed that MC was relatively consistent between specimens. Table 1 shows the average percentage MC during initial installation and during each subsequent site visit.

Table 1. Percentage moisture content at the end and center of the specimens by months of exposure

Location	0 months	6 months	12 months	17 months
End of specimen	~25	24.0	25.5	27.9
Center of specimen	11.3	19.1	19.4	18.1

A set of typical time domain and frequency domain plots collected by the GPR unit are shown in Figure 6. The specimen examined was C13. The plots were collected with the antenna on the top surface of the specimen (the surface with two drilled holes as shown in Figure 2a). To facilitate data clarity in Figure 6a, the time domain magnitude data shown are natural logs of the absolute values of the time domain data multiplied by the original sign for the individual data points. The process enhances the visibility of low magnitude peaks and valleys. Figure 6b has the frequency domain data subsequently described. Figure 6c is a side view of the specimen constructed from CT images. The CT images were collected on July 25, 2017. The bright object on the top surface of the specimen is the metal ID tag. In the CT image, pixel brightness is directly and linearly proportional to density. The four drilled fungal cavities illustrated in Figure 2 are clearly visible. The bright areas around the fungal cavities are moisture that has moved into the wood from the cavities. The CT image and time domain plots are aligned such that the vertical black dashed lines across the plots and CT image represent the same location within the specimen. The 0-month plot (top) shows a relatively small amount of variation along the length. There are distinct positive peaks and distinct negative valleys. The 6-month plot (second from top) has variation in the signal visible near the ends where the fungal cavities are present, although distinct peaks and valleys are still visible. In the 12-month plot, the time domain signals around both fungal cavities have shifted positively causing the loss of distinct negative valleys. The 17-month time domain plot shares many characteristics with the 12-

month plot. The fungal cavities have caused a loss of positive peaks on one end and a loss of negative valleys on the other. The fungal cavity at the 6-in. (15-cm) mark causes peaks that are mainly negative, whereas the cavity at 26 in. (66 cm) has peaks that are mainly positive. One complicating factor of the time domain plots is the high potential of internal features to clutter the image. Knots, voids, and moisture cavities are all reflectors that are visible to the GPR unit. Although the raw time domain data plots reveal the location of internal features, identifying what the feature represents can be a challenge.

In an effort to find a more consistent identifier for internal moisture and fungal decay, the time domain data were converted into the frequency domain. The associated frequency domain plots computed from the time domain signal data are shown in Figure 6b. The GPR antenna has a center frequency of 2 GHz. The red dashed line in Figure 6b shows the 2-GHz frequency band. The majority of the signal energy in the 0-month plot was at 2 GHz, as expected. All frequency domain plots were normalized to the maximum value present in the 0-month plot; therefore, a loss of magnitude in later months is visible as a shift from red to yellow, then to green, and finally to blue. As the moisture increased from field exposure, the magnitude of the 2-GHz signal decreased. There was a noticeable drop in the 2-GHz magnitude between the 0- and 6-month scans along with an associated increase in MC in the center of the specimens according to Table 1. Between the 6- and 12-month scan, there was another drop of 2-GHz magnitude and a shifting of the center frequency slightly lower, both of which were expected results of increased MC, but no increase in MC was recorded between those visits. During the 6-month visit, the 3-day inspection period had several passing showers. The passing showers probably increased the recorded MC results from the 6-month visit. At the 12- and 17-month visits, the magnitude of the signal along the 2-GHz signal was relatively consistent compared with the 0- and 6-month data; however, the regions of moisture caused the signal magnitude to noticeably decrease along the 2-GHz band. In addition, signal magnitude above 2 GHz decreased to a greater extent than signal magnitude below 2 GHz. This was expected because the electromagnetic wave speed through water is slower than through air or dry wood. The drop in magnitude associated with the fungal cavities was largely consistent for all specimens examined, indicating that MC was probably the source of the signal magnitude loss. Cross-sectional hardness profiles of the 6-month group have shown no indication of internal decay. Time of flight measurements taken during the 17-month visit, likewise, showed no indication of internal decay. The changes in the frequency magnitude are probably attributable to internal moisture. All CT scans of specimens retrieved from the field show the presence of moisture around the fungal cavities (Fig. 7).

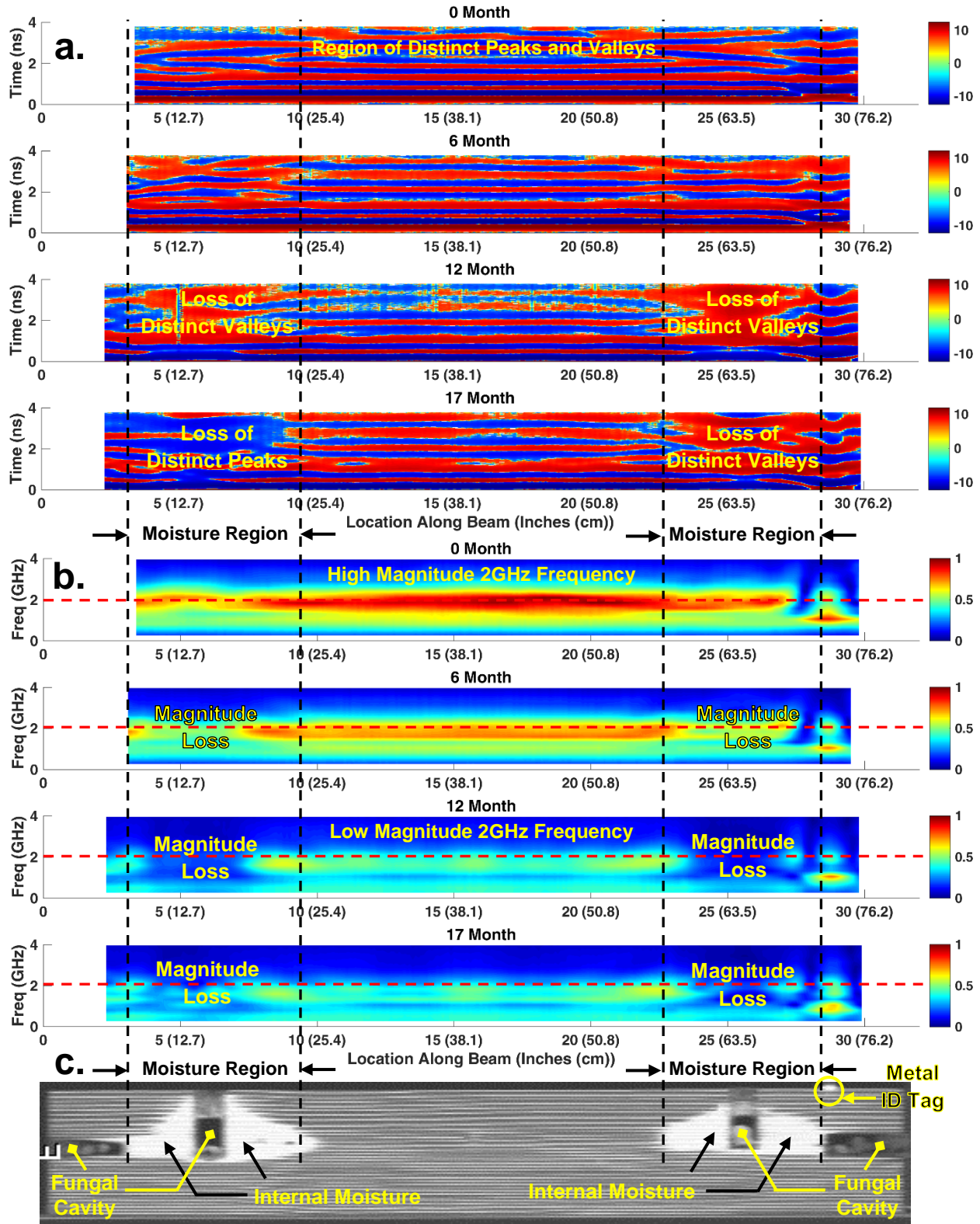


Figure 6. Through depth time and frequency domain plots at 0, 6, 12, and 17 months: (a) top four plots are time domain; (b) lower four plots are frequency domain (red dashed lines show the 2-GHz frequency band); (c) CT cross section of the specimen in which fungal cavities are visible and bright areas are internal moisture. Black dashed vertical lines show the boundary of moisture regions across all plots and images.

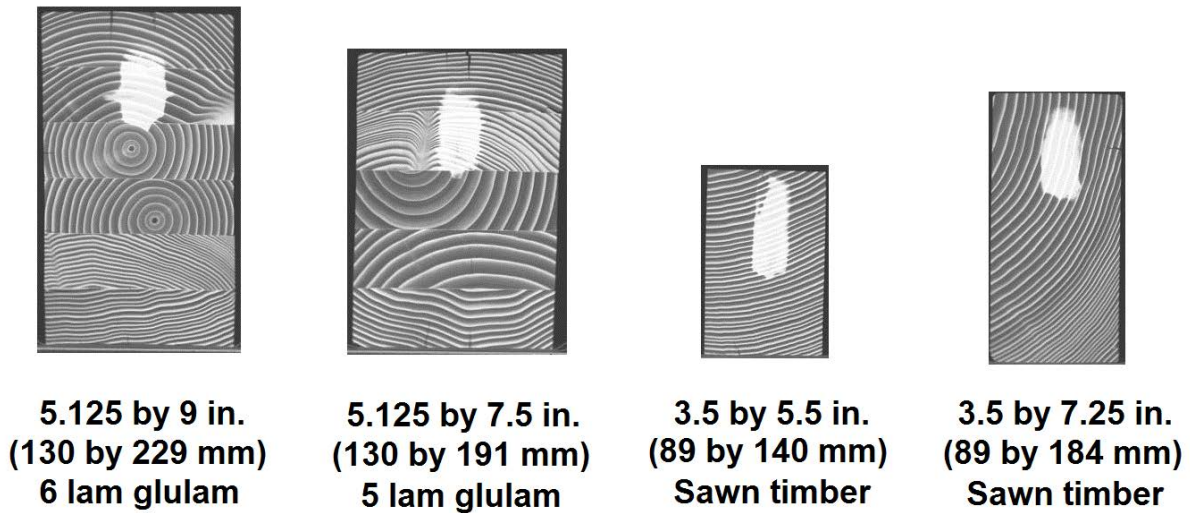


Figure 7. CT images of specimen cross sections after 17 months of field exposure showing internal moisture.

Summary

In this study, GPR was investigated for suitability for inspecting large timber bridge components. One focus of the study was the efficacy of using GPR to detect fungal decay and moisture pockets within Douglas-fir beams. A total of 96 specimens were created from two sizes of glulam beams and two sizes of sawn timber beams. The beams selected were of sizes typically used in covered timber bridge applications. Initially, the beams were assessed using a variety of physical, mechanical, and NDE test methods including, microresistance drilling, Janka hardness, stress wave transmission, and GPR. These data provided a baseline to which field-exposed specimens were compared. The specimens were inoculated with brown-rot fungus, *Fomitopsis pinicola*, and transported to HEF, 22 miles (35.4 km) north of Gulfport, Mississippi, USA. In January 2016, the specimens were placed outside at HEF to promote fungal growth. FPL researchers returned after 6, 12, and 17 months to evaluate the specimens using GPR scanning, stress wave, and visual assessment. During each visit, a subset of the specimens were retrieved from the field and returned to FPL. The returned specimens were subjected to visual assessments, NDE evaluation, CT imaging, and hardness profile mapping of specimen cross sections. At the time of this report (17+ months of field exposure), no testing method showed indications of internal decay in the specimens. Time domain and frequency domain data collected from the specimens using GPR showed a strong connection between signal magnitude and internal moisture pockets. Future work on this study will focus on developing a metric to positively identify internal moisture as well as assess the ability of GPR to detect internal fungal decay within the Douglas-fir specimens when it develops.

Acknowledgments

This study was conducted under a joint agreement between the Federal Highway Administration (FHWA) — Turner–Fairbank Highway Research Center and the USDA Forest Service, Forest Products Laboratory (FPL). The study is part of the Research, Technology, and Education portion of the National Historic Covered Bridge Preservation (NHCBP) program administered by the FHWA. The NHCBP program includes preservation, rehabilitation, and restoration of covered bridges that are listed or are eligible for listing on the National Register of Historic Places; research for better means of restoring and

protecting these bridges; development of educational aids; and technology transfer to disseminate information on covered bridges to preserve the Nation's cultural heritage.

Many people have assisted in this project. We acknowledge their contributions: Bessie Woodward (retired) and Stan Lebow of FPL for inoculation of the specimens; Andrea Gilich, C. Dana Nelson, and Chance Parker of Forest Service Harrison Experimental Forest for assistance in preparing a field location and preparing the specimens for exposure; GPR consultant Francisco Romero of Romero NDT&E, LLC, for his assistance and training in the use of the GPR; Lon A. Yeary of University of Wisconsin-Platteville, Marcela Cordeiro Barbosa of Federal University of Brasilia (Brazil), Alex Costa of São Paulo State University (Brazil), and Lujing Zhou of Beijing Forestry University (China) for their assistance during the initial assessment of the specimens; and Zhanguo Wei of the Central-South University of Forestry and Technology (China) for assisting in the laboratory assessment of the retrieved specimens.

References

- Green, D.W.; Begel, M.; Nelson, W. 2006. Janka hardness using nonstandard specimens. Res. Note FPL–RN–0303. Madison, WI: U.S. Department of Agriculture, Forest Service, Forest Products Laboratory: 13 p.
- Hans, G.; Redman, D.; Leblon, B.; Nader, J.; La Rocque, A. 2015a. Determination of log moisture content using early-time ground penetrating radar signal. *Wood Material Science & Engineering*. 10(1): 112-129. DOI: 10.1080/17480272.2014.939714.
- Hans, G.; Redman, D.; Leblon, B.; Nader, J.; La Rocque, A. 2015b. Determination of log moisture content using ground penetrating radar (GPR). Part 1. Partial least squares (PLS) method. *Holzforschung*. 69(9): 1117-1123.
- Hans, G.; Redman, D.; Leblon, B.; Nader, J.; La Rocque, A. 2015c. Determination of log moisture content using ground penetrating radar (GPR). Part 2. Propagation velocity (PV) method. *Holzforschung*. 69(9): 1125-1132.
- Maï, T.C.; Razafindratsima, S.; Sbartai, Z.M.; Demontoux, F.; Bos, F. 2015. Non-destructive evaluation of moisture content of wood material at GPR frequency. *Construction and Building Materials*. 77: 213-217.
- Maï, T.C.; Sbartai, Z.M.; Bos, F.; Razafindratsima, S.; Demontoux, F. 2014. Nondestructive evaluation of timber structures using GPR technique. In: *Proceedings of the 15th International Conference on Ground Penetrating Radar*. June 30–July 4, 2014. Brussels, Belgium. New York: Institute of Electrical and Electronics Engineers: 218-222.
- Martínez-Sala, R.; Rodríguez-Abad, I.; Diez Barra, R.; Capuz-Lladro, R. 2013. Assessment of the dielectric anisotropy in timber using the nondestructive GPR technique. *Construction and Building Materials*. 38: 903-911.
- Muller, W. 2003. Timber girder inspection using ground penetrating radar. *Insight — Non-Destructive Testing and Condition Monitoring*. 45(12): 809-812.
- Riggio, M.; Anthony, R.W.; Augelli, F.; Kasal, B.; Lechner, T.; Muller, W.; Tannert, T. 2014. In situ assessment of structural timber using non-destructive techniques. *Materials and Structures/Materiaux et Constructions*. 47(5): 749-766.
- Rodriguez-Abad, I.; Martinez-Sala, R.; Garcia-Garcia, F.; Capuz-Lladro, R.; Diez Barra, R. 2011. Non-destructive characterization of maritime pine sawn timber dielectric anisotropy by means of GPR. In: *6th International Workshop on Advanced Ground Penetrating Radar, IWAGPR 2011*. June 22–24, 2011. Aachen, Germany. New York: Institute of Electrical and Electronics Engineers: 129-134.
- Ross, R.J. (ed.). 2015. *Nondestructive evaluation of wood: second edition*. Gen. Tech. Rep. FPL–GTR–238. Madison, WI: U.S. Department of Agriculture, Forest Service, Forest Products Laboratory: 169 p.

Ross, R.J. 2010. Wood handbook: wood as an engineering material. Centennial ed. Gen. Tech. Rep. FPL–GTR–190. Madison, WI: U.S. Department. of Agriculture, Forest Service, Forest Products Laboratory.

Senalik, C.A.; Wacker, J.P.; Wang, X.; Jalinoos, F. 2016. Assessing the ability of ground-penetrating radar to detect fungal decay in Douglas-fir beams. In: 25th ASNT Research Symposium: Summaries and Abstracts. April 11-14, 2016, New Orleans, Louisiana. Columbus, OH: American Society for Nondestructive Testing: 7 p.

USDOT. 2014. Table of bridges by deck structure type. <http://www.fhwa.dot.gov/bridge/nbi/no10/deck14.cfm>. U.S. Department of Transportation, Federal Highway Administration, Programs Office, Office of Infrastructure, Office of Bridges and Structures, National Bridge Inventory Library.

Wacker, J.P.; Senalik, C.A.; Wang, X.; Jalinoos, F. 2016. Effectiveness of several NDE technologies in detecting internal moisture and artificial-decay in sawn timber and glulam. In: Proc. WCTE 2016 World Conference on Timber Engineering. Aug. 22-25, 2016. Vienna, Austria.

Assessment of Deterioration in Timbers with Time and Frequency Domain Analysis Techniques

C. Adam Senalik

USDA Forest Service, Forest Products Laboratory
Madison, Wisconsin, USA, christopherasenalik@fs.fed.us

Lujing Zhou

Beijing Forestry University, Beijing, China, lujingzhou6@gmail.com

Robert J. Ross

USDA Forest Service, Forest Products Laboratory
Madison, Wisconsin, USA, rjross@fs.fed.us

Abstract

The research reported here focuses on the use of time and frequency domain analysis techniques for assessing the internal condition of timbers. Several large timbers obtained from a historic public viewing tower were evaluated with acoustic-based nondestructive testing techniques. Waveforms were captured and analyzed using both time and frequency domain techniques. The slope of the phase with respect to frequency shows potential to be a metric that is more sensitive to the presence of internal decay than time of flight.

Keywords: timber, deterioration, acoustic signals, time domain, frequency domain, phase

Introduction

Wood is used extensively for both interior and exterior applications in the construction of a variety of structures. The deterioration of an in-service wood member may result from a variety of causes during the life of a structure. It is important, therefore, to periodically assess the condition of wood used in structures to determine the extent of deterioration so that degraded members may be replaced or repaired to avoid structural failure.

Assessment of the condition of wood in a structure can be conducted for a variety of reasons. Code compliance, historic preservation, or alternative uses of a structure are frequently cited reasons for conducting a condition assessment. A structural condition assessment consists of the following: (1) a systematic collection of data pertaining to the physical and mechanical properties of materials in use; (2) analysis and evaluation of the data collected; and (3) developing recommendations regarding portions of an existing structure that affect its current or proposed use. Such an assessment relies on an in-depth inspection of the wood members in the structure. During these inspections, a wide variety of techniques are used to assess the condition of the wood. Visual, resistance drilling (probing), and stress wave or ultra-sound-based techniques are all used either individually or collectively to inspect in-service wood.

These techniques are discussed in detail in *Wood and Timber Condition Assessment Manual, Second Edition* (White and Ross 2014).

A significant volume of research has been devoted to the use of sound waves for locating areas of deterioration in timber structures, and a practical set of guidelines for their use has been prepared by the USDA Forest Service, Forest Products Laboratory (FPL) (Ross et al. 1999). In summary, the transmission of sound in wood is affected significantly by the presence of deterioration. Consequently, ultrasound and stress-wave-based technologies have been developed and are widely used to inspect wood structures (Allison et al. 2008; Brashaw et al. 2005; Clausen et al. 2001; Emerson et al. 2002; Franca et al. 2015; Ross et al. 1999, 2006) and have been used for the assessment of culturally significant historic ships and artifacts (Ross et al. 1998, Wang et al. 2008, Dundar and Ross 2012).

A simple, inexpensive stress-wave timer is commonly used in inspections. Sensors are placed on opposite sides of a timber. The timber is then struck, generating a stress wave. The time it takes for the wave to travel between the sensors is measured by the timer and recorded. Transmission times for wood from several species are known and are used as a baseline. Transmission times significantly longer than baseline values indicate the presence of deteriorated wood.

Currently used stress-wave timing equipment uses simple electronic circuitry to process the waveforms, with simple time domain evaluation techniques. Information on the use of more advanced signal processing techniques, specifically those that use frequency domain analysis techniques, for evaluating wood exposed to in-service conditions is lacking. One laboratory study using frequency analysis was McGovern et al. (2011) in which the wave dispersion qualities of 1-in. (25-mm) loblolly pine cubes of varying decay were assessed. The objective of the research described here was to examine the use of both time and frequency domain stress wave techniques to evaluate several large timbers that were exposed to a variety of in-service conditions for more than 80 years.

Background on tower

FPL was contacted in late 2015 to assist engineers from the Wisconsin Department of Natural Resources (DNR) in evaluating the condition of timbers in a historic viewing tower located in Wisconsin's Peninsula State Park. Located in Door County, Eagle Tower (Fig. 1a) was a 75-ft (22.9-m) tall observation tower that sat atop a 180-ft (54.9-m) limestone bluff. From its top platform, one could see Peninsula State Park, surrounding islands in Lake Michigan, and Michigan's Upper Peninsula.

The tower structure was built in 1932. It replaced the original tower built on Eagle Bluff, which was constructed in 1914. This iconic tower stood as one of the most unique landmarks in Wisconsin. Peninsula State Park is visited by more than a million people every year.

The DNR periodically examined the structure using visual inspection techniques. Engineers looked for signs of distress, such as failed members and those showing evidence of attack by decay fungi or carpenter ants or nesting activity by local bird populations. After an extensive inspection, the DNR concluded that the main structural members were severely deteriorated and, consequently, closed the structure. The tower was dismantled September 19, 2016.

History of tower

The original tower on Eagle Bluff was constructed in 1914 at a cost of \$1,061.92. The tower was 76 ft (23.2 m) tall, and it stood 225 ft (68.9 m) above Lake Michigan. It was constructed during the summer of 1914 to serve as a fire tower with the expectation it would become a tourist attraction. The ledger of Peninsula's first manager, A.E. Doolittle, lists payment to men for fire watch duty.

A construction crew cut logs and boards from timber in the park using tools and saws available at the time. To erect the tower, they first raised the center pole. Then they used the center pole to raise other support poles. Three trees composed each corner pole, with platforms between the separate trees. Horizontal landing support beams were added, followed by planks for decking at the three levels.

A telephone line connected the tower to the manager's residence and the local exchange so that fires could be quickly reported. Historical records indicate there was a large buildup of fire-prone material in the park. Peninsula's last significant fire was in 1921.

The original tower was dismantled. Eagle Tower was built in 1932. Foreman Sam Erickson and crew used horses, tractors, trucks, and other machinery. They wrapped cable around nearby trees to raise poles. A stump wrapped with rusty cable can still be seen a short distance from the tower, along the road leading towards Eagle Terrace (GPS coordinates N45.16275 W 87.19730). Untreated western redcedar poles were shipped from Washington State.

Eagle Tower was 75 ft (22.9 m) tall and stood 250 ft (76.2 m) above water level. Safety improvements were made in 1972, including slanting the top deck railings. Hardware and decking were replaced and stained in subsequent years.



a.



b.

Figure 1. Eagle Tower prior to and after disassembly; (a) Eagle Tower just prior to disassembly; (b) sections cut from the four vertical supports of Eagle Tower.

Materials and methods

This study focused on six sections taken from the four western redcedar support legs of the tower as shown in Figure 1b. Timber inspection was performed on February 6th, 2017, at Peninsula State Park in Door County Wisconsin. The sections measured between 3 (0.9) and 6 ft (0.9 and 1.8 m) in length. The diameters of the sections measured between 12.5 and 16.5 in. (31.8 and 41.9 cm). The poles were given the identifiers B1, B2, B3, G1, G2, and G3. Two nondestructive testing tools were used in the inspections: a Fakopp Microsecond Timer from Fakopp Enterprise Bt. (Agfalva, Hungary) and Tree Check Sonic Wave Tree Decay Detector from Allison Tree, LLC (Verona, Wisconsin). Measurements were taken perpendicular to grain orientation, 6 in. (15.2 cm) from the end of the pole and then at 1-ft (30.5-cm) increments starting 1 ft (30.5 cm) from the end of the pole.

The Fakopp Microsecond Timer records the time of flight (ToF) of mechanical waves between two probes that are driven into the surface of the poles. The probes were installed on opposite sides of the pole at the locations described, and the ToF values of the waves were recorded and are shown in Tables 1 and 2. Tables with SI units are in the Appendix.

The Tree Check Sonic Wave Tree Decay Detector records the ToF between two accelerometers that are installed on awls that are driven into the surface of the poles. In addition, the waveform signal is recorded. The signal is recorded as 1,280 data points at a sampling rate of 20 kHz. Recording begins after a threshold voltage is surpassed; therefore, the recorded signal does not contain lead zeros. The probes were installed on opposite sides of the pole at the locations described above and the ToF values of the waves were recorded as shown in Table 1 for B group and Table 2 for G group. The waveforms were recorded for time and frequency analysis. A representative recorded waveform, the magnitude plot, and the phase plot are shown in Figure 2.

The recorded points were also given a designation based on a combination of the visible characteristics of the poles and ToF measurements. There were six designations: rot, transition, end of log, above hole, below hole, and good. A designation of rot indicated there was evidence of decay. Evidence of decay included visible indications of decay or a ToF above 400 $\mu\text{s}/\text{ft}$ (1,300 $\mu\text{s}/\text{m}$). ToF measurements above 400 $\mu\text{s}/\text{ft}$ (1,300 $\mu\text{s}/\text{m}$) are indicative of internal decay. A designation of transition was given to points between areas with the designation of rot and other areas. A test location adjacent to the end of the poles was given the designation of end of log. Previous experience of the authors (Senalik et al. 2010) with frequency analysis of signals collected near the end of beams and poles led to the creation of the end of log group because proximity to the end can create unique signal content unseen elsewhere in the log. At some locations, holes existed that had been part of the timber's use within the tower. For a pole section with a drilled hole, the original vertical orientation of the pole section was determined. The test location that was located above the hole was given the designation above hole, and the two test locations below the hole were given the designation below hole. In the absence of any visible signs of rot, decay indications from ToF, or drilled holes, a test location was designated as good. There was a caveat to the designation process. A rot designation preempted all others. For example, a test location at the end of a log with visible signs of rot would be designated rot rather than end of log.

The frequency analysis occurred in two parts: magnitude and phase. The two plots are shown in Figure 2b. In a nondispersive material, all frequency components of a signal travel at the same rate; therefore, the signal received is similar in frequency content to the source signal. In a dispersive material, such as wood, the frequency content alters as it passes through the material. In a dispersive material, waves can have

frequency-dependent velocities; however, the bulk of the energy signal travels at a speed known as the group velocity. Group velocity for dispersive materials is given in the following equation (Sachse 1978):

$$V_g(\omega) = \frac{d_o}{\left(\frac{d\phi}{d\omega} - t_o\right)}$$

where group velocity, V_g , is dependent on three unknowns: the distance between the source and receiver, d_o , the amount of time the wave is in the material (which is the ToF), t_o , and the slope of the line relating the frequency to phase, $d\phi/d\omega$. For brevity, this term will be referred to in this report as the phase–frequency slope (PFS).

The ToF has been used as a metric for gauging internal decay of in-service wood for several decades, but PFS has not been examined for that purpose. Because wood becomes more dispersive as decay advances and PFS relies on more signal information than ToF, it was believed that PFS may provide a metric more sensitive to the presence of decay than ToF. To determine PFS, the upper and lower frequencies must be defined. The lower bound frequency was taken to be 1 Hz. The upper bound frequency was chosen such that 80% of the signal energy was below the upper bound frequency. The limit of 80% was chosen because it encompassed the majority of the signal energy, was normally within a relatively narrow range of frequencies between 1,500 and 2,000 Hz, and the range of frequencies that made up the final 20% of the signal energy varied widely between measurement locations and had a disproportionately large influence on the final slope values.

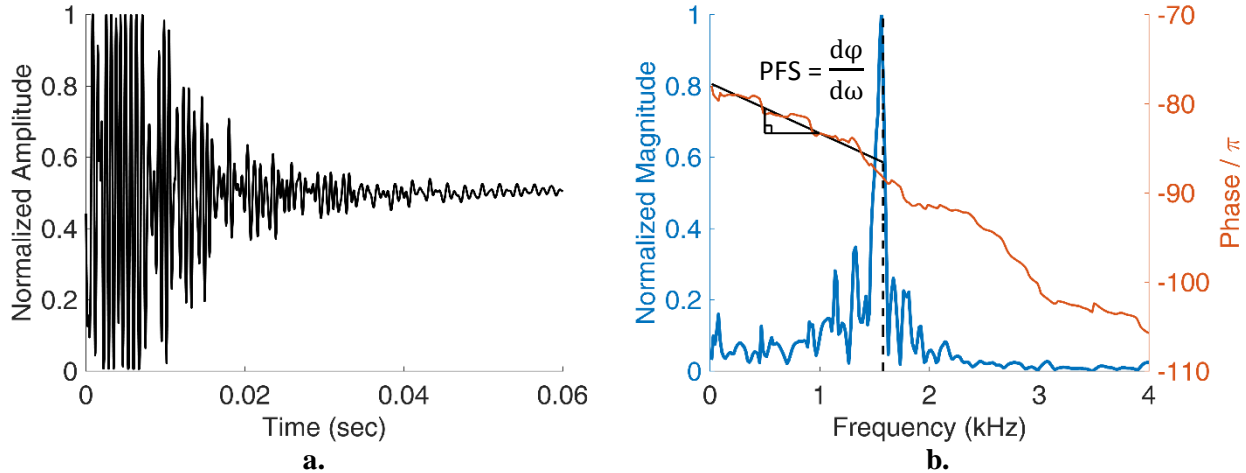


Figure 2. Representative (a) time domain and (b) frequency domain plots. Thick blue line is the normalized magnitude. The thin orange line is phase angle. The vertical dashed line is at the frequency that 80% of the signal energy is below. The solid black line shows the phase–frequency slope (PFS).

The expectation of the results was that the rot group would have the highest PFS and ToF and the transition group would have the second highest PFS and ToF. After those groups, expectations were not clear. Experience indicated that the group with the next highest amount of decay was likely to be the below hole group, or the area immediately below drilled bolt holes. Water intruding into the pole around the bolt hole would probably pool in the hole and create an environment conducive for decay. The next group would probably be the above hole group but only if enough water entered the drilled hole to wet

both above and below the bolt. The good group would probably have the lowest PFS and ToF. No expectation could confidently be made regarding the end of log group. Because the pole sections were cut from larger poles, the top and bottom cross-sectional surfaces were not exposed to the elements during the 80-year service. The pole sections were placed on their sides so water was not allowed to pool on the newly cut top cross sections or come in contact with the newly cut bottom cross sections.

Results

The data collected in Tables 1 and 2 are shown in Figure 3. Individual data points are shown as small symbols. The large symbol is the average for the group. As expected, the rot group had both the highest average ToF and PFS. The second highest average PFS was the below hole B group; however, the average ToF was comparable with the good G group. The transition group had the third highest average PFS and the second highest average ToF. The end of log, above hole, and good groups had closely overlapping ToF and PFS values.

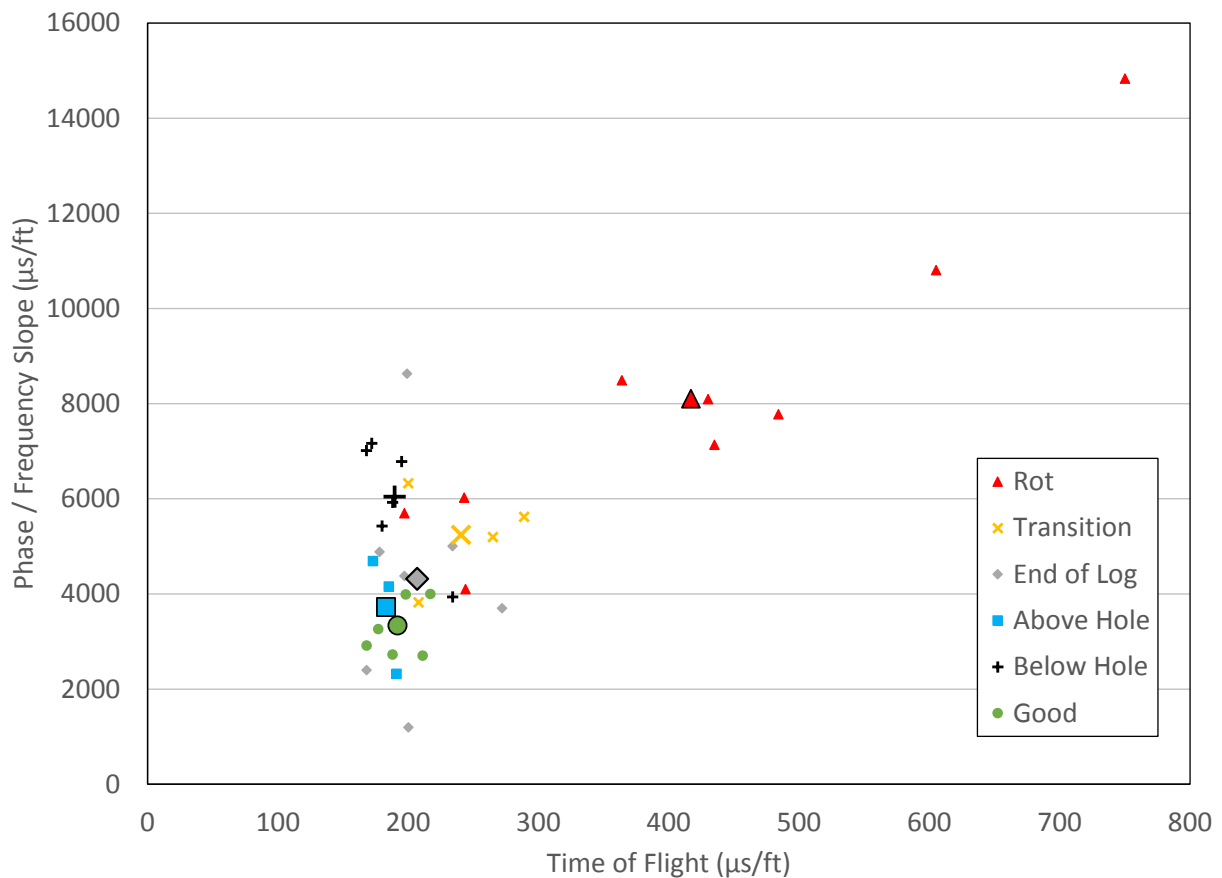


Figure 3. Time of flight versus phase–frequency slope. The small symbols represent the data points within each designation group. The large symbols represent the average value for the group.

Table 1. Time of flight (ToF), phase–frequency slope (PFS), and designation groups for poles B1, B2, and B3

Loc. (ft)	Fakopp ToF (μs/ft)			Tree Check ToF (μs/ft)			Tree Check PFS (μs/ft)			Designation group ^a		
	B1	B2	B3	B1	B2	B3	B1	B2	B3	B1	B2	B3
0.5	244	372	4,101	484	778	7,775	200	325	1,198	R	R	E
1	197	296	5,695	364	428	8,493	188	320	2,728	R	R	G
2	208	317	3,822	289	500	5,623	184	297	3,748	T	T	G
3	217	316	3,999	272	395	3,702	211	340	2,703	G	E	G
3.5	—	—	—	—	—	—	265	392	5,199	—	—	T
4	200	290	6,325	—	—	—	430	538	8,095	T	—	R
4.5	—	—	—	—	—	—	605	844	10,805	—	—	R
5	435	535	7,137	—	—	—	750	929	14,835	R	—	R

^aDesignation groups: R = rot, T = transition, E = end of log, A = above hole, B = below hole, G = good.

Table 2. Time of flight (ToF), phase–frequency slope (PFS), and designation groups for poles G1, G2, and G3

Loc. (ft)	Fakopp ToF (μs/ft)			Tree Check ToF (μs/ft)			Tree Check PFS (μs/ft)			Designation group ^a		
	G1	G2	G3	G1	G2	G3	G1	G2	G3	G1	G2	G3
0.5	168	265	2,401	197	304	4,379	178	290	4,886	E	E	E
1	168	276	2,918	191	306	2,322	177	283	3,260	G	A	G
2	195	302	6,784	188	293	5,927	168	271	7,013	B	B	B
3	180	287	5,429	234	345	3,940	172	284	7,168	B	B	B
4	—	—	—	—	—	—	—	—	—	A	G	A
5	185	282	4,159	198	296	3,990	173	281	4,691	R	E	E

^aDesignation groups: R = rot, T = transition, E = end of log, A = above hole, B = below hole, G = good.

Concluding comments

Six pole sections from the disassembled Eagle Tower in Peninsula State Park in Door County, Wisconsin, were studied using advanced frequency analysis techniques that examined the magnitude and phase within the frequency domain. During inspection, data were separated based on a combination of visible characteristics and ToF values at the measurement location. The six groups were rot, transition, end of log, above hole, below hole, and good. Expected results were obtained for each group except for the below hole group. Although it was considered likely that rot was present below the drilled holes because of the intrusion of water during the service life, it is unknown as to why the ToF measurement would be similar to the good group. A more in-depth inspection has been deemed necessary to evaluate the use of PFS as a nondestructive inspection method. Permission has been obtained to retrieve the six pole sections inspected in this project and transport them to FPL in Madison, Wisconsin, for further study, including the use of microresistance drilling. If the test locations of the below hole group are shown to possess decay, then the PFS method appears to be more sensitive to the presence of internal decay than the currently accepted method of using ToF.

Appendix

Figure 3 and Tables 1 and 2 are reproduced here in SI units as Figure A1 and Tables A1 and A2, respectively. Two data points are not shown on Figure A1 that are shown in Figure 3; the two data points that have the highest ToF and PFS values were excluded in Figure A1. The two excluded points were clearly indicated as rot by ToF, PFS, and visual inspection. As such, they were omitted in favor of producing a figure in which the other data points could be more clearly viewed.

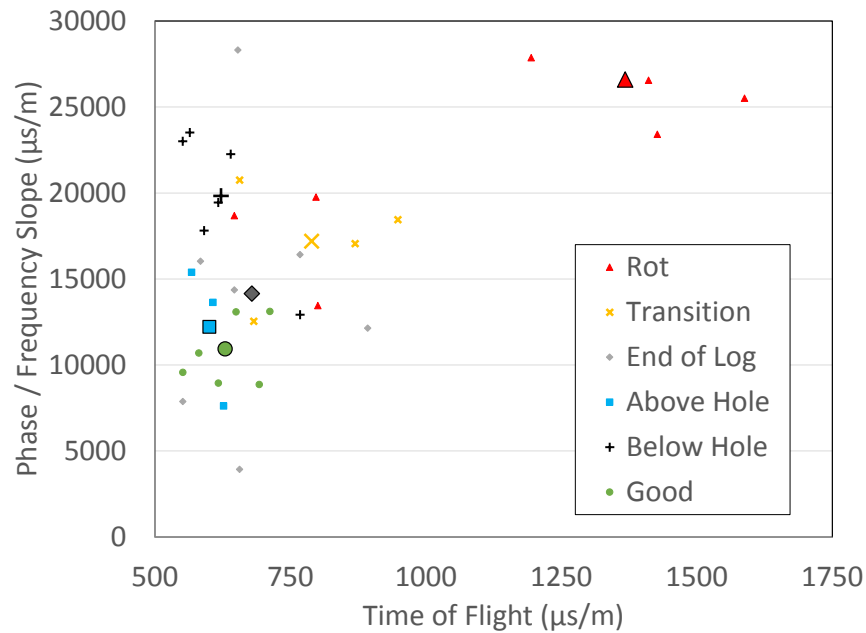


Figure A1. Time of flight versus phase–frequency slope. The small symbols represent the data points within each designation group. The large symbols represent the average value for the group.

Table A1. Time of flight (ToF), phase–frequency slope (PFS), and designation groups for poles B1, B2, and B3

Loc. (m)	Fakopp ToF (µs/m)			Tree Check ToF (µs/m)			Tree Check PFS (µs/m)			Designation group ^a		
	B1	B2	B3	B1	B2	B3	B1	B2	B3	B1	B2	B3
0.15	801	1,220	13,455	1,588	2,552	25,509	656	1,066	3,930	R	R	E
0.30	646	971	18,684	1,194	1,404	27,864	617	1,050	8,950	R	R	G
0.61	682	1,040	12,539	948	1,640	18,448	604	974	12,297	T	T	G
0.91	712	1,037	13,120	892	1,296	12,146	692	1,115	8,868	G	E	G
1.07	—	—	—	—	—	—	869	1,286	17,057	—	—	T
1.22	656	951	20,751	—	—	—	1,411	1,765	26,558	T	—	R
1.37	—	—	—	—	—	—	1,985	2,769	35,449	—	—	R
1.52	1,427	1,755	23,415	—	—	—	2,461	3,048	48,671	R	—	R

^aDesignation groups: R = rot, T = transition, E = end of log, A = above hole, B = below hole, G = good.

Table A2. Time of flight (ToF), phase–frequency slope (PFS), and designation groups for Poles G1, G2, and G3

Loc. (ft)	Fakopp ToF ($\mu\text{s/m}$)			Tree Check ToF ($\mu\text{s/m}$)			Tree Check PFS ($\mu\text{s/m}$)			Designation group ^a		
	G1	G2	G3	G1	G2	G3	G1	G2	G3	G1	G2	G3
0.15	551	869	7,877	646	997	14,367	584	951	16,030	E	E	E
0.30	551	906	9,573	627	1,004	7,618	581	928	10,696	G	A	G
0.61	640	991	22,257	617	961	19,446	551	889	23,009	B	B	B
0.91	591	942	17,812	768	1,132	12,927	564	932	23,517	B	B	B
1.22	607	925	13,645	650	971	13,091	568	922	15,390	A	G	A
1.52	797	1,188	19,767	768	1,115	16,417	653	889	28,314	R	E	E

^aDesignation groups: R = rot, T = transition, E = end of log, A = above hole, B = below hole, G = good.

References

- Allison, R.B.; Wang, X.; Ross, R.J. 2008. Visual and nondestructive evaluation of red pines supporting a ropes course in the USFS Nesbit Lake Camp, Sidnaw, MI. Proceedings, 15th Nondestructive Testing of Wood Symposium, September 10–12, 2007, Duluth, MN: Forest Products Society: 43-48.
- Brashaw, B.K.; Vatalaro, R.J.; Wang, X.; Ross, R.J.; Wacker, J.P. 2005. Condition assessment of timber bridges. 2. Evaluation of several stress wave tools. Gen. Tech. Rep. FPL–GTR–160. Madison, WI: U.S. Department of Agriculture, Forest Service, Forest Products Laboratory: 11 p.
- Clausen, C.A.; Ross, R.J.; Forsman, J.W.; Balachowski, J.D. 2001. Condition assessment of roof trusses of Quincy mine blacksmith shop in Keweenaw National Historical Park. Res. Note FPL–RN–0281. Madison, WI: U.S. Department of Agriculture, Forest Service, Forest Products Laboratory. 4 p.
- Dundar, T.; Ross, R.J. 2012. Condition assessment of 2500 year old wood coffin. Res. Note FPL–RN–0327. Madison, WI: U.S. Department of Agriculture, Forest Service, Forest Products Laboratory. 3 p.
- Emerson, R.; Pollock, D.; McLean, D.; Fridley, K.; Pellerin, R.; Ross, R.J. 2002. Ultrasonic inspection of large timber bridge members. *Forest Products Journal*. 52(9): 88-95.
- Franca, F.; Franca, T.; Yeary, L.A.; Hohnholt, C.; Forsman, J.W.; Ross, R.J. 2015. Condition assessment of a historic trout rearing station in upper Michigan. Res. Note. FPL–RN–334. Madison, WI: U.S. Department of Agriculture, Forest Service, Forest Products Laboratory. 5 p.
- McGovern, M.; Senalik, A.; Chen, G.; Beall, F.C.; Reis, H. 2011. Effect of decay on ultrasonic velocity and attenuation measurements in wood. In: *SPIE smart structures and materials - nondestructive evaluation and health monitoring*. Bellingham, WA: International Society for Optics and Photonics. Vol. 7910: 79810N-1–79810N-13.
- Ross, R.J.; Brashaw, B.K.; Wang, X. 2006. Structural condition assessment of in-service wood. *Forest Products Journal*. 56(6): 4-8.

Ross, R.J.; Soltis, L.A.; Otton, P. 1998. Assessing wood members in the USS Constitution using nondestructive evaluation methods. *APT Bulletin*. 29(2): 21-25.

Ross, R.J.; Volny, N.; Pellerin, R.F.; Salsig, W.W.; Falk, R.H. 1999. Inspection of timber bridges with stress wave nondestructive evaluation tools. A guide for use and interpretation. Gen. Tech. Rep. FPL–GTR–114. Madison, WI: U.S. Department of Agriculture, Forest Service, Forest Products Laboratory.

Sachse, W. 1978. Measurement of phase and group velocities of dispersive waves in solids. In: Proceedings of the ARPA/AFML review of progress in quantitative NDE. Sept. 1976–June 1977. 24.

Senalik, A.; Beall, F.C.; Reis, H. 2010. Detection and assessment of wood decay in glulam beams using a decay rate approach. *Insight - Non-Destructive Testing and Condition Monitoring*. 52(10): 553-560.

Wang X.; Wacker, J.P.; Ross, R.J.; Brashaw, B.K. 2008. Condition assessment of main structural members of steam schooner WAPAMA. Gen. Tech. Rep. FPL–GTR–177. Madison, WI: U.S. Department of Agriculture, Forest Service, Forest Products Laboratory. 29 p.

White, R.H.; Ross, R.J. 2014. Wood and timber condition assessment manual. Second Edition. Gen. Tech. Rep. FPL–GTR–324. Madison, WI: U.S. Department of Agriculture, Forest Service, Forest Products Laboratory. 102 p.



Session 9

**Wood Material
Characterization II**

Correlations between the Mechanical Properties of Scots Pine Wood Determined by Micro-Size and Standard-Size Test Specimens

Türker Dündar *

Faculty of Forestry, Istanbul University, Istanbul, Turkey, dundar@istanbul.edu.tr

Ümit Büyüksarı

Faculty of Forestry, Duzce University, Duzce, Turkey, umitbuyuksari@duzce.edu.tr

Nusret As

Faculty of Forestry, Istanbul University, Istanbul, Turkey, nusretas@istanbul.edu.tr

* Corresponding author

Abstract

The aim of this study was to investigate the correlations between the mechanical properties determined by micro-size and standard-size test specimens in Scots pine (*Pinus sylvestris* L.) wood. Eight trees with straight stems were selected as sample trees. Logs of 3 m in length were cut from each tree at a height of 0.30 m, and then 6-cm-thick planks, including the central pith, were cut from these logs. The micro-size and standard-size specimens for bending, tensile and compression tests were prepared from these planks. The bending strength, modulus of elasticity in bending, tensile strength and compression strength values were determined using micro- and standard-size samples. A regression analysis was used to determine the relationship between the standard- and the micro-size specimens in individual trees and all trees. The regression analyses indicated a strong, positive linear relationship between the mechanical properties of the micro- and standard-size specimens. The correlation coefficients ranged from 74.9 to 83.9 for bending strength, ranged from 73.7 to 79.8 for modulus elasticity, ranged from 71.9 to 82.1 for tensile strength, and ranged from 72.0 to 85.2 for compression strength.

Keywords: micro-size test, standard-size test, mechanical properties, scots pine

Introduction

To determine the mechanical properties of wood, the approach to use both structural-size and small-size clear specimens has grown in popularity. In recent years, micro-size specimens have been used to evaluate the mechanical properties of earlywood and latewood sections, wood strands, and fibers (Plagemann 1982; Hunt et al. 1989; Deomano and Zink-Sharp 2004; Zink-Sharp and Price 2004; Wu et al. 2005; Cai et al. 2007; Hindman and Lee 2007; Jeong 2008; Jeong et al. 2009; Roszyk et al. 2016; Büyüksarı et al, 2016). In previous studies, researchers used various specimen dimensions and loading rates according to the purpose of the study.

Micro-size specimens have the ability to be used to determine the mechanical properties of wood when obtaining standard-size test specimens is not possible. To avoid damaging the wood material for use in

various applications, the mechanical properties could be determined using micro-size test specimens. Moreover, the test specimens of structural wood material could be taken periodically and their mechanical properties determined. Thus, changes in the mechanical properties of the wood over time could be observed. With the development of micro-size tests, the strength losses from the length of exposure could be determined for the structural applications of the wood. This information would provide a solid base for a true assessment of the necessity of wooden structure renewal (Buyuksari et al, 2016).

There is limited information concerning a comparison of the mechanical properties of micro- and standard-size specimens. In previous studies, researchers compared their findings for micro-size test specimens with the published values in the *Wood Handbook* (Green *et al.* 1999) for standard-size specimens (Deomano 2001; Zink-Sharp and Price 2006; Cai *et al.* 2007). Deomano (2001) reported that the bending strength (MOR) and modulus elasticity (MOE) values of the micro-size specimens were lower than those of standard-size specimens for southern yellow pine, sweet gum, and yellow poplar, except for the MOR of yellow poplar. Cai *et al.* (2007) found that for willow, yellow poplar, red oak, and loblolly pine strands, the tensile strengths were, respectively, 31.1%, 44.2%, 36.2%, and 73.4% lower than that of standard-size specimens. Zink-Sharp and Price (2006) stated that the compression strength of the micro-size specimens was close to, but lower than, the handbook values for the sweet gum, yellow poplar, and maple wood species. The aim of this paper is to investigate the correlations between the mechanical properties determined by micro-size and standard-size test specimens in Scots pine (*Pinus sylvestris* L.) wood.

Materials and methods

Materials

Sample trees were harvested from Bolu Forest Enterprises in the northwestern part of Turkey. Eight trees with straight stems were selected as sample trees. Logs of 3 m in length were cut from each tree at a height of 0.30 m, and then 6-cm-thick planks, including the central pith, were cut from these logs. The micro- and standard-size test specimens were prepared from these planks. The cutting plan of the test specimens is shown in Fig. 1. All of the specimens were conditioned in a climate chamber at a temperature of 20 °C and a relative humidity of 65% for three weeks to reach a target moisture content of 12% prior to testing.

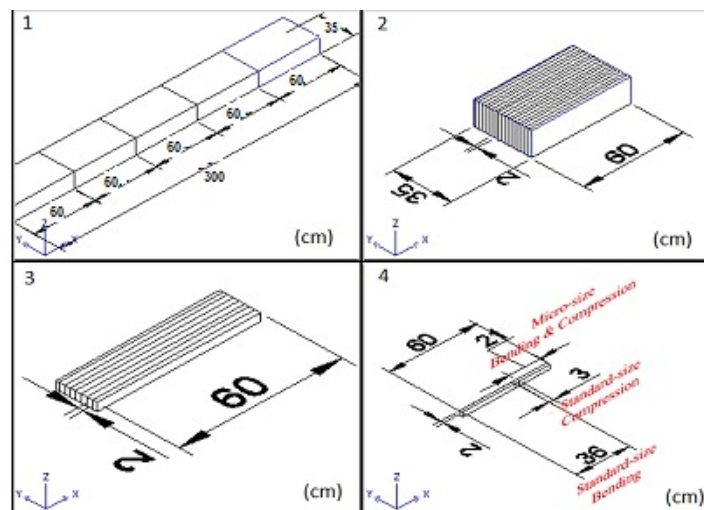


Figure 1. Cutting plan of standard- and micro-size flexural test specimens

Methods

The specimens were cut according to the International Organization for Standardization (ISO) to determine the bending strength (ISO 13061-3 2014) and modulus of elasticity in bending (ISO 13061-4 2014). The standard-size test specimens were prepared with dimensions of 20 mm × 20 mm × 360 mm for the flexural test. In the three-point bending test, the load was applied tangential to the annual rings, and the span/thickness ratio was 15. A Lloyd (Lloyd Instruments, LS100, FL, USA) universal testing machine with a 10-kN load cell was used for the standard-size tests.

The micro-size tests were performed with a Zwick (Zwick GmbH & Co., ZO50TH, Ulm, Germany) universal testing machine using a 100-N load cell. The same ISO standards were used as a guide for the micro-size specimens. The micro-size flexural test specimens were approximately 0.8 to 1.2 mm × 5.0 mm × 50.0 mm. The tests were performed with a three-point bending fixture. The same span/thickness ratio, 15, was used for both the micro-size and standard-size bending tests. The micro-size bending test specimen and test setup are shown in Fig. 2.

Data Analyses and Statistical Methods

A regression analysis was used to determine the relationship between the standard- and the micro-size specimens. The correlation coefficient, equation, F value and significance values between the mechanical properties of standard- and the micro-size specimens.

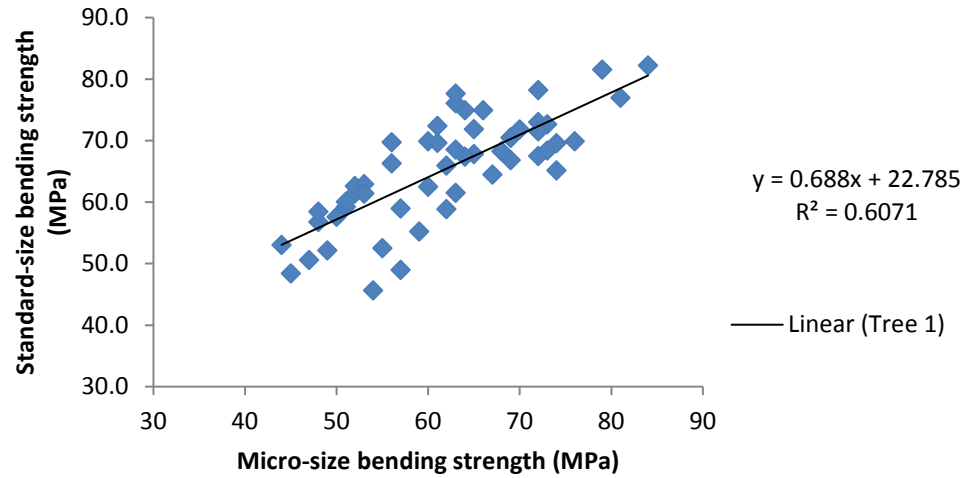
Results and Discussion

The correlation coefficients, equations, F values, and significance between bending strength of micro- and standard-size samples of Scots pine wood are shown in Table 2.

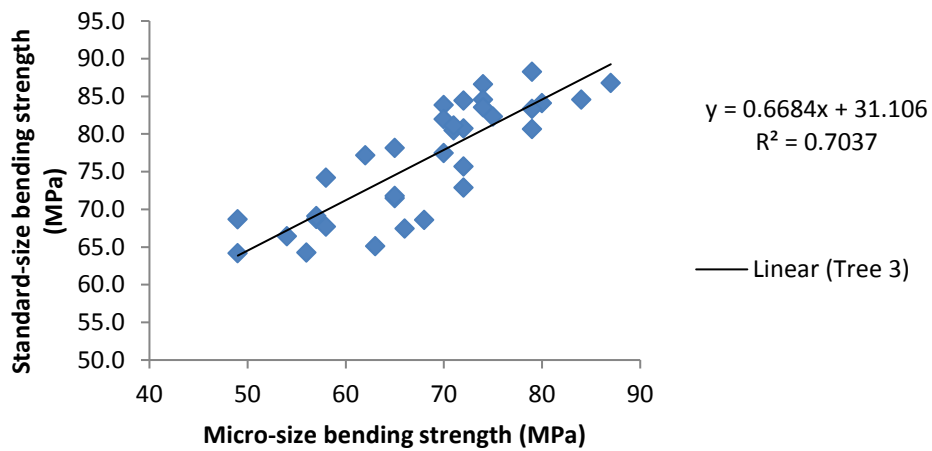
Table 2. The correlations between bending strength of micro- and standard-size samples of Scots pine wood

Tree Number	Correlation coefficient	Equation	F value	Sig.
1	0,78	$y = 0,688x + 22,785$	80,4	0,000
2	0,80	$y = 1,0064x + 5,4949$	39,5	0,000
3	0,84	$y = 0,6684x + 31,106$	76,0	0,000
4	0,78	$y = 0,5143x + 41,226$	78,3	0,000
5	0,75	$y = 0,5673x + 37,213$	43,5	0,000
6	0,78	$y = 0,6764x + 37,864$	51,2	0,000
7	0,80	$y = 0,6271x + 30,519$	50,8	0,000
8	0,83	$y = 0,6468x + 34,127$	55,0	0,000
All	0,78	$y = 0,736x + 25,83$	460,5	0,000

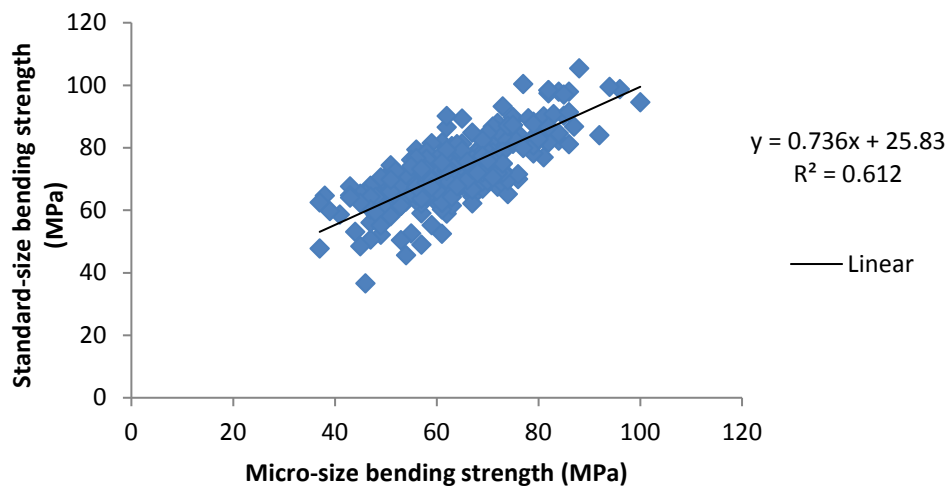
The correlation graphs of tree 1, tree 3 and all values between bending strength of micro- and standard-size samples of Scots pine wood are shown in Figure 2 a, b, and c, respectively.



(a)



(b)



(c)

Figure 2. Correlation graphichs of tree 1 (a), tree 3 (b) and all trees (c) between bending strength of micro- and standard-size samples of Scots pine wood

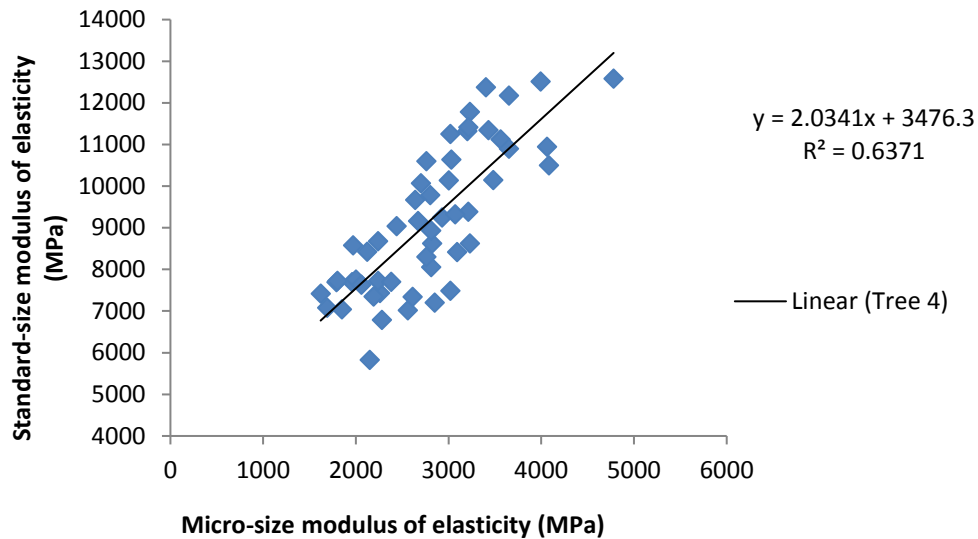
The regression analyses indicated that the bending strength of micro- and standard-size samples of Scots pine wood had a good relationship at the 95 % confidence level. The correlation coefficients ranged from 0.75 to 0.84.

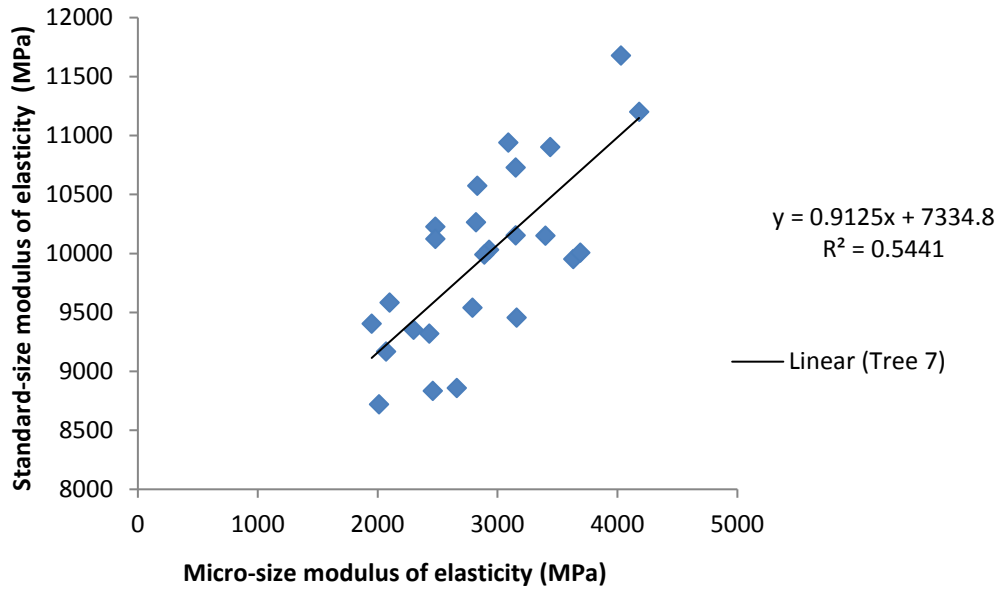
The correlation coefficients, equations, F values, and significance between the modulus of elasticity of micro- and standard-size samples of Scots pine wood are shown in Table 3.

Table 3. The correlations between the modulus of elasticity of micro- and standard-size samples of Scots pine wood

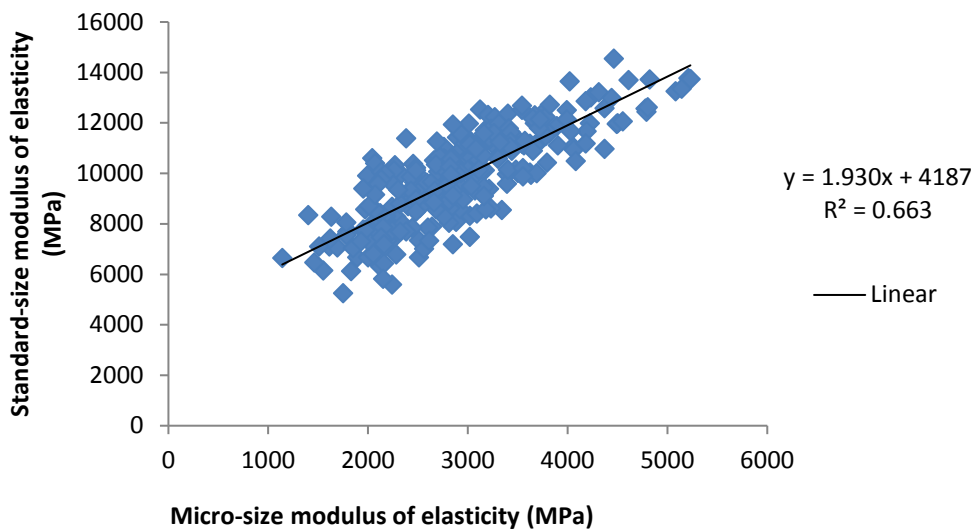
Tree Number	Correlation coefficient	Equation	F value	Sig.
1	0,77	$y = 2,4999x + 2693,8$	68,3	0,000
2	0,79	$y = 1,7055x + 3508,1$	35,0	0,000
3	0,78	$y = 1,3309x + 6498,9$	49,8	0,000
4	0,80	$y = 2,0341x + 3476,3$	87,8	0,000
5	0,74	$y = 2,3976x + 3818,7$	41,6	0,000
6	0,80	$y = 1,3493x + 6818,6$	48,1	0,000
7	0,74	$y = 0,9125x + 7334,8$	27,5	0,000
8	0,77	$y = 2,201x + 3137,3$	29,9	0,000
All	0,81	$y = 1,930x + 4187$	535,2	0,000

The correlation graphichs of tree 4, tree 7 and all values between the modulus elasticity of micro- and standard-size samples of Scots pine wood are shown in Figure 3a, b, and c, respectively.





(b)



(c)

Figure 3. Correlation graphs of tree 4 (a), tree 7 (b) and all trees (c) between modulus elasticity of micro- and standard-size samples of Scots pine wood

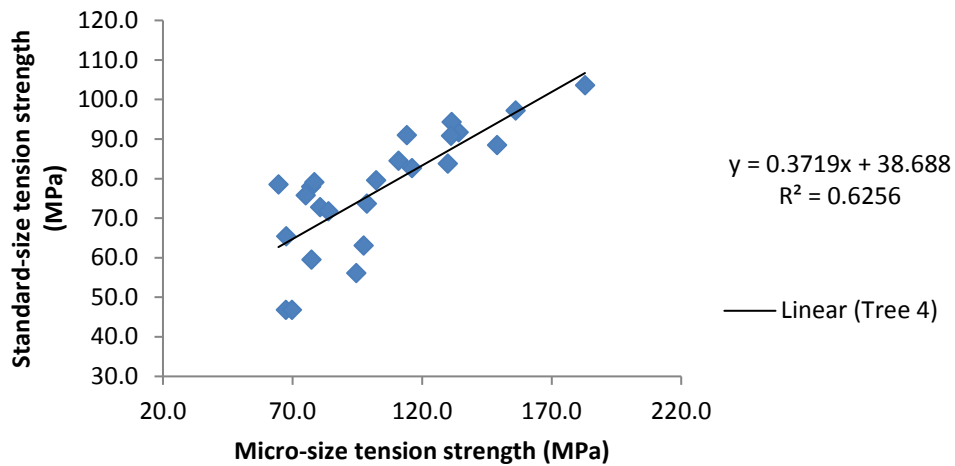
The regression analyses indicated that the modulus of elasticity of micro- and standard-size samples of Scots pine wood had a good relationship at the 95 % confidence level. The correlation coefficients ranged from 0.74 to 0.81.

The correlation coefficients, equations, F values, and significance between tensile strength of micro- and standard-size samples of Scots pine wood are shown in Table 4.

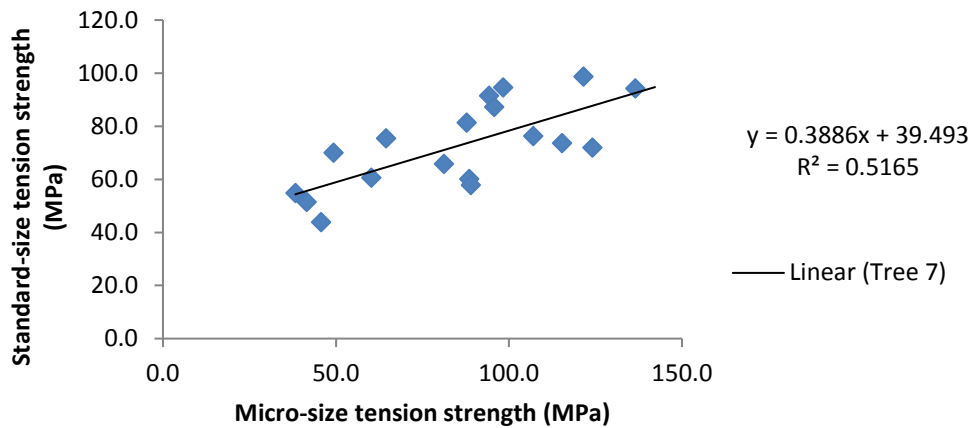
Table 4. The correlations between tensile strength of micro- and standard-size samples of Scots pine wood

Tree Number	Correlation coefficient	Equation	F value	Sig.
1	0,77	$y = 0,853x - 3,3481$	24,3	0,000
2	0,81	$y = 0,651x + 29,62$	15,8	0,004
3	0,75	$y = 0,812x + 6,470$	18,3	0,000
4	0,79	$y = 0,371x + 38,68$	36,8	0,000
5	0,82	$y = 0,8159x + 7,8908$	28,9	0,000
6	0,77	$y = 0,4148x + 44,865$	25,4	0,000
7	0,72	$y = 0,3886x + 39,493$	17,1	0,000
8	0,73	$y = 0,351x + 30,01$	19,2	0,000
All	0,71	$y = 0,486x + 30,10$	141,6	0,000

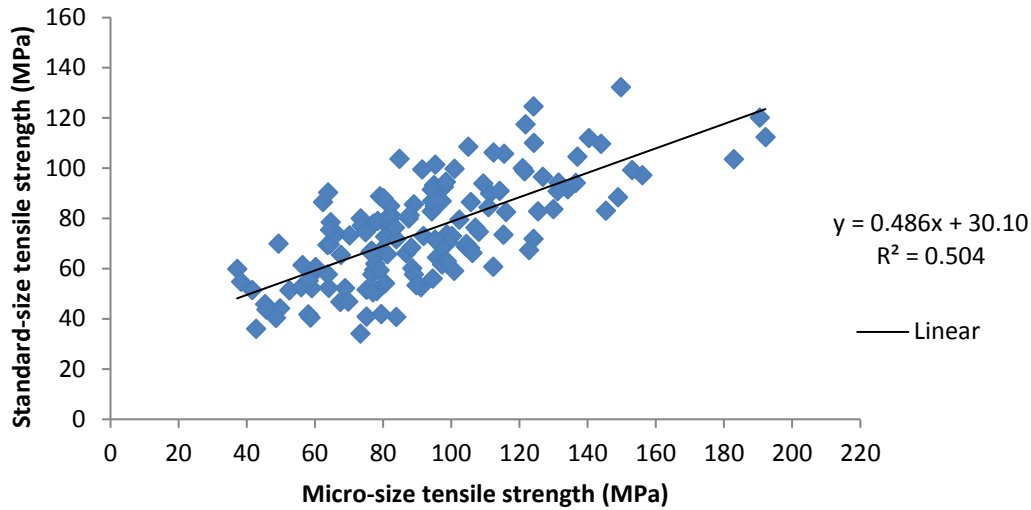
The correlation graphichs of tree 4, tree 7 and all values between tensile strength of micro- and standard-size samples of Scots pine wood are shown in Figure 4a, b, and c, respectively.



(a)



(b)



(c)

Figure 4. Correlation graphichs of tree 4 (a), tree 7 (b) and all trees (c) between tensile strength of micro- and standard-size samples of Scots pine wood

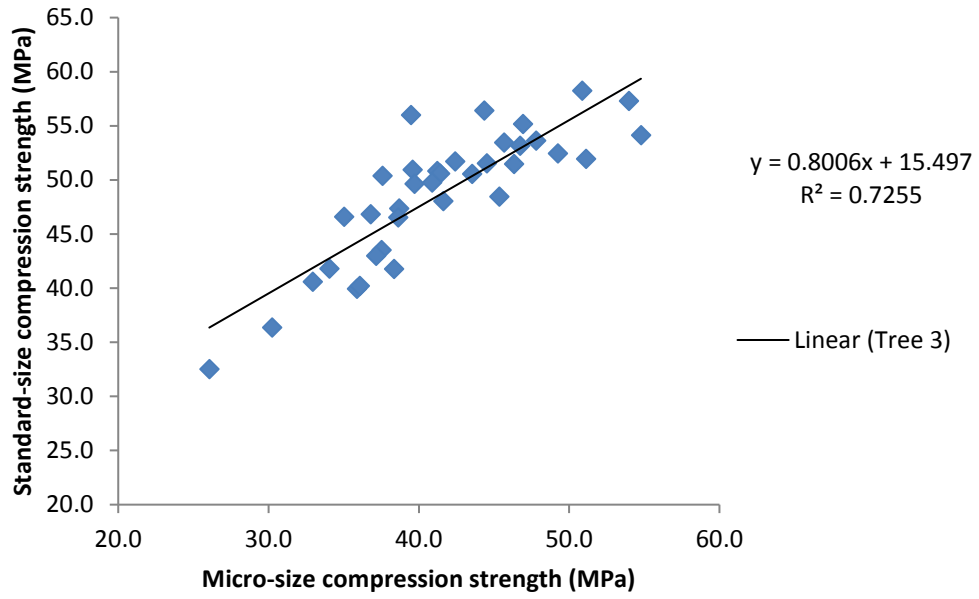
The regression analyses indicated that the tensile strength of micro- and standard-size samples of Scots pine wood had a good relationship at the 95 % confidence level. The correlation coefficients ranged from 0.71 to 0.82.

The correlation coefficients, equations, F values, and significance between compression strength of micro- and standard-size samples of Scots pine wood are shown in Table 5.

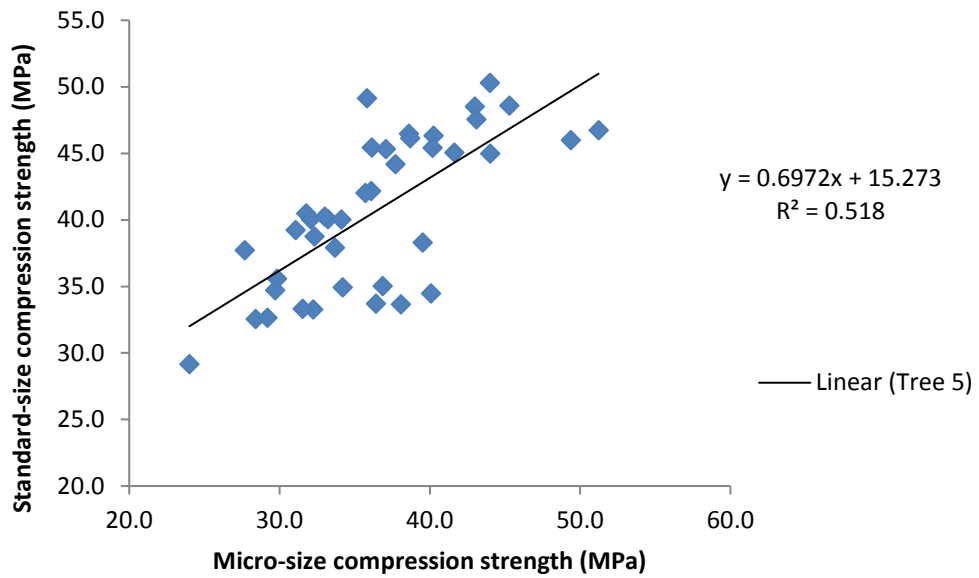
Table 5. The correlations between compression strength of micro- and standard-size samples of Scots pine wood

Tree Number	Correlation coefficient	Equation	F value	Sig.
1	0,81	$y = 0,7913x + 12,085$	70,4	0,000
2	0,78	$y = 0,763x + 10,785$	55,8	0,000
3	0,85	$y = 0,8006x + 15,497$	89,8	0,000
4	0,81	$y = 0,8538x + 9,5309$	81,8	0,000
5	0,72	$y = 0,6972x + 15,273$	40,8	0,000
6	0,79	$y = 0,8609x + 15,194$	68,9	0,000
7	0,79	$y = 1,0309x + 3,4012$	56,1	0,000
8	0,78	$y = 0,6349x + 19,08$	59,1	0,000
All	0,82	$y = 0,938x + 7,651$	636,4	0,000

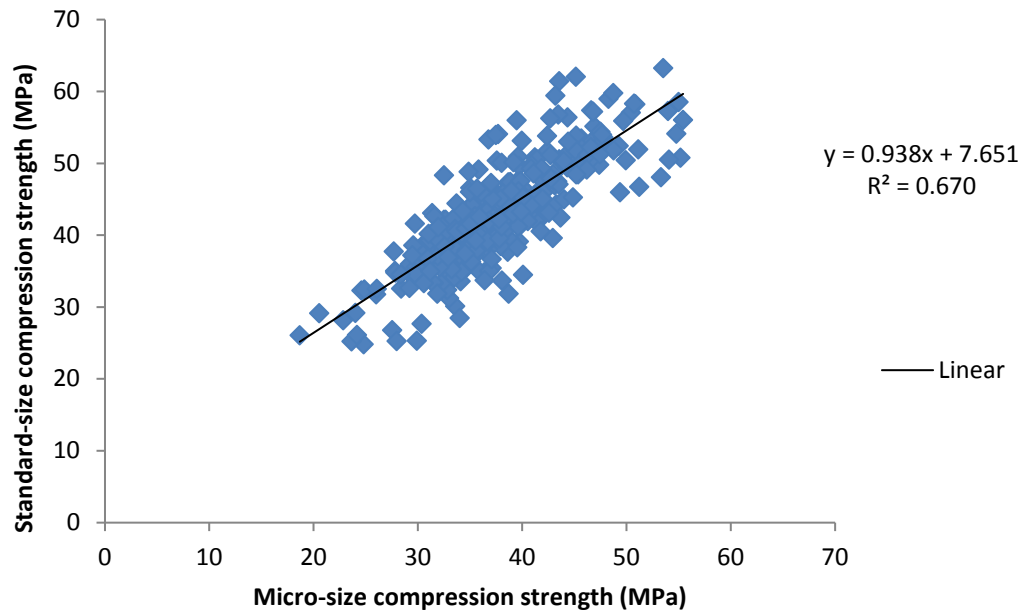
The correlation graphichs of tree 3, tree 5 and all values between compression strength of micro- and standard-size samples of Scots pine wood are shown in Figure 5a, b, and c, respectively.



(a)



(b)



(c)

Figure 5. Correlation graphics of tree 3 (a), tree 5 (b) and all trees (c) between compression strength of micro- and standard-size samples of Scots pine wood

The regression analyses indicated that the compression strength of micro- and standard-size samples of Scots pine wood had a good relationship at the 95 % confidence level. The correlation coefficients ranged from 0.72 to 0.85.

Conclusions

The regression analyses indicated that the bending strength, modulus of elasticity, tension strength, and compression strength of micro-size and standard –size samples had a good relationship at the 95 % confidence level. The correlation coefficients ranged from 74.9 to 83.9 for bending strength, ranged from 73.7 to 79.8 for modulus elasticity, ranged from 71.9 to 82.1 for tensile strength, and ranged from 72.0 to 85.2 for compression strength.

References

- Buyuksari, U.; As, N.; Dündar, T.; Sayan, E. 2016. Comparison of micro- and standard-size specimens in evaluating the flexural properties of scots pine wood. *BioResources* 11(4), 10540-10548.
- Cai, Z.; Wu, Q.; Han, G.; Lee, J.N. 2007. Tensile and thickness swelling properties of strands from Southern hardwoods and Southern pine: Effect of hot-pressing and resin application. *Forest Products Journal* 57(5): 36-40.
- Deomano, E.C. 2001. Mechanism of Flake Drying and Its Correlation to Quality, Ph. D. Dissertation, Virginia Polytechnic Institute & State University, Blacksburg, VA.
- Deomano, E.C.; Zink-Sharp, A. 2004. Bending properties of wood flakes of three southern species. *Wood Fiber Sci.* 36(4), 493-499.

Green, D.W.; Winandy, J.E.; Kretschmann, D.E. 1999. Mechanical properties of wood. In: Wood handbook-Wood as an engineering material, Gen. Tech. Rep. FPL–GTR–113, Chapter 12. U.S. Department of Agriculture, Forest Service, Forest Products Laboratory: Madison, WI, 463 p

Hindman, D.P.; Lee, J.N. 2007. Modeling wood strands as multi-layer composites: Bending and tension loads. *Wood Fiber Sci.* 39(4), 516-526.

Hunt, M.O.; Triche, M.H.; McCabe, G.P.; Hoover, W.L. 1989. Tensile properties of yellow-poplar veneer strands. *Forest Products Journal* 39(9): 31-33.

Jeong, G.Y. 2008. Tensile Properties of Loblolly Pine Strands Using Digital Image Correlation and Stochastic Finite Element Method, Ph. D. Dissertation, Virginia Polytechnic Institute & State University, Blacksburg, VA.

Jeong, G.Y.; Zink-Sharp, A.; Hindman, D.P. 2009. Tensile properties of earlywood and latewood from loblolly pine (*Pinus taeda*) using digital image correlation. *Wood Fiber Sci.* 41(1), 51-63.

Plagemann, W.L. 1982. The response of hardwood flakes and flakeboard to high temperature drying. Master's thesis, Washington State University, Pullman, WA

Roszyk, E.; Molinski, W.; Kaminski, M. 2016. Tensile properties along the grains of earlywood and latewood of Scots pine (*Pinus sylvestris* L.) in dry and wet state. *BioResources* 11(2), 3027-3037.

Wu, Q.; Cai, Z.; Lee, J.N. 2005. Tensile and dimensional properties of wood strands made from plantation southern pine lumber. *Forest Prod J* 52(2):1-6.

Zink-Sharp, A.G.; Price, C. 2006. Compression strength parallel to the grain within growth rings of low density hardwoods. *Maderas: Ciencia y Tecnologia* 8(2): 117-126.

Effects of Polyhedral Specimen Reduction in Wood Characterization by Ultrasound

Cinthy Bertoldo*

Laboratory of Nondestructive Testing - LabEND, School of Agricultural Engineering - FEAGRI - University of Campinas – UNICAMP, Brazil. E-mail: cinthya.bertoldo@feagri.unicamp.br

Renata Flores

Laboratory of Nondestructive Testing - LabEND, School of Agricultural Engineering - FEAGRI - University of Campinas – UNICAMP, Brazil. E-mail: renata_flores_@hotmail.com

Raquel Gonçalves

Laboratory of Nondestructive Testing - LabEND, School of Agricultural Engineering - FEAGRI - University of Campinas – UNICAMP, Brazil. E-mail: raquel@feagri.unicamp.br

Carlos Vazquez

Department of Agroforestry Engineering, University of Santiago de Compostela, Campus Universitario, 27002 Lugo, Spain. E-mail: carlosenriquevazquezvazquez@gmail.com

* Corresponding author

Abstract

This research aimed to study the influence of reduction the polyhedral specimen, in dimension and number of faces, in values of the twelve elastic parameters involved in the wood characterization by ultrasound. For achieve the objective we used polyhedral specimens with 26 faces with two different sizes and also polyhedral specimens with 18 faces. One of polyhedral specimen with 26 faces had the face dimension greater than the transducer diameter and the other one smaller. The polyhedral with 18 faces has the face dimension greather than the transducer diameter. The tests were performed using ultrasound equipment and longitudinal and shear 1000-kHz transducers. The results indicated that only two (E_R and G_{LT}) of the twelve elastic parameters calculated showed statistically significant differences according to the size and/or the specimen geometry used. The remaining parameters have values statistically equivalent using the three polyhedral specimens.

Keywords: Poisson's ratio, elastic constants, modulus of elasticity.

Introduction

Brazil has part of the largest tropical forest in the world, as well as other large forest reserves, although wood does not stand out as a fundamental material in the construction sector. This is due to the traditions of masonry construction, a lack of constructive techniques and a lack of knowledge of the mechanical properties of wood. The use of wood has the advantages of comfort, durability, energy savings, and fast assembly, as well as wood is a sustainable material, come from a renewable resource and bringing nature to urban environments.

Increasingly precise and potent computer programs have made knowledge of material properties essential. Acquiring this knowledge is particularly difficult when dealing with wood, because as an orthotropic material it has different proprieties in the three main directions (Longitudinal, Radial and

Tangential). Knowing its behavior implies determining 12 elastic parameters – 3 longitudinal elasticity modules (E_L , E_R , E_T), 3 shear modules (G_{LR} , G_{LT} , G_{RT}) and 6 Poisson ratios (ν_{LR} , ν_{LT} , ν_{RL} , ν_{RT} , ν_{TL} , ν_{TR}).

All these properties can be determined through static testing, but such tests are costly and arduous. Mascia (1991) and Furlani (1995) presented a methodology for determining compliance matrix using static compression test. For such test, 6 prismatic specimens were used in each sample. From the three specimens retrieved from the symmetry axis, the three Young modules can be obtained, as well as the six Poisson ratios. The three shear modules can be found using specimens obtained out of axes on the three symmetry planes. Six strain gages are bonded to each specimen.

François (1995) suggested a 26-faced polyhedron as a specimen to determine the elastic constants of wood using wave propagation. The advantage of this specimen is that it allows obtaining all the elements of the stiffness matrix using a single polyhedron.

Trinca (2011) evaluated the test's methodology using ultrasound to determine the elastic constants in wood using three specimen geometries: prismatic, multi-faced disc, and 26-faced polyhedron. The author concluded that all three geometries present equivalent results, but the 26-faced polyhedron implies in reduced sampling and is easier to product.

Although the polyhedral test specimen, used in the characterization of the wood, is already well established (Trinca, 2011; Gonçalves et al., 2011, Bertoldo et al., 2013, Gonçalves et al., 2014 and Vázquez et al., 2015) and presents good results for calculate the properties of longitudinal and transverse modulus of elasticity, the values obtained for the Poisson ratio still show some divergences. The difficulty of obtaining these parameters (Poisson ratio) is mainly related to the slope of the growth rings, which can only be greatly minimized in very small test specimens. Therefore, the challenge of this work was to evaluate the possibility of reducing the size of the test piece, which nowadays is limited to the size of the transducer face. This reduction has the purpose of decrease the slope of the growth rings, which hampers the wave propagation in a unidirectional way, mainly in the radial and tangential directions.

Considering what was presented, the objective of this research was to compare the results of the complete characterization of the wood using polyhedron of 26 faces with dimensions traditionally used with polyhedrons of 26 faces with reduced face dimensions and with polyhedron with 18 faces.

Metodology

The polyhedrons were obtained from Amazonian's specie *Dinizia excels Ducke*. The wood was used to make the three types of polyhedral, one of them with 26 faces, traditionally used in our research group, with 55 mm face-to-face distance; the second with 26 faces and 30 mm face-to-face distance, and the last one with 18 faces and 35 mm face-to-face dimension.

We used 5 specimens for each type and dimension of polyhedron. Only for the polyhedron with 55 mm face-to-face distance we used 6 specimens, totaling 16 polyhedral specimens (Figure 1).

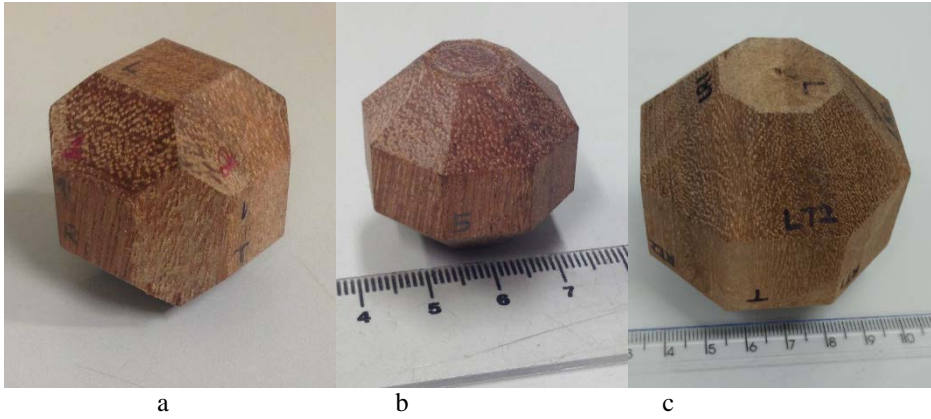


Figure 1 – Polyhedron with 18 faces (a), polyhedron with 26 faces and reduced size (b) and polyhedron with 26 faces and 55 mm face-to-face distance (c).

After the specimens' preparation, we performed ultrasonic tests (EPOCH 4, Panametrics, USA) to obtain the wave propagation velocities.

Ultrasound tests were performed using compression and shear transducers, with flat faces, and 1.0 MHz-frequency. For the tests with compression waves we used medical gel as coupling media between the material and the transducer and for the tests with shear transducers we used glucose syrup as coupling media (Figure 2).

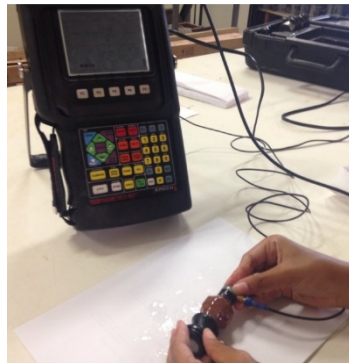


Figure 2 – Ultrasound test on polyhedron.

From the ultrasonic tests we obtained the time of wave propagation (t) between opposite faces of the polyhedron (L) and calculate the propagation velocity (V_{LL}) using Equation 1.

$$V_{LL} = \frac{L}{t} \quad (1)$$

The velocity results were used to determine the stiffness matrix $[C]$, using the Christoffel equations (Equations 2 to 10).

$$[C] = \begin{bmatrix} C_{11} & C_{12} & C_{13} & 0 & 0 & 0 \\ C_{21} & C_{22} & C_{23} & 0 & 0 & 0 \\ C_{31} & C_{32} & C_{33} & 0 & 0 & 0 \\ 0 & 0 & 0 & C_{44} & 0 & 0 \\ 0 & 0 & 0 & 0 & C_{55} & 0 \\ 0 & 0 & 0 & 0 & 0 & C_{66} \end{bmatrix}$$

$$C_{11} = C_{LL} = \rho \cdot V_{LL}^2 \quad (2)$$

$$C_{22} = C_{RR} = \rho \cdot V_{RR}^2 \quad (3)$$

$$C_{33} = C_{TT} = \rho \cdot V_{TT}^2 \quad (4)$$

$$C_{44} = C_{RT} = \rho \cdot ((V_{RT} + V_{TR}) / 2)^2 \quad (5)$$

$$C_{55} = C_{LT} = \rho \cdot ((V_{LT} + V_{TL}) / 2)^2 \quad (6)$$

$$C_{66} = C_{LR} = \rho \cdot ((V_{LR} + V_{RL}) / 2)^2 \quad (7)$$

$$(C_{12} + C_{66}) n_1 \cdot n_2 = [(C_{11}n_1^2 + C_{66}n_2^2 - \rho V_\alpha^2) \cdot (C_{11}n_1^2 + C_{66}n_2^2 - \rho V_\alpha^2)]^{1/2} \quad (8)$$

$$(C_{23} + C_{44}) n_2 \cdot n_3 = [(C_{22}n_2^2 + C_{44}n_3^2 - \rho V_\alpha^2) \cdot (C_{44}n_2^2 + C_{33}n_3^2 - \rho V_\alpha^2)]^{1/2} \quad (9)$$

$$(C_{13} + C_{55}) n_1 \cdot n_3 = [(C_{11}n_1^2 + C_{55}n_3^2 - \rho V_\alpha^2) \cdot (C_{55}n_1^2 + C_{33}n_3^2 - \rho V_\alpha^2)]^{1/2} \quad (10)$$

Where ρ ($\text{kg} \cdot \text{m}^{-3}$) is the apparent density ($\cong 12\%$ moisture content) of the wood; in equations 8, 9 and 10, V_α is the wave velocity out of axes with angle α , $n_1 = \cos \alpha$, $n_2 = n_3 = \sin \alpha$, where $\alpha = 45^\circ$ due to the shape of the specimen. The sub-indexes L, R and T indicate the longitudinal, radial and tangential directions of wave propagation and polarization, respectively.

After the stiffness matrix [C] calculation, we performed its inversion $[C]^{-1}$ obtaining the compliance matrix [S], which allows to calculate the elastic parameters and the Poisson ratios.

$$[S] = \begin{bmatrix} \frac{1}{E_1} & -\frac{\nu_{21}}{E_2} & -\frac{\nu_{31}}{E_3} & 0 & 0 & 0 \\ -\frac{\nu_{12}}{E_1} & \frac{1}{E_2} & -\frac{\nu_{32}}{E_3} & 0 & 0 & 0 \\ -\frac{\nu_{13}}{E_1} & -\frac{\nu_{23}}{E_2} & \frac{1}{E_3} & 0 & 0 & 0 \\ 0 & 0 & 0 & \frac{1}{G_{23}} & 0 & 0 \\ 0 & 0 & 0 & 0 & \frac{1}{G_{13}} & 0 \\ 0 & 0 & 0 & 0 & 0 & \frac{1}{G_{12}} \end{bmatrix}$$

On compliance matrix [S] the axes 1, 2, 3 can be replaced by the three wood directions: Longitudinal (L), Radial (R) and Transversal (T), respectively.

Results

The average density of *Dinizia excelsa* Ducke, used in this research, was $1124 \text{ kg} \cdot \text{m}^{-3}$ with coefficient of variation (CV) of 2.2%.

According to the Brazilian standard (ABNT NBR 7190/97), the coefficient of variation (CV) acceptable for stiffness is 28% and for wood strength is 18%. In the same standard, there is no reference value for the coefficient of variation of the Poisson ratio. Considering the data of this research, the coefficient of variation of the modulus of elasticity range from 1.0 for the transverse modulus in the LR plane (longitudinal-radial) for the polyhedron with 18 faces, until 12.6 for the longitudinal modulus (E_L) for the polyhedron with 26 faces of traditional size (Table 1).

Table 1 – Average elastic parameters and coefficients of variation (CV) for the different shapes and sizes polyhedrons used in the research.

Elastic parameters	26 faces of tradicional size		26 faces of reduced size		18 faces	
	Mean	CV (%)	Mean	CV (%)	Mean	CV (%)
E_L (MPa)	8477	12.6	7359	6.6	8456	4.8
E_R (MPa)	2368	6.4	2043	3.9	2138	9.7
E_T (MPa)	2284	6.6	2195	4.0	2274	5.0
G_{RT} (MPa)	851	10.6	925	1.8	918	2.0
G_{LT} (MPa)	1806	7.4	1540	7.8	1540	7.0
G_{LR} (MPa)	1773	6.2	1796	5.5	1857	1.0
ν_{RL}	0.34	8.3	0.33	5.4	0.32	1.4
ν_{TL}	0.21	11.1	0.24	11.1	0.22	9.9
ν_{LR}	1.22	5.8	1.27	5.3	1.28	8.4
ν_{TR}	0.14	26.6	0.14	32.8	0.14	12.8
ν_{LT}	0.80	8.5	0.79	6.9	0.80	12.0
ν_{RT}	0.13	22.4	0.13	29.6	0.14	16.4

E_L is the Young's modulus in the longitudinal direction, E_R is the Young's modulus in the radial direction, E_T is the Young's modulus in the tangential direction, G_{RT} is the shear modulus in the radial–tangential plane, G_{LT} is the shear modulus in the longitudinal–tangential plane, G_{LR} is the shear modulus in the longitudinal–radial plane, ν_{LR} is the longitudinal–radial Poisson's ratio, ν_{LT} is the longitudinal–tangential Poisson's ratio, ν_{RT} is the radial–tangential Poisson's ratio, ν_{RL} is the radial–longitudinal Poisson's ratio, ν_{TL} is the tangential–longitudinal Poisson's ratio, and ν_{TR} is the tangential–radial Poisson's ratio.

The reduction of polyhedral specimen size, by reducing the face size or by reducing the number of faces (18 faces), was able to reduce the coefficient of variation of eleven from twelve parameters obtained through the characterization of the wood by ultrasound (Table 1). This reduction probably occurs due to the slope decrease of the growth rings.

The Poisson ratios values, obtained using ultrasound tests (Table 1), were superior to those proposed by Bodig and Jayne (1982). This result has also been found by Preziosa et al. (1981 and 1982), Bucur and Archer (1984), Bucur (2006), Trinca (2011), Gonçalves (2011), Ozyhar (2013), Bertoldo et al. (2013) and Vázquez et al. (2015).

Considering the values of the elastic parameters, obtained through the 26-faces polyhedrons with 55mm face to face distance (commonly used for the characterization of the wood by ultrasound), as reference, the statistical indicated that only for two elastic parameters (E_R , G_{LT}) there was statistically significant difference (P-value <0.05) among specimens' formats evaluated (Table 2).

Table 2 – Elastic and statistical parameters for the three formats of specimens evaluated.

Elastic parameters	26 faces of tradicional size	26 faces of reduced size	18 faces
E_L (MPa)	8477 (a)	7359 (b)	8456 (a)
E_R (MPa)	2368 (a)	2043 (b)	2138 (b)
E_T (MPa)	2284 (a)	2195 (a)	2274 (a)
G_{RT} (MPa)	851 (a)	925 (a)	918 (a)
G_{LT} (MPa)	1806 (a)	1540 (b)	1540 (b)
G_{LR} (MPa)	1773 (a)	1796 (a)	1857 (a)
ν_{RL}	0.34 (ab)	0.33 (b)	0.32 (a)
ν_{TL}	0.21 (a)	0.24 (a)	0.22 (a)
ν_{LR}	1.22 (a)	1.27 (a)	1.28 (a)
ν_{TR}	0.14 (a)	0.14 (a)	0.14 (a)
ν_{LT}	0.80 (a)	0.79 (a)	0.80 (a)
ν_{RT}	0.13 (a)	0.13 (a)	0.14 (a)

* Letters in parentheses indicate the result of the statistical analysis of comparisons of mean (multiple range test).

In the case of polyhedron with 26 faces and reduced size, although the size of the face is smaller than the size of the transducer diameter, violating one of the theory aspects related to wave propagation, this infraction was not enough to bring differences on results for the elastic parameters of the wood obtained by ultrasound.

The reduction of the number of polyhedral faces to 18, eliminating unused faces from the polyhedron with 26 faces (commonly used in the characterization of wood by ultrasound), reduce the complexity and time to the specimen preparation.

Conclusion

The results of the research indicated that only two (E_R and G_{LT}) from twelve elastic parameters involved in wood characterization, presented a statistically significant difference due to size reduction and/or shape alteration on test specimen. The reductions of the coefficients of variation, obtained with the reduction of the polyhedron size and consequent decrease of the growth rings inclination, increase the reliability of the ultrasonic method to obtain the elastic parameters of the wood, especially for the Poisson ratios.

Further research using other species should be carried out considering the polyhedral shapes adopted in this work, in order to verify if the same behavior is repeated.

Acknowledgment

The authors thank the São Paulo Research Foundation (FAPESP, Process nº 2016/ 00658-4) and the Support Fund for Teaching, Research and Extension (FAEPEX/UNICAMP, Process nº 2200/16) by funding research and to the Student Support Service (SAE/UNICAMP) and to the National Council for Scientific and Technological Development (CNPq) by Scientific Initiation scholarship.

References

- Bertoldo C.; Gonçalves, R.; Merlo, E. S.; Santaclara, O.; Ruy, M.; Moreira, M. E. M. 2013. Elastic constants of *Pinus pinaster* wood determined by wave propagation. In: 18th International Nondestructive Testing and Evaluation of Wood Symposium. Madison, EUA, p. 656-662.
- Brazilian Association of Technical Standards - NBR 7190/97 - Design of wooden structures 107p. 1997. Rio de Janeiro (RJ).
- Bucur, V; Archer R. R. 1984. Elastic constants for wood by an ultrasonic method. *Wood Sci. Technol* 18: 255-265.
- Bodig, J.; Goodman, B. A. 1973. *Mechanics of wood and wood composites*. 2. ed. Malabar, Flórida: Krieger, 712 p.
- Bodig J, Jayne B. A. 1982. *Mechanics of wood and wood composites*. Van Nostrand Reinhold, New York, p 419
- François, M. 1995. Identification des symmetries matérielles de matériaux anisotropes. França, Tese de Doutorado –Universidade de Paris, 137p.
- Furlani, J.E. 1995. Um estudo sobre a variação numérica do coeficiente de Poisson na madeira, considerando a anisotropia do material. Campinas, Tese de Mestrado –Faculdade de Engenharia Civil, Departamento de Construção Civil/ UNICAMP.
- Gonçalves, R.; Trinca, A. J.; Cerri, D. G. P. 2011. Comparison of elastic constants of wood determined by ultrasonic wave propagation and static compression test. *Wood and Fiber Science*, v. 43 (1), p. 64-75.
- Gonçalves, R.; Trinca, A. J.; Pellis, B. P. 2014. Elastic constants of wood determined by ultrasound using three geometries of specimens. *Wood Science and Technology*. 48:269–287.
- Mascia, N.T. 1991. Considerações à respeito da anisotropia na madeira. São Carlos, Tese de Doutorado - Escola de Engenharia de São Carlos/USP, 295p.
- Ozyhar, T.; Hering, S.; Sanabria, S.J.; Niemz, P. 2013. Determining moisture-dependent elastic characteristics of beech wood by means of ultrasonic waves. *Wood Sci Technol*, 47: 329-341. DOI 10.1007/s00226-012-0499-2.
- Preziosa, C.; Mudry, M.; Launay, J.; Gilletta, F. 1981. Détermination des constantes élastiques du bois par une méthode acoustique goniométrique. *CR Acad Sci Paris* 293(2):91-94.
- Preziosa, C. 1982. Méthode de détermination des constantes élastiques du matériau bois par utilisation des ultrasons. Université d'Orléans (Orléans).
- TRINCA, A. J. 2011. Metodologia para determinação das constantes elásticas da madeira por ultrassom. Tese (Doutorado em Engenharia Agrícola) – Na área de concentração de Construções Rurais e Ambiente, Faculty of Agricultural Engineering, University of Campinas, Campinas (SP).
- Vázquez, C.; Gonçalves, R.; Bertoldo, C.; Baño, V.; Veja, A.; Guaita, M. 2015. Determination of the mechanical properties of *Castanea sativa* Mill. using ultrasonic wave propagation and comparison with static compression and bending methods. *Wood Sci Technol*, 49: p. 607-622.

Correlations between Nondestructive and Destructive Test Results of Bent Beech Wood at Different Radii

Ümit Büyüksarı *

Department of Wood Mechanics and Technology, Duzce University, Duzce, Turkey, umitbuyuksari@duzce.edu.tr

Nusret As

Department of Wood Mechanics and Technology, Istanbul University, Istanbul, Turkey, nusretas@istanbul.edu.tr

Daniel Hindman

Department of Sustainable Biomaterials, Virginia Tech, Blacksburg, Virginia, USA, dhindman@vt.edu

Türker Dündar

Department of Wood Mechanics and Technology, Istanbul University, Istanbul, Turkey, dundar@istanbul.edu.tr

* Corresponding Author

Abstract

The aim of this study was to investigate the relationships between non-destructive and destructive test results of bent Beech wood at different radii. The sample trees were harvested from Duzce Forest Enterprises in the northwestern part of Turkey. Two trees from each wood species having straight stems and with approximately 40 cm diameter were selected and two 4-m long logs from each tree were cut. The logs were sawn to timber at 8 cm thickness. Samples having 2x2 cm cross-sections and different lengths were prepared from this timber. The prepared samples except for control group were steamed, bended and setted. The steaming was carried out at two different steam pressures (0.2 and 1.3 atm) and steaming times (36 and 6 min). The samples were bended at 300 mm, 200 mm and 100 mm radius. The setting process was performed with a drying room setting and a high frequency setting. Non-destructive (ultrasonic velocity) and micro-mechanical (modulus of elasticity, bending, tension and compression strength parallel to fibers) properties of bended and unbent samples were determined. Non-destructive measurements in the parallel direction were taken on one surface of unbent samples and in the two (convex and concave) surfaces of bended samples. Micro-mechanical test samples were cut from convex and concave surfaces of bent wood. Relationships between nondestructive and micro-mechanic tests were determined with regression analyses. The regression analyses indicated that the velocity parallel to the fibers and the bending strength, modulus of elasticity in bending, tension strength, and compression strength on both surfaces had a good relationship at the 95 % confidence level.

Keywords: bent wood, bending radii, non-destructive test, destructive test

Introduction

Bending of solid wood is a well-known process that has been used for many years. Bent wood are used in production of furniture, arched windows and doors, baskets, barrels, boats and ships, tool handles,

sporting goods, agricultural implements and musical instruments (Stevens and Turner 1970). Bending of wood demonstrates variations depending on many factors such as radius of bending, species, moisture content, thickness and width of wood, steaming time, fiber direction and defects (Niemiec and Brown 1995). Some pre-treatments such as steaming, immersion in boiling water, pre-compression application and chemical substances are used to improve the bending qualities of wood. Steaming is the most commonly used method for softening of wood. When a piece of wood is bent, tension stress occurs in the outer (convex) side due to fiber elongation while compression stress occurs in the inner (concave) side as the fibers contract (Stevens and Turner 1970). Thus, convex and concave sides of bent wood are differently affected in bending process. However, there is no study about how these sides are affected. After being bent, the piece should be cooled and dried while held in by a setting method to maintain the curved shape (Rowell 1999).

Mechanical properties of wood can be determined using destructive and non-destructive evaluation (NDE). The structural size samples, small size clear samples, and microscale size samples are used destructively. In recent years, microscale size samples have been used to determine mechanical properties of earlywood and latewood sections, wood strands, and fibers (Groom et al. 2002; Mott et al. 2002; Deomano and Zink-Sharp 2004; Hindman and Lee 2007; Jeong 2008; Jeong et al. 2009; Buyuksari et al. 2016; Roszyk et al. 2016). The NDE is defined as the science of identifying the physical and mechanical properties of a piece of a given material without altering its ultimate usability (Ross 1992). NDE is an important tool for the characterization of wood. It has been used for sorting or grading structural products, in situ assessment of wood members, detection of defects and predicting mechanical properties of wood (Zombori 2001). NDE offers advantages compared to conventional wood characterization methods, such as the possibility of evaluating the properties of wood without extracting test specimens, faster analysis of large populations, and adaptability to standardized production line routines (Oliveira 2002).

There are lots of studies about the correlations between non-destructive and destructive test results and generally used standard size wood samples in the destructive tests. However, there is no information on the correlation between non-destructive tests and micro-size samples destructive test. The aim of this study was to investigate the relationships between non-destructive and destructive test results of bent Beech wood at different radii.

Materials and methods

Materials

Sample trees were harvested from Duzce Forest Enterprises in the northwestern part of Turkey. Two trees having straight stems and with approximately 40 cm diameter were selected and 4-m in length were cut from each tree at a height of 0.30 m. The logs were sawn to 8 cm thickness timbers. Samples with a 2 x 2 cm cross-section and varying lengths (31.4 cm for groups F and I, 62.8 cm for groups E, H and J, 94.2 cm for groups D and G) were prepared from these timbers sources. Cutting plan of the different groups from the trees is shown in Figure 1. The study plan used is shown in Table 1.

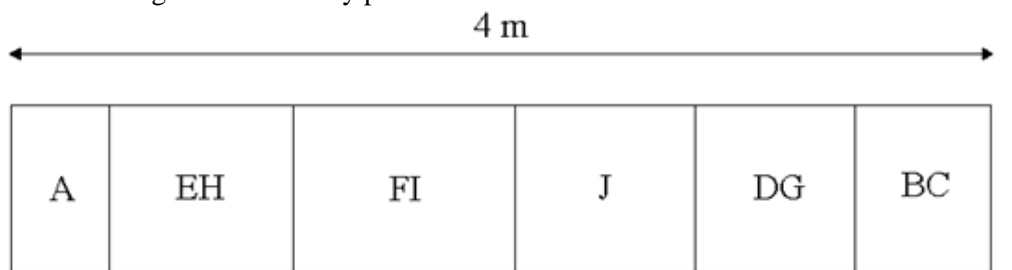


Figure 1. Cutting plan of the different groups from the lumbers

Table 1. Experimental design

Group	Steaming pressure (atm)	Setting method	Bending radii (mm)
A	Non-steamed	-	-
B	0.2	-	-
C	1.3	-	-
D	0.2	Drying Room (DR)	300
E	0.2	DR	200
F	0.2	DR	100
G	1.3	High Frequency (HF)	300
H	1.3	HF	200
I	1.3	HF	100
J	1.3	DR	200

The prepared samples except for control group were steamed, bended and setted. The steaming was carried out at two different steam pressures (0.2 and 1.3 atm) and steaming times (36 and 6 min). The samples were bended at 300 mm, 200 mm and 100 mm radius. The setting process was performed with a drying room setting and a high frequency setting.

Methods

Determination of velocity parallel to the fibers

Measurements in the parallel direction were taken with a Fakopp Ultrasonic Timer on one surface of the unbent samples and on the convex and concave surfaces of the bent samples. The velocity parallel to the fibers was calculated by the following equation:

$$V = (d * 1000) / (t - 6.1) \quad (1)$$

where V is velocity parallel to the fibers (m/s); d is distance (mm); t is transit time (μ s); 6.1 is time correction.

Determination of micro-mechanical properties

The micro-size test samples were cut from convex and concave sides of bent wood samples. Bending strength, modulus of elasticity (MOE) in bending, compression strength and tension strength were determined. A Minimat 2000 Miniature Materials Tester from Rheometric Scientific, Inc. was used for bending and tension tests. The Minimat tester contained an integral 200 N load cell. Data acquisition software was used with testing machine to continually monitor the load and displacement. Compression test was performed MTS universal testing machine with 1000 N load cell.

Bending tests used samples that were approximately 50.0 mm long, 5.0 mm wide and 1.3 mm thick. The tests were performed flatwise with a three-point bending fixture. The load was applied in the direction tangential to the annual rings. Spans were 18.11 mm and 24.4 mm for convex and concave sides, respectively. The span was greater for concave side samples due to increased deflection of samples. The maximum load and load-deflection curve were used to calculate the bending strength and MOE using following formulas:

$$\sigma_B = (3 * P_{max} * L_s) / (2 * b * h^2) \quad (2)$$

$$MOE = (\delta P * L_s^3) / (4 * b * h^3 * \delta f) \quad (3)$$

where, σ_B is bending strength, P_{max} is maximum load, L_s is span, b is width (radial) of sample, h is thickness (tangential) of the sample, δF is change of force, and δf is deflection in elastic region.

Tension test specimens were approximately 50 mm (L) \times 5.0 mm (R) \times 1.3 mm (T) and the 5 mm width of the specimen was reduced to 0.8 mm with a sanding drum to get dog-bone shape. From the ultimate load, the tensile strength was calculated. Compression test specimens had 3 x 3 x 5 mm dimensions. Tension and compression strengths were calculate from following formulas:

$$\sigma_{T,C} = P_{max} / A \quad (4)$$

where, $\sigma_{T,C}$ is tension and compression strength, P_{max} is maximum load and A is cross section area of the samples.

Statistical Analyses

Relationships between nondestructive and micro-mechanic tests were determined with regression analyses. The correlation coefficient, equation, F value and significance values between velocity values and micro-mechanical properties on both concave and convex sides.

Results and Discussion

The correlation coefficients, equations, F values, and significance between velocity parallel to fibers and bending strength on both convex and concave side of Beech wood are shown in Table 2 and Table 3, respectively.

Table 2. The correlations between convex side velocity parallel to fibers and bending strength of Beech wood

Group	Correlation coefficient	Equation	F value	Sig.
A	0.84	$y = 0.0972x - 286.08$	22.37	0.001
B	0.89	$y = 0.0639x - 147.64$	33.75	0.000
C	0.90	$y = 0.0978x - 288.95$	64.41	0.000
D	0.83	$y = 0.0618x - 157.91$	26.15	0.000
E	0.82	$y = 0.1044x - 272.56$	22.43	0.001
F	0.91	$y = 0.0663x - 137.29$	70.49	0.000
G	0.82	$y = 0.1068x - 378.71$	23.65	0.001
H	0.80	$y = 0.3525x - 1291.2$	17.54	0.002
I	0.80	$y = 0.0771x - 174.57$	17.83	0.002
J	0.83	$y = 0.0959x - 256.56$	22.07	0.001

Table 3. The correlations between concave side velocity parallel to fibers and bending strength of Beech wood

Group	Correlation coefficient	Equation	F value	Sig.
A	0.84	$y = 0.0972x - 286.08$	22.37	0.001
B	0.89	$y = 0.0639x - 147.64$	33.75	0.000
C	0.90	$y = 0.0978x - 288.95$	64.41	0.000
D	0.85	$y = 0.0638x - 186.84$	30.98	0.000
E	0.82	$y = 0.0721x - 170.03$	18.69	0.002
F	0.89	$y = 0.081x - 164.66$	37.42	0.000
G	0.79	$y = 0.0901x - 298.66$	16.82	0.002
H	0.81	$y = 0.0699x - 164.89$	19.84	0.001
I	0.82	$y = 0.0278x - 20.149$	13.76	0.008
J	0.85	$y = 0.0694x - 178.75$	23.68	0.001

The correlation graphs of convex side of group C and concave side of group G between bending strength and velocity parallel to the fibers are shown in Figure 2 and Figure 3.

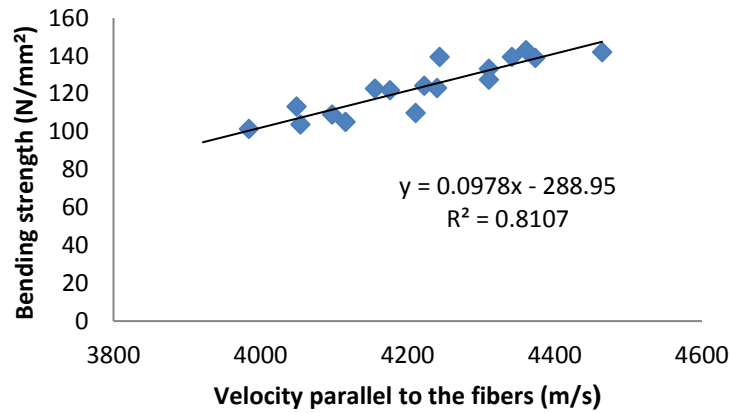


Figure 2. The correlation graphich of convex side of group C

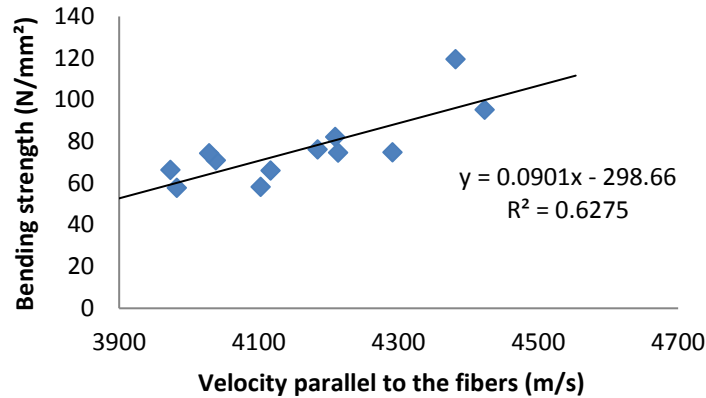


Figure 3. Correlation graphich of concave side of group G

The regression analyses indicated that the velocity parallel to the fibers and the bending strength on both surfaces had a good relationship at the 95 % confidence level. The correlation coefficients ranged from 0.80 to 0.91 for convex side, and from 0.81 to 0.90 for concave side.

The correlation coefficients, equations, F values, and significance between velocity parallel to fibers and MOE on both convex and concave side of Beech wood are shown in Table 4 and Table 5, respectively.

Table 4. The correlations between convex side velocity parallel to fibers and MOE of Beech wood

Group	Correlation coefficient	Equation	F value	Sig.
A	0.86	$y = 10.487x - 34637$	29.05	0.000
B	0.83	$y = 4.4314x - 8942.1$	26.45	0.000
C	0.94	$y = 9.0197x - 27976$	90.30	0.000
D	0.86	$y = 7.0513x - 23378$	33.30	0.000
E	0.84	$y = 8.4336x - 22369$	33.61	0.000
F	0.88	$y = 8.4423x - 25815$	31.38	0.000
G	0.87	$y = 9.3075x - 35322$	32.30	0.000
H	0.85	$y = 16.199x - 56965$	31.03	0.000
I	0.79	$y = 6.4816x - 18175$	11.50	0.012
J	0.85	$y = 7.4298x - 20210$	36.09	0.000

Table 5. The correlations between concave side velocity parallel to fibers and MOE of Beech wood

Group	Correlation coefficient	Equation	F value	Sig.
A	0.86	$y = 10.487x - 34637$	29.05	0.000
B	0.83	$y = 4.4314x - 8942.1$	26.45	0.000
C	0.94	$y = 9.0197x - 27976$	90.30	0.000
D	0.82	$y = 2.3798x - 7154$	20.69	0.001
E	0.81	$y = 2.584x - 6112.5$	19.17	0.001
F	0.90	$y = 1.8839x - 3367.7$	49.05	0.000
G	0.84	$y = 1.7428x - 4534.5$	28.83	0.000
H	0.83	$y = 4.9471x - 13737$	22.71	0.001
I	0.78	$y = 2.5477x - 4946.7$	11.10	0.013
J	0.95	$y = 1.9878x - 4285.4$	77.40	0.000

The correlation graphs of convex side of group D and concave side of group E between MOE and velocity parallel to the fibers are shown in Figure 4 and Figure 5.

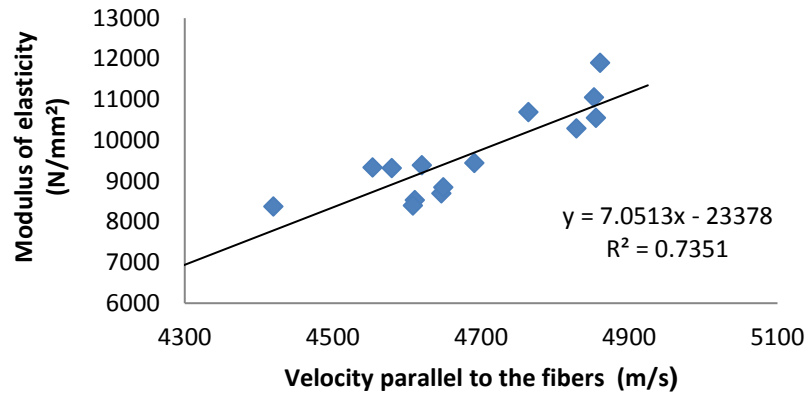


Figure 4. The correlation graphich of convex side of group D

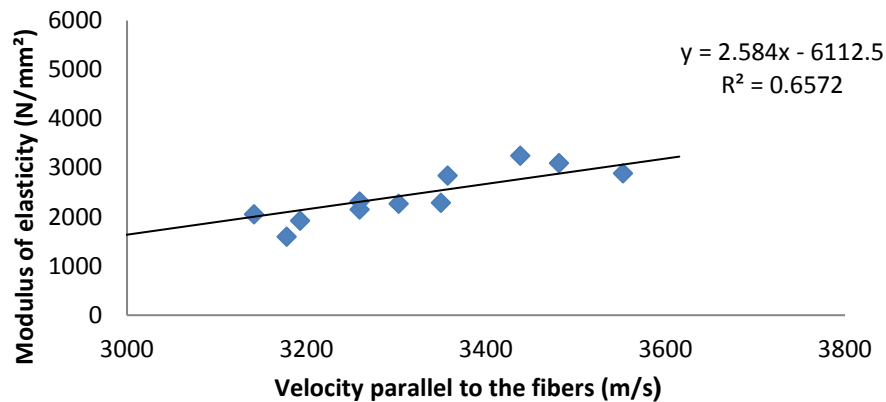


Figure 5. Correlation graphich of concave side of group E

The regression analyses indicated that the velocity parallel to the fibers and the MOE on both surfaces had a good relationship at the 95 % confidence level. The correlation coefficients ranged from 0.79 to 0.94 for convex side, and from 0.78 to 0.95 for concave side.

The correlation coefficients, equations, F values, and significance between velocity parallel to fibers and tensile strength on both convex and concave side of Beech wood are shown in Table 6 and Table 7, respectively.

Table 6. The correlations between convex side velocity parallel to fibers and tensile strength of Beech wood

Group	Correlation coefficient	Equation	F value	Sig.
A	0.79	$y = 0.3874x - 1485.9$	17.12	0.002
B	0.87	$y = 0.1096x - 325.44$	29.13	0.000
C	0.87	$y = 0.1611x - 542.81$	41.17	0.000
D	0.81	$y = 0.17x - 643.61$	19.11	0.001
E	0.79	$y = 0.1406x - 400.69$	20.61	0.001
F	0.84	$y = 0.0809x - 196.14$	26.61	0.000
G	0.86	$y = 0.1793x - 707.66$	37.20	0.000
H	0.89	$y = 0.3824x - 1399.6$	41.16	0.000
I	0.84	$y = 0.094x - 262.24$	17.45	0.004
J	0.84	$y = 0.1053x - 285.02$	22.94	0.001

Table 7. The correlations between concave side velocity parallel to fibers and tensile strength of Beech wood

Group	Correlation coefficient	Equation	F value	Sig.
A	0.79	$y = 0.3874x - 1485.9$	17.12	0.002
B	0.87	$y = 0.1096x - 325.44$	29.13	0.000
C	0.87	$y = 0.1611x - 542.81$	41.17	0.000
D	0.82	$y = 0.1434x - 517.03$	29.70	0.000
E	0.86	$y = 0.1272x - 327.72$	43.52	0.000
F	0.87	$y = 0.1201x - 271.69$	21.00	0.003
G	0.81	$y = 0.0791x - 218.47$	13.03	0.009
H	0.81	$y = 0.3774x - 1179.1$	14.86	0.005
I	0.82	$y = 0.1868x - 457.03$	12.86	0.012
J	0.87	$y = 0.1109x - 283.41$	29.10	0.000

The correlation graphichs of convex side of group G and concave side of group J between tensile strength and velocity parallel to the fibers are shown in Figure 6 and Figure 7.

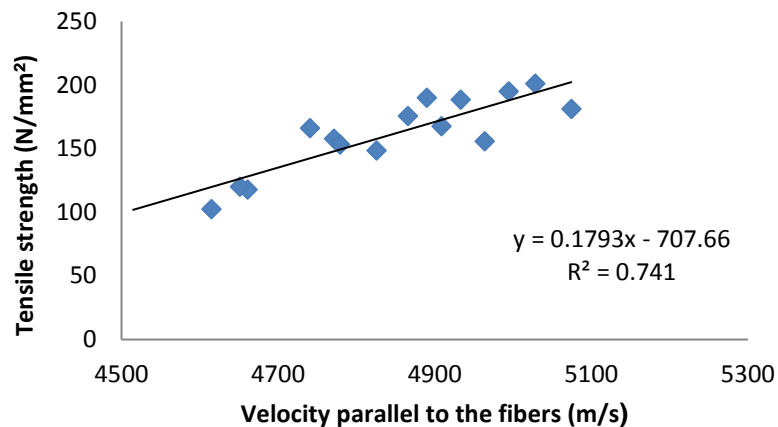


Figure 6. The correlation graphich of convex side of group G

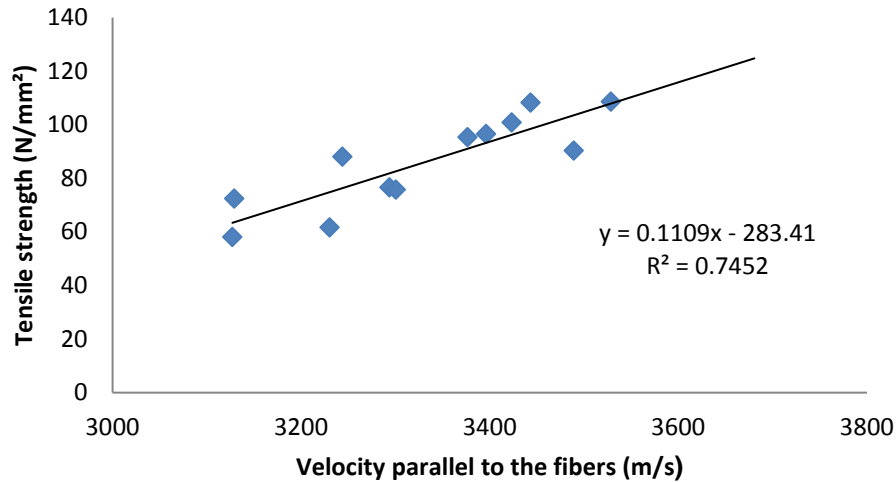


Figure 7. Correlation graphich of concave side of group J

The regression analyses indicated that the velocity parallel to the fibers and the tensile strength on both surfaces had a good relationship at the 95 % confidence level. The correlation coefficients ranged from 0.79 to 0.89 for convex side, and from 0.79 to 0.87 for concave side.

The correlation coefficients, equations, F values, and significance between velocity parallel to fibers and compression strength on both convex and concave side of Beech wood are shown in Table 8 and Table 9, respectively.

Table 8. The correlations between convex side velocity parallel to fibers and compression strength of Beech wood

Group	Correlation coefficient	Equation	F value	Sig.
A	0.86	$y = 0,0763x - 267,88$	34,05	0,000
B	0.87	$y = 0,0657x - 230,47$	19,02	0,005
C	0.88	$y = 0,0541x - 168,72$	36,54	0,000
D	0.87	$y = 0,0335x - 96,054$	22,60	0,002
E	0.85	$y = 0,0419x - 103,91$	41,75	0,000
F	0.85	$y = 0,0243x - 33,961$	30,68	0,000
G	0.85	$y = 0,0407x - 141,87$	23,95	0,001
H	0.89	$y = 0,0721x - 224,96$	32,47	0,000
I	0.85	$y = 0,0496x - 136,01$	18,92	0,003
J	0.88	$y = 0,047x - 128,87$	32,66	0,000

Table 9. The correlations between concave side velocity parallel to fibers and compression strength of Beech wood

Group	Correlation coefficient	Equation	F value	Sig.
A	0.86	$y = 0,0763x - 267,88$	34,05	0,000
B	0.87	$y = 0,0657x - 230,47$	19,02	0,005
C	0.88	$y = 0,0541x - 168,72$	36,54	0,000
D	0.81	$y = 0,024x - 52,969$	16,51	0,003
E	0.79	$y = 0,0171x - 6,6584$	18,93	0,001
F	0.87	$y = 0,039x - 54,709$	28,90	0,000
G	0.84	$y = 0,0405x - 121,68$	19,32	0,002
H	0.88	$y = 0,0727x - 190,81$	42,89	0,000
I	0.87	$y = 0,1095x - 246,34$	25,90	0,001
J	0.88	$y = 0,0263x - 37,121$	32,07	0,000

The correlation graphs of convex side of group H and concave side of group I between compression strength and velocity parallel to the fibers are shown in Figure 8 and Figure 9.

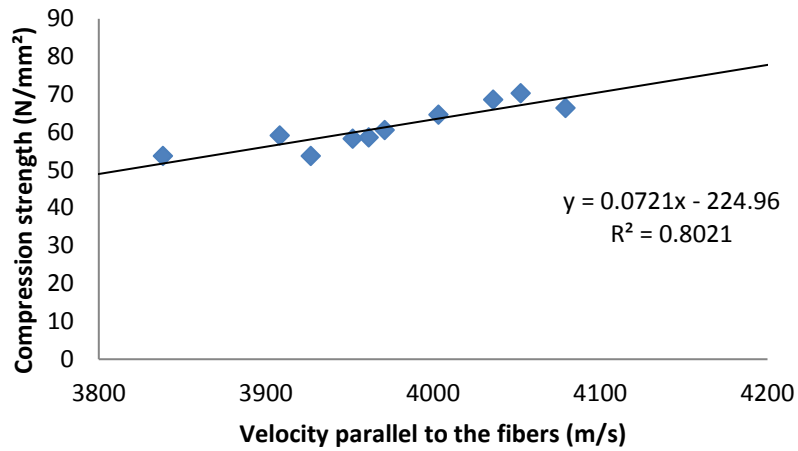


Figure 8. The correlation graphich of convex side of group H

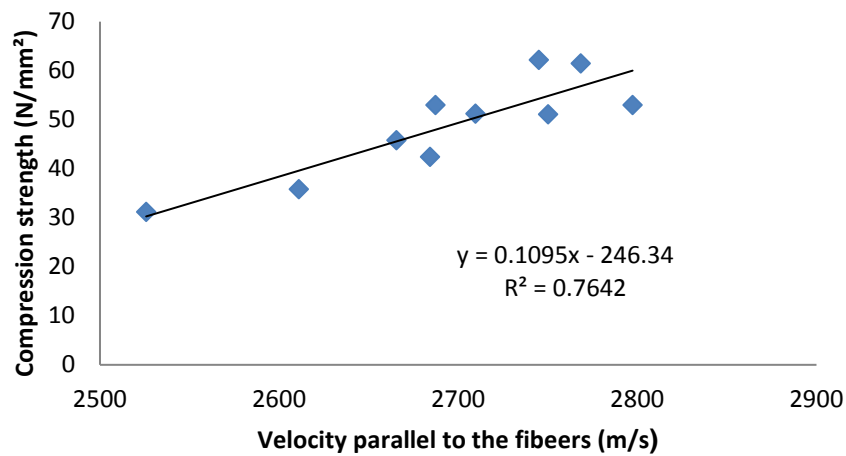


Figure 9. Correlation graphich of concave side of group I

The velocity parallel to the fibers and the compression strength on both surfaces had a good relationship at the 95 % confidence level. The correlation coefficients ranged from 0.85 to 0.89 for convex side, and from 0.79 to 0.88 for concave side.

Conclusions

The regression analyses indicated that the velocity parallel to the fibers and the bending strength, modulus of elasticity in bending, tension strength, and compression strength on both concave and convex sides had a good relationship at the 95 % confidence level.

References

Buyuksari, U.; As, N.; Dündar, T.; Sayan, E. 2016. Comparison of micro- and standard-size specimens in evaluating the flexural properties of scots pine wood. *BioResources* 11(4), 10540-10548.

- Deomano, E.C.; Zink-Sharp, A. 2004. Bending properties of wood flakes of three southern species. *Wood Fiber Sci.* 36(4), 493-499.
- Groom, L.; Shaler, S.; Mott, L. 2002. Mechanical properties of individual southern pine fibers. Part III. Global relationships between fiber properties and fiber location within an individual tree. *Wood Fiber Sci.* 34(2), 238-250.
- Hindman, D.P.; Lee, J.N. 2007. Modeling wood strands as multi-layer composites: Bending and tension loads. *Wood Fiber Sci.* 39(4), 516-526.
- Jeong, G.Y. 2008. Tensile Properties of Loblolly Pine Strands Using Digital Image Correlation and Stochastic Finite Element Method, Ph. D. Dissertation, Virginia Polytechnic Institute & State University, Blacksburg, VA.
- Jeong, G.Y.; Zink-Sharp, A.; Hindman, D.P. 2009. Tensile properties of earlywood and latewood from loblolly pine (*Pinus taeda*) using digital image correlation. *Wood Fiber Sci.* 41(1), 51-63.
- Mott, L.; Groom, L.; Shaler, S. 2002. Mechanical properties of individual southern pine fibers. Part II. Comparison of earlywood and latewood fibers with respect to tree height and juvenility. *Wood Fiber Sci.* 34(2), 221-237.
- Niemiec, S.S.; Brown, T.D. 1995. Steam Bending Red Alder, In: Green, D.; von Segen W.; Willits, S. Western hardwoods-value-added research and demonstration program. Gen. Tech. Rep. FPL-GTR-85. Madison, WI: U.S. Department of Agriculture, Forest Service, Forest Products Laboratory. 43 p.
- Oliveira, F.G.R.; Campos, J.A.O.; Sales, A. 2002. Ultrasonic measurements in Brazilian hardwood. *Mater Res* 5:51-55.
- Ross, R.J. 1992. Nondestructive testing of wood. In: Proceedings of nondestructive evaluation of civil structures and materials. University of Colorado Boulder; p. 43-46.
- Roszyk, E.; Molinski, W.; Kaminski, M. 2016. Tensile properties along the grains of earlywood and latewood of Scots pine (*Pinus sylvestris* L.) in dry and wet state. *BioResources* 11(2), 3027-3037.
- Rowell, R.M. 1999. Specialty Treatments, Chapter 19. In: *Wood Handbook-Wood as an Engineering Material*, Forest Products Laboratory Gen. Tech. Rep. FPL-GTR-113, Madison.
- Stevens, W.C.; Turner, N. 1970. *Wood bending handbook*. Woodcraft & Supply Corp., Parkersburg.
- Zombori, B. 1992. In situ nondestructive testing of built in wooden members. In: The 12th international symp of NDT of wood, vol. 6; p. 134.

Relation between Thermal Expansion Coefficient and Sound Velocity in Solid Wood

Ferenc Divos

Professor, Institute of Physics and Electronics, University of Sopron, Hungary.
divos.ferenc@uni-sopron.hu

Marton Pribelszki

Student, University of Sopron, Hungary. pribelszki.marton@gmail.com

Abstract

The linear thermal expansion coefficient of robinia pseudoacacia material is measured in fiber direction. Measured data are compared with sound velocity in fiber direction. All together 18 pieces of 5 by 5 by 300 mm specimen are tested, representing a wide velocity range from 4400 m/s to 5500 m/s. The resolution of the displacement sensor is under 100 nm and it was a reliable and sensitive tool for testing minor displacement in the range of 0,4 mm. The applied temperature interval for the thermal expansion coefficient determination was 25 to 45°C. High correlation coefficient of 0.93 was found between the two quantities. An increasing sound velocity is related to a decreasing thermal expansion coefficient. This experimental result is indirectly supporting our hypothesis that linear thermal expansion coefficient and sound velocity in fiber direction are depending on the microfibril angle of wood, but direct verification of the hypothesis is necessary.

Introduction

The linear thermal expansion coefficient of solid wood in fiber direction is rather low, lower than metals. Temperature change results minor dimension changes, much less, than shrinkage in case of moisture content change. For this reason, little attention was focused on the determination of thermal expansion coefficient of solid wood. The definition of the linear thermal expansion coefficient (α) is:

$$\alpha = \frac{1}{l_0} \frac{dl}{dt}; \quad (1/^\circ\text{C}) \quad (1)$$

here: l_0 initial length (m)
 dl change in length due to temperature change (m)
 dt temperature change ($^\circ\text{C}$)

In fiber direction the linear thermal expansion coefficient of yellow birch is $3.57 \cdot 10^{-6} \text{ } 1/^\circ\text{C}$, in radial direction $32.2 \cdot 10^{-6} \text{ } 1/^\circ\text{C}$ and in tangential direction $39.4 \cdot 10^{-6} \text{ } 1/^\circ\text{C}$. Data are from Richard C. Weatherwax (1956), Forest Product Laboratory. Similar values can be found in F. Kolmann (1968). Thermal expansion coefficient is strongly depends on anatomical orientation. Values perpendicular to fiber direction are roughly 10 times higher than in fiber direction.

The aim of our investigation is to find a link between thermal expansion coefficient and microfibril angle. However, because we had no access to MFA determination instrument, we selected sound velocity determination as indirect indicator of MFA. Our hypothesis is that thermal expansion coefficient is

increasing with decreasing sound velocity in fiber direction. The paper presents the results of the experiment that supports this hypothesis.

Materials and methods

Robinia pseudo acacia (black locust) was selected as raw material for the experiment. The sample dimensions were 5 by 5 by 300 mm. Small cross-sectional dimensions were used to achieve thermal equilibrium relative quickly. All of the 18 samples were defect free, no slope of grain and conditioned at room temperature before the experiment. Moisture content was rather uniform, between 10.5 and 11.7%. Samples were wrapped by thin plastic layer before the start of the test procedure to prevent moisture content change during the whole procedure. An important specimen selection criteria was to cover a wide range of sound velocities in fiber direction which was between 4400 and 5500 m/s. Samples representing low velocities were taken from juvenal wood section.

Measurements were done inside a Sapratin made climate chamber. The air temperature was controlled. The selected temperature levels were 25, 30, 35, 40 and 45 °C. After moving to the next temperature level, roughly 30 minutes was necessary to reach equilibrium state, where dimension change stopped. For safety the duration of each temperature step was around 1 hour. Figure 1 shows the sample inside the climate chamber.



Figure 1. The experimental setup inside a climate chamber. The sensor on the left is a capacitor type extensometer. The specimen is placed on rubber foam. A steel frame is holding the extensometer, sample and the reference point on the right.

The sample is standing on a foam support. On the left-hand side of the sample there is a sensor. The sensor is a prototype version of a high sensitivity displacement sensor. The working range of the displacement sensor is only 0.4mm, but the resolution is around 100 nm. The sensor is a capacitor type displacement sensor. The sensitive component is a capacitor in parallel plate arrangement where one plate is moving

together with the sample. The plate size is 100 by 100 mm. The calibration curve of the displacement sensor is shown on figure 2.

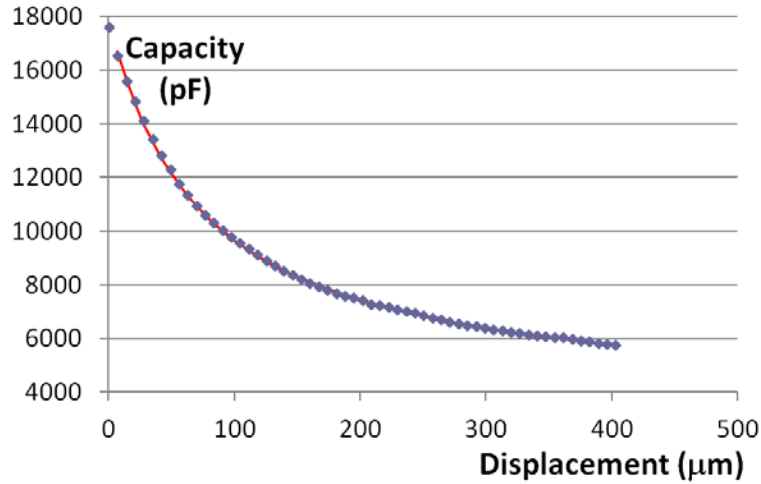


Figure 2. The calibration curve of the prototype displacement sensor.

The pink line on Figure 2 is the theoretical calibration curve, given by next formula:

$$Displacement (\mu m) = \frac{1\ 060\ 000}{capacity(pF) - 3500} - 73.6 \quad (2)$$

The actual resolution depends on the position of the capacitor plate. The resolution is 10 nm at the sensitive end, just before the plates are in contact while it is 100 nm at the other end of the working range. This resolution is sufficient to measure minor displacements of the specimens during temperature change because one step of 5°C temperature change results in a displacement of around 10 μm. Figure 3 indicates the sample displacement versus time.

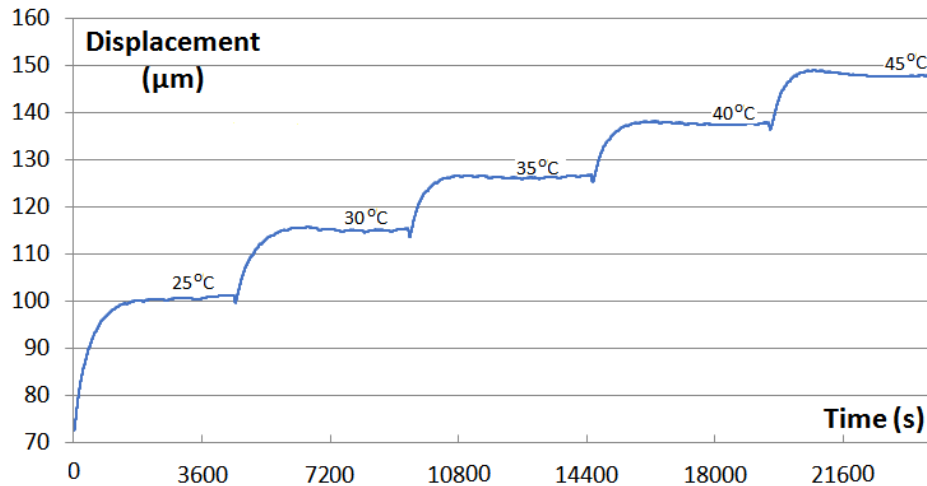


Figure 3. Robinia pseudoacacia specimen displacement versus time over the whole measurement process which took about 7 hours.

We had only one high sensitivity displacement sensor, so we measured displacement of the 18 samples one by one, so we spent 1 month with data collection. After cooling down the sample, we determined the sound velocity in fiber direction using ultrasonic time of flight, the applied frequency was 45 kHz.

Results and discussion

The basis of the evaluation is formula (1). Dimensional change occurred not only on wood sample, but also on the steel frame shown on Figure 1. To compensate this effect, the following formula was used:

$$\alpha_{\text{apparent}} = \alpha_{\text{steel}} - \alpha_{\text{wood}} \quad (3)$$

where α_{apparent} is the apparent thermal expansion coefficient determined by the data collected, shown on Figure 3, α_{steel} is the thermal expansion coefficient of steel: $12.5 \cdot 10^{-6} \text{ 1/}^\circ\text{C}$ and α_{wood} is the thermal expansion coefficient of the wood sample. The accuracy of the wood material linear thermal expansion coefficient depends on the accuracy of the steel data taken from the Tipler (2008). Our result, the linear thermal expansion coefficient of robinia in fiber direction as a function of sound velocity is shown on Figure 4. We assumed linear relationship. The correlation coefficient between the two quantities is 0.93.

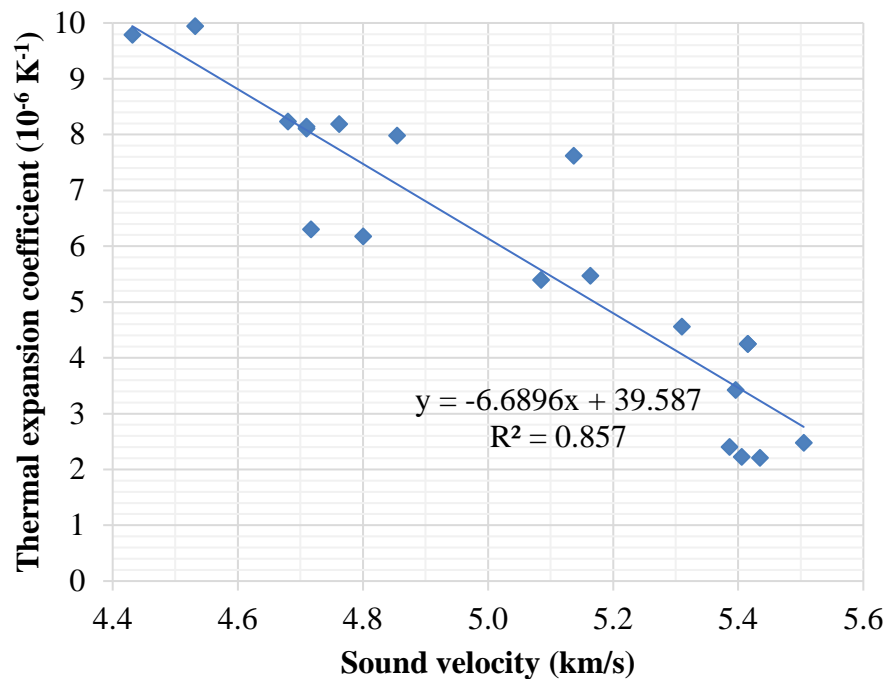


Figure 4. The linear thermal expansion coefficient of robinia in fiber direction as a function of sound velocity

The linear relationship and the high correlation coefficient gives us the possibility for predicting the thermal expansion coefficient from the measured sound velocity using the following empirical formula:

$$\alpha_{\text{robinia,parallel}}(10^{-6} \text{ 1/}^\circ\text{C}) = 39.6 - 6.69 \cdot V_{\text{sound}}\left(\frac{\text{km}}{\text{s}}\right) \quad (4)$$

The above formula gives us the thermal expansion coefficient in fiber direction in the temperature range between 25 and 45 °C and is valid for robinia pseudoacacia only.

Conclusion

The high correlation of 0.93 strongly supports the hypothesis that thermal expansion coefficient and sound velocity in wood material are not independent physical properties. Thermal expansion coefficient is increasing with decreasing sound velocity in fiber direction. It is very likely that micro fibril angle is the link between the two measured quantities, but more experimental data would be necessary to verify hypothesis.

Acknowledgments

This article was made in frame of the „EFOP-3.6.1-16-2016-00018 – Improving the role of research+ development+innovation in the higher education through institutional developments assisting intelligent specialization in Sopron and Szombathely”.

References

- Weatherwax R.C., Stamm A.J. (1956). The Coefficients of Thermal Expansion of Wood and Wood Products, Forest Products Laboratory, March 1956, No. 1487
ir.library.oregonstate.edu/xmlui/bitstream/handle/1957/1597/FPL_1487ocr.pdf
- Kollmann F.F.P; Cote W. A.: (1968). Principles of wood science and technology, ISBN: 978-3-642-87930-2 Berlin, Heidelberg, New York, Springer-Verlag
- Tipler P.A.; Mosca G. (2008). *Physics for Scientists and Engineers, Volume 1* (6th ed.). New York, NY: Worth Publishers. pp. 666–670. ISBN 1-4292-0132-0.

Ultrasound Characterization of Brazilian Tropical Wood

Recieli Knoner Santos Gorski

Master Student, School of Agricultural Engineering (FEAGRI), Laboratory of Nondestructive Testing (LabEND), University of Campinas (UNICAMP), Campinas, São Paulo, Brazil, reciksanos@gmail.com

Monica Ruy

PhD student, School of Agricultural Engineering (FEAGRI), Laboratory of Nondestructive Testing (LabEND), University of Campinas (UNICAMP), Campinas, São Paulo, Brazil, monica.ruy@hotmail.com

Rejane Costa Alves

PhD student, Federal University of Espírito Santo (UFES), Department of Forestry and Wood Sciences, Espírito Santo, Brazil, rejane.alves@ufes.br

Cinthya Bertoldo Pedroso

Assistant Professor, College of Agricultural Engineering (FEAGRI), Laboratory of Nondestructive Testing (LabEND), University of Campinas (UNICAMP), Campinas, São Paulo, Brazil, cinthya.bertoldo@feagri.unicamp.br

Raquel Gonçalves

Professor, College of Agricultural Engineering (FEAGRI), Laboratory of Nondestructive Testing (LabEND), University of Campinas (UNICAMP), Campinas, São Paulo, Brazil, raquel@feagri.unicamp.br

Abstract

There is a wide variety of tropical species in Brazil whose could be used on a sustainable way for timber, but it is necessary to know their elastic properties. This research aimed to characterize wood tropical species using ultrasonic waves propagation. For the tests, we used 18 polyhedrons with 26 faces from 6 tropical species grown in Amazon Forest. The stiffness matrix was determined using ultrasound equipment and 1000-kHz frequency longitudinal and transverse wave transducers. The elastic properties and Poisson's ratio, obtained by non-destructive tests, were compared with the results from Literature and also analyzed using expected relations among elastic parameters. The elastic parameters obtained by ultrasound present values in agreement with other researches and inside expected ranges for a material with great variability, showing the potential of the technique in characterizing the wood.

Keywords: modulus of elasticity, Poisson ratio, elastic parameters

Introduction

The use of wood in civil construction has become an important alternative for the global sustainability. There are some researches focused on some species from Brazilian Amazonian Forest that has possibility

of being reforested for commercial uses. In addition, there are companies that use tropical wood in a sustainable way. But the proper use of wood as structural members requires the knowledge of its properties. The complete characterization of the wood is performed through the achievement of 12 constants to describe its elastic behavior: three longitudinal moduli, three shear moduli and six Poisson ratios.

The methodology to the compliance matrix determination through compression tests requires a high quantity of material (Mascia 1991, Furlani 1995). For only one sample it is necessary 6 prismatic specimens. Three specimens removed on symmetric axes (Longitudinal (L), Radial (R) and Tangential (T)) allow to calculate the three longitudinal modulus of elasticity and the six Poisson's ratio, while three samples taken out of symmetric plans (LR, LT and RT) allows obtaining the three shear moduli.

François (1995) proposes a polyhedron with 26 faces as specimen to the determination of the elastic constants of the wood through acoustic tests. This geometry has the advantage of allowing the achievement of all stiffness matrix elements using only one specimen.

Gonçalves et al (2014) compared the results obtained by the characterization of wood using three geometries for the specimens (prism, multifaceted disk and 26-surface polyhedron). For the tests, the authors used three species of wood (*Eucalyptus saligna*, *Apuleia leiocarpa*, and *Goupia glabra*). To compare the results with static tests, the prismatic specimens were tested also in compression. In general, for the three geometries evaluated, the authors found longitudinal and shear modulus obtained by ultrasound statistically equivalent to those obtained by compression tests. The polyhedral specimen showed better results and were considered the best option by the authors, considering the results and also the reduction of the number of specimen's necessary to the tests (one for polyhedron, 3 for disks and 4 for prismatic ones).

Several studies (González et al., 2001; Bucur, 2006; Gonçalves et al., 2011) emphasize that the absolute values of the elastic constants obtained by the acoustic method are higher than those obtained by the static test. This behavior is explained by the process of the tests – while the tests using wave propagation is an adiabatic process, the static one is isothermal (Gonçalves et al. 2014).

Considering the importance of the knowledge of the properties of different species of tropical wood and the results obtained in Literature using wave propagation to access the stiffness matrix, this study aimed to characterize 6 species of wood from the Amazon region using ultrasound.

Material and Methods

Six species of tropical wood were used (*Bertholletia excelsa*, *Hymenolobium petraeum* Ducke, *Caryocar brasiliense*, *Peltogyne lecointei* Duckei, *Dinizia excelsa* Ducke, *Apuleia leiocarpa*). For each specie were prepared 18 polyhedron with 26 faces (FRANÇOIS, 1995; TRINCA, 2011). The polyhedrons were made with the faces oriented on the axes longitudinal (L), radial (R) and tangential (T), with 60 mm between opposite sides.

The specimens were tested with ultrasound (EP1000, Olympus, EUA) (Figure 1), with longitudinal and transversal 1000-kHz frequency transducers, flat faces. The ultrasonic tests were performed to obtain the parameters of the stiffness matrix and its inversion, compliance matrix.

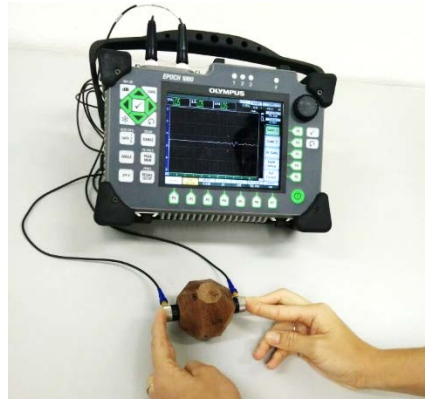


Figure 1 — Ultrasound test.

The longitudinal velocities on L (or 1), R (or 2) and T (or 3) axes (V_{11} , V_{22} and V_{33}) were obtained by positioning the longitudinal transducers on parallel faces. Likewise, using the same position but shear transducers were obtained shear velocities in planes: V_{44} , V_{55} , V_{66} . To obtain the velocities outside the symmetry axes (V_{12} , V_{13} and V_{23}), the shear transducers were positioned on the 45° faces of the polyhedral.

The equations of Christoffel (Equation 1) were used to obtain terms of the diagonal of the stiffness matrix [C]: C_{11} , C_{22} , C_{33} , C_{44} , C_{55} , C_{66} .

$$C_{ii} = \rho \cdot V_{ii}^2 \quad (1)$$

Were: $i = 1, 2, 3, 4, 5$ e 6 ; ρ = density and V = Velocity of wave propagation in respective directions

The numbering is related to the axes as follows $1 = L$; $2 = R$; $3 = T$; $44 =$ planes 2 and 3; $55 =$ planes 1 e 3 e $66 =$ planes 1 e 2. In the same way, the 3 non-diagonal terms (C_{12} , C_{13} and C_{23}) deduced from the Christoffel tensor were calculated by Equations 2, 3 and 4 respectively.

$$(C_{12} + C_{66}) n_1 n_2 = \pm [(C_{11} n_{12} + C_{66} n_{22} - \rho V \alpha^2) (C_{66} n_{12} + C_{22} n_{22} - \rho V \alpha^2)]^{1/2} \quad (2)$$

$$(C_{23} + C_{44}) n_2 n_3 = \pm [(C_{22} n_{22} + C_{44} n_{32} - \rho V \alpha^2) (C_{44} n_{22} + C_{33} n_{32} - \rho V \alpha^2)]^{1/2} \quad (3)$$

$$(C_{13} + C_{55}) n_1 n_3 = \pm [(C_{11} n_{12} + C_{55} n_{32} - \rho V \alpha^2) (C_{55} n_{12} + C_{33} n_{32} - \rho V \alpha^2)]^{1/2} \quad (4)$$

Were:

α = ultrasound wave propagation angle (outside the symmetric axes)

$n_1 = \cos \alpha$; $n_2 = \sin \alpha$ and $n_3 = 0$ when α is taken related to axis 1 (Plane 12)

$n_1 = \cos \alpha$; $n_3 = \sin \alpha$ and $n_2 = 0$ when α is taken related to axis 1 (Plane 13)

$n_2 = \cos \alpha$; $n_3 = \sin \alpha$ and $n_1 = 0$ when α is taken related to axis 2 (Plane 23)

After obtaining all stiffness matrix components [C], the components of the compliance matrix [S] were obtained by [C] inversion, with which the elastic constants were determined.

$$[S] = \begin{bmatrix} \frac{1}{E_1} & -\frac{\nu_{21}}{E_2} & -\frac{\nu_{31}}{E_3} & 0 & 0 & 0 \\ -\frac{\nu_{12}}{E_1} & \frac{1}{E_2} & -\frac{\nu_{32}}{E_3} & 0 & 0 & 0 \\ -\frac{\nu_{13}}{E_1} & -\frac{\nu_{23}}{E_2} & \frac{1}{E_3} & 0 & 0 & 0 \\ 0 & 0 & 0 & \frac{1}{G_{23}} & 0 & 0 \\ 0 & 0 & 0 & 0 & \frac{1}{G_{13}} & 0 \\ 0 & 0 & 0 & 0 & 0 & \frac{1}{G_{12}} \end{bmatrix}$$

The elastic constants of wood are compared with values obtained in Literature and also with values expected to relation between the constants. These comparisons allow verify if the results are compatible with the basis of wood behavior.

Results and discussions

The data obtained through ultrasound tests using the polyhedron specimen allowed to obtain the 12 elastic parameter of the six tropical species tested (Table 1).

Preliminary analysis showed that, as expected, the values of modulus of elasticity obtained for the longitudinal direction are greater than the values of the radial direction followed by the tangential direction (Table 1). As also expected, the coefficients of variation than those obtained for Poison ratio was higher than for longitudinal and shear modulus.

Table 1. Acoustic parameters obtained by the flexibility matrix from the ultrasonic tests of the six species studied.

	AM	AV	R	P	G	CA
E_L	15404 (5%)	12307 (1%)	16260 (13%)	12981 (5%)	15993 (12%)	11434 (9%)
E_R	2438 (8%)	2908 (7%)	2493 (1%)	2553 (5%)	2619 (7%)	1839 (7%)
E_T	1619 (1%)	2296 (3%)	1874 (2%)	1447 (2%)	1908 (7%)	1298 (6%)
G_{RT}	552 (3%)	739 (2%)	630 (2%)	506 (5%)	552 (6%)	419 (1%)
G_{LT}	1117 (2%)	1345 (7%)	1171 (1%)	859 (4%)	804 (2%)	955 (5%)
G_{LR}	1429 (10%)	2282 (9%)	1892 (3%)	1216 (25%)	1918 (5%)	1178 (1%)
V_{RL}	0,13 (26%)	0,19 (17%)	0,11 (32%)	0,17 (7%)	0,14 (2%)	0,11 (5%)
V_{TL}	0,08 (36%)	0,12 (23%)	0,09 (17%)	0,09 (40%)	0,10 (15%)	0,06 (49%)
V_{LR}	0,84 (12%)	0,82 (19%)	0,73 (22%)	0,88 (12%)	0,87 (4%)	0,70 (4%)
V_{TR}	0,28 (43%)	0,37 (5%)	0,43 (7%)	0,32 (4%)	0,42 (5%)	0,38 (8%)
V_{LT}	0,75 (32%)	0,62 (22%)	0,77 (4%)	0,78 (36%)	0,84 (11%)	0,55 (61%)
V_{RT}	0,42 (38%)	0,47 (5%)	0,58 (9%)	0,56 (5%)	0,57 (5%)	0,54 (4%)

*Values in parentheses is the coefficient of variation

AM- *Hymenolobium petraeum* Ducke; AV- *Dinizia excelsa* Ducke; R- *Peltogyne lecointei* Duckei; P- *Caryocar brasiliense*; G- *Apuleia leiocarpa*; CA- *Bertholletia excelsa*

According to the literature there are expected relations between elastic parameters. The relations between E_L/E_T were much smaller (Table 2) than proposed by Bodig and Jayne (1982), around 20, but in the same magnitude order than Gonçalves et al. (2011) who obtained 8.0, 6.8 and 5.9 for two tropical wood and one Eucalyptus. Keunecke et al (2007) obtained ratios of $E_L/E_T = 7.26$ and 11.8 for the spruce and yew species and Vazquez et al. (2015) 12.6 for *Castanea sativa*.

Considering the relation E_R/E_T (Table 2) the values were closer to 1.6 expected by Bodig and Jayne (1982). For hardwoods, the difference between properties in radial and tangential directions are smaller than in softwoods (Gonçalves 2011), so the values are in agreement with this condition.

Gonçalves et al. (2011) shows results from Bucur (2006) for 11 species whose G_{LR}/G_{RT} ratios ranged from 3.3 to 20.8, G_{LT}/G_{RT} between 1.9 and 21.4, and E_L/G_{LR} between 4.1 and 21.2; from Bucur and Archer (1984) with results for six species: G_{LR}/G_{RT} ratios between 2.89 and 16.9, G_{LT}/G_{RT} between 2.6 and 13.1, and E_L/G_{LR} between 5.6 and 8.8 and Keunecke et al (2007): $G_{LR}/G_{RT} = 4.7$ for yew and 11.6 for spruce, $G_{LT}/G_{RT} = 4.5$ for yew and 11.1 for spruce, and $E_L/G_{LR} = 9.6$ for yew and 22.4 for spruce. These values demonstrate the great variability of results for these wood parameters and show that our results are within these intervals.

Table 2. Relationship between elastic parameters obtained by ultrasound in different axis or planes.

	E_L/E_T	E_R/E_T	G_{LR}/G_{RT}	G_{LT}/G_{RT}	E_L/G_{LR}
AM	9.51	1.51	2.59	2.02	10.78
AV	5.36	1.27	3.09	1.82	5.39
R	8.68	1.33	3.00	1.86	8.59
P	8.97	1.76	2.40	1.70	10.68
G	8.38	1.37	3.47	1.46	8.34
CA	8.81	1.42	2.81	2.28	9.71

AM- *Hymenolobium petraeum* Ducke; AV- *Dinizia excelsa* Ducke; R- *Peltogyne lecointei* Duckei; P- *Caryocar brasiliense*; G- *Apuleia leiocarpa* ; CA- *Bertholletia excelsa*

There are also relations expected to Poisson ratio and modulus of elasticity. Also for these relations the results obtained in this research are within expected values (Table 3) and values showed in literature. Vazquez et al. (2015) obtained values very close to this paper for v_{RL}/E_R (4.58) and v_{LR}/E_L (5.04) and greater for the other relations, mainly for v_{TR}/E_T (48.11) and v_{RT}/E_R (47.74) although both are within values expect by Bodig and Jayne (1982).

Table 3. Relationship between terms of the compliance matrix (10-5) obtained with ultrasound an interval proposed by Bodig and Jayne (1982)

	v_{RL}/E_R	v_{LR}/E_L	v_{TL}/E_T	v_{LT}/E_L	v_{TR}/E_T	v_{RT}/E_R
AM	5.3	5.5	4.9	4.9	17.3	17.2
AV	6.5	6.7	5.2	5.0	16.1	16.2
R	4.4	4.5	4.8	4.7	22.9	23.3
P	6.7	6.8	6.2	6.0	22.1	21.9
G	5.3	5.4	5.2	5.3	22.0	21.8
CA	6.0	6.1	4.6	4.8	29.3	29.4
Bodig and Jayne (1982)	1.52 a 5.13	1.37 a 4.27	1.79 a 6.14	1.59 a 6.48	20.7 a 128	21 a 104

AM- *Hymenolobium petraeum* Ducke; AV- *Dinizia excelsa* Ducke; R- *Peltogyne lecointei* Duckei; P- *Caryocar brasiliense*; G- *Apuleia leiocarpa* ; CA- *Bertholletia excelsa*

Conclusion

Using ultrasound tests, it was possible determine the 12 elastic parameters of 6 Brazilian tropical species allowing obtain important parameter to give information about the potentiality of these species. The elastic parameters obtained by ultrasound present values in agreement with other researches and inside expected ranges for a material with great variability, showing the potential of the technique in characterizing the wood.

References

Associação Brasileira de Normas Técnicas. NBR 7190: Projeto de estruturas de madeira. Rio de Janeiro, 1997.

Bodig J, Jayne BA (1982) Mechanics of wood and wood composites. Van Nostrand Reinhold, New York, NY. 712 pp.

Bucur, V. (2006) *Acoustics of wood*, 2nd edn. Springer, New York, p 393.

Bucur V, Archer RR (1984) Elastic constants for wood by an ultrasonic method. *Wood Sci Technol* 18:255-265.

Gonçalez. J.C; Valle AT, Costa AF (2001) Estimativas das constantes elásticas da madeira por meio de ondas ultrassônicas (The use of ultrasonic method for estimating wood elastic constants). *Revista Cerne* 7(2):81–92

Gonçalves R, Trinca AJ, Cerri DGP (2011) Comparison of elastic constants of wood determined by ultrasonic wave propagation and static compression testing. *Wood Fiber Sci* 41(1):64–75

François, M. Identification des symmetries matérielles de matériaux anisotropes. França, Tese de Doutorado –Universidade de Paris, 137p., 1995.

Furlani. J. E. Um estudo sobre a variação numérica do coeficiente de Poisson na madeira. 1995. 144 p. Dissertação (Mestrado em Engenharia Civil) – Universidade de Campinas. Faculdade de Engenharia Civil, Campinas.

Keunecke D, Sonderegger W, Pereteanu K, Lüthi T, Niemz P (2007) Determination of Young's and shear moduli of common yew and Norway spruce by means of ultrasonic waves. *Wood Sci Technol* 41:309-327.

Mascia, N. T. Considerações a respeito da anisotropia da madeira. 1991. 293 p. Tese (Doutorado em Engenharia de Estruturas) - Universidade de São Paulo. Escola de Engenharia de São Carlos, São Carlos.

Trinca, A. J. Metodologia para determinação das constantes elásticas da madeira por ultrassom. 129p. Tese (Doutorado em Engenharia Agrícola) – Na área de concentração de Construções Rurais, Faculdade de Engenharia Agrícola, Universidade Estadual de Campinas, Campinas (SP), 2011.

Vázquez, C.; Gonçalves, R.; Bertoldo, C.; Baño, V.; Veja, A.; Guaita, M. 2015. Determination of the mechanical properties of *Castanea sativa* Mill. using ultrasonic wave propagation and comparison with static compression and bending methods. *Wood Sci Technol*, 49: p. 607-622.

Investigating Fire Performance of Heat-Treated Bamboo Scrimber Flooring

Zhijia Liu

International Centre for Bamboo and Rattan, Beijing, China, Liuzj@icbr.ac.cn

Jingxin Wang*

School of Natural Resources, West Virginia University, Morgantown, WV, USA,
Jingxin.Wang@mail.wvu.edu

Benhua Fei*

International Centre for Bamboo and Rattan, Beijing, China, feibenhua@icbr.ac.cn

Changle Jiang

School of Natural Resources, West Virginia University, Morgantown, WV, USA, chjiang@mix.wvu.edu

Tao Zhang

International Centre for Bamboo and Rattan, Beijing, China, 1204624557@qq.com

Fang Liang

International Centre for Bamboo and Rattan, Beijing, China, 577759813@qq.com

***Corresponding author**

Abstract

Fire characteristics of bamboo scrimber flooring produced from different heat-treated processes were investigated by thermogravimetric analysis (TGA) and cone calorimeter in this research. The results showed that the combustion process of samples included moisture removal, oxidative and char combustion. All characteristic temperatures had shifted to higher ones with the increase of heating rates. The activation energy of oxidative combustion stage was lower than that of char combustion stage. Compared with untreated samples, LBSF had a lower activation energy in both combustion stages. HBSF had a higher activation energy in the oxidative stage and a lower activation energy in the char stage. LBSF and HBSF had lower heat release rates and larger time to ignition. However, both had a higher total heat release, total suspended particulate, and higher heating value. The results will be rather helpful for guiding and promoting the utilization of bamboo scrimber flooring.

Keywords: Bamboo; Bamboo scrimber flooring; Heat-treatment; Thermogravimetric analysis; Cone calorimeter

1. Introduction

Recently, the environment-friendly decorative materials have drawn increasing attention (Song et al. 2013). Bamboo is considered as an important non-wood forest resource and has become one of the alternatives to timber materials due to easy propagation and fast growth (Shao 2009). It has widely been used to produce flooring decoration materials. There are two main types of commercial bamboo floorings, bamboo scrimber flooring and laminated bamboo flooring. The utilization percentage of bamboo for laminated flooring is lower than 50% due to its special structure. However, bamboo scrimber flooring can use about 90% bamboo materials during manufacturing process. Yu and Yu (2013) reported that bamboo reconstituted processing method was one of the most effective ways to use plantation bamboo. Bamboo scrimber flooring has some excellent natural decorative properties. However, poor dimensional stability and uneven color change have also affected the development of bamboo scrimber flooring, especially for outdoor environment. Heat treatment is a thermal modification technology which is considered as a potential solution to solve the problems above. Therefore, many scientists have been working on a variety of studies on heat treatment to improve the properties of final bamboo products. Salim et al. (2010) found the heat-treated bamboo retained majority of their original physical and strength properties after undergoing the heat treatment. Zhang et al. (2013) found that the color of heat-treated bamboo was darkened and all color parameters (L^* , a^* , b^*) were significantly changed. Meng et al. (2016) found that hemicellulose contents of bamboo decreased after heat treatment. Ester formation linked to lignin decreased the hygroscopicity of bamboo and improved dimensional stability and durability. Qin et al. (2012) found that thickness swelling of bamboo boards treated by heat decreased and total color difference apparently changed with increasing in heat-treatment temperature.

One of the key parameters to evaluate bamboo flooring is fire performance, which limits the application of bamboo flooring to a given area. Liu et al. (2014) found that bamboo with higher content of volatiles was easier to be burned rapidly, which led to a security risk. Shu et al. (2007) found that bamboo floor covering was easier to ignite and held higher flashover risk as well as greater CO yields (in early burning) than wood floor covering. Mena et al. (2012) investigated fire behavior of *Guadua angustifolia kunth* (a.k.) bamboo and found that it would be qualified as structural and indoor finishing building material. Yu et al. (2017) investigated the combustibility of boron-containing fire retardant treated bamboo filaments. It was also found that boron-containing flame retardants had excellent smoke suppression efficacy and total smoke release was decreased by 86.1% and 9.1%, respectively. To the best of our knowledge, there is the lack of sufficient information concerning fire performances of heat-treated bamboo scrimber flooring. Therefore, fire properties of bamboo scrimber flooring with different heat-treated processes were studied by thermogravimetric analysis (TGA) and cone calorimeter in this work. The outcome will be beneficial for the development and guidance of bamboo scrimber flooring utilization.

2. Materials and methods

2.1 Materials

Bamboo scrimber flooring were purchased from factory of bamboo flooring in Zhejiang Province, China. The raw materials, 5 years old moso bamboo (*Phyllostachys heterocycla*), were sampled from a bamboo plantation. Moso bamboo was firstly made to bamboo fiber bundles. They were heat treated with low temperature of 140°C for 3 hours (LBSF) and high temperature of 190°C for 10 hours (HBSF), respectively. Heat-treated bamboo fiber bundles were impregnated using phenolic formaldehyde adhesive then pressed firmly together in a hot press to manufacture bamboo scrimber flooring.

2.2 Determination of combustion characteristics

Bamboo scrimber flooring was broken down to particles using a Wiley Mill (Thomas-Wiley). Samples were screened to obtain the particles with a size of 250-425 μm and were dried at temperature of 105°C until mass stabilized. Combustion characteristics were observed in terms of the materials mass loss through TA Instrument TGA Q 500 thermogravimetric analyzer (TA Instrument, USA). The particles were evenly and loosely distributed in an open sample pan and the initial sample weight was about 5-10mg. The temperature change was controlled from room temperature (30±5°C) to 800°C with different heating rates of 5°C/min, 10°C/min, 20°C/min and 30°C/min. The air stream with flow rate of 60 mL/min was continuously passed into the furnace to investigate combustion characteristics. Three replicates of each TGA experiment were performed. The combustion kinetics of bamboo scrimber were calculated based on the Coats-ReDFern (CR) model. The CR model is a kinetic model based on different heating rates. It is suitable to calculate the frequency factor and reaction order by using the activation energy (Yorulmaz et al. 2009).

$$\ln\left(\frac{-\ln(1-\alpha)}{T^2}\right) = \ln\left[\frac{A \cdot R}{\beta \cdot E_a} \left(1 - \frac{2R \cdot T}{E_a}\right)\right] - \frac{E_a}{R \cdot T} \quad (n = 1)$$

Where, α is the conversion rate, β is the heating rate, R is the universal gas constant (8.314J/mol·K), T is the reaction temperature, E_a is the activation energy.

2.3 Determination of fire performances

Bamboo scrimber flooring was cut into pieces with a size of 100 mm (length) \times 100 mm (width) \times about 10 mm (thickness) according to the requirement of ISO standard (5660-1:2002). All samples were dried at temperature 105°C until mass stabilized. Fire performance of bamboo scrimber flooring were determined using a cone calorimeter (Fire Testing Technology LTD., UK). The tests were carried out at the horizontal orientation with a 50 kW/m² flux, using an edge frame. Three replicates of each cone experiment were performed.

2.4 Proximate and ultimate analysis

Proximate and ultimate analyses of materials were determined according to the standard method. The determination of moisture and volatiles were performed according to GB/T 212-2008. The determination of inorganic ash was performed according to D1102-84. The determination of high heating value was performed according to ASTM E 711. The determination of C, H and N was performed according to GB/T 476-2008. The oxygen content was obtained by calculating the difference.

3. Results and discussion

3.1 Combustion characteristics

Figure 1 showed combustion processes of bamboo scrimber flooring at heating rates of 5°C/min, 10°C/min, 20°C/min and 30°C/min. There were three stages during combustion process of all samples. The mass loss at the first stage was due to moisture removal, which occurred at temperature below 150°C. The second stage was oxidative combustion with a temperature range from 150°C to 350°C. The release and oxidative combustion of volatiles resulted in mass loss at this stage. The mass loss at the third stage was due to char combustion, which occurred at the temperature range from 350°C to 500°C. **Table 1** showed proximate and ultimate analysis of samples. There were about 80% volatiles and 20% fixed carbon for bamboo scrimber flooring. This indicated that oxidative combustion of volatiles was the main combustion stages. With the increase of heat-treatment temperature and time, volatiles of samples gradually decreased by 72.78% and 68.26%. Meanwhile, the main combustion of LBSF and HBSF also gradually shifted to

char combustion. It was found that the combustion process of bamboo scrimber flooring also shifted to high temperature with the increase of heating rates. This phenomenon was similar with the results of Munir et al. (2009) and Tonbul et al. (2009). There were also higher content of ash and lower content of moisture after bamboo scrimber flooring was treated by heat. The release of volatiles during heat-treatment process resulted in ash increase. Bamboo is mainly composed of cellulose, hemicelluloses and lignin. These chemical compositions were subject to thermal degradation and hydroxyl groups were destroyed during heat-treatment process. The process decreased water absorption properties of LBSF and HBSF.

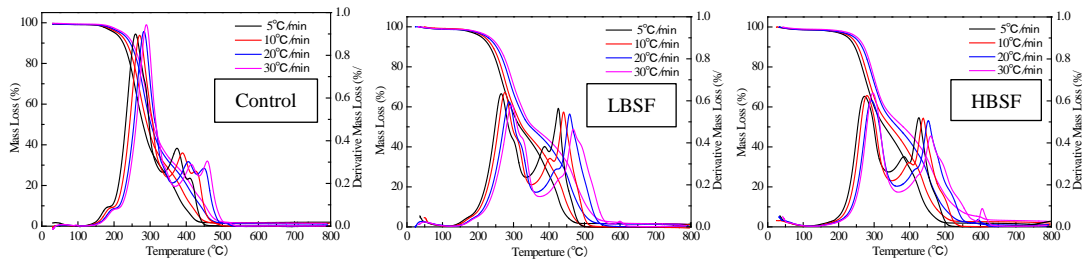


Figure 1—Combustion process of bamboo scrimber flooring at different heating rates

Table 1—Proximate and ultimate analysis of samples

Samples	Proximate analysis (%)			Ultimate analysis (%)				HHV (MJ/kg)
	Volatiles	Ash	Moisture	C	H	O	N	
Control	79.56	1.44	4.13	49.58	5.60	44.54	0.28	19.59
LBSF	72.78	2.00	3.75	53.08	5.58	41.20	0.14	21.03
HBSF	68.26	2.64	3.97	55.72	5.48	38.62	0.18	22.13

HHV is higher heat value.

Thermogravimetric analysis (TGA) can be used to determine characteristic points during biomass combustion (García et al. 2015). **Table 2** showed combustion characteristics of all samples. It was found that all characteristic temperatures shifted to higher ones with the increase of heating rates. Ignition temperatures of bamboo scrimber flooring were 221°C, 228°C, 244°C and 250°C corresponding to heating rate of 5°C/min, 10°C/min, 20°C/min and 30°C/min. Similarly, peak temperatures of that corresponding to the maximum mass loss rates were 259°C, 271°C, 283°C and 290°C at the oxidative combustion stages, then 374°C, 389°C, 406°C and 458°C during the char combustion stages. The burnout temperatures of that were 455°C, 498°C, 525°C and 540°C for untreated bamboo scrimber flooring. The maximum mass loss rate of samples was higher at oxidative combustion stage than that at char combustion stage, indicating there was a higher reaction activity at the oxidative combustion stage. There was about 70% mass loss at the oxidative combustion stage while about 30% mass loss at the char combustion stage. When bamboo scrimber flooring was treated by heat, characteristic temperatures at both combustion stages also shifted to higher ones. However, the difference of the maximum mass loss rate between oxidative combustion stage and char combustion stage was not significant compared with untreated bamboo scrimber flooring.

Table 2—Combustion characteristics of samples

Samples	Hr (°C/min)	T _i (°C)	Oxidative combustion			Char combustion			T _b (°C)
			T _p (°C)	DTG _{max} (mg/min)	W ₁ (wt.%)	T _p (°C)	DTG _{max} (mg/min)	W ₁ (wt.%)	
Control	5	221	259	0.90	71.03	374	0.36	26.16	455
	10	228	271	0.89	69.92	389	0.34	27.68	498
	20	244	283	0.91	69.22	406	0.30	28.43	525
	30	250	290	0.94	68.95	458	0.30	28.64	540
LBSF	5	224	265	0.63	52.55	426	0.56	44.27	502
	10	233	276	0.64	54.69	441	0.55	42.60	520
	20	248	287	0.59	51.05	458	0.54	45.88	556
	30	256	295	0.58	51.31	468	0.46	44.85	573
HBSF	5	239	273	0.62	50.93	426	0.52	45.51	518
	10	243	280	0.63	48.86	438	0.52	46.90	554
	20	254	292	0.60	47.83	453	0.51	48.92	594
	30	262	296	0.64	46.38	459	0.43	49.01	639

T_i is ignition temperature, T_p is the peak temperature of this stage, W₁ is the weight loss of this stage, Hr is heating rate and T_b is burnout temperature.

The reaction kinetics of biomass materials is critical to predict the combustion characteristics (Islam et al. 2015). As an isothermal integral model, the CR model had widely been used to investigate the biomass combustion kinetics. Table 3 showed the kinetic parameters of bamboo scrimber flooring at different heating rates. The correlation coefficient of the linear relationship (R² value) was higher, indicating that CR model could accurately calculate the activation energy of the samples. The activation energy of oxidative combustion stage was apparently lower than that of char combustion stage. The activation energy of bamboo scrimber flooring varied in the range of 79.77-84.81KJ/mol in the oxidative stage and 139.85-122.21 KJ/mol in the char combustion stage. LBSF had a lower activation energy than those of untreated samples in both combustion stages, with a value of 71.82-73.18KJ/mol in the oxidative stage and 106.17-110.97 KJ/mol in the char combustion stage. However, compared with untreated samples, HBSF had a higher activation energy in the oxidative stage (80.44-90.44KJ/mol) and a lower activation energy in the char stage (84.98-98.81KJ/mol). This was mainly attributed to the release of volatiles during the heat-treatment process. It also indicated that the heat-treatment decreased the reaction reactivity of bamboo scrimber flooring and required a higher energy to fire. For untreated samples and HBSF, the activation energy gradually increased in the oxidative stage and decreased in the char stage as heating rates increased.

Table 3—The kinetic parameters of samples at different heating rates (C-R model)

Samples	Combustion stage	Hr (°C/min)	Linear function	R ²	Ea (KJ/mol)	A (1/min)
Control	Oxidation combustion	5	y=-9595x+4.8573	0.99368	79.77	1.23E+07
		10	y=-9689x+4.6597	0.99386	80.56	2.05E+07
		20	y=-9926x+4.7313	0.99428	82.53	3.38E+07
		30	y=-10201x+5.0337	0.99448	84.81	6.26E+07
	Char combustion	5	y=-16821x+12.3880	0.96066	139.85	4.04E+10
		10	y=-15854x+10.1666	0.96389	131.81	8.25E+09
		20	y=-14778x+7.8424	0.96842	122.86	1.13E+09
		30	y=-14699x+7.3750	0.97283	122.21	9.38E+08
LBSF	Oxidation combustion	5	y=-8755x+3.1327	0.99514	72.79	2.01E+06
		10	y=-8639x+2.6003	0.99579	71.82	2.33E+06
		20	y=-8802x+2.5768	0.99721	73.18	3.47E+06
		30	y=-8781x+2.3149	0.99809	73.00	3.56E+06
	Char combustion	5	y=-12970x+5.7070	0.99058	107.83	3.90E+07
		10	y=-13348x+5.6317	0.9935	110.97	7.45E+07
		20	y=-12848x+4.1920	0.99713	106.82	2.55E+07
		30	y=-12770x+3.6375	0.99871	106.17	1.94E+07
HBSF	Oxidation combustion	5	y=-9676x+4.4936	0.987	80.44	4.33E+06
		10	y=-10157x+5.1095	0.98533	84.45	1.68E+07
		20	y=-10319x+4.9781	0.98765	85.79	3.00E+07
		30	y=-10878x+5.8679	0.98463	90.44	1.15E+08
	Char combustion	5	y=-11885x+3.8868	0.98964	98.81	2.90E+06
		10	y=-11609x+3.0107	0.99153	96.51	2.36E+06
		20	y=-11513x+2.2956	0.99065	95.72	2.29E+06
		30	y=-10222x+0.1737	0.98025	84.98	3.65E+05

Hr is heating rate; R² is correlation coefficient value; Ea is activation energy; A is exponential factor.

3.2 Fire performances

The heat release rate (HRR) is a key factor for evaluating fire safety of materials. **Figure 2** displayed the HRR of bamboo scrimber flooring. There were two HRR peaks. The first peak resulted from the

burning of the accumulated flammable pyrolysates on the decomposed material surface and the second one is primarily from the flashover of the bottom layers (Xiao et al. 2016). It was found that HRR peaks of LBSF and HBSF shifted to right in the graph and the interval of two peaks increased. Furthermore, the second HRR peaks of heat-treated samples also delayed with the increase of heat-treatment temperature and time. This phenomenon was mainly due to the thermal decomposition of volatiles during heat-treatment process. Liu et al. (2016) found that volatiles of bamboo had a higher reactivity and was easier to be ignited. **Table 3** showed that the time to ignition (TTI) of bamboo scrimber flooring was 20s. When it was heat-treated, TTI of LBSF and HBSF gradually increased to 50s and 54s. The average HRR values of samples was respectively 232.94kW/m², 163.02kW/m² and 131.27kW/m². HRR indicates fire intensity of the materials. Higher HRR means lower safety in the fire. The peak of HRR value is also considered as important parameter that best expresses maximum intensity of HRR (Seo et al. 2016). Heat-treated bamboo scrimber flooring had a higher value of the first HRR peak and lower value of the second HRR peak. Grexa and Lübke (2001) reported that the second HRR peak indicated the heat release rate of samples. The lower value of the second HRR peak further confirmed that heat-treated bamboo scrimber flooring had a better fire performance.

The total heat release (THR) represents the combustion heat of the material. Higher THR indicates higher potential of heat energy available for material combustion. **Figure 3** showed THR of bamboo scrimber flooring. Heat-treated samples had a higher THR compared with untreated samples. The THR values of samples was 106.00MJ/m², 187.50MJ/m² and 231.10MJ/m². A longer time to reach the flashover stage of heat-treated samples resulted in this phenomenon. **Table 4** showed that the time to reach the flashover stage of untreated samples was from 20s to 458s. However, that of LBSF and HBSF was respectively 50-1199s and 54-1810s. It is well known that the longer combustion time, the higher THR. Furthermore, the higher carbon content of heat-treated samples was also responsible for its higher THR. Demirbas (2004) reported that carbon atoms of materials mainly affected the heating value. Results in **Table 1** indicated that heat-treated samples had a higher HHV, such as 19.59MJ/kg (untreated samples), 21.03MJ/kg (LBSF) and 22.13MJ/kg (HBSF). There were in accordance with the results of THR.

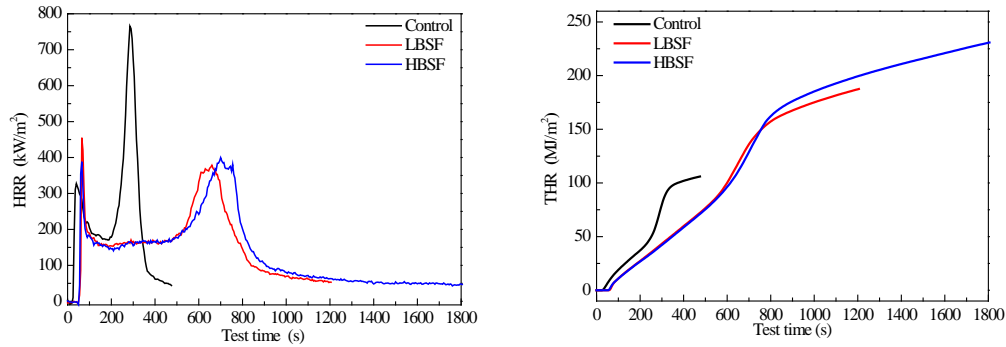


Figure 2—HRR curves of bamboo scrimber flooring **Figure 3**—THR curves of bamboo scrimber flooring

Table 4—Fire characteristics of bamboo scrimber flooring

Samples	TTI (s)	TTF (s)	HRR _{mean} (kW/m ²)	THR (MJ/m ²)	TSP (m ²)	CO _{mean} kg/kg	CO _{2 mean} kg/kg
Control	20	458	232.94	106.00	3.20	0.0119	1.77
LBSF	50	1199	163.02	187.50	5.60	0.0218	1.67
HBSF	54	1810	131.27	231.10	8.30	0.0502	1.89

TTI is time to ignition, HRR is heat release rate, THR is total heat release, MLR is mass loss rate.

Smoke suppression properties are crucial in terms of fire safety, because the toxic smoke generated from fire is more lethal than heat (Chu et al., 2017). Being consistent with the results of HRR curves, the smoke production rate (SPR) curve of samples also exhibited two main peaks, as showed in **Figure 4**. The smoke primarily consisted of incompletely combusted polymeric fragments and steam produced from decomposed cell wall of biomass materials (Xiao et al., 2016). Total suspended particulate (TSP) is also an important parameter to describe the fire hazard of materials. **Figure 5** showed TSP of bamboo scrimber flooring. The TSP values of samples apparently increased when they were heat-treated, respectively corresponding to 3.20m² (control), 5.60m² (LBSF) and 8.30m² (HBSF). Bamboo, as a type of biomass, is mainly composed of cellulose, hemicelluloses and lignin. These chemical compositions can release CO and CO₂ when they were fired in air environment. The CO and CO₂ yield of untreated samples was 0.0119kg/kg and 1.77kg/kg during the combustion process. Similar, the CO and CO₂ yield of LBSF was 0.0218kg/kg and 1.67kg/kg and that of HBSF was 0.0502kg/kg and 1.89kg/kg, respectively. The high CO and CO₂ yield of heat-treated samples could resulted in its high TSP value.

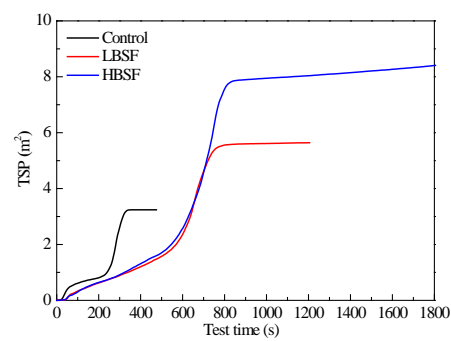
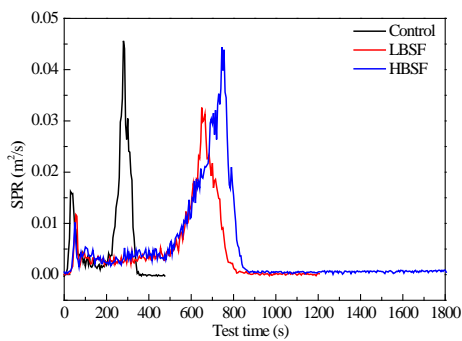


Figure 4—SPR curves of bamboo scrimber flooring **Figure 5**—TSP curves of bamboo scrimber flooring

4. Conclusions

The combustion process of bamboo scrimber flooring included moisture removal, oxidative and char combustion. All characteristic temperatures shifted to higher ones with the increase of heating rates. The activation energy of oxidative combustion stage was significantly lower than that of char combustion stage. LBSF had a lower activation energy than that of untreated samples in both combustion stages. HBSF had a higher activation energy in the oxidative stage and a lower activation energy in the char stage. LBSF and HBSF had a lower HRR and a larger TTI. Both had a higher THR, TSP, and HHV.

Acknowledgments

This research was financially supported by ‘13th Five Years Plan-Study on manufacturing technology of bamboo wastes and its mechanism (Grant No. 2016YFD0600906) and ‘Basic Scientific Research Funds of International Centre for Bamboo and Rattan-Co-combustion technology of torrefied bamboo and coal’ (Grant No. 1632016011).

References

- Chu, D.; Mu, J.; Zhang, L.; Li, Y. 2017. Promotion effect of NP fire retardant pre-treatment on heat-treated poplar wood. Part 1: color generation, dimensional stability, and fire retardancy. *Holzforschung*, 71: 207-215.
- Demirbas, A. 2004. Combustion characteristics of different biomass fuels. *Progress in energy and combustion science*, 30: 219-230.

- García, R.; Pizarro, C.; Álvarez, A.; Bueno, J.L. 2015. Study of biomass combustion wastes. *Fuel*. 148: 152-159.
- Grexa, O.; Lübke, H. 2001. Flammability parameters of wood tested on a cone calorimeter. *Polymer Degradation and Stability*. 74: 427-432.
- Liu, Z.; Fei, B.; Jiang, Z.; Liu, X. 2014. Combustion characteristics of bamboo-biochars. *Bioresour Technol*. 167: 94-99.
- Liu, Z.; Hu, W.; Jiang, Z.; Mi, B.; Fei, B. 2016. Investigating combustion behaviors of bamboo, torrefied bamboo, coal and their respective blends by thermogravimetric analysis. *Renewable Energy*. 87: 346-352.
- Mena, J.; Vera, S.; Correal, J.F.; Lopez, M. 2012. Assessment of fire reaction and fire resistance of *Guadua angustifolia* kunth bamboo. *Construction and Building Materials*, 27: 60-65.
- Meng, F.D.; Yu, Y.L.; Zhang, Y.M.; Yu, W.J.; Gao, J.M. 2016. Surface chemical composition analysis of heat-treated bamboo. *Applied Surface Science*. 371: 383-390.
- Munir, S.; Daood, S.S.; Nimmo, W.; Cunliffe, A.M.; Gibbs, B.M. 2009. Thermal analysis and devolatilization kinetics of cotton stalk, sugar cane bagasse and shea meal under nitrogen and air atmospheres. *Bioresour Technol*. 100: 1413-1418.
- Li, Q.; Yu, W.J.; Yu, Y.L. 2012. Research on properties of reconstituted bamboo lumber made by thermo-treated bamboo bundle curtains. *Forest products journal*. 62: 545-550.
- Salim, R.; Ashaari, Z.; Samsi, H.W.; Wahab, R.; Alamjuri, R.H. 2008. Effect of oil heat treatment on physical properties of semantan bamboo (*Gigantochloa scortechinii gamble*). *Modern Applied Science*. 1: 91.
- Seo, H.J.; Park, J.E.; Son, D.W. 2016. Combustion and thermal characteristics of Korean wood species. *BioResources*. 11: 7537-7550.
- Shao, S.; Jin, Z.; Wen, G.; Iiyama, K. 2009. Thermo characteristics of steam-exploded bamboo (*phyllostachys pubescens*) lignin. *Wood science and technology*. 43: 643-652.
- Shu, Z.; Chen, Q. 2007. Fire performances of bamboo floor covering compared to wood floor covering by cone calorimeter test. *Fire Safety Science*. 3: 005.
- Song, L.; Sun, X.; Miao, J. 2013. Exploration about new green building materials-the new decorative materials of water printing ecological wood. *International Conference on Structures and Building Materials*. 1805-1808.
- Tonbul, Y.; Saydut, A.; Yurdakoç, K.; Hamamci, C. 2009. A kinetic investigation on the pyrolysis of Seguruk asphaltite. *Journal of Thermal Analysis and Calorimetry*. 95: 197-202.
- Xiao, Z.; Xu, J.; Mai, C.; Militz, H.; Wang, Q.W.; Xie, Y.J. 2016. Combustion behavior of Scots pine (*Pinus sylvestris* L.) sapwood treated with a dispersion of aluminum oxychloride-modified silica. *Holzforschung*. 70: 1165-1173.
- Yu, L.L.; Lu, F.; Qin, D.C.; Ren, H.Q.; Fei, B.H. 2017. Combustibility of boroncontaining fire retardant

treated bamboo filament. *Wood and Fiber Science*. 49: 125-133.

Yu, W.; Yu, Y. 2013. Development and prospect of wood and bamboo scrimber industry in China. *China Wood Industry*. 27: 5-8.

Zhang, Y.M.; Yu, Y.L.; Yu, W.J. 2013. Effect of thermal treatment on the physical and mechanical properties of *Phyllostachys pubescens* bamboo. *European Journal of Wood and Wood Products*. 71: 61-67.



Session 10

**Evaluation of Seedlings
and Young Trees for
Genetic Improvement**

Ultrasonic Method for Evaluating Wood Quality of Poplar Seedlings

Houjiang Zhang

School of Technology, Beijing Forestry University, Beijing, China, hjzhang6@bjfu.edu.cn

Dan Feng

School of Technology, Beijing Forestry University, Beijing, China, 853078861@qq.com

Xiping Wang

USDA Forest Service Forest Products Laboratory, Madison, Wisconsin, USA, xwang@fs.fed.us

Abstract

In China, quality of seedlings is typically evaluated based on physical index such as root-collar diameter, seedling height, root length and width etc.; while wood properties of the seedlings are not taken into consideration. Latest research have shown that wood properties of seedlings such as stiffness and micro-fibril angle are highly heritable and they determine the wood quality of future plantations. Ultrasonic velocity, as a nondestructive measure, is closely related to wood quality and has been recognized as a reliable predictor of stiffness. In this study, we investigated the use of an ultrasonic device as a potential nondestructive tool to monitor and assess the wood quality of poplar (*Populus×euramericana* cv.'74/76') seedlings, a common plantation species in China. A total of 200 poplar seedling samples were selected and their ultrasonic velocities were measured at four times during the first growth year. Following ultrasonic measurements, 61 seedlings were randomly selected and cut down and the acoustic velocity of each sample was measured using a resonance method. The ultrasonic velocity of the seedlings measured each time was in a normal distribution and it had a strong positive correlation with the number of growth days. The coefficient of determination for the linear relationship between average velocity and growth days was 0.991. No significant correlation was found between ultrasonic velocity and root-collar diameter of the seedlings. Ultrasonic velocity measured on the seedlings was found to have a strong correlation with the velocity of the cut samples measured using resonance method ($R^2=0.805$). The results of this laboratory study indicate that ultrasonic measurement can be used to assess quality traits of young seedlings in future genetic programs.

Key words: Poplar seedlings; resonance acoustic velocity; ultrasonic velocity; wood quality

Introduction

The quality of seedlings determine survival rate of afforestation and quality of plantation growth. Scientific and accurate evaluation of seedling quality and reasonable grading of the seedlings play an important role in improving effectiveness of the afforestation. In China, quality of seedlings is

typically evaluated based on physical index such as root-collar diameter, seedling height, root length and width etc. (GB 6000-1999); while wood properties of the seedlings are not taken into consideration. Latest research have shown that wood properties of seedlings such as stiffness and micro-fibril angle are highly heritable and they determine the wood quality of future plantations (Xu 2011), so it is very meaningful to carry out nondestructive testing and evaluation of wood quality of the seedlings.

Ultrasonic velocity and acoustic velocity, as nondestructive measures, are closely related to wood quality and has been recognized as a reliable predictor of stiffness (Liang et al. 2008, Divos 2010). Generally, the larger velocity is, the better the wood density and mechanical properties are. In recent years, New Zealand scholars started to evaluate radiata pine (*Pinus radiata*) seedling quality using stress wave, two miniature accelerometers were coupled to the bark of a growing seedling stem to record the acoustic signals and a small striker to generate an acoustic pulse. The result shows good promise as a rapid and cost-effective tool for early screening of wood quality in clonal trials (Emms et al. 2012, 2013). In China, the stress wave has been used to study and evaluate wood mechanical properties of plantations (Guan and Zhao 2013, Liu et al. 2016). In essence, ultrasonic and acoustic waves propagating in solids all belong to stress wave (Sheng 2014), but so far, research on using ultrasonic to screen the seedling quality was very few.

The research work presented in this paper was to measure the ultrasonic propagation velocity in poplar (*Populus×euramericana* cv.'74/76') seedlings, a common plantation species in China, and analyze the measuring results, to do some basic work for future developing a rapid screening method of poplar seedling wood quality.

Material and methods

Poplar seedlings

Poplar (*Populus×euramericana* cv.'74/76') seedlings were grown in Seedling Base of Beijing Forestry University. They were cottage planted in April 13, 2015, with 80 cm of row space and 30 cm of column space. A total of 22 rows of poplar seedlings were planted, in which 200 seedlings of them were randomly selected as our investigation samples. Before the measuring, the 200 seedling samples were numbered as P-01, P-02, ..., P-200.

Testing instruments

The instrument used was an ultrasonic device, Fakopp Ultrasonic Timer made in Hungary, has two identical sensors and one electronic box. The two sensors, a starter sensor and a receiver sensor, are pressed to the seedling stem, providing acoustic coupling between the seedling and sensor. The box generates ultrasonic signals for the starter sensor and receives the ultrasonic signals from the receiver sensor, and calculates and displays ultrasonic propagation time between the two sensors in the seedling stems. The ultrasonic device operated by battery, is suitable for outdoor field measurements. Figure 1 shows an example of measuring using Fakopp Ultrasonic Timer.



Figure 1—Field measuring

Experimental methods

The investigation was taken place as three experiments, including proper distance determination between the two sensors, ultrasonic velocities measuring in the seedling stems and acoustic velocities measuring using a resonance method.

Proper distance determination between the two sensors

The purpose of this experiment is to determine a proper distance between the two sensors when measuring ultrasonic velocity in poplar seedling stems. To fully reflect the wood properties of seedlings, it is better to set a bigger distance between the two sensors, but the ultrasonic pulse signal emitted by the electronic box will continue to weaken during propagation in the seedling stems, if the distance is too large, the receiver sensor may not trigger the timer, resulting in no measurement results.

6 seedlings were selected to do the determination. The starter sensor was put at 200 mm position above root ground, and the receiver sensor was put at 100 mm, 200 mm, 300 mm, 400 mm, 500 mm, 600 mm, 700 mm, 800 mm, 900 mm and 1000 mm above the starter sensor respectively. The ultrasonic propagation times were measured and analyzed, then the proper distance between the two sensors will be chosen.

Ultrasonic velocities measuring in the seedling stems

After determining the proper distance between the two sensors, ultrasonic propagation times of 200 seedling samples selected were measured, and the ultrasonic propagation velocity of each seedling was calculated. To reduce effects of environmental factors on the test results, the 200 seedlings measurements were completed on the same day. Total 4 time measurements were conducted in July 27, September 5th, September 23rd and November 8th of year 2015, i.e. 105 days, 145 days, 165 days and 209 days after they were cottage planted. Simultaneously, root-collar diameters of the seedlings were measured and recorded.

Acoustic velocities measuring using a resonance method

Acoustic resonance techniques have been used for a long time to determine the stiffness of construction materials. In many respects, acoustic resonance techniques provide a more useful result, as is evident by correlations of time-of-flight measurement results on stems to resonance results on logs (Wang et al. 2007). Resonance techniques are more accurate and repeatable than time-of-flight techniques, and generally do not require calibration and do not greatly depend on how the operator performs the measurements. Figure 2 shows setup of acoustic velocities measuring using a resonance method, the formula for acoustic velocity is

$$v = \frac{2l}{t} = 2lf$$

Where l is specimen length, t is time of an impacting pulse travel a round trip through the specimen, and f is frequency of the impacting pulse travel between two ends of the specimen.

61 seedlings were selected and cut to measure acoustic velocities and compare these velocities with ultrasonic velocities. For each selected seedling, ultrasonic propagation time and its diameter were measured before logging. Length of a seedling specimen for the resonance test was 15 times of its root-collar diameter.

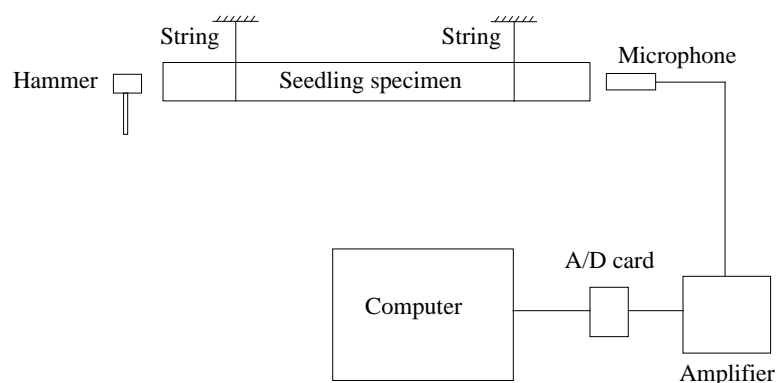


Figure 2—Setup of acoustic velocities measuring using a resonance method

Results and analysis

Proper distance between two sensors

Figure 3 shows experimental results of relationship between sensor space and ultrasonic velocity. It can be seen that when sensor spacing is less than 300mm, the velocity values are lower; when distance of the two sensors is from 300mm to 700mm, the ultrasonic velocity basically keeps stable; when the sensor spacing is greater than 700mm, some seedlings can not be measured ultrasonic propagation times. Therefore, considering the convenience of measuring operation, the proper distance between two sensors was finally set to 400 mm.

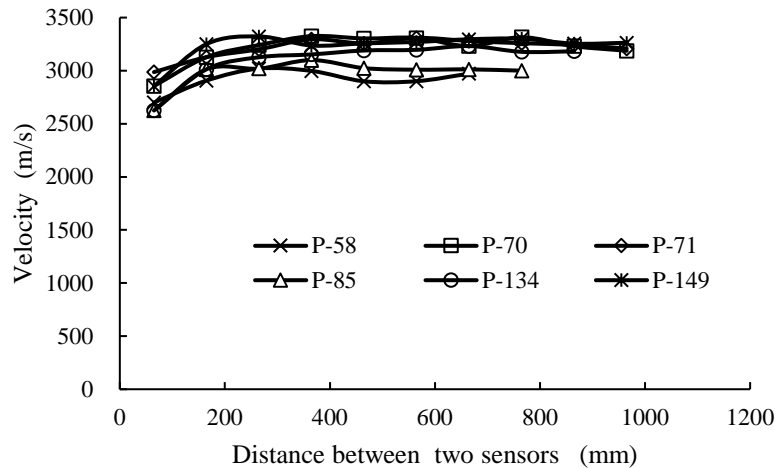


Figure 3—Relationship between sensor space and ultrasonic velocity

Ultrasonic velocities of seedlings

Ultrasonic velocities and root-collar diameters were measured 4 times, which conducted in July 27, September 5th, September 23rd and November 8th of year 2015 respectively. Table 1 shows the measuring results.

Table 1—The results of ultrasonic velocity and root-collar diameter of the 200 seedlings

Date	Root-collar diameter	Quantity	Average diameter	Maximum root-collar diameter	Minimum root-collar diameter	Average velocity	Maximum velocity	Minimum velocity
	(mm)		(mm)	(mm)	(mm)	(m/s)	(m/s)	(m/s)
July 27	$d \leq 10$	18	8.2	10.0	4.9	1928	2321	1476
	$10 < d \leq 20$	135	15.3	20.0	10.2	2001	2382	1680
	$20 < d \leq 30$	31	20.2	25.0	20.1	1898	2083	1341
Sept. 5	$d \leq 10$	7	7.6	9.4	5.7	2389	2513	2195
	$10 < d \leq 20$	68	15.6	20.0	10.2	2516	2739	2131
	$20 < d \leq 30$	84	20.6	29.9	20.2	2312	2699	1992
	$d > 30$	5	33.3	33.3	30.5	2140	2278	2036
Sept. 23	$d \leq 10$	7	7.7	9.7	5.7	2464	2659	2292
	$10 < d \leq 20$	60	11.8	19.5	10.2	2701	2914	2321
	$20 < d \leq 30$	78	20.9	29.6	20.1	2483	2824	2222
	$d > 30$	19	31.0	35.0	30.1	2326	2397	2182
Nov. 8	$d \leq 10$	7	8.0	9.9	6.4	2735	3341	2496
	$10 < d \leq 20$	59	11.9	19.9	10.2	2952	3223	2699
	$20 < d \leq 30$	76	21.5	29.8	20.5	2882	3341	2621
	$d > 30$	22	32.5	36.3	30.1	2733	2961	2566

Analysis of ultrasonic velocity distribution

Figure 4 shows statistical distribution results of two times ultrasonic velocities measured in July 27th and November 8th, 2015. The abscissa is ultrasonic velocity, and left ordinate is frequency which is seedling numbers in each velocity range, and right ordinate is probability of normal distribution. It can

be seen that for each time measuring result, the ultrasonic velocity distribution is an approximately normal distribution, that is, although the 200 seedlings are cottage planted on the same day, the growth time is the same, the wave velocities are not same, mostly concentrated near the mean velocity. The difference of ultrasonic velocities reflects the difference of mechanical properties, density and other material indexes among the seedlings. In September 5th and September 23rd, the two measuring results showed the similar distribution of the velocities.

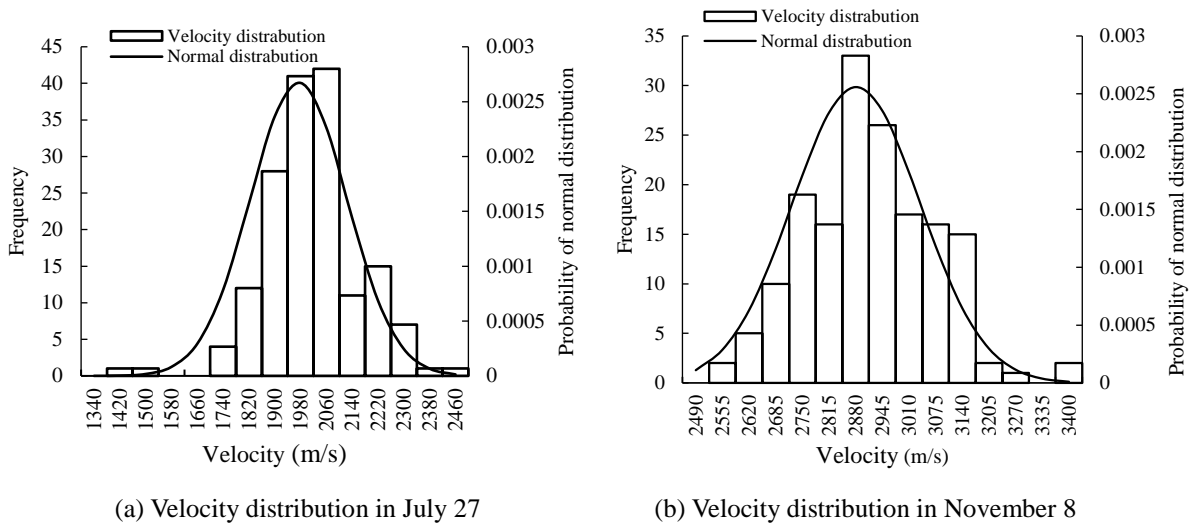


Figure 4—Distribution of ultrasonic velocities

Relationship between the velocity and growth days

Table 2 shows average velocity, standard deviation, upper bound velocity and lower bound velocity calculated by normal distribution formula for the 4 time measurements.

Table 2—Statistic results of the 4 time ultrasonic velocities measured

Date	Average velocity		Upper bound velocity	Lower bound velocity
	(m/s)	standard deviation	(m/s)	(m/s)
July 27	1974	149	2420	1527
Sept. 5	2395	177	2926	1863
Sept. 23	2544	182	3090	1998
Nov. 8	2881	155	3348	2415

Growth days, from cottage planting to 4 times measuring, were 105 days, 145 days, 165 days and 209 days respectively. The relationships between the ultrasonic velocities and seedling growth days were shown in Figure 5. It can be seen that there are good correlations between the three kinds of velocities (average velocity, upper bound velocity and lower bound velocity) and the growth days. The coefficient of determination between the average velocity and growth days is 0.991. The average velocity increases gradually, reflecting a batch of seedlings, with same planting day and same growth days, their mechanical properties and densities become better with their growth.

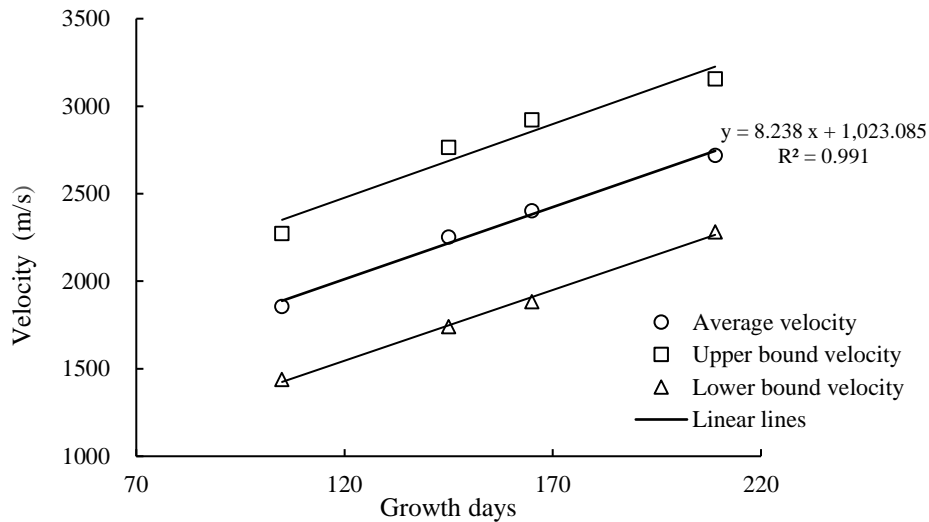


Figure 5—Relationship between ultrasonic velocity and seedling growth days

Relationship between the velocity and root-collar diameter

As shown in Figure 6, diameters of the 200 seedlings have a certain range of distribution, and with the increase of the root-collar diameter, the velocity changes very little, i.e. there is almost no correlation between the velocity and the root-collar diameter. With increase of seedling age, the root-collar diameter and velocity all increase, and because there is no obvious correlation between velocity and diameter, so it can be concluded that a batch of seedlings, with same planting day and same growth days, has no obvious relationship between their wood properties and their root-collar diameters.

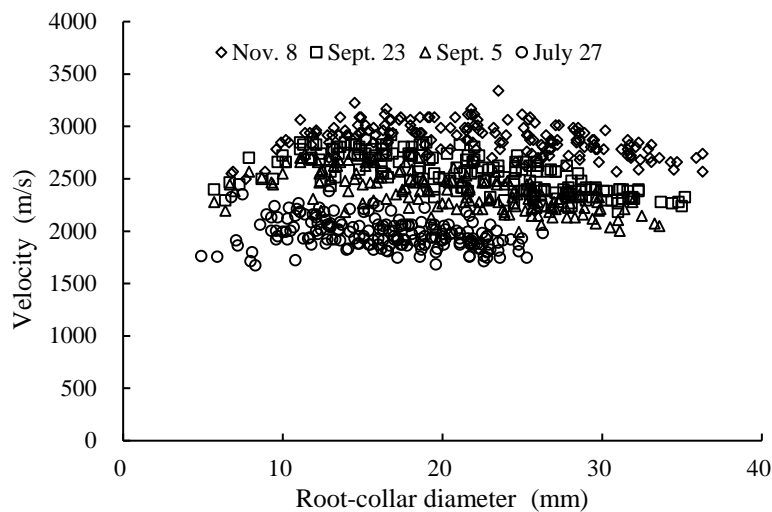


Figure 6—Relationship between the velocity and root-collar diameter of seedlings

Although there is no obvious correlation between the ultrasonic velocity and root-collar diameter of the seedlings, for seedlings with similar size of root-collar diameter, their velocities are quite different. Figure 7 shows the velocity distribution of seedlings that their root-collar diameters in 15~20 mm measured in July 27th. As you can see, this batch of seedlings velocity distribution is in range of

1600~2432 m/s, i.e. a batch of seedlings with same age and similar physical index such as root-collar diameter and seedling height, their wood properties are quite different, furthermore ultrasonic velocity can detect differences between emergence of the seedling wood properties.

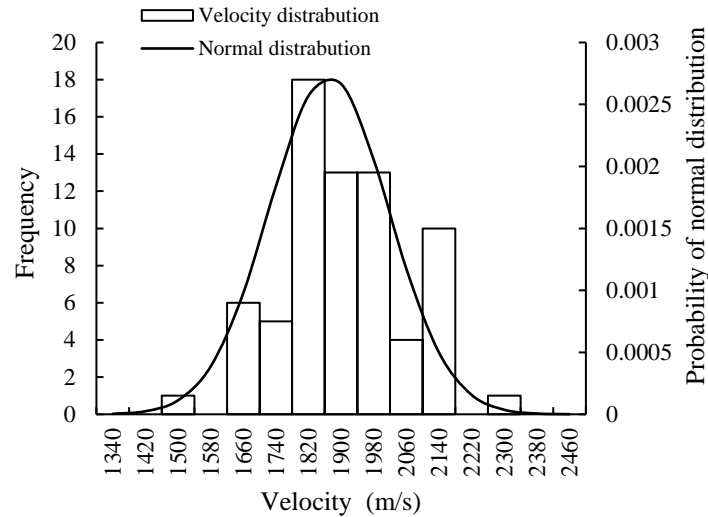


Figure 7—Distribution of ultrasonic velocity (July 27th, root-collar diameter 15~20 mm)

Relationship between ultrasonic velocity and resonance acoustic velocity

Figure 8 shows experimental results of relationship between ultrasonic velocity and acoustic velocity measured by the resonance method. It can be seen although ultrasonic velocity of a seedling is smaller than its resonance acoustic velocity, correlation between these two velocities is significant, and the coefficient of determination is 0.805. As the resonance method is generally accepted as an accurate method for measuring acoustic velocity of wood, it indicates that ultrasonic measurement can be used to assess quality traits of young seedlings in future genetic programs.

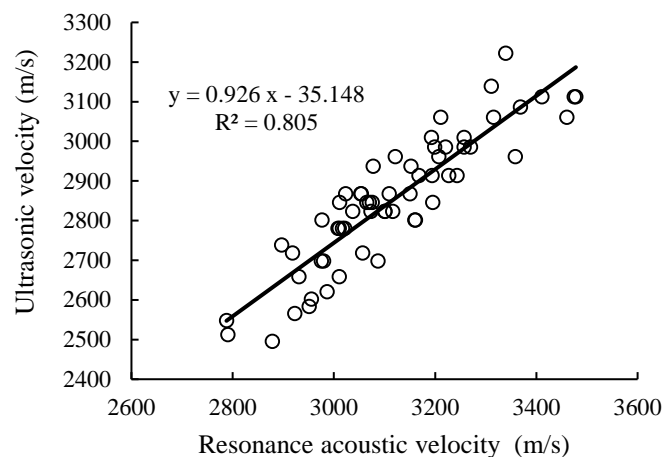


Figure 8—Relationship between the ultrasonic velocity and resonance acoustic velocity

Conclusions

When distance of the two sensors was from 300mm to 800mm, the ultrasonic velocity basically kept stable. Considering the convenience of measuring operation, the proper distance between two sensors in this study was finally set to 400 mm.

The 200 seedlings were measured 4 times after they were cottage planted 105 days, 145 days, 165 days and 209 days respectively. The ultrasonic velocities of every time measuring result appear an approximately normal distribution. i.e. although a batch of seedlings are cottage planted on the same day, the growth time is the same, they have the difference of mechanical properties, density and other material indexes among the individual seedlings.

There are good correlations between the three kinds of velocities (average velocity, upper bound velocity and lower bound velocity) and the growth days. The coefficient of determination between the average velocity and the growth days is 0.991. It means the mechanical properties and densities of the seedlings become better with their growth.

There is almost no correlation between the ultrasonic velocities and the root-collar diameters for a batch of seedlings with same planting day and growth days.

Ultrasonic velocity of seedlings has a very good linear correlation relationship with resonance acoustic velocity, and the coefficient of determination is 0.805. As the resonance method is generally accepted as an accurate method for measuring the wave velocity of wood, it indicates that ultrasonic measurement can be used to assess quality traits of young seedlings in future genetic programs.

References

Divos F. 2010. Acoustic tools for seedling, tree and log selection. ‘The Future of Quality Control for Wood & Wood Products’, 4-7th May, Edinburgh, The Final Conference of COST Action E53.

Emms Grant, Nanayakkara B., Harrington, J. 2012. A novel technique for non-damaging measurement of sound speed in seedlings. *Eur. J. For. Res.* 131(5): 1449-1459

Emms Grant W., Nanayakkara Bernadette, Harrington Jonathan J. 2013. Application of longitudinal-wave time-of-flight sound speed measurement to *Pinus radiata* seedlings. *Canadian Journal of Forest Research.* 43(8): 750-756

GB 6000-1999. 1999. Tree seedling quality grading of major species for afforestation. Standardization Administration of the People’s Republic of China, Beijing, China.

Guan Xun, Zhao Maocheng. 2013. Advances in the researched of wood quality testing and stress grading based on the acoustic technology in north America. *Journal of Northwest Forestry University*. 28(2): 178-181.

Liang Shanqing, Cai Zhiyong, Wang Xiping, Robert J. Ross, Fu Feng. 2008. Developments and applications of nondestructive tests for wood in North America. *China Wood Industry*. 22(3): 5-8

Liu Fenglu, Jiang Fang, Wang Xiping, Zhang Houjiang, Yang Zhihui. 2016. Stress wave propagation in larch plantation tress: numerical simulation. *Journal of Northwest Forestry University*. 31(4): 201-205.

Sheng Liying. 2014. *Ultrasonic detection technology*. Chemical Industry Press, Beijing, China.

Wang Xiping, Ross Robert J., Carter Peter. 2007. Acoustic evaluation of wood quality in standing trees. Part I. Acoustic wave behavior. *Wood and Fibre Science*. 39(1): 28-38.

Xu Youming. 2011. *Wood science*. China Forestry Publishing House, Beijing, China.

Evolution of Eucalyptus Clone's Parameters Obtained Nondestructively in Nursery Seedlings up to Cutting Age

Rafael Gustavo Mansini Lorensani

Laboratory of Nondestructive Testing – LabEND, College of Agricultural Engineering – FEAGRI – UNICAMP, Campinas, São Paulo, Brazil, rafaelmansini@hotmail.com

Raquel Gonçalves

Laboratory of Nondestructive Testing – LabEND, College of Agricultural Engineering – FEAGRI – UNICAMP, Campinas, São Paulo, Brazil, raquel@feagri.unicamp.br

Gabriela Müller

Laboratory of Nondestructive Testing – LabEND, College of Agricultural Engineering – FEAGRI – UNICAMP, Campinas, São Paulo, Brazil, gabicesar_3@hotmail.com

Cilene da Silva Alves

Laboratory of Nondestructive Testing – LabEND, College of Agricultural Engineering – FEAGRI – UNICAMP, Campinas, São Paulo, Brazil, cilenealves7@gmail.com

Guilherme Alonso Martins

Laboratory of Nondestructive Testing – LabEND, College of Agricultural Engineering – FEAGRI – UNICAMP, Campinas, São Paulo, Brazil, guimartins93@gmail.com

Mônica Ruy

Laboratory of Nondestructive Testing – LabEND, College of Agricultural Engineering – FEAGRI – UNICAMP, Campinas, São Paulo, Brazil, monica.ruy@hotmail.com

Nádia Schiavon da Veiga

Laboratory of Nondestructive Testing – LabEND, College of Agricultural Engineering – FEAGRI – UNICAMP, Campinas, São Paulo, Brazil, nadiasveiga@gmail.com

ABSTRACT

The anticipation of knowledge of properties for the wood processing industries is important in management of the wood production chain. So, it is important to know how some characteristics propagate over time. The objective of this research was to analyze the evolution of velocity of ultrasonic wave propagation, diameter, height and basic density, from 3- months-old nursery seedlings to 6-years-old trees, cutting age used in pulp and paper companies in Brazil. The tests were conducted in 121 seedlings and 270 trees of three *Eucalyptus* clones. The velocity of ultrasonic wave propagation was the only property that maintained, at the cutting age (6-years-old), the coherence of the differentiation between clones obtained on seedlings. The diameter and height maintained coherence from 12-months-old up to the cutting age, while the basic density since 24-months-old.

Key words: velocity of ultrasonic wave propagation; basic density; height and diameter of the stem

Introduction

In the advanced programs of genetic improvement, the velocity of wave propagation, obtained by indirect measurement in standing trees, has been considered efficient to select the trees by stiffness

(Lindström et al. 2002, Gapare et al. 2009, Gonçalves et al. 2013, Sharma et al. 2016) as for the juvenile wood quality (Wielinga et al. 2009). However, any parameter that is included in this type of analysis, especially in young trees, requires the knowledge of its behavior during the tree growth, or its ability to propagate with age. In this sense, there is in the literature, indicative results that the acoustic waves propagation velocity increases with age, especially until the transition period from juvenile to adult wood (Bucur 2006, Nogueira & Ballarin 2006, Oliveira et al. 2006, Innes 2007, Gonçalves et al. 2013). The basic density was the first variable used as a parameter to select wood quality in the genetic improvement programs, almost 30 years ago (Merlo et al. 2008 and Santaclara et al. 2011). The causes for this variable has been selected as a property par excellence is its high correlation with other properties of interest, and its high degree of genetic propagation (Merlo et al. 2008 and Santaclara et al. 2011). Inheritance and density correlation with several properties are also reported by Padua 2009 in mentioning parameters of quality selection. Apiolaza 2009 adds that the correlation between the basic density of juvenile and adult wood makes it an important parameter for the early selection in the main programs of genetic improvement. The basic density usually increases abruptly in the juvenile period, more slowly during the transition period, remaining more or less constant at maturity. However, researchers have obtained another pattern, with uniform variation, increase or decrease during life, or decrease during the juvenile period and increase from maturity (Haygreen and Bowyer 1982, Phashin et al. Zeeuw 1982 apud Padua 2009 and Lorensani et al. 2015). These discrepant results show that there is no definite or consolidated pattern for the density variation along the tree growth. The height of the trees and their diameter at the breast height (DBH), present a gradual increase with age, being influenced by several factors, such as spacing between individuals (Simões et al. 1980 and Alves Ferreira et al. 2014), geographic localization (Bhat et al. 1987) and clonal differences (Neves et al. 2013), demonstrating the high sensitivity of this trait to changes from the environment. Considering the mentioned aspects and aiming the anticipation of wood selection, the objective of this research was to verify if the seedlings grading based on diameter, height, basic density and velocity of ultrasonic wave propagation would remain consistent throughout the trees growth until 6 years old (cutting age used in pulp and paper companies in Brazil).

Material and Methods

The sample was composed by 3 clones named in this study as clones A, B and C (Table 1). The number of nursery seedlings and trees at each age was determined according to the availability and logistics of the company that was the partnership in this research (*International Paper*). For all clones, it was possible to obtain nursery seedlings with 3-months-old, whereas for the trees the available ages were 12, 24, 48 and 72-months-old. As clone C was adopted, from the beginning of the research, as validation material, its tests were only planned in the nursery seedling (3-months-old) and in trees at the cutting age (72-months-old). From each site, 30 trees were chosen randomly, avoiding the ones of edge because they are more likely to have reaction wood. All seedlings and trees (Table 1) were submitted to ultrasonic tests as well as basic density calculation and diameter and height measurements.

Table 1. Sampling of seedlings and trees used for ultrasound tests and basic density calculations

Clone/age	3	12	24	48	72	Total
A	51	30	30	30	30	171
B	20	30	30	30	30	140
C	50	-	-	-	30	80
Total	121	60	60	60	90	391

To measure the height of the nursery seedlings, the stem was considered from ground line to its extremity, region where a budding area was located, disregarding extreme leaves. For the trees (from 12 months onwards) the height was measured with a hypsometer (Vertex IV, Haglölf, Switzerland). The diameter of the nursery seedlings was measured at the ground line while in the trees at the breast height (DBH), considered 1.30 m from the ground, using caliper.

Ultrasound equipment (USLab, Agricef, Brazil) with 45-kHz-frequency exponential tips transducers were used in the tests. The transducers tips are interchangeable, allowing the seedlings tests were made with needle tips and the tree tests with 3-mm rounded tips. The needle tips were made by the research group itself. For the test in the nursery seedlings a wooden support was constructed to positioned the probes with 150-mm distance in all measurements. The distance between the probes (wave propagation length) was previously established to contain at least 3 wavelengths (λ) avoiding wave disturbance. The seedlings were tested indirectly by ultrasound, with the transducers positioned at 45° with the stem axis. The indirect test allows the nursery seedling be tested alive and is the same methodology applied on trees. As in the case of nursery seedlings, the ultrasound test on trees was performed indirectly, with the transducers positioned at 45° with the trunk axis. In trees the distance between the transducers was 0.7 m, always adopting 0.35 m above and below the breast height (1.3 m from the ground line). The ultrasound test on each tree was repeated in two diametrically opposite positions of the trunk. With the times of waves propagation and the distances between the transducers, velocities were calculated for both nursery seedlings and trees.

From the seedlings stem, which were approximately 150-mm long, samples from 30 to 50-mm long were used for basic density determination. In the case of the trees, increment borer was used to get cylindrical samples, 6-mm diameter, at breast height. Each sample was packed in a plastic bag and refrigerated for maintenance of moisture to subsequent laboratory measurements. The volume of the specimens was obtained in saturated condition, and then the specimens were taken to an oven at $103 \pm 2^\circ\text{C}$ until reaching to constant mass (oven dry condition), in which the weights were obtained.

The parameters (diameter, height, velocity and basic density) were analyzed to verify if there are statistical differences among ages and among clones. Using actual average values and regression models (parameters x age) we also analyze if the differences among clones observed in nursery seedlings are maintained until the cutting age.

RESULTS AND DISCUSSIONS

Ultrasound

For clones A and B, for which are obtaining velocities at different ages, it was possible evaluate that the average velocity (obtained at each age) increased linearly with age and that the order of velocities magnitude obtained on seedlings (velocities in clones B < A) remained at the cutting age. The slope of the linear regression model shows that the velocity-age variation in Clone A is about 6% higher than that of Clone B. Ikeda et al. (2015) obtained, in Japanese cedar trees tests performed in trees growth in different sites, 25% increase in stress wave velocity propagation measured from 2 and 6-years-old and 14% in trees from 4 to 7-years-old. Statistical analysis using all the data obtained at each age (Table 1), and not with the average values, shows that, in addition to increasing, velocities were statistically different at different ages (Table 2). It was also statistically shown that, for clones A and B, the velocities obtained at the same age differ from each other in all age range (Table 2), indicating potential of the tool to differentiate properties among clones. Nursery seedlings of Clones B and C presented velocities statistically equal each other and both inferior (on average 9%) to that of Clone A (Table 2). This same behavior was repeated at the cutting age (Table 2), but at this age the difference increase to about 20%, showing that the grading of nursery seedling clones by velocities remained until cutting age. This same result is obtained by analyzing the velocities in Clones A and B at 12, 24 and 48 months, showing that at these ages it would also be possible to grading clones by velocity.

Density

Basic density is expected to increase with age, but this parameter is very variable within and between trees up to 3-years-old (Raymond 2002 cited by Padua 2009). The multiple comparison test indicated that basic density of Clone A at 3 and 12-months-old were statistically different from each other and different from the densities in other ages (Table 3), while the density of Clone B was different from other ages only at 3-months-old (Table 3). Numerically, the selection at 3-months (seedling) or 12-months (tree) were not consistent with the density at the cutting age. From 24-months on, Clone A presented higher density than Clone B until the cutting age.

Table 2. Average values of velocity of ultrasound wave propagation (in m.s^{-1}) and coefficient of variation (CV in %) and analysis of statistical differences between ages (letters in lines) and between clones (numbers in the columns)

Clone	Parameter	Age (months)				
		3	12	24	48	72
A	Average	2249 (10.1)	2697 (7.7)	3130 (16.7)	3811 (9.2)	4654 (8.1)
	Statistical	(a) (1)	(b) (1)	(c) (1)	(d) (1)	(e) (1)
B	Average	2048 (4.7)	2475 (5.6)	2835(10.5)	3133(12.3)	3852(9.6)
	Statistical	(a) (2)	(b) (2)	(c) (2)	(d) (2)	(e) (2)
C	Average	2095 (7.7)			3954 (5.9)	
	Statistical	(a) (2)			(b) (2)	

Different letters/numbers indicate statistically different values

Table 3. Average values of basic density (in kg.m^{-3}) and coefficient of variation (%) for clones A, B and C at different ages (in months) and statistical analysis differences between ages (letters in lines) and between clones (numbers in columns).

Clone	Parameters	Ages (months)				
		3	12	24	48	72
A	Average	350 (17.8)	430 (5.2)	480 (6.8)	470 (3.8)	480 (4.6)
	Statistical	(a) (1)	(b) (1)	(c) (1)	(c) (1)	(c) (1)
B	Average	360 (15.7)	460 (4.1)	470 (10.0)	460 (5.8)	460 (5.0)
	Statistical	(a) (1)	(b) (2)	(b) (1)	(b) (1)	(b) (2)
C	Average	270 (17.0)			470 (4.8)	
	Statistical	(a) (2)			(b) (2)	

Different letters/numbers indicate statistically different values

Diameter and height

It is expected that the diameter and height of the trees increase over the years, however, the rate of this growth is dependent from site and species. Downes et al. (1993) found 1.24 m to average height increment for fast growing *Pinus radiata* from 13 to 24 months-old. Even for clones, the coefficient of variation of the diameter (from 7.2% to 16.1%) and of the height (from 2.6% to 14.9%) were high (Tables 4 and 5). The diameter presented statistical differences for all ages in both clones (Table 4). There was also a statistical difference between clones at different ages (Table 4). Clone B was statistically different from Clones A and C having larger average diameter. At the cutting age the three clones differed statistically, however there was an inversion and Clone A presented the largest average diameter (Table 4). The height also differed statistically for all ages and clones, but among the clones, differentiation did not occur for all ages (Table 5). In addition, the nursery seedlings did not differ statistically and, during growth, the position of differences were not maintained, with inversion at 72 months (Table 5). As previously discussed, it is important to point out that the values are not obtained in same trees at different ages, but are averages among tree, that can help to explain some unexpected behavior.

Table 4. Average values of diameter * (in mm) and coefficient of variation (%) of clones A, B and C at different ages (in months) and analysis of statistical differences between ages (letters in the lines) and between clones (numbers in the columns).

Clone	Parameters	Ages (months)				
		3	12	24	48	72
A	Average	2.5 (7.2)	64.7 (7.6)	110.6 (14.3)	124.5 (9.2)	190.1 (8.9)
	Statistical	(a) (1)	(b) (1)	(c) (1)	(d) (1)	(e) (3)
B	Average	2.8 (12.5)	81.2 (16.1)	119.9 (12.2)	143.0 (9.1)	168.7 (6.4)
	Statistical	(a) (2)	(b) (2)	(c) (2)	(d) (2)	(e) (2)
C	Average	2.5 (10.1)			139.5 (12.4)	
	Statistical	(a) (1)			(b) (1)	

Different letters/numbers indicate statistically different values. *In the case of trees corresponds to the diameter at breast height (DBH)

Table 5. Average values of height (in m) and coefficient of variation (%) of clones A, B and C at different ages (in months) and analysis of statistical differences between ages (letters in Lines) and between clones (numbers in the columns).

Clone	Parameters	Ages (months)				
		3	12	24	48	72
A	Average	0.31 (9.3)	7.78 (13.7)	16.12 (2.8)	17.52 (2.6)	28.72 (3.6)
	Statistical	(a) (1-2)	(b) (1)	(c) (1)	(d) (1)	(e) (3)
B	Average	0.28 (4.5)	10.66 (5.8)	16.47 (14.9)	20.87 (3.0)	26.75 (2.6)
	Statistical	(a) (1)	(b) (2)	(c) (1)	(d) (2)	(e) (2)
C	Average	0.31 (10.1)			20.45 (5.7)	
	Statistical	(a) (2)			(b) (1)	

Different letters/numbers indicate statistically different values

Conclusions

The velocity of ultrasound waves propagation allows to differentiate clones from the nursery seedling, and the differentiation order is maintained, in a coherent way, up to the cutting age. The velocity of ultrasound waves used as tool to grading clones at 12 or 24-months-old present the same behavior, showing that these ages could also be used to differentiate clones by acoustic methods. The density age-related followed the same statistical regression model of mechanical properties age-related, but only after 24-months-old, maintaining from this age the differentiation among the clones up to cutting age. The height and diameter age-related was represented by the same statistical regression model and the differentiation of the clones could be made from 12-months-old. In general, the results allows to conclude that all parameters have the potential to be used in a predictive model to anticipate grading clones, but the degree of this anticipation would not be the same.

Acknowledgements

The authors would like to thank Sao Paulo Research Foundation (FAPESP) - Proc. 2013/03449-9 and 2015/05692-3 for research funding and scholarship. They also thank the *International Paper* from Brazil for the nursery seedlings and trees donation and for the logistic support for forest trials.

References

- Alves Ferreira, D. H. A., Feles, P. S. S., Machado, E. C., Abreu, A. H. M. and Abílio, F. M. Growth of clone of *Eucalyptus urophylla* x *E. Grandis* in different spacings. *Floresta*, [s.l.], v. 44, n. 3, p. 431-440, mar. 2014. Issn 1982-4688.
- Apiolaza, L. A. (2009). Very early selection for solid wood quality: screening for early winners. *Ann For Sci* 66:601.
- Bhat, K. M., Bhat, K. V. and Dhamodaran, T. K. Effect of age and location on pulpwood quality of *Eucalyptus Grandis*. Kerala Forest Research Institute. V. 49, 19p. Division of Wood Science, Kerala Forest Research Institute, 1987.
- Bucur, V. 2006. ACOUSTICS OF WOOD. Springer, Berlin, pp 223–225.
- Downes G. M., Beckers E. P. J, Turvey N. D. and Porada H. Strength and structure of stems from fast grown *Pinus radiata*. *Trees* 1993,7: 131 – 6
- Gapare, W. J., Baltunis, B. S., Ivkovi´C, M. and Wu, H. X. 2009. Genetic correlations among juvenile wood quality and growth traits and implications for selection strategy in *Pinus radiata* D. Don. *Ann. For. Sci.* 66 (6) 606.
- Gonçalves, R., Batista, F. and Lorensani, R. G. M. 2013, Selecting Eucalyptus Clones Using Ultrasound Test on Standing Trees. *Forest Products Journal*, Vol. 63, pp.112-118.
- Haygreen, J. G. and Bowyer, J. L. *Forest products and wood science: an introduction*. Ames: Iowa State University, 1982. 495 p.
- Innes, T. C. 2007. Processing and wood properties of four ages of *Eucalyptus obliqua*. *Holz Roh Werkst.* 65:197–200
- Ikeda, K., Yamamoto, S., Hakamata, T., Yamada, S. and Kondo, A. Early age evaluation by the stress wave speed for the breeding of high Young's modulus Japanese cedar. In: 19th International Nondestructive Testing and Evaluation of Wood Symposium. Rio de Janeiro, Brasil, Setembro de 2015.
- Lindström, H., Harris, P., and Nakada, R., 2002. Methods for measuring stiffness of young trees. *Holz Roh. Werkst.* 60: 165–174.
- Lorensani, R. G. M., Alves, C. S. and Gonçalves, R. Prediction of basic density using parameters measured on trees. In: 19th International Nondestructive Testing and Evaluation of Wood Symposium. Rio de Janeiro, Brasil, September 2015.
- Merlo, E., Zas, R., Piñeiro, G. and Pedras, F. 2008. Variability of wood quality parameters between and within provenances of *Pseudo Tsugamenziesii*. *Cuadernos de la Sociedad Española de Ciencias Forestales*, 24 262 - 266.
- Neves, T. A., Protásio, T. P., Trugilho, P.F., Valle, M. L. A., Sousa, L. C. and Vieira, C. M. Wood quality of Eucalyptus clones at different ages for the production of bioenergy. *Revista de Ciências Agrárias* 2013, 56(2):139-148. doi:10.4322/rca.2013.022
- Nogueira, M. and Ballarin A. W. 2006. Ultrasound as a tool in the classification of parts of *Pinus taeda*. In: Seminário END Madeira, Itatiba, SP, CD-ROM 2006.

Oliveira, F. L., Lima, I. L., Garcia, J. N. and Florsheim, S. M. B. 2006. Wood properties of *Pinus taeda* depending on the age and the radial position in the log. *Revista Instituto Florestal* 18:59–70.

Santaclara, O., Álvarez, J. G. and Merlo, E. 2011. Modeling structural lumber quality for *Pinus pinaster* Ait. in northwestern Spain using standing tree acoustic assesment, tree characteristics and stand variables. *Proceedings of the 17th International Non destructive Testing and Evaluation of Wood Symposium*. University of West Hungary, Sopron, Hungary.

Sharma, M., Apiolaza, L.A., Chauhan, S., Mclean, J. P. and Wikaira, J. Ranking very young *Pinus radiata* families for acoustic stiffness and validation by microfibril angle. *Annals of Forest Science*. 2016. 73: 393. doi:10.1007/s13595-015-0529-y

Simões, J. W., Coelho, A. S. R., Mello, H. A. and Couto, H. T. Z. Growth and production of eucalyptus wood. Piracicaba: IPEF. N.20, p.77-97, 1980

Wielinga, B., Raymond, C. A., James, R., and Matheson, A. C. 2009. Genetic parameters and genotype by environment interactions for green and basic density and stiffness of *Pinus radiata* d. don estimated using acoustics. *Silvae Genet* 58:112–122

Prediction of Wood Properties in Trees from Parameters Obtained Nondestructively in Nursery Seedlings

Rafael Gustavo Mansini Lorensani

Laboratory of Nondestructive Testing – LabEND, College of Agricultural Engineering – FEAGRI – UNICAMP, Campinas, São Paulo, Brazil, rafaelmansini@hotmail.com

Raquel Gonçalves

Laboratory of Nondestructive Testing – LabEND, College of Agricultural Engineering – FEAGRI – UNICAMP, Campinas, São Paulo, Brazil, raquel@feagri.unicamp.br

Esther Merlo

MADERAPlus, Ourense, Spain, maderaplus@maderaplus.es

Oscar Santaclara

MADERAPlus, Ourense, Spain, maderaplus@maderaplus.es

Manuel Touza

CIS-MADERA, Ourense, Spain, manuel.cesareo.touza.vazquez@xunta.gal

Manuel Guaita

Department of Agroforestry Engineering, University of Santiago de Compostela, Lugo, Spain, m.guaita@usc.es

Francisco José Lario

Tragsa, Ourense, Spain, flario@tragsa.es

Abstract

The early selection of trees allows accelerating the processes of genetic improvement, as well as those related to the forest management aiming improving the quality of the wood produced. The goal of this research was to study parameters, measurable nondestructively in seedlings, that could be used in models to predict stiffness (E_{ts}), strength (f_{ts}) and basic density (BD_t) of wood from trees. The trials were performed in 240 nursery seedlings and in 52 72-months-old trees. In the nursery seedlings, the longitudinal velocity of ultrasonic wave propagation (V_{Ls}), the height (H_s) and the diameter (D_s) were measured, while in the trees BD_t , the f_{ts} and the E_{ts} . The multiple regression model involving H_s and V_{Ls} in the nursery seedlings was the most adequate for the prediction of E_{ts} from the wood from trees. For f_{ts} and BD_t it was not possible to obtain statistical significant models using only parameters obtained nondestructively in nursery seedlings.

Key words: velocity of ultrasound waves propagation, basic density, wood stiffness, wood strength, stem diameter, stem height

Introduction

The early selection of wood from young trees is very important for forest-based companies. In companies that aim to use wood as a material, prior grading allows material selection and its destination to application in function of its properties, avoiding unnecessary spending to process or benefit ones that wouldn't have the minimum properties for which processing would be required. For paper and pulp companies and producers of forest plants, prior selection allows anticipating the

knowledge of genotypes that do not have the necessary properties to be commercially viable, avoiding unnecessary investments (Apiolaza et al. 2013, Gonçalves et al. 2013, Sharma et al. 2016).

In order for this early selection to be made, it is necessary to use prediction models that involve properties that have the characteristic of propagation with age and that have a correlation with the future property that one wants to infer. Among the properties of interest of the forest-based companies are the stiffness, strength and density of the wood. On the other hand, among measurable properties in seedlings or in young trees, with characteristics of propagation with age and correlation with the properties of interest, are the acoustic properties (Lindström et al. 2002, Bucur 2006, Wang et al. 2007, Gapare et al. 2009, Gonçalves et al. 2012, Chauhan et al. 2013, Gonçalves et al. 2013); the density (Wielinga et al. 2009, Lorensani et al. 2015) and the diameter and height (Simões et al. 1980, Neves et al. 2013).

The development of nondestructive methods for evaluating young trees in order to select for adult wood quality is becoming increasingly important. For this reason, researchers have recently sought to propose protocols for this anticipation (Merlo & Santaclara 2012, Apiolaza et al. 2013, Chauhan et al. 2013, Lorensani et al. 2015). Models of prediction of wood properties in trees have been developed (Santaclara et al. 2011, Merlo et al. 2014) but, in general, not comparing properties with those of trees of the same genotypes in other trials, nor proposing the use of models using properties obtained in nursery seedlings.

The objective of this research was to study parameters, measurable in nursery seedlings, that could be used in models of prediction of stiffness, strength and density in trees.

Materials and methods

Sampling

Sampling for the analysis of the prediction models consisted of nursery seedlings and trees of 7 genotypes of two distinct species: 3 *Eucalyptus* clones and 4 *Pinus pinaster* progenies (Table 1).

Table 1. Seedlings and Trees sampling

Species	Seedlings*	Trees†
Clone 1	50	6
Clone 2	20	6
Clone 3	50	6
Progeny 15	30	8
Progeny 18	30	9
Progeny 19	30	8
Progeny 23	30	9
Total	240	52

*Seedling 1, 2 and 3 were 3 months old, and seedling 15, 18, 19 and 23 were 6 months old. †All the trees were 72 months old

Methodology

Nursery Seedling trials

The height measurement of the seedlings (H_s) considered the entire stem, disregarding the leaves at the extremities (Figure 1). The diameter (D_s) was measured at the interface with the soil, or region of the collar.



Figure 1. Scheme for measuring the height of the seedlings

To determine the longitudinal velocity of ultrasonic waves in stem of the nursery seedlings (Figure 2), a minimum distance (L) of 150 mm between the transducers was delimited from the root collar in order to maintain a ratio of path length (L) and wave length (λ) around 3.

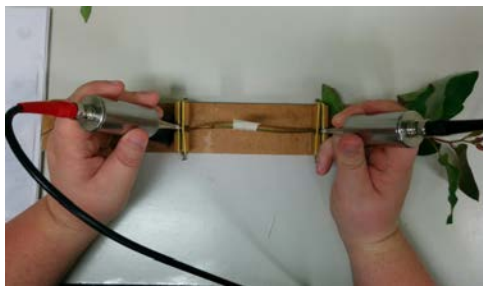


Figure 2. Ultrasound test in *Eucalyptus* (a) and *Pinus pinaster* (b) seedlings

The tests were performed with ultrasound equipment (USLAB, Agricef, Brazil) and 45 kHz transducers, with tapered and pointed tips designed and produced by the research group. For the tests, the transducers were positioned at 45° (indirect test), allowing the nursery seedling to be analyzed without destroying it and constituting a methodology compatible with that applied to trees. With the ultrasonic wave propagation time, the velocity of the ultrasonic pulse that travels through the stem of the seedlings (V_{Ls}) was calculated.

From the stem of the seedlings samples of lengths ranging from 30 to 50 mm were taken for the determination of the basic density. The volume of the samples was obtained in the saturated condition, and then the samples were taken to an oven with a temperature of $103 \pm 2^\circ\text{C}$ until reaching the anhydrous condition, in which the weights were obtained. The dry mass and the saturated volume values were used to determine the basic density of the seedlings (BDs).

With the velocity (V_L s) and the basic density (DBs) in the seedling, the stiffness coefficient (CLLs - Equation 1) was obtained.

$$CLL_s = DB_s VL_s^2 \quad \text{Equation 1}$$

The stiffness coefficient is determined using the apparent density. However, the use of the apparent density of saturated wood (in the case of seedling) is not adequate, since it induces results contrary to those expected physically for stiffness (Sobue 1993, Mishiro 1996, Bucur 2006, Gonçalves & Leme da Costa 2008). Thus, we choose to calculate the stiffness coefficient using the basic density. Wielinga et al. (2009) obtained good correlations ($R = 0.9$) between the stiffness coefficient (called “dynamic modulus of elasticity” by the authors) calculated using the density in the green condition (as in this research) and calculating using the basic density.

Trials on trees

From each cut tree, a log for the static bending test and one disk for determining the basic density (BD_t) were removed from the base. Static bending tests were conducted according to EN 408 (2010),

with the piece on two supports and the application of two-point loading on the thirds of the length (Figure 3). The distance between supports was at least 18 times the diameter in the central section of the log. During the test, the load (P) and the vertical displacement (f) were measured simultaneously. The modulus of rupture (f_{mt}) (Equation 2) and the modulus of elasticity (E_M) (Equation 3) of the logs were calculated according to EN 408 (2010) adapted for the round wood.

$$f_m = \frac{3F_{max}a}{bh^2} = \frac{3F_{max}a}{AD} \quad \text{Equation 2}$$

$$E_M = \frac{3aL^2 - 4a^3}{2bh^3 \left(2 \frac{f_{40\%} - f_{10\%}}{P_{40\%} - P_{10\%}} - \frac{6a}{5Gbhh} \right)} = \frac{3aL^2 - 4a^3}{48 I \left(\frac{f_{40\%} - f_{10\%}}{P_{40\%} - P_{10\%}} \right)} \quad \text{Equation 3}$$

Where: F_{max} is the maximum load (N); $a = L/3$; $L = \text{span}$; $A = \text{transversal section area of the round timber} = \frac{\pi D^2}{4}$; $D = \text{diameter of the cross - section of the log at the centre point under bark}$; $P_{40\%}$ and $P_{10\%}$ are 40% and 10%, respectively, of the maximum load applied to the log during the bending tests; $f_{40\%}$ and $f_{10\%}$ are the vertical displacements corresponding to the loads $P_{40\%}$ and $P_{10\%}$, respectively; $I = \text{Inertia of round timber} = \frac{\pi D^4}{64}$



Figure 3. Static bending test in logs

Data analysis

In order to obtain predictive models of tree properties (dependent variables) from properties obtained in nursery seedlings (independent variables), the simple correlations between these variables (dependent and independent) were initially evaluated. From this analysis, the linear correlation models were evaluated, as well as the statistic provided from the software, which evaluates several alternatives of simple regression models, indicating the one with the best coefficient of correlation (R) and determination (R^2). The number of independent variables (k) to be used in multiple regression models should be adopted as a function of the number of observations of the sample (n), so that at least 2 degrees of freedom (GL) are obtained for residues ($GL = n - k - 1$) (Volpato and Barreto 2011). Thus, in this research, although there were 4 variables obtained in the seedlings (independent), multiple regressions should contain only 2 of them, since the sampling was composed of 7 species (Table 1). In order to increase the possibility of using all the parameters measured in the seedlings, the analysis of the models also counted on the use of the stiffness coefficient (CLLs - Equation 1) and the relationship between height and diameter (Hs/Ds). These three parameters were also evaluated in an isolated way in the simple regression models. Before the multiple correlation analysis, we verified the existence of correlations between the independent variables that would be tested in the multiple regression models. Independent variables are considered to be self-correlated when the correlation coefficient (R) between them is greater than 0.5. In this case ($R > 0.5$) there will be multi-collinearity, undesirable in multiple correlation models. The parameters considered not auto correlated were used in the software to select the independent variables that allow better adjustment of the multiple regression model. This selection is made by the software based on the highest coefficient of determination (R^2) and the lowest value of the Mallows C_p statistic, which is a measure of the deviation of the model, based on the comparison of the average total square error with the variance of the true error.

Results and discussion

The normality, tested by the parameters: asymmetry, kurtosis and normal probability graph was statistically verified for all parameters listed in Table 2.

Table 2. Average values (first row) and coefficient of variation (second row) of the parameters measured in the seedling: longitudinal velocity ($V_{L,s}$), diameter (D_s) and height of the seedling (H_s) and the wood properties obtained in the trees: Basic density (DB_t), modulus of elasticity ($E_{M,t}$) and modulus of rupture ($f_{m,t}$).

Species	Seedlings (3* e 6 months)			Trees (72 months)			
	V_{L_s} $m.s^{-1}$	D_s mm	H_s m	DB_s $kg.m^{-3}$	DB_t $kg.m^{-3}$	$f_{m,t}$ MPa	$E_{M,t}$ MPa
Clone 1	2249	2.48	0.31	350	480	46	8257
	10.1	7.2	9.3	17.8	4.6	12.0	18.3
Clone 2	2048	2.83	0.29	360	460	44	7346
	4.7	12.5	7.5	15.7	5.0	16.0	8.6
Clone 3	2095	2.51	0.31	270	470	48	7295
	7.7	10.1	9.2	17.0	4.80	5.7	30.6
Progenie 15	1816	3.30	0.33	430	440	50	2797
	9.9	11.0	7.4	11.7	7.7	16.1	25.2
Progenie 18	1789	3.59	0.33	430	460	59	3183
	8.2	9.2	10.4	6.4	9.0	11.3	14.1
Progenie 19	1735	3.46	0.31	440	460	54	2721
	11.0	9.9	11.5	16.7	11.5	28.4	31.1
Progenie 23	1930	3.75	0.36	440	480	49	2964
	11.1	11.32	9.7	6.3	7.8	29.8	16.8

*Seedling 1, 2 and 3 were 3 months old, and seedling 15, 18, 19 and 23 were 6 months old.

From the parameters obtained in the seedlings (Table 2), relationships were determined (Table 3) and also analyzed in prediction model of wood properties in the tree.

Table 3. Values of relations between parameters obtained in the seedlings

Species	CLL_s	H_s/D_s
Clone 1	1770	125.0
Clone 2	1510	102.5
Clone 3	1185	123.5
Progenie 15	1417	100.0
Progenie 18	1376	91.9
Progenie 19	1324	89.6
Progenie 23	1639	96.0

Note: Stiffness coefficient of seedling $CLL_s = DB_s (V_{L,s})^2$, Longitudinal velocity ($V_{L,s}$), seedling diameter (D_s), seedling height (H_s) and basic density in seedling (DB_s).

Considering in isolation each parameter obtained in the seedling (independent variables), as well as the variables obtained from the relationships of these parameters (Table 3), it was possible to obtain statistically significant predictive models of the modulus of elasticity of the tree (EM_t), except for the variable height (H_s) and stiffness coefficient (CLL_s) - Table 4. The linear model correlating EM_t with seedlings parameters was not the one with the best coefficients of correlation (R) and determination (R^2) for any case (Table 4) but, in the case of the independent variables velocity ($V_{L,s}$), basic density (DB_s) and diameter (D_s), were the ones that presented the smallest prediction errors (Table 4). The models to predict modulus of elasticity of the wood from trees (EM_t) using only one variable obtained in the seedling, in general presents high values of prediction errors.

Table 4. Simple regression models correlating modulus of elasticity (EM_t in MPa) of the wood from the tree with each parameter obtained in the seedling: longitudinal velocity (V_{Ls} in $m.s^{-1}$), basic density (DB_s in $kg.m^{-3}$), diameter (D_s in mm), height (H_s in m), stiffness coefficient (CLL_s in MPa) and relationship between height and diameter (H_s/D_s dimensionless).

Parameters	Model	P-value	R ² (%)	R	Error*
VLs	$EM_t = -19671 + 12.6 V_{Ls}$	0.0025	86.3	0.93	1033
VLs	$EM_t = \sqrt{-1.02E8 + 34.3V_{Ls}^2}$	0.0017	88.2	0.94	1272
DBs	$EM_t = 18154 - 34.0 * DB_s$	0.0121	74.7	-0.86	1402
DBs	$EM_t = 1 / (-0.0000911 + 2.23E-9 * DB_s^2)$	0.0047	82.4	0.91	3422
Ds	$EM_t = 19278 - 4760 D_s$	0.0018	88.0	-0.94	964
Ds	$EM_t = \sqrt{-1.18E8 + 4.5E8/D_s}$	0.0011	90.1	0.95	1154
Hs		ns	-	-	-
CLL _s		ns	-	-	-
Hs/Ds		ns	-	-	-
Hs/Ds	$MOEt = \sqrt{2.12 E8 - 1.86 E7/Hs/Ds}$	0.012	74.8	-0.86	1490

*Standard error of estimative; The non-linear regression models were those proposed by the statistical program as being those with the highest coefficient of correlation and determination; "ns" indicates that no statistically significant model was found (with P-value ≤ 0.05)

For the bending strength obtained in the wood of the trees (fm_t) only the velocity obtained in the seedlings, had statistically significant correlations (Table 5). Apiolaza (2009) indicates that acoustic tools produce better results for wood selection than density. Linear models presented lower coefficients of determination and correlation and higher prediction errors than models with variable transformation (Table 5).

Table 5. Simple regression models correlating the modulus of rupture (fm_t in MPa) of the wood from the tree with each parameter obtained in the seedling: longitudinal velocity (V_{Ls} in $m.s^{-1}$), basic density (DB_s in $kg.m^{-3}$), diameter (D_s in mm), height (H_s in m), stiffness coefficient (CLL_s in MPa), height to diameter ratio (H_s/D_s dimensionless).

Parameters	Model	P-value	R ² (%)	R	Error*
VLs	$fm_t = 90.4 - 0.0207 * VLs$	0.0447	58.6	-0.76	3.56
VLs	$fm_t = 1 / (0.037 - 32.1 / VLs)$	0.0304	64.2	-0.80	3.37
DBs		ns	-	-	-
Ds		ns	-	-	-
Hs		ns	-	-	-
CLL _s		ns	-	-	-
Hs/Ds		ns	-	-	-

For the basic density obtained in the wood of the trees (DB_t) no parameter obtained in the seedlings presented a statistically significant correlation. Apiolaza (2009) points out that below 15-years-old, density has a very weak correlation with acoustic properties. This result may be related to the radial variation pattern of this parameter, which is very large (Lenz, 2011). Watt et al. (2010) and Lindström et al. (2002) showed that for clones with ages varying from 3 to 12-years-old, there are strong correlations between MOE and microfibril angle, but that the correlations between MOE and density are very weak or moderate.

Considering the 6 independent variables (parameters measured in the seedlings - Table 2 and composition of these parameters - Table 3) that can be used in the models, the only ones that are not auto correlated ($R < 0,50$) are CLL_s (with no variable) and H_s with VL_s .

With the unrelated independent variables, the statistical software selected the most appropriate variables to be inserted in the multiple regression model. In no case the C_{LLs} variable was selected for the multiple regression models. It is important to remember that the calculation of C_{LLs} was made based on the basic density of the seedlings, which, according to several authors mentioned earlier, is a very unstable parameter in such young plants. For the modulus of elasticity obtained in the wood from trees (EM_t), one model was selected, considering independent variables not correlated with each other (Table 6). From a practical point of view, obtaining these parameters (speed and height) is easy and

nondestructive. Kijidani et al. (2014) in a study with the species *Chamaecyparis obtusa* concluded that the greater height of the young plant correlates with the greater stiffness of the adult wood, because it has negative effect on the microfibril angle, a result that corroborates the height of the plant as a significant variable in the model obtained in our research. Li et al. (2007) found a statistically significant correlation between tree height and wood stiffness.

Table 6. Multiple regression models correlating the modulus of elasticity (EM_t in MPa) of the wood from the tree with parameters, without collinearity, obtained in the seedling: longitudinal velocity (V_{LS} in $m.s^{-1}$) and height (Hs in m).

Model	P-valor					R ²	Error*
	Regression	VLs	Hs	Hs/Ds	CLLs*		
$EM_t = -2504 + 10.8*VLs - 42572*Hs$	0.0002	0.0003	0.0048		ns	98.5	384

*Coefficient of stiffness of seedling ($CLL_s = DB_s * VL_s^2$) where, DB_s is the basic density obtained in the seedling. "ns" non-significant variable in the model

Comparing the statistical parameters of the multiple regression models (Table 6) with those of the simple regression (Table 4), it is verified that the variability of the modulus of elasticity of the tree wood (EM_t) is better explained by the multiple correlation. Watt et al. (2010) point out that, since the MOE is the criterion for which wood is classified, it is preferable that genetic selection be made taking this parameter directly and not the density or the microfibril angle. Watt and Zoric (2010) analyzed models of correlation between modulus of elasticity and dimensional (diameter, height, height/diameter) and environmental (temperature and rainfall occurrence) parameters, age and planting density for *Pinus radiata*. The authors concluded that age, height/diameter ratio and minimum autumn temperature accounted for 96% of the variability of the modulus of elasticity.

For the bending strength (fm_t) and basic density (DB_t) obtained in the wood of the tree, no multiple regression model involving independent variables not auto correlated were statistically significant. The magnitude of variation of these parameters may explain this result. The coefficient of variation of the density and of the bending strength of the clones and progenies varied 3% and 10%, respectively, while for the modulus of elasticity the CV was 52%. A similar result was obtained by Lindström et al. (2002), with great differences of density variation (19%) and modulus of elasticity (89%). Lindström pointed out that density alone did not allow differentiate clones, but if associated with the microfibril angle the differentiation is possible.

The wood stiffness is increasing from the pith to the bark, but the most significant variations occur in the wood near the pith (Xu and Walker 2004, Wu et al. 2004), validating the good prediction results obtained in this research, as well as future prospects of anticipation of the knowledge of wood properties still in very young trees.

Conclusions

The multiple regression model involving the height and the longitudinal velocity of ultrasonic waves along the grain direction of the seedlings stem, was the most adequate for the prediction of the wood stiffness from trees. To the prediction of the wood bending strength from trees, the simple regression model, using the longitudinal velocity of ultrasonic waves allowed a statistically significant prediction. However, the wood density from the trees cannot be predicted by any model involving parameters obtained in seedlings of the same clones or progenies.

Acknowledgments

The authors are grateful to Sao Paulo Research Foundation (FAPESP; Processes 2013/03449-9 and 2015/11926-7) for financial support and scholarship; To the International Paper of Brazil for the donation of seedlings and trees of the Eucalyptus clones and logistic support for forest trials; To the "IMAGINE" Project FEDER INNTERCONNECTA n°:ITC-20151167 developed at the Madera Plus

Calidad Forestal and the Tragsa company, Galicia, Spain, for financial support; To the Trees4Future Project developed at the Center of Innovation and Technological Services of Wood of Galicia (CISMADEIRA), Spain and to the Laboratory of Structures of the Superior Polytechnic School of Lugo, University of Santiago de Compostela, Lugo, Spain.

References

Apiolaza, L. A. 2009. Very early selection for solid wood quality: screening for early winners. *Annals of Forest Science* 66:601.

Apiolaza, L., Chauhan, S., Hayes, M., Nakada, R., Sharma, M. and Walker, J. 2013. Selection and breeding for wood quality. A new approach. *New Zealand Journal of Forestry* 58(1): 32-37.

Bucur, V. 2006. *ACOUSTICS OF WOOD*. Springer, Berlin, pp 223–225.

Chauhan, S. S., Sharma, M., Thomas, J., Apiolaza, L. A., Collings, D. A. and Walker J. C. F. 2013. Methods for the very early selection of *Pinus radiata* D. Don for solid wood products. *Ann. For. Sci.* 70: 439-449

European Standards. EN 408. Structural timber and glued laminated timber. Determination of some physical and mechanical properties, 2010.

Gapare, W. J., Baltunis, B. S., Ivkovi´c, M. and Wu, H. X. 2009. Genetic correlations among juvenile wood quality and growth traits and implications for selection strategy in *Pinus radiata* D. Don. *Ann. For. Sci.* 66 (6) 606 (2009)

Gonçalves, R., Batista, F. A. F. and Lorensani, R. G. M. Selecting eucalyptus clones using ultrasound test on standing trees. *Forest Products Journal*, v.63 (3/4), pp. 119-118. 2013.

Gonçalves, R. and Costa, O. A. L. 2008. Influence of the moisture content on longitudinal, radial and tangential ultrasonic velocity for Brazilian wood species. *Wood and Fiber Science*, v. 40, p. 580-586.

Gonçalves, R., Pedroso, C. B. and Massak, M. V. 2012. Acoustic and bending properties in *Pinus elliottii* beams obtained from trees of different ages. *J. Wood Sci.* Vol.59 pp.127-132.

Kijidani, Y., Kawasaki, Y., Matsuda, D., Nakazono, F., Hayakawa, M., Mutaguchi, H. and Sakagami, H. 2014. Tree heights in the ring-formed years affect microfibril angles in the rings from juvenile to mature wood at breast height in hinoki trees (*Chamaecyparis obtusa*). *Journal of Wood Science*. 60: 381. doi:10.1007/s10086-014-1426-y

Lenz, P. Breeding for wood quality: the impact of cambial age on the genetics of White Spruce wood traits. 2011. 180 f. (Thesis) Doctorate. Faculty of Forestry, Geography and Geomatics, University Laval, Quebec.

Li, X., Huber, D. A., Powell, G.L., White, T. L. and Peter, G. F. 2007. Breeding for improved growth and juvenile corewood stiffness in slash pine. *Can J For Res* 37:1886–1893. doi:10.1139/x07-043

Lindström, H., Harris, P. and Nakada, R. 2002. Methods for measuring stiffness of young trees. *Holz Roh. Werkst.* 60: 165–174.

Lorensani, R. G. M., Alves, C. S. and Gonçalves, R. Prediction of basic density using parameters measured on trees. In: 19th International Nondestructive Testing and Evaluation of Wood Symposium. Rio de Janeiro, Brasil, September 2015.

- Merlo, E. S. and Santaclara, O. E. Wood quality screening with acoustic methods in 3 years old pinaster pine progenies. Madera Plus Calidad Forestal S.L. 2012.
- Merlo, E., Alvarez-Gonzalez, J. G., Santaclara, O. and Y Riesco, G. 2014. Modelling modulus of elasticity of *Pinus pinaster* Ait. in northwestern Spain with standing tree acoustic measurements, tree, stand and variables. Forest Systems 23 (1) 1-14.
- Mishiro, A. 1996a. Ultrasonic velocity and average moisture content in wood II. Mokuzai Gakkaishi 42(10):612–617.
- Neves, T. A., Protásio, T. P., Trugilho, P. F., Valle, M. L. A., Sousa, L. C. and Vieira, C. M. Qualidade da madeira de clones de *Eucalyptus* em diferentes idades para a produção de bioenergia. *Revista de Ciências Agrárias*. 2013, 56(2):139-148. doi:10.4322/rca.2013.022
- Santaclara, O., Álvarez, J. G. and Merlo, E. 2011. Modeling structural lumber quality for *Pinus pinaster* Ait. in northwestern Spain using standing tree acoustic assesment, tree characteristics and stand variables. Proceedings of the 17th International Non destructive Testing and Evaluation of Wood Symposium. University of West Hungary, Sopron, Hungary.
- Sharma, M., Apiolaza, L.A., Chauhan, S., Mclean, J. P. and Wikaira, J. Ranking very young *Pinus radiata* families for acoustic stiffness and validation by microfibril angle. *Annals of Forest Science*. 2016. 73: 393. doi:10.1007/s13595-015-0529-y
- Simões, J. W., Coelho, A. S. R., Mello, H. A. and Couto, H. T. Z. Crescimento e produção de madeira de eucalipto. Piracicaba: IPEF. N.20, p.77-97, 1980
- Sobue, N. 1993. Simulation study on stress wave velocity in wood above fiber saturation point. Mokuzai Gakkaishi 39(3):271-276
- Volpato, G. and Barreto, R. 2011. Estatística sem dor. Besting Writting. Botucatu. 64p.
- Wang, X., Carter, P., Ross, R.J. and Brashaw, B. K. 2007. Acoustic assessment of wood quality of raw forest materials – A path to increased profitability. *Forest Prod J* 57(5):6-14.
- Watt, M. S., Sorensson, C., Cown, D. J., Dungey, H. S. and Evans, R. 2010. Determining the main and interactive effect of age and clone on wood density, microfibril angle and modulus of elasticity for *Pinus radiata*. *Can. J. For. Res.* 40: 1550-1557
- Watt, M. S. and Zoric, B. 2010. Development of a model describing modulus of elasticity across environmental and stand density gradients in plantation-grown *Pinus radiata* within New Zealand. *Can. J. For. Res.* 40: 1558-1566.
- Wielinga, B., Raymond, C. A., James, R. and Matheson, A.C. 2009. Genetic parameters and genotype by environment interactions for green and basic density and stiffness of *Pinus radiata* d. don estimated using acoustics. *Silvae Genet* 58:112–122
- Wu, H. X., Yang, J., McRae, T. A., Li, L. and Powell, M. B. 2004. Genetic relationship between breeding objective and early selection criterion traits in Australia radiata pine population, CSIRO CFFP Technical Report 1402 and STBA Technical Report TR04-01, 51p.
- Xu, P. and Walker, J. 2004. Stiffness gradients in radiata pine trees. *Wood Science and Technology* 38(1): 1-9

Effects of the Clone Differences and Initial Plant Density on the Acoustic Measurements in Hybrid Poplar Trees

Türker Dündar

Faculty of Forestry, Istanbul University, Istanbul, Turkey, dundar@istanbul.edu.tr

Hüseyin Akkılıç

Faculty of Forestry, Istanbul University, Istanbul, Turkey, hakkilic@istanbul.edu.tr

Ümit Büyüksarı

Faculty of Forestry, Duzce University, Duzce, Turkey, umitbuyuksari@duzce.edu.tr

Abstract

We examined the effect of clone differences and initial plant density on the acoustic measurements and the mechanical properties in hybrid poplar wood from different clones; I-214 (*Populus nigra*×*P. deltoides*), I-45/51 (*Populus nigra*×*P. deltoides*), I-77/51 (*P. deltoides*), 89M (*P. nigra*), and S307 (*P. nigra*). The experiments were carried out on a 12 years old stand composed of adjacent part to be planted with initial spacing of 2×2 m, 3×2 m, 3×3 m, and 4×3 m. Twenty five sample trees for every clones and initial spacing, 500 trees in total, were measured by Fakopp Microsecond Timer to determine the wave velocity parallel to grain and dynamic modulus of elasticity (E_D) in standing trees. Total of 100 sample trees, five from every clones and initial spacing, were cut down and a 1m-length-logs were taken from where the acoustic measurements were performed. The standard size test specimens were tested for the basic density at 12% moisture content (MC), bending strength, static modulus of elasticity in bending (E_S) and compression strength parallel to grain. The results showed that the basic density varied from 0.32 to 0.42 g/cm³. The lowest wood density was determined in I-214 clone while the highest value was determined in 77/51 clones. We found significant differences between the clones in terms of the wave velocity. The lowest velocity values were obtained in I-214 and I-45/51 clones while the highest values were found in 77/51, S307. The basic density and the destructive tests results also confirmed the acoustic measurement results obtained from the standing trees. As for the plant density, the results were complicated. We couldn't observed any comprehensible results in nondestructive and destructive test in terms of plant density. Strong correlations were found between the E_D and E_S , MOR and compression strength. The results showed that the acoustic velocity measurements performed on the standing trees have a promising potential to use for managing hybrid poplar plantations by monitoring the wood properties.

Keywords: acoustic measurmenets, poplar clones, plant density, wood density, wood strength

Introduction

In Turkey, as well as all over the world, industrial plantations with fast growing species are of high priority to tackle the shortage of wood supply. Poplar (*Populus* spp.) represent the fastest growing trees in the temperate regions. Turkey is one of the major country for poplar plantations with an area of 125.000 ha which represents a remarkable increase in past two decades (FAO 2012). Planted poplar forests are primarily owned by the private sector (98% of total area) and are largely used for production purposes (≈80.000 ha for roundwood production). The registration and identification of poplar clones of different

origins have continued in the experimental nurseries of the Poplar Research Institute, Izmit. Programs concerning the genetic modification of poplars continue to enhance resistance against pests, diseases and other stresses, namely drought or flooding, and to improve technical properties as well as growth and yield. Breeding programs focus on black poplars (*Populus nigra* L.) as one of the main poplar species in the country. *P.x euramericana* “I-214”, *P.x euramericana* “I-45/51” and *P.deltoides* “Samsun” clones have been successfully planted in hybrid poplar plantations, which are composed of 75% “I-214” and “I-45/51” clones, and 25% “Samsun” clones, the latter being preferred in the Black Sea region due to its rapid growth (IPC 2012). In planted poplar forests, including highly productive poplar clones, growth rates are reported to range from 2.75 to 41 m³/ha/yr mean annual increment, on average 17 m³/ha/yr. Rotation periods are rather short and span in most cases 10 to 20 years for the production of industrial roundwood, and 2 to 30 years, on average 20 years, for the production of fuelwood and biomass (IPC 2012).

Poplar wood production continues to increase on or close to agricultural land. More than 80% of black poplar wood is utilized as roundwood for rural construction purposes and for the daily needs of the rural people. Additionally, poplar wood industries have developed, producing fiber boards and chip boards, furniture, packing material, particle boards, plywood, and matches, mainly from hybrid poplars (*P.x euramericana*). Turkey is one of the top producers of poplar wood with reported removals of 3.5 million m³ (IPC 2012).

As forest products companies are interested in hybrid poplar clones for the manufacture of a variety of products, the selected clones must meet the needs of the forest industry for diverse end uses. The physical and mechanical properties of hybrid poplar wood may show great variations depending on the growing site factors as well as the genetic differences between the clones. It is widely reported in the literature that significant variation in physical and chemical composition exists among hybrid poplar clones depending on the genetic makeup (Chantre 1995; Ivkovich, 1996; Matyas and Peszlen 1997; Hernández et al. 1998; Peszlen, 1998; Goyal et al 1999; DeBell et al 2002). Information on basic wood properties of poplar grown in short-rotation plantations and on opportunities to alter such properties through silvicultural practices and management decisions is limited. Reports on the relation of wood density or specific gravity to growth rate are inconsistent. Beaudoin et al. (1992) and Hernández et al. (1998) pointed out significant but weak negative correlations between wood density or mechanical properties and growth rate in *P. deltoides*×*nigra*. Peszlen (1998) found no effect of growth on specific gravity or mechanical wood properties of three poplar clones.

Significant efforts have been devoted to develop robust nondestructive evaluation (NDE) technologies capable of predicting the intrinsic wood properties of individual trees, stems, and logs, and to assess the value of stands and forests. Such technologies can help foresters make wise management decisions, grow higher quality wood, and lead to greater profitability for the forest industry. Acoustic technologies have been well established as material evaluation tools in the past several decades. Recent research developments on acoustic sensing technology offer further opportunities for wood manufacturers and forest owners to evaluate raw wood materials (standing trees, stems, and logs) for general wood quality and intrinsic wood properties. This provides strategic information that can help make economic and environmental management decisions on treatments for individual trees and forest stands, improve thinning and harvesting operations, and efficiently allocate timber resources for optimal utilization (Wang et al. 2007).

The aim of this study is to evaluate the hybrid poplar trees from different clones by stress wave nondestructive test techniques in order to determine the effects of clone differences and initial plant density on the wood quality of standing trees. The changing in the mechanical properties of the poplar wood depending on the clones and planting density was also investigated by destructive tests performed on small clear specimens. The results from destructive and non-destructive tests were compared to evaluate the reliability of the acoustic measurements.

Materials and Methods

Experimental stand

An experimental poplar plantations planted by The Izmit Poplar Research Institute for research purposes in Izmit district was selected as the sample site. These plantation was composed of adjacent parts where five hybrid poplar clones that are I-214 (*Populus nigra*×*P. deltoides*), I-45/51 (*P. nigra*×*P. deltoides*), I-77/51 (*P. deltoides*), S307 (*P. nigra*), and 89M (*P. nigra*) were planted with initial spacing of 2×2 m, 3×2 m, 3×3 m, and 4×3 m. Figure 1 shows the plantation plan of the experimental site. Each part of the stand had 25 poplar trees at the age of 12. Therefore, 500 trees were sampled for the acoustic measurements.

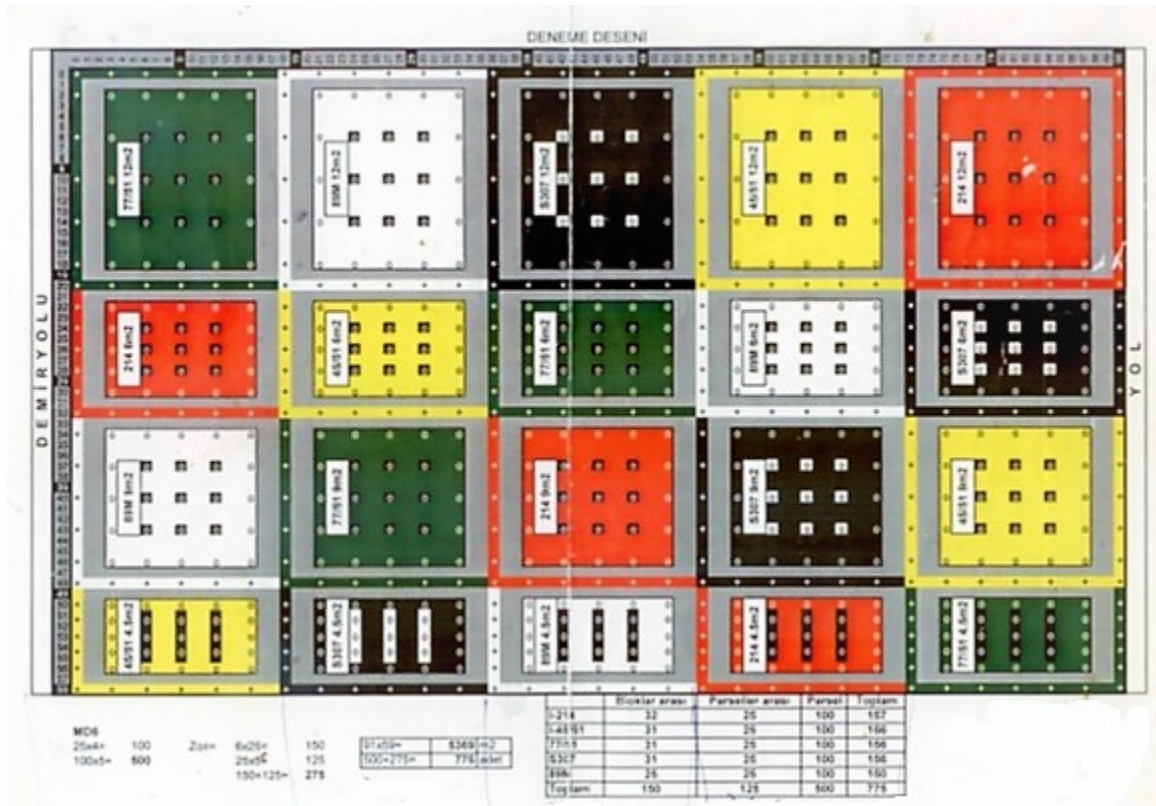


Figure 1— The plantation plan of the experimental sites.

Measurements on the standing trees

Time-of-flight (TOF) acoustic method was employed to determine the acoustic velocity of the standing poplar trees. A total of 500 poplar trees were measured with Microsecond Timer device developed by FAKOPP Enterprise.

The system includes two probes containing piezoelectric sensors (start sensor and stop sensor), a portable timer, and a hand-held hammer. The probes are inserted into the tree trunk (into sapwood) with an angle of less than 45° with the stem and aligned within a vertical plane on the same face. The lower probe is placed about 0.5-0.6 m above the ground. The distance between the lower and upper probes was 1 m (Figure 2). The acoustic energy is then directed into the tree trunk by hammer on the input probe. The resulting acoustic waves are detected by the sensors and transmitted to the timer and hence, time-of-flight was measured. After TOF measurement, acoustic velocities were calculate by;

$$C_T = \frac{S}{TOF}$$

where, C_T is tree acoustic velocity (m/s), and S is distance between the two probes (sensors) (m).

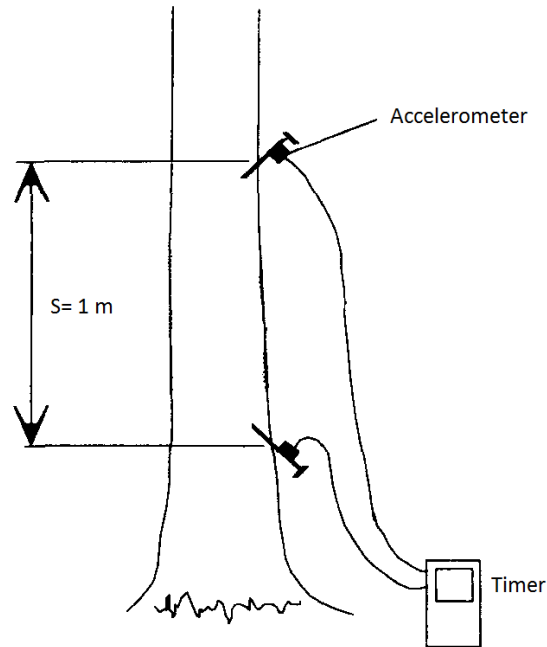


Figure 2— Experimental setup for acoustic measurements.

Tree measurements were taken from a randomly selected side of the tree trunk. Three readings were collected from each tree to derive average acoustic velocity. Diameter at breast height (DBH) of each tree was also measured.

The dynamic modulus of elasticity values of the trees were calculated via acoustic velocity by a well-known equation:

$$E_D = C_T^2 \times \rho$$

where ρ is the wood density. In this study, we used the average basic density values at 12% MC determined on the small clear specimens in calculating the E_D values.

Mechanical tests on the small clear specimens

Following the acoustic measurements, five sample trees representing the average diameter of the stands with cylindrical straight stem were felled from every clones and initial spacing for the destructive mechanical tests. A 1m-length-log was cut from where the acoustic measurements were made (around breast height (1.3 m)) on each tree and a 6 cm-thick-plank including the central pith was sawn from each log. For each mechanical property, thirty standard sized defect-free test specimens were prepared from these planks. Thus, for each property, 150 specimens from each planting density and clone, totally 3000 samples, were conditioned at 65% relative humidity (RH) and 20°C temperature to reach 12% equilibrium moisture content (EMC).

Basic wood density at 12% EMC was determined on the clear specimens with dimensions of 20 mm by 20 mm by 30 mm by measuring their mass and volume as indicated in ISO 13061-2 (2014). Static bending strength (MOR) and static MOE (E_s) were determined on the small clear samples with dimensions of 20 mm by 20 mm by 300 mm by a three-point static bending test with a span/thickness ratio of 15 as described by ISO 13061-3 and ISO 13061-4 (2014). The formulas used to calculate MOR and E_s are given in related standards. The compressive strength parallel to the grain was measured by following ISO 3787 (1976). The dimension of the specimens was 20 mm by 20 mm by 30 mm and crosshead motion or rate of loading was 0.6 mm/min. The formula used to calculate compression strength is given in related standards.

Data analysis

Analysis of Variance (ANOVA) was used to determine the effect of clone differences and the planting density on the acoustic velocity of standing trees and the mechanical properties. Duncan test was applied to determine the homogeneity groups.

Results and discussions

Table 1 shows the results of the acoustic velocity measurements of the standing poplar trees. The letters below the numbers indicate the homogeneity groups. The results showed that the acoustic velocity values of the trees changed significantly between the clones at a confidence level of 95%. The acoustic velocity of the I-214 and I-45/51 clones (*P. nigra* × *P. deltoides*) were found significantly lower than the I-77/51 (*P. deltoides*), S307 and 89M clones (*P. nigra*) at low planting densities (9 m² and 12 m²) where the latter clones were identical. However, when the planting space reduced to 4.5 m² and 6 m² the differences between the clones have become insignificant except for S307 clone which had significantly higher velocity than the others. When the effect of planting density within the clones is examined, a significant decrease is seen in the velocities of I-214 and I-45/51 clones with the decreasing planting density to 9 m² and 12 m², while it was not found a comprehensible change in the velocity values depending on the planting density in the other clones. This finding also may explain why I-214 and I-45/51 clones had significantly lower velocity values than others when planted sparsely while there were no remarkable difference between the clones when they were planted densely.

Table 1—Acoustic velocity measurements results

Clones	Planting density (m ²)			
	4.5	6	9	12
I-214	3861,8 (263,9) DE*	3784,2 (280,4) CD	3610,8 (251,1) B	3437,2 (228,1) A
I-45/51	3840,8 (338,8) DE	3646,8 (244,7) BC	3659,1 (271,7) BC	3538,2 (140,6) AB
I-77/51	3811,5 (296,8) CD	4123,4 (236,6) FGH	4162,0 (220,4) GH	4004,8 (198,2) EFG
S307	4198,3 (250,2) H	3991,4 (277,4) EF	4118,1 (175,9) FGH	3897,7 (192,5) DE
89M	3843,3 (248,7) DE	3775,6 (330,8) CD	3992,3 (235,3) EF	3844,3 (285,6) DE

*p<0,05

Table 2 shows the results of the basic wood density measurements. As in the velocity values, clear differences were found between the poplar clones. The wood density of the I-214 clone (*P. nigra*×*P. deltoides*) was found significantly lower than the others followed by the I-45/51 (*P. nigra*×*P. deltoides*) at all planting densities. The I-77/51 and S307 clones had the higher density values than the other clones. When we examined the effect of planting space on the wood density, even if some exceptions were seen in the I-77/51 and 89M clones, it can be concluded that the planting density did not affect the wood density.

Table 2—Basic wood density measurements results

Clones	Planting density (m ²)			
	4.5	6	9	12
I-214	0,324 (0,013) A*	0,328 (0,006) A	0,328 (0,010) A	0,320 (0,008) A
I-45/51	0,396 (0,016) BC	0,389 (0,012) B	0,393 (0,009) BC	0,388 (0,010) B
I-77/51	0,397 (0,007) BC	0,418 (0,017) DE	0,424 (0,009) E	0,452 (0,011) F
S307	0,415 (0,015) DE	0,407 (0,015) CD	0,417 (0,013) DE	0,414 (0,012) DE
89M	0,382 (0,011) B	0,383 (0,010) B	0,409 (0,012) CDE	0,396 (0,011) BC

*p<0,05

Table 3 shows the MOR and E_S values obtained from the small clear specimens. As seen on the Table, both the MOR and the E_S values of I-214 and I-45/51 clones were found lower than the other clones. However, the MOR and E_S values obtained from I-77/51, S307 clones were significantly higher than the others. As mentioned before the same trend were also observed in density and velocity values. When we consider the planting density, it can be said that the MOR and ES were not affected by planting density. This finding was also compatible with the results obtained for acoustic velocity and density.

Table 3—The results of bending strength (MOR) and static modulus of elasticity (E_s)

Clones	Planting density (m ²)							
	4.5		6		9		12	
	MOR	E _s	MOR	E _s	MOR	E _s	MOR	E _s
I-214	44,9 (2,8) A*	5492,7 (381,0) W	42,6 (2,7) A	5772,0 (339,0) W	44,4 (3,3) A	5579,3 (272,2) W	44,4 (1,9) A	5529,9 (372,0) W
I-45/51	50,7 (1,9) C	5620,7 (330,8) W	48,9 (1,6) C	5388,3 (453,5) W	45,4 (1,8) AB	5173,6 (555,4) W	48,3 (3,0) BC	5267,9 (549,1) W
I-77/51	58,3 (2,2) EF	7083,6 (652,8) XYZ	60,5 (2,2) EFG	7428,7 (465,7) Z	59,7 (3,5) EF	7472,0 (383,9) Z	57,2 (1,8) DE	7063,4 (295,3) XYZ
S307	63,3 (2,0) G	8175,8 (387,2) Q	59,4 (1,7) EF	7195,5 (341,9) YZ	61,4 (2,7) FG	7445,3 (399,6) Z	58,9 (3,8) EF	6771,8 (559,1) XY
89M	54,1 (1,3) D	6701,7 (306,6) XY	49,2 (2,9) C	5818,6 (514,1) W	59,3 (2,8) EF	7201,8 (559,1) YZ	54,3 (2,3) D	6480,9 (416,2) X

*p<0,05

Table 4 show the results of compression strength parallel to grain. As in the other properties, it is clear that the lowest compression strengths were determined in I-214 and I-45/51 clones at all planting spaces where I-45/51 was slightly higher than the I-214. In general, the other clones were found close to each other, but the S307 clone stood out slightly from the others. Conflicting results were obtained about the effect of planting density on the strength values of hybrid poplars. Although the some significant differences were found between the planting densities, the results were not comprehensible. For instance, the compression strength of S307 clone tends to be lower as the planting space increase while I-77/51 tends to be higher. No significant differences were found in I-214 depending on the planting density.

Table 4—The results of compression strength

Clones	Planting density (m ²)			
	4.5	6	9	12
I-214	23,1 (0,72) A	22,5 (1,56) A	21,9 (1,801) A	23,1 (0,976) A
I-45/51	25,1 (1,11) BC	23,5 (0,99) AB	23,1 (1,042) A	25,6 (1,645) C
I-77/51	29,9 (1,71) DEFG	28,7 (0,712) DE	30,9 (1,685) FG	30,4 (0,678) EFG
S307	32,9 (1,57) H	31,7 (1,472) GH	30,8 (1,432) FG	30,6 (0,662) EFG
89M	29,0 (0,98) DEF	25,2(1,711) BC	30,3 (1,288) EFG	28,3 (2,725) D

*P<0,05

Figure 3 shows the relationship between the E_D calculated by the velocity of standing trees and the mechanical properties for all poplar trees from all clones and planting density. As seen in the figure strong linear correlations were found between the E_D and E_S and MOR with R^2 of 0,64 and 0,59, respectively. Also a good linear correlations was found between the E_D and compression strength with a R^2 of 0,49.

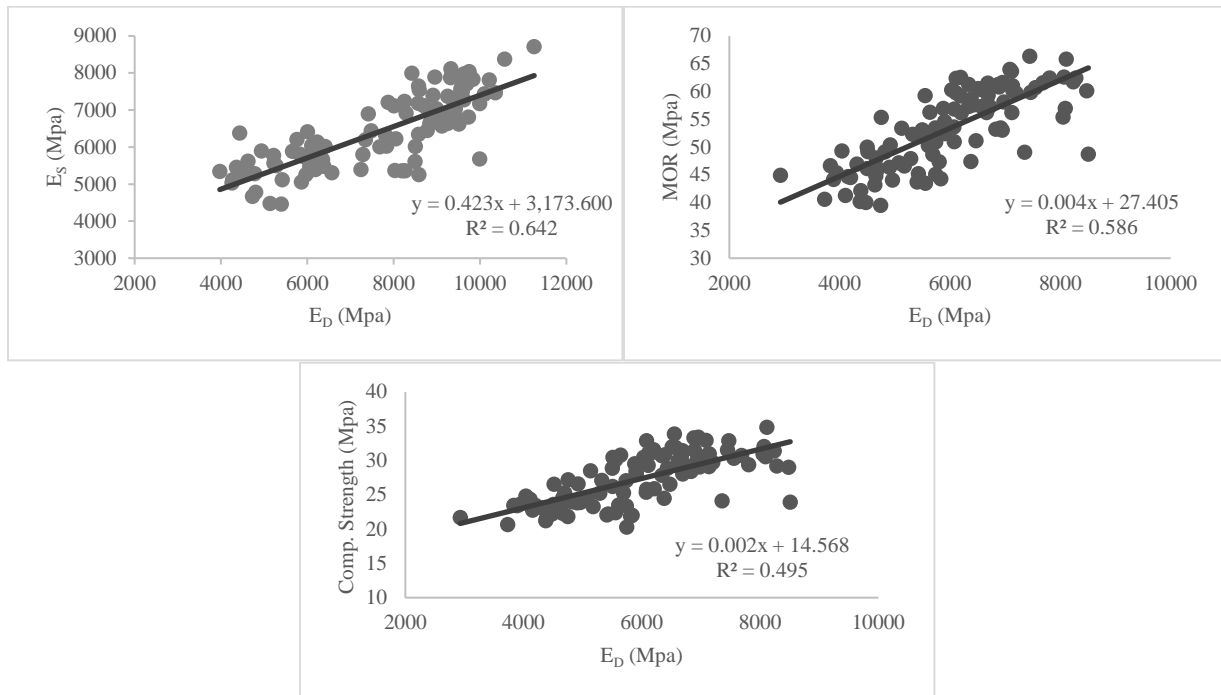


Figure 3— The relationship between the E_D obtained from standing measurements and the mechanical properties for all poplar trees

When we make a general assessment, it seems that the acoustic velocity measurements on the standing poplar trees were able to determine the differences in wood properties between the clones. The basic density and destructive test results were verified the results of acoustic measurements that the wood quality of I-214 and I-45/51 clones were relatively lower than the other clones while the I-77/51 and S307 clones stood out slightly from the others. However, we could not find any comprehensible differences in the acoustic velocity depending on the initial planting density. This finding was also verified by the basic density values and the destructive test results. Consequently, we can expressed that the acoustic measurements performed on the standing trees have a promising potential to use for managing hybrid poplar plantations by monitoring the wood properties.

Conclusions

The acoustic velocity values of the hybrid poplar trees changed significantly between the clones at a confidence level of 95%. In general, the acoustic velocity of the I-214 and I-45/51 clones were found significantly lower than the I-77/51 (*P. deltoides*), S307 and 89M clones (*P. nigra*). The same results were also obtained by bending and compression tests performed on the small clear specimens where the lowest strength values were determined again in I-214 and I-45/51 clones. Conflicting results were obtained about the effect of plant density on both the velocity and the strength values. We found strong correlations between the ED obtained from standing trees and the strength values with R^2 of varying from 0,49 to 0,64. The results showed that the acoustic velocity measurements performed on the standing trees have a promising potential to use for managing hybrid poplar plantations by monitoring the wood properties.

Acknowledgments

“This work was supported by Scientific Research Projects Coordination Unit of Istanbul University. Project number BEK-2017-25531.

References

Beaudoin, M.; Hernandez, R.E.; Koubaa, A. [and others]. 1992. Interclonal, intraclonal and within-tree variation in wood density of poplar hybrid clones. *Wood and Fiber Science*. 24(2): 147-153.

Chantre, G. 1995. Variabilite clonale des caracteristiques technologiques chez le peuplier. *CR Acad Agric Fr*. 81 (3): 207-224.

DeBell, D.S.; Singleton, R.; Harrington, C.A. [and others]. 2002. Wood density and fiber length in young populus stems: relation to clon, age, growth rate, and pruning. *Wood and Fiber Science*. 34(4): 529-539.

FAO International Poplar Commission Report. 2012. Improving lives with poplars and willows, synthesis of country progress reports - activities related to poplar and willow cultivation and utilization-2008 through 2011.

Goyal, G.C.; Fisher, J.J.; Krohn, M.J. [and others]. 1999. Variability in pulping and fiber characteristics of hybrid poplar trees due to their genetic makeup, environmental factors and tree age. *Tappi Journal*. 82 (5): 141-147

Hernandez, R.E.; Koubaa, A.; Beaudoin, M. [and others]. 1998. Selected mechanical properties of fast-growing poplar hybrid clones. *Wood and Fiber Science*. 30(2): 138-147.

Ivkovich, M. 1996. Genetic variation of wood properties in Balsam Poplar (*Populus balsamifera* L.). *Silvae Genetica*. 45(2): 119-124.

Matyas, C.; Peszlen, I. 1997. Effect of age on selected wood quality traits of poplar clones. *Silvae Genetica*. 46(2-3): 64-72.

Peszlen, I. 1998. Variation in specific gravity and mechanical properties of poplar clones. *Drevarsky Vyskum*. 43(2): 1-17.

Wang, X.; Carter, P.; Ross, R.J. [and others]. 2007. Acoustic assessment of wood quality of raw forest materials – a path to increased profitability. *Forest Products Journal*. 57(5): 6-14.

Solid Wood Quality Prediction Capacity with Acoustic Methods in Young Trees

Esther Merlo Sánchez *

Department I+D+i, Madera Plus Calidad Forestal S.L., Ourense, España, maderaplus@maderaplus.es

Gonzalo Caballé

Instituto Nacional de Tecnología Agropecuaria (INTA), Bariloche, Argentina, caballe.gonzalo@inta.gob.ar

Raquel Gonçalves,

Laboratório de Ensaios Não Destrutivos, FEAGRI, UNICAMP, Campinas, Brasil, raquel@feagri.unicamp.br

Rafael Mansini

Laboratório de Ensaios Não Destrutivos, FEAGRI, UNICAMP, Campinas, Brasil, rafaelmansini@hotmail.com

Oscar Santaclara

Department I+D+i, Madera Plus Calidad Forestal S.L., Ourense, España, maderaplus@maderaplus.es

Manuel Guaita,

Plataforma de Ingeniería de la Madera Estructural (PEMADE) de la USC, Lugo, España, m.guaita@usc.es

Francisco J. Lario Leza,

TRAGSA, Sección Viveros, UT1 Maceda, España, flario@tragsa.es

* Corresponding author

Abstract

Making a prediction of the technological wood properties from non-destructive methods on the standing tree at early ages, allows to accelerate the processes of selection and genetic improvement of a Species or improve the forest management efficiency aiming the production of high quality timber. The present study was carried out on 9 years old *Pinus pinaster* (n:40). The measurements were made in standing trees and then they were felled. In each tree, growth and shape variables were measured and the acoustic wave velocity propagation in the longitudinal and radial directions was also measured. Standard test method for elasticity (MOE) and rupture modulus (MOR) of entire stem and other variables like wood density were performed in all trees. Subsequently, multivariate regression models were developed to predict these properties. The three models developed have coefficient of determination close or greater than 50%. The slenderness, the inclination of the tree and the wave velocity propagation in the longitudinal direction are the variables that best relate to MOR, MOE. As for density, the diameter of the branches and the velocity of propagation in the face of compression were relevant. These variables should be taken into account in the silvicultural management and genetic selection in order to obtain high quality structural timber.

Keywords: models, wood properties, *Pinus pinaster*, wave velocity

Introduction

The *Pinus pinaster* Ait. is one of the most important coniferous species used by the Spanish forestry industry, especially in Galicia, where more than 2.8 million cubic meters of wood are produced annually in this species. The main destination in this region is the crushing industry for the production of different types of panels. However, *P. pinaster* presents mechanical properties suitable for use as structural wood with medium-high resistant class (Riesco, et al 2007; Carballo et al, 2009 ,Merlo et al, 2014). The possibility of making a prediction of the technological properties that define its suitability for structural use, from the measurement of non-destructive variables on the standing tree at early ages, allows to accelerate the genetic improvement processes of this species and at the same time , to improve the efficiency of the tasks of forest management aiming the production of wood of structural quality.

The objective of the present work was to develop predictive models for the main variables that define the structural use of wood (modulus of elasticity, flexural strength and basic density) using non destructive measures on standing trees in juvenile stage (9 years).

Materials and methods

The present study was carried out on 40 trees of *P. pinaster* of 9 years of age that were part of a test of provenances of the species, installed in the forest nursery of the company TRAGSA (42°16'43"N, 7°37'29' O), Maceda, Orense, Spain. 3-5 trees of the 10 provenances with the best performance (rate of growth and volume) were randomly selected from a total of 25 provenances. In each tree the following variables were measured:

Total height (m)

Height of crown (m)

Diameter (DAP, 1.3 m; cm)

Angle of inclination (Ang; °)

Depth of the arc in 1.8m (De;mm)

Slenderness (H m/DAP cm)

Number of whorls (Wh)

Whorls dead

Branches by whorls at 1.3 m

Diameter of branches at a 1.3 m (Dr; mm)

Angle of branches at 1.3 m (°)

The propagation velocity of the acoustic wave (time-of-flight method) was measured in standing trees using ultrasound equipment USLab (AGRICEF, Brazil), and sonic equipment ST300 (FibreGen, New Zealand) and MST Microsecond Timer (Fakopp, Hungary) in the longitudinal direction and in the radial direction with USLab and MST equipments. With these three equipments a measurement was made on the opposite side of the compression wood. Only the MST and USLab equipment were also used on the side of compression wood. In the radial direction the measurement was made by placing the transducers from compression wood to opposite wood.

At the end of the standing measurements, the trees were cut, and the entire stems (approximately 3 m in length) were sent to the PEMADE laboratory at the Polytechnic University of Lugo (University of Santiago de Compostela) to the mechanical tests. At the end of the test, a defect-free slice was extracted for determination of wood density and humidity according to norm EN 13.183-1.

Equations 1 and 2 were used to calculate the MOR and MOE.

$$MOR = \frac{16P_{max}L}{3\pi D^3} \quad \text{Equation 1}$$

$$MOE = \frac{1,33L^3(P_{40\%}-P_{10\%})}{\pi D^4(f_{40\%}-f_{10\%})} \quad \text{Equation 2}$$

Where: MOR = modulus of flexural rupture (MPa); Pmax = maximum load (N); L = free space between supports (mm); MOE = modulus of elasticity (MPa); P40% = 40% of the maximum load (N); P10%=10% of the maximum load (N); F40% = vertical displacement corresponding to P40% (mm); F10% = vertical displacement corresponding to P10% (mm)

Subsequently, multiple regression models were developed to predict MOR, MOE and wood density. The "stepwise" procedure was used and possible collinearity problems between variables were discarded by keeping the variance inflation factor (VIF) below 10. Data with studentized residues smaller than or equal to -2 and 2 were eliminated as aberrant. For the case of propagation velocity of the acoustic wave the differences between the equipments were evaluated by the Students test.

Results

The average growth rate was 0.88 cm/year in diameter and 0.49 cm/year in height. There was a poor correlation between both parameters. The trees with the highest height growth showed the lowest growth in diameter. Consequently, the slenderness was higher in the trees with higher growth in height. The angle of inclination was the variable with the greatest dispersion data (Table 1).

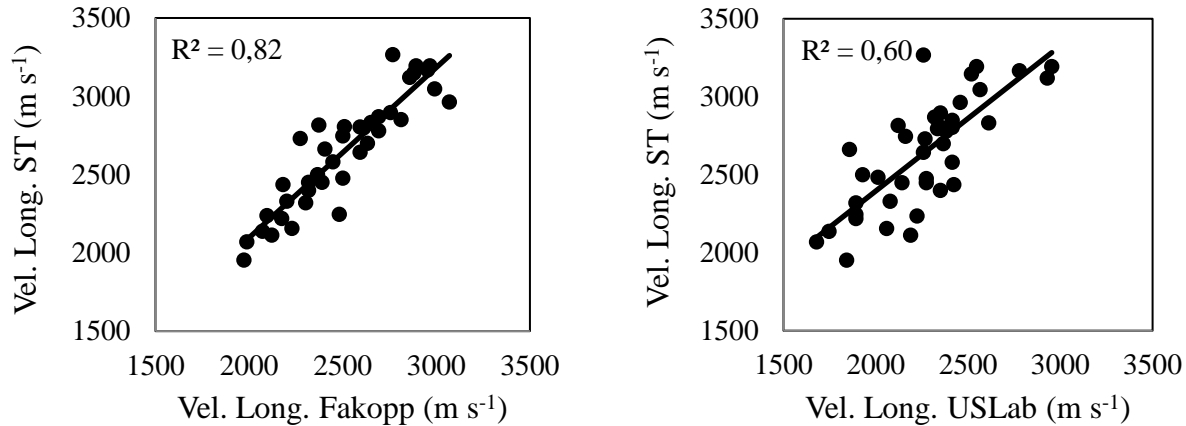
The data obtained by the sonic equipments (ST300 and MST Fakopp) were similar (R2 = 0.82, Fig. 1) whereas the data obtained by ultrasonic equipment (USLab) deviated R2 = 0.60, Fig. 1).

Table 1. Average values (EE), maxima and minima of the main growth traits evaluated on 9-year-old *Pinus pinaster* trees.

Variable	n	Mean	SE	Min	Max
Total height (m)	40	4,44	0,09	3	5,85
Height of crown (m)	40	1,11	0,07	0,25	2,25
Diameter (DAP, 1,3 m; cm)	40	7,93	0,15	5,99	10,24
Angle of inclination (Ang; °)	40	12,15	1,13	1,4	36,3
Depth of the arc in 1,8m (De;mm)	40	53,73	4,17	8	124
Slenderness (H m/DAP cm)	40	56,78	1,54	42,25	75,62
Number of whorls (Wh)	36	11,94	0,42	7	17
Whorls dead	39	4,59	0,29	0	8
Branches by whorls at 1,3 m	39	5,1	0,22	2	8
Diameter of branches at a 1,3 m (Dr; mm)	36	14,67	0,65	6,64	22,44
Angle of branches at 1,3 m (°)	39	64,77	2,25	6	85

The propagation velocity in the longitudinal direction on the opposite side of wood compression was a little higher (2465 m/s) than on the side of wood compression (2365 m/s). The propagation velocity in transversal direction was 2050 m/s and in the tangential direction it was somewhat lower (1870 m/s).

Figure 1. Relation between acoustic wave propagation velocity values in longitudinal sense with sonic equipment ST300 and MST Fakopp (left) and between sonic equipment ST300 and ultrasonic USLab (right).



The average modulus of elasticity (MOE) was 1655.8 N.mm⁻² (\pm 675.4), the average flexural strength (MOR) 18.5 N.mm⁻² (\pm 5.4) and the average density 0.36 g.cm⁻³ (\pm 0.05). The wood density did not show a significant correlation with the MOE ($r = 0.16$, $p = 0.34$) nor with MOR ($r = 0.2$, $p = 0.22$). The propagation velocity in longitudinal and tangential directions had a significant positive correlation with both MOE and MOR. On the contrary, the radial velocity presented a non-significant correlation with the same parameters. The propagation velocity, in any of the senses, presented non significant correlations with the wood density.

The predictive models for the MOE and MOR for each equipment, are presented in Table 2. The values of the coefficient of determination, R², fluctuated between 0.58 and 0.68, with the ST300 equipment being the best fit presented with both variables (Table 2).

Table 2. Estimated equations and parameters for prediction of MOR and MOE with ST 300 (FibreGen, New Zealand), MST (Fakopp (Hungary) and USLad (AGRICEF, Brazil) on 9 year old Pinus pinaster trees.

Estimated equations	R ² _{Aj}	ECMP
ST300		
$MOE = -1948,11 + 0,98VL + 21,46H/DAP - 21,24Ang$	0,63	222829,5
$MOR = -11,21 + 0,01VL - 0,04De + 1,73H$	0,68	11,06
MST Fakopp		
$MOE = -2103,86 + 1,03VL + 24,97H/DAP - 20,64Ang$	0,59	237971,1
$MOR = -13 + 0,01VL + 2,83H - 0,05De$	0,59	14,33
USLab		

$MOE = -1555,18 + 0,93VL + 23,94H/DAP - 5,32De$	0,60	241045,6
$MOR = -10,56 + 0,01VL + 2,80H - 0,05De$	0,58	14,48

MOE: global modulus of elasticity (N.mm⁻²), MOR: flexural strength (N.mm⁻²), VL: propagation velocity of acoustic wave longitudinally on the opposite side of wood compression (ms⁻¹), H/DAP: slenderness (dimensionless), Ang: stem inclination angle (°), De: Depth of the arc in 1,8m (mm) and H: Total height (m). ECMP: Mean mean square error.

It was only possible to find a model to predict the wood density (R² = 0.5) with the velocity data obtained by the USLab ultrasonic equipment on the side of compression wood together with other tree variables.

Table 3. Equation and estimated parameters for prediction of basic density with USLab ultrasonic equipment (AGRICEF, Brazil) on 9-year-old *Pinus pinaster* trees.

Equation and estimated parameters	R ² _{Aj}	ECMP
USLab		
$Den. básica = 0,31 + 5,7.10^{-5}VL_c + 2,9.10^{-3}Ang - 4,2.10^{-3}D_b - 0,01DAP + 4,2.10^{-3}Wh$	0,50	0,002
<i>Den. Basic: basic density (grcm⁻³), VLc: acoustic wave propagation velocity in the longitudinal direction on the side of wood compression (ms⁻¹), Ang: stem inclination angle (°), Db : Mean diameter of the branches of the whorl closest to DAP (mm), DAP: diameter at breast height (cm) and Wh: number of total whorls. ECMP: Mean mean square error.</i>		

Discussion

The propagation velocity of acoustic wave, especially in the longitudinal direction, together with the slenderness or height and the straightness of the tree (angle or arrow) are the variables that best predict the technological characteristics of *P. pinaster* wood at juvenile stage.

The positive correlation between slenderness and mechanical properties is probably based on Euler's buckling formula. The leaner individuals avoid Euler buckling by increasing the MOE / density ratio, mainly through increments in the MOE, since the density is relatively constant (Watt et al, 2010; Lasserre et al, 2005).

The relationship between tree straightness and the internal characterization of wood has been a widely studied topic, especially when examining the spatial distribution of wood of reaction or compression. Radi and Castera (1992) in maritime pine, found that the percentage of compression wood and eccentricity, defined as the ratio between maximum and minimum radius, showed a positive correlation up to 6 m in height. Beyond this height the relations became less evident. More recently, Alteyrac et al. (1999) also analyzed *P. pinaster* and based on computer simulations of tree shape and wood characteristics (MOE, basic density, moisture content), concluded that the current shape of the stem is a good indicator of the location of the wood compression, but the relationship is complex and difficult to evaluate without any knowledge of the history of the tree. The inverse relation between the tree straightness and the elastomechanical variables (MOE and MOR) and direct relation with the basic density found in the present study, possibly respond to the small size of the trees (> 6 m height) and to the significant effect that the wood of compression has on these parameters.

Numerous studies explored the relationship between the propagation velocity of the acoustic wave and the wood density. However, the conclusions differ considerably. In some cases the speed of propagation does not depend on the density of the wood (Oliveira and Sales, 2006) and in others, it is proven that speed increases are related to higher density (Bucur and Chivers, 1991), or on the contrary, decreases speed against density increases (Zobel and Buijtenen, 1989). The predictive model developed contemplates a positive linear relationship between the propagation velocity of the wave and the basic density of *P. pinaster* juvenile wood only with the ultrasonic equipment on the wood compression side. The sonic equipment did not present an acceptable fit.

The wavelength, λ , is directly proportional to the wave velocity and inversely proportional to the acoustic pulse frequency. For a given propagation speed, as the frequency increases the wavelength decreases, providing the possibility of higher resolution. The increase of the compression wood on the face of compression and the higher resolution of the ultrasonic equipment, apparently, allow to capture the differences in density of the wood and to incorporate the measure of speed in the predictive model.

The increment growth in diameter and its effect on wood density is controversial. Zobel and van Buijtenen (1989) mention that the variation of the wood density among trees due to genetic causes is so great that the variability due to other external factors such as site quality, level of competence, structure of crown or geographic location. The predictive model developed contemplates an inverse relationship between DAP and the basic density of *P. pinaster* juvenile wood. This response is especially due to the increase in the proportion of latewood to early wood within each growth ring (data not shown). Similar response was found by Merlo et al (2014) in adult *P. pinaster* trees.

Conclusion

It is possible to predict the technological properties that define the structural suitability of *P. pinaster* wood, from the measurement of non-destructive variables on the standing tree at early ages. These models will serve as a basis for the selection and genetic improvement of this species aiming at the production of quality wood for structural use.

Acknowledgments

This work has been carried out within the framework of different research projects defined as follows: Project "TOPWOOD" Call for papers H2020-MSCA-RISE-2014, n°: 645654 with title "Wood phenotyping tools: properties, functions and quality"; Project "IMAGINE" call, FEDER INNTERCONNECTA n°: ITC-20151167 with title "Innovation in the synergy of the value chain of the Galician coniferous wood for a more efficient industry" and grant FAPESP. 2015 / 11926-7 entitled "Anticipation of knowledge of wood properties using wave propagation test in young plants". Special thanks to the technical support of the staff of the TRAGSA nursery and staff of the PEMADE laboratory, at the Polytechnic University of Lugo, University of Santiago de Compostela.

References

- Alteyrac, J., Fourcaud, T., Castera, P., Stokes A. Analysis and simulation of stem righting movements in Maritime pine (*Pinus pinaster* Ait.), in Proc. 3rd Workshop IUFRO WP S5.01-04, La Londe-Les-Maures, France (1999) 644 p.
- Bucur, V. y Chivers, R.C. Acoustic properties and anisotropy of some Australian wood species. *Acou stica* 75 (1991) 69-75. Riesco, G. y Díaz González J. Características físicas de la madera de pino procedente de raleos en el noroeste de España. *Maderas, Ciencia y Tecnología*, 9 (2007) 233-244.
- Bucur, V. 1995. *Acoustic of wood*. New York: CRC Press I
- Carballo, J, Hermoso, E., Fernández-Golfín, J.I. Mechanical properties of structural maritime pine sawn timber from Galicia (*Pinus pinaster* Ait. ssp. *atlantica*). *Invest Agrar Sist Recur For* 18 (2009) 152-158.

Lasserre, J.P., Mason, E. y Watt, M. The effects of genotype and spacing on *Pinus radiata* (D. Don) corewood stiffness in a 11 year old experiment. For *Ecol Manage* 205 (2005) 375-383.

Merlo, E, Alvarez-Gonzalez, J.G., Santaclara, O., y Riesco, G. Modelling modulus of elasticity of *Pinus pinaster* Ait. in northwestern Spain with standing tree acoustic measurements, tree, stand and variables. *Forest Systems* 23 (1) (2014) 1-14.
nc.

Oliveira, F.G.R. y de Sales, A. Relationship between density and ultrasound velocity in Brazilian tropical woods. *Bioresour Technol* 97 (2006) 2443-2446.

Radi M., Castera P., Qualification de deux pins maritimes en liaison avec la structure de leur bois, *Ann. Sci. For.* 49 (1992) 185–200

Watt, M.S., Moore, J.R., Façon, J.P., Downes, G.M., Clinton, P.W., Coker, G., Davis, M.R., Simcock, R., Parfitt, R.L., Dando, J., Mason, E.G. y Bown, H.E. Modelling the influence of stand structural, edaphic and climatic influences on juvenile *Pinus radiata* dynamic modulus of elasticity. For *Ecol Manage* 229 (2006): 136-144.

Zobel, B.J. y Van Buijtenen, J.P. *Wood variation: Its causes and control*. Springer-Verlag, Berlín. Germany (1989) 363 p.

Session 11

Evaluation of Roundwood

Eucalyptus Wood Poles Grading Using Ultrasound

Yann Benoit

CBT SA, Head of Technology, Saint-Sulpice, Switzerland, benoit@cbs-cbt.com

Michel Njankouo

National Advanced School of Engineering, Timber engineering, Yaoundé, Cameroon, njankouo@gmail.com

Abstract

Wood poles are largely used around the world to carry power and telecom lines. If species and impregnation of those poles are key factors for overhead networks design, the mechanical properties variability within a same species requires a specific grading to ensure both a reliable design and an extended life time expectancy.

Luxpole is a non-destructive concept using ultrasound to optimize new wood poles grading. This objective technique is based on the measurement of the time of flight of low frequency ultrasonic waves (22kHz).

ENEO, the national energy provider of Cameroon, uses local wood poles for their overhead networks and wishes to continue so. ENEO receives the rough poles from their suppliers before impregnating them in their own facilities.

This paper presents the project led jointly by the National Advanced School of Engineering of Yaounde, ENEO and CBT SA. The goal was to validate Luxpole concept on the local Eucalyptus species and ensure the traceability of the measurements.

The outcomes show that non-destructive ultrasonic measurements are a real solution for tropical-wood poles grading.

Keywords: ultrasound, eucalyptus, wood poles, grading

Introduction

ENEO, the national power provider in Cameroun, is using wood poles for their low and medium voltage overhead lines all over the country. The company counts about 200'000 wood poles in the field.

The species is local Eucalyptus and mainly:

- Saligna
- Robusta
- Grandis
- Hybride

Wood poles suppliers deliver rough poles at ENEO's impregnation site located in Bafoussam in the Western region (Figure 1). All the poles are then impregnated by ENEO before they are shipped to be used.

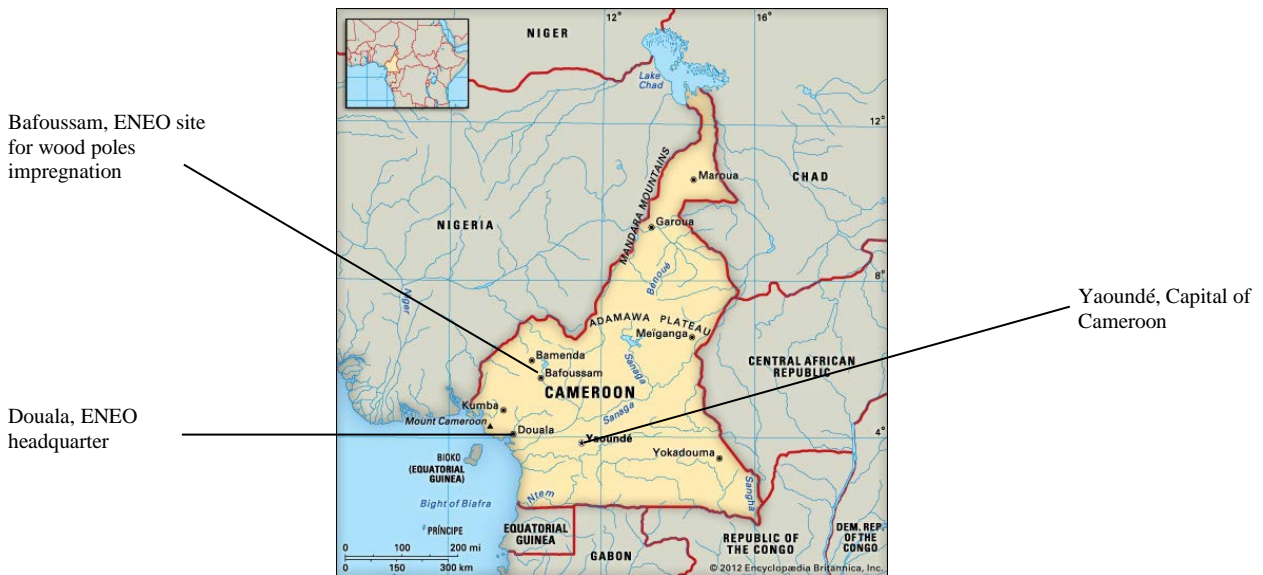


Figure 1 – Map of Cameroon with ENEO’s headquarter and treatment plant.

To improve the quality management of their poles and especially qualify their suppliers, ENEO wants to organize a mechanical quality control when they do receive the poles.

CBT SA has developed the concept Luxpole to grade the new wooden pole. This concept, based on ultrasonic nondestructive measurements, has been used in Europe for a decade to select the best poles, but more importantly, to purge the weakest ones.

ENEO has contacted CBT SA to check if a similar concept is possible with their local concerns.

This project presents this mission held in Fall 2016 with the cooperation of the National Advanced School of Engineering in Yaoundé.

The technology

Luxpole concept is the application of the Sylvatest Trio (Figure 2) for new wooden poles.



Figure 2 – Nondestructive technology using ultrasound: Sylvatest Trio device with its two transducers.

Ultrasound technology

The technology is using low frequency ultrasound waves (22kHz). A transducer is installed at each pole's end (Figure 3). The time of flight is registered and converted into a speed thanks to the pole's length (1). This speed of ultrasound is corrected with the pole's moisture content (2 and Figure 4) that is measured with a standard wood moisture meter.

The speed of ultrasound reflects the mechanical pole's strength as illustrated by the equation (3)

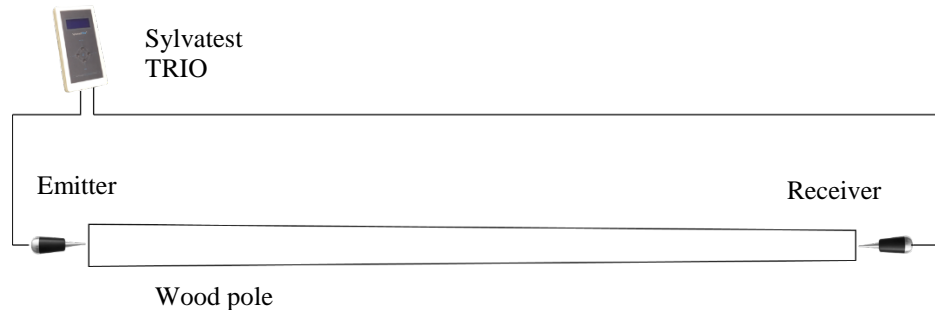


Figure 3 – Illustration of a measurement on a wood pole with Sylvatest TRIO

$$S_M = \frac{L}{t} \times 10^6 \quad (1)$$

where S_M is the speed of ultrasound [m/s], L is the pole's length [m] and t the time of flight [μ s] measured by Sylvatest TRIO.

$$S_0 = S_M + K_{MC} \quad (2)$$

where S_0 is the speed of ultrasound [m/s] corrected by the moisture content and K_{MC} is the factor obtained on the Figure 4.

$$S_0 \approx \sqrt{\frac{MOE}{k \cdot \rho}} \quad (3)$$

where MOE is the Modulus of Elasticity [MPa] and $k \cdot \rho$ is the material density property.

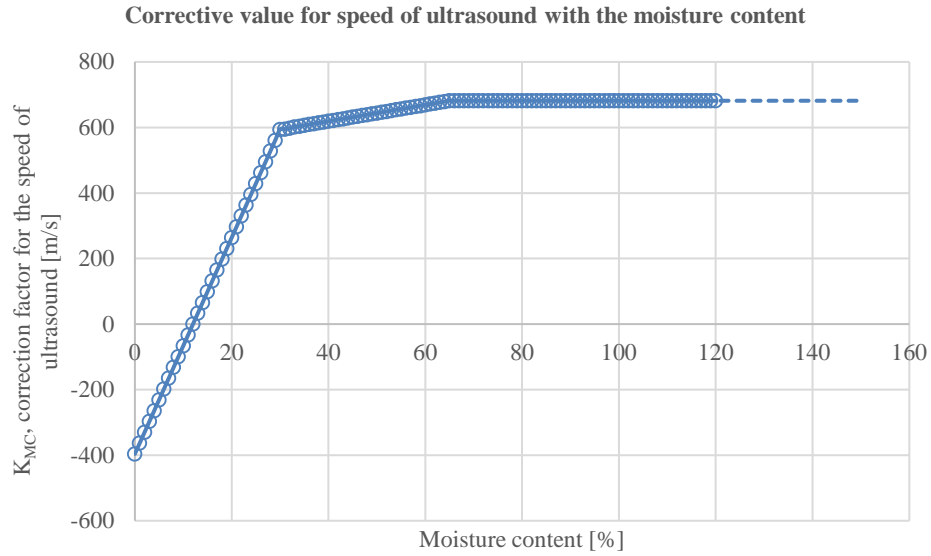


Figure 4 – Corrective factor for the moisture content on the speed of ultrasound.

Luxpole concept

Luxpole concept uses the nondestructive technology based on ultrasound to assess new wooden poles quality.

The speed of ultrasound is correlated to the wood poles mechanical properties (Figure 5).

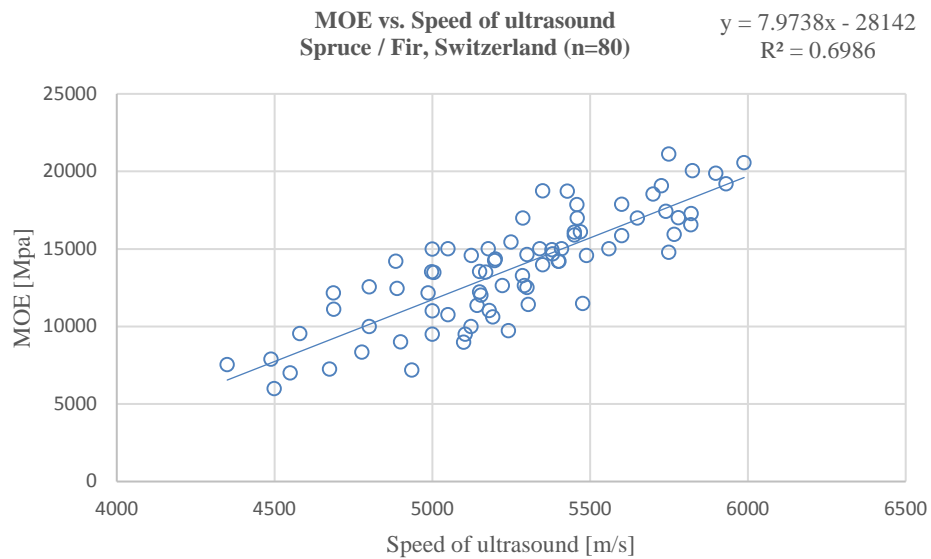


Figure 5 – Correlation between speed of ultrasound [m/s] and Modulus of Elasticity [MPa] of new wooden poles (not impregnated, Spruce and Fir from Switzerland)

The models are built thanks to destructive tests in Cantilever bending mode. Additionally, parameters that are taken into account for Luxpole are:

- Wood species
- Moisture content
- Temperature
- Impregnation

Thanks to the speed of ultrasound that is measured a strength class category is assigned to a wood pole. Luxpole proposes three strength class categories (Figure 6):

- XL: Best poles
- L: Good poles
- S: Weakest poles

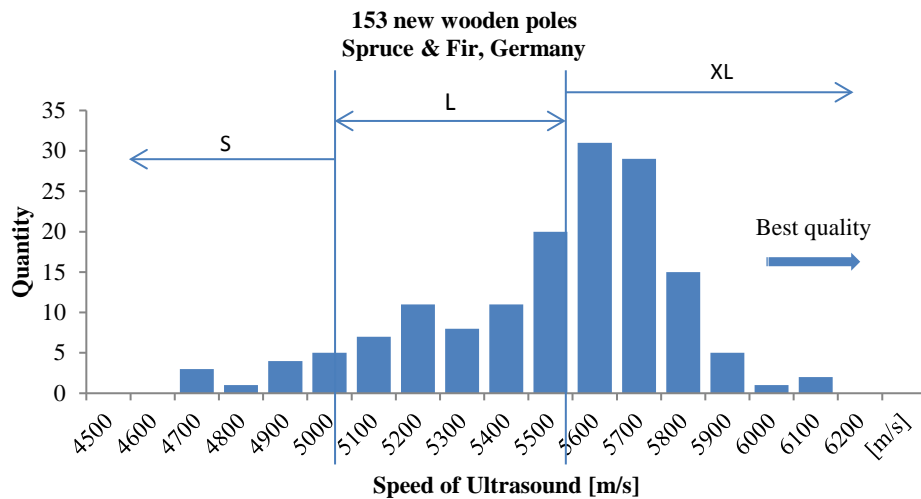


Figure 6 – Distribution of the Speed of ultrasound [m/s] vs. Luxpole classes. 153 new wood poles, Spruce and Fir, Germany

S class is usually considered as the class of poles to be rejected and XL class the one that offers better opportunities to extend either the load to be carried or the span between two poles in keeping the same pole's geometric dimensions.

The sample

The challenge with tropical wood

If Luxpole is usually used with Western softwoods, ENEO's request deals with local tropical species as Eucalyptus and more precisely:

- Saligna
- Robusta
- Grandis
- Hybride

Ultrasonic mechanical grading had already been studied in the past on Eucalyptus especially in Brazil. But the researches were mainly done with other frequencies (but still low frequencies) and in a radial mode as Luxpole is performed in lengthwise measurements.

Additionally, in order to have stabilized measurements, both transducers are usually coupled to the wood with a small hole. This is not a big problem with western softwoods but with tropical wood, this issue could be a challenge as the poles are very hard.

The sample and conditions of measurement

The tests have been performed on 148 poles of Eucalyptus Saligna and Robusta issued from three local suppliers.

Poles were from 6 to 14m long and were not impregnated.

The moisture content has been measured for each pole thanks to two moisture content meters (Gann) in order to compare their values. All the poles were in wet conditions with a moisture content higher than 50%.

The measurements have been performed in September 2016. The temperature was about 25-30°C during the day (Figure 7).



Figure 7 – Luxpole measurements in Bafoussam, ENEO's treatment plant. Cameroun, 2016.

The results

The first measurements have shown that holes were not required to install the transducers in the poles. This is a great advantage as the poles are really hard and performing two holes per pole requires a huge effort.

In other terms, the signal of the ultrasounds can clearly be measured without any hole for the transducers, even for poles up to 14m long, what is not always the case for Western softwoods.

The distribution of the speed of ultrasounds is illustrated by the figure 8.

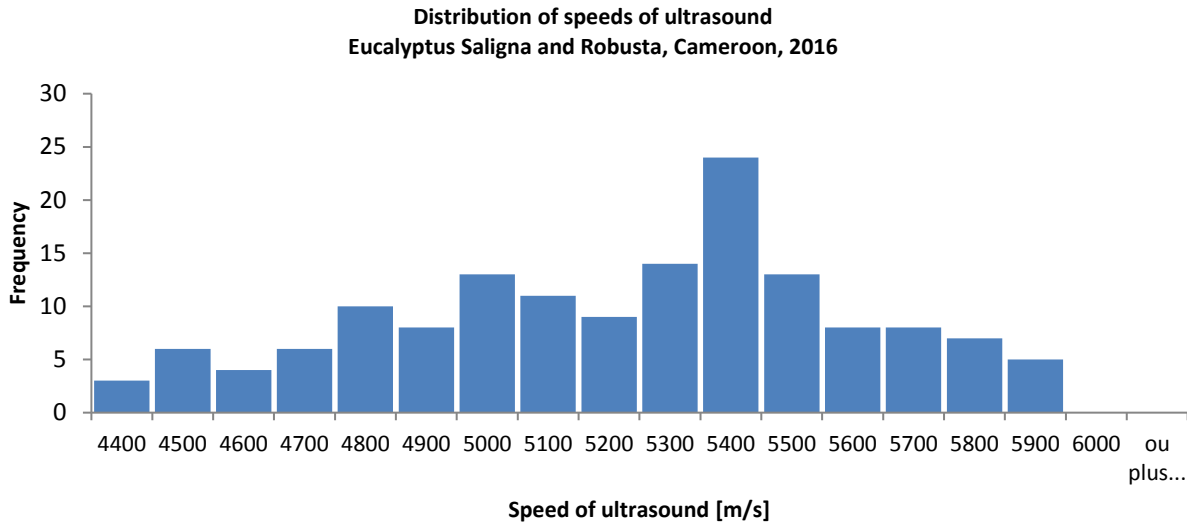


Figure 8 – Distribution of the speeds of ultrasound (Luxpole) for 148 wood poles of Eucalyptus Saligna and Robusta, Cameroon, 2016.

This figure shows that grading the Eucalyptus (Saligna and Robusta) poles with ultrasound is clearly possible as the distribution can be identified.

Sorting the three suppliers is then possible as illustrated by the Table 1 and the figure 9.

Table 1 – Statistical distribution of ultrasonic speeds according to ENEO's suppliers. Eucalyptus Saligna and Robusta, Sept. 2016, Bafoussam, Cameroun

Supplier	n	Min [m/s]	Mean [m/s]	Max [m/s]	Std. Dev. [m/s]
B	49	4049	4862	5716	342.2
E	46	4359	5464	5879	290.5
H	53	4497	5190	5846	274.0
Total	148	4049	5166	5879	386.3

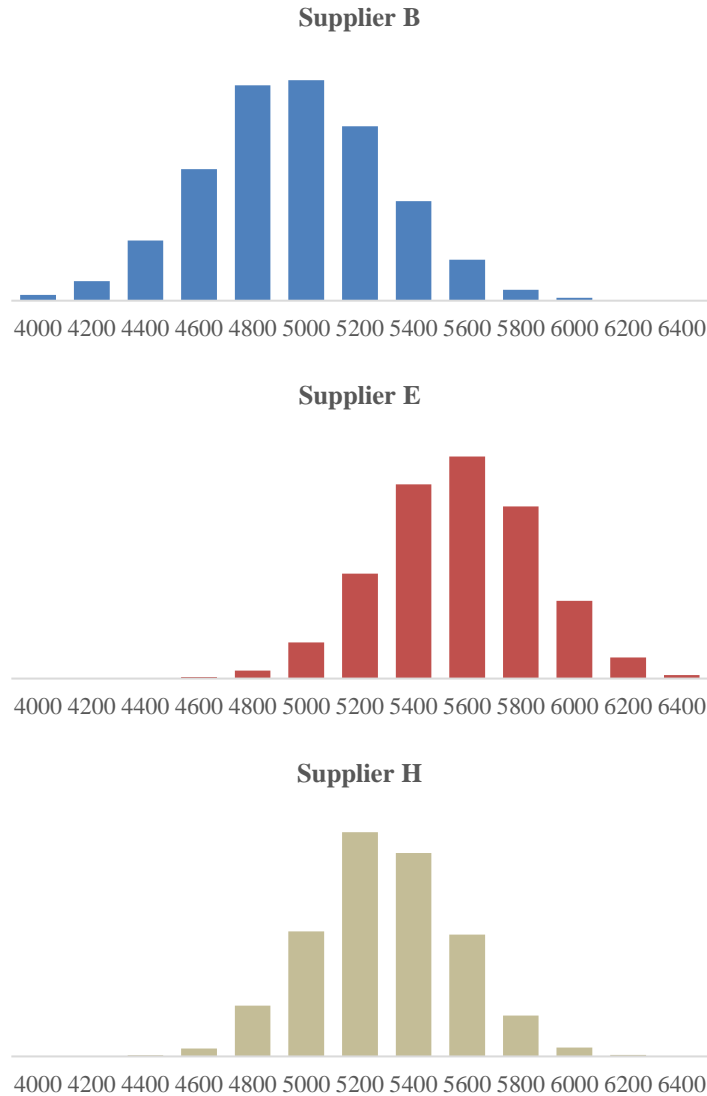


Figure 9 – Statistical distribution of the ultrasonic speeds according to ENEO’s suppliers. Eucalyptus Saligna and Robusta, Bafoussam 2016, Cameroon.

These results are aligned to ENEO’s expectation as the supplier E, with the best quality during the tests, usually have the best poles thanks to favorable growing conditions.

In order to assign strength classes to the poles, complementary tests should be performed, and more precisely, Cantilever bending strength according the EN14229. The ultrasonic speeds distribution should reflect the mechanical performances one.

As a first step, and based on the rejection rate known by ENEO’s experience, limits have been decided to split the different qualities as follow:

- XL poles: ultrasonic speed $S_0 > 5350$ m/s
- L poles: $4600 \text{ m/s} \leq \text{ultrasonic speed } S_0 < 5350$ m/s
- S poles: ultrasonic speed $S_0 < 4600$ m/s

with S_0 the speed of ultrasound corrected with the moisture content.

With these limits, the results obtained on the sample measured during this first experiment give the following illustration (Figure 10).

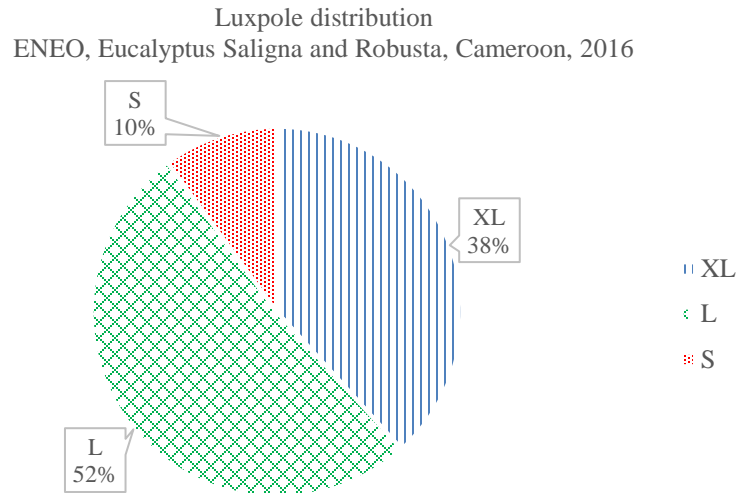


Figure 10 – Distribution of the Luxpole classes, first model. Eucalyptus Saligna and Robusta, Cameroon, 2016

Conclusion

This first experimentation of Luxpole on tropical wood in Cameroon confirms that new wood poles grading is possible with nondestructive measurements using low frequency ultrasound as proposed by Luxpole concept.

The scope of values obtained without any hole is completely in the range of values known for other species from other origins: from 4000m/s to 6000m/s.

A software for the traceability of this Luxpole quality insurance concept has been customized especially for ENEQ's concerns (LuxSoft). Each supplier is then qualified according to the quality he delivers. This promotes the delivery of a global higher quality.

The next step will be to launch destructive tests at the National Advanced School of Engineering, in Yaoundé, Cameroon, to confirm the strength classes according to the ultrasonic speeds measured on the poles.

Additionally, some other tests need to be performed on other species from Cameroon and especially Eucalyptus Grandis and Hybrid. There is no reason why it wouldn't work as their biological structures are close to the species tested in this first local experimentation.

Acknowledgments

CBS would like to thank ENEO staff and the co-author of this article, Dr. Michel Njankouo for his precious help on the local issues.

Additionally, CBS is thankful to Prof. Dr. Raquel Gonçalves, from the University of Unicamp, Brazil, who was very positive about the outcomes before the project has started.

References

Gonçalves, R. 2005. Using ultrasonic to predict the modulus of rupture and modulus of elasticity of wooden poles. In: International Symposium on Nondestructive Testing of Wood, 14. Hanover, Germany.

Drill Bit Friction and Its Effect on Resistance Drilling Measurements in Logs

Evgenii Sharapov*

Volga State University of Technology, Yoshkar-Ola, Mari El Republic, Russian Federation

Xiping Wang

USDA Forest Service Forest Products Laboratory, Madison, Wisconsin, USA

Elena Smirnova

Volga State University of Technology, Yoshkar-Ola, Mari El Republic, Russian Federation

*Corresponding author, e-mail: sharapoves@volgatech.net

Abstract

The objectives of this study were to determine the effect of drill bit shaft friction on resistance drilling measurements on green logs and assess the potential of using drilling resistance and feeding force to predict density and hardness of wood in logs, and ultimately in standing trees. Two freshly-cut yellow birch (*Betula alleghaniensis*) logs, one with internal decay and the other of decay free, were used as test specimens. Drilling measurements were conducted on the logs using an IML-RESI PD 400 tool equipped with a standard spade-type drill bit. Following drilling measurements, nine 5.1-cm-thick disks were cut from the decayed log, one at each drilling location, and then a 5.1-cm-wide strip was cut from each disk. A series of hardness tests were conducted on each strip based on a procedure modified from ASTM D 143-2012. Then each strip was cut into 1.8-cm segments to determine wood density using a volumetric method. In addition, 195 drilling measurements were conducted on the decay-free log to characterize shaft friction variations and its relationship with drilling depth. The mean shaft friction observed on the defect-free yellow birch log was 19.2% with a coefficient of variation of 17.5%. A linear relationship was found between shaft friction and drilling depth in the defect-free log. Linear models were used to make a correction to the original drilling resistance profiles by subtracting the shaft friction along the entire drilling path. The adjusted resistance profiles showed better contrast between decayed zone and intact wood than the original resistance profile, which could be an advantage in tree inspection. The results also indicated that removing shaft friction from the original resistance profiles increased the prediction power of the drilling resistance as a nondestructive measure of wood density and hardness. Feeding force exhibited similar patterns with drilling resistance which is useful in decay detection, but it has limited prediction power if it is used to assess wood density and hardness.

Keywords: Drilling resistance, resistance profile, wood density, feeding force, hardness, logs

Introduction

Since introduction of the first prototype of resistance-based drilling machine in Germany in the 1980's, resistance drilling technique has quickly evolved into sophisticated electronic tools that simultaneously measure, display, and record relative resistance profile as a long drilling needle is driven into wood. The relative resistance profile (hereafter refers to resistance profile) is obtained through direct measurement of the electric power consumption (EPC) of a direct-current needle-rotation motor. So far, the resistance

drilling method has been successfully used in various applications such as tree ring analysis (Rinn et al. 1996; Chantre and Rozenberg 1997; Wang and Lin 2001; Wang et al. 2003; Guller et al. 2012), tree decay detection (Wang and Allison 2008; Allison and Wang 2015), and structural timber condition assessment (Rinn 1990, 2012; Ceraldi et al. 2001; Ross et al. 2004). Research has progressed to evaluate the potential of resistance drilling as an indirect method to measure density or specific gravity of dry wood. Some early studies demonstrated that there was a strong linear correlation between the mean drilling resistance and gross density of dry wood (Görlacher and Hättich 1990; Rinn et al. 1996). More recent studies on structural wood members also showed moderate to strong relationships between measured resistance values and wood density (Ceradi et al. 2001; Park et al. 2006; Bouffier et al. 2008; Zhang et al. 2009; Sharapov and Chernov 2014).

There has also been a growing interest in using resistance drilling method to obtain wood density information from standing trees, particularly in tree genetic improvement and wood quality survey programs where hundreds or even thousands of trees must be sampled (Gao et al. 2017). One of the concerns on the use of resistance drilling tool on trees is the accuracy of measured resistance (amplitude in resistance profile, %) as an indirect measure of the wood density (Sharapov et al. 2015; Gao et al. 2017). Isik and Li (2003) evaluated the use of Resistograph tool for rapid assessment of relative wood density of live loblolly pine trees in progeny trials. They reported strong correlations among average drilling resistance value and wood density and strong genetic control at the family level. However, individual phenotypic correlations were found to be weak. Similar results have also been reported by Gants (2002), Charette et al (2008), Gwaze and Stevenson (2008), and Eckard et al. (2010).

In principle, resistance drilling in wood is a wood cutting process (Bershadskii and Tsvetkova 1975). The cutting forces are typically measured by the total power consumption. Friction is an important parameter that affects the measurement precision. The boring drill bits employed in the existing commercial drilling tools are thin needle, spade-type drill bits with a triangular-shape cutting head, which includes a tip and two symmetrical cutting edges that are perpendicular to the rotating axis. Similar to other wood cutting tools, friction force in a resistance drilling process can be generally resolved into chip friction with the rake face of the cutting edges, clearance-face friction with the wood cutting surface, side surfaces of the drill bit cutting part with the drilling hole surface, and shaft friction with wood chips and the drilling hole surface. Generally, friction is influenced by wood species, moisture content, cutting speed parameters, and angle and blunting parameters of the cutting edges. While most of the friction forces remain constant during a single drilling, the drill bit shaft friction increases with increased drilling depth. Rinn (2012) reported that the systematic errors in the profiles caused by shaft friction tend to increase for specimens with a wood density higher than 600 kg/m³. Nutto and Biechele (2015) conducted resistance drilling measurements on six different tropical wood species and found that drill bit shaft friction ranged from 4% to 70%. There is little knowledge on how the drilling bit friction will affect sensitivity of resistance profiles in terms of decay detection and wood property prediction.

The research reported herein was a continuation of the previous study on investigating the wear behavior and blunt effect on resistance drilling measurements on wood (Sharapov et al. 2015). The objectives of this paper were to characterize the drilling friction in drilling green yellow birch logs, determine the effect of shaft friction on resistance drilling measurement, and evaluate the potential of using resistance drilling tools to assess wood density in green logs, and ultimately in standing trees.

Materials and Methods

Two freshly-cut yellow birch (*Betula alleghaniensis*) logs were obtained for resistance drilling experiments, one contained internal rot and the other was defect free. The decayed log was 2.53-meter long with a diameter of 32 cm at the large end and 30 cm at the small end, and had an average moisture

content (MC) of 39.8% and average density of 589 kg/m³. The defect-free log was 2.58-meter long with a diameter of 35 cm at the large end and 29 cm at the small end, and had an average MC of 55.5% and an average wood density of 710 kg/m³.

An IML-RESI PD 400 tool (IML System GmbH, Wiesloch, Germany) was used to conduct resistance drilling measurement on two log samples. This Resistograph tool was equipped with standard spade-type drill bits. The drilling profiles obtained from each measurement include a relative resistance curve reflecting the torsion force on the drill bit and a feeding force curve reflecting the pressure put on the tool, both recorded in percentage of the amplitude. The drilling force parameters were measured and recorded once every 0.1 mm of drilling depth. The Resistograph data was saved and processed using the PD-Tools PRO software (IML System GmbH, Wiesloch, Germany).

Resistance drilling experiments included two parts: 1. Conduct extensive drilling tests on the defect-free log to study the wear behavior and shaft friction of the drill bit. The wear behavior of the drill bit in wood resistance drilling was reported in a previous presentation (Sharapov et al. 2015). In this paper, we analyzed the resistance profiles obtained through this extensive drilling experiment to determine the shaft friction and its relationship with drilling depth. 2. Conduct drilling tests at selected locations on the decayed log to study the sensitivity of measured drilling parameters (drilling resistance and feeding force) to wood property changes (wood density and hardness). All resistance drilling measurements were conducted at a room temperature of about 20 °C.

Resistance Drilling Procedures

Drilling Experiment —Part 1: A total of 195 resistance drilling measurements were conducted on the defect-free yellow birch log using a new drill bit, with a feed rate of 0.508 m/min and a rotational speed of 2500 rpm (nominal feed rate per cutting edge was about 0.1 mm). These speed parameters were selected based on several preliminary drilling tests with different feed rate and rotational speed combinations so that the amplitudes of the drilling resistance and feeding force were not very low and within the measurement scale. All drillings were made across the log diameter in the radial-longitudinal section, with a 1-1.5 cm spacing between any neighboring drillings.

Drilling Experiment —Part 2: Nine resistance drilling measurements were conducted on the decayed log with a feed rate of 0.99 m/min and a rotational speed of 2500 rpm (nominal feed rate per cutting edge was about 0.2 mm). The large end appeared solid, but a significant central rot was observed on the small end. The drilling measurement was started at a location 12.7 cm (5 in.) from the small end, followed by the second drilling 5.1 cm (2 in.) apart from the first one, then the remaining seven drillings were made with a 30.5 cm increment. Figure 1 shows the locations of resistance drilling measurements.

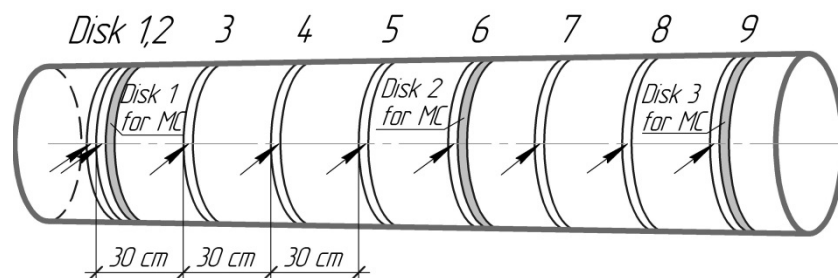


Figure 1—Schematic diagram of the decayed yellow birch (*Betula alleghaniensis*) log showing the locations of a series of resistance drilling measurements (arrows on the figure) and the disk sample at each location. Three moisture content disks are shown in gray color.

Janka Hardness Test and Wood Density Measurements

Upon completion of the resistance drilling measurements, the decayed log was dissected and a 5.1-cm-thick disk was obtained at each drilling location for further laboratory evaluation (Figure 1). For each disk, a 5.1-cm-wide strip was cut through the center of the disk along the drilling path. All strips were placed at the conditioning room of 20 °C and 65% relative humidity (RH) till the equilibrium moisture content (EMC) of 12% was reached.

To map the hardness along the drilling path, we conducted a series of Janka ball hardness tests on each strip sample based on a procedure modified from ASTM D 143-2012 (ASTM 2012). The hardness test was conducted on the end-grain face (TR plane) of the strip. On each strip sample, 2-cm grid lines were drawn on the end-grain face with the pith located in the center grid. Hardness test was then conducted on each grid using an Instron universal testing machine (Model 5566, Instron Corporation, Norwood, MA, USA) with a 10 kN load cell and a loading rate of 5.08 mm/min. A total of 13 Janka hardness tests were performed on each wood strip. The hardness value obtained from this specialized test was defined as end-hardness. After Janka ball hardness tests, each strip was cut into 1.8-cm segments for determining basic wood density using volumetric method (ASTM 2012).

Wood Moisture Content Determination

For decayed log, three additional disks were obtained next to drilling location no.1, no.5 (middle of the log), and no.9 respectively. A 5.1-cm-wide strip was cut from each of these disks and used as moisture content sample. The moisture contents of the strips were then determined based on the initial (green) weight and the oven-dry weight (ASTM 2007). The same procedure was used to determine the average MC of the defect-free log.

Data Processing and Analysis

During each resistance drilling measurement, two cutting-force parameters were measured and recorded: drilling resistance (torque moment acting on the drill bit cutting-head) and feeding force (external force acting on the Resistograph tool by the operator). It is hypothesized that variations in the output amplitudes of both drilling resistance and feeding force are directly related to the changes in wood density and mechanical properties along the drilling path. The exact unit of resistance amplitude is not specified by the tool manufacturer and expressed as a relative value in percentage (%). For regression analysis with the wood density and hardness data, the resistance amplitude data was averaged over each wood segment where the actual wood density and end hardness value were obtained. The amplitude of feeding force curves was calibrated to actual feeding force in Newton (N) based on the calibration data obtained in a universal testing machine (MTS 810, MTS Systems Corporation, Eden Prairie, MN USA) with a 1-kN load cell. The feeding force data obtained from each drilling measurement was then converted into actual force.

Results and Discussion

Drilling Friction

Figure 2 shows the last portion (drilling depth beyond 280 mm) of a typical drilling profile obtained from the birch logs, with drilling resistance displayed with higher amplitude (in grey shade) and the feeding force displayed in lower amplitude (in dark shade). It was observed that a residual drilling-resistance existed after the drill bit cutting-head exited the log at 305 mm. This residual resistance remained relatively constant as the drill bit continued feeding through and it is caused by the friction between the

drill bit shaft and the wood chips remained within the drilling hole. During a drilling process, wood chips remain inside the drilling hole and can be compacted and cause friction along the shaft. The magnitude of this friction theoretically depends on wood species, basic wood density, moisture content, size and forms of the chips, as well as drilling parameters such as cutting speed and feed rate. In Figure 2, the drill bit shaft friction is characterized by the residual amplitude of the resistance profile, which is 15%. The feeding force, on the other hand, reduced significantly after the cutting-head exited the log and fluctuated between 0 and 3% like a sine wave. This fluctuation in residual feeding force is believed to be related to the feeding mechanism of the screw gear in the drilling tool.

Table 1 summarizes the statistical data of the residual drilling-resistance (shaft friction) and the residual feeding-force for both decayed and defect-free birch logs. The mean residual drilling-resistance observed on decayed log is 16.8 (amplitude in %), which is 12 percent lower than the mean shaft friction observed on defect-free log (19.2). Based on wood density data obtained from the disks, the density of decayed log is 17% lower than the decayed log. It is apparent that the lower wood density of the decayed log contributed to the decrease in shaft friction during the resistance drilling. The mean residual feeding-force for both decayed and defect-free logs is below 3%. This translates into a direct feeding force of less than 2.5 N. Coefficient of variation for normalized (COV_N) residual drilling resistance (shaft friction) in relation to the drilling depth (log diameter) is less than the standard COV which is consistent with the interaction between shaft friction and drilling depth. At the same time decreasing of COV_N for the residual feeding force is negligible.

Figure 3 shows the linear relationship observed between the drill bit shaft friction and the drilling depth for the defect-free yellow birch log, with a coefficient of determination (R^2) of 0.45. The empirical regression model indicates a 1.5% increase in friction for every 10 mm increase in drilling depth. Nutto and Biechele (2015) examined the drilling friction in several tropical species and the observed friction ranged from about 5% for Parana pine (*Araucaria angustifolia*) (with 30 cm in diameter) to about 65% for Pau Ferro (*Caesalpinia ferrea*) (with 32 cm in diameter). Among the species investigated, the Arueira (*Lithraea molleoides*) had a wood density of 725 kg/m³, which is close to the density of the defect-free yellow birch log in this study. When the empirical regression model for yellow birch was applied to Arueira, we obtained a friction of 19.7%, which is close to the actual friction 18% reported by Nutto and Biechele (2015). It is therefore hypothesized that the empirical friction model developed for a species can be used to predict the drilling friction at any point of the drilling path for the same species or a species with similar wood density.

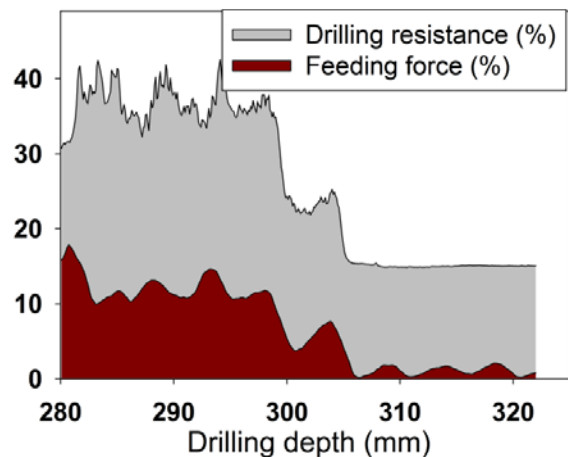


Figure 2—Typical drilling profiles obtained from the yellow birch logs (showing later portion), with drilling resistance displayed in grey shade and feeding force displayed in in dark shade.

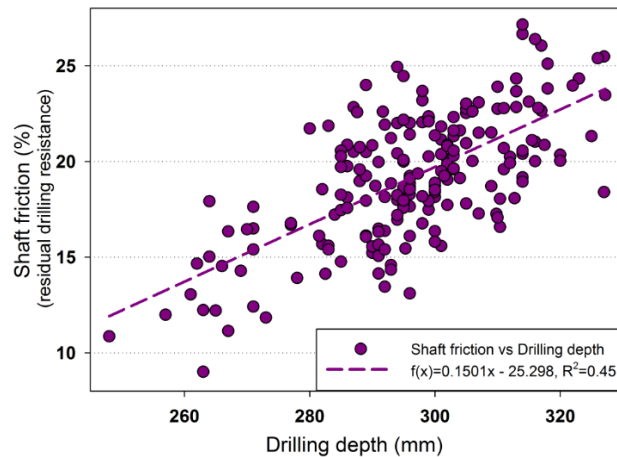


Figure 3—Relationship between shaft friction (residual drilling resistance, %) and drilling depth for the defect-free yellow birch log.

Table 1—Statistical data of residual drilling resistance (shaft friction) and residual feeding force for decayed and defect-free yellow birch logs.

Log sample	Residual drilling resistance (%) (Needle shaft friction)			Residual feeding force (%)			Basic wood density (kg/m ³)	
	Mean	COV ^a	COV _N ^b	Mean	COV	COV _N	Mean	COV
	Decayed log	16.8	22.2	20	1.65	90.9	89.1	589
Defect-free log	19.2	17.5	14.9	2.43	50.5	50.1	710	5.6

^aCOV – coefficient of variation; ^bCOV_N – coefficient of variation for normalized residual drilling resistance and residual feeding force

Sensitivity of Drilling Resistance Profiles to Internal Decay

Comparison of drilling-resistance profiles for decayed and defect free-logs is presented in Figure 4. The drilling resistance in defect-free log was relatively consistent within the first radius (0-150 mm), with a slight increase as the drill bit moved towards the pith; then it increased significantly in the second radius (150-300 mm). This might indicate nonlinearity of the drilling friction, but it could also be caused by the wood property differences between two halves of the log. Overall, the drilling-resistance profile in defect-free log did not show significant drops through the entire drilling path. In contrast, the drilling resistance in decayed log showed different patterns comparing to the defect-free log. The drilling-resistance profile exhibited sharp drops in the central area of the log, from 90 to 225 mm. The Janka hardness and wood density data obtained from the disk also showed significant reduction in the same central area, which indicated a good agreement with the resistance profile. With respect to direct interpretation of the resistance profile obtained from decayed log, the starting boundary of the central decay can be readily recognized by the sharp drop in drilling resistance at a drilling depth of about 90 cm. However, as the drill bit penetrated through the decay zone and reached the intact wood, the drilling resistance showed a gradual increase, not a sharp transition. Consequently, identifying the other side of the decay boundary might not be straightforward. The extent of the central decay can only be estimated approximately.

The accuracy of drilling-resistance profiles recorded in the resistance drilling tool is affected by the shaft friction. Although shaft friction are dependent of many factors as we discussed early, for green yellow birch logs/trees, a linear model of shaft friction in relation to drilling depth can be used to make a correction in original resistance profiles by subtracting the friction along the entire drilling path. Figure 5 shows the original resistance profile (1) superimposed with the adjusted resistance profile (2), as well as the original feeding-force curve for the decayed log. The adjusted resistance profile essentially had a pattern very similar to the original resistance profile. But from visual appearance, adjusted resistance profile had better contrast between decayed zone and intact wood. This may be an advantage in tree inspection. The feeding force curve for the decayed log also exhibited a similar pattern comparing to the resistance profiles (original and adjusted), but the contrast in amplitude between intact wood and decay zone is much smaller than those seen in the resistance profiles.

Both 3D surface and 2D contour graphs of the drilling resistance for the entire decayed log were created through approximation and interpolation of eight sets of the measured resistance profile (drilling no. 2 to no. 9) (Figure 6). In the graphs, low resistance values are highlighted by red colour, and high resistance values are highlighted by green colour. These graphs provide an overall assessment of the log condition and demonstrate resistance/wood density variations through the RL plane of the log.

Relationships between Drilling Parameters and Wood Properties

Figure 7 is the data plot of Janka hardness measured in the wood strips of the decayed log and wood density of the corresponding small segments cut from the strips. Regression analysis indicated a strong linear relationship between hardness and wood density ($R^2=0.79$), which is in agreement with the results reported in Forest Products Laboratory (2010).

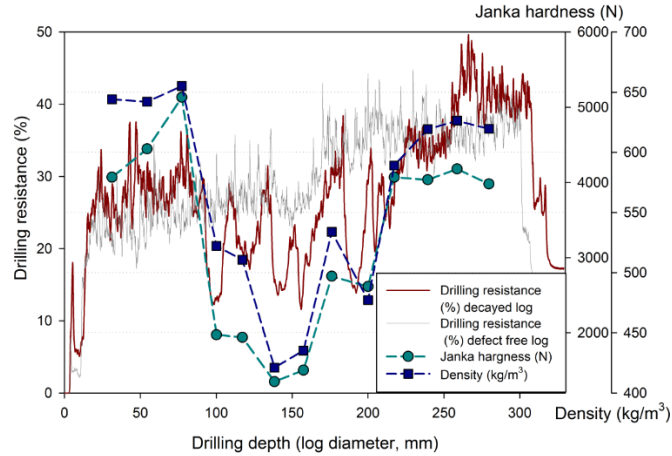


Figure 4—Comparison of the drilling resistance profiles for decayed and defect free yellow birch logs. Data points shows the distribution of Janka hardness and wood density along the drilling path for the decayed log.

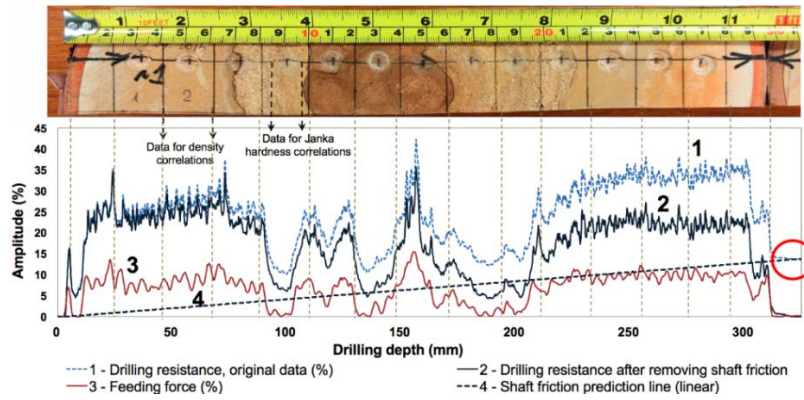


Figure 5—Resistance drilling profiles of the decayed yellow birch log and image of the wood strip cut along the drilling path (Disc no. 2).

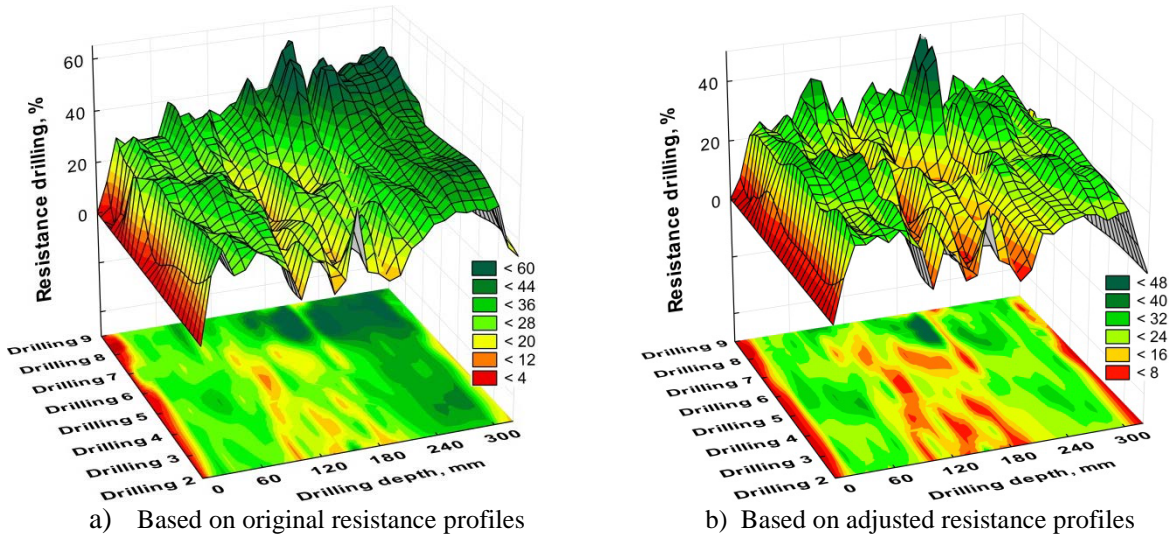


Figure 6—3D surface map and 2D contour map of drilling resistance for the decayed yellow birch log. a) Developed from the original resistance profiles; b) developed from the adjusted resistance profile.

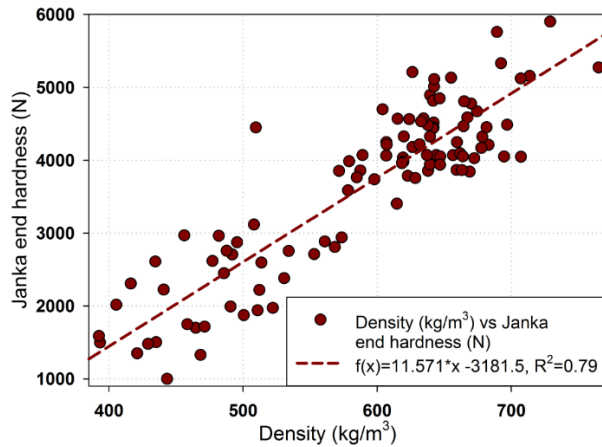


Figure 7— Relationship between hardness measured in the wood strips of the decayed yellow birch log and wood density of the corresponding segments cut from the strips.

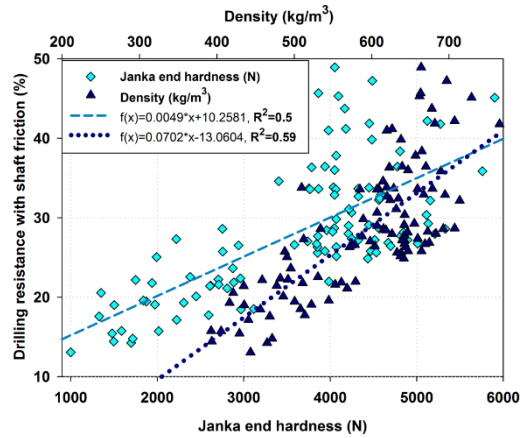


Figure 8— Relationships between the original drilling resistance (shaft friction included) measured in decayed log and hardness and wood density of the corresponding segments in the drilling path.

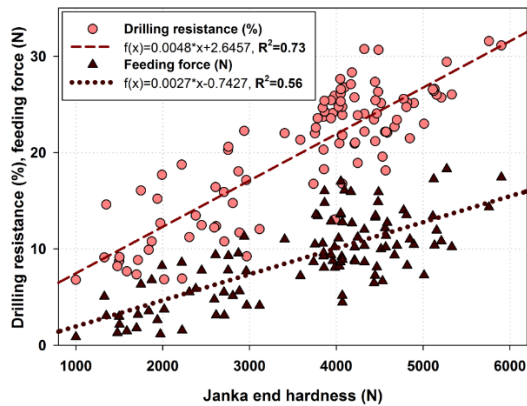


Figure 9— Relationships between drilling parameters (adjusted drilling resistance and feeding force) of the decayed log and the corresponding hardness.

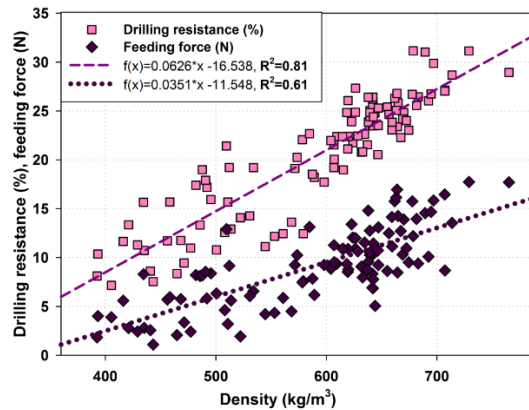


Figure 10— Relationships between drilling parameters (adjusted drilling resistance and feeding force) of the decayed log and the corresponding wood density.

Figure 8 shows the relationships between the original drilling-resistance (shaft friction included) measured in the decayed log and hardness and wood density of the corresponding segments in the drilling path. Regression analysis indicated positive linear relationships with a moderate strength ($R^2 = 0.5$ for hardness, $R^2 = 0.59$ for density).

Figure 9 shows the relationships between drilling parameters (adjusted drilling-resistance and feeding force) of the decayed log and the corresponding hardness. The adjusted drilling-resistance had a relatively strong correlation with hardness with a R^2 of 0.73, which is a significant improvement comparing to the original drilling resistance ($R^2 = 0.5$). Feeding force showed a moderate correlation with hardness ($R^2 = 0.56$).

Figure 10 shows the plots of the drilling parameters (adjusted drilling-resistance and feeding force) and the corresponding wood density for the decayed log. The adjusted drilling-resistance had a strong linear relationship with wood density with a R^2 of 0.81, which is a significant improvement comparing to the

original drilling resistance ($R^2 = 0.59$). Again, feeding force showed a moderate correlation with wood density ($R^2 = 0.61$).

Conclusion

In this study we characterized the drill bit shaft friction in resistance drilling green yellow birch logs through extensive laboratory experiments. It was found that a residual drilling-resistance existed after the drill bit cutting head exited the log. This residual resistance was caused by the friction between the drill bit shaft and the wood chips within the drilling hole and remained relatively constant as the drill bit continued feeding through. The mean shaft friction observed on the defect-free yellow birch log was 19.2% with a coefficient of variation of 17.5%. A linear relationship was found between shaft friction and drilling depth in the defect-free yellow birch log. The empirical regression model indicates a 1.5% increase in shaft friction for every 10 mm increase in drilling depth. The mean residual feeding force for both decayed and defect-free logs was below 3% (or less than 2.5 N).

The accuracy of drilling-resistance profiles recorded in the resistance drilling tool is affected by drill bit shaft friction. For green yellow birch logs, a linear model of shaft friction in relation to drilling depth can be used to make a correction to the original resistance profiles by subtracting the friction along the entire drilling path. The adjusted resistance profiles showed better contrast between decayed zone and intact wood than the original resistance profile, which could be an advantage in tree inspection.

The results also indicated that removing shaft friction from the original resistance profiles increased the prediction power of the drilling resistance as a nondestructive measure of wood density and hardness. Resistance data adjustment can be carried out directly on the resistance drilling tool by adding a data correction module or accomplished during post data processing. Feeding force parameter, although exhibited similar patterns with drilling resistance, has limited prediction power if it is used to assess wood density and hardness.

Acknowledgments

This research work was supported by the Council for International Exchanges of Scholars (CIES) Fulbright Visiting Scholar Program (Grant ID 68140222).

References

- Allison RB, Wang X (2015) Nondestructive testing in the urban forest. In: Ross RJ (ed) *Nondestructive Evaluation of Wood*, 2nd edn. General Technical Report FPL-GTR-238. U.S. Department of Agriculture, Forest Service, Forest Products Laboratory, Madison, WI, pp 77–86
- ASTM (2012) D 143 Standard methods of testing small clear specimens of timber. *Annual Book of ASTM Standards*. ASTM, Philadelphia.
- ASTM (2007) D4442 Standard test methods for direct moisture content measurement of wood and wood-base materials. *Annual Book of ASTM Standards*. ASTM, Philadelphia.
- Bershadskii AL, Tsvetkova NI (1975) *Rezanie drevesiny [Wood cutting]*. Minsk, 303 pp.
- Bouffier L, Charlot C, Raffin A, Rozenberg P, Kremer A (2008) Can wood density be efficiently selected at early stage in maritime pine (*Pinus pinaster Ait.*)? *Ann For Sci* 65(1): 106-113.

Chantre G and Rozenberg P (1997) Can drill resistance profiles (Resistograph) lead to within-profile and within-ring density parameters in Douglas-fir wood? In: Proceedings of CTIA – International Union of Forestry Research Organizations (IUFRO) International Wood Quality Workshop: Timber Management Toward Wood Quality and End-Product Value. Forintek Canada Corp., Sainte-Foy, Québec, Canada. pp 41–47.

Charette P, Lu P, Tang F, Zhang SY (2008) Evaluation of the resistograph for wood density estimate and the use of multi-trait selection index for genetic selection in jack pine. In: Proceedings of the 31st Meeting of the Canadian Forest Genetics Association: Adaptation and Conservation in the Era of Forest Tree Genomics and Environmental Change, Quebec City, Quebec, 25-28 August 2008. Edited by J.D. Simpson. Natural Resources Canada, Canadian Forest Service, Fredericton, N.B. p. 88.

Ceraldi C, Mormone V, Russo-Ermolli E (2001) Resistographic inspection of ancient timber structures for the evaluation of mechanical characteristics. Mater Struct 34: 59-64.

Eckard JT, Isik F, Bullock B, Li BL, Gumpertz M (2010) Selection efficiency for solid wood traits in *Pinus taeda* using time-of-flight acoustic and micro-drill resistance methods. Forest Sci 56(3): 233-241.

Forest Products Laboratory (2010) Wood handbook - Wood as an engineering material. General Technical Report FPL-GTR-190. Madison, WI: U.S. Department of Agriculture, Forest Service, Forest Products Laboratory. 508 pp.

Gantz CH (2002) Evaluating the efficiency of the Resistograph to estimate genetic parameters for wood density in two softwood and two hardwood species, MA thesis, North Carolina State University, 78 pp.
Gao S, Wang X, Wiemann MC, Brashaw BK, Ross RJ, Wang L (2017) A critical analysis of methods for rapid and nondestructive determination of wood density in standing trees. Annals of Forest Science. DOI 10.1007/s13595-017-0623-4.

Gao S, Wang X, Wiemann MC, Brashaw BK, Ross RJ, Wang L (2017) A critical analysis of methods for rapid and nondestructive determination of wood density in standing trees. Annals of Forest Science. DOI 10.1007/s13595-017-0623-4.

Görlacher R, Hättrich R (1990) Untersuchung von altern Konstruktionsholz - Die Bohrwiderstandsmessung. Bauen mit Holz 455-459.

Guller B, Guller A, Kazaz G (2012) Is Resistograph an appropriate tool for the annual ring measurement of *Pinus brutia*? In: Proceedings of the International Conference NDE Safety, Czech Republic, pp 89-94.

Gwaze D, Stevenson A (2008) Genetic variation of wood density and its relationship with drill resistance in shortleaf pine. Southern Journal of Applied Forestry 32(3): 130-133.

Isik F, Li B (2003) Rapid assessment of wood density of live trees using the Resistograph for selection in tree improvement programs. Can J Forest Res 33(12): 2426-2435.

Nutto L and Biechele T (2015) Drilling resistance measurement and the effect of shaft friction – using feed force information for improving decay identification on hard tropical wood. Gen. Tech. Rep. FPL – GTR – 239. In: Proceedings of the 19th International Nondestructive Testing and Evaluation of Wood Symposium, pp 154-161.

Park CY, Kim SJ, Lee JJ (2006) Evaluation of specific gravity in post member by drilling resistance test. Mokchaek Konghak 34(2): 1-9.

Rinn F (1990) Device for material testing, especially wood inspection by drill resistance measurements. German Patent 4122494

Rinn F, Schweingruber FH, Schar E (1996) Resistograph and X-ray density charts of wood comparative evaluation of drill resistance profiles and X-ray density charts of different wood species. *Holzforschung* 50(4): 303-311.

Rinn F (2012) Basics of micro-resistance drilling for timber inspection. *Holztechnologie* 53(3): 24-28.

Ross RJ, Brashaw BK, Wang X, White RH and Pellerin RF (2004) *Wood and Timber Condition Assessment Manual*, Forest Products Society, Madison, WI.

Sharapov ES, Chernov VY (2014) Sravnitel'nyi analiz sposobov opredeleniya plotnosti drevesiny s pomoshch'yu rentgenovskogo izlucheniya i ustroistva dlya izmereniya soprotivleniya sverleniyu [Comparative analysis of wood density techniques determination with using X-ray and device for drilling resistance measurements]. *Moscow State Forest University Bulletin – Lesnoy vestnik* 2(101): 89-95.

Sharapov E, Wang X, Smirnova E, Wacker JP (2015) Wear behavior of drill bit and its blunting effect on force parameters in drilling resistance measurement on wood. Poster presentation at the 19th International Nondestructive Testing and Evaluation of Wood Symposium, September 22-25, 2015. Rio de Janeiro, Brazil.

Wang SY and Lin CJ (2001) Application of the drill resistance method for density boundary evaluation of earlywood and latewood of *Taiwania* (*Taiwania cryptomerioides* Hay.) plantation wood. *Taiwan J For Sci* 16(3):196-199.

Wang SY, Chiu CM, Lin CJ (2003) Application of the drilling resistance method for annual ring characteristics: evaluation of *Taiwania* (*Taiwania cryptomeribides*) trees grown with different thinning and pruning treatments. *J Wood Sci* 49(2): 116-124.

Wang X and Allsion RB (2008) Decay detection in red oak trees using a combination of visual inspection, acoustic testing, and resisatnce microdrilling. *Arboriculture & Urban Forestry* 34(10): 1-4.

Zhang H, Guo Z, Su J (2009) Application of a drill resistance technique for rapid determining wood density. *Progress of Machining Technology. Key Engineering Materials* 407-408: 494-499.

Grading Round *Eucalyptus* Timber by Ultrasound

Mônica Ruy

PhD student, Laboratory of Nondestructive Testing - LabEND, School of Agricultural Engineering - FEAGRI - University of Campinas - UNICAMP, Campinas, São Paulo, Brazil – monica.ruy@hotmail.com.

Raquel Gonçalves

Professor, LabEND - FEAGRI, UNICAMP, Campinas, São Paulo, Brazil, raquel@agr.unicamp.br

Douglas Pereira Moraes

Undergraduate student, LabEND - FEAGRI, UNICAMP, Campinas, São Paulo, Brazil, douglaspm1409@gmail.com

Rafael Mansini Lorensani

Doctor, LabEND - FEAGRI, UNICAMP, Campinas, São Paulo, Brazil,

Abstract

The use of logs in its original shape, as round timber, has been considered economically competitive and sustainable, turning the development of techniques that allow their classification important. The objective of this research was to evaluate the viability of the use, for round timber, the Brazilian's ultrasonic lumber grading standard. Ultrasound tests were performed in round wood at green and air-dry equilibrium moisture content. Static bending tests were performed only under the equilibrium moisture content. In addition to the ultrasound and bending tests, the diameters of the round wood were measured. The diameter showed a negative correlation with the acoustic and static parameters. Although it is necessary to validate the conclusions with a larger data set, the results indicate that the classes proposed by the Brazilian standard can be used to grading round *Eucalyptus* timber applying velocity correction coefficient according to the diameter of the pieces.

Keywords: strength in bending, modulus of elasticity in bending, wave propagation, logs.

Introduction

Wood grading is extremely important for the commercialization, because it facilitates distinction between pieces with higher or lower incidence of defects and greater or lower strength and /or stiffness. To sort timber according to their defects and properties make the material more valuable, because it allows the material to be used according to its characteristics. Due to the high natural variability of timber, the use of tables containing average of properties is important in the design process, but it does not solve the problem of the acquisition and use of timber with compatible strength with a project. To solve this problem, it is necessary that all the pieces are mechanically graded.

Wave propagation techniques have been studied to be applied in freshly cut logs in order to sort them before sawing process (Rais *et al* 2013; Amishev and Murphy 2008; Wang *et al* 2007; Carter *et al* 2005; Pelizan 2004; Tsehayve 2000; Sandoz 1994). These techniques have become an important part of the wood grading process.

An economic analysis was made by Carter *et al* 2005 and it indicated that there is an increase of 5% in the yield of the production and the commercialization of the structural wood when a preliminary analysis through acoustic tests is carried out. Likewise, pre-grading with longitudinal acoustic waves of 154 trees (*Douglas-fir*), from two experimental forests of Southern of Germany, showed that there was a mean increase of 10% in the yield for structural boards production (Rais *et al* 2013). The

methodology was performed by Rais *et al* (2013) at different levels of wood processing (standing trees, long logs and beams).

In standards, usually mechanical grades of wood are established according to bending tests performed on structural pieces (modulus of elasticity and bending strength). Other wood properties (compression, tension, shear, etc.) are proposed by correlations with values obtained in bending. The general procedure to propose mechanical grades for structural wood consists to sort pieces into visual and mechanical classes according to data obtained by nondestructive methods (classification machines, wave propagation methods, etc.). Visual and nondestructive parameters are usually associated with modulus of elasticity (E_M) and strength (f_M) obtained in static bending.

In Brazil, NBR 15521 (2007) specifies requirements for the use of ultrasound technique in grading sawn timber and defines criteria for this sorting based on acoustic parameters (velocity and stiffness coefficient C_{LL}). This standard was proposed based on ultrasonic and bending tests of sawn timber from tropical species with about 45-years-old. Considering the possibility of structural uses for wood from planted and fast-growing forest in Brazil, Lorensani 2013 evaluated the possibility of using NBR 15521 to grade timber from 4 *Eucalyptus* species. The author concluded that applying a 0.85 reduction coefficient to the velocity values obtained in the ultrasound tests, rendered the classes proposed by Brazilian standard appropriate for grading lumber.

The log resistance, low energy consumption for its processing, availability and easy handling make the round wood a highly competitive and sustainable material (Calil Jr. and Brito, 2010) and can be directly used as structure (poles, beams, columns etc.). Considering these issues, this research intends to contribute to provide basis for the discussion of important aspects to propose mechanical classes for round timber.

Material and Methods

We used three species of eucalyptus (*Eucalyptus grandis*, *Eucalyptus cloeziana* and *Eucalyptus saligna*) that are usual for structural uses in São Paulo, Brazil. For each species, we use 18 round pieces approximately 3.6 m in length. These pieces were segregate in 3 diameters ranges. Different diameters were adopted to evaluate the influence of this parameter on the propagation of ultrasound waves, and consequently, in the grades proposal.

Non-destructive tests were performed with ultrasound equipment (USLab, Agricef, Brazil) and 45-kHz longitudinal transducers. The measurements were made directly and parallel to the fibre (lengthwise). The first ultrasound measurement of the round pieces was made at saturated moisture content (MC), which was defined in this study as MC greater than 30%.

The round pieces were stored for drying in a place protected from weather. When the measurements indicated a MC of approximately 12%, the pieces were tested again via ultrasound and then static bending tests were performed in a frame with 500 kN load capacity. The round pieces are supported at two points and loads were applied at thirds of the span (EN 408).

After static bending test, three discs 100 mm thick were removed along the length of each log (base, middle and top). The discs were used to determine the density and actual MC of the logs. The moisture data were used to verify that the pieces had MCs of $12 \pm 4\%$, which was considered as equilibrium condition (Íñiguez-González *et al* 2015).

The velocity (V_{Eq}) and the density (ρ) obtained under equilibrium conditions were used to calculate C_{LL} using Equation 1, as follows:

$$C_{LL} = \rho \times V_{Eq}^2 \times 10^{-6} \quad \text{Equation 1}$$

where C_{LL} is expressed in MPa; ρ is the apparent density of the wood at EMC ($12\% \pm 4\%$), expressed in kg.m^{-3} , and V_{Eq} is the wave propagation velocity in the wood at the EMC ($12\% \pm 4\%$), expressed in m.s^{-1} .

From the bending tests, modulus of elasticity (E_M) were calculated according to EN 408.

For sawed lumber classification, Brazilian standard (NBR 15521 2007) uses, as an input parameter, the velocity under saturated condition (V_{sat}) or the stiffness coefficient (C_{LL}) obtained at equilibrium MC. In the classes proposed by NBR 15521 (2007) one of these acoustic parameters are used to predict the range of values expected to the modulus of elasticity in static bending (E_M) of the tested piece. Thus, to verify the appropriateness of the use of these standard classes to round timber, the V_{sat} and the C_{LL} obtained in the ultrasound tests were used to predict the ranges of E_M .

To evaluate the pieces individually, the actual value of E_M (obtained in the bending tests) was compared to the range of values predicted in NBR 15521 (2007) using V_{sat} and C_{LL} . The result of the comparison was classified into one of the following three categories proposed by Kretschmann and Hernandez (2006):

- Category 1 – The E_M value obtained in the test is within the expected interval by the grading;
- Category 2 – The E_M values obtained in the test are lower than those expected by the grading;
- Category 3 – The E_M values obtained in the test are higher than those expected by the grading.

Results in Categories 1 and 3 were considered hits using the analysis of Kretschmann & Hernandez (2006) because it was expected that the use of characteristic curve (using model prediction errors) for the calculation of the classes in classification standards would consequently yield elevated assignments to Category 3, which would indicate an underestimation of the stiffness, representing an error in favor of safety but against economics aspects. The results in Category 2 were considered errors because they indicated an overestimation of the stiffness; therefore, they represented a safety error.

Results and discussions

The apparent densities obtained for *E. cloeziana* and *E. saligna* under the equilibrium condition, 822 and 731 kg.m^{-3} , respectively (Table 1), were very close to the average values indicated by the Brazilian standard (NBR 7190 1997). In the present study, *E. grandis* had higher density, 640 kg.m^{-3} (Table 1), than that indicated in NBR 7190 (1997).

NBR 7190 (1997) does not present strength or stiffness values obtained in bending, nor does it present values of properties for round timber. For *E. cloeziana*, there are reference values in Molina (2009) *apud* Calil Jr. & Brito (2010) for round timber, indicating a modulus of elasticity of 24,660 MPa, which is close to the average value obtained in the present study (Table 1). This value is approximately 1.7-fold the value indicated in the table of properties from NBR 7190 (1997) for the modulus of elasticity in compression of sawed lumber for this specie. Ranta-Maunus (1999) suggested that the properties obtained in round timber are much higher than those obtained in sawed lumber, which could explain the superiority of the stiffness values obtained for the species evaluated in the present study and in the study by Calil Jr. & Brito (2010).

Eucalyptus cloeziana had pieces with highly variable diameters. Therefore, its E_M was the most variable (Table 1). Using asymmetry and kurtosis (between -2 and +2), the frequency distribution for all of the parameters was considered normal (Table 1).

Table 1 - Average parameters and statistics for the saturated velocity (V_{sat}), the coefficient of rigidity (C_{LL}), the modulus of elasticity (E_M) in static flexion of the diameter and the apparent density under the equilibrium condition (ρ) for the 3 tested species.

Species	Parameters	V_{LLsat} $m.s^{-1}$	C_{LL} MPa	E_M MPa	Diameter mm	ρ $kg.m^{-3}$
<i>Eucalyptus grandis</i>	Average	4,560	18,452	15,844	207	751
	CV (%)	6.7	9.1	38.3	24.6	7.0
	Asymmetry	-0.41	0.54	-0.13	0.95	-1.17
	Kurtosis	-1.14	-1.03	-0.80	-0.69	0.27
<i>Eucalyptus cloeziana</i>	Average	4,517	23,431	20,091	151	820
	CV (%)	8.7	17	55.0	58.0	7.0
	Asymmetry	0.39	1.75	-0.76	0.62	-0.35
	Kurtosis	-0.54	0.47	0.08	-1.44	-0.83
<i>Eucalyptus saligna*</i>	Average	4,148	17,470	13,003	182	740
	CV (%)	10.9	12	20.0	32.0	14.0
	Asymmetry	0.11	-0.40	-0.37	-1.05	-1.08
	Kurtosis	-0.43	-1.12	-0.54	-0.90	-0.40

* Obtained from the velocity measured under a moisture condition (U) below saturation point (V_U) and the density under the same moisture condition (ρ_U), using the equation from the Brazilian standard NBR15521 (2007): $V_{sat} = -1745 + V_U + 16 MC + \rho_U$.

Individual analyses of the pieces according to the categories proposed by Kretschmann & Hernandez (2006) indicated that many of the moduli of elasticity had been overestimated (Category 2) with the use of the classification by V_{sat} or by C_{LL} (Figures 1, 2 and 3).

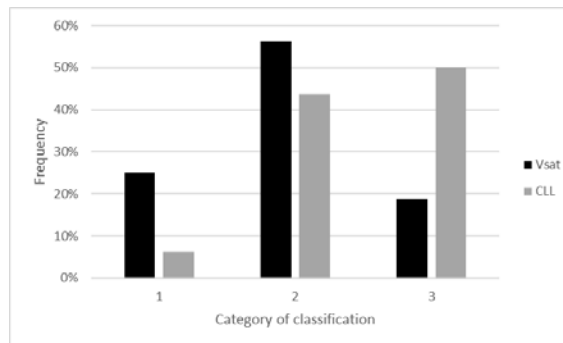


Figure 1. Framing categories of sorting by velocity in saturated condition (V_{sat}) and by stiffness coefficient (C_{LL}) for the batch of wood composed by *Eucalyptus grandis*. Category 1 - Actual values within the range expected by classification; Category 2 - Real values lower than expected by classification and Category 3 - Real values higher than expected by classification.

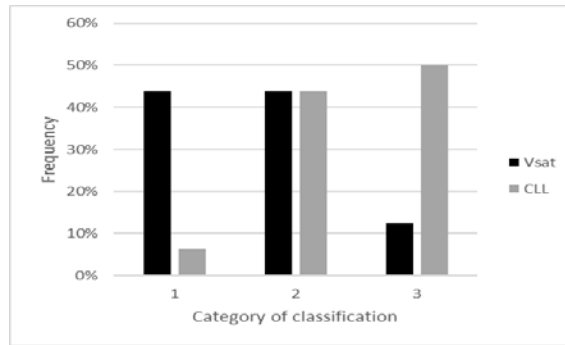


Figure 2. Framing categories of sorting by velocity in saturated condition ($V_{LL,sat}$) and by stiffness coefficient (C_{LL}) for the batch of wood composed by *Eucalyptus cloesiana*. Category 1 - Actual values within the range expected by classification; Category 2 - Real values lower than expected by classification and Category 3 - Real values higher than expected by classification.

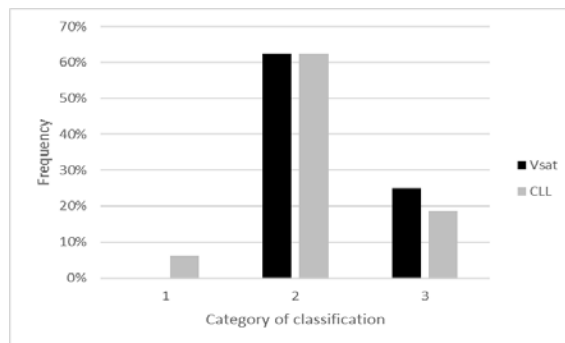


Figure 3. Framing categories of sorting by velocity in saturated condition ($V_{LL,sat}$) and by stiffness coefficient (C_{LL}) for the batch of wood composed by *Eucalyptus saligna*. Category 1 - Actual values within the range expected by classification; Category 2 - Real values lower than expected by classification and Category 3 - Real values higher than expected by classification

Considering the 3 lots used in the present study, the diameter of the round pieces was significantly correlated (P -value < 0.05) with the V_{sat} ($R = -0.51$), C_{LL} ($R = -0.45$) and E_M ($R = -0.78$). In all cases, an increase in the diameter caused a reduction in the acoustic and static parameters. This result indicates that it is necessary to consider the diameter class of the round pieces in sorting process (Table 2).

Table 2 – Groups of logs by diameters range.

Group	Diameter range (mm)
1	50 to 109
2	110 to 169
3	170 to 229
4	>230

For each round piece, the expected saturated velocity and stiffness coefficient were calculated according to the classification range based on the modulus of elasticity obtained in the static bending test (E_M). Because the calculations involved a range of values, the maximum value of the range was adopted for the saturated velocity and for the stiffness coefficient considering the adequate framework of the E_M . With this procedure, the relationships between the expected velocity and the actual velocity obtained in the test were calculated. Using the average values of these relationships for each diameter group, velocity correction factors (under the saturated and equilibrium moisture conditions) were

proposed for the diameter groups of the round pieces (Table 3). Consistent with the previously discussed behavior, the correction coefficient decreased with the increase diameter (Table 3)

Table 3. Velocity correction coefficients (under the saturated and equilibrium conditions) according to the diameter group of the round piece.

Diameter group*	Velocity correction factor
1	0.85
2	0.85
3	0.80
4	0.70

Diameter group 1: diameters between 50 and 109 mm; Diameter group 2: diameters between 110 and 169 mm; Diameter group 3: diameters between 170 and 229 mm; and Diameter group 4: diameters greater than 230 mm.

Applying the correction coefficients (Table 3) to the saturated and equilibrium velocities (which affected the calculation of the stiffness coefficient) led to a significant reduction of pieces in Category 2 (against safety). The sorting varied among species; however, approximately 95% of the pieces would be sorting in favor of safety using the velocity under the saturated condition and 93% using the stiffness coefficient (Table 4).

Table 4 - Average framework percentages in the grading categories for the 3 species of *Eucalyptus* with the application of the velocity reduction coefficients according to the diameter range.

Category	V _{sat}	C _{LL}
1	23%	9%
2	5%	7%
3	72%	84%

Category 1 – actual values within the interval expected by the grading; Category 2 – actual values lower than those expected by the grading; and Category 3 – actual values higher than those expected by the grading.

*Diameters less than 169 mm – coefficient 1.0; diameters between 170 and 229 mm – coefficient 0.80; and diameters larger than 230 mm – coefficient 0.70.

The velocity under the saturated condition is a simple and direct parameter for grading wood by ultrasound, whereas the stiffness coefficient depends on knowledge of density. The velocity under the saturated condition showed, on average, more pieces in Category 1 (correct range) and fewer in Category 2 (against safety) (Table 4). This result confirms that, for round *Eucalyptus* timber, the saturated velocity as input in the ranges classes of the Brazilian standard (NBR 15521 2007) would be the most appropriate and simple means of classification.

Conclusions

In the present study, we evaluated the viability of applying the Brazilian ultrasound-based grading standard for round wood *Eucalyptus* timber. The sorting parameters analyzed were the velocity under saturated condition and the stiffness coefficient, which was calculated with the velocity and the density under equilibrium condition ($12 \pm 4\%$). Although it is necessary to validate the conclusions with a larger data set, the results indicate that:

- The diameter of the round timber is associated with its acoustical and mechanical properties. Considering this association, the gradung of round timber must consider the diameter of the pieces.
- The velocity under saturated condition is the simplest and most appropriate parameter for the acoustical classification of round *Eucalyptus* timber.

- The classes proposed by the Brazilian standard (NBR 15521 2007) can be used in round Eucalyptus timber grading by applying reduction coefficient to the velocity. The correction coefficients decrease as the diameters of the round wood increase.

Acknowledgments

We thank FAPESP for financially supporting research group (Proc. 2012 / 22599-9) and for the PhD scholarship (Proc. 2011 / 00904-1). We also thank CNPq for the Master's scholarships and undergraduate research.

References

- Amishev, D.; Murphy, G. E. "In-forest assessment of veneer grade Douglas-fir logs based on acoustic measurement of wood stiffness". *Forest Products Journal*, 58, 42-47. 2008.
- Associação Brasileira De Normas Técnicas. NBR 15521: Ensaio não destrutivo — Ultra-som — Classificação mecânica de madeira serrada de dicotiledôneas. Rio de Janeiro, 2007.
- Associação Brasileira de Normas Técnicas. NBR 7190: Projeto de estruturas de madeira. Rio de Janeiro, 1997.
- Calil Jr., C.; Brito, L.D. "Manual de Projeto e Construção de Estruturas com Peças Rolijas de Madeira de Reflorestamento". Universidade de São Paulo, Escola de Engenharia de São Carlos, 2012.
- Carter, P.; Briggs, D.; Ross, R. J.; Wang, X. "Acoustic testing to enhance western forest values and meet customer wood quality needs". *Productivity of Western Forests: A Forest Products Focus*, 121-129, 2005.
- European Standards. EN 408: Structural timber and glued laminated timber. Determination of some physical and mechanical properties, 2010.
- Íñiguez-González G., Arriaga, F., Esteban M., Llana, D.F. "Reference conditions and modification factors for the standardization of nondestructive variables used in the evaluation of existing timber structures". *Constr Build Mater*, 2015
- Kretschmann, D.; Hernandez, R. "Grading timber and glued structural members". *Primary wood processing: principles and practice*. Dordrecht, Springer, 339-390, 2006.
- Lorensani, R. G. M. "Classificação de peças estruturais de eucalipto utilizando ultrassom". Dissertação (Mestrado) - Curso de Engenharia Agrícola, Universidade Estadual de Campinas, Campinas, 2013.
- Molina, J.C. "Relatório final da caracterização dos eucaliptos". Projeto: Centro de Educação Ambiental (CEAM), Votorantin Metalurgia, Unidade Florestal, 2009.
- Pelizan, T.R. "Estudo de propriedades mecânicas de peças roliças de Eucalipto Citridora utilizando a técnica de ultra-som". Dissertação (Mestrado) – Universidade de São Paulo, São Carlos, 2004.
- Rais, A., Pretzsch, H, & Van de Kuilen, j. "Roundwood pre-grading with longitudinal acoustic waves for production of structural boards". *European journal of wood and wood products*, 72, 87-98, 2013.
- Ranta-Maunus, A. "Round Small-diameter timber for constructions". Final report of project FAIR CT-95-0091. Espoo 1999, Technical Research Centre of Finland, VTT Publications 383, 191, 1999.

Sandoz, J.L. "Ultrasound applications to structural timber". Pacific Timber Engineering Conference – PTEC'94, Gold Coast, Australia, 740-744, 1994.

Tsehayve, A.; Buchanan, A.H.; Walker, J.C.F. "Sort of logs using acoustics". Wood Science and Technology, 34, 337-344, 2000.

Wang, X. et al. "Acoustics assessment of wood quality of raw forest materials". Forest Products Journal, 57, 6-14, (Maio) 2007.

Detecting Internal Defects in Hardwood Logs Using Ultrasonic Tomography Based on Distorted Born Iterative Algorithms

Feng Xu *

College of Information Science and Technology, Nanjing Forestry University, Nanjing, China, xufeng@njfu.com.cn

Yunfei Liu

College of Information Science and Technology, Nanjing Forestry University, Nanjing, China, lyf@njfu.com.cn

Dan Zhang

College of Information Science and Technology, Nanjing Forestry University, Nanjing, China, zhangdan@njfu.edu.cn

Ling Jiang

College of Information Science and Technology, Nanjing Forestry University, Nanjing, China, jiangling@njfu.edu.cn

Xiping Wang

USDA Forest Service Forest Products Laboratory, Madison, Wisconsin, USA, xwang@fs.fed.us

* Corresponding author

Abstract

Accurate determination of location and nature of internal defects in hardwood logs can provide significant benefit to the wood industry in terms of making accurate quality assessments, making accurate volume estimates, and optimizing utilization of hardwood resources. The objective of this study was to develop an ultrasonic tomography technique based on an inverse scattering theory for accurately detecting internal defects in hardwood logs. Poplar and camphorwood log sections were obtained and subjected to multipath ultrasonic measurements. Wave equations in scattered field and whole field were established based on the characteristics of ultrasonic wave propagation. The equations were discretized using the method of moment and then reconstructed using the distorted Born iterative (DBI) and Born iterative (BI) algorithms. The resulting tomograms showed high contrast between severely defected areas (such as a void) and the surrounding area. A defect was detectable in tomogram images when the defect area exceeded 5% of the cross section. Both location and size of internal defects in logs can be detected using ultrasonic tomography. Compared with acoustic tomography, ultrasonic tomography has greater accuracy because of the high frequency and short wavelength.

Keywords: Ultrasonic tomography, internal defect, inverse scattering, log, scattered field, inversion algorithm

Combining Acoustic and Laser Scanning Methods to Improve Hardwood Log Segregation

Xiping Wang

USDA Forest Service, Forest Products Laboratory, Madison, Wisconsin, USA, xwang@fs.fed.us

Ed Thomas

USDA Forest Service, Northern Research Station, Princeton, West Virginia, USA, ethomas@fs.fed.us

Feng Xu

Yunfei Liu

College of Information Science and Technology, Nanjing Forestry University, Nanjing, China, xufeng@njfu.com.cn, lyf@njfu.com.cn

Victor Krause

Natural Resources Research Institute, University of Minnesota Duluth, Duluth, Minnesota, USA, vkrause@d.umn.edu

Brian K. Brashaw

Robert J. Ross

USDA Forest Service, Forest Products Laboratory, Madison, Wisconsin, USA, bbrashaw@fs.fed.us, rjross@fs.fed.us

Abstract

The objective of this research was to examine the technical feasibility of combining acoustic wave data with high-resolution laser scanning data to improve accuracy of hardwood log defect detection and segregation. Using acoustic impact testing and high-resolution laser scanning techniques, 21 yellow-poplar logs obtained from the central Appalachian region were evaluated for internal and external defects. These logs were then sawn into boards, and the boards were visually graded based on National Hardwood Lumber Association grading rules. The response signals of the logs from acoustic impact testing were analyzed through moment analysis and continuous wavelet transform to extract time domain and frequency domain parameters. The results indicated that acoustic velocity, time centroid, damping ratio, as well as the combined time and frequency domain parameters are all effective quality predictors for segregating low-end logs. Acoustic data combined with high-resolution laser scanning data provide a more complete picture of the log in terms of size, shape, surface defects, and degree of soundness. Indications of “soundness” in a particular log allow the internal prediction system to flag suspicious defects as potentially unsound. Thus, a combined system would be able to discriminate much more exactly with respect to log quality and potential lumber recovery than either method independently.

Keywords: acoustic velocity, damping ratio, impact testing, laser scanning, log defects, wavelet analysis, yellow-poplar

Introduction

The quality of hardwood logs varies widely within species, harvest site, and even the same tree. Holes, knots, wounds, and other growth defects on logs decrease the strength and appearance of any resulting products and thus decrease the value of the log and its products (Carpenter et al. 1989). The location, type, and size of defects on hardwood logs dictate the potential grade and value of the resulting lumber. Hardwood lumber is bought and sold using National Hardwood Lumber Association (NHLA) grades reflecting the value of each board. The fewer the defects, the greater the length and width of clear areas, which results in higher lumber grade and value. Hardwood log sawing begins with the log face that is clearest and will yield the highest valued boards. The sawyer attempts to saw the log such that any defects will be on the edges of boards. Such defects can then be edged from the sides of the board to make a higher valued board. Thus, scanning systems that find defects on and inside hardwood logs could dramatically improve the sawing process and the grade and value of sawn lumber.

Another important reason for early defect detection in hardwood logs is to remove logs from the processing stream that have little or no profitability. This concept is commonly known as the “break-even log” because processing a log with quality lower than the break-even log results in a loss for the company. Ideally, logs that give no real financial return from processing should be sold to other processors that can economically process these logs into products such as railroad ties, pallet lumber, pulp, fuel, or other similar products to realize target profit maximization.

Research in the field of nondestructive testing and evaluation of wood has resulted in an array of tools for detecting internal defects. Technologies such as X-ray, computed tomography (CT), and nuclear magnetic resonance (NMR) offer cross-sectional images with sufficient details but are not cost-effective for hardwood mills and are too slow to be considered suitable for on-line implementation (Wagner et al. 1989, Chang 1992, Guddanti and Chang 1998, Li et al. 1996, Bhandarker et al. 1999). Laser scanning, however, is an inexpensive, fast, and accurate method of measuring log diameter, length, and volume. As a by-product, the scanning systems measure the crook, sweep, and eccentricity of the log to a fraction of a millimeter. In addition, most surface defects regarded as degrade defects by the Forest Service grading rules are detected during laser data image processing. This permits logs that have been laser-scanned to be sorted not only by diameter and length but by quality as well. A high-resolution laser scanning system has been developed by the USDA Forest Service (Thomas et al. 2006, 2008). This system shows promise for improving internal defect predictions and greatly improving lumber value. This system, however, has some limitations on predicting unsound areas within a log based solely on solid-appearing surface defects.

Acoustic wave methods use a mechanical impact to generate low-frequency stress waves that propagate longitudinally through a log. Then, the reverberation of the waves within the log are recorded and analyzed. At the microstructure level, energy storage and dissipation properties of the log are controlled by orientation of wood cells and structural composition, factors that contribute to stiffness and strength of wood. Such properties are observable as frequency of the wave reverberation and rate of wave attenuation. Research has shown that propagation velocity of acoustic waves in wood is a good predicting parameter for wood deterioration caused by any wood decay mechanism (Pellerin et al. 1985, Wang et al. 2004). Commercial acoustic tools are now widely accepted in the forest products industry for on-line quality control (structural lumber, veneer) and field or in-plant segregation of incoming softwood logs (Harris et al. 2002; Carter et al. 2005; Wang et al. 2007, 2013; Wang 2013).

Acoustic waves and laser scanning methods operate under different principles. Each addresses the weaknesses or inabilities of the other. The main objective of this study was to determine the technical feasibility of combining acoustic wave data with high-resolution laser scanning data to improve the accuracy of defect detection and quality assessment in hardwood logs.

Materials and methods

Materials

A random sample of 15 yellow-poplar (*Liriodendron tulipifera*) trees were harvested from a Mead WestVaco leased and managed forest near Rupert, West Virginia, USA, in the central Appalachian region in late January 2015. Each tree was bucked to commercial lengths with 3 to 5 logs being cut from each tree, resulting in a total of 52 logs. All logs were tagged and transported to the Forest Service wood laboratory located in Princeton, West Virginia, USA, for laboratory scanning and testing. From visual observation, these logs ranged in quality level. Some of the logs had very obvious rot after bucking, some had deeply grown wounds with significant encapsulated decay pockets, and some were very high quality.

Physical diagramming and 3D laser scanning

The yellow-poplar logs were first put on a rack for physical diagramming of all surface defect indicators shortly after arriving at the lab. All surface defects were manually located and measured according to the characteristics as defined in Carpenter et al. (1989). For each log, the following information was recorded to create a ground-truth defect map: defect type, surface width (across grain) and length (along grain), growth rate, bark thickness, and surface height rise. Photos were also taken of each log for visual documentation.

A high-resolution laser scanner (Thomas and Thomas 2011) was then used to scan each log to obtain measurements, shape, and surface data. This log scanning system electronically digitizes the surface of logs with a scan line every 1.59 mm (0.0625 in.) along the length. Each scan line describes the circumference of the log and consists of 250 to 450 points, depending on the size of the log. At each reference point, the scanner records the laser energy reflected from the surface as 10-bit grayscale value. Average resolution around a log's circumference is 8 points per inch. This resolution is significantly higher than the scanner currently used in sawmills in which typically one scan line every 30 to 60 cm (12 to 24 in.) is used. Figure 1 shows the laser scanning system and an example of a 3D rendering of log data using the laser energy data for false color. The log shape as well as defect positions and relative sizes are easily discerned.

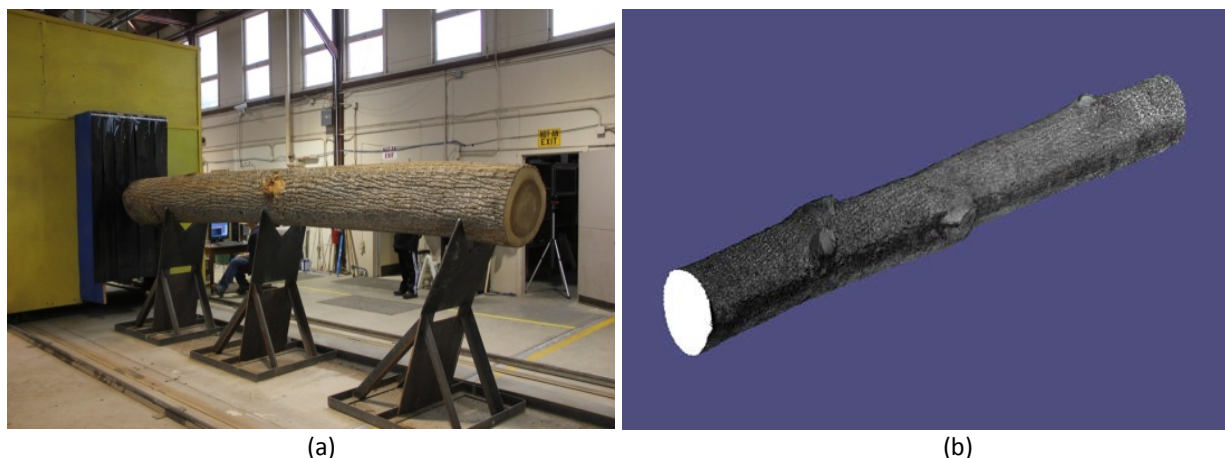


Figure 1—Laboratory laser scanning of yellow-poplar logs: (a) high-resolution laser scanning system; (b) high-resolution scanned imagery of yellow-poplar log (log no. 1161).

Acoustic impact test

Following physical diagramming and laser scanning, each log was placed on the ground and acoustically tested to obtain nondestructive parameters for potential detection of internal defects. An acoustic impact test was conducted in two different ways: (1) using a resonance acoustic tool to directly measure the acoustic velocity of each log and (2) using a laboratory impact testing system to obtain and record the response signals from each log following a mechanical impact. All acoustic tests were conducted under a condition of 21 °C (70 °F) and 50% relative humidity.

A hand-held resonance acoustic tool (Hitman HM200, Fibre-Gen, Inc., Auckland, New Zealand) was used to directly measure the acoustic velocity of each log. Following a hammer impact, the HM200 tool immediately processes the received acoustic signals through the Fast Fourier Transform (FFT) program built into the tool and calculates log acoustic velocity (V) based on the resonant frequency and log length:

$$V = 2 f_n L/n \quad (1)$$

where f_n is the n th harmonic frequency (Hz) of the response signal, L is the full length of a log, and n is the order of harmonic frequency.

To collect the response signals from each log, a sensor probe (Fakopp spike sensor, Fakopp Enterprise Bt., Agfalva, Hungary) was inserted into the end grain at the log end (close to the center). The impact acoustic waves were generated through a 5.44-kg (12-lb) sledge hammer blow on the opposing end, and the response signals were recorded through a data acquisition card (NI 5132) connected to the laptop, with a sampling frequency of 20 kHz and a sampling length of 1,000 points.

Sawing and visual grading

After laboratory scanning and testing, 21 logs were selected and sawn into boards using a portable sawmill. This subsample of logs was systematically selected based on visual assessment and resonant acoustic testing results such that they represent the quality range of the 52 logs. The resulting boards were visually graded according to NHLA rules (NHLA 2015).

Data processing and analysis

Laser scan data

The laser scan data of each log was processed by a defect detection system developed to locate severe defects on hardwood logs (Thomas and Thomas 2011, 2013). As an example, Figure 2 presents defect detection results for log no. 1161. This is the same log shown in Figure 1. The defect detection begins by fitting a circle to each laser scan line. Next, a residual image is generated using the residual, or distances between the fitted circle and circular scan line (Fig. 2a). In the residual image, bumps or high spots are presented as lighter gray, whereas low areas, such as holes, are shown as darker gray. Performing a contour analysis on the residual image yields a contour map (Fig. 2b) that defines the bumps and depressions that correspond to defective areas, for example, severe log degrade defects. An expert system was developed to process the contour map and recognize, classify, and measure the defective areas. Figure 2c is the graphical output from this final detection step. The sawing process for each log was also replicated using the RAYSAW sawing simulator. The size and positions of internal defects were estimated using the models developed by Thomas (2008, 2013). These methods use the size and type of the surface indicator to predict the size and location of the internal defect. When RAYSAW processes a log, it reports the overall shape of each board, as well as the positions and sizes of all predicted defects that fall on the board faces.

Acoustic wave data

A series of physical and acoustic properties of the logs were obtained and used as potential quality indicators for predicting the soundness of the logs and grade yields of the resulting boards. The predicting parameters we examined included acoustic velocity (V), dynamic modulus of elasticity (E_d), time centroid

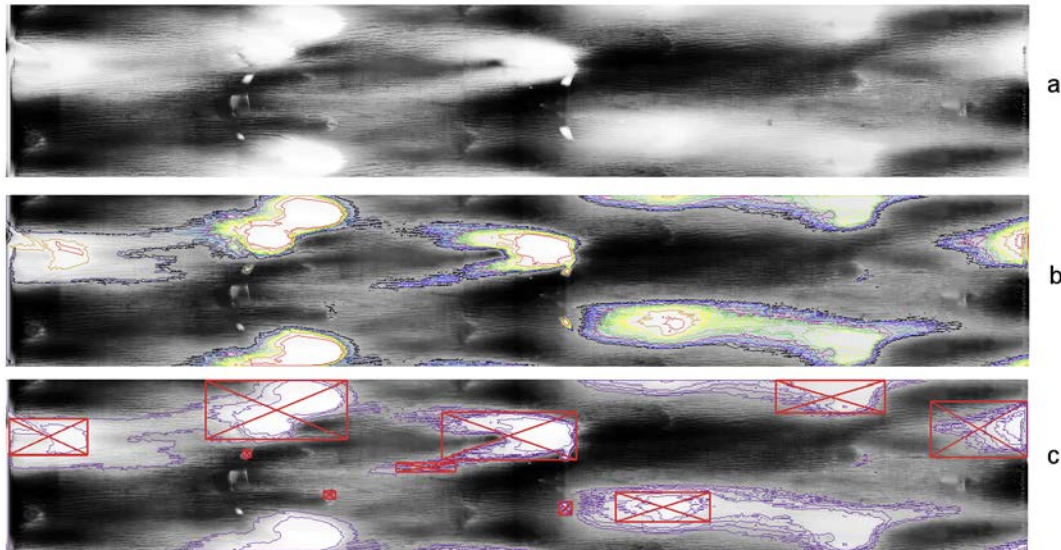


Figure 2—Defect detection results for log no. 1161: (a) residual image generated; (b) image resulting from contour analysis of residual image; (c) defects detected in contour map are identified using red boxes.

(T_c), and damping ratio (ζ), as well as two combined parameters of the response signals (Wang et al. 2016). The following procedures were followed in acoustic data analysis:

- 1) Compute dynamic modulus of elasticity of the logs using one-dimensional wave equation:
 $E_d = \rho V^2$ (2)
- 2) Determine time centroid (T_c) of the response signals through first moment analysis;
- 3) Perform continuous wavelet transform (CWT) of the response signals and compute the wavelet ridge by maximizing the modulus of wavelet skeleton at each time instant;
- 4) Compute instantaneous natural frequency (f_i) and damping ratio (ζ_i) according to wavelet ridge and skeleton;
- 5) Determine the relationships between each individual predictor and actual board grade yield;
- 6) Determine the relationships between the combined parameters and actual board grade yield.
- 7) Rank logs based on individual and combined parameters.

Results and discussion

Table 1 shows the dimensional and physical measures of the 21 selected logs and the sawing results (board volume, cant volume, and board grades). The NHLA rules are based on the size and number of cuttings (pieces) that can be obtained from a board when it is cut up and used in the manufacture of a hardwood product. Therefore, the grades provide a measurable percentage of clear, defect-free wood for each grade. The board grades determined based on NHIA rules include the upper grades (FAS, FIF, and Select), common grades (No. 1 Common, No. 2 Common, and No. 3 Common), and below grade (BG).

Table 1—Dimensional and physical measures of the yellow-poplar logs and the sawing results^a

Log no.	Length (ft)	Diameter (in.)			Weight (lb)	Sweep (in.)	Volume (board footage)			Grade yield (board footage)				
		Large end	Small end	Avg.			Debarked	Board	Cant	High ^b	1C	2C	3C	BG ^c
1123	11.4	18.60	17.19	18.83	923	1.62	219.82	106	34.47	17	29	42	18	0
1126	13.1	20.39	20.39	19.72	1183	1.36	288.92	158	32.04	138	8	7	0	5
1128	13.1	23.58	20.70	21.46	1823	1.05	339.20	219	29.76	187	19	0	5	8
1129	15.2	20.27	20.27	21.02	1810	0.87	380.26	198	34.99	59	121	6	6	6
1131	16.4	15.18	13.99	14.51	855	2.13	186.80	66	34.01	30	16	20	0	0
1133	14.7	19.30	18.76	18.96	1097	0.96	293.33	157	38.29	32	56	41	28	0
1134	16.8	17.03	15.58	16.20	926	0.83	243.36	116	44.08	23	70	23	0	0
1136	14.0	12.90	12.90	12.98	368	0.52	115.58	36	28.16	0	7	12	17	0
1137	13.5	19.29	17.18	18.01	1209	0.79	236.95	137	21.25	129	8	0	0	0
1138	11.1	16.96	16.39	16.61	801	1.69	168.90	87	25.18	61	26	0	0	0
1140	11.1	15.11	15.11	15.08	641	2.09	135.31	36	33.30	0	12	12	12	0
1141	13.4	14.27	14.27	14.28	686	1.7	143.64	38	41.13	0	10	28	0	0
1147	12.5	14.43	13.76	14.23	632	1.65	137.12	60	31.25	38	6	4	0	12
1153	11.8	21.29	20.56	21.50	1487	1.53	312.18	160	33.92	88	57	5	10	0
1154	9.5	21.09	21.09	20.75	1418	1.23	233.26	126	30.95	76	32	18	0	0
1155	11.4	20.36	18.37	19.22	1151	2.48	235.54	112	59.13	23	36	46	7	0
1161	16.5	17.29	15.29	16.14	1208	1.81	235.73	99	46.90	5	47	47	0	0
1166	17.0	23.85	23.29	23.06	2649	0.91	528.00	290	31.25	192	58	40	0	0
1167	11.4	18.50	17.02	17.86	1012	1.44	198.91	100	30.20	19	20	32	29	0
1169	16.1	17.55	14.94	15.63	1046	1.59	215.58	98	43.20	54	15	29	0	0
1170	14.5	14.77	14.77	14.68	793	1.25	171.59	85	26.79	32	39	9	0	5

^a1 ft = 0.3048 m; 1 in. = 2.54 cm; 1 lb = 0.454 kg; 1 board foot = 0.00235974 m³.^bHigh includes grade FAS, F1F, and Select.^cBG, below grade.

Table 2 shows the physical and acoustic properties of the 21 selected yellow-poplar logs. The moisture contents of the wood samples were found to be 45% to 60%. Therefore, all acoustic parameters discussed in this paper are considered “green log” parameters. The results of the acoustic impact test were

Table 2—Physical and acoustic properties of the yellow-poplar logs

Log no.	Density (lb/ft ³) ^a	V (km/s)	E _d (GPa)	Scale	f (Hz)	Time centroid (10 ⁻²)	Damping ratio (10 ⁻²)	E _d /ζ ² (10 ³)	ρ/T _c ² (10 ⁵)
1123	42.79	3.34	7.65	115	521.74	1.74	3.59	5.93	1.41
1126	41.98	3.37	7.65	145	413.79	1.64	3.43	6.52	1.57
1128	55.29	3.04	8.18	157	382.17	1.47	3.61	6.27	2.56
1129	48.91	3.05	7.29	174	344.83	1.93	4.25	4.04	1.31
1131	45.54	3.27	7.81	181	331.49	2.08	4.26	4.31	1.05
1133	38.14	3.83	8.98	141	425.53	1.90	4.12	5.29	1.06
1134	38.36	3.78	8.79	161	372.67	1.88	4.41	4.51	1.08
1136	31.03	3.59	6.42	141	425.53	1.98	3.73	4.61	0.79
1137	51.74	3.65	11.05	134	447.76	1.41	3.16	11.04	2.59
1138	47.92	3.88	11.57	104	576.92	1.44	3.02	12.71	2.32
1140	47.45	3.76	10.72	107	560.75	1.75	3.16	10.76	1.56
1141	47.43	3.67	10.21	131	458.02	1.57	3.83	6.95	1.92
1147	45.91	2.91	6.22	154	389.61	1.80	3.88	4.14	1.42
1153	49.06	3.38	8.98	125	480.00	1.48	4.17	5.17	2.25
1154	50.57	2.93	6.95	107	560.75	1.21	3.75	6.08	3.44
1155	49.96	3.32	8.85	126	476.19	1.51	4.53	4.30	2.18
1161	51.63	3.23	8.64	188	319.15	2.04	4.27	4.75	1.24
1166	51.88	3.30	9.06	189	317.46	1.69	4.06	5.50	1.82
1167	51.65	2.98	7.35	140	428.57	1.88	4.14	4.29	1.46
1169	48.71	3.63	10.28	155	387.10	1.53	3.16	10.27	2.07
1170	46.23	3.73	10.31	143	419.58	1.70	4.13	6.06	1.59

^a1 lb/ft³ = 16.0185 kg/m³.

reported in a previous report (Wang et al. 2016). Log acoustic velocity was able to identify the very low-end logs that had the most severe internal rot or other unsound defects but failed to identify the logs with poor geometry that resulted in very low recovery. The time domain parameters (time centroid and ρ/T_c^2) and frequency domain parameters (damping ratio and E_d/ζ^2) were identified as log quality predictors with positive correlation with the board grade yields.

Log visual grades based on laser scan data

The high-resolution laser scanning system was able to accurately measure all log size and shape characteristics. The size, sweep, weight, and volume of each log are listed in Table 1. By examining the center points of each scan line, the scanner can measure the departure of the log from a straight line. This allows the crook and sweep of the log to be measured. A crooked log is one with an end that has a dramatic bend to one side. A swept log has a bow to one side along the length. A log with a crook or sweep will yield less lumber than a straight log of the same diameter and length. In addition, the lumber sawn from a crooked or swept log will generally be weaker than lumber sawn from a straight log. This is because the fiber angles in swept or crooked logs are not aligned along the length of the board.

Using the log measurement data combined with the log surface defect information (position, size, and type of every surface defect) allowed the RAYSAW program (Thomas 2013) to grade each log to U.S. Forest Service hardwood log grading rules (Rast et al. 1973). The U.S. Forest Service log grades are based on the number and type of defects present on a log and the predicted impact they will have on the value and volume of lumber that log should produce. As such, they provide a method of classifying logs based on their observed characteristics, regardless if the inspection is made by machine or human.

Ranking logs based on acoustic parameters

To evaluate the effectiveness of the time domain and frequency domain parameters as log quality predictors, we ranked the 21 yellow-poplar logs using time centroid, damping ratio, ρ/T_c^2 , and E_d/ζ^2 , respectively. Table 3 lists the logs rated as high and low quality according to each acoustic predictor. The volume recovery and board grade yields of individual logs were tabulated in Table 4 for high-quality logs and in Table 5 for low-quality logs.

Table 3—Yellow-poplar logs rated as high quality and low quality based on different NDE predictors^a

Predictor	Logs rated as high quality					Logs rated as low quality								
T_c	1154	1137	1138	1128	1153	1131	1161	1136	1129	1133	1134	1167		
ζ	1138	1140	1137	1169	1126	1155	1134	1161	1131	1129	1153	1167	1170	1133
ρ/T_c^2	1154	1137	1128	1138		1136	1131	1133	1134	1161	1129	1123	1147	1167
E_d/ζ^2	1138	1137	1140	1169	1141	1126	1129	1147	1167	1155	1131	1134	1136	1161

^aThe log marked with a box indicates an abnormal case with a false prediction.

Table 4—Volume recovery and grade yield of high-quality yellow-poplar logs

Log no.	Volume (footage)								Recovery (%)		Board grade yield (%)				
	Board	Cant	Debarked	High	1C	2C	3C	BG	Total	Board	High	1C	2C	3C	BG
1137	137	21.25	236.95	129	8	0	0	0	66.8	57.8	94.2	5.8	0	0	0
1138	87	25.18	168.90	61	26	0	0	0	66.4	51.5	70.1	29.9	0	0	0
1128	219	29.76	339.20	187	19	0	5	8	73.3	64.6	85.4	8.7	0	2.3	3.7
1154	126	30.95	233.26	76	32	18	0	0	67.3	54.0	60.3	25.4	14.3	0	0
1126	158	32.04	288.92	138	8	7	0	5	65.8	54.7	87.3	5.1	4.4	0	3.2
1153	160	33.92	312.18	88	57	5	10	0	62.1	51.3	55.0	35.6	3.1	6.3	0

Time centroid vs. ρ/T_c^2

Time centroid (T_c) and combined parameter ρ/T_c^2 resulted in similar predictions in both high-quality and low-quality ratings, with the exception that when log density (ρ) was taken into consideration, log no. 1153 was excluded from high-quality class and logs no. 1123 and no. 1147 were added into low-quality class per ρ/T_c^2 rating. Considering that log no. 1153 was only marginally rated as high quality per time centroid rating and could be excluded by adjusting T_c threshold, the effectiveness of the combined parameter ρ/T_c^2 for rating high-quality logs was not substantially different from that of single parameter T_c . However, in rating low-quality logs, the combined parameter can be considered more effective because the two added low-quality logs (no. 1123 and no. 1147) per ρ/T_c^2 rating did yield high percentage of low grade (3 Common and BG) boards as shown in Table 5.

Table 5—Volume recovery and grade yield of low-quality yellow-poplar logs.

Log no.	Volume (footage)								Recovery (%)		Board grade yield (%)				
	Board	Cant	Debarked	High	1C	2C	3C	BG	Total	Board	High	1C	2C	3C	BG
1134	116	44.08	243.36	23	70	23	0	0	65.8	47.7	19.8	60.3	19.8	0	0
1167	100	30.20	198.91	19	20	32	29	0	65.5	50.3	19.0	20.0	32.0	29.0	0
1136	36	28.16	115.58	0	7	12	17	0	55.5	31.1	0	19.4	33.3	47.2	0
1131	66	34.01	186.80	30	16	20	0	0	53.5	35.3	45.5	24.2	30.3	0	0
1129	198	34.99	380.26	59	121	6	6	6	61.3	52.1	29.8	61.1	3.0	3.0	3.0
1133	157	38.29	293.33	32	56	41	28	0	66.6	53.5	20.4	35.7	26.1	17.8	0
1161	99	46.90	235.73	5	47	47	0	0	61.9	42.0	5.1	47.5	47.5	0	0
1123	106	34.47	219.82	17	29	42	18	0	63.9	48.2	16.0	27.4	39.6	17.0	0
1147	60	31.25	137.12	38	6	4	0	12	66.5	43.8	63.3	10.0	6.7	0	20.0
1153	160	33.92	312.18	88	57	5	10	0	62.1	51.3	55.0	35.6	3.1	6.3	0
1155	112	59.13	235.54	23	36	46	7	0	72.7	47.6	20.5	32.1	41.1	6.3	0
1170	85	26.79	171.59	32	39	9	0	5	65.2	49.5	37.6	45.9	10.6	0	5.9

Damping ratio vs. E_d/ζ^2

In selecting high-quality logs, damping ratio and combined parameter E_d/ζ^2 resulted in similar predictions with slight change in the ranking order and inclusion of log no. 1141 in E_d/ζ^2 rating. This could be because the defects presented in high-quality logs were too small to have a significant influence on global modulus of elasticity of the logs. However, in rating low-quality logs, the predictions of damping ratio and combined parameter E_d/ζ^2 were quite different as shown in Table 3. Three low-quality logs (no. 1133, no. 1153, and no. 1170) by damping ratio rating were not present in E_d/ζ^2 rating, whereas two low-quality logs (no. 1147 and no. 1136) in E_d/ζ^2 rating were not picked up by damping ratio. The sawing results indicated that logs no. 1147 and no. 1136, rated low quality by E_d/ζ^2 , yielded a relatively large proportion of low-grade boards (20% BG for log no. 1147, 47.2% 3 Common for log no. 1136). Particularly for log no. 1147, which had the lowest acoustic velocity of 2.91 km/s (1.8 miles/s) and the

largest proportion of BG boards among all the logs, defects significantly decreased the stiffness (E) and thus, this log was effectively rated as the second worse log. However, log no. 1147 was not picked up by damping ratio. Similarly for log no. 1136, the defects that resulted in 47.2% 3 Common boards had a significant impact on stiffness (E) and therefore was picked up by E_d/ζ^2 rating but not by damping ratio.

For three logs (no. 1153, no. 1170, and no. 1133) rated low quality by damping ratio, two of them (no. 1133 and no. 1170) were dominated by 1 Common and 2 Common boards (79.6% and 56.5%, respectively) and should be considered intermediate quality logs, and one log (no. 1153) was dominated by high grade and 1 Common boards (90.6%) and should be considered a high-quality log.

Tables 6 and 7 list the logs that were rated as high quality and low quality, respectively, using four different predictors and the frequency of positive ratings. The more positive ratings, the higher the probability of the log being rated accurately. However, it should be noted that the logs with lower rating frequency still have a probability of being rated accurately. Overall, rating of low-quality logs was more accurate than rating of high-quality logs.

Table 6—Frequency of positive ratings for high-quality logs using four predictors

Log no.	Logs rated as high quality									
	1137	1138	1128	1154	1126	1169	1140	1153	1141	
Frequency of positive rating	4/4	4/4	2/4	2/4	2/4	2/4	2/4	1/4	1/4	

Table 7—Frequency of positive ratings for low-quality logs using four predictors

Log no.	Logs rated as low quality											
	1134	1131	1161	1129	1167	1136	1133	1155	1147	1153	1170	1123
Frequency of positive rating	4/4	4/4	4/4	4/4	4/4	3/4	3/4	2/4	2/4	1/4	1/4	1/4

Abnormal cases

Logs no. 1140 and no. 1141 are abnormal cases in which the sawing results showed very low recovery (26.5%) and poor grade yields (1, 2, and 3 Common) but all acoustic predictors failed in prediction. In fact, two frequency-domain parameters (damping ratio and E_d/ζ^2) mistakenly rated these two logs as high quality. From visual examination and laser scan data, we found that these two logs were relatively small in diameter and had a significant amount of sweep or crook (Table 1).

When logs with significant amounts of crook (an abrupt bend), sweep (log is bowed in one or more directions), or taper are sawn, more wood must be removed from the surface to establish a flat board face. This piece of wood from each log face is called a slab. Log no. 1140 had 7.3-cm (2.89-in.) of crook along the red–blue axis (man-made mark for sawing). Log no. 1141 had 4.5-cm (1.79-in.) of sweep primarily along the red–blue axis, but the bow also twisted around the log toward the black face on the large end. To true up the logs, the slabs had to be cut thicker than usual with 10.5-cm- (4.125-in.-) and 10.8-cm- (4.25-in.-) thick slabs sawn from log no. 1140. Slab thicknesses on log no. 1140 were 8.6, 9.8, and 6.7 cm (3.375, 3.875, and 2.625 in.) on the black, blue, and red faces. A similar sawing operation occurred to log no. 1141. In short, these two logs had poor geometry. Significant sweep or taper always significantly decreases the volume of lumber recovered. However, the impact is much more severe on small-diameter logs. Apparently, no acoustic parameters were able to detect logs of poor geometry.

Comparison of acoustic sorting and log scanning results

Table 8 lists the logs that belong to the high- and low-quality acoustic sorts. High-resolution scanning can sense visible features such as bumps, holes, log shape, and size. These observations are based on precise

and exact measurements from the laser system. For each log scanned, the number of severe or degrade defects encountered on that log are listed, along with a brief summary, characterizing the defects present. A degrade defect is a defect of a type and/or size that will impact the grade of the log.

Table 8—Defect detection results by high- and low-quality log sorts

Quality sort	Log number	Log grade	Severe defect count	Defect summary
Low	1134	F2	0	Medium bark distortions
Low	1131	F3	14	Multiple wounds and knots
Low	1161	F3	7	Overgrown, unsound, and sawn knots
Low	1129	F2	1	Large overgrown crack–seam
Low	1167	F2	1	Overgrown knot
Low	1136	F3	5	Overgrown knots
Low	1133	F1	0	Several small adventitious clusters
Low	1155	F2	3	Unsound knots and an overgrown knot
Low	1147	F2	6	Wound and five overgrown knots
Low	1170	F1	1	Sawn knot
Low	1123	BG	4	Sawn knot and three overgrown knots
Average		2.27	3.82	
High	1137	F1	0	Clear
High	1138	F2	1	Large wound
High	1128	F1	0	Clear
High	1154	F2	3	Large overgrown knots
High	1126	F2	2	Large wound and a large gouge
High	1169	F1	1	Small wound
High	1140	F2	5	Overgrown knots
High	1153	F1	0	Clear
High	1141	F3	5	Overgrown and unsound knots
Average		1.78	1.89	

For each log scanned, the Forest Service log grade was determined using the RAYSAW sawing analysis program (Thomas 2013). Within the Forest Service grading rules, the highest grade or high-quality sawlog is Factory 1 or F1. Factory 2 or F2 is the middle quality level and Factory 3 or F3 is the lowest quality level for sawlogs. As log grade or quality decreases, the number of degrade defects increase and the lengths of the clear areas between defects decrease. If enough defects are present, or the extent of crook or sweep is severe enough, the log will fail to meet the lowest grade, F3. If this happens, the log is graded as BG.

Assigning numeric values to the log grades (where 1 = F1, 2 = F2, 3 = F3, and 4 = BG) allows us to determine an average log grade within each acoustic quality sort. For the low-grade logs, the average grade is 2.27, or slightly lower than Factory 2. For the high-grade logs, the average grade is 1.78, or slightly better than Factory 2. Thus, with our small sample, there is little difference between the visual log grades of the high- and low-quality sorts. Similarly, there is little difference in the number of severe or degrade defects encountered between the samples. Therefore, it is not evident that developing a correlation between log grade or severe defects and acoustic assessment will yield a distinct advantage in sorting or processing capabilities.

Although it is difficult to correlate results from one scanning system to another, the complementary nature of the two systems negate this need. In Table 8, we see that two logs, no. 1133 and no. 1170, in the low-quality acoustic sort were graded as Factory 1, a high-quality visual grade. Examining the grade yield for these two logs (Table 5), we see that the lumber produced was much lower quality than one would expect for a high-grade sawlog. This indicates the presence of one or more internal defects that significantly impacted recovery. For the medium-quality (Factory 2) logs (no. 1129, 1134, 1147, 1155, and 1167) in

the low-quality acoustic sort, most logs had lumber yields consistent with low-quality logs (Table 5), which was less than would be expected from a Factory 2 log. The one exception was no. 1147, which had a lumber grade yield that would be expected of a Factory 1 log. We have no explanation for this anomaly. For the high-quality acoustic log sort, lumber grade yields (Table 4) were what would be expected of high-quality sawlogs, with two exceptions, logs no. 1140 and no. 1141. These two logs had significant crook and sweep that drastically decreased their yields. They were also smaller logs for which any fault, shape, or surface defect caused a greater yield decrease.

Conclusions

Acoustic velocity, time centroid, damping ratio, as well as the combined time and frequency domain parameters are all effective quality predictors of hardwood logs in terms of internal soundness. Acoustic parameters combined with high-resolution laser scanning results provide a more complete data picture of the log: size, shape, surface defects, and degree of soundness. A high-quality acoustic assessment coupled with low visual grade indicates a sound log, but the lumber will either have significant numbers of knots or recovery will be low because of poor log shape. In contrast, a high visual grade coupled with a low-quality acoustic sort indicates a log with hidden deficiencies that will decrease lumber value and volume. Thus, a combined system would be able to discriminate much more exactly with respect to log quality and potential lumber recovery than either method independently.

Acknowledgment

This project was conducted under the cooperative research agreement (14-JV-1111133-089) between the Natural Resources Research Institute of the University of Minnesota Duluth (UMD) and the USDA Forest Service, Forest Products Laboratory (FPL). Mr. Feng Xu's participation in this project was supported by the Priority Academic Program Development (PAPD) of Jiangsu Higher Education Institutions and the Nanjing Forestry University (NFU) Innovation Grant for Outstanding PhD Dissertations (grant no. 163070682). We thank Neal Bennett and Deborah Conner for their technical assistance during the project.

References

- Bhandarkar, S.; Faust, T.; Tang, M. 1999. Catalog: a system for detection and rendering of internal log defects using computer tomography. *Machine Vision and Applications*. 11(4): 171-190.
- Carpenter, R.D.; Sonderman, D.L.; Rast, E.D. 1989. Defects in hardwood timber. *Agric. Handb. No. 678*. Washington, DC: U.S. Department of Agriculture, Forest Service. 88 p.
- Carter, P.; Briggs, D.; Ross, R.J.; Wang, X. 2005. Acoustic testing to enhance western forest values and meet customer wood quality needs. PNW-GTR-642. Portland, OR: USDA Forest Service, Pacific Northwest Research Station: 121-129.
- Chang, S. 1992. External and internal defect detection to optimize cutting of hardwood logs and lumber. *Transferring technologies for industry No. 3*. Beltsville, MD: U.S. Department of Agriculture, National Agriculture Library. 24 p.
- Guddanti, S.; Chang, S. 1998. Replicating sawmill sawing with topsaw using CT images of a full length hardwood log. *Forest Products Journal*. 48(1): 72-75.

Harris, P.; Petherick, R.; Andrews, M. 2002. Acoustic resonance tools. In: Proceedings of the 13th international symposium on nondestructive testing of wood. August 19-21, 2002, Berkeley, CA: 195-201.

Li, P.; Abbott, A.; Schmoldt, D. 1996. Automated analysis of CT images for the inspection of hardwood log. In: Proceedings IEEE conference on neural networks. Washington, DC: 3:1744-1749.

NHLA. 2015. Rules for the measurement and inspection of hardwood and cypress. Memphis, TN: National Hardwood Lumber Association. 104 p.

Pellerin, R.F.; DeGroot, R.C.; Esenther, G.R. 1985. Nondestructive stress wave measurements of decay and termite attack in experimental wood units. In: Proceedings, 5th international symposium on nondestructive testing of wood, September 9-11, 1985, Pullman, WA: Washington State University: 319-353.

Rast, E.D.; Sonderman, D.L.; Gammon, G.L. 1973. A guide to hardwood log grading. Gen. Tech. Rep. NE-1. Upper Darby, PA: U.S. Department of Agriculture, Forest Service, Northeastern Forest Experiment Station. 32 p.

Thomas, L.; Mili, L.; Thomas, R.E.; Shaffer, C.A. 2006. Defect detection on hardwood logs using laser scanning. *Wood and Fiber Science*. 38(4): 682-695.

Thomas, L.H.; Thomas, R.E. 2011. A graphical automated detection system to locate hardwood log surface defects using high-resolution three-dimensional laser scan data. In: Fei, S.L.; Lhotka, J.M.; Stringer, J.W.; Gottschalk, K.W.; Miller, G.W., eds. Proceedings, 17th central hardwood forest conference. April 5-7, 2010. Lexington, KY. Gen. Tech. Rep. NRS-P-78. Newtown Square, PA: U.S. Department of Agriculture, Forest Service, Northern Research Station: 92-101.

Thomas, R.E. 2008. Predicting internal yellow-poplar log defect features using surface indicators. *Wood and Fiber Science*. 40(1): 14-22.

Thomas R.E. 2013. RAYSAW: a log sawing simulator for 3D laser-scanned hardwood logs. In: Proceedings, 18th central hardwood forest conference. March 26-28, 2012. Morgantown, WV; Gen. Tech. Rep. NRS-P-117. Newtown Square, PA: U.S. Department of Agriculture, Forest Service, Northern Research Station: 325-334.

Thomas, R.E.; Thomas, L.H. 2013. Using parallel computing methods to improve log surface defect detection methods. In: Ross, R.J.; Wang, X., eds. Proceedings, 18th international nondestructive testing and evaluation of wood symposium. September 24-27, 2013, Madison, WI. Gen. Tech. Rep. FPL-GTR-226. Madison, WI: U.S. Department of Agriculture, Forest Service, Forest Products Laboratory: 196-205.

Thomas, R.E.; Thomas, L.; Shaffer, C. 2008. Defect detection on hardwood logs using high-resolution laser scan data. In: Proceedings of the 15th International Symposium on Nondestructive Testing of Wood, September 10-12, 2007, Duluth, MN. Duluth, MN: Natural Resources Research Institute, University of Minnesota: 163-167.

Wagner, F.; Taylor, F.; Ladd, D.; McMillin, C.; Roder, F. 1989. Ultrafast CT scanning of an oak log for internal defects. *Forest Products Journal*. 39(11/12): 62-64.

Wang, X. 2013. Acoustic measurements on trees and logs: a review and analysis. *Wood Science and Technology*. 47: 965-975.

Wang, X.; Carter, P.; Ross, R.J.; Brashaw, B.K. 2007. Acoustic assessment of wood quality of raw forest materials – a path to increased profitability. *Forest Products Journal*. 57(5): 6-14.

Wang, X.; Divos, F.; Pilon, C.; Brashaw, B.K.; Ross, R.J.; Pellerin, R.F. 2004. Assessment of decay in standing timber using stress wave timing nondestructive evaluation tools — a guide for use and interpretation. Gen. Tech. Rep. FPL–GTR–147. Madison, WI: U.S. Department of Agriculture, Forest Service, Forest Products Laboratory. 12 p.

Wang, X.; Verrill, S.; Lowell, E.; Ross, R.J.; Herian, V.L. 2013. Acoustic sorting models for improved log segregation. *Wood Science and Technology*. 45(4): 343-452.

Wang, X.; Thomas, E.; Krause V.; Xu, F.; Liu, Y.; Brashaw, B.K.; Ross, R.J. 2016. Improving log defect detection accuracy by complementary scanning methods. Final report NRRI/TR-2016/38. Natural Resources Research Intitute (NRRI). Duluth, MN: University of Minnesota Duluth. 23 p.

Assessing Internal Soundness of Hardwood Logs by Acoustic Impact Testing

Feng Xu

College of Information Science and Technology, Nanjing Forestry University, Nanjing, China,
xufeng@njfu.com.cn

Xiping Wang

USDA Forest Service Forest Products Laboratory, Madison, Wisconsin, USA, xwang@fs.fed.us

Yunfei Liu

College of Information Science and Technology, Nanjing Forestry University, Nanjing, China,
lyf@njfu.com.cn

Brian K Brashaw

USDA Forest Service Forest Products Laboratory, Madison, Wisconsin, USA, bbrashaw@fs.fed.us

Lon A Yeary

Natural Resources Research Institute, University of Minnesota Duluth, Duluth, Minnesota, USA,
yearyl@uwplatt.edu

Abstract

The quality of hardwood logs varies widely within species, harvest site, and even the same tree. Internal decay, holes, knots and other growth defects on logs reduce the grade and yield of the resulting boards and cause a substantial monetary loss to timber buyers and wood manufacturers. Early detection of internal defects in hardwood logs could provide significant benefits to wood industry in terms of making accurate quality assessment and volume estimates and optimal utilization of the hardwood resource. In this study, we explored the potential of acoustic impact testing as a nondestructive evaluation procedure to assess the soundness of hardwood logs in terms of internal rot, void and defect ratio. Fifteen hardwood logs including black cherry, white oak, red oak and cottonwood were obtained and subjected to acoustic impact testing. The logs were subsequently dissected for visual examination and physical mapping of the internal defects. The response signals were analyzed using a modern signal processing method, continuous wavelet transform, to derive first and second order damping ratio. Our results indicated that acoustic velocity had a negative relationship with defect ratio in general, but lacked sensitivity to small defects and were affected by species. Wavelet based damping ratio was found to have a close linear relationship with log defect ratio. Comparing with the first order damping ratio, the second order damping ratio had a better predicting power and was not affected by type and location of defects and log species.

Keywords: Acoustic velocity, damping ratio, defect ratio, hardwood log, wavelet transform, wood quality

Introduction

The quality of hardwood logs varies widely within species, harvest site, and even the same tree. Decay, holes, knots, wounds, and other growth defects on logs reduce the strength and appearance of any resulting products and thus reduce the value of the log and its products (Carpenter et al. 1989). The location, type, and size of these defects on hardwood logs dictate the potential grade and value of the resulting boards. Researches have shown that the value of hardwood lumber can be improved as much as 10%-21% if internal defect information in hardwood logs such as location, type, size, and shape is used efficiently during the sawing process (Steele et al. 1994; Thomas 2010). Thus, early detection of internal defects in hardwood logs could provide significant

benefits to wood industry in terms of making accurate quality assessment and volume estimates and optimal utilization of the hardwood resource.

Over the past decades, several nondestructive imaging techniques were investigated for detecting internal defect in logs, including X-ray, CT (computed tomography), and NMR (nuclear magnetic resonance) (Chang 1992; Sarigul et al. 2003). These imaging technologies can provide high quality cross section images of a log with sufficient details, but are not cost effective for most hardwood mills, and too slow to be considered suitable for on-line implementation (Wagner et al. 1989; Chang 1992; Guddanti and Chang 1998; Li et al. 1996; Bhandarker et al. 1999). As an alternative method, laser scanning has been investigated to detect surface defects regarded as degrade defects by the visual grading rules. In addition, models were developed to predict internal defects based on external features (Thomas 2008, 2009). However, a system based entirely on log surface inspection may incorrectly predict internal quality. Some defects give the appearance of being solid or sound and effectively hide an unsound or rotten area, thereby reduce the accuracy of predicted internal product quality and value.

Acoustic technologies have been well established as material evaluation tools in the past several decades and are becoming widely accepted in the forest products industry for online quality control and products grading. For example, acoustic velocity as a nondestructive measure has been proved to be related to the basic wood and fiber properties such as stiffness, density, micro-fibril angle (Carter et al. 2005; Wang et al. 2007; Wang 2013). It has also been recognized as a predicting parameter for wood deterioration caused by any wood decay mechanism (Pellerin et al. 1985). But most of the predictive parameters, including acoustic velocity, transmission time, attenuation, etc., are derived from time or frequency domain analysis of the acoustic signals, and they offer limited information regarding internal quality features. The objective of this study was to further explore the information within the acoustic signals of hardwood logs using the modern signal processing technique—continuous wavelet transform (CWT) and identify new signal features for assessing the internal soundness of hardwood logs.

Background

Damping is one of the important dynamic characteristics of a material that affect its dynamic responses and influence the mechanical performance of the material. Damping ratio provides a mathematical means of expressing the level of damping in a material relative to its critical damping. Damping ratio is usually used in dynamic analysis to reflect the inherent capacity of dissipating dynamic forces imposed in a material.

Continuous wavelet transform (CWT) has been widely used in modal parameter identification and damage detection of structures in recent decades because of its good time-frequency localization features and capability of decoupling vibration modes of multiple-degree-of-freedom system (Staszewski 1997; Slavic et al. 2003; Teng et al. 2009). Pawlus et al. (2012) applied wavelet-based methodology to vehicle collision with a pole for estimating vehicle modal parameters and reported that the method was capable of identifying the frequency components of the recorded crash pulses and estimating the damping ratio. However, to improve the accuracy of estimated vehicle modal parameters, a complete scalogram of the crash pulse should be analyzed. Le and Paultre (2013) approximately identified damping ratio of the simulated responses and recorded data from a real structure based on the CWT and the singular value decomposition algorithm. They also indicated that there existed some discrepancies in the damping estimation in the lower modes, in comparison with other operational modal analysis techniques. Uhl and Klepka (2005) confirmed that the wavelet transform was a useful tool to support the identification process of non-stationary systems, and can significantly reduce the computation time of modal parameters due to the use of analytical formulas for damping ratio and natural frequencies and facilitated hardware implementation of the algorithm.

Ülker-Kaustell and Karoumi (2011) applied CWT to study the amplitude dependency of the natural frequency and equivalent viscous modal damping ratio of the first vertical bending mode for a ballasted, single spanned concrete-steel composite railway bridge. The results have implications on the choice of damping ratios for theoretical studies aiming at upgrading existing bridges and in the design of new bridges for high speed trains.

Materials and Methods

Hardwood Log Specimens

Fifteen hardwood logs of mixed species were obtained from a local wood company in Madison, Wisconsin for this study. The log specimens included two black cherry, five white oak, six red oak, and two cottonwood. These logs were selected from company’s log stocks based on visual appearances so that they included both sound and unsound logs. The unsound logs had a range of defects (voids, cracks, ring shake, internal rot, etc.) and were in different deterioration levels. Upon delivery to the laboratory, the logs were placed on the ground inside the building (Figure 1). Each log was assigned a log number and the basic dimensions were measured. Table 1 shows the species information and dimensions of the logs.

Experimental Procedures

All logs were first subject to acoustic impact tests in longitudinal directions. A laboratory impact testing system was used to obtain and record the response signals from each log following a mechanical impact. Figure 2 shows the schematic diagram of the acoustic impact testing system. Two sensor probes (Fakopp Microsecond Meter sensors, Fakopp Enterprise) were inserted into the opposing ends of each log (close to the center), one on each end. The impact acoustic waves were generated through a hammer impact at one end. The response signals were recorded through a data acquisition card (NI 5132) connected to the laptop, with a sampling frequency of 20 kHz.



Figure 1—Hardwood log samples used in the study.

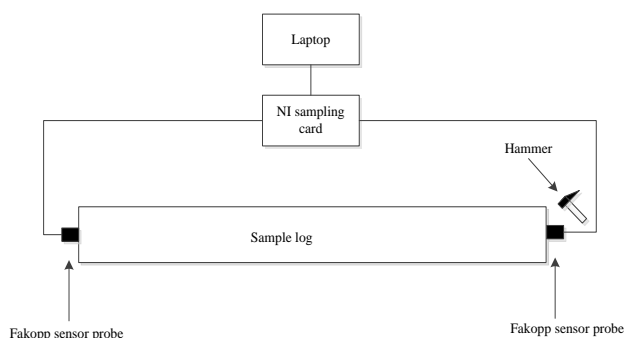


Figure 2—Schematic diagram of acoustic impact testing on a log

Table 1—Physical characteristics of the hardwood logs.

Log No.	Species	Length (cm)	Diameter (<i>D</i>) (cm)						MC (%)	Defect ratio (%)
			<i>D_L</i>		<i>D_S</i>		Average			
			<i>D_{L1}</i>	<i>D_{L2}</i>	<i>D_{S1}</i>	<i>D_{S2}</i>	<i>D_{Avg}</i>	<i>D_{Avg}</i>		
FPL 1	Black cherry	243.8	45.40	39.05	38.00	38.10	42.23	38.05	48.4	0
FPL 2	Red oak	253.9	53.98	53.34	40.64	38.74	53.66	39.69	39.7	28.6
FPL 3	White oak	262.1	38.58	38.10	38.42	28.58	38.34	33.50	80.8	14.6
FPL 4	Red oak	249.0	34.13	25.56	23.18	20.64	29.85	21.91	61.6	3.3
FPL 5	Black cherry	262.1	48.58	43.18	44.29	38.56	45.88	41.43	58.3	4.6
FPL 6	White oak	248.1	38.10	35.88	33.02	33.02	36.99	33.02	31.3	31.7
FPL 7	Red oak	267.0	61.91	59.21	51.75	51.44	60.56	51.59	75.9	6.4
FPL 8	Cottonwood	260.0	36.20	35.56	35.72	35.56	35.88	35.64	95.6	0
FPL 9	Red oak	253.0	51.44	45.72	43.50	40.96	48.58	42.23	86.0	15.1
FPL 10	White oak	246.0	30.96	30.64	26.04	23.81	30.80	24.92	52.5	13.5
FPL 11	White oak	255.1	55.72	50.80	38.10	37.78	53.26	37.94	77.4	20.3
FPL 12	White oak	234.1	38.89	35.56	31.12	30.48	37.23	30.80	46.6	5.4
FPL 13	Cottonwood	243.8	33.02	31.43	31.43	28.10	32.23	29.77	76.8	8.0
FPL 14	Red oak	259.1	38.42	38.10	35.88	35.56	38.26	35.72	68.8	10.0
FPL 15	Red oak	264.0	43.97	39.21	45.50	43.50	41.59	44.50	70.3	3.7

Following impact test, a series of stress wave transmission tests were conducted on each log in radial direction, starting from the cross section 30-cm from the large end, then at cross sections with a 30-cm increment throughout the entire length of each log. This test was mainly to provide a detailed nondestructive assessment of the physical conditions of each log which was later used to determine the dissecting locations for each log to reveal the major internal defects.

Upon completion of the nondestructive tests, each log was dissected at locations where internal defect was either started or stopped based on the mapping of stress wave transmission time in each log. Figure 3 shows the dissected log sections revealing internal defects. Visual inspection and physical measurements were conducted at each opened cross-section to determine the locations and sizes of the defects. A high-resolution digital image was subsequently obtained for each cross-section to document the internal conditions at specific locations. Based on the physical measurements, a ground-truth defect map was created for each log and total volume of the defected area was estimated. The defect ratio of each log was subsequently determined by dividing the volume of defect area by the total log volume.

To determine the moisture levels of the logs, we cut one to two 5-cm-thick discs from each log. The moisture contents (MC) of each disk was determined in accordance with the ASTM Standard D4442-92 (ASTM 2003).

Signal Processing and Analysis

The acoustic signals of the logs were first processed using the fast Fourier transform (FFT) program to obtain the natural frequencies of each log. The acoustic velocity of each log was then determined using the following equation:

$$C_L = \frac{2f_n L}{n} \quad (1)$$

Where C_L is longitudinal acoustic velocity (m/s), f_n is the n^{th} -order natural frequency (Hz) of the acoustic waves, L is log length.

A modified Morlet wavelet was then used to perform continuous wavelet transform (CWT) of the response signals and compute the wavelet ridge by maximizing the modulus of wavelet skeleton at each time instant. The modified Morlet used is defined as

$$\varphi(t) = \frac{1}{\sqrt{\pi f_b}} e^{j2\pi f_c t} e^{-t^2/f_b} \quad (2)$$

Where f_b is the wavelet bandwidth parameter, f_c is wavelet center frequency. The center frequency f_c of the Morlet wavelet is approximately bounded by $2\pi f_c \geq 5$ in order to fulfill the condition of admissibility (Kronland-martinet et al. 1987).

Following the CWT calculation, the instantaneous frequency and damping ratio of the response signals were estimated according to the wavelet ridge and skeleton.



Figure 3—Dissected log sections revealing internal defects.

Results and Discussion

Physical Characteristics of Hardwood Logs

The moisture content of the logs ranged from 31.3 to 95.6% based on the MC disk measurements (Table 1). All logs were well above the fiber saturation point (30% MC) except log FPL no.6 (white oak) having a MC of 31.1%. Therefore the logs tested were considered in green condition at the time of testing and the acoustic parameters discussed in this paper are treated as “green log” parameters.

The fifteen hardwood logs were in a wide range of conditions in terms of internal defects and soundness. Based on the ground-truth defect maps created by dissecting at multiple locations and measuring the defected areas on each cross-section, the estimated defect ratio (k) of the logs ranged from 0 to 31% (Table 1). Two logs (no.1 and no.8) were solid logs with no defects ($k=0$); three logs (no.4, no.5, and no.15) had minor defects ($k<5\%$); three logs (no.7, no.12, no.13) had moderate defects ($k=5-10\%$); four logs (no.3, no.9, no.10, and no.14) had significant defects ($k=10-20\%$); and three logs (no. 2, no.6, and no.11) had the most severe defects ($k>20\%$).

Relationships between Defect Ratio and Acoustic Velocity

Table 2 shows the various acoustic measures of the response signals. Acoustic velocity of the mixed species logs ranged from 2047 to 3317 m/s with a coefficient of variation of 14.3%. If we divided logs into five classes based on the defect ratios, we then observed the average log velocity of each class as follows:

Class 1 ($k=0$):	V=3,284 m/s
Class 2 ($k<5\%$):	V=3,118 m/s
Class 3 ($5\%<k<10\%$):	V=2,656 m/s
Class 4 ($k=10-20\%$):	V=2,557 m/s
Class 5 ($k>20\%$):	V=2,266 m/s

The small sample size of the logs in each class does not lend to a meaningful statistical comparison among classes, but the decreasing trend of acoustic velocity with increasing defect ratio is obvious. Figure 4a shows the data plot of log defect ratio and log acoustic velocity for all fifteen hardwood logs we tested. The relationship between defect ratio and log velocity can be best described by a polynomial regression model,

$$k (\%) = 167.04 - 0.0945V + 10^{-5} V^2 \quad (R^2=0.75) \quad (3)$$

Table 2—Acoustic measures of the response signals received from the hardwood logs.

Log No.	Species ID	Velocity V (m/s)	Scale s_1	1 st order freq. ^a f_1 (Hz)	Damping ratio (ζ_1)		Scale s_2	2 nd order freq. ^b f_2 (Hz)	Damping ratio (ζ_2)	
					Original	Revised			Original	Revised
FPL 1	Black cherry	3250	143	699.3	0.0187	0.0187	74	1351.4	0.0279	0.0279
FPL 2	Red oak	2047	250	400.0	0.0324	0.0990	117	854.7	0.0365	0.0911
FPL 3	White oak	2697	193	518.1	0.0346	0.0630	96	1041.7	0.0341	0.0574
FPL 4	Red oak	3273	137	729.9	0.0385	0.0353	76	1315.8	0.0252	0.0266
FPL 5	Black cherry	3000	175	571.4	0.0199	0.0298	89	1123.6	0.0251	0.0363
FPL 6	White oak	2290	218	458.7	0.0232	0.0539	115	869.6	0.0360	0.0869
FPL 7	Red oak	2600	204	490.2	0.0207	0.0420	100	1000.0	0.0255	0.0466
FPL 8	Cottonwood	3317	150	666.7	0.0187	0.0206	74	1351.4	0.0272	0.0272
FPL 9	Red oak	2320	217	460.8	0.0214	0.0493	114	877.2	0.0269	0.0638
FPL 10	White oak	2790	173	578.0	0.0332	0.0486	89	1123.6	0.0340	0.0492
FPL 11	White oak	2460	208	480.8	0.0208	0.0440	106	943.4	0.0299	0.0614
FPL 12	White oak	2667	168	595.2	0.0258	0.0356	87	1149.4	0.0268	0.0370
FPL 13	Cottonwood	2700	151	662.3	0.0329	0.0367	83	1204.8	0.0344	0.0433
FPL 14	Red oak	2420	210	476.2	0.0198	0.0427	111	900.9	0.0188	0.0423
FPL 15	Red oak	3080	167	598.8	0.0261	0.0356	86	1162.8	0.0251	0.0339

^{a,b} $f_i = \frac{f_c \times f_s}{s_i}$, f_c is the central frequency of complex Morlet wavelet, f_s is the sampling frequency, s_i and f_i are scale and its corresponding frequency of wavelet transform respectively.

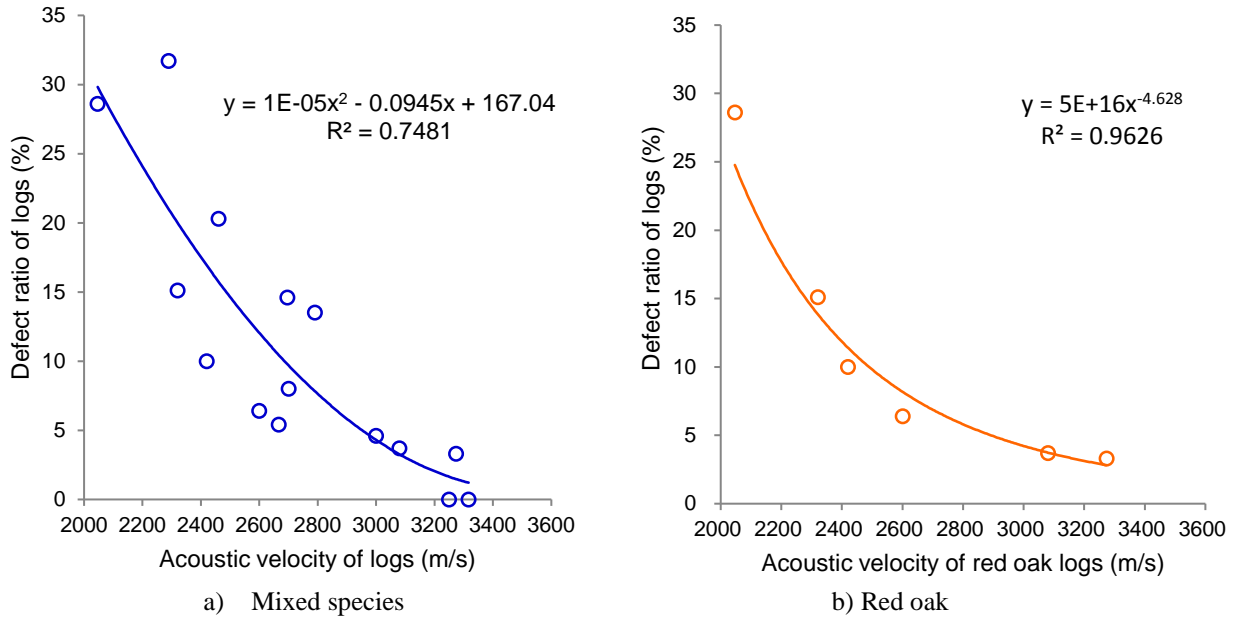


Figure 4—Relationships between log defect ratio and log acoustic velocity of hardwood logs.

Disregard the species and MC effect, it appeared that in general, as log velocity dropped below 3,000 m/s, the severity of the internal decay increased in a much higher rate as log velocity continuously decreased.

Among the four hardwood species in the log specimens, red oak had the largest sample size—6 logs. When red oak logs were examined alone, we observed a similar decreasing trend of acoustic velocity with increasing defect ratio (Figure 4b), except mathematically a power model best fit to the data ($R^2=0.96$). It appeared that species did have an effect on the defect ratio and acoustic velocity relationships.

Estimation of Damping Ratio

Figure 5 illustrates the procedures for estimating another important acoustic measure, damping ratio, of the hardwood logs. Using FPL no 1 log as an example, Figure 5a shows the response signal of the log; the wavelet moduli were obtained through continuous wavelet transform using a complex Morlet wavelet function and are shown in Figure 5b in the form of two-dimensional contour map and in Figure 5c in the form of three-dimensional contour map. The wavelet ridge and skeleton were then calculated from the wavelet modulus and are shown in Figure 5b marked in redline and in Figure 5c marked as black line. Figure 5e, and 5g show the instantaneous frequency and damping ratio of the response signals of the log. The instantaneous frequencies obtained were instantaneous natural frequency and the second-order harmonic frequency and the damping ratios were also referred to both the first mode and second mode.

As shown in Figure 5e, the case of a high quality log with no defects, the instantaneous frequency did not vary much within the finite duration of the response signal, implying that the reflection and refraction of acoustic waves that are typically associated with internal defects did not exist. As a result, the frequency conversion phenomena did not occur, and the estimated damping ratio deduced from the instantaneous frequency did not vary significantly. However, in the case of low quality logs with internal defects, variation of damping ratio was evident. For ease of use, a high order polynomial fitting was performed on damping ratio data and the fitting curve (marked as “red”) is also shown in Figure 5e. The estimated damping ratios for all hardwood logs are summarized in Table 2. To reduce the effect of frequency (scale) difference on damping ratio, the adjusted damping ratio was calculated as follows:

$$\zeta_i^j = \frac{(s_i^j)^2}{(s_i^1)^2} \times \zeta_i^1, \quad i = 1,2; j = 1,2, \dots, 15. \quad (4)$$

Where s_i^j and ζ_i^j denote the scale and damping ratio of the i^{th} order mode shape from the j^{th} sample log. Revised damping ratio also listed in the Table 2.

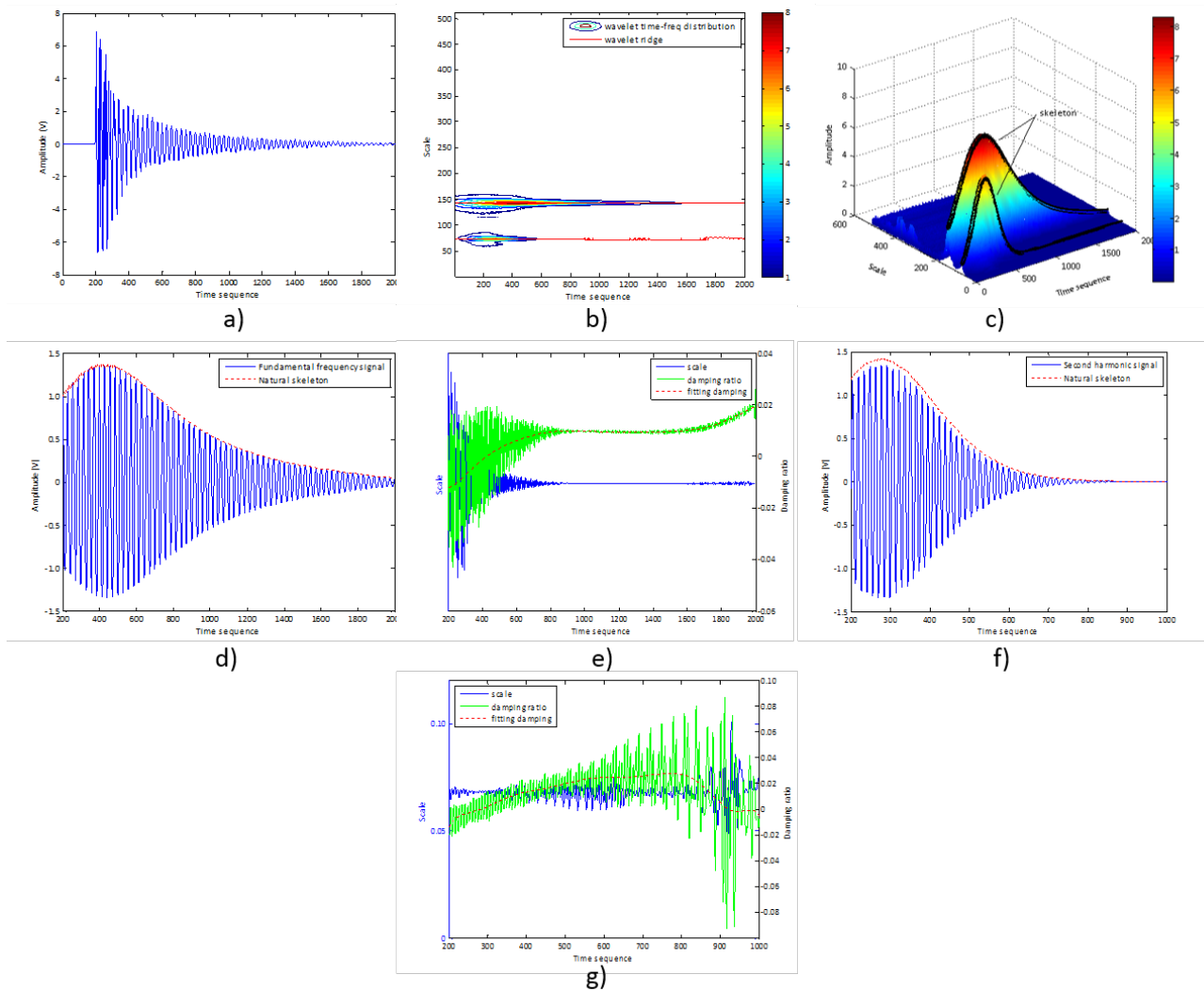


Figure 5— Illustration of procedures for estimating damping ratio of acoustic signals (log FPL no.1). a) Time history of the acoustic signal; b) time-scale distribution of wavelet modulus and wavelet ridge (red line) of the acoustic signal obtained through CWT; c) time-scale distribution of wavelet modulus and wavelet skeleton (black line); d) fundamental frequency component of the acoustic signal and its skeleton (red dash line); e) instantaneous frequency (scale), damping ratio and fitted damping ratio curve based on fundamental frequency component of the signal; f) second-order harmonic component of acoustic signal and its skeleton (red dash-line); g) instantaneous frequency (scale), damping ratio, and fitted damping ratio curve based on the 2nd-order harmonic component of the signal.

Relationships between Defect Ratio and the First-Order Damping Ratio

Figure 6 shows the data plot of defect ratio and first-order damping ratio of the hardwood logs. Regression analysis showed a moderate linear relationship ($R^2=0.65$), with two seemingly outliers (logs no. 6 and no.11). Examining the dissected cross-sections of these two logs, we found that they both contained a big single void that extended very deep, resulting in a defect ratio of 20.3% (no.11) and 31.7% (no.6) respectively. The voids in these logs were concentrated in the heartwood while the sapwood were left relatively intact. Although the acoustic velocity in these two logs had been reduced significantly as a result of the center rot, the acoustic energy had still been effectively transferred through the solid sapwood path and the energy dissipation due to the center void was much less than we would expect for a log with such a high defect ratio. As a result, the corresponding damping ratios were smaller than we expected from logs with such high defect ratios. Another factor that might have influenced the damping ratio is log moisture content. In Figure 6, log no.6 exhibited the largest deviation of damping ratio from the linear regression model. It turned out the log no.6 had the lowest moisture content (31.3%) among all the hardwood logs tested. The drier wood of log no.6 could have contributed to the low damping ratio value we observed.

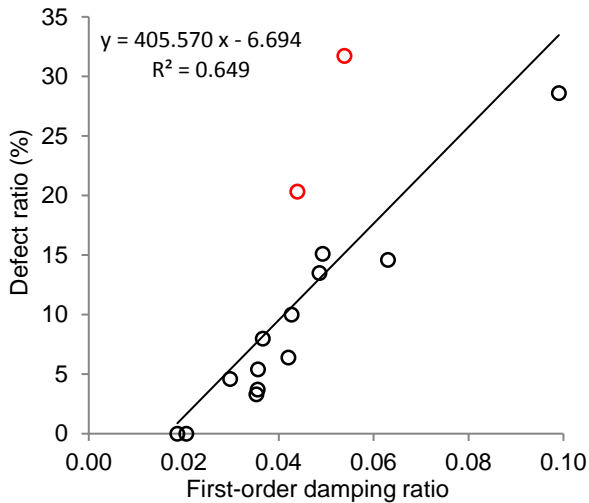


Figure 6—Relationship between defect ratio and the first-order damping ratio of the hardwood logs.

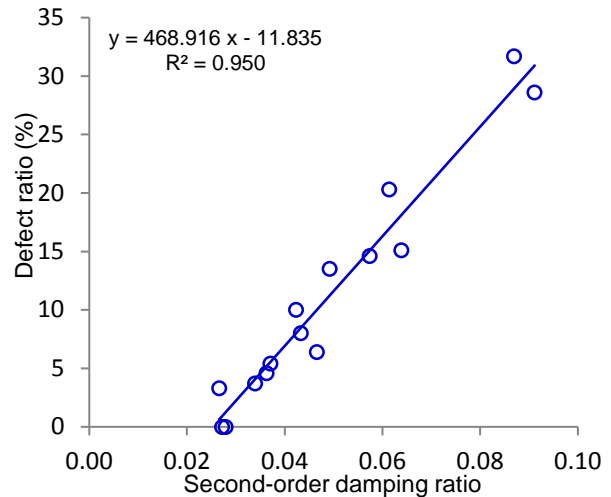


Figure 7—Relationship between defect ratio and the second-order damping ratio of the hardwood logs.

Based on the observed relationship between defect ratio and first-order damping ratio and the above analysis, it can be concluded that the first-order damping ratio not only depends on the size and volume of defects, but also related to the type of defects, wood MC, and how defects are distributed within a log.

Relationships between Defect Ratio and the Second-Order Damping Ratio

Similar to analysis of the first-order damping ratio, a linear regression analysis was also performed between the second-order damping ratio and log defect ratio. The results showed that the second-order damping ratio had an excellent linear relationship with the log defect ratio ($R^2 = 0.95$) (Figure 7). Comparing to the first-order damping ratio, the second-order damping ratio appeared not affected by the types of defects and how were they distributed in a log, but only relevant to the extent of the damage. Therefore, the second-order damping ratio of the response signal can characterize the defect condition of hardwood logs more accurately than the first-order damping ratio. Comparing to the acoustic velocity of a log, second-order damping ratio predicted the degree of damage in a log more accurately, and was not influenced by species.

Conclusion

In this study, we investigated the potential of an acoustic impact testing method for evaluating the soundness of hardwood logs. In addition to analyzing the log acoustic velocity as a predictor of defect ratio, a continuous wavelet transform (CWT) based method was used to determine the damping ratios of the first and second natural frequencies and their relationships with the extent of internal damage in a log. Based on the results and analysis, we drew the following conclusions:

1. Acoustic velocity measured in hardwood logs are negatively affected by the internal defects of the logs. Log acoustic velocity generally decreased with increasing severity of internal defects. When log velocity dropped below a critical value, the severity of internal decay increased at a much higher rate as log velocity continuously decreased. This critical velocity value can be different for different species, but 3,000 m/s can be used as a threshold for logs of mixed species.
2. Damping ratios of the natural frequencies are good indicators of hardwood log quality in terms of predicting the defect ratio. The first-order damping ratio not only depends on the extent of defects, but also related to the type of defects, wood MC, and how defects are distributed within a log.
3. Comparing to the first-order damping ratio, the second-order damping ratio appeared not affected by the types of defects and how were they distributed in a log, but only relevant to the extent of the damage.

Therefore, the second-order damping ratio of the response signal can characterize the defect condition of hardwood logs more accurately than the first-order damping ratio.

4. Comparing to the acoustic velocity, second-order damping ratio predicted the degree of damage of a log more accurately, and was not influenced by species.

The hardwood logs examined in this study contained a wide range of deterioration levels which were difficult to quantify with precision. The response signals from impact testing of the logs were complex and variable. Although the results and analysis indicated a very good potential of using the impact testing method, coupled with advanced signal analysis, to predict the existence and extent of internal defects in hardwood logs, large scale experiments with commercial-size logs need to be carried out in future to test the feasibility and applicability of the technique in production lines.

Acknowledgement

This project was conducted through research collaborations between the USDA Forest Service Forest Products Laboratory (FPL), Natural Resources Research Institute of University of Minnesota Duluth, and Nanjing Forestry University (NFU) in Nanjing, China. Feng Xu's research visit at FPL was supported by a project funded by the Priority Academic Program Development (PAPD) of Jiangsu Higher Education Institutions and the NFU Innovation Grant for Outstanding PhD Dissertations (Gant No. 163070682).

Reference

ASTM 2003. Standard test methods for direct moisture content measurement of wood and wood-base materials. ASTM D4442-92. America Society for Testing and Materials. Philadelphia, PA.

Bhandarkar S, Faust T, Tang M. 1999. Catalog: a system for detection and rendering of internal log defects using computer tomography. *Machine Vision and Applications* 11(4): 171-190.

Carpenter RD, Sonderman DL, Rast ED. 1989. Defects in hardwood timber. *Agricultural Handbook*, No. 678. Washington, DC: U.S. Department of Agriculture, Forest Service. 88 p.

Carter P, Briggs D, Ross RJ, Wang X. 2005. Acoustic testing to enhance western forest values and meet customer wood quality needs. PNW-GTR-642. USDA Forest Service, Pacific Northwest Research Station, Portland, OR. p 121-129.

Chang S. 1992. External and internal defect detection to optimize cutting of hardwood logs and lumber. *Transferring Technologies for Industry* No. 3. Beltsville, MD: U.S. Department of Agriculture, National Agriculture Library. 24 p.

Guddanti S, Chang S. 1998. Replicating sawmill sawing with topsaw using CT images of a full length hardwood log. *Forest Products Journal* 48(1): 72-75.

Kronland-martinet R, Morlet J, Grossmann A. 1987. Analysis of sound patterns through wavelet transforms. *International Journal of Pattern Recognition and Artificial Intelligence* 1(2): 273-302.

Le TP, Paultre P. 2013. Modal identification based on the time-frequency domain decomposition of unknown-input dynamic tests. *International Journal of Mechanical Sciences* 71: 41-50.

Li P, Abbott A, Schmoldt D. 1996. Automated analysis of CT images for the inspection of hardwood log. In: *Proceedings IEEE Conference on Neural Networks*. Washington, DC. 3:1744-1749.

- Pawlus W, Karimi HR, Robbersmyr KG. 2012. Multiresolution wavelet-based approach to identification of modal parameters of a vehicle full-scale crash test. 2012 IEEE International Symposium on Intelligent Control (ISIC) Part of 2012 IEEE Multi-conference on Systems and Control, October 3-5, 2012. Dubrovnik, Croatia.1172-1177.
- Pellerin, RF, DeGroot RC, Esenther GR. 1985. Nondestructive stress wave measurements of decay and termite attack in experimental wood units. In: Proceedings, 5th International Symposium on Nondestructive Testing of Wood, September 9-11, 1985, Pullman, WA. Washington State University. p 319-353.
- Sarigul E, Abbott A, Schmoldt DL. 2003. Rule driven defect detection in CT images of hardwood logs. In: International Conference on Image Processing and Scanning of Wood, August 21, 2000, Mountain Lake, Virginia. pp. 37-49.
- Slavič J, Simonovski I, Boltežar M. 2003. Damping identification using a continuous wavelet transform: application to real data, *Journal of sound and Vibration* 262:291-307.
- Staszewski WJ. 1997. Identification of damping in MDOF systems using time-scale decomposition. *Journal of Sound and Vibration* 203(2):283-305.
- Steele PH, Harless TEG, Wagner FG, Kumar L, Taylor FW. 1994. Increased lumber value from optimum orientation of internal defects with respect to sawing pattern in hardwood logs. *Forest Products Journal* 44(3): 69-72.
- Teng J, Zhu Y, Zhou F, Li H, Ou J, Fu X, Gu L. 2009. Modal parameters identification of large-span spatial structures based on complex Morlet wavelet transform. *Journal of Vibration and Shock* 28(8): 25-29.
- Thomas, RE. 2008. Predicting internal yellow-poplar log defect features using surface indicators. *Wood and Fiber Science* 40(1): 14-22.
- Thomas RE. 2009. Modeling the relationships among internal defect features and external Appalachian hardwood log defect indicators. *Silva Fenn.* 43(3):447-456.
- Thomas RE. 2010. Validation of an internal hardwood log defect prediction model. In: Fei et al. eds. Proceedings of the 17th Central Hardwood Forest Conference, April 5-7, 2010, Lexington, KY. Gen. Tech. Rep. NRS-P-78. Newtown Square, PA: U.S. Department of Agriculture, Forest Service, Northern Research Station: 77-82.
- Uhl T, Klepka A. 2005. Application of wavelet transform to identification of modal parameters of nonstationary systems. *Journal of Theoretical and Applied Mechanics* 43(2): 277-296.
- Ülker-Kaustell M, Karoumi R. 2011. Application of the continuous wavelet transform on the free vibrations of a steel-concrete composite railway bridge. *Engineering Structures* 33: 911-919.
- Wagner F, Taylor F, Ladd D, McMillin C, Roder F. 1989. Ultrafast CT scanning of an oak log for internal defects. *Forest Products Journal* 39(11/12): 62-64.
- Wang X, Carter P, Ross RJ, Brashaw BK. 2007. Acoustic assessment of wood quality of raw forest materials – A path to increased profitability. *Forest Products Journal* 57(5): 6-14.
- Wang X. 2013. Acoustic measurements on trees and logs: a review and analysis. *Wood Science and Technology* 47:965-975.

Nondestructive 3D Measurement of Roundwood for Volume and Quality Determination

Udo H. Sauter

Department of Forest Utilisation, Forest Research Institute, Baden-Wuerttemberg, Wonnhaldestr. 4, Freiburg, Germany, udo.sauter@forst.bwl.de

Joerg Staudenmaier

Department of Forest Utilisation, Forest Research Institute, Baden-Wuerttemberg, Wonnhaldestr. 4, Freiburg, Germany, Joerg.staudenmaier@forst.bwl.de

Franka Bruechert

Department of Forest Utilisation, Forest Research Institute, Baden-Wuerttemberg, Wonnhaldestr. 4, Freiburg, Germany, franka.bruechert@forst.bwl.de

Abstract

The importance of electronic roundwood measurement systems used in saw mills for accounting and optimizing purposes has increased continuously in the past decades. Today many softwood processing sawmills are equipped with 3D scanning systems. Based on the recorded high-resolution data, the outer shape of each single log can be described in detail. Volume and relevant log dimensions can be derived from this information, as well as certain quality parameters which are important key factors for further optimization of the break-down processes from logs to sawn timber.

Keywords: Roundwood measurement, scaling, grading, log quality

Introduction and background

Today electronic three-dimensional (3D) roundwood measurement systems are mainly used in modern European softwood mills and represent the key technology for accounting and further optimization of the sawing process at mill gate. Measurements are focused on log dimensions, derived log volume as well as quality parameters related to the outer log shape, such as taper and sweep. Three-dimensional measurement units are nowadays based on laser scanners which are using the laser scattering (tracheid effect). State-of-the-art digital cameras catch the reflected laser light signals which are subsequently processed and transferred to complete 3D-log shapes with high resolutions. This kind of data basis for each log provides any needed surface information for further data processing. Praxis oriented algorithms can be applied for calculating log volumes or information on taper resp. sweep of the logs which gain importance for accounting purposes but also for optimizing the value output of high grade sawn products. This type of the 3D scanning technology is well established and can be seen as the base NDT technology in terms of reasonable investment costs. Any further demand on especially solid inner log structure information leads to x-ray based scanning devices whereas a combination of single static installed x-ray-sources deliver first information of main structures but the high end solution is a real CT designed for industrial uses and standard log yard processing speeds. Only a CT for logs delivers sufficient information for precise sawing optimization in terms of lumber quality and value.

Nondestructive assessment by 3D measurement of roundwood

3D scanning technology

State-of-the-art 3D laser scanners at the mill gates are based on the projection of a laser ring and its detection by sensors, mostly high resolution digital cameras. The measurement principle is the so-called laser triangulation, whereas the laser light scatters on the log surface which makes it possible to identify the right position of the surface point. This type of surface measurement is possible for logs with bark as well as for debarked logs. The 3D scanners are static and the logs are travelling on the conveyer belt through the measurement unit up to a speed of 240 m/min. This provides additionally the log length and the continuous measurement enables measurements of short and long logs. The result is a high-resolution 3D scan.

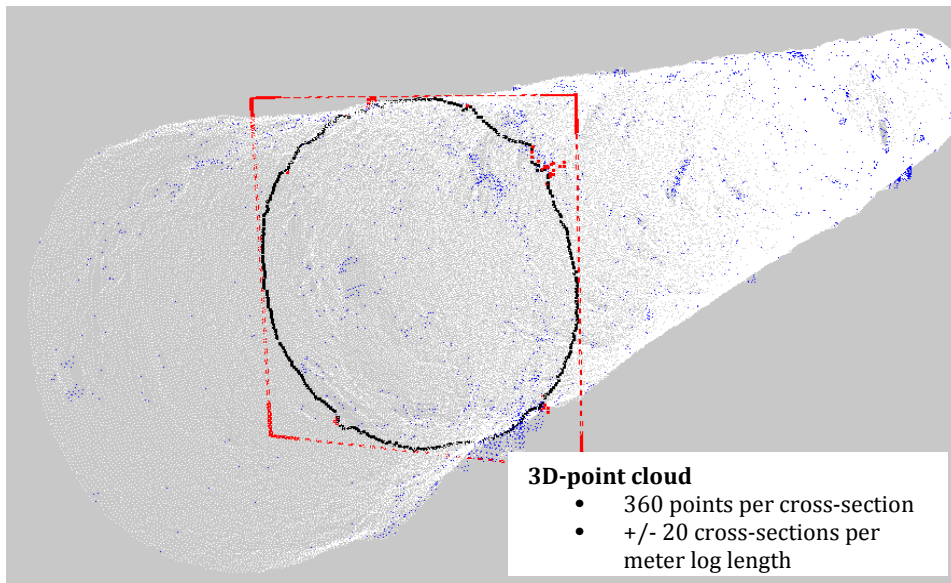


Figure 1—High resolution 3D-point cloud (Staudenmaier 2012)

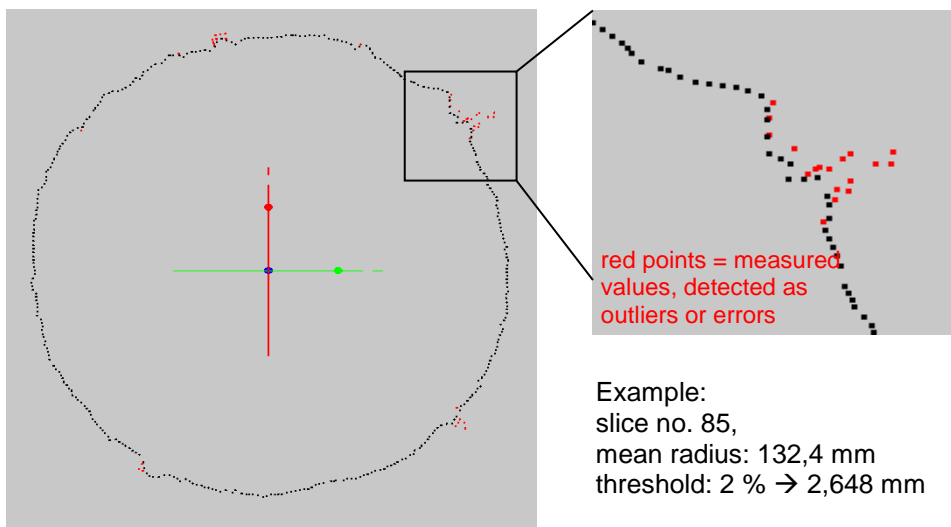


Figure 2—Outliers and smoothing algorithm (Staudenmaier 2012)

Data quality and data processing

To obtain reliable results, a distinct pre-processing of the raw data is essential. Because of the natural rough log surface and due to the technical issues like unavoidable influences of parts of the conveyer belt, quite often expected data of a contour are missing or “false” data is observed. The rough log surface is caused by manipulation gear, de-barker knives etc. which leads to ripped bark or ripped wood. The raw data survey shows often measured points as outliers which would cause misleading results. Therefore detected outliers (by introducing adapted thresholds) are exchanged by new computed surface values. The used algorithms are tested by their effect on aimed values. In any case, a thoroughly applied quality control has to be adapted before further calculations are made on that data basis.

Log surface and diameters

The log surface and its typical deviations from a strong regular geometrical form of a truncated cone plays the important role of all further going derivations like diameters needed as basis for volume calculations. The 3D-shape of a typical softwood log shows for example clearly identifiable branch whorls. But also irregular bark specifications or damages on the wood surface caused throughout the rough log manipulation are easily visible and detectable by 3D-scanning devices. That raises the question where to withdraw reliable contour measurements as basis for volume, taper and sweep calculation algorithms. The graphs in Figures 3 and 4 show exemplarily the problem for the “right” diameter measurement and the indirect influence of the surface parameters on the diameter measurements.

Conclusions

The presented details show clearly the high sensitivity of the aimed calculation results like volume or the quality parameter taper derived from 3D-laser scanner data. The detailed knowledge basis is necessary for the development of reliable algorithms for determining log volume and quality parameters as taper and sweep. On the basis of further research in that field the wide range of influences of log surface characteristics should be made transparent for a solid discussion of praxis solutions for the forest and wood industry branch.

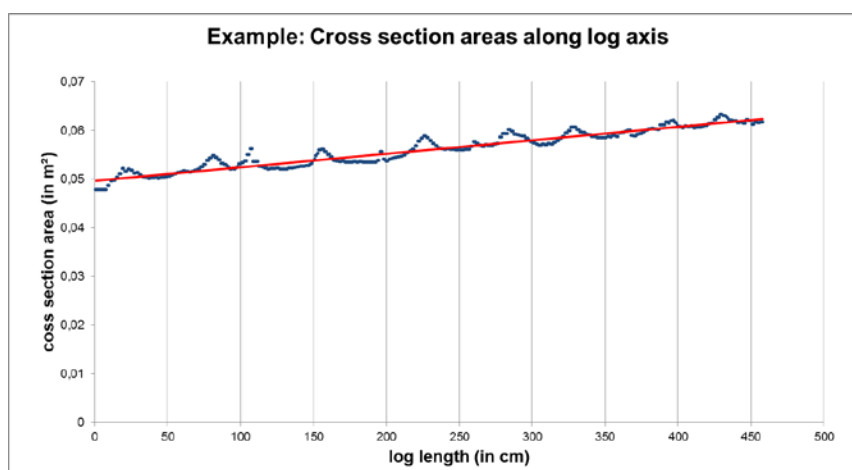


Figure 3—Typical log surface including clearly visible branch whorls, indicated are 50 cm sections along the total log length

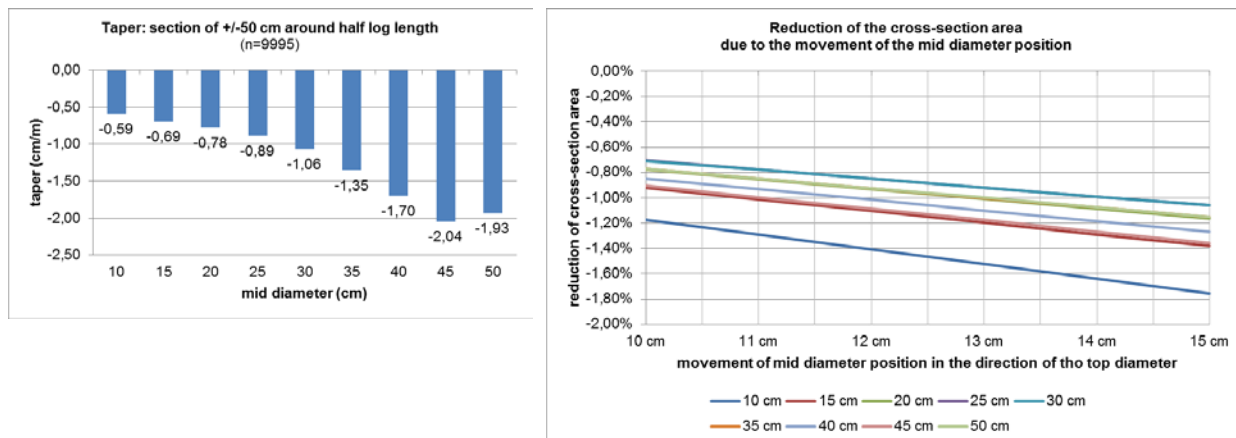


Figure 4—Taper depending on mid diameter of typical softwood logs and the influence of a moved mid diameter on the measured cross section area as basis of the volume calculation for accounting (Sauter and Staudenmaier, 2017)

Acknowledgments

We thank our science partners from several common research projects. Special thank goes to our industry partners for strong research cooperation and providing some pictures of this publication. We thank all authors for their cooperation.

References

- Bruechert, F.; Baumgartner, R.; Laudon, N.; Breinig, L. and Sauter, U.H. 2017. Roundwood sawing optimisation based on x-ray based computed tomography. Proceedings, IUFRO Division V Conference, June 12-16 2017, Vancouver
- Sauter, U.H.; Staudenmaier, J. und Verhoff, S. 2010. Mehr Transparenz im Rundholzgeschäft – Elektronische Rundholzvermessung: Wie groß sind die Volumenunterschiede wirklich? Holz-Zentralblatt Nr. 50 1269-1270
- Sauter, U.H. and Staudenmaier, J. 2017. Methods for precise scaling and grading of sawlogs using 3D-scanning system. Proceedings, IUFRO Division V Conference, June 12-16 2017, Vancouver
- Staudenmaier, J. 2012: Verfahren zur einzelstammweisen Volumen- und Konturermittlung von Stammholz am Beispiel von Nadel-Rundholzabschnitten. Schriftenreihe Freiburger Forstliche Forschung; Bd. 54. ISBN 978-3-933548-55-9

Wood I-beams Manufactured From Small Diameter Logs

Thomas Gorman

Univ. of Idaho, Moscow, Idaho, USA, tgorman@uidaho.edu

Bradley Miller

Retired, Missoula, Montana, USA, bradmillermt@gmail.com

David Kretschmann

USDA FPL, Madison, Wisconsin, USA, dkretschmann@fs.fed.us

Abstract

An innovative new concept for structural use of small diameter logs is a solid wood I-beam produced from a single log. We tested a set of 28 I-beams made from 15.25 cm diameter lodgepole pine (*Pinus contorta*) logs in bending to determine the MOE and MOR, to demonstrate the concepts and to determine if conventional stress design values for lodgepole pine logs could be applied. We also non-destructively assessed the MOE of individual logs prior to processing to determine if stress rating logs could predict final I-beam properties. I-beam stiffness was reasonably-well correlated with the stiffness of the log it was produced from; suggesting that non-destructive evaluation of raw logs offers a method for sorting to select high strength components.

Keywords: I-beam, small log utilization, non-destructive evaluation, timber construction, beetle killed pine

Introduction

Harvests to control pine beetle infestations in the Intermountain Western United States should increase the availability of small diameter logs that could be used for manufacturing building products. An innovative new concept with potential for efficient use of this material is a solid wood I-beam produced from a single, small diameter log. This structural product could serve as a locally produced substitute for glued laminated beams, window and door headers, components for pedestrian and short span road bridges, or other beam applications.

Objectives

The main objective of this study was to demonstrate and test the concept of manufacturing structural I-beams from small diameter lodgepole pine (*Pinus contorta*) logs. We tested a set of I-beams in bending to determine the modulus of elasticity (MOE) and modulus of rupture (MOR), in order to determine if conventional stress design values for lodgepole pine logs could be applied. A second objective was to non-destructively assess the stiffness of individual logs prior to processing to determine if stress rating raw logs could be used to predict final I-beam properties and thus offer a procedure for selecting logs with the best potential for making I-beams.

Background

By using small diameter logs as structural components themselves, rather than sawing into dimension lumber, more complete utilization of the log is achieved. This concept has been successfully demonstrated in several pavilions, kiosks, a library, and a pedestrian bridge (Green et al. 2005).

Non-destructive grading methods for determining allowable design stresses for small diameter roundwood in the United States have been developed (Green *et al.* 2006, Green *et al.* 2008, Green *et al.* 2007). These methods are based on the machine stress grading evaluation procedure, for which the stiffness of components is evaluated as a mechanically measurable predictor of suitability for end use. Mechanical grading systems also employ some form of visual “override,” a visual appraisal of specified characteristics that affect piece strength and stiffness, as well as limitations to end use performance such as warp and wane. Because machine stress grading sorts lumber into grades using a mechanically measurable predictor, such as MOE, grades are less variable in the predictor compared to similar visual grades (Galligan and Snodgrass 1970). When deflection criteria is the controlling limit to long span beams, preselecting logs with high stiffness characteristics to make structural components should be useful.

Green *et al.* (2006) established the technical basis for mechanical grading 228 mm diameter logs. The material for that study was 236 logs of the Englemann spruce (*Picea engelmannii*)-alpine fir (*Abies lasiocarpa*)-lodgepole pine (*Pinus contorta*) species grouping (ES-AF-LP). The logs were cut from fire-killed trees and were at a moisture content of about 15 to 17 percent at time of test. Bending tests were conducted on 169 logs and short column compression tests on 67 logs. The relationships between properties are the basis for the mechanical grading of structural lumber. For machine stress rated lumber bending strength is estimated from modulus of elasticity. The coefficient of determination (r^2) between MOE determined by transverse vibration (E_{tv}) and determined by static test in third-point bending (MOE) was 0.83 for these 923 cm diameter logs. The r^2 value for the correlation between MOR and E_v , was 0.53, and that between MOR and MOE was 0.68. These correlations are similar to the results expected for softwood dimension lumber (Green and McDonald 1993) and thus confirmed the potential for mechanical grading these logs for structural applications. The 90 percent lower confidence limit on the MOE-MOR relationship excludes 5 percent of the data on the lower side of the regression, and provides the regression equivalent to the 5th percentile traditionally used to assign properties to visually graded lumber.

Stepwise regression indicated that if MOE is measured, then addition of characteristics such as knot size and slope of grain provide only a marginal increase in the ability to predict MOR. In the initial phase of the study (Green *et al.* 2004) the value between MOR and MOE increased from 0.61 to 0.67 with the addition of knot size (root mean square error increased from 4.46 MPa to 4.80 MPa). It was recommended that MOE be the primary sorting criteria for the proposed grading system but that the maximum allowable knot size and slope of grain be limited to those allowed in No. 3 visual grade; knot size $\leq 3/4$ of the diameter and slopes ≤ 1 in 6. Factors that might affect serviceability such as degree of roundness and warp were also set at the limits given for the No. 3 visual grade.

Green *et al.* (2006) concluded the following from their research on mechanical grading of structural roundwood:

- Property assignment procedures for visually graded logs using *ASTM D 3957/D 245* [12] produce slightly conservative assignment of MOE values and quite conservative assignment of allowable bending and compression strengths parallel to grain.
- A good correlation exists between static MOE in third-point bending and MOE determined by transverse vibration and between static bending strength, static MOE, and MOE by transverse vibration.
- Procedures traditionally used to assign allowable compressive strength parallel to grain to mechanically graded lumber also appear applicable to round timbers.
- There are apparently no technical barriers to developing a mechanical grading system for 228 mm diameter round timber beams.

- Additional research is needed to clarify anticipated grade yields at higher mechanical grades and the applicability of the proposed methods to logs of other sizes and species. Some of this research is in progress.
- Mechanical grading offers an opportunity to improve the precision of the property assignment for round timber beams and significantly increase grade yield for a given property specification.

In addition, earlier work demonstrated that mid-span, single point loading used to non-destructively determine the MOE of doweled logs gave good correlation ($r^2 = 0.94$) to the static MOE determined by ASTM D-198 third-point bending tests procedures (ASTM 2014). The advantage of using single-point loading as a non-destructive method to determine MOE is the simplicity with which a measurement can be obtained, as well as the possibility for future implementation in an industrial setting.

In general, machining small-diameter logs to a constant diameter removes much of the mature wood on the outside of the beam, thus exposing more of the juvenile wood core. It also tends to expose more knots, especially in species that readily self-prune limbs on the lower part of the stem as the tree grows. The net effect of the machining is to lower both MOR and MOE. In a study on the effect of machining on small-diameter Douglas-fir (*Pseudotsuga menziesii*) and ponderosa pine (*Pinus ponderosa*) logs (Green *et al.* 2005), suppressed-growth Douglas-fir logs, the MOR of 76- to 152-mm logs machined to a uniform diameter was reduced by about 8%, whereas the MOE was reduced about 15%. For 76- to 152-mm ponderosa pine logs, the MOR was reduced about 12% and the MOE about 33%. The greater effect of processing on the properties of ponderosa pine compared with those of Douglas-fir was probably a result of the respective ages of the trees, coupled with the relatively larger juvenile wood core of the shade-intolerant ponderosa pine. The suppressed-growth Douglas-fir trees had an average age of 67 years, whereas the average age of the ponderosa pine was only 42 years.

The concept of using small diameter logs to manufacture I-beams was developed to produce structural components that exceed the carrying capacity of individual structural logs (Figure 1). The conversion from roundwood to wood I-beams can potentially utilize over 80 percent of the material from a doweled log. For a tapered log, the conversion ratio would be reduced. The cross sectional moment of inertia increases nearly five times when converting roundwood to wood I-beams, effectively doubling the allowable span length. Table 1 provides examples of the estimated weights and cross sectional properties for six different small diameter timber sizes when converted to wood I-beams. If small diameter wood-I beams can perform at anticipated structural capacities, there is an opportunity to encourage beam production facilities in rural areas where pine beetle infestations have created the need for harvesting trees that are not large enough to be suitable for use as dimension lumber but adequate for production into I-beams.

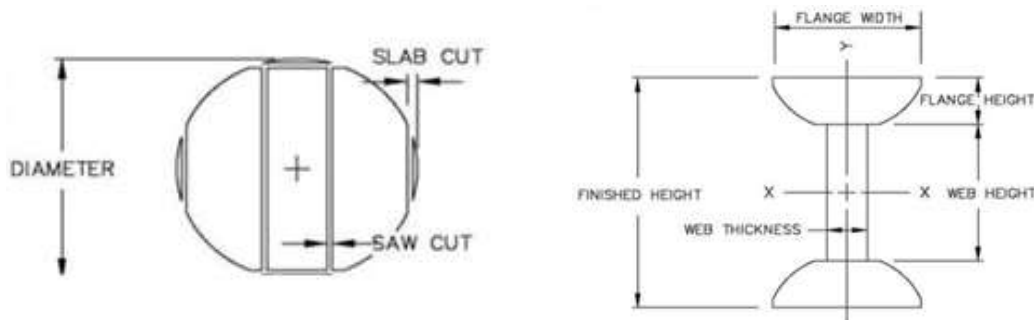


Figure 1-- Cutting pattern (left) for converting a small diameter log into components to produce an I-beam (right).

Table 1 -- Examples of the weights and cross sectional properties of six different diameter round wood I-Beams. Roundwood values are shown above wood I-beam values.

Initial Roundwood Diameter & Finished Height (cm)	Area (cm ²)	Weight (kg/m)	Web Thick. (cm)	Web Height (cm)	Flange Width (cm)	Flange Thick. (cm)	Axis X-X		C.G. (cm)	Axis Y-Y	
							I	S		I	S
							(cm ⁴)	(cm ³)		(cm ⁴)	(cm ³)
10.2	81.1	6.5					523	103		523	106
15.2	69.7	5.6	2.5	9.2	9.2	3.0	2,013	263	4.9	261	91
14.6	167.5	13.4					2,233	305		2,233	219
22.9	148.9	11.9	3.2	13.3	13.3	4.8	10,003	873	7.6	1,254	195
19.1	285.0	22.8					6,465	677		6,465	373
30.5	257.7	20.6	3.8	17.5	17.5	6.5	31,300	2,048	10.3	3,855	337
21.3	355.4	28.5					10,052	942		10,052	465
33.8	325.7	26.1	4.4	19.7	19.7	7.3	49,715	2,891	11.5	6,004	426
23.5	433.6	34.7					14,959	1,270		14,958	567
38.1	401.6	32.2	5.1	21.9	21.9	8.1	75,209	3,936	12.7	8,933	525
26.0	532.4	42.6					22,551	1,727		22,553	697
41.9	492.0	39.4	5.7	24.1	24.1	8.9	111,054	5,284	13.9	13,390	644

Methods

Logs used in the study were purchased from a cooperating post and pole manufacturer and preselected by measuring the stress wave velocity of logs using Fiber-gen Director HM200 acoustic log stress wave equipment (Carter et al. 2006). The intent was to select logs that represented a range of stiffness values and to establish the correlation between stress wave velocities of logs and the MOE of I-beams produced from them. A total of 40, 15.25 cm diameter logs, measuring 4.9 m in length, were selected and brought to the laboratory. The logs were then non-destructively evaluated using a single-point, mid-span bending test to predict MOE, and from those results, we selected 28 logs that represented the 10 most stiff and 10 least stiff, plus 8 logs from the mid-range stiffness. The Equation (1) used to determine MOE from a single-point, mid-span load/deflection relationship is:

$$\text{MOE} = (L^3/48)(P/\Delta I) \quad (1)$$

where P/Δ = slope of load-deformation relationship, L = span, and I = moment of inertia

In addition, the stress wave velocity, as well as the volume and mass, of each log was measured in the laboratory to calculate the dynamic MOE (MOE_{dyn}), using the Equation (2) provided by Carter *et al.* (2006):

$$\text{MOE}_{\text{dyn}} = \rho V^2 \quad (2)$$

where ρ = nominal density and V = acoustic velocity

A portable bandsaw mill was used to cut each of the logs into three sections as shown in Figure 1, marked to identify the specific log that each component was made from, stacked, and air dried to approximately 12% moisture content. The components were then machined to create smooth surfaces for gluing, and a groove was machined into each of the flanges to assist with later assembly (Figure 2). I-beams were

assembled by brushing a room temperature curing phenol-resorcinol adhesive into each groove, stacking four I-beam assemblies at a time, and clamping overnight. Final dimensions of the I-beams were 21 cm high, 12.75 cm wide, and 3.66 m long.



Figure 2 -- Machined components prior to gluing. The groove cut in the flanges was made to assist with positioning the webs during assembly.

After curing, the I-beams were kept in a conditioning room to maintain a 12% moisture content. Bending tests were then carried out using ASTM D 198 third-point loading procedures (ASTM 2014) to determine MOE and ultimate bending stress for each I-beam.

Results

The average cross sectional area for the 28 I-beams was 131.7 cm^2 (COV = 2.0). This area represents a utilization of 72% of the available wood fiber present in the raw logs obtained for the study. The bandsaw mill sawing and subsequent profile machining procedures used to prepare the components likely impacted the ratio of fiber utilization, such that a more precise sawing and machining procedure could improve the yield.

The average moment of inertia for the 28 I-beams was 7582.4 cm^4 (COV = 2.2). A higher moment of inertia could have been achieved by reducing the depth of the groove used to position the web members (shown in Figure 2). This reduction would have improved the fiber yield and increased the carrying capacity of the I-beams.

Moisture content of the I-beams at the time of the bending tests averaged 12.7%. The mean static MOE for the 28 I-beams was 8.87 GPa (COV = 10.6).

The stress wave velocities measured in the field with the Director HM200 did not correlate well ($r^2 = 0.3477$) with the static MOE of the I-beams produced from them (Figure 3). However, when log density measurements were combined with stress wave velocity to predict MOE_{dyn} using Equation (2), the correlation was significantly improved ($R^2 = 0.840$) (Figure 4).

The static MOE of raw logs, determined by imposing a single-point, mid-span load on each log and measuring deflection, also correlated well ($r^2 = 0.839$) with the static MOE of the manufactured I-beams (Figure 5).

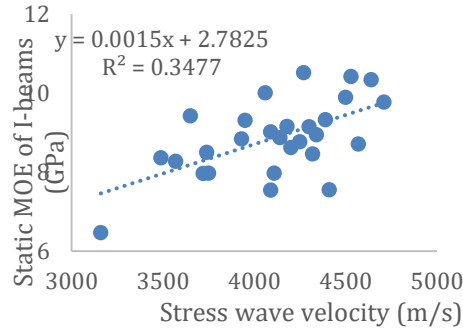


Figure 3 -- Relationship between field measurements of the stress wave velocities of logs and the static MOE of I-beams produced from the logs.

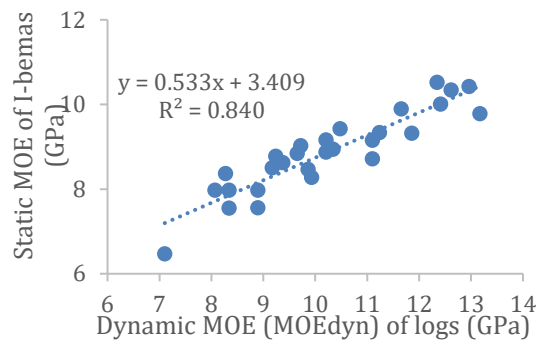


Figure 4 -- Relationship between dynamic MOE of logs, as determined by stress wave velocity and density measurements, and the static MOE of I-beams produced from the logs.

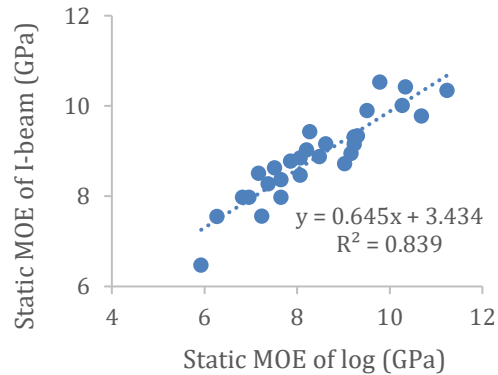


Figure 5 -- Relationship between static MOE of logs, as determined by single-point, mid-span loading, and the static MOE of I-beams produced from the logs.

Seven of the 28 I-beams tested in bending failed due to shear in the web members (Figure 6). The ultimate bending loads on 5 of these samples were the highest recorded for all I-beams; the ultimate loads for the remaining 2 samples that failed in shear were the 10th and 11th highest recorded. The association of the shear failures with some of the highest levels of bending stresses suggest that the ultimate shear resistance of the wood-I beams was well balanced with the ultimate bending stress resistance. Average

shear stress at failure for the 7 specimens that failed in shear was 5,492 kPa (COV = 9.3), which is slightly higher than the value of 4,200 kPa reported for shear parallel to grain reported in the Wood Handbook (Forest Products Laboratory 2010) for lodgepole pine. No glueline failures were observed in any of the specimens.



Figure 6 -- Seven of the 28 I-beams tested to failure in bending exhibited shear failure in the webs.

The mean Modulus of Rupture (MOR) value for all of the I-beams was 59,623 kPa (COV = 22.4), which is somewhat lower than that reported in the Wood Handbook (Forest Products Laboratory 2010) for clear, straight-grained lodgepole pine bending samples (65,000 kPa), but consistent with the values found for No. 1 and Select Structural visually graded lodgepole pine dimension lumber in a previous study (Erikson et al 2000). The correlation between static MOE and the 21 beams that failed in bending was poor ($r^2 = 0.227$) (Figure 7).

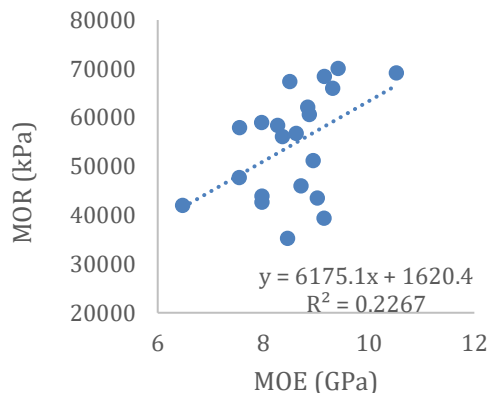


Figure 7 – Relationship between the static MOE and the MOR of the 21 I-beams that failed in bending.

Conclusions

I-beams were successfully made from doweled roundwood by sawing each log into 3 pieces and assembling the components into I-beams using structural glues. Since an I-beam made from a small diameter log has a significantly larger moment of inertia than the log it was produced from, this concept has the potential to significantly increase the structural use of small diameter roundwood. It is suggested that an improvement in the shear resistance of these I-beams can be made if the thickness of the web is increased slightly.

I-beam stiffness was reasonably-well correlated with the stiffness of the log it was produced from, suggesting that non-destructive evaluation of raw logs offers a method for sorting to select high strength

components. There appears to be potential to predict, and therefore, assign, stiffness and strength values for I-beams made from beetle killed small diameter logs.

Acknowledgement

We would like to recognize the assistance of Dr. Carl Morrow in the preparation and testing of this material. Funding for this study was provided by the Coalition for Advanced Structures.

References

American Society for Testing and Materials (ASTM). 2014. Standard methods of static tests of lumber in structural sizes, D 198-02; Standard practices for establishing structural grades and related allowable properties for visually graded lumber, D245-00; Standard practice for establishing stress grades for structural members used in log homes, D 3957-90. *In: Annual Book of Standards, Volume 04.10.* Wood. ASTM, West Conshohocken, PA, USA.

Carter, P., S. Chauhan, and J. Walker. 2006. Sorting logs and lumber for stiffness using Director HM200. *Wood and Fiber Science*, 38(1): 49-54.

Erikson, R.G., T. M. Gorman, D.W. Green, and D. Graham. 2000. Mechanical grading of lumber sawn from small-diameter lodgepole pine, ponderosa pine, and grand fir trees from Northern Idaho. *Forest Products J.* 50(7/8): 59-65.

Forest Products Laboratory. 2010. Wood handbook - Wood as an engineering material. General Technical Report FPL-GTR-190. Madison, WI: U.S. Department of Agriculture, Forest Service, Forest Products Laboratory: 508 p.

Galligan, W.L. and D.V. Snodgrass. 1970. Machine stress rated lumber: Challenge to design. *In: Proceedings, American Society of Civil Engineering. Journal of Structural Division.* (ST12)96: (Pap. 7772): 2639–2651.

Green, D.W., J. W. Evans, J. F. Murphy, C. A. Hatfield, and T. M. Gorman. 2005. Mechanical grading of 6-inch-diameter lodgepole pine logs for the travelers' rest and rattlesnake creek bridges. Research Note FPL-RN-0297. U.S. Department of Agriculture, Forest Service, Forest Products Laboratory, Madison, WI, USA.

Green, D.W., T.M. Gorman, J.W. Evans, and J.F. Murphy. 2004. Improved grading system for structural logs for log homes. *Forest Products J.* 54(9):52-62.

Green, D.W., T. M. Gorman, J. W. Evans, and J. F. Murphy. 2006. Mechanical grading of round timber beams. *J. of Materials in Civil Engineering.* 18(1):1-10.

Green, D.W., T. M. Gorman, J. W. Evans, and J. F. Murphy. 2008. Grading and properties of small-diameter Douglas-fir and ponderosa pine tapered logs. *Forest Prod. J.* 58(11):33-41.

Green, D.W., T. M. Gorman, J. F. Murphy, and M. B. Wheeler. 2007. Moisture content and the properties of lodgepole pine logs in bending and compression parallel to the grain. Research Paper, FPL-RP-639. USDA Forest Service, Forest Products Laboratory, Madison, WI, USA.

Green, D.W. and K.A. McDonald. Mechanical properties of red maple structural lumber. 1993. *Wood and Fiber Sci.* 25(4):365-374.

Session 12

Poster Session

Relationship between Drilling Resistance and Wood Anatomy in Young Eucalypt

José Tarcísio da Silva Oliveira*

Forest and Wood Science, Federal University of Espírito Santo, Jerônimo Monteiro, ES, Brazil,
jose.t.oliveira@ufes.br

Xiping Wang

USDA Forest Service, Forest Products Laboratory, Madison, WI, USA, xwang@fs.fed.us

Brunela Pollastrelli Rodrigues

Forest and Wood Science, Federal University of Espírito Santo, Jerônimo Monteiro, ES, Brazil,
brunelafloresta@yahoo.com.br

Graziela Baptista Vidaurre

Forest and Wood Science, Federal University of Espírito Santo, Jerônimo Monteiro, ES, Brazil,
grazividaurre@gmail.com

* Corresponding author ,+552835582513, jose.t.oliveira@ufes.br

Abstract

The objective of this study was to evaluate the relationship between Resistograph amplitude and wood anatomy along the stem diameter of trees at a young *Eucalyptus* plantation grown for pulpwood production. The genetic material used in this study consisted of two trees, one 34 months old and one 62 months old, from *Eucalyptus grandis* × *Eucalyptus urophylla* hybrid clonal plantations located in the north of Espírito Santo State, Brazil. The relationship between drilling resistance and wood anatomical parameters in the clone hybrid wood from two ages changed with tree age; the correlation coefficients between Resistograph amplitude and anatomical parameters were better in the 62-month-old tree than in the younger tree. In the older tree, the anatomical parameter that better correlated with drilling resistance was fiber wall thickness. When all data from the two ages were combined, all anatomical parameters were correlated with drilling resistance. The wood of both ages showed a good correlation between drilling resistance and wood specific gravity.

Keywords: eucalypt wood, Resistograph® amplitude, anatomical parameters, correlations.

Relationship between Wood Moisture Content and Drilling Resistance in Eucalypt Trees

José Tarcísio da Silva Oliveira*

Forest and Wood Science, Federal University of Espírito Santo, Jerônimo Monteiro, ES, Brazil,
jose.t.oliveira@ufes.br

Xiping Wang

USDA Forest Service, Forest Products Laboratory, Madison, WI, USA, xwang@fs.fed.us

Graziela Baptista Vidaurre

Forest and Wood Science, Federal University of Espírito Santo, Jerônimo Monteiro, ES, Brazil,
grazividaurre@gmail.com

Brunela Pollastreli Rodrigues

Forest and Wood Science, Federal University of Espírito Santo, Jerônimo Monteiro, ES, Brazil,
brunelafloresta@yahoo.com.br

* Corresponding author, +552835582513, jose.t.oliveira@ufes.br

Abstract

The objective of this study was to evaluate the relationship in the radial sense to moisture content with drilling resistance along the stem diameter in trees at a young *Eucalyptus* plantation grown for pulpwood production. The genetic material used in this study consisted of 50 trees of age 34 months and 50 trees of age 62 months of the clonal hybrid *Eucalyptus grandis* x *Eucalyptus urophylla* from a forest plantation situated in the north of Espírito Santo State, Brazil. In 34-month-old trees, correlation coefficients between drilling resistance and wood moisture content were low, and in some situations not significant at 1% probability. In 62-month-old trees, correlation coefficients between drilling resistance and moisture content improved, with correlation coefficients of -0.65 and 0.81 at diametric distances of 10 and 15 mm in the first half of the diameter. When the trees were combined, good correlation coefficients were found in the different diametric distances for the first half of the diameter. The best correlation coefficient when combining the trees of two ages was -0.75 between amplitude and wood moisture content in the first half of the diameter at 5 mm of the periphery of the stem. The good correlations were found mainly in the 64-month-old trees, and when combined, the two tree groups confirm the possibility of a successful use of the Resistograph to evaluate moisture content of eucalypt logs with good accuracy and relatively low cost.

Keywords: eucalypt wood, Resistograph® amplitude, wood moisture contents, correlations.

Evaluation of the Modulus of Elasticity of the Wood Using a Portable Device Based on Stress Wave Method

Antonio Alves Dias

Department of Structural Engineering, São Carlos School of Engineering-São Paulo University, São Carlos, São Paulo State, Brazil, dias@sc.usp.br

Jairo Ribas de Andrade Jr.

Department of Structural Engineering, São Carlos School of Engineering-São Paulo University, São Carlos, São Paulo State, Brazil, jairoribasjr@gmail.com

Pedro Gutemberg de Alcântara Segundinho

Department of Forestry and Wood Sciences, Federal University of Espírito Santo, Jerônimo Monteiro, Espírito Santo, Brazil, pedro.segundinho@ufes.br

Abstract

The objective of this study was to evaluate the modulus of elasticity of timber using a stress wave method and to compare the results with values obtained from static bending tests. Tests were performed in 260 visually graded pieces of *Pinus elliottii* specie, from São Paulo State-Brazil, with nominal dimensions 45mm x 105mm x 2500mm. Dynamic modulus of elasticity (E_{MTG}) were obtained by non destructive testing of longitudinal vibration, using a portable device Brookhuis Microeletronic Timber Grader (MTG), based on stress wave method. Static modulus of elasticity (MOE) were obtained from a three points static bending test. Results show a good estimative of MOE from the results obtained using MTG device (E_{MTG}). The correlation coefficient ranged from 0.76 (S3 grade) to 0.91 (SS grade) and was 0.86 for the complete lot.

Keywords: stress wave, Microeletronic Timber Grader, structural grading

Introduction

Sawn timber of structural dimensions is a heterogeneous material, which presents defects that reduce its resistance. A non-destructive mechanical test should be based on known correlations between the resistances and other properties that can be evaluated without damaging the material. Modulus of elasticity is the mechanical property that is evaluated most of cases.

The modulus of elasticity can be obtained by means of static bending tests or by dynamic methods such as transverse vibration, longitudinal vibration or ultrasound, which are faster and easier to perform.

The objective of this work was to evaluate the nondestructive test by means of longitudinal vibration using the MTG BrookHuis portable device to obtain the modulus of elasticity of boards of *Pinus elliottii*,

visually graded according to the rules of the Southern Pine Inspection Bureau (SPIB), presented by Carreira 2003.

The American Society for Testing and Materials (ASTM D4761) presents the procedures of the four points static bending test for sawn wood beams with structural dimensions. Relation between support span and height of the beams must be between 18 and 21. In this test shear stresses don't have significant influence in the MOE (Bodig and Jayne, 1993).

Dynamic methods based on natural frequency measurements can be used to determine the dynamic modulus of elasticity (Ed). An advantage of dynamic measurements is the short duration of the test. In general, the dynamic modulus of is slightly higher than those obtained from static tests, but the differences are small, on the order of 5% to 15% (Kollman and Cote 1968).

Segundinho et al. 2012 evaluated the effectiveness of test based on the natural vibration frequencies, using the Sonelastic® device, on beams of Pinus oocarpa. The dynamic modulus of elasticity was more than 10% higher than the MOE obtained in static bending tests.

Horacek and Tippner 2012 obtained the dynamic modulus of elasticity (Ed) using the longitudinal stress wave method for the specie Pinus sylvestris L., with density between 370kgf / m³ and 543kgf / m³. The results showed higher values for Ed and significant correlation ($R^2 = 0.96$) between the Ed and the MOE obtained from static bending tests.

Material and methods

The tests and procedures were carried out at the Laboratory of Wood and Timber Structures (LaMEM), of the Department of Structural Engineering (SET) of the São Carlos School of Engineering (EESC), University of São Paulo (USP). Firstly, the visual structural grading of timber boards was performed. After that, the dynamic modulus of elasticity (E_{MTG}) was evaluated using MTG device. Then, static bending tests were performed to determine the edgewise modulus of elasticity (MOE).

Material

Two hundred sixty boards of Pinus elliottii from the Southwest of São Paulo State, Brazil, were used, with nominal dimensions of 45mm x 105mm x 2500mm, previously oven dried. Forty seven boards that presented wane, resin pocket and excessive warp were discarded, remaining 213 board for the tests.

Methods

Visual grading

Timber boards were visual graded using Southern Pine Inspection Bureau rules. Table 1 presents defects limits related each visual grade.

Table 1—Defect limits for each visual grade

Grade	Knot diameter (mm)		Grain orientation (%)	Surface Ring shake	Split
	wide face	narrow face			
SS	9 mm	37 mm	8%	600 mm	105 mm
S1	11 mm	47 mm	10%	600 mm	105 mm
S2	15 mm	53 mm	12.5%	625 mm	157 mm
S3	23 mm	79 mm	25%	-	416 mm

Dynamic tests

Dynamic modulus of elasticity (EMTG) were obtained by longitudinal vibration test, using a portable device Brookhuis Microeletronic Timber Grader (MTG), based on stress wave method (Rozema 2013). Figure 1 shows this device in use. Through a internal software, imputing the moisture content and wood specie, the MTG device evaluate the modulus of elasticity for a moisture content equal to 12%.



Figura 1—Portable device Brookhuis Microeletronic Timber Grade (MTG)

Obtaining the dynamic modulus of elasticity from the natural frequency is the basis of formulation used by MTG. This equipment applies a correction to modify the dynamic modulus obtained, depending on the species, resulting in estimated values of the modulus of elasticity (E_{MTG}). Previously, the following characteristics of the piece should be reported: dimensions, moisture content, temperature and weight. Results are transferred to a PC/laptop by Bluetooth. These results can be "translated" into one of the many international standards used for mechanical graded of timber.

Static bending tests

Modulus of elasticity (MOE) was obtained through the static bending test showed in Figure 2. Span between supports was 18 times the height of the timber board.



Figura 2—Static bending test to determine edgewise modulus of elasticity (MOE)

Results

The average moisture content was 9.5%. The mean apparent density at 12% moisture content was 484 kg/m³, varying between 470 kg/m³ and 502 kg / m³. Tables 2 and 3 present the descriptive statistics of the results obtained for MOE and the E_{MTG}, respectively, considering the totality of boards and each visually graded group.

Table 2—Descriptive Statistic of the static modulus of elasticity (MOE)

	Totality	SS	S1	S2	S3
Mean (MPa)	7270	8250	7071	7019	6875
Standard deviation (MPa)	1960	2112	1652	1938	1709
Minimum value (MPa)	3183	4076	3183	3325	3349
Maximum value (MPa)	14728	14728	10715	14366	12341
Coefficient of variation (%)	27	26	23	28	25
Quantity of boards	213	72	43	42	56

Table 3—Descriptive Statistic of the dynamic modulus of elasticity (E_{MTG})

	Totality	SS	S1	S2	S3
Mean (MPa)	7558	8611	7214	7162	7254
Standard deviation (MPa)	2203	2489	1861	2084	1950
Minimum value (MPa)	3432	3769	3541	3432	3845
Maximum value (MPa)	16006	15999	12545	16006	12831
Coefficient of variation (%)	29%	29%	26%	29%	27%
Quantity of boards	213	72	43	42	56

A simple linear regression model was used to compare the dynamic modulus of elasticity obtained with the MTG device (E_{MTG}) and the static modulus of elasticity (MOE). The analysis was done determining the linear regression equation, the correlation coefficient and analyzing the residues, to verify compliance with the requirements. Afterwards, the variance analysis was performed to verify the condition of the adjusted model. Figure 3 shows: (A) linear regression analysis for the totality of data; (B) residual analysis, where can be observed the homogeneity of variance.

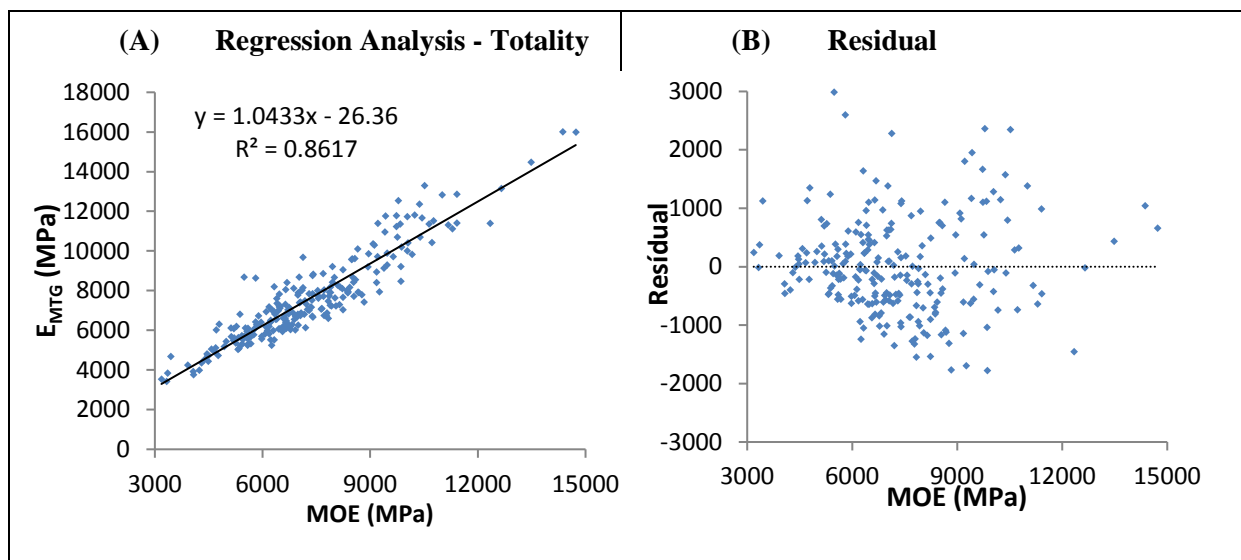


Figure 3—(A) Regression Analysis and (B) residual for the totality of boards

Figure 4 shows the regression analysis for each visually graded group. Table 4 presents a summary of the values obtained in all regression analysis.

Table 4—Summary of regression analysis

Grade	Correlation	Equation
	coefficient	
Totality	0.86	1.043 MOE-26,36
SS	0.91	1.125 MOE-672,5
S1	0.85	1.036 MOE-115,3
S2	0.88	1.009 MOE+78,9
S3	0.74	0.982 MOE+500,8

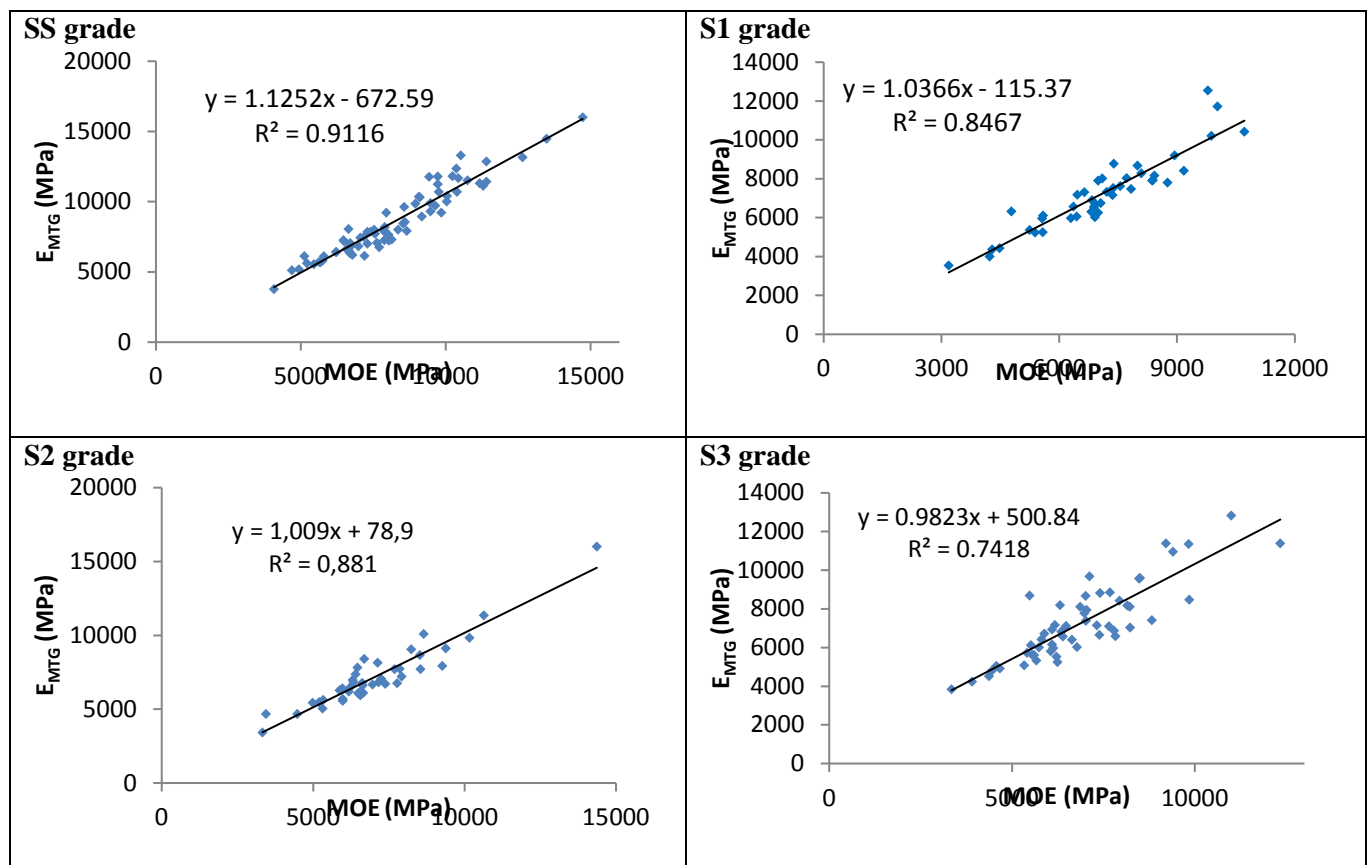


Figura 4—Regression analysis .

Conclusion

For the totality of pieces, mean value of dynamic modulus of elasticity (E_{MTG}) was 4% higher than the static modulus of elasticity (MOE) obtained from static bending tests. In each visually graded group, mean values of E_{MTG} were always higher than the mean values of MOE: SS (+4.4%), S1 (+2%), S2 (+2%) and S3 (+5.5%).

The regression analyzes showed a good correlation for all cases: 0.86 (totality), 0.91 (SS), 0.85 (S1), 0.88 (S2) and 0.74 (S3). The best correlation was for the SS group, and a decrease in the correlation coefficient with the decrease in the quality of the group of boards could be observed.

The portable MTG device presented good results for the evaluation of MOE, and his use is recommended for the mechanical grading of timber boards.

Acknowledgments

The authors thank CNPq (National Counsel of Technological and Scientific Development) and CAPES (Coordination for the Improvement of Graduated People) for financial support and grants.

References

- Bodig, J.; Jayne, B. A 1993. *Mechanics of Wood and Wood Composites*. New York: Van Nostrand Reinhold. 712 p.
- Kollmann, F.F.P.; Cote, W. A. 1968. *Principles of wood science and technology*. Vol 2: Solid Wood. New York, Springer Verlag. 592 p.
- ROZEMA, P. 2013. *TimberGrader MTG: Operational instructions*. Holanda: Enschede Institutenweg, 93p.
- Carreira, M. R. 2003. *Critérios para classificação visual de peças estruturais de Pinus sp.* São Carlos School of Engineering- São Paulo University. São Carlos-SP-Brazil. 95p. M S Thesis.
- Segundinho, P. G. A. (and others) 2012. *Aplicação do método de ensaio das frequências naturais de vibração para obtenção do módulo de elasticidade de peças estruturais de madeira*. *Revista Arvore*. 36(6): 1155-1162.
- Horáček, P.; Tippner, J. 2012. *Nondestructive Evaluation of Static Bending Properties of Scots Pine Wood using stress wave technique*. *Wood Research*. 57(3): 359-366.

Prediction of Compression Strength of Timber Posts in Ancient Timber Buildings by Using Resistograph and Screw Withdrawal Tests

Shuo Xue

Research Institute of Wood Industry, Chinese Academy of Forestry, Beijing 100091, China; 1040260800@qq.com

Haibin Zhou*

Research Institute of Wood Industry, Chinese Academy of Forestry, Beijing 100091, China; zhouhb@caf.ac.cn

Xiaona Liu

Research Institute of Wood Industry, Chinese Academy of Forestry, Beijing 100091, China; 1325017341@qq.com

Weibin Wang

Shanxi Supervision Station on Maintenance Quality of Traditional Construction, Taiyuan 030001, China

Abstract Ultimate compression strength parallel to grain (UCS) of timber is one of important performance to evaluate the structural security of old timber buildings. Poplar wood (*Populus tomentosa*), Chinese larch wood (*Larix gmelinii* (Rupr.) Kuzen.) and Chinese fir wood (*Cunninghamia lanceolata* (Lamb.) Hook) were selected as the models in this paper. The aim of study is to predict UCS of timber by using Resistograph and screw withdrawal methods, establishing the relationships of the UCS and the density with the resistographic measure (RM) and the screw withdrawal strength by regression models. The results showed that the correlation coefficient between the RM and the UCS ranged from 0.5 to 0.7. The correlation coefficient between the double-start thread screw withdrawal strength (SW_{DST}) and the UCS distributed from 0.1 to 0.65, while the values of coefficients for the single-start thread screw withdrawal (SW_{SST}) differed from 0.4 to 0.65. The correlation coefficient of poplar for the regression model of screw withdrawal strength with the UCS and the density were higher than those of Chinese fir and larch. By comparison with the screw withdrawal test, the Resistograph test method was more reliable for predicting the UCS of timber.

Keywords Compression strength parallel to grain · Density · Resistograph · Screw withdrawal

Introduction

A number of buildings of wooden construction rank as important historic relics, such as the Yingxian Tower (1056, China), Horinji (682, Japan) and the South Gate of Seoul (1448, Korea) [1,2]. These types of architecture, mainly based on wood, represent significant inventions in history. As wood is made of natural polymers it has some drawbacks, in particular it is prone to deformation as it ages, leading to a weakening of its properties [3].

In order to investigate the effect of the variation of wood properties on the structural deformation of ancient buildings, Chen et al. [4] Compared the physical properties of old original timbers with modern

replacement timbers that had been installed during maintenance work. The results showed that tensile strength and compression strength transverse to grain of ancient timber was significantly reduced compared with the modern timbers. Chinese fir and poplar exhibited a 50 percent reduction of tensile strength and an 80 percent reduction of compression strength transverse to grain. The researchers measured the mechanical properties of common species used in ancient buildings, including beech (service life of 240, 650 years), red pine (service life of 115, 270, 290 years), and cypress (service life of 35 up to 1300 years) [5-8]. The compression strength parallel to grain, bending strength, and Young's modulus of cypress were higher than the corresponding fresh wood. However, the beech presented a 10.8 percent reduction of compression strength parallel to grain, and an evident 50 percent reduction of bending strength. This resulted from the gradual development of bending, splitting and fracturing in timber from ancient buildings. Therefore, having an understanding of the structural properties of timber helps to ensure that the most appropriate measurements can be made on ancient wooden structures to enhance their protection.

The methods used to estimate the mechanical properties of wood were divided into two types: destructive and non-destructive [9]. While the destructive method enabled the mechanical properties to be determined accurately, it was not considered appropriate for use on in situ ancient timbers [10]. Non-destruction was therefore considered the optimal approach [9]. When historical constructions are repaired, the original materials including timber, which may have sufficient mechanical properties to continue to be in function, is often replaced without reasonable evaluation. This phenomenon can be prevented if in-situ and non-destructive testing (NDT) technology is applied to diagnose timber. The most frequently used NDT devices are currently semi-destructive devices which identify the range and location of degradation by means of material resistance to various tools (Resistograph, screw) [11]. In order to apply these semi-destructive methods (Resistograph, screw), it is mandatory to investigate the relationship among resistographic measurements, wood properties and screw withdrawal strength [12]. It has been known that wood density is statistically correlated to screw withdrawal strength and screw diameter since 1926 [15]. Subsequently, Mclain et al. [13] proved that the screw diameter, screw depth in wood, and the wood grain had a significant influence on this linear correlation. Ceraldi et al. [14] and Cai et al. [15] evaluated density and mechanical properties by using Resistograph and screw withdrawal methods, respectively. The results showed that there was a strong linear relationship between density and the mechanical properties. To determine internal cavity morphology, Briank et al. [16] studied Hungarian wooden buildings by using stress wave and screw withdrawal; they showed that these methods accurately

predicted the bending strength and internal cavity morphology of individual in situ timbers in ancient buildings. With the development of sophisticated instruments and the improvement of testing regimes, Resistograph and screw withdrawal methods were widely used to estimate the mechanical properties and Young's modulus of wood [17-19]. However, the relationship was affected by many factors including screw pitch and wood species, which was barely studied in previous researches. As a result, the aim of this work is to use different species (as tangential sections) as the raw materials for measuring the compression strength parallel to grain, density, RM, as well as screw withdrawal strength. The results are used to establish the models for predicting the practical properties of wood by RM and screw withdrawal strength, and to explore the influence of species and screw pitch on the modeling equations.

Materials and Methods

Materials

The test clear wood specimens were obtained from the plainsawn boards. The dimension, physical properties and test size of test specimens from three species (poplar, Chinese larch, Chinese fir) are listed in Table 1. Each specimen was divided into two parts, L1 and L2, as shown in Fig. 1. Three test points (h1, h2, h3) were selected at the outside tangential section of the L1 for testing, and the L1 length was equally divided by these test points. Test points h1 and h3 were used to test screw withdrawal while h2 was used for Resistograph testing. The L2 was used to determine the density and the ultimate compression strength parallel to grain (UCS) with a size of 20mm by 20mm by 30mm (R × T × L).

Table 1 Specification and physical properties of specimens.

	Specimen dimensions (mm)	Annual ring width (mm)	Moisture content (%)	Number
Poplar (<i>Populus tomentosa</i>)	R	50	12.76	30
	T	50		
	L	300		
Chinese fir (<i>Cunninghamia lanceolata</i> (Lamb.) Hook.)	R	40	3.8	30
	T	50		
	L	280		
Chinese larch (<i>Larix gmelinii</i> (Rupr.) Kuzen.)	R	40	0.64	30
	T	50		
	L	280		

Note: R represents the radial direction of the specimens; T represents the tangential direction of the specimens; L represents the length direction of the specimens.

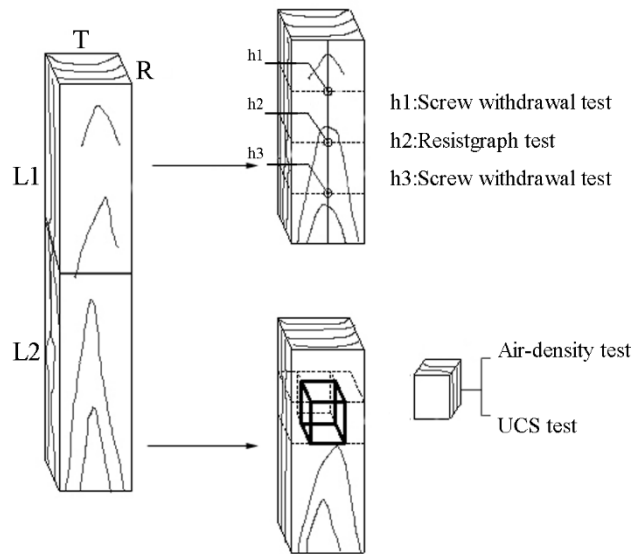


Fig. 1 Test specimens

Testing Methods

Density and UCS testing

Air density was measured in accordance with the Chinese Standard GB/T 1933-2009 [20]. The density was calibrated to the value under the moisture content of 12 percent by using equation 1.

$$P_{12} = P_m [1 - 0.01(1 - K)(W - 12)] \quad (1)$$

Where, K refers to the volume shrinkage coefficient with 1 percent variation of moisture content; W refers to moisture content (%); P_{12} refers to the air density at a moisture content of 12 percent (g/cm^3); and P_m refers to air density with a moisture content of m (g/cm^3).

The UCS was tested in accordance with GB/T 1935-2009 [21] by using INSTRON 5582. The UCS results were calibrated using equation 2.

$$\delta_{12} = \delta_w [1 + 0.05 \times (W - 12)] \quad (2)$$

Where δ_{12} refers to compression strength parallel to grain (MPa); δ_w refers to compression strength parallel to grain with moisture content of 12 percent (MPa); and W refers to moisture content (%).

Resistograph testing

In this paper, RESISTOGRAPH 4453-S (Germany, RINNTECH company) was used to obtain the RM. The RM distribution was collected by using microdrilling, perpendicularly drilling through the sample surface with a constant speed (resistance distribution is shown in Fig. 2). The testing sites and repeat times are given in Table 1 and Fig. 1. The RM was calculated using equation 3:

$$Rm = \frac{\int_0^l Area}{l} \quad (3)$$

where Rm is RM; L is the distance penetrated by microneedles (mm) and $\int_0^l Area$ is the integral area of RMs.

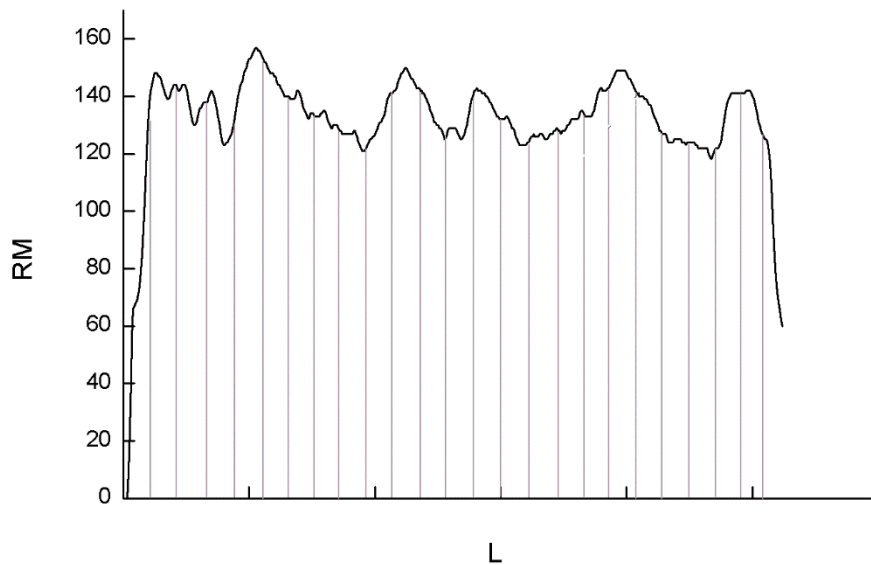


Fig. 2 The resistance distribution

Screw withdrawal testing

The screw withdrawal strength was measured in accordance with the Chinese Standard LY/T 2377-2014[22], using sites h1 and h3. The testing times are listed in Table 1. The screw satisfied the standard of GB/T 14210-93[23], as shown in Table 2. The screw was driven into the sample at a constant speed up to a depth of 18 mm. The screw was pulled out by using INSTRON 5582 with a speed of 2mm/min. The maximum loading was recorded as F_{max} . The screw withdrawal strengths were calculated by equation 4. The critical displacement was determined by increasing the loading until it decreased to $0.85 \cdot F_{max}$ (shown in Fig. 3). The ductility coefficient was calculated by equation 5 [24]. The loading

corresponding with the maximum displacement was as the F_{max} in the loading-displacement curve. The loading corresponding with the displacement of 15 mm was as the F_{max} if the displacement is over 15 mm. The rigidity was determined by the slope of curve between 10 % F_{max} and 40 % F_{max} [25]. The rigidity was calculated by equation 6.

$$f = \frac{F_{max}}{d \times l_p} \quad (4)$$

Where, f is the screw withdrawal strength, N/mm^2 , F_{max} is the maximum loading, N , d is the screw diameter, mm , l_p is the depth of screw in sample, mm .

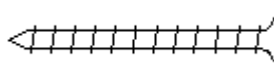
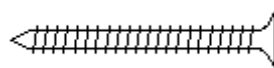
$$\mu = \frac{\Delta u}{\Delta y} \quad (5)$$

Where, μ is ductility coefficient, Δu is the critical displacement, mm , Δy is the displacement corresponding with the maximum yield loading, mm .

$$K = (F_{0.4} - F_{0.1}) / (S_{0.4} - S_{0.1}) \quad (6)$$

Where, K is the screw connecting rigidity, N/mm , $F_{0.4}$ is the 40 percent of F_{max} , N , $F_{0.1}$ is the 10 percent of F_{max} , N .

Table 2 Major specifications of screws.

Screw type	Nominal diameter (mm)	Nut diameter (mm)	Pitch(mm)	Nominal length(mm)	Screw sketch
Single-start thread screw	3.5	5	2.8	40	
Double-start thread screw	3.5	5	1.4	40	

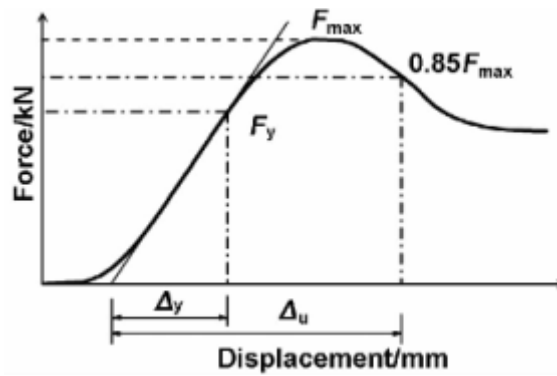


Fig. 3 Loading-displacement curve [26]

Results and Discussions

The correlation of density with RM and screw withdrawal strengthen

Fig.4 shows the regression model of density with RM and screw withdrawal strength, (a), (b), (c) exhibited the relationship of density and single-start screw withdrawal, density and double-start screw withdrawal, density and RM, respectively. The results showed that RM represented a high correlation coefficient with a range of 0.6~0.8 in three species. The correlation coefficient for screw withdrawal was in a range of 0.35~0.85. Different species had significant influence on the testing results, which was flavor for the density. The Resistgraph testing method is prior to screw withdrawal testing with the unobvious effect on the species. The correlation coefficients between density of Chinese larch and screw withdrawal strength with two methods (single- and double- start) were only 0.35 and 0.52, respectively, while the correlation coefficient of density and RM reached to 0.70. The reason was the different testing mechanism caused by Resistgraph and screw withdrawal. The max pulling force was recorded in screw withdrawal testing, while an average value was collected during the driving screw in Resistograph test [15,18]. The correlation coefficient between density of poplar and single-, double- start screw withdrawal strength, RMs were 0.74, 0.81, 0.79, respectively, which were totally higher than those of larch and fir. It was due to the various microstructure of softwood and hardwood [27]. A considerable researches had shown that the correlation coefficients between density and results with micro-destruction, non-destruction were mainly in a range of 0.35~0.85 [9, 28]. The results in this study, therefore, were considerable. Resistgraph testing was considered as the optimal method to predict the density of wood.

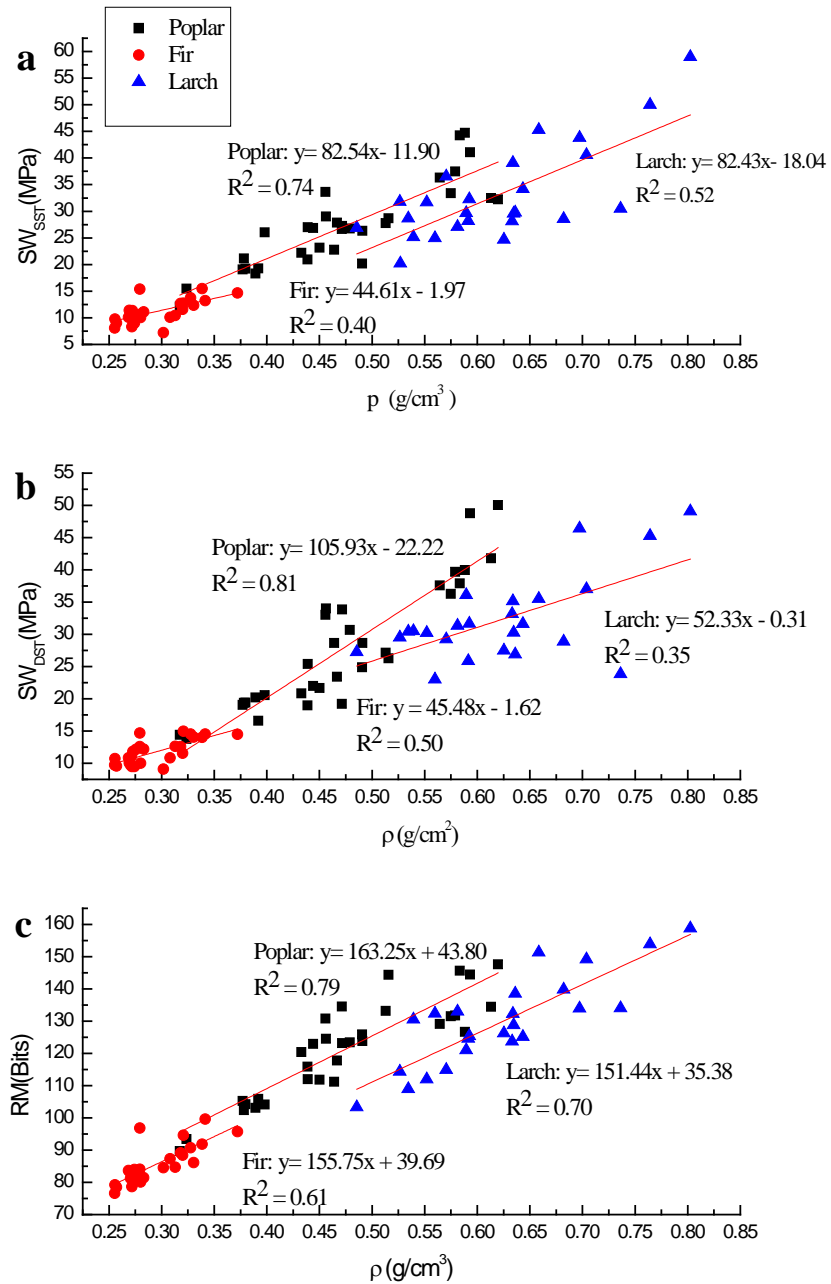


Fig. 4 The regression model of density with RM and screw withdrawal strength, (a) the relationship of density and single-start screw withdrawal strength (SW_{SST}), (b) the relationship of density and double-start screw withdrawal strength (SW_{DST}), (c) the relationship of density and RM

The correlation of UCS with RM and screw withdrawal strength

Fig.5 shows the regression model of UCS with RM and screw withdrawal strength, (a) (b), (c), exhibited the relationship of UCS and single-start screw withdrawal, UCS and double-start screw withdrawal, UCS and RM, respectively. With the various microstructure of species, such as fiber size and cell type [29-31], the feasible testing method existed huge differences as well. About the relationship between UCS and testing methods, the highest correlation coefficient between UCS and RM for Chinese fir and Chinese larch was 0.70 and 0.60, respectively, but the maximum correlation coefficient between UCS and single-start screw withdrawal strength for poplar was 0.65. The coefficient distribution of three species were all in a range of 0.5~0.7. Fig.5 shows the coefficient of UCS of samples and single-start screw withdrawal strength distributed in 0.4~0.65, while that of with double-start screw withdrawal strength was in a range of 0.10~0.61. Therefore, Resistgraph and single-start screw withdrawal testing were considered as the optimal choice. For the species, the correlation coefficient with the two screw withdrawal to predict density and UCS was: poplar > fir and larch. Screw withdrawal testing was considered to determine the UCS of hardwood with a high coefficient. Resistgraph method was for UCS of softwood. The common correlation coefficients of UCS with micro-destruction or non-destruction were in range of 0.3~0.7 [9, 19, 32]. It illustrated that both methods were used to determine the UCS with a high coefficient. A further research need be done to ensure the effect of screw pitch on the correlation coefficient of predicting model.

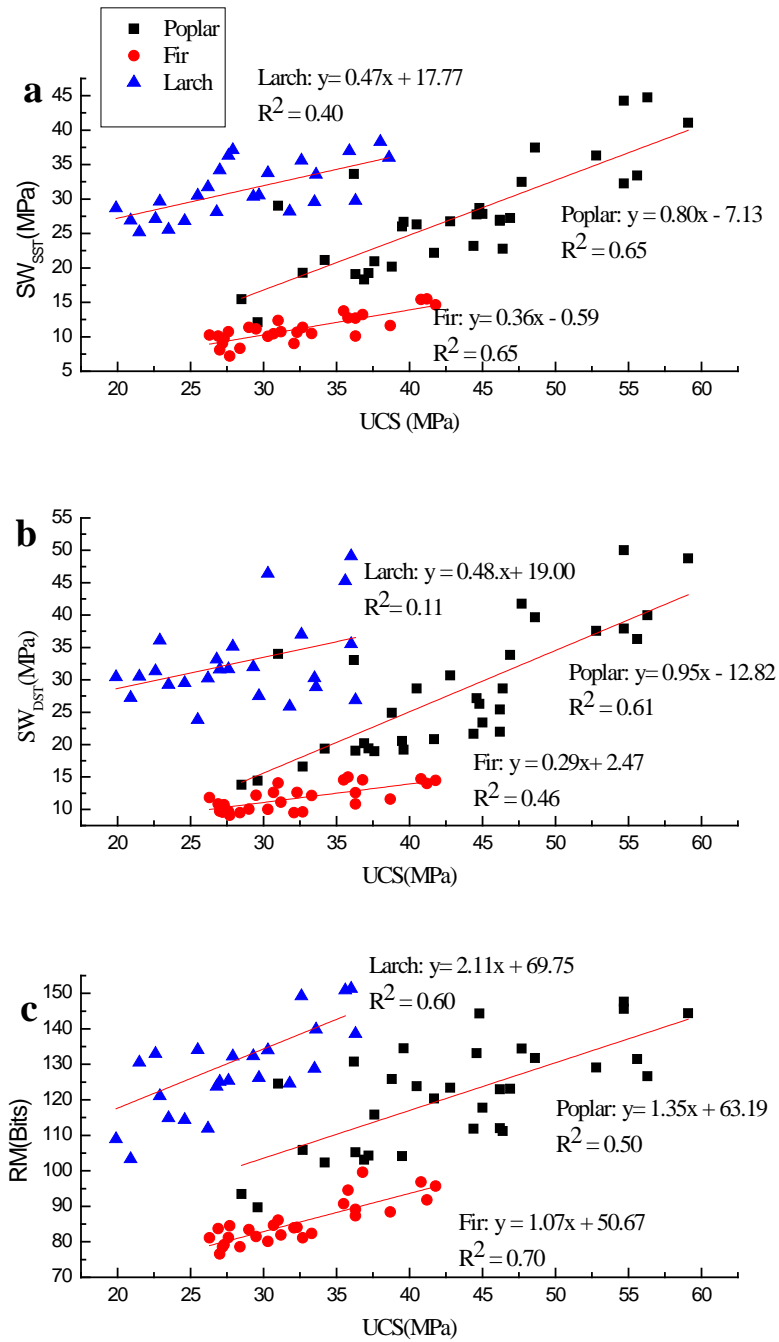


Fig. 5 The regression model of UCS with RM and screw withdrawal strength, (a) the relationship of UCS and single-start screw withdrawal strength (SW_{SST}), (b) the relationship of UCS and double-start screw withdrawal strength (SW_{DST}), (c) the relationship of UCS and RM

Table 3. Experiment results

	Poplar	Chinese fir	Chinese larch
Density (g/cm ³)	0.473(17.54)	0.293(10.41)	0.620(12.81)
UCS (MPa)	43.034(18.83)	32.171(14.85)	28.412(17.82)
SW _{SST} (MPa)	27.176(29.15)	11.155(18.64)	33.067(26.89)
SW _{DST} (MPa)	27.937(34.83)	11.953(18.77)	31.728(22.71)
RM	121.088(12.54)	85.460(6.99)	129.298(10.93)

Note: Values in parentheses are coefficients of variation (%); UCS is the ultimate compression strength parallel to grain; SW_{SST} is the single-start screw withdrawal strength; SW_{DST} is the double-start screw withdrawal strength; RM is the resistographic measure.

The analysis of single- and double- start screw withdrawal strengths

Tab.3 shows the average density, UCS, single- and double- start screw withdrawal strength of three species and their resultant variable coefficient. Fig.6 shows the screw withdrawal strength-replacement curves of three species with two screw withdrawal testing. (a), (b), (c), referred to poplar, fir, larch, respectively. The yield strength, critical strength with different screw pitches were different in screw withdrawal testing, resulting from the screw being vertical to tracheid and wood fiber, leading to the wood cell divided into two parts. A partial of tracheid and wood fiber underwent the shear force to break when the screw was pulling. The broken fibers were absorbed in screw gap with scatter distribution, integral fibers were warped along with the pulling force. The degree of warping gradually increased from the inner to surface, owing to the shear times increasing from inner to surface. Large screw pitch led to a large connecting area with stronger shear force and friction force. Small screw pitched resulted in a breakage of wood fiber, affecting the pulling strength [33].

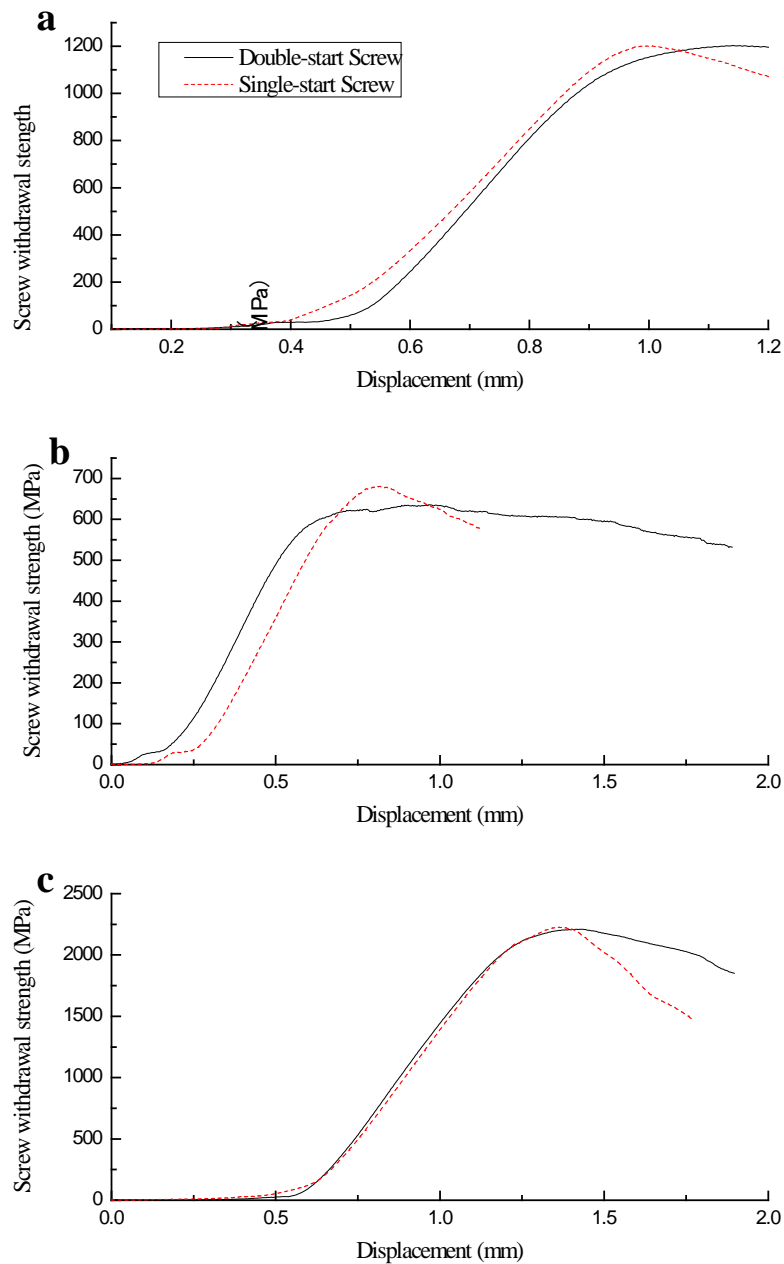


Fig. 6 Screw withdrawal strength -displacement curves of three species of wood. (a): Poplar, (b): Chinese fir, (c): Chinese larch

As shown in Fig.6, the correlation coefficients of UCS of three species and single-start screw withdrawal strength were higher than those of with double-start screw withdrawal strength. Ductility coefficient referred to the max replacement of timber divided to yield replacement, reflecting the plastic

deformation capacity before breakage. The high ductility coefficient implied the excellent plastic deformation capacity, leading to a high correlation coefficient of UCS and screw withdrawal strength.

Double-start screw had a small pitch, increasing the force acting on wood fiber, which was prone to decline the plastic strength [34], leading to the correlation coefficient was smaller than that of single-start screw withdrawal. Fig.7 shows the ductility distribution of three species. The results presented that the ductility coefficient of poplar obtained from single- or double- start screw withdrawal was higher than those of larch and fir. The linear relationship between density, UCS, and the screw withdrawal strength in three species presented the similar values, implying that ductility was a key factor that affecting the results.

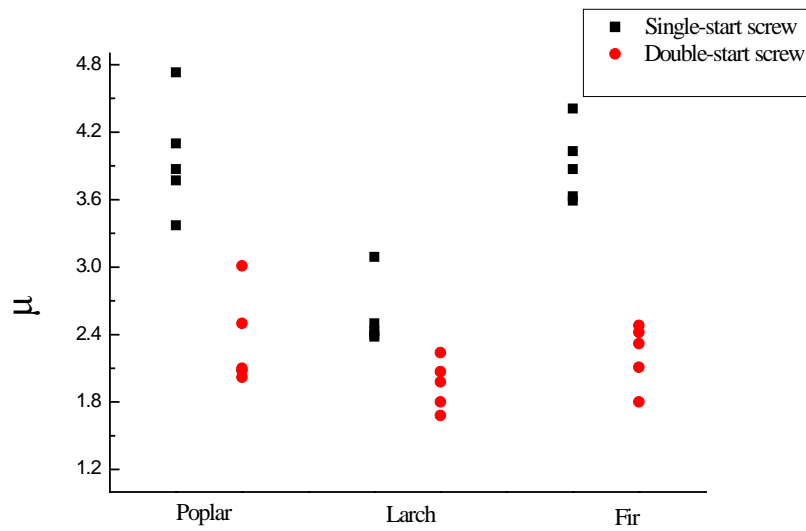


Fig. 7 Ductility coefficient distribution

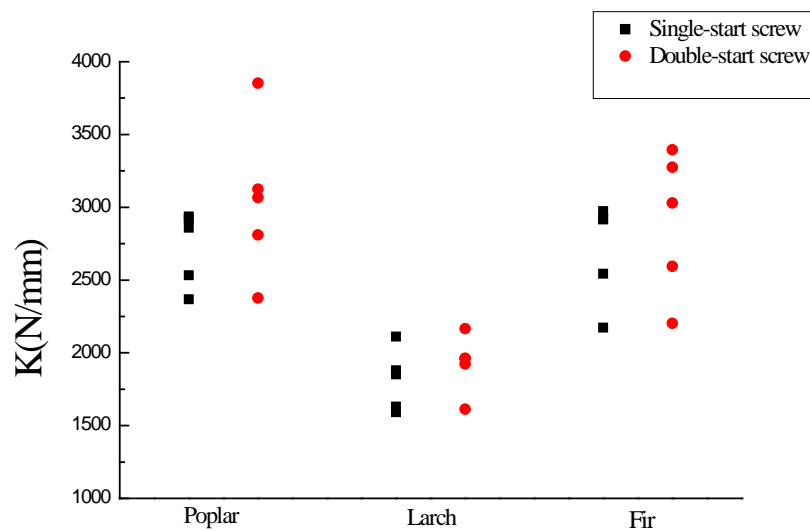


Fig. 8 Rigidity distribution

Fig. 8 shows the rigidity distribution of three species. The rigidity reflected the resistance deformation capacity of timber under the external force. Higher rigidity indicated stronger capacity of resisting the deformation. For one species, the rigidity determined by single- and double- start screw withdrawal were similar, the rigidity of larch was higher than that of fir, the rigidity of fir and poplar were almost the same. Combined with Fig 3 and 4, the correlation coefficient of fir between density, UCS, and screw withdrawal strength were higher than those of larch, while lower than those of poplar. Therefore, the rigidity of wood was not considered as a valued parameter to predict the density and UCS.

Conclusion

Wood species determined the correlation coefficient between density and RM, and between density and screw withdrawal strength. The correlation coefficient values were poplar > fir and larch. Resistograph method was able to investigate the correlation coefficient in a high fitting rate, leading to modeling the relationship of density and UCS well. Compared with the screw withdrawal method, Resistograph method had the inconspicuous wood species influence on correlation coefficient. In screw withdrawal method, the screw pitch affected the test results, greater pitch resulting in higher correlation coefficient.

References

- 1 Tollefson J (2017) The wooden skyscrapers that could help to cool the planet. *Nature*, 545(7654), 280
- 2 Fang DP, Iwasaki S, Yu MH, Shen Q, Miyamoto Y, Hikosaka H (2001) Ancient Chinese timber architecture. I: Experimental study. *Journal of structural engineering*, 127(11), 1348-1357
- 3 Lin L, Qin L, Fu F(2015) Development of Micromechanical Technique and Application on Wood Science. *Scientia silve sinicae*, 51(2), 121-128
- 4 Chen GY (2004) Study on the change of old building timber and its influence on building deformation (in Chinese). *Traditional Chinese Architecture and Gardens*,21(3),49-52
- 5 Hirashima Y, Sugihara M, Sasaki Y, Ando K, Yamasaki M (2004) Strength properties of aged wood i : tensile strength properties of aged keyaki and akamatsu woods. *Journal of the Japan Wood Research Society*, 50(8), 301-309
- 6 Hirashima Y, Sugihara M, Sasaki Y, Ando K, Yamasaki M (2004) Strength properties of aged wood ii : compression strength properties, shearing strength and hardness of aged keyaki and akamatsu woods. *Journal of the Japan Wood Research Society*, 50(6), 368-375
- 7 Hirashima Y, Sugihara M, Sasaki Y, Ando K, Yamasaki M (2005) Strength properties of aged wood iii: static and impact bending strength properties of aged keyaki and akamatsu woods. *Mokuzai Gakkaishi*, 51(3), 146-152
- 8 Shizhu Ni, Yuanzhe Li (1994) Survey of timber species and analysis of main wood properties in ancient buildings, *Build Sci Res Sichuan*, 20(1),11-14
- 9 Kloiber M, Tippner J, Hrivnák J (2014) Mechanical properties of wood examined by semi-destructive devices. *Materials and Structures*,47(1), 199-212
- 10 Kasal B (2003) Semi-destructive method for in-situ evaluation of compression strength of wood structural members. *Forest Products Journal*, 53(11), 55-58
- 11 Kloiber M, Drdácý M, Tippner J, Hrivnák J (2015) Conventional compressive strength parallel to the grain and mechanical resistance of wood against pin penetration and microdrilling established by in-situ semidestructuve devices. *Materials and*

- Structures, 48(10), 3217-3229
- 12 Bo K, Anthony R W (2004) Advances in in situ evaluation of timber structures. *Progress in Structural Engineering and Materials*, 6(2), 94-103
 - 13 Mclain TE (1997) Design axial withdrawal strength from wood: I. Wood screws and lag screws. *Forest products journal*, 47(5), 77-84
 - 14 Ceraldi C, Mormone V, Russo, Ermolli E (2001) Resistographic inspection of ancient timber structures for the evaluation of mechanical characteristics. *Materials and structures*, 34(1), 59-64
 - 15 Cai Z, Hunt MO, Ross R J, Soltis L A, Cai Z, Hunt MO (2003) Screw withdrawal: a means to evaluate densities of in-situ wood members. *Proceedings of the 13th International Symposium on Nondestructive Testing of Wood*, Madison, USA
 - 16 Briank B, Voichita B, Ferenc D, Raquel G, Lu J, Roger M (2009) Nondestructive testing and evaluation of wood: a worldwide research update. *Forest Products Journal*, 59(3), 7-14
 - 17 Feio A (2005) *Inspection and Diagnosis of Historical Timber Structures: NDT Correlations and Structural*, PhD thesis, Universidade do Minho, Braga, Portugal
 - 18 Lechner T, Nowak T, Kliger R (2014) In situ assessment of the timber floor structure of the skansen lejonet fortification, Sweden. *Construction and Building Materials*, 58(4), 85-93
 - 19 Zhang J, Xu QF, Xu YX, Zhang M (2015) Research on residual bending capacities of used wood members based on the correlation between non-destructive testing results and the mechanical properties of wood. *Journal of Zhejiang University-SCIENCE A*, 16(7), 541-550
 - 20 GB/T1933-2009 (2009) Test method for density of small clear wood (in Chinese). Standardization Administration of the People's Republic of China (SAC), Haidian District, Beijing
 - 21 GB/T 1935-2009(2009) Method of testing in compression strength parallel to grain of wood (in Chinese). Standardization Administration of the People's Republic of China (SAC), Haidian District, Beijing
 - 22 LY/T 2377-2014 (2014) Test methods for the joint performance with dowel type fasteners used in wooden structural material (in Chinese). State Forestry Administration, Dongcheng district, Beijing, China
 - 23 GB/T 14210-1993 (1993) Dry wall screws (in Chinese) General Administration of Quality Supervision Inspection and Quarantine of the People's Republic of China (CSBTS) Haidian District, Beijing
 - 24 Sture, S (2005) *Dynamics of Structures: Theory and Applications to Earthquake Engineering* by Anil K. Chopra. Prentice Hall, 31 (6) :719-720
 - 25 EN26891 (2001) *Timber Structures-Joints made with mechanical fasteners-general Principles for the Determination of Strength and Deformation Characteristics*. European committee for standardization, Brussels
 - 26 Zhong Y, Zhou HB, Ren H (2013) The effect of Temperature on compression properties of wood fiber composites in the LVL. *Functional Materials*, 44(23), 3397-3400
 - 27 Cheng JQ (1985) *Wood science* (in Chinese). China Forestry Publishing House, Beijing, China
 - 28 Feio AO, Lourenço PB, Machado JS (2007) Non-destructive evaluation of the mechanical behavior of chestnut wood in tension and compression parallel to grain. *International Journal of Architectural Heritage*, 1(3), 272-292
 - 29 Bai MF, Liu SQ, Zhou LA, Liu Q (2009) Tracheid morphology characteristics and microfibrillar angle and their variation patterns of *larix gmelinii* (in Chinese). *Journal of Anhui Agricultural University*, 36(2), 189-193
 - 30 Zhu J, Jiang F (1994) A study on regularity of the change of fiber length of wood in poplar shelterbelts and its application in shelterbelt management (in Chinese). *Scientia SilvaeSinicae*, 30(1), 50-56
 - 31 Ren HE, Wang HF (2009) Cell image of wood classification and identification algorithm (in Chinese). *Computer Engineering and Applications*, 45(28), 246-248
 - 32 eraldi C, Mormone V, Ermolli ER (2001) Resistographic inspection of ancient timber structures for the evaluation of mechanical characteristics. *Materials and Structures*, 34(1), 59-64
 - 33 Liu Y, Zhao G (2012) *Wood Science* (in Chinese). China Forestry Publishing House, Beijing, China
 - 34 Li H (2013) *The Study on C Joints Property of Hollow Screw in Cunninghamia Lanceolata Component* (in Chinese) Master's thesis, Central South University of Forestry and Technology. Changsha. China, pp 34-35

Ultrasonic Tomography in Detecting Knots

Dr. Alex J. Trinca*

**Director of Research & Development, Trinca Research & Development, Jundiai, Sao Paulo, Brazil,
ajtrinca@mxb.com.br**

Ms. Ney B. A. Sidou

**Coordinator of Automation, Trinca Research & Development, Jundiai, Sao Paulo, Brazil,
neysidou@gmail.com.**

Railson S. Ferreira

Application Engineer, Trinca Research & Development, Jundiai, Sao Paulo, Brazil, ajtrinca@mxb.com.br

*** Corresponding author**

Abstract

Non-destructive tests continuously have been rolling; for that development, it is essential that results should express as accurate as possible measures. For that precision we have developed equipment capable of expressing the real perimeter of the element to be measure, feeding the tomograph the exact data needed for accurate reports.

The research has been conducted to make a portable device, with a connectable platform to other software, measuring in a quick and reliable way the profile of the element from sclerometric techniques, using software, to generate interchangeable data with other systems. The system can even identify precisely the length between two aleatory points when requested. The results obtained generate the perimeter delineation with millimetrical precision, which allows the elaboration of images with the real proportions of this sample, giving a greater accuracy to the non-destructive tests.

Keywords: perimeter of trees, measures of trees, profilemeter.

Introduction

Nondestructive ultrasonic tests are based on the velocity of wave propagation, obtained through the relation between time and distance. When structures or trees with an inhomogeneous profile are analyzed then it is considered that wood is a circumference, or even an ellipse, causing substantial interference in the results obtained. We therefore conclude that these distances used for calculation must be as accurate as possible. According to Trinca, (*et al.*, 2013) it was proven that laser profilometry allows us to reconstitute the profile of objects.

According to Wang (*et al.*, 2007) the precision obtained with the ultrasound technology allows to predict the intrinsic quality and properties of the wood from the measurements made in the live tree and also to correlate with the structural performance of the product's final results. In addition, the authors also say that with advances and continuous improvements, this technology could help in the management of wood quality, allowing the evaluation of forest stands and improving the quality of future plantations.

Wang (*et al.*, 2007) also said stated that wave propagation in wood is a dynamic and complex process, controlled by the properties, orientation and microstructure of the wood fiber and, more importantly, by the geometric shape of the material.

Because the wood is a material of biological origin, it's subject to variations in its conformation (nodes, marrow, grain slope) that can cause changes in its properties. Nodes, for example, originating from the branches modify the linearity of the fibers in the trunks of the wood. The influence on the linearity of a tree interferes with the resistance of the part depending on its size and location. In the analysis of the defects of the wood one must take into account the singular anisotropy of the wood which is a compound with oriented fibers.

According to Bucur (*et al.*, 2005), the propagation of waves is affected by the presence of materials with different acoustic impedance characteristics, such as defects induced by irregularities of different natural growth patterns (grain deviation, nodes, resin bags, etc.) and anomalies caused by biological attacks of fungi and insects. These differences in the material cause variation in the propagation velocity of the wave and in the amplitude of the emitted signal. These variations can be detected by the ultrasound equipment and studied for the elaboration of a behavioral profile that can be associated to algorithms for imaging by performing the ultrasound tomography. Puccini (*et al.*, 2002) evaluated the influence of nodes, marrow and fiber deviation on the propagation velocity of ultrasound waves. The results indicated that the velocity variation was highly significant for the models involving, as independent variable, the presence of nodes, marrow and grain mismatch. With these results, the authors concluded that the velocity is a parameter that can be associated to the characteristics analyzed, and that; therefore, it can be used as an analysis tool for the detection of defects in wood.

Therefore, it is important to determine the correct profile in the image construction using the variation of the propagation velocity of the ultrasonic waves (ultrasonic tomography) in wood.

Methodology

For the determination the perimeter on trees, we used urban, native, and reforestation trees.

Initially, a laser was used to trace the profile line and the ImageJ program to generate the image of this profile, as presented by Trinca (*et al.*, 2013).

Due to the difficulties of the acquisition of the images with the use of the laser, with the interference of the luminosity of the external environment, we decided to change the method using a colored ribbon emphasizing the perimeter independently of the external luminosity (Figure A).

The actual method to obtaining the profile is slowness, transforming a fieldwork into a laboratory work, it was necessary to develop dedicated software (Avallye®) for the graphical composition of the profile and spreadsheet, with the possibility of feeding other equipment, e. g: tomograph.

For the verification of the results of the tests, the methodology proposed by Divos and Szalai (2002), diffraction mesh, (Figure B) was followed, where the distance between the points was mentioned.



Fig. A

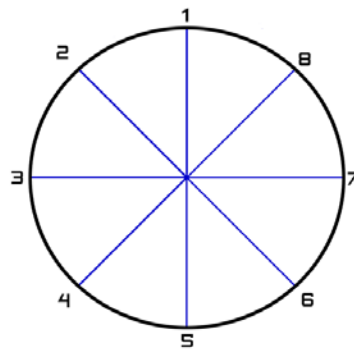


Fig. B

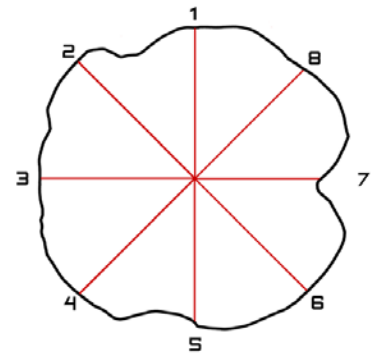


Fig. C

After data collection, it was possible to generate the actual image of the profile, (Figure C). A table with the data obtained the distances between the model using circumference and the real model was then generated (Figure D).

Results

With the possession of the measurement results it was possible to prepare a spreadsheet previously mentioned.

Distance Between Points	Approximated Circumference (m)	Using the actual profile (m)	Variation (%)
1-5	0.1642	0.1516	7.67
2-6	0.1642	0.1675	2.01
3-7	0.1642	0.1446	11.94
4-8	0.1642	0.163.7	0.31

Figure D: Distances using circumference and real model.

CONCLUSION

It is concluded that using the proposed model to approximate the profile of a tree to a circumference produces values that generate a significant deviation of velocity, incurring errors in the evaluation of the element.

It's impossible determine the deviation or variation statistics, because there aren't a model that represents the comparison between a real profile and a hypothetical circumference.

BIBLIOGRAPHY

BUCUR, Voichita. Acoustics of wood. Springer-Verlag, Berlin, Germany. P. 223-225, 2006.

DIVOS, F.; SZALAI, L. 2002. Tree evaluation by acoustic tomography. In: Proceedings of the 13th International symposium on nondestructive testing of wood; 2002 August 19. 21; Berkeley, CA. Madison, WI: Forest Products Society: 251.256. 2002.

PUCCINI, Carlos Teixeira, Avaliação de aspectos de qualidade da madeira utilizando o ultrassom, Campinas, Brasil, fevereiro 2002

TRINCA, A. J.; Lino, A.C.L.; Gonçalves, R; Silva, M.V.G.. Use of laser to determine profile of trees. In: 18th International Nondestructive Testing and Evaluation of Wood Symposium, 2013, Madison Wisconsin U.S.A. 18th International Nondestructive Testing and Evaluation of Wood Symposium USDA forest Products Laboratory. Washington DC: USDA's TARGET center, 2013.

WANG, X.; ROSS, R. J.; BRASHAW, B. K.; ERICKSON, J. R.; FORSMAN, J. W.; PELLERIN, R. F.. Diameter effect on stress-wave evaluation of modulus of elasticity of logs. Wood Science and Technology, v. 36, p. 368-377, 2004.

Estimation of the Moisture Content of Japanese Cedar (*Cryptomeria japonica*) Large Diameter Logs by Measuring Relative Permittivity and Phase Attenuation of Low Frequency (52 Mhz) Electromagnetic Wave

Kiyohiko IKEDA

Shizuoka Prefectural Research Institute of Agriculture and Forestry, Negata2542-8 Hamakita, Hamamatsu, Shizuoka Japan, kiyohiko1_ikeda@pref.shizuoka.lg.jp

Youki SUZUKI

Forestry and Forest Products Research Institute, Tsukuba, Ibaraki, Japan, youki@ffpri.affrc.go.jp

Akihiro SUGIYAMA

Micro Measure Co., Ltd. Shimada, Shizuoka, Japan, sugia@micromes.com

Takeshi HOSHIKAWA

Shizuoka Prefectural Research Institute of Agriculture and Forestry, Hamakita-ku, Hamamatsu, Japan, hoshikawa.T@gmail.com

Abstract

The purpose of this research is to develop a method and device for evaluating large variations in moisture content, particularly heartwood moisture content distribution. High correlation was found between the relative permittivity of the logs and the heartwood moisture content (MC). We investigated whether it is possible to estimate from the phase and attenuation when the log moves between the transmitting and receiving antennas of low frequency electromagnetic waves (52 MHz) as a non - contact MC evaluation method for logs. In the model test of Japanese cedar logs, a high correlation was found between the phase and the laminated whole MC, between the attenuation and the sapwood MC. A significant correlation was found between the value obtained by subtracting the voltage output value of the attenuation from the voltage output value of the phase, and the heartwood MC. From these results, it was suggested that the MC evaluation of the entire log and the inside of the outer periphery or heartwood could be performed nondestructively.

Keywords: Moisture content, Electromagnetic wave, Relative permittivity, Phase, Attenuation, Japanese cedar,

Introduction

It is known that the quality of Japanese cedar varies widely among individuals, and in particular, the moisture content of heartwood in standing trees and logs are greatly different. For this reason, when manufacturing lumber products of large cross section such as beams or girders from middle and large diameter logs of heartwood, the proportion that the target moisture content cannot be satisfied after drying increases. In addition, since the yield may decrease due to the occurrence of cracks in the drying process, it is an obstacle in stably producing products of a certain quality and performance.

For these reasons, authors have evaluated the high moisture content in the high moisture content of Japanese cedar by the phase of the electromagnetic wave (Ikeda, K. 2013), the impedance (Suzuki, Y. 2011), and the dielectric constant (Suzuki, Y. 2003) and we have also worked on the development of a device to evaluate the moisture content of logs on scaling line. Others, For the moisture evaluation in the high moisture content region, impedance by intermediate electrode insertion (Sobue N. 2011), microwave scanning (Johansson, J. 2003), acoustic method (Dieste, A 2013) have been studied. In this study, we

established methods to evaluate moisture content of whole logs and sapwoods by phase and attenuation of low frequency (52 MHz) electromagnetic waves, and moisture content of heartwood by relative permittivity, and try to implement of device development and improvement.

Method and Specimen

Evaluation of moisture content of logs by phase (non-contact) and relative permittivity (contact) of low-frequency electromagnetic waves

Figure 1 was showed the outline of the relative permittivity measuring device used for evaluating the heartwood moisture content of logs. In the device, an electrical circuit with a transmission frequency of 20 MHz is connected to a terminal with a needle length of 45 mm, the relative permittivity when the terminal is driven into the core material of the log roof surface is displayed, the power supply voltage is 9 v, the display value range of the relative dielectric constant is 0 to 200. The relative permittivity was measured at two places outer heartwood and near the pith with the heartwood of the cedar logs.

An electromagnetic wave transmission / reception sensor (dipole antenna: one side length 1400 mm) and the like with a transmission frequency of 52 MHz was used for non-contact evaluation of moisture content of log (whole) is shown Figure 1(Right). The phase was calculated from the difference in voltage output between when there was nothing between the sensors and when log was placed.

Approximately two months after logging, we tested a total of 90 Japanese cedar logs with a length of 4 m and a diameter of 30 to 42 cm. After that, cedar logs measured apparent density, cut at the site of 1 m in length from the end, and picked up a disk with a thickness of 5 cm. Cubic specimens of heartwood and sapwood were sampled from the disk and the moisture content and oven-dried density of the samples were measured by the oven dried method. In addition, timber beams with a width of 130 mm and a thickness of 300 - 390 mm according to the diameter from the logs; they were subjected to kiln drying by steam for 10 days. After drying, the moisture contents of them were measured using a high-frequency type and microwave type moisture meter.

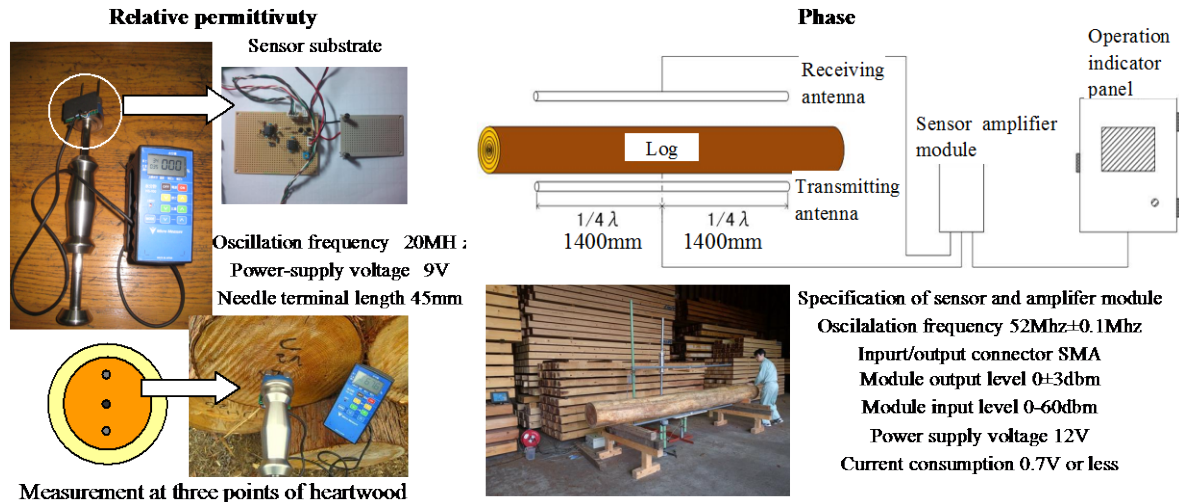


Figure 1 -Outline of the sensor used for relative permittivity measurement of heartwood MC (Left) and sensor used for phase measurement of log MC. (Right),

Non-contact evaluation of wood moisture content by phase and attenuation of low frequency electromagnetic waves

The electromagnetic wave sensor device used in the previous section was improved so that it can measure fluctuation data of phase and attenuation when a log or the like is moved between the sensors.

The difference between the minimum value and the maximum value of the voltage output value during the movement process of a log or the like was defined as phase and attenuation

Model test A: Using the Japanese cedar plate (150 mm in width, 35 mm in thickness, 4 m in length) classified into 4 groups with moisture content adjusted, the phases when 4 grating lumbers of the same moisture content group were laminated attenuation was measured, and the phase and attenuation were measured when gradually stacking up to ten layers one by one respectively.

Model test B: Using a cedar lumber divided into six MC groups with moisture content adjusted, 6 outer layers assuming sapwood and 7 inner layers assuming heartwood were combined so that the moisture content groups were different 8 types of model specimens with a width of 225 mm and a thickness of 315 mm were prepared and the phase and attenuation were measured.

Actual size Japanese cedar log test A: The phase and attenuation were measured similarly to the model test on five cedar logs (preliminary relative permittivity, apparent density) having a diameter of 30 to 32 cm and a length of 4 m passed two months after harvesting. The phase and attenuation were measured for cases where the log edge of the same log was changed by 15 degrees and when the feed speed of the log was changed, and the influence of them were examined. Also, after placing these logs outdoors for another two months, we measured phase, attenuation and apparent density.

Actual size Japanese cedar log test B: After measuring the phase and attenuation for 8 cedar logs of 30-32 cm in diameter and 4 m in length logs a section of 1 m from the end was cut and then disc samples were collected, and then, the sapwood MC and heartwood MC were measured by oven-dried method.

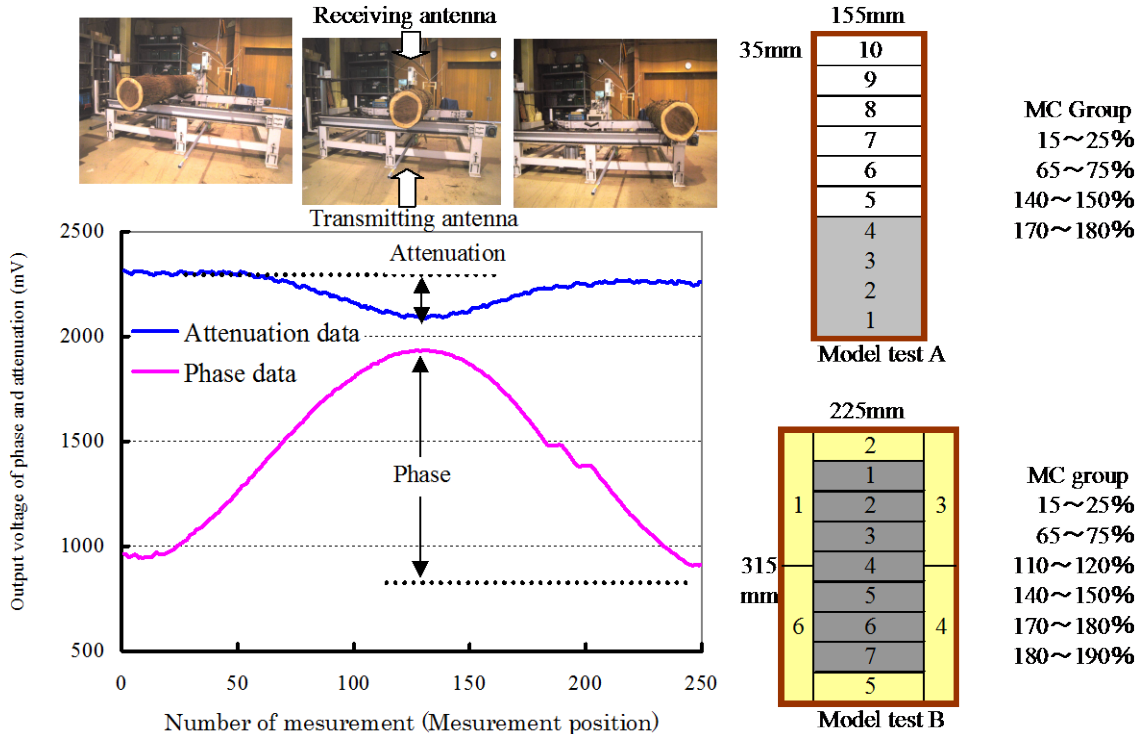


Figure 2- Method of measuring method of attenuation and phase of Sugi logs or timber model test samples. Model test A: Measurement of attenuation and phase when laminating 4 to 10 layer of Sugi lumber of the same MC group. Model test B: Measurement of attenuation and phase when laminating Sugi lumbers different MC groups on the outer layer (6:assumed sapwood) and the inner layer (7: assumed heartwood)

Result and Discussion

Evaluation of Japanese cedar logs moisture content by the phase (non-contact) and relative permittivity (contact) of low frequency electromagnetic waves

The relative permittivity measured at three heartwood parts of 90 Japanese cedar logs fluctuated over a wide range of 50 to 180 and the difference between within the same individual were appeared to large (**Figure 3**). In addition, the relative permittivity showed a tendency that the majority of individuals tended to be higher at the center part (near Pith) of heartwood. A high correlation was found between the average value of relative dielectric constant measured at six heartwood parts and heartwood MC by oven drying method the correlation coefficient of 0.824 (**Figure 4**). In addition, a significant correlation (correlation coefficient $r = 0.713$) was also found for the relative permittivity of heartwood and the apparent density of the log. Even in another test in which the author examined the relationship between the relative permittivity and the core material MC of each part of the core material separately carried out, the correlation coefficient by the exponential approximation between them is 0.91, and from the relative permittivity, MC could be estimated.

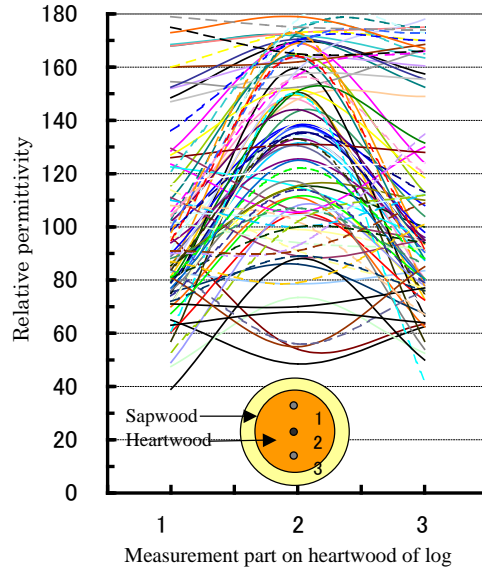


Figure 3- Difference in relative permittivity at heartwood measurement 3 part of Japanese cedar

Figure 5 was showed the relationship between the phase of cedar logs with a 52 MHz electromagnetic wave transmission / reception sensor and the MC by oven-dried method using disc samples sampled from logs. The correlation coefficient between the phase and the whole MC was 0.814, and it seemed that the moisture content of the whole log could be estimated from the phase difference. On the other hand, although the correlation coefficient between phase and moisture content of sapwood or heartwood were significant, it were lower than that of the whole logs. The dotted line in the Figure 4 and Figure 5 shows the heartwood moisture content and the relative permittivity, which are presumed to remain in the

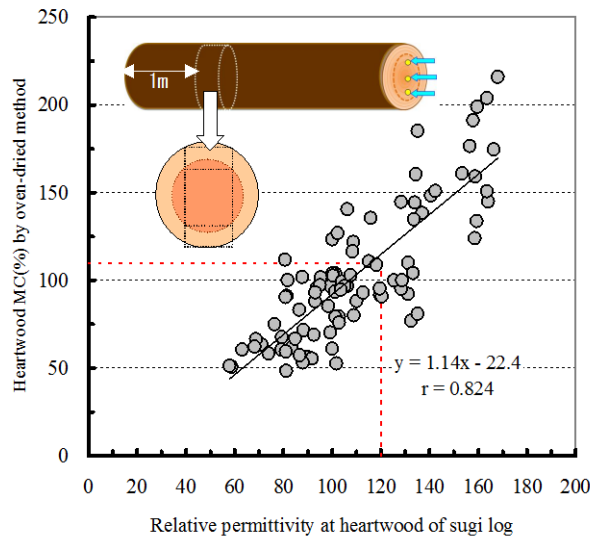


Figure 4- Relationship between relative permittivity and heartwood MC by oven-dried method.

Red dotted line: A line connecting the moisture content with a high possibility that the MC after drying from the artificial drying test of the past cedar beam material is 20% or less and the relative permittivity corresponding to that value.

lumber after kiln drying, and the total moisture content and phase, respectively.

Relationship between the relative permittivity of the log and the MC of kiln dried sawn timber made from them (measured using high frequency and microwave moisture meter) are shown.

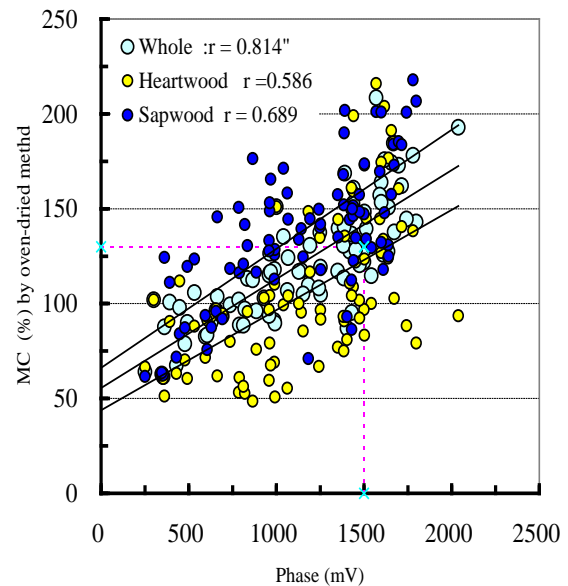


Figure 5- Relationship between phase and MC by oven-dried method

In the figure, 90 Japanese cedar logs were divided into two groups with the relative permittivity of 120 and the phase of 1500 mV as threshold values (see Figure 4 and 5), and showed MC after drying, respectively. The MC measured with high frequency moisture meter (average value measured at 6 points in a wide core material part), when sawn from a log with a relative dielectric constant less than 120 or a phase less than 1500 mV, mostly showed 20% or less. Likewise, in the MC by the microwave moisture meter, a large MC difference appeared between the two categories. On the other hand, logs with large specific permittivity (presumed to have a high heartwood moisture content) were presumed to have a high possibility of leaving the moisture content gradient after drying even if the phase of log is low (**Figure 6**).

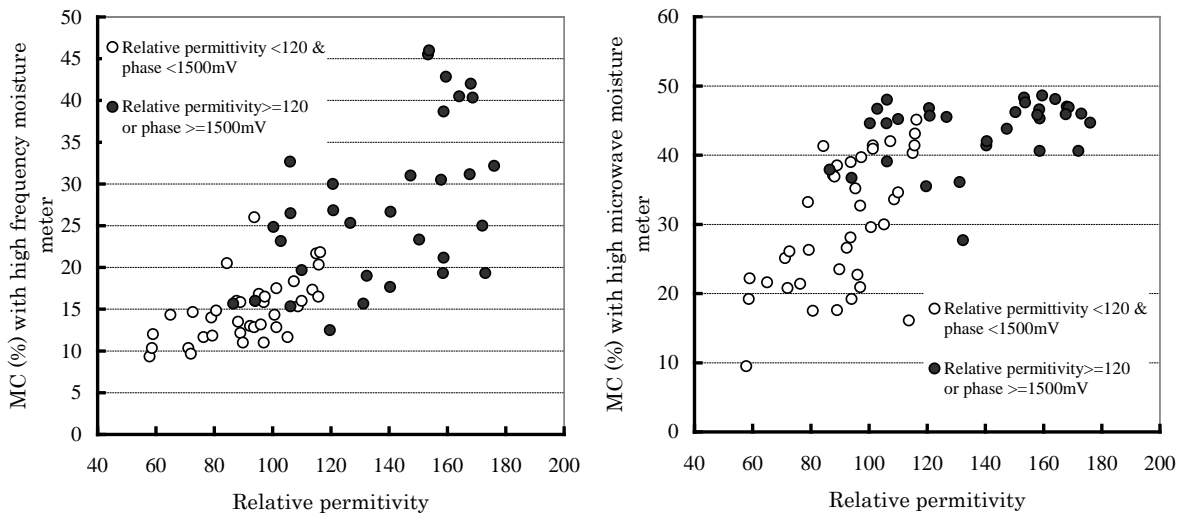


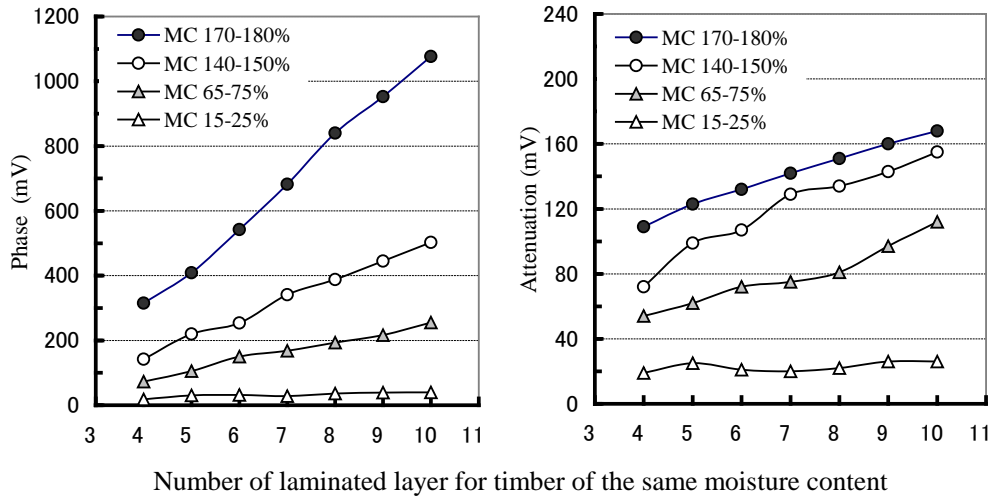
Figure 6- Relationship between relative permittivity of logs and MC of large timber beams which were sawn and kiln dried from logs.

From these results, the effectiveness of moisture evaluation at the log-grading were verified using two electric signals of relative permittivity and phase as division thresholds. However, since the measurement of the relative dielectric constant is a contact type, it is necessary to measurement time (necessary to stop the log and measure it), and the reliability of the system (needle terminal: such as breakage and durability etc.), leaves problems.

Non-Contact Evaluation Method of Moisture Content of Raw Wood by Phase and Attenuation of Low Frequency Electromagnetic Wave

Model test in which MC adjusted Japanese cedar lumbers laminated on each other

Figure 7 was showed the phase and attenuation fluctuations when the cedar lumbers of the same moisture content group were laminated with 4 lumbers and then increased one by one and gradually laminated up to 10 layers. Both phase and attenuation showed a tendency to increase almost linearly in proportion to the number of layers stacked lumber in the 4 moisture content groups. In the electromagnetic wave sensor with the frequency 116 Mhz tested in the previous report, the proportional relationship was not obtained due to the attenuation (Ikeda, K. 2013), but the possibility of the evaluation in the high moisture region was obtained even with the attenuation in this sensor. **Figure 8** was showed the relationship between MC and phase and attenuation of a model specimen in which 6 lumbers on the outer circumference assuming sapwood, 7 lumbers in the inner layer assuming a heartwood, and combinations of Japanese cedar lumbers with different moisture content groups, respectively.



Number of laminated layer for timber of the same moisture content
Figure7- Changes in phase and attenuation, when increasing the number of Japanese cedar lumber laminates of the same MC level

The correlation coefficient between the attenuation and the MC at the outer circumference was 0.943, and the correlation coefficient of the whole MC and the correlation coefficient was 0.972, both high correlation was confirmed respectively. When comparing the types of magnitude discrimination of the outer layer (sapwood) and the inner layer (heartwood) with magnitude (○ and ● in the Figure 8) of MC, the difference between them is either the phase and the MC of the whole, attenuation and the MC of the outer circumference could not see any difference. A significant correlation (correlation coefficient 0.791) was found between the MC of the inner layer and the value obtained by subtracting the attenuation voltage from the phase. However, the relationship between the two was noticeably different depending on the difference in elevation of MC between the outer and inner layers, and the correlation coefficient was not higher than the above phase and the total MC. It will be a future task, but by obtaining means to evaluate the difference between the MC height and the inner and outer layers, it is thought that further accuracy improvement can be achieved when estimating the MC of the inner layer.

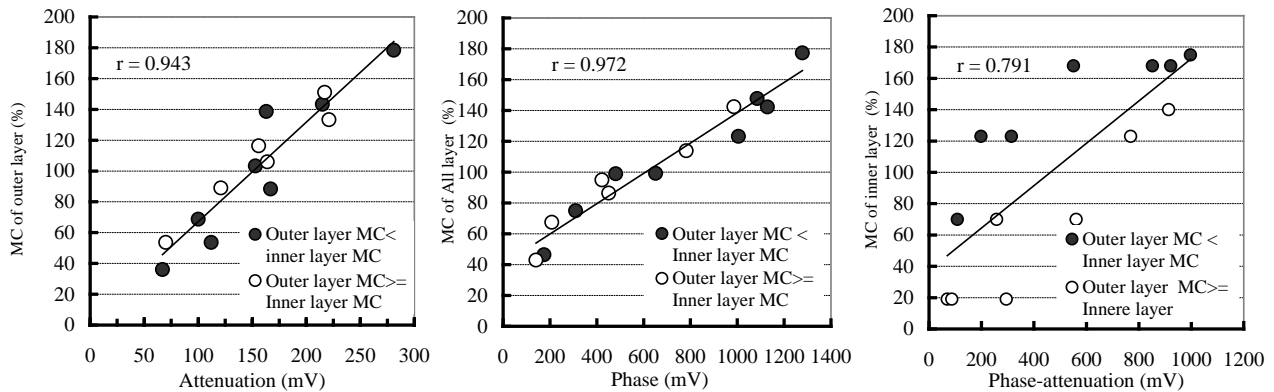


Figure 8 -Relationship between attenuation and phase of MC with laminated Japanese cedar lumbers of different MC groups on the outer circumference (6 layers: assumed sapwood) and the inner layer (7 layers: assumed heartwood).

Evaluation by large diameter Japanese cedar log

The phase, attenuation and apparent density of Japanese cedar logs measured at 2 months and 4 months after harvesting were compared. Between 2 months the apparent density and phase of the logs both fluctuated (**Figure 9**). Also, the correlation coefficient between the decrease in apparent density and the decrease in attenuation was higher than the decrease in phase (**Figure 10**). From these results, it was

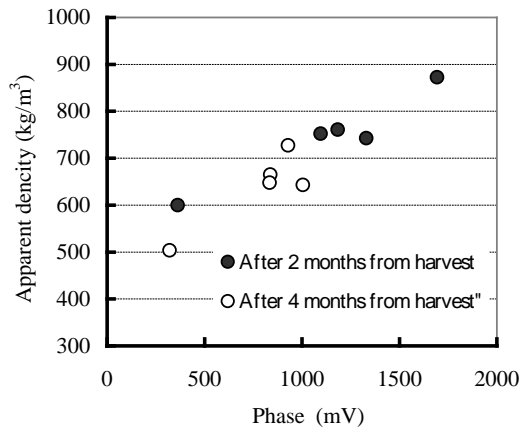


Figure 9- Apparent density and phase at the end of 2 months and 4 months after harvesting of cedar log

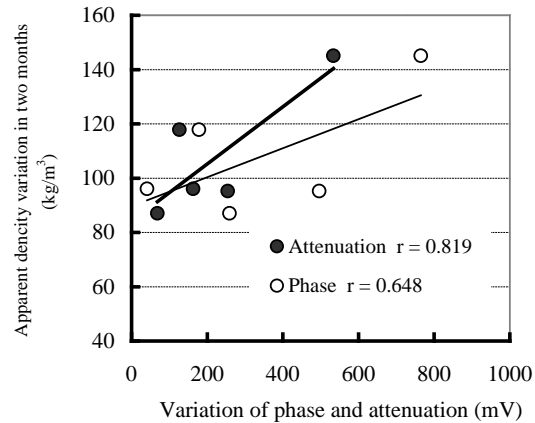


Figure 10- Relationship between apparent density and attenuation or phase variation in 2 months

inferred that the decrease of the apparent density appeared in the decrease of mainly the attenuation and further the decrease in the phase that the moisture release from the sapwood (the outer periphery of the log) was large. For the same cedar logs, it was confirmed that the phase and attenuation in (4 directions) when the direction of the butt end relative to the sensor was changed by 15 degrees at the time of measurement movement were compared. In addition, it was confirmed that there was hardly any influence on the measurement values of phase and attenuation even when the measurement was performed by changing the feed speed (1 to 20 m / min) on the line. Figure 11 was showed relationship between the phase and attenuation of logs and the MC measured with discs by oven-dried method. The correlation coefficients were attenuation and sapwood MC 0.844, phase and whole MC 0.944, phase - attenuation and heartwood MC 0.844.

Compared to the result of model test B, the correlation coefficient between core material MC and phase-attenuation was high. Comparing the results of the actual size cedar log with the model test B, the regression equation of the sapwood MC and attenuation was somewhat different from the regression formula of the phase and the total MC or the phase - attenuation and the heartwood MC were similar. From the above results, it was confirmed that the MC evaluation of the log can be performed efficiently by non-contact in the process of moving the scale measure lines.

In addition, when considering the results of model test B, it is expected to improve accuracy by measuring in high-moisture moisture content state only in those with less time lapse after harvesting. In future, we will increase the number of samples of nondestructive moisture indicator such as phase etc for logs of different diameters, and will carry out the verification accompanied with the evaluation of non-destructive moisture index and the MC of kiln-dried lumber.

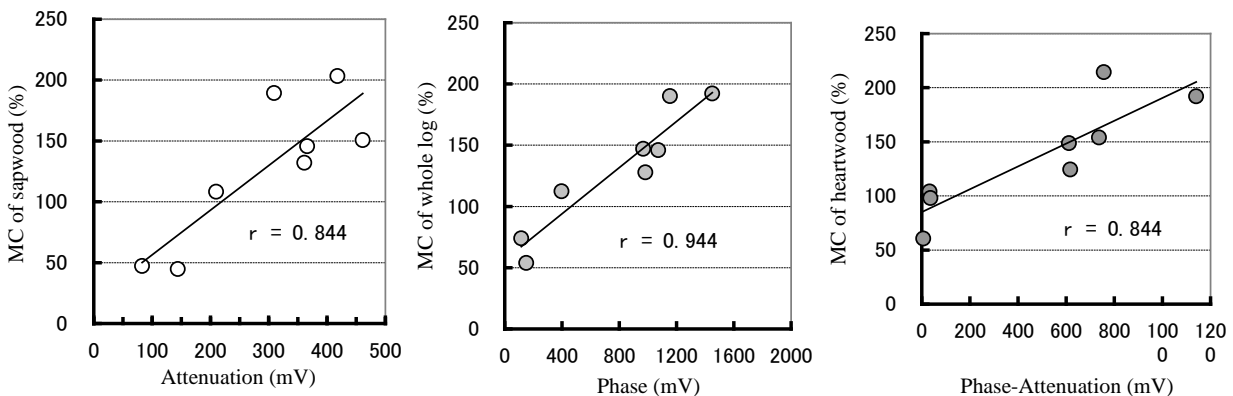


Figure 11- Relationships of each part MC in Sugi Logs with different elapsed time after logging and the phase, attenuation. MC: A value obtained by dividing a disk collected from logs into sapwood and heartwood and measuring them by oven-dried method

Conclusions

The relative permittivity when a needle-type terminal is driven into a heartwood at butt end of a Japanese cedar (Sugi) log and a device for measuring the phase attenuation when the log moves between the transmitting and receiving antenna of the low-frequency (52MHz) electromagnetic, were developed. High correlation was found between the relative permittivity of Sugi logs and the heartwood moisture content. We investigated whether it is possible to estimate from the phase and attenuation when sugi log moves between the transmitting and receiving antennas of low frequency electromagnetic waves as a non-contact MC evaluation method for Sugi logs. In the model test of Sugi logs, a high correlation was found between the phase and the laminated whole MC, between the attenuation and the sapwood MC. A significant correlation was found between the value obtained by subtracting the voltage output value of the attenuation from the voltage output value of the phase, and the heartwood MC. From these results, it was confirmed that the MC evaluation of the entire log and the inside of the outer periphery can be performed nondestructively and by non-contact.

Acknowledgments

This research was supported by grants from the project of the Bio-oriented technology research Advancement Institution, NARO (the special scheme project on advanced research and development for next-generation technology). In addition, we gave great cooperation and support to Ooigawa Small diameter Wood Processing Cooperative Association and Fujiichi Co.,Ltd. in this research project.

References

- Ikeda, K.; Hoshikawa, T.; Watai, J.; Suzuki, Y.; Sugiyama, A. 2013. Evaluation of high moisture content of Japanese cedar (*Cryptomeria Japonica*) log using the phase detector of electromagnetic wave transmitter. 18th International nondestructive testing and evaluation of wood symposium. 723-728.
- Suzuki, Y.; Ikeda, K. 2011. Evaluation of moisture content in a log using impedance Model. ISMAE11th. 269-274.
- Suzuki, Y.; Kuroda, N. 2003. Dielectric properties of wood with High Moisture Content (in Japanese). Mokuzai Gakkaishi. 49(3):161-170.
- Dieste, A.; Gonzalez, L.; Vega, A.; Bano, V. 2013. Moisture content above fiber saturation point estimated by an acoustic method in freshly cut Radiata pine logs. 18th International nondestructive testing and evaluation of wood symposium.180-185.
- Suzuki, Y. 2005. Evaluation of moisture content of wood by Electrical measurements (in Japanese). Wood Industry. 60(10): 483-488.
- Sobue, N.; Doi, K.; Date, M. 2011. New impedance measurement system estimating cross-sectional moisture distribution in cylindrical and electric network modeling. J wood Sci. 57(5): 395-400.
- Johanson, J.; Hagman, O.; Fjellner, B. A.; 2003 Predicting moisture content and density distribution of Scots pine by microwave scanning of sawn timber. J wood Sci. 49(5): 312-316.

Applying Discriminate Analysis and Acoustic Tool to Assign Loblolly Pine Families into Susceptibility Classes

Charles Essien¹, Brian Via¹, Thomas Gallagher¹, Timothy McDonald², Lori G. Eckhardt¹

1 School of Forestry & Wildlife Sciences, Auburn University, 602 Duncan Drive, Auburn, AL 36849, USA

2 Biosystems Engineering Department, Engineering Drive Auburn University Auburn, AL 36849.USA

Charles Essien Email: cze0017@auburn.edu ; Brian K.Via Email: brianvia@auburn.edu

Thomas T Gallagher Email: gallatv@auburn.edu;

Timothy Mcdonald Email: mcdonpt@auburn.edu; Lori G. Eckhardt Email: eckhalg@auburn.edu

Abstract

Loblolly pine is one of the most important tree species in the southeastern USA. However, root-feeding fungi continue to be one of the major challenges confronting pine production in this country. Little information exists on the use of rapid nondestructive wood quality assessment techniques to differentiate between families susceptible and tolerant to root-feeding fungi. In this study, we explore the possibility of using an acoustic tool and statistical techniques to differentiate between 17-year-old loblolly pine trees susceptible and tolerant to root feeding fungi. The results indicated that the effect of the root feeding fungi on the wood quality properties differs widely between the families studied. The acoustic tool was successfully used to differentiate between the susceptible and tolerant families.

Keywords: Discriminate analysis, Root-feeding fungi, acoustic tools

Introduction

Loblolly pine is an important tree species in the United States. It dominates on approximately 13.4 million ha throughout the southeastern forests and accounts for over 50% of the standing pine volume of this region (Schultz 1997). Loblolly pine is native to fourteen states extending from southern New Jersey, down to central Florida and west to eastern Texas. Due to its adaptability, it has also been successfully planted along the periphery of its natural range, and even on other continents (Moya et al. 2013). In the southeastern U.S., loblolly pine (*Pinus taeda*) is the most dominant tree species in the southern yellow pine (SYP) group in terms of cultivation, utilization and genetic improvement (McKeand et al. 2003). One of the most important premium products from this species is still dimension lumber for structural applications.

Over the last six decades, Southern Pine Decline (SPD) has been causing reduced growth, decline and eventual premature deaths of loblolly pine, especially in the southeastern United States.

Recently, loblolly pine decline has become one of the major challenges confronting plantation development in the southern USA. This decline has been linked to a complex interaction among fungi, insect, environment, and host. There are several studies exploring the underlying causal and the nature of relationships among the factors causing this decline. However, little information exists on the use of rapid nondestructive wood quality assessment techniques to help differentiate between trees susceptible and tolerant to root-feeding fungi. We hypothesized that the susceptible and tolerant families will exhibit different morphological, physical and anatomical properties hence if acoustic velocity is sensitive to these properties coupled with wood chemistry (Essien et al. 2017), then velocity will vary significantly between the families. Furthermore, anatomical properties will show a significant effect on velocity as the distance between the acoustic probes decreased due to a progressive reduction in a heterogeneity of the wood material. The objective of this study was to explore the possibility of using acoustic velocity determined at different between distances and statistical techniques to differentiate trees susceptible and tolerant to root feeding fungi.

Materials and Methods

Materials

In this study, 17 – year – old loblolly pine plantation located in Eufaula, Alabama (N32°03'85" and W85° 21'30") were selected. The topography of site was relatively flat with a slope less than 2% and 20m altitude above sea level. The soil was very fine sandy loam, poorly drained and generally poor in nutrients which formed from loamy and silty Coastal Plain sediments. The mean annual temperature ranged 17 to 19°C and the annual precipitation from 1981 to 2010 averaged 1315mm (NOAA 2016).

The total size of the site was 6744m² which was divided into four blocks, and four different families were randomly planted in each block on a bed at 1.6 m x 3.2 m. The same planting design and silvicultural treatments were applied to the blocks. The stands had not received any commercial thinning since establishment at the time of data collection. The experiments were established to compare the stability and growth performance of different loblolly pine families. Two of the families were susceptible (S1 and S2) to SPD while the remaining two were tolerant (T1 and T2) to SPD. Twenty-five trees each were randomly selected from each family for this study. The diameter at breast height (DBH) and tree height were measured using diameter tape and clinometer respectively. Tree morphological characteristics such as diameter at breast height (DBH) and height were measured using diameter tape and clinometer respectively. The taper of each tree was determined according to Eqn. 1 (Lasserre et al. 2007)

$$Taper = \frac{Total\ tree\ height}{DBH} \quad Eqn. 1$$

Acoustic measurements of standing trees

All the selected trees from family were acoustically tested using FAKOPP Treasonic Microsecond Timer acoustic tool (Fakopp Enterprise, Agfalva, Hungary) which relied on the time-of-flight (ToF) principle (Essien et al 2016; Essien et al 2017). Basically, the accelerometers (the transmitter and the receiver probes) were positioned on the same side of the tree at 120, 100, 80, 60, 40, 20 and 10cm apart with the center of the path occurring at breast height (Fig. 1). Both probes were positioned 45° to the tree axis and the stress wave was generated by striking the transmitter probe with a steel hammer at a steady force. The generated wave was detected by the receiver and the time lapse for the sound wave to travel the distance between the probes was recorded by the data logger. Ten readings each were taken on each tree and tree velocity was estimated as the ratio of the distance to time (Eqn. 2).

$$Velocity = \frac{Distance}{time} \quad Eqn. 2$$

Physical properties measurement

The physical properties were determined using core samples taken from each of the selected trees at breast height. Moisture content, green, and oven dried densities of all the 100 selected trees were determined following ASTM D2395 protocols. The volume of the core samples was determined using a digital caliper to the nearest 0.025mm and the weight measured to the nearest 0.001g using electronic balance while the core samples were green. The core samples were dried to a constant weight at 102°C. The moisture content (MC), oven dried density (ODD) and green density (GD) of the core samples were determined using Eqns. 4, 5 and 6

$$MC = 100 * \left(\frac{Mi - Mo}{Mo} \right) \quad \text{Eqn. 4}$$

$$ODD = \frac{Mo}{Vo} \quad \text{Eqn. 5}$$

$$GD = \frac{Mi}{Vi} \quad \text{Eqn. 6}$$

where MC = moisture content, Mi = initial mass, Mo = oven-dried mass, v_o = oven dried volume, v_i = green volume, ODD= oven dried density, GD = green density.

Anatomical properties determination

Thin core samples measuring about 100µm in thickness were macerated using equal volumes of hydrogen peroxide (30%) and glacial acetic acid at 80°C for 24 hours for thorough maceration (Essien 2011; Peter et al. 2003). The macerated cells were then rinsed with water to remove the excess solution and stop the maceration reaction. Temporary slides were prepared from the macerated fibers. Fiber length, lumen diameter, wall thickness and MFA were measured following the procedure described by Peter et al. (2003). Measurements were performed on twenty full fibers selected from both the earlywood and latewood using Differential Interference Contrast (DIC) Microscope (Olympus BX53) (Essien et al. 2017). The MFA measurements were performed using ImageJ software.

Data analysis

The parameters determined were DBH, total height, slenderness (taper), MC, green density, fiber length, fiber lumen diameter, and fiber wall thickness. The dataset was analyzed using SAS (SAS Institute 2014). Simple descriptive statistics and charts were generated for each of the parameter studied for each family. Due to the strong correlation between some of the anatomical and physical properties variables, principal components regression were used with the velocity determined at seven distance as the response and the principal component loadings as the predictors. This step helped to identify the most important components affecting the velocity. Multiple linear regressions with the raw parameters were used to validate the results from the principal component regression. After confirming that most of the variation in the velocity can be explained by the measured parameters or the derived components, the velocities were then used to perform allocate the families into their respective rate code (either susceptible or tolerant) using linear discrimination method. Seventy percent of the dataset was used to develop the model and 25% used to test the model. Five-fold cross-validations were performed using subsamples from the whole dataset (Acquah et al. 2016, Johnson and Wichern, 2007).

Results and discussion

Physical, anatomical, morphological, and acoustic properties of the four families

The results of the morphological, anatomical, physical, and acoustic properties of the four loblolly pine families are presented in Figs 1 – 4 respectively. Generally, families have statistically similar diameter at breast height but they are significantly different in terms of height growth and slenderness (taper). T1 is the tallest and the T2 is the shortest (Fig.1). From Fig 2, the anatomical properties of the susceptible families (S1 and S2) are statistically similar as compared to the tolerant families (T1 and T2). For instance, there is no significant difference between the susceptible families (S1 & S2) in terms of fiber length, lumen diameter and wall thickness (Fig 2) but fiber length and wall thickness are significantly different within the tolerant families (T1 & T2). A similar trend is observed in the acoustic velocity. The susceptible families and one tolerant family (T1) are statistically similar as compared to T2. Since there is no distinct pattern in the studied parameters between susceptible and tolerant families. However, one of the tolerant families (T2) seems distinctively different from the rest for most of the parameters studied. This suggests that the families can be separated.

Principal component, multiple linear regression, and linear discriminate analysis

The results of the multiple linear regression and the principal component analysis are shown in Tables 1 - 2. From 1, the first 5 principal components (PCs) explained about 92% variations in the dataset hence 5 PCs were used for further analysis (Johnson and Wichern 2007). The adjusted R^2 for both the multiple linear and principal component regressions ranged from 36% to 66% for velocities estimated from 10 cm to 120 cm. This implies that the independent variables explained more than half the variations in the dependent variables (V 10 to V 120), the velocities can be used as a discriminant factor. The results from the linear discriminate analysis are presented in Table 3 – 4. The generalized squared distances (Table 4) indicate the extent of separation between groups in space. Therefore, an unknown sample from the group is classified into a given category if it is similar enough to the other members in that category, else it is rejected. From Table 3, T2 offered the best separation family hence it will be easier to classify members into this family as indicated in Table 5. Contrarily, the other families are very close (Table 3) hence difficult to correctly allocate member (Table 4). The error rate of classification is 35% for V120 and 40% for V60. This suggests between 60 to 65 % correct classification rates despite the close semblance between the susceptible families (S1 & S2). This time – of – flight tool has been calibrated to function effectively within a certain distance between the probes hence 120 cm offered the best correct classification rate. Though the 35% error rate of classification is high but it indicated the possibility of using the acoustic technique to segregate susceptible and tolerant families during tree breeding programs.

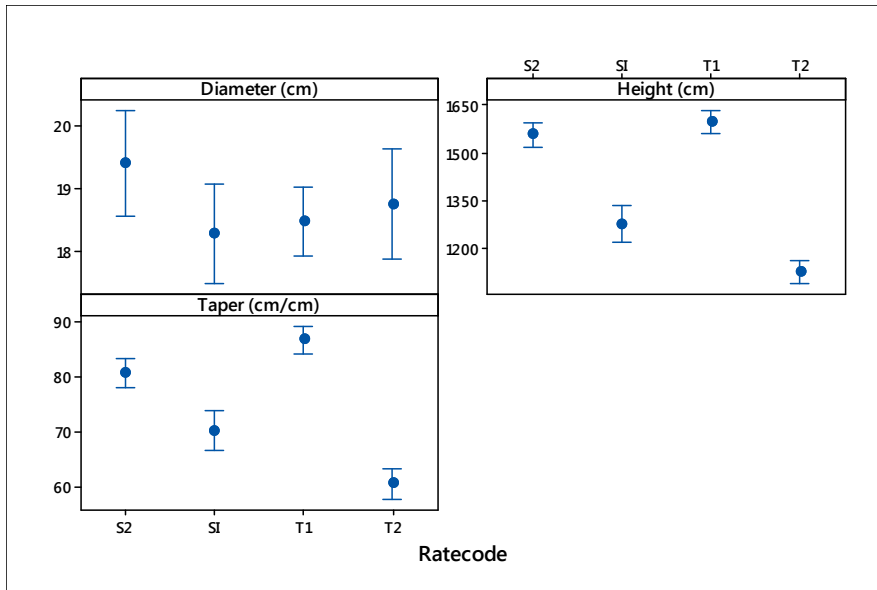


Fig 1 - Tree morphological parameters of the four mature loblolly pine families. T1 & T2 are tolerant while S1 & S2 are susceptible. The error bars indicate 95% confidence interval.

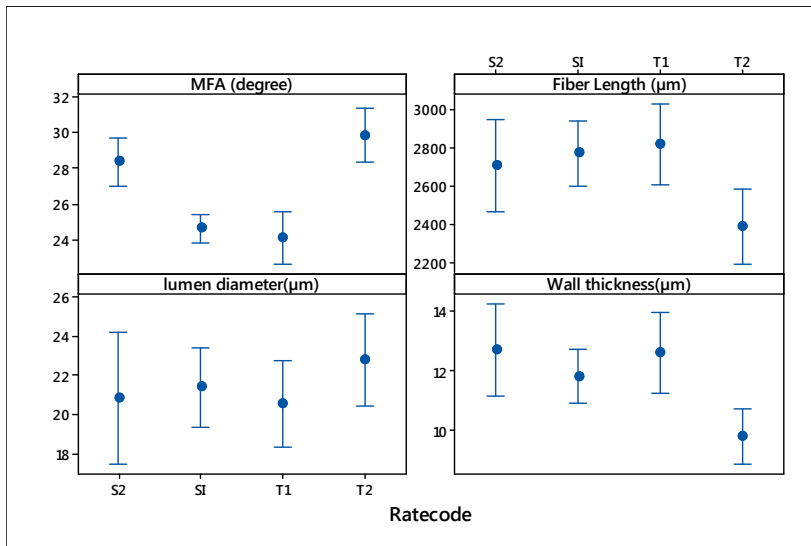


Figure 3. The wood anatomical parameter of the four mature loblolly pine families. T1 and T2 are tolerant while S1 & S2 are susceptible. The error bars indicate 95% confidence interval.

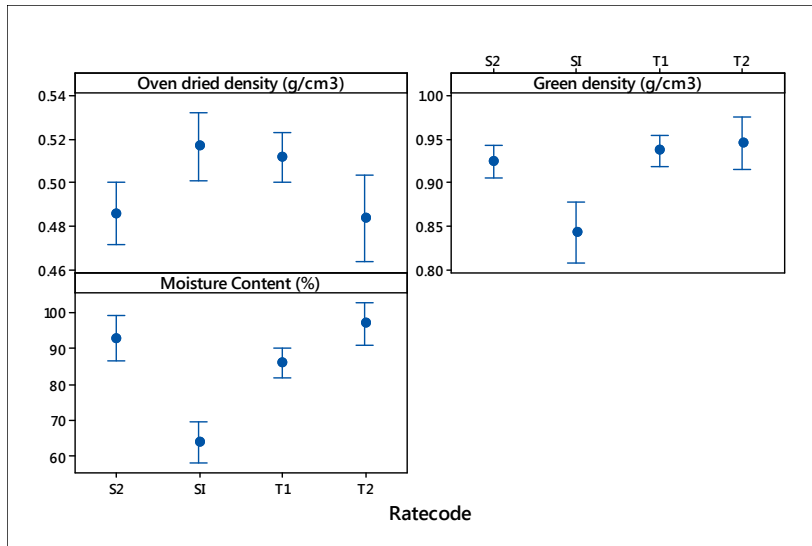


Figure 4. Physical properties of the four mature loblolly pine families. T1 and T2 are tolerant while S1 & S2 are susceptible. The error bars indicate 95% confidence interval.

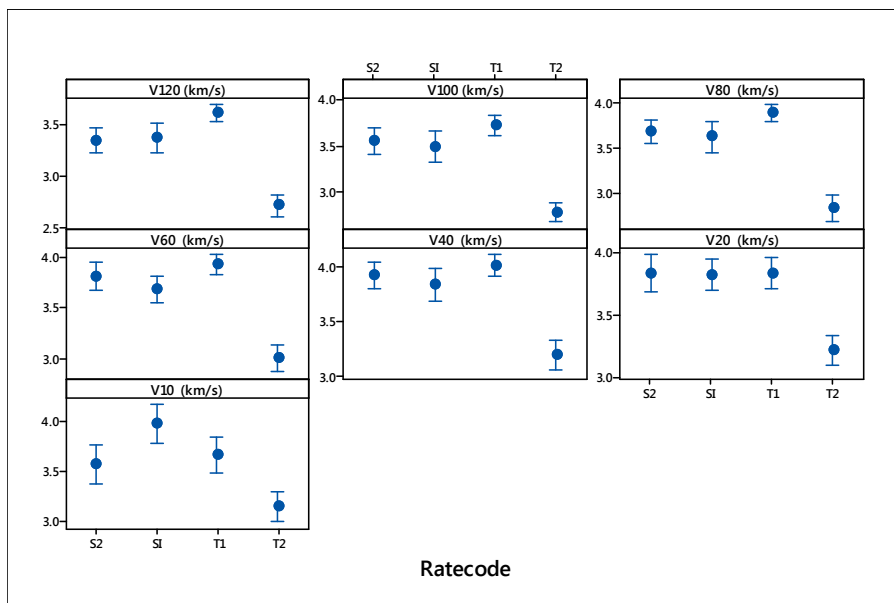


Figure 4. Acoustic velocities determined at various between probes distances for the four mature loblolly pine families. T1 and T2 are tolerant while S1 & S2 are susceptible. The error bars indicate 95% confidence interval.

Table 1 – Eigen values, proportion and cumulative variance explained, and dominant variable for Principal components.

PC	Eigen value	Proportion of variance explained (%)	Cumulative variance explained (%)	Dominant Variable(s) in PC
1	2.781	39.7	39.7	Fiber length, MFA, wall thickness, lumen diameter
2	1.558	22.3	62.0	Moisture content, oven dried density

3	0.954	13.6	75.6	Taper
4	0.700	10.0	85.6	MFA, lumen diameter
5	0.450	6.4	92.0	Fiber length, MFA, lumen diameter
6	0.379	5.4	97.5	Moisture content, oven dried density
7	0.178	2.5	100.0	wall thickness

Table 2 – Principal component regression analysis

	Significant PCs	Coefficients (SE)	SER	R ² adj
V120	PC1	0.085 (0.021)	0.257	66.15
	PC2	0.067 (0.025)		
	PC3	-0.168 (0.054)		
V100	PC1	0.101 (0.025)	0.302	62.46
	PC2	0.088 (0.029)		
	PC3	-0.159 (0.053)		
V80	PC1	0.097 (0.025)	0.299	66.63
	PC2	0.076 (0.029)		
	PC3	-0.185 (0.053)		
V60	PC1	0.077 (0.024)	0.294	61.43
	PC2	0.067 (0.028)		
	PC3	-0.113 (0.05)		
V40	PC1	0.076 (0.022)	0.292	56.76
	PC2	0.053 (0.028)		
V20	PC1	0.065 (0.024)	0.304	45.84
	PC3	-0.123 (0.054)		
	PC4	0.076 (0.038)		
V10	PC1	0.084 (0.032)	0.407	39.76
	PC3	-0.173 (0.072)		
	PC4	0.138 (0.051)		

Table 3 - Generalized squared distances matrixes for the four families with rate code (susceptible S1 S2) and tolerant (T1 and T2)

From / To	V120				V100				V80				V60			
	S1	S2	T1	T2	S1	S2	T1	T2	S1	S2	T1	T2	S1	S2	T1	T2
S1		0.03	1.10	4.10	0.01	0.33	4.41		0.01	0.51	6.57		0.128	0.27	5.40	
S2			0.76	4.84		0.48	3.93			0.68	5.99			0.76	3.87	
T1				9.45			7.14				10.7				8.07	
T2																

Table 4 – Summary of percentage error rate for individual family and mean model error rate from five – fold cross - validation method

	V120				V100				V80				V60			
	S1	S2	T1	T2	S1	S2	T1	T2	S1	S2	T1	T2	S1	S2	T1	T2
Error Rate (%)	74	55	0	10	75	100	29	0	85	64	20	18	92	45	33	15
Mean error rate (%)	35				40				39				40			

Conclusion

In this study, we used time – of – flight acoustic tool to classify trees identified to be susceptible or tolerant to root feeding fungi. The results indicated the susceptible families were very similar in terms of their morphological, physical, anatomical, and acoustic attributes while the tolerant families vary significantly in these attributes. Both the multiple linear regression and the principal component regressions indicated the acoustic velocity can be used to separate the families. Using the acoustic velocity as the discriminant, we achieved 35% error rate of classification indicating 65% success rate of classifying new member into the families. It was, however, impossible to separate the members within the susceptible families (S1 and S2).

Reference

- Acquah G.E., Via B.K., Billor N., Fasina O.O., and Eckhardt L.G.2016. Identifying plant part composition of forest logging residue using infrared spectral data and linear discriminant analysis. *Sensor* 16: 1375
doi:10.3390/s16091375
- ASTM Standard D2395. 2007. Standard Test Methods for Specific Gravity of Wood and Wood-Based Materials ASTM International, West Conshohocken, Pa
- Essien, C., Cheng, Q., Via, B.K., Loewenstein, E.F., Wang, X.2016. An Acoustic operations study for loblolly pine standing saw timber with different thinning history *BioResources* 11(3): 7512 – 7521
- Essien C. 2011. Physical, Anatomical and Treatment characteristics of the wood of *Cola gigantea* and *Ficus sur*. Master of Philosophy Thesis, Faculty of Renewable Natural Resource - Kwame Nkrumah University of Science and Technology, Kumasi, Ghana. Pp 196
- Essien, C., Via BK, Wang, X., Gallagher T, McDonald T, Eckhardt LG (2017) Multivariate Modeling of Acousto-mechanical Response of Fourteen Year Old Suppressed Loblolly Pine (*Pinus taeda*) to Variation in Wood Chemistry, Microfibril Angle, and Density *Wood Sci Technol* 51: 475 – 492.
- Johnson, R.A. & Wichern, D.W. 2007. Applied multivariate statistical analysis. Pearson Education Inc. Upper Saddle River, NJ. USA.
- Peter, G.F., Benton, D.M., Bennett, K.2003.A simple direct method for measurement of microfibril angle in single fibers using differential interference contrast microscopy. *J. Pulp and Paper Sci.* 29: 274 – 280
- Lasserre JP, Mason EG, and Watt MS (2007) Assessing corewood acoustic velocity and modulus of elasticity with two impact based instruments in 11-year-old trees from a clonal-spacing experiment of *Pinus radiata* D. Don. *For. Ecol. Manage.* 239:217–221.
- McKeand S, Mullin T, Byram T and White T (2003) Deployment of genetically improved loblolly and slash pine in the South. *J. For.* **101**: 32-37.
- National Oceanic and Atmospheric Administration (NOAA 2016) State, regional and national monthly precipitation: area weighted monthly normal, 1981 – 2015. *Historical Climatology*
- Statistical Analysis Software (SAS) version 9.4 (2014) Cary, NC, USA
- Moya L, Laguarda ML, Cagno M, Cardoso A, Gatto F, O'Neill (2013) Physical and mechanical properties of loblolly and slash pine wood from Uruguayan plantations. *For. Pro. J.* 63 (3/4): 128 – 137.
- Schultz, R. P. 1997. Loblolly pine, the ecology and culture of loblolly pine (*Pinus taeda* L.). U.S. Dep. Agric., Forest Service, Agric. Handb -713 Washington, D.C. pp 1 – 16.

Friction of Drill Bit and Its Effect on Resistance Drilling Measurements in Logs

Evgenii Sharapov*

Volga State University of Technology, Yoshkar-Ola, Mari El Republic, Russian Federation, sharapoves@volgatech.net

Xiping Wang

USDA Forest Service, Forest Products Laboratory, Madison, Wisconsin, USA, xwang@fs.fed.us

Elena Smirnova

Volga State University of Technology, Yoshkar-Ola, Mari El Republic, Russian Federation, smirnovaev@volgatech.net

* Corresponding author

Abstract

The main objectives of this laboratory study were to determine the effect of drill bit friction on resistance drilling measurements conducted on green logs and to assess the potential of using relative resistance and feeding force to predict density and hardness of wood in logs, and ultimately in standing trees. Two freshly cut yellow birch (*Betula alleghaniensis*) logs, one with central rot and the other decay free, were used as test specimens. Drilling measurements were conducted on the logs using an IML-RESI PD 400 tool equipped with a standard spade needle drill bit. Following drilling measurements, nine 5.1-cm-thick disks were cut from the decayed log, one at each drilling location, and a 5.1-cm-wide strip was cut from each disk. A series of hardness tests was conducted on each strip based on a procedure modified from ASTM D 143-2012. Then each strip was cut into 1.8-cm segments to determine wood density using volumetric method. In addition, 195 drilling measurements were conducted on the decay-free log to specifically examine the friction effect. Statistical analysis was conducted to determine friction variations along the drilling path and develop density and hardness prediction models using measured resistance and feeding force as predictors.

Keywords: drilling resistance, feeding force, Janka hardness, logs, wood density

Acoustic Characterization of Wood from Tree Branches

Gustavo Garcia

Master student, UNICAMP, Valinhos–SP, Brazil, gustavohlgarcia@hotmail.com

Raquel Gonçalves

Professor, LabEND - FEAGRI, UNICAMP, Campinas, São Paulo, Brazil, raquel@agr.unicamp.br

Mônica Ruy

PhD student, Laboratory of Nondestructive Testing - LabEND, University of Campinas - UNICAMP, Campinas, São Paulo, Brazil –monica.ruy@hotmail.com

Rafael Gustavo Mansini Lorensani

Doctor, LabEND - FEAGRI, UNICAMP, Campinas, São Paulo, Brazil

Abstract

With the extreme events caused by climate change, there is significant growth of breaking and falling branches in urban trees. The falling of big branches in urban area can cause serious accidents. The branches have great importance in analysis of trees behavior using biomechanics but, in general, the properties of these elements are not specifically evaluated but considerate as the same of the stem.

The objective of this paper is to present preliminary results of acoustic characterization of wood from branches. To achieve this goal we collected sections of branches using six species of trees. In a same branch, specimens were collected in different positions. Readings were taken longitudinally with direct measurements (transducers positioned on opposite faces of the branch section) and with indirect measurements (transducers positioned at 45 degrees on the same face).

The results showed that there are variation in velocities among species, indicating that this easy tool could be used to grading, by stiffness, branches from different species of trees or branches from different position of the same tree. The results also allow us to obtain statistically significate correlations between velocities obtained in direct and indirect tests. This result is important to the use of the technology in live trees in standing trees inspections aiming the analysis of fall risk through biomechanical studies. This data will be compared with the characterization of wood from roots and stem.

Keywords: Strength of branches wood, Stiffness of branches wood, Ultrasound in wood characterization, Chestnut wood, Pine wood

Air-Coupled Ultrasound and Electrical Impedance Spectroscopy Applications for Wood

Markku Tiitta *

Department of Applied Physics, Univ. of Eastern Finland, Kuopio, Finland, email markku.tiitta@uef.fi

Laura Tomppo

Department of Applied Physics, Univ. of Eastern Finland, Kuopio, Finland, email laura.tomppo@uef.fi

Third author first and last names

Department of Applied Physics, Univ. of Eastern Finland, Kuopio, Finland, email reijo.lappalainen@uef.fi

* Corresponding author

Abstract

The overall goal was to develop efficient methods to improve the quality assessment of wood. Air-coupled ultrasound and electrical impedance spectroscopy were the studied measurement methods. The ultrasound method is based on mechanical waves and is affected by the mechanical properties and defects of wood. Density affects both methods, and the electrical impedance method is especially affected by moisture content and the chemical properties of wood. The relations between the methods and the properties of several wood species were examined, both softwoods and hardwoods. Several studies were also conducted for modified wood. According to the results, electrical impedance spectroscopy, air-coupled ultrasound, and combined method are efficient nondestructive techniques for estimating quality properties of hardwood, softwood, and modified wood. Recently, industrial tests have also been conducted.

Keywords: Air-coupled ultrasound, electrical impedance spectroscopy, quality assessment

Determination of Modulus of Elasticity of Wood Particleboard by Nondestructive and Destructive Testing Methods

Felipe Silva Bastos

Federal University of Viçosa, Viçosa, Minas Gerais, Brazil, felipe.bastos@ufv.br

Marcos Oliveira de Paula *

Federal University of Viçosa, Viçosa, Minas Gerais, Brazil, modepaula@gmail.com

Camila Batista da Silva Lopes

Federal University of Viçosa, Viçosa, Minas Gerais, Brazil, camila.batista@ufv.br

Matheus Fernandes de Carvalho Reis

Federal University of Viçosa, Viçosa, Minas Gerais, Brazil, matheusfcreis@gmail.com

Vinícius Resende de Castro

Federal University of Viçosa, Viçosa, Minas Gerais, Brazil, vinicius.castro@ufv.br

* Corresponding author

Abstract

The transverse vibration method offers great potential for nondestructive wood testing and evaluations due to the precision of the mathematical model associated with this method and the possibility of application in pieces of structural dimensions. However, there is a lack of study about the utilization in wood particleboard. Particleboards of *Pinus caribaea* were produced at Federal University of Viçosa, in the Mechanical Properties Laboratory, with density of 0.60 g cm^{-3} and final dimensions of 38 by 38 by 1 cm. Phenol-formaldehyde (PF) and sodium silicate (SS) adhesives were used with different proportions: 100% PF; 96% PF, 4% SS; 94% PF, 4% SS; 92% PF, 8% SS; 90% PF, 10% SS, for a total of five treatments. The particleboards were cut into samples for modulus of elasticity determination by a destructive method using a universal mechanical test machine and by the transverse vibration method. This nondestructive testing was performed using a prototype with a microphone and the software Fast Fourier Transform Spectrum Analyzer to capture the mechanical wave vibration through each sample. Then the dynamic modulus of elasticity was calculated. The values obtained for modulus of elasticity using the transverse vibration method were equivalent to the destructive method, showing no significant difference. Therefore, such a tool is a potential alternative for wood particleboard mechanical characterization. It is necessary to emphasize the need to improve this technique, developing new equipment and creating models with adequate parameters and coefficients, so that this method can be more effectively used.

Keywords: modulus of elasticity, mechanical testing, nondestructive method, wood particleboard, transverse vibration technique

Plant Health Evaluation and Fall Risk in Urban Trees in the City of Belo Horizonte, Brazil

Aderbal Gomes da Silva^{1*}, Luis Miguel Martins²

¹Departament of Agrarian Sciences – DCIAG – Federal University of São João Del Rei, Rod. MG-424, Km 47, CEP: 35701-970, Cx.P: 56. Sete Lagoas, MG, Brasil

* +55 31 99180 9322, +55 31 3697 2041, aderbalsilva@ufsj.edu.br

²Department of Forest Sciences and Landscape Architecture – University of Trás-os-Montes e Alto Douro, Quinta dos Prados, 5000 911, Vila Real, Portugal

Abstract

The objectives of this study were to evaluate the plant health and the risk of fall of 20 trees of four species frequent in Brazilian public roads. The evaluation was performed through visual inspection and the use of internal prospecting instruments. The trees were located on public roads in the city of Belo Horizonte, Minas Gerais, Brazil. Initially, dendrological characteristics were observed and dendrometric parameters such as diameter at breast height (DBH), median canopy radius, total height, and height of the canopy base were evaluated. Visual inspection was carried out, evaluating the condition of the trees and local conditions, using as basis the VTA (visual tree assessment) method. In the diagnostic process, tools such as rubber hammer, binoculars, and internal prospecting instruments were also used. Five individuals were evaluated from each species: *Jacaranda mimosaeifolia*, *Ligustrum lucidum*, *Michelia champaca*, and *Poicicanella pluviosa*. The evaluated trees were older than 40 years, and had diameter at breast height greater than 45 cm and height between 10 and 16 m. At the end of the evaluation process, suppression was recommended for four individuals of *Ligustrum lucidum*, three of *Jacaranda mimosaeifolia*, and two of *Poicicanella pluviosa* due to irreversible damages, characterizing low phytosanitary condition and high risk of fall. In general, it was observed that cavities, cancers, codominances, and biotic agents (fungi) affected the safety of the trees. The individuals of *Michelia champaca* evaluated presented medium phytosanitary quality with small necroses in the trunk, but without structural damages. The presence of the cochineal pest was also identified, but the species was tolerant.

Keywords: hazard tree, risk assessment, plant health, visual inspection

Nonconventional Approach to Evaluate the Quality of Heartwood and Sapwood

Sabrina Cherelli*

Department of Rural Engineering, School of Agriculture, São Paulo State University (Unesp), Botucatu, SP, Brazil, sabrina_galetti@hotmail.com

Adriano Ballarin

Department of Rural Engineering, School of Agriculture, São Paulo State University (Unesp), Botucatu, SP, Brazil, awballarin@fca.unesp.br

* Corresponding author

Abstract

This study evaluated the quality of heartwood and sapwood from mature trees of two species (*Corymbia citriodora* and *Eucalyptus tereticornis*) by means of the qualification of their proportion, determination of basic and apparent density using nondestructive attenuation of gamma radiation technique, and calculation of the density uniformity index. The heartwood and sapwood were delimited by macroscopic analysis, and the calculations of areas and percentage of heartwood and sapwood were performed using digital image analysis. The uniformity index was calculated following methodology that numerically quantifies the dispersion of punctual density values of the wood around the mean density along the radius. The percentage of heartwood was higher than that of sapwood in all species studied. The density results showed no statistical difference between heartwood and sapwood. In contrast, in all species studied there were statistical differences between uniformity indexes for heartwood and sapwood regions, making justifiable the inclusion of the density uniformity index as a quality parameter for *Eucalyptus* wood.

Keywords: *Eucalyptus*, density uniformity index, nonconventional approach

Comparison between Eucalyptus and Oak Woods with a View to Application in Wooden Shims

Pedro Gutemberg de Alcântara Segundinho*

Department of Forestry and Wood Sciences, Federal University of Espírito Santo, Jerônimo Monteiro, Espírito Santo, Brazil, p_gutemberg2001@yahoo.com.br, pedro.segundinho@ufes.br

Thais de Souza Marcchiori

Department of Forestry and Wood Sciences, Federal University of Espírito Santo, Jerônimo Monteiro, Espírito Santo, Brazil, thaismarcchiori@gmail.com

Fabricio Gomes Gonçalves

Department of Forestry and Wood Sciences, Federal University of Espírito Santo, Jerônimo Monteiro, Espírito Santo, Brazil, fabricio.goncalves@ufes.br

* Corresponding author

Abstract

It is remarkable how important the construction sector is in any country, along with sustainability in current times. In Brazil, wood material is not yet widely used in buildings, compared to countries in North America and Europe. Eucalyptus and oak woods were evaluate in this study to deepen the knowledge about them and to compare the two species of wood. The analysis was carried out by comparing physical and mechanical properties of the wood species; in almost all tests, the oak wood presented higher property values than eucalyptus wood. However, the eucalyptus wood also shows suitability for the manufacture of wooden shims.

Keywords: nondestructive tests, physical properties, mechanical properties, timber structures.

Characterization of the Dynamic MOE by Transverse Vibration Method in Glulam of Thermal Treated *Eucalyptus grandis*

César Polanco-Tapia *

Forestry Engineer Program, Universidad Distrital Francisco José de Caldas, Bogotá, D.C., Colombia, cpolanco@udistrital.edu.co

Diana Peña

Forestry Engineer Program, Universidad Distrital Francisco José de Caldas, Bogotá, D.C., Colombia, dianay.ps@gmail.com

Jose Nivaldo Garcia

Forestry Engineer Program, ESALQ, Universidad de Sao Paulo, Piracicaba, SP, Brazil, jngarcia@usp.br

* Corresponding author

Abstract

Eucalyptus grandis species is recognized in Latin America because of its rapid growth and high mechanical resistance. Thermal treatment of biological materials is gaining importance in the scientific literature and in industrial processes to acquire advantages such as natural durability, waterproofness, dimensional stability, and color homogenization. Unfortunately, some authors found disadvantages in this process, especially regarding the loss of mechanical strength. The effect of heat treatment on the adhesive line stability is unknown. The present paper evaluated the effect in glulam of heat treatment in *E. grandis* through the transverse vibration nondestructive technique. It compared the obtained values of the dynamic modulus of elasticity (MOE) in treated and untreated wood. The FFT Analyzer program was used to measure vibration frequencies; for the transformations, the USDA equations were followed. All the wood underwent bending test in three points (ASTM D 143) to determine static MOE. The pieces used had PRF (phenol resorcinol formol) in the adhesive line localized in the thickness middle with 350 g m⁻² of spread. Finally, we found differences for MOEs between treated and untreated wood, and between transverse vibration and bending static methods. In the case of the destructive tests, the failure did not occur on the adhesive line, and it can be anticipated that temperature conditions and time intervals used in the heat treatment did not cause serious damage to adhesive lines but rather to the wood.

Keywords: Phenol resorcinol formol, glue line, Fast Fourier Test (FFT), bending test

Comparison among Velocity of Ultrasound Wave Propagation in Roots, Branches and Stem

Cândida P. da Costa*

PhD, Post-doctoral researcher, Laboratory of Nondestructive Testing - LabEND, School of Agricultural Engineering - FEAGRI - University of Campinas - UNICAMP, Brazil
E-mail: candidapcosta@gmail.com

Raquel Gonçalves

Professor, Laboratory of Nondestructive Testing – LabEND, School of Agricultural Engineering - FEAGRI - University of Campinas - UNICAMP, Brazil –
E-mail: raquel@agr.unicamp.br

Cinthy Bertoldo*

Professor, Laboratory of Nondestructive Testing – LabEND, School of Agricultural Engineering - FEAGRI - University of Campinas - UNICAMP, Brazil –
E-mail: cinthya.bertoldo@feagri.unicamp.br

Nina M. O. Cavalcanti

Master student, Laboratory of Nondestructive Testing – LabEND, School of Agricultural Engineering - FEAGRI - University of Campinas - UNICAMP, Brazil
E-mail: nina.ocavalcanti@gmail.com

Mariana N. Reis

Master student, Laboratory of Nondestructive Testing – LabEND, School of Agricultural Engineering - FEAGRI - University of Campinas - UNICAMP, Brazil
E-mail: ma.nagle.reis@gmail.com

Gustavo H. Garcia

Master student, Laboratory of Nondestructive Testing – LabEND, School of Agricultural Engineering - FEAGRI - University of Campinas - UNICAMP, Brazil
E-mail: gustavohlgarcia@hotmail.com

* Corresponding author

Abstract

Trees are very important to the urban welfare but, on the other hand, can cause accidents. Because of this dichotomy, nowadays people wants to preserve the trees but require safety. So, it is very important studies that have as objective the improvement in tree inspections, given more objectivity to the diagnosis. Wave propagation methods are very used to infer elastic properties of wood mainly that linked with its stiffness. At the same time, the stiffness is one very important property related to the biomechanics behavior of the tree. As the stiffness is linked with velocity of wave propagation, the objective of this research was to determine and compare velocity of wave propagations obtained in roots, branches and stem. The aim is to contribute to increment information about properties of wood from different parts of the tree, to support studies of tree risk assessment from biomechanics. Considering the preliminary results, we could not find a pattern to represent the behavior of the velocity in different organs (root, branches and stem) of the tree.

Key words: ultrasound; velocity of wave propagation; trees

Introduction

Trees are fundamental to the well-being of urban communities and, among many others features, it plays an important role in reducing temperature and pollution and so in interception of rainwater (Silva Filho et al. 2002; Silva et al. 2008 Brazolin 2009 and 2010, Rollo et al 2013). On the other hand, trees can be protagonists of accidents, producing conflicts, since there is ecological pressure for preservation and the need to guarantee personal and patrimonial security (Silva Filho et al 2002; Brazolin 2009). Thus, it becomes important studies that make feasible the use of technology, associated with visual and biological analysis, allowing greater objectivity in the diagnoses of the condition of the tree.

Several methods have been used to help identify the phytosanitary and biomechanical conditions of trees, and the risk of their fallen (Nicolotti et al 2003). Among them are the visual analyzes of the tree and the environment and the nondestructive analysis techniques, which originated from the need to solve practical problems without compromising the integrity of the standing trees (Nicolotti et al. 2003; Bucur 2005). Among the nondestructive methods, the acoustic tomography is one of the most indicated for applications in tree inspection (Nicolotti et al 2003; Bucur 2005).

However, in general, the acoustic properties of the sound wood from species used in urban areas are not known. Still less known are properties obtained from different parts of the tree (roots, branches and stem). These properties are very important to the correct application of acoustic tomography, mainly to the image interpretation, contributing to the decision about the falling tree risk. The mechanical characterization of trees has been carried out mainly on stems, with scarce works on the properties of wood from root and branches. In general, it is assumed that all wood of the tree is structurally similar. However, studies aiming analyzing possible variations in mechanical properties of the wood among different organs from trees are important for the holistic understanding of the trees biomechanics.

Objective

The objective of this paper was to determine and compare the radial velocities of ultrasound wave propagation obtained in wood from roots, stems and branches of five species present in urban arborization in Brazil.

Methods

Samples from root, stem and branches used in the trials were extracted from trees of the species Tamboril (*Enterolobium contortisiliquum* (Vell.) Hauman), Ingá (*Inga sessilis* (Vell.) Mart), Mogno (*Swietenia macrophylla* King), Pau d'alho (*Galesia integrifolia* (Spreng.) Harms) and Aroeira salsa (*Schinus molle* (Anacardiaceae)), fallen during the micro-bursts phenomenon (Figure 1), occurred in the region of Campinas (São Paulo state, Brazil), in June 2016.



Figure 1— Image of trees fallen during the micro-busters phenomenon and withdrawal of samples

The roots analyzed were taken from portions corresponding to lateral roots of support, found just after the trunk flare region. The stem samples were removed in the DAP zone (1.30 m from the soil tree) and the branches were cut from the branch insertion region in the longitudinal growth direction.

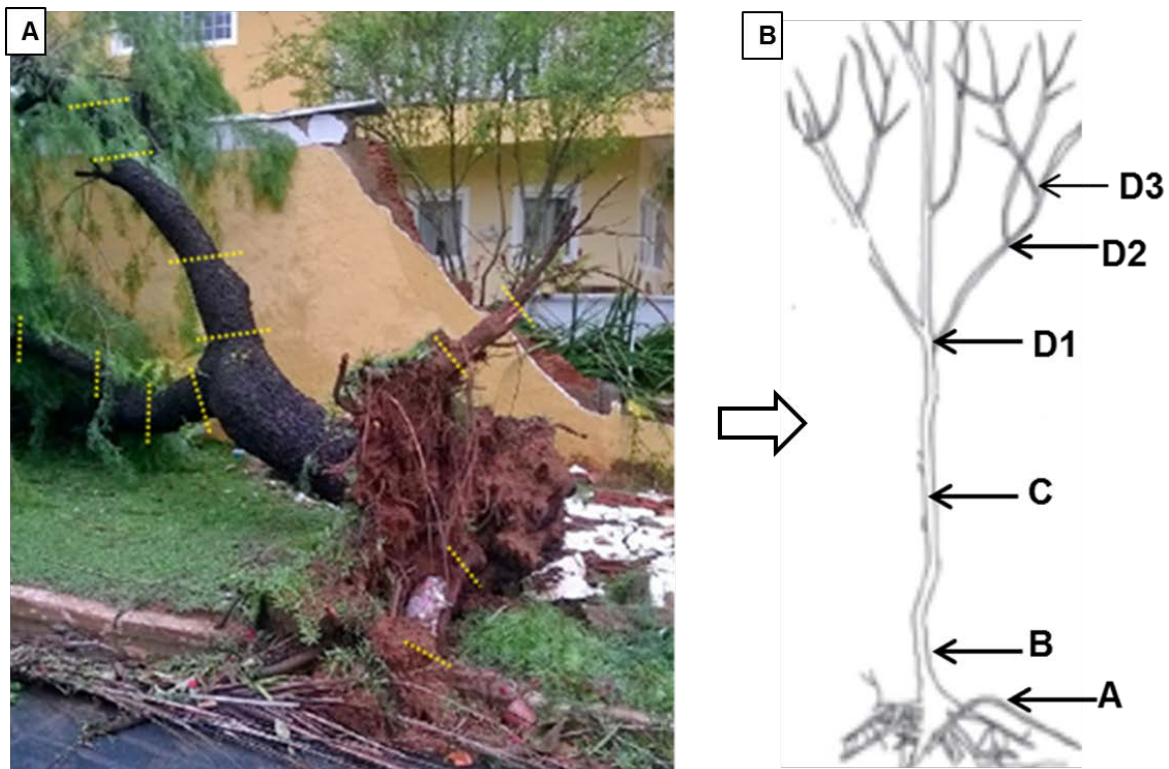


Figure 2—A) Yellow lines mark cutting site for root and branch sample B) Profile diagram showing the sampled region of trees. The arrows indicate: A) root; B) and C) stem and from D1 to D3 the main ramifications of branches.

All pieces were measured for the determination of the diameter and were submitted to ultrasound tests, with determination of the propagation times (t). The wave propagation tests were performed with ultrasound (USLab, Agricef, Brazil) and 45-kHz exponential face longitudinal transducers. Ultrasound tests were performed in the radial direction and directly (transducers coupled on opposite

faces) – Figure 3. Radial velocities (V_R) were calculated from the diameters and propagation times. The radial velocity was adopted because is that used in ultrasonic tomography.



Figure 3—Example of ultrasound test in a wood specimen from root .

For analysis of the results, it was first verified if the radial velocity could be considered as having normal distribution. This analysis was made based on values of asymmetry and kurtosis, which, when between -2.0 and +2.0 indicate the possibility of acceptance of the normal frequency distribution. Accepting the normal distribution, we proceed with the statistical analysis of average comparison considering radial velocities in different species and different organs (root, stem and branches) using multifactor analysis of the variance (Multifactor ANOVA) with 95% of confidence level.

Results and Discussion

Analysis of the frequency distribution of the radial velocities indicated that the normal distribution can be accepted for the velocities obtained in the roots, stem and branches.

The roots present the greatest variability among species (5 groups in 6 species) while the stem the smallest (3 groups and 4 species in the same group) (Table 1).

Velocities in root were different from velocities in stem to 67% of species and from branches in only 33% of species (Table 1). A velocity in stem and branches differs in 50% of species (Table 1).

Velocities in stem were greater than in root and branches for 50% of the species and roots are greater in 33% of them.

Table 1—Mean values of radial velocity ($m.s^{-1}$) obtained in different organs of the same tree

Species	Root	Stem	Branches
<i>Enterolobium contortisiliquum</i>	1441cA	1567bA	1316aA
<i>Inga sessilis</i>	1852eA	1787cB	1802bcAB
<i>Swietenia macrophylla</i>	1513cC	992aA	1242aB
<i>Gallesia integrifolia</i>	1363bA	1831cB	1420abA
<i>Schinus molle</i> *	1708dA	1897cC	1999cAB
<i>Schinus terebinthifolia Raddi</i>	1229aA	1862cAB	1570abB
All species	1520	1690	1611

* Average considering two trees

Lower cases indicate the statistical analyses in columns (among species) and capital letters the statistical analyses in rows (among organs). Same letters indicate homogenous groups.

Considering the preliminary results, we verify that there is not a pattern to represent the behavior of the velocity in different organs (root, branches and stem) of the tree. We need to add the density of each organ to verify if we can see a pattern on stiffness coefficient ($C_{RR} = \rho V_{RR}^2$). As a part of this research project we are also testing polyhedral specimens by ultrasound to calculate the stiffness matrix and all elastic parameter of wood from roots, branches and stem; testing specimens from each organ in compression to determine Young modulus and Poisson ratio and testing by ultrasound the tree components in longitudinal directions (direct and indirect). So, we expect obtain more information about properties (acoustics and mechanics) of each part of the tree.

Conclusions

In our preliminary results we could not find a pattern to represent the behavior of the velocity in different organs (root, branches and stem) of the tree.

Acknowledgments

The authors are grateful to FAPESP (Proc. 2015/05692-3) for the financial support and MEC/CAPES for granting scholarships to the Master students. We thank the School of Agricultural Engineering – FEAGRI (University of Campinas - UNICAMP, Brazil) for providing logistical support. This study is a contribution of the Laboratory of Nondestructive Testing (LabEND)

References list

- Brazolin, S. Biodeterioração, anatomia do lenho e análise de risco de queda de árvores de tipuana, *Tipuana tipu* (Benth.) O. Kuntze, nos passeios públicos da cidade de São Paulo, SP. Piracicaba, 2009. 267p. Tese (Doutorado em Recursos Florestais) – Escola Superior de Agricultura “Luiz de Queiroz”, Universidade de São Paulo.
- Brazolin, S.; Tomazello-Filho, M.; Amaral, R.D.A.M; Oliveira-Neto, M.A. 2010. Associação entre fungos apodrecedores e cupins subterrâneos no processo de biodeterioração do lenho de árvores de *Tipuana tipu*, na cidade de São Paulo, SP. *Scientia Forestalis*, Piracicaba, v.38, n. 86, p.215-224.
- Bucur, V. 2005. Ultrasonic techniques for nondestructive testing of standing trees. *Ultrasonics*. 43:237-239.
- Nicolotti, G; Socco, L. V., Martinis, R.; Godio, A.,Sambuelli, L. 2003. Application and comparison of three tomographic techniques for detection of decay in trees. *Journal of Arboriculture* 29(2): 66-78.
- Rollo, F.M.A., Soave Júnior, M.A., Viana, S.M., Rollo, L.C.P., Couto, H.T.Z., Silva Filho, D.F.2013. Comparação entre leituras de resistógrafo e Imagens Tomográficas na avaliação interna de troncos de árvores. 2013. *Cerne*, Lavras, v. 19, n. 2, p. 331-337.
- Silva Filho, D.F., Pizetta, P.U.P., Almeida, J.B.S.A, Pivetta, K.F.L., Ferraudo, S. 2002. Banco de dados relacional para cadastro, avaliação e manejo da arborização em vias públicas. *R. Árvore*, v.26, n.5,p.629-642.
- Silva, L.F., Lima, A.M.P., Silva Filho, D.F., Couto, H.T. 2008. Interceptação da chuva pelas copas das espécies de *Caesalpinia pluviosa* DC. (Sibipiruna) e *Tipuana tipu* O. Kuntze (Tipuana) em arborização urbana. *Sci. For.*, Piracicaba, v. 36, n. 80, p. 307-315.

The Potential of Portable NIRS Devices for Rapid, Nondestructive Measurement of Basic Wood Density on Standing Trees

Esther Merlo Sánchez *

Department I+D+i, Madera Plus Calidad Forestal S.L., Ourense, España, maderaplus@maderaplus.es

Jean Paul Charpentier

UR0588 Amélioration, Génétique et Physiologie Forestières. INRA Val-de-Loire, jean-paul.charpentier@inra.fr

Vincent Segura

UR0588 Amélioration, Génétique et Physiologie Forestières. INRA Val-de-Loire, vincent.segura@inra.fr

Ines Bertoldi

Instituto Nacional de Tecnología Agropecuaria (INTA), Bariloche, Argentina, bertoldi.ines@inta.gob.ar

Gonzalo Caballé

Instituto Nacional de Tecnología Agropecuaria (INTA), Bariloche, Argentina, caballe.gonzalo@inta.gob.ar

Oscar Santaclara

Department I+D+i, Madera Plus Calidad Forestal S.L., Ourense, España, maderaplus@maderaplus.es

* Corresponding author

Abstract

NIRS (near infrared spectroscopy) has been used quite successfully in measuring many wood properties. As a result, NIRS calibration has recently been developed for wood basic density. To what extent can NIRS be used as an alternative tool for estimating precisely defined wood microdensity variables? Recently, portable NIRS devices have emerged on the market. Such devices offer the potential of acquiring NIR spectra on standing trees, but the way of collecting the spectra and the extent to which they compare with spectra collected in the laboratory remain to be explored. In this work, we explored and tested the potential of these devices for rapid, nondestructive measurement of basic wood density on standing trees. Measurements were carried out with a portable NIR device on two clonal eucalyptus trees in Spain, from which cores were previously extracted and basic density determined. Microdensity profiles were analyzed and NIR spectra were obtained in the laboratory.

Keywords: Near infrared spectroscopy, eucalyptus, calibration

Dendrochronology Application: Potential of the X-Ray Microdensitometric and μ -EDXRF in Tree-Rings Physical and Chemical Analysis of *Pinus Taeda* Wood

Daigard Ricardo Ortega Rodriguez*

Department of Forest Sciences, Luiz de Queiroz College of Agriculture (ESALQ)-University of São Paulo (USP), Piracicaba, SP, Brazil, dai.ricardo.or@gmail.com.

Elton E. Novais Alves

Soil Science Department, Universidade Federal de Viçosa (UFV), Viçosa, MG, Brazil, elton.alves@ufv.br.

Pablo de Azevedo Rocha

Soil Science Department, Universidade Federal de Viçosa (UFV), Viçosa, MG, Brazil, pab_zulu@yahoo.com.br

Liovando Marciano da Costa

Soil Science Department, Universidade Federal de Viçosa (UFV), Viçosa, MG, Brazil, liovandomc@yahoo.com.br.

Mario Tomazello Filho

Department of Forest Sciences, Luiz de Queiroz College of Agriculture (ESALQ)-University of São Paulo (USP), Piracicaba, SP, Brazil, mtomazel@usp.br.

Abstract

The use of NDTE in dendrochronology is a novel alternative to assess wood properties and silvicultural metrics in a wide range of trees growing conditions. The X-ray microdensitometric and fluorescence microanalysis (μ -XRF) techniques provide intra-annual ring data of physical and chemical availability. Our aim was to evaluate the potential use of the X-ray microdensitometric and μ -EDXRF analysis to assess the carbon accumulation and detect the presence of chemical elements in the wood of *Pinus taeda* of 17 years old. One radial sample at DHB were obtained from six *P. taeda* trees varying in their nutritional state (0, 20, 40, 60, 80 and 100 t/ha of cellulosic residues). Samples were analyzed in the QTRS-01X X-ray equipment, for continuous radial scanned density of the wood. It was constructed the radial density profiles and related to the tree-ring width growth to obtain the annual carbon accumulation by allometric equations. X-ray transmission intensity and microchemistry maps were obtained from twin radial samples in μ -EDXRF spectrometer. The nutritional treatments had a significant effect on the carbon accumulation. The highest carbon accumulation in the wood was found for the sample with 80 t/ha of cellulosic residues. The main chemical elements found were P, S, K, Ca, Mn and Fe. This exploratory testing, using X-ray techniques in the *P. taeda* wood, show potential value for evaluating the carbon accumulation and detection of chemical elements in wood. In addition, this NDTE may provide an interesting tool for interpreting the trees physical and chemical response to their silvicultural growing conditions.

Keywords: X-ray fluorescence, densitometry, carbon accumulation, dendrochemistry.

Methods for Evaluating Mechanical Properties of Wood–Plastic Composite Pallets

Zhanguo Wei

College of Logistics & Transportation, Central-South University of Forestry & Technology, Changsha, Hunan, China, jackwzg007@163.com

Abstract

Wood–plastic composite (WPC) pallets are commonly used in logistic operations in developed countries. In China, the performance requirement and test methods have been developed for general purpose pallets. Because of the unique characteristics of WPC, the test methods developed for general purpose pallets cannot be adopted for the WPC pallets. This paper reports an ongoing study of developing new test methods for evaluating the mechanical performance of WPC pallets.

Keywords: Wood–plastic composite, pallet, test standard, standardization system

Introduction

The pallet is widely used in the production, transportation, storage and circulation, Play an important role in the modern logistics. Compare with the developed country, our country has little forest resource, pallet market is under considerable pressure to go green including road transportation pallet market, and considering the road transportation conditions and road freight cost, characteristics of light and high strength must be taken into account in the pallet (Soury et al. 2009), This paper reports an ongoing study of developing new test methods for evaluating the mechanical performance of WPC pallets.

Structure of WPC pallet

WPC pallet structure diagram is shown in Figure 1. The deck boards of a WPC pallet are made from wood-plastic composites, cushion blocks are made from same material, and it is prepared with thin metal sheets made by pressing, cushion block has hollow structure, compared with traditional wooden structure of the same structure and size, it can not only save wood, but also decrease the total weight greatly (Takahara 2005).

The size of a pallet is 1200 x 1000 mm according to the BB/T 0020-2001, upper and lower board and carling plate are made from the WPC boards of 12-mm thick and 100-mm wide.



Figure 1—WPC pallet structure

For this WPC pallet, since the load properties of pallet largely depend on the compressive strength of cushion block, the appropriate result can be obtained only when with fine enough meshing in finite element model. Cushion block, upper board, lower board and longitudinal beam are connected with spiny of cushion block by pressing, when dividing the mesh, irregular grid appear in the junction, Virtual Topology can be used to remove those irregular grid at this time.

Choosing Wood-Plastic Composites as the material of pallet, compared with woodwork swan, it has a higher strengthen, toughness and other properties, and moreover, it has a good stability and accurate specification (Cardoso 2013). Physical parameters are shown in Table 1.

Mechanical model of Pallet was simplified, when upper board subject to distributed load. Since static load of pallet $W=2 \times 104 \text{ N}$ and distributed load $q=W/S$, meaning of S is total bearing area of upper board, according to the size parameters of pallet, distributed load can be obtained, $q=W/S=3330 \text{ Pa}$ (Kim et al. 2007).

Mechanical properties testing of materials and equipment

Raw materials are mainly WPC pallet material properties and physical mechanical properties are shown in Table 2 and Table 3.

Table 1—Compare with Wood-Plastic Composites and woodwork swan

Parameter	MOE (MPa)	MOR (MPa)	Poisson's ratio	Density (g/mm ³)
Wood-plastic composites	2611	25	0.211	0.45
Woodwork swan	7480	67	0.31	0.8

Table 2— Composite raw material properties of WPC pallets

Items	Reference Standards	Performance index
Flexural modulus (GPa)	ASTMD790-09	3.6~4.2
Bending flexural strength (MPa)	ASTMD790-09	48.8~52.6
Breaking elongation (%)	ASTMD790-09	3.6~4.2
Modulus of elasticity in compression (MPa)	ASTMD790-09	1.2~1.8
Compression strength (MPa)	ASTMD790-09	30~40
Non-notched impact strength (I•m ⁻¹)	ASTMD790-09	163.9~179.5
Screw pull-out strength (kg)	FT1	342

Table 3—Basic demands for properties of WPC pallet samples

Properties	Value	Properties	Value
Density (g/cm ³)	0.96~1.1	Recoverability	100%
Water absorption (24h)	0.2%		
Bending and compressive strength	Equivalent to hardwood	Raw material	
Impact strength	Can withstand various shocks during handling	Existing	Wide 60~140
Operating temperature	-25°C~45°C	Size (mm)	Height 15~100
Structure size	Small tolerance, High stability		
Standard pallet load	2~5 t	Weight (kg)	17~35
Shelves carry	1~2 t		1200×800
			1200×1000
Maximum deflection (cm)	Under normal temperature static load 0.4	Common pallet specifications (mm)	1219×1016
(Load 3-5t)	45°C static load 1.3		1140×1140
	dynamic load 0.4		1100×1100
			1067×1067

The main test experiments are shown in Figure 2.



Figure 2—Main experimental equipment.

Summary of test methods on static tests

Static tests are performed to determine the strength and stiffness of the pallet under specified load and support conditions (Patricio1 et al. 2006). For all static tests described in Compression Tests, Bending Tests on Pallet and Bending Tests, the test load applied shall include the mass of all load applicators supported by the pallet. The performance criteria in Table 2 and Table 3 may be used to determine the safe working load of a pallet.

4.1 Compression Tests on Pallet Deck Spacers or Supports—the purpose of this test is to determine the resistance to compression of deck spacers (stringers, blocks, and posts) of pallets.

Deformation Measurements—When tested in accordance with the procedure specified in 4.1.2, record the change in the height, y , at Locations A, B, C, and D, as shown in Figure 3, relative to the ground (or test frame), (1) at the datum load (see 4.1.2 and 4.1); (2) at the beginning and end of the full-load period; and (3) upon unloading, at the datum load (see 4.1.2), every 5 min until successive readings are practically identical (limited to a maximum period of 1 h).

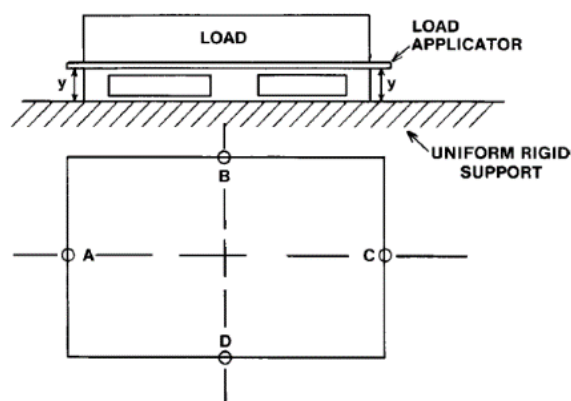


Figure 3—Load and Support Conditions and Locations of Deflection Measurements for Compression Tests of Pallet Deck Spacers or Supports.

4.1.1 When, due to test procedure, the deflections at Locations A, B, C, and D, are not identical, the average of the four observations shall be used as the test measure (see Figure 3).

4.1.2 Test Procedure:

4.1.2.1 Place the pallet in a normal position on a flat, hard, rigid, and horizontal surface. Place a rigid load applicator of sufficient size to overlap the pallet edges and ends, as shown in Figure 3.

4.1.2.2 Gradually apply the test load at a uniform rate of 0.5 ± 0.1 in./min from 0 to 0.10 R, where R is the preliminary safe working load based on the preliminary test or on that determined from tests to failure. This value of 0.10 R shall be the datum load for subsequent deflection measurements. Apply the full test load of $1.1 \cdot M \cdot R$, where M is the maximum number of pallet loads expected in a stack during use. The datum as well as the full test loads shall be applied in not less than 1 min or more than 5 min. maintain the full test load for a period of at least 24h. Reduce the test load to the datum load for the necessary period (see 4.1.1). Take deflection measurements at A, B, C, and D (see Figure 3).

4.1.2.3 If because of the unavailability of a suitable testing machine, dead weights are used for the test load, they shall be symmetrically placed during loading and unloading. Dead weights shall be carefully placed, without dropping, within a 1 to 5-min loading period.

4.1.2.4 An alternative to the full pallet compression test is the test of an individual spacer as in block or post pallets or a portion of the spacer as in stringer pallets (see Figure 4). The datum load shall be adjusted by the ratio of the bearing area of the individual spacers or portions of spacers tested and the bearing area of all spacers in the pallet. For non-uniform loading, only the most severely stressed spacers shall be tested.

4.1.2.5 The average of the deflections measured at A1 and A2 shall be used (see Figure 4). When testing only a portion of the pallet, at least three tests shall be performed at different locations of the pallet, such as at A, B, and C in Figure 4.

4.1.2.6 Observe and record any structural damage or failures. The pallet has failed the test if the observed damage in any pallet tested would affect pallet stiffness, strength, or functionality. The rate of deformation is expected to decrease during the full-load static test.

4.1.2.7 During preliminary testing and to determine the preliminary safe working load R (see Table 3), this test shall be continued to a load level causing structural failure. In such a case, the failed pallet is no longer suitable for use in sequential testing.

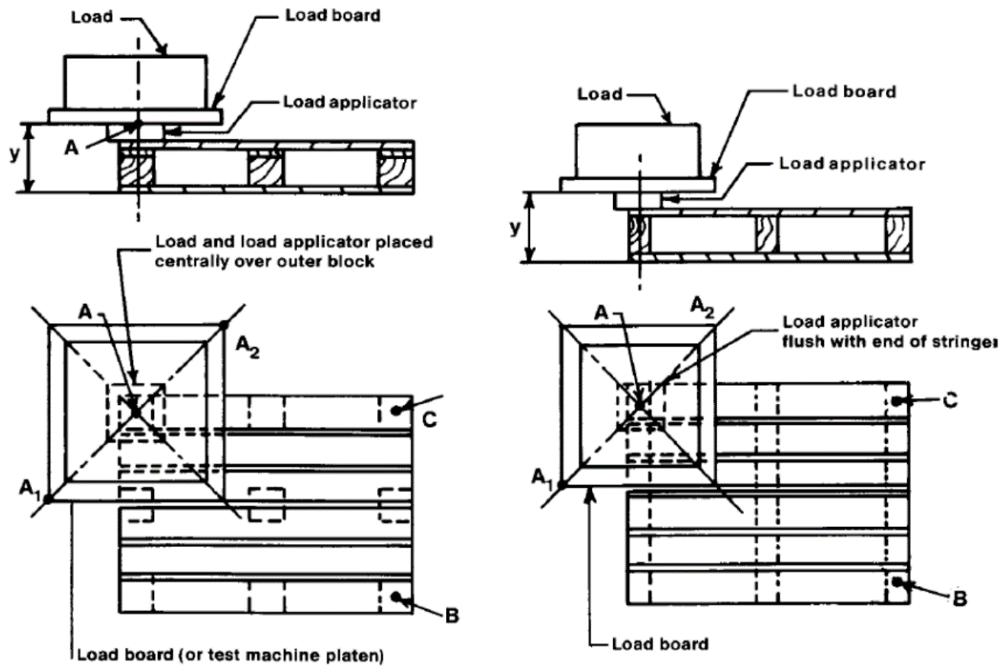
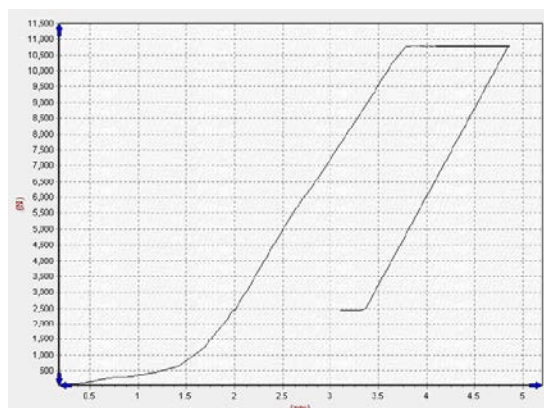


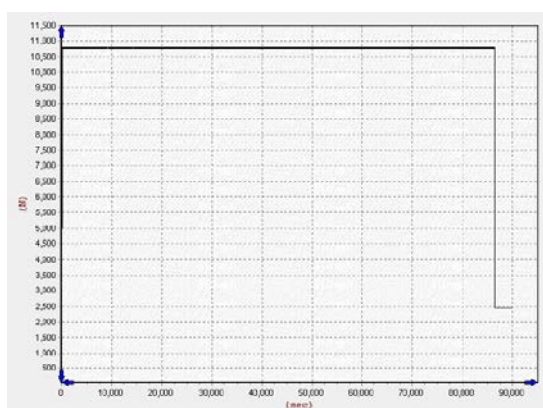
Figure 4—Load Application and Deflection-Measurement Locations for Compression Tests of Individual Pallet-Deck Spacers or Portions of Spacers.



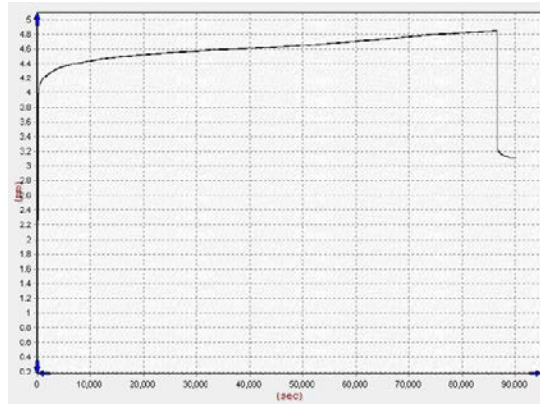
Figure 5—Measure WPC pallet sample in Compression tests



(a) Load-displacement curve



(b) Load-time curve



(c) Displacement-time curve

Figure 6—Curve in Compression tests

4.2 Bending Tests on Pallet—the purpose of this test is to determine the flexural stiffness and strength of the whole pallet.

4.2.1 Test Loads—typical representative loads (case goods, bagged goods, blocks, barrels, etc.) shall be used in pallet bending tests. Where various loads will be placed on pallets that load type resulting in the greatest stress shall be used. When actual loads cannot be used, simulated loads are acceptable. Uniformly distributed case goods or bag loads are simulated using an inflatable bag or a tube restrained in a testing rig or by using a vacuum chamber. Concentrated loads on pallets are simulated with load applications exhibiting the same geometric interface between the load and the pallet deck as the actual in-service load.

4.2.2 Supports—Placement of rigid supports for pallet bending tests shall be based on the mode of support during use. When more than one mode of support is likely to occur, that which most limits the functionality of the pallet under load shall be used for testing. That support which limits pallet functionality in bending shall be used which causes greatest deflection or structural failure at the lowest load levels. This is typically the support that results in the greatest unsupported free span. Support modes are shown in Figure 7 and described as follows:

4.2.2.1 Fork-Tine Support—under the top deck or in the stringer notch in stringer pallets.

4.2.2.2 Rack Support—under the bottom deck or outside of the deck spacers in wing pallets.

4.2.2.3 Sling Support—under the top deck, outside of the deck spacers such as in wing pallets. For sling tests, support modes shall be determined by the intended distribution cycle and the sling equipment used in that distribution environment. (Test devices may include wire, tape, or chain slings and rigid, round, or rectangular spreader bars.)

4.2.2.4 With the exception of very long or wide pallets, which exhibit large cantilevers beyond the supports, the rack mode generally represents the greatest span and corresponding deflection.

4.2.3 Deformation Measurements—When tested in accordance with the method specified in 4.3, the deflection at Locations A, B, and C, as shown in Figure 7, when measured relative to the upper (or lower) surface of the top (or bottom) decks and the ground (or test frame), shall be observed and recorded as follows:

4.2.3.1 At the datum load (see 4.3).

4.2.3.2 Upon unloading, at the datum load (see 4.3), every 5 min until successive readings are practically identical (limited to a maximum period of 1 h).

4.2.3.3 The distance between the decks, h , at mid-span between deck spacers, measured in order to obtain data on the minimum fork entry heights under given loads.

4.2.3.4 Between the decks, similar measurements made at Locations C, D, and E when the test is repeated along the second horizontal axis of the pallet (see 4.3).

4.3 Test Procedure:

4.3.1 For most pallets stressed in bending, the support mode which limits functionality is the rack support or the support under the bottom deck in double-face pallets or under the top deck in single-face pallets. Under these conditions of support, place the pallet top deck uppermost on rigid support beams with square or semicircular cross section. If the span between the supports is unknown, place the inside edges of the supports (or centerline in semicircular cross-section supports) 51 mm (2 in.) from the outer edges of the pallet (see Figure 7).

4.3.2 Gradually apply the test load at a uniform rate from 0 to 0.1 R, where R is the preliminary safe working load per pallet and 0.1 R is the datum load for subsequent deflection measurements. Apply the full test load of $1.25 \cdot M \cdot R$, where M is the maximum number of pallet loads expected when supported or tested. Maintain the full test load for a period of at least 24 h.

4.3.3 Reduce the test load to the datum load for the necessary period (see 4.2.3) and observe the deflection measurements at Locations A, B, and C (see Figure 7).

4.3.4 If, because of the unavailability of a suitable testing machine, dead weights are used for the test load, they shall be symmetrically placed during loading and unloading. Dead weights shall be carefully placed, without dropping, and within a 1 to 5-min loading period.

4.3.5 Repeat the test along the second horizontal axis of the pallet (that is, when both length and width are to be tested). A further set of deflection measurements shall be taken at Locations C, D, and E. Observe and record any damage and structural failure. The pallet has failed the test if the observed damage in any pallet tested affects pallet stiffness, strength, or functionality. The rate of deformation is expected to decrease during the full-load static test.

4.3.6 During preliminary testing and to determine the preliminary safe working load R, this test shall be continued to a load level causing structural failure. In such a case, the failed pallet shall not be used for further testing.

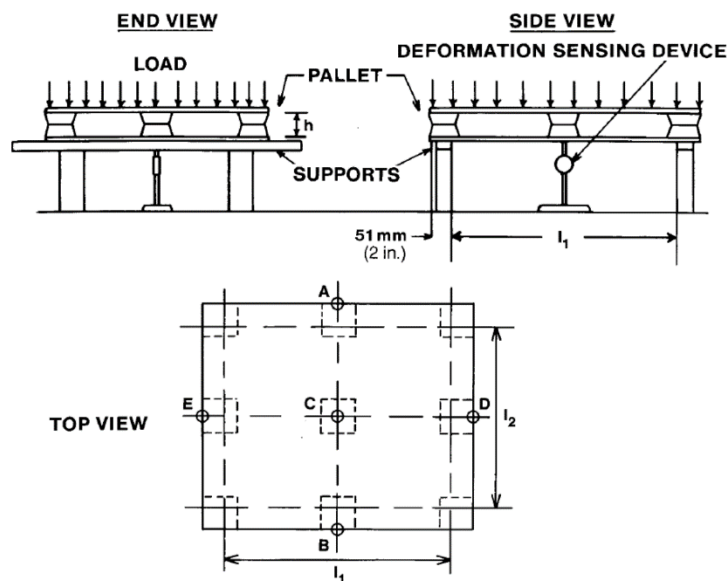


Figure 7—Schematic diagram of pallet bending test using uniformly distributed load.

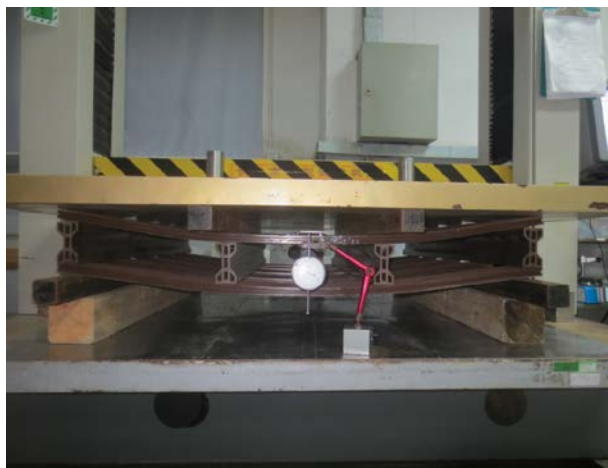


Figure 8—Measured WPC pallet sample of pallet bending test.

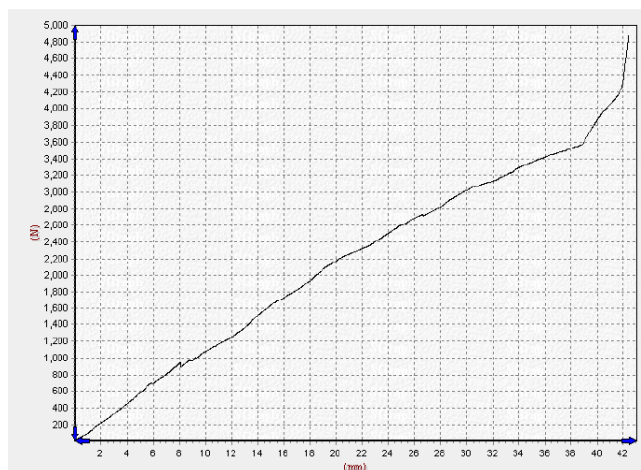


Figure 9—Curve of pallet bending test.

Summary of test methods on dynamic tests

Dynamic tests are performed to determine the stability of the pallet and unit load on the pallet when exposed to elements of the handling and shipping environments (Ratnam et al. 2005). These tests shall be sequentially performed in the order described and each represents one hazard element. A hazard element is a specific event that occurs in the distribution cycle that may pose a hazard to the pallet and the unit load. If any deviations are made from this sequence to meet specific requirements or limitations, they shall be indicated and explained in the report.

5.1 Free-Fall Drop Tests on Pallet Corners and Edges along Pallet Ends and Sides—the purpose of these tests is to determine the resistance to impacts of the pallets, including its decks and blocks, as a result of free-fall pallet drops during handling. Such drops occur during unstacking or removal of pallets. For those non-rigid pallets which may deform as a result of dropping, this test can be used to measure the relative diagonal pallet rigidity (see Figure 10).

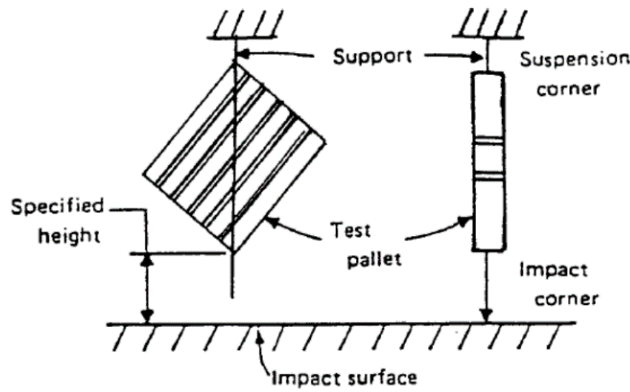


Figure 10—Free-fall drop tests.



Figure 11—Measured WPC pallet sample in free-fall drop tests.

5.2 Incline Impact Tests on Pallet Deck Edges, Blocks or Posts, and Stringers—The purpose of these tests is to determine the resistance of the pallet and its components (deck board, blocks, and stringers) to impact forces resulting from interaction with a variety of material handling equipment, such as forklift trucks and pallet jacks. These tests simulate impact conditions resulting from the following conditions:

Fork heel impacts when the fork heels of the forklift truck impact the pallet deck edges; Fork impact when the tip of misaligned forks strike the corner post or stringer on entry; Fork-tine tip pressure, which causes pallets to collapse horizontally.

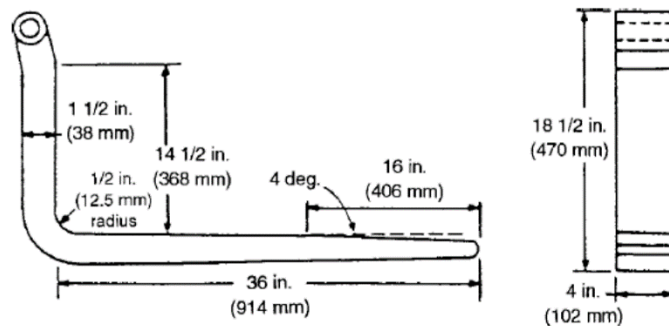


Figure 12—Standard fork used for leading-edge deck-board-separation impact test.

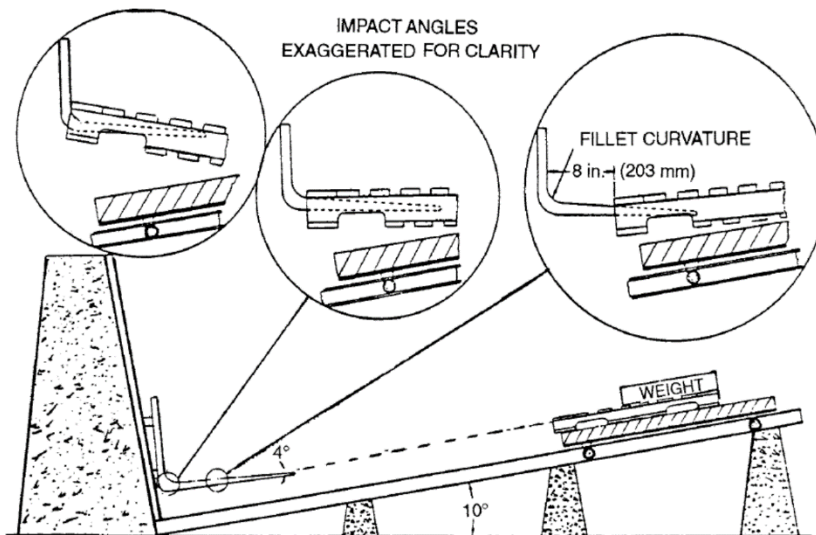


Figure 13—Test setup for determination of incline-impact resistance of leading-edge deck board of pallet.



Figure 14—Measured WPC pallet sample in incline impact tests on pallet deck edges, blocks or posts, and stringers.

Conclusion

As an alternative to the traditional pallets, wood-plastic pallets are gradually gaining market shares in China. Compared to the pallets made of other materials (such as wood, plastic, metal etc.), wood-plastic pallets have certain advantages such as lower cost, environmentally friendly, high water and fire resistance. However, current feedback from the industry and our laboratory testing all indicated that wood-plastic pallets have lower mechanical performance than the traditional wooden pellets, thus add constrains on its application. In order to promote the use of this environmentally friendly product and better regulate its production and circulation in the market, technical standards and specifications need to be established for wood-plastic pallets.

Acknowledgments

The paper is supported by The National Forestry Science and Technology Achievements Promotion Project (No.2015-51) of China State Forestry Administration & The Science Research Project of The China Hunan Province Education Department(No.13A127) .

Reference

E. Soury, A.H. Behraves, E.Rouhani Esfahani, A.Zolfaghari. ,2009.Design, optimization and manufacturing of wood–plastic composite pallet, *Materials & Design*, 30(10):4183-4191.

Kim H-S, Lee B-H, Choi S-W. 2007.The effect of types of maleic anhydride-grafted polypropylene (MAPP) on the interfacial adhesion properties of bio-flour-filled polypropylene composites. *Compos A* 38:1473–1482.

M.M. Ratnam, J.H. Lim, et al. 2005.Study of Three-dimensional Deformation of a Pallet Using Phase-shift Shadow Moir and Finite-element Analysis. *Society for Experimental Mechanics*:9-18.

M.A. Patricio¹, D. Maraval, et al. 2006. Crack Detection in Wooden Pallets Using the Wavelet Transform of the Histogram of Connected Elements. DOI 10.1007/s00107-005-0072-x.*Holz als Roh- und Werkstoff* 64:172–177.

S.R. Cardoso, A.P.F. Barbosa-Póvoa, S. Relvas. 2013.Design and planning of supply chains with integration of reverse logistics activities under demand uncertainty. *European Journal of Operational Research*.226 (3):436-451.

S.Takahara. 2005.Loading Problem in Multiple Containers and Pallets. *EJOR*.123:373-381.

Identification and Evaluation of Historic Timber Buildings in the Dominican Republic by Nondestructive Testing (NDT)

Virginia Flores Sasso *

Department of Architecture, Pontificia Universidad Catolica Madre y Maestra (Pucmm), Santo Domingo, Dominican Republic, vfloressasso@gmail.com

Raquel Carrera Rivery

Department of Architecture, Pontificia Universidad Catolica Madre y Maestra (Pucmm), Santo Domingo, Dominican Republic,

Esteban Prieto Vicioso

Department of Architecture, Pontificia Universidad Catolica Madre y Maestra (Pucmm), Santo Domingo, Dominican Republic, eprietovicioso@gmail.com

* Corresponding author

Abstract

All the Caribbean islands possess abundant wood architecture that are part of its cultural heritage and of the historical landscape of the region, most of them constructed between XIX and XX centuries, product of the commercial boom between the Greater Caribbean with the United States and Europe. Now, most of these buildings are in a poor condition and lack of maintenance. Also the Caribbean weather conditions accelerate the deterioration process. In the Dominican Republic, the timber buildings are not properly protected and there is no regulations or policies that controls the preservation, causing inadequate interventions that affect their construction systems and historical value. The cause is a product of ignorance of the properties of the woods and absence of appropriate methodology to evaluate and study it. The lack of a useful and consistent inspection method to detect damage and decayed parts of the timber structural elements, and the interest of saving the maximum amount of historic fabric, motivated this study. For that reason, the aim of the research is to characterize the type of wood and develop a methodology to evaluate the state of the historic timber fabric by nondestructive testing. A methodology was designed for “in situ” and laboratory evaluation. The intend are to integrate research techniques and new processes together with traditional methods. The used methods are: visual inspection for quality, nondestructive testing and a minimum of destructive testing (just to determine a few parameters) to assessment the structural elements mechanical characteristics as a resistography readings and impulse tomography images.

Keywords: historic timber, resistography, Arbotom impulse tomography, Caribbean timber

Feasibility and marketing channels of a mobile phone application that brings nondestructive techniques to job sites

Songyi Han *

Department of Sustainable Bioproducts, Mississippi State University, Starkville, Mississippi, U.S.,
sh2350@msstate.edu

R. Daniel Seale

Department of Sustainable Bioproducts, Mississippi State University, Starkville, Mississippi, U.S.,
rds9@msstate.edu

Rubin Shmulsky

Department of Sustainable Bioproducts, Mississippi State University, Starkville, Mississippi, U.S.,
rs26@msstate.edu

Abstract

This work proposes to 1) conduct market research on the use of mobile phones and mobile phone apps in the forest products industry and academia and 2) project how well an app that measures stiffness of wood board is welcomed and used on job sites. An online survey was conducted to collect data adopting convenience sampling method. Participants were who work with wood or wood-based products, and the sample was compiled from publicly available online sources, online directories, and print of Big Book by Random Length. A questionnaire was specifically developed to this study. Out of 1,221 email invitations 311 responses were returned at the response rate of 27 percent. Data were analyzed using SPSS. Nearly all of the respondents (95.7%) had smartphones and over half of them were iOS users (52.3%). Higher personal use of mobile phone apps was observed than for working purposes. In which, academia and research users showed higher app uses. More respondents had purchased paid apps (45.2%) than in-app services on free apps (28.5%) that indicates paid apps can be more likely of respondents' interests than in-app purchase. The respondents were asked if they would be interested in an app that measures stiffness of wood boards. The result showed that the app could be useful for them. Millennial respondents were more interested in the app than Baby Boomer and Generation X, whereas, respondents in academia showed higher level of interest than those in industry.

Keywords: mobile phone use, mobile phone application, forest products industry, stiffness of wood board, email survey